The Role of F_{420}-dependent Enzymes in *Mycobacteria*

A thesis submitted for the degree of Doctor of Philosophy of the Australian National University

Australian National University

Brendon M. Lee

December 2017

Declaration

The work presented in this thesis has been performed by the author except were stated in the text before the chapter. This work was primarily done at the Australian National University under the supervision of Associate Professor Colin Jackson. Some experimental work was performed at the Commonwealth Scientific and Industrial Research Organisation at Black Mountain under the supervision of Dr. Matt Taylor and at the University of Otago under the supervision of Professor Gregory Cook. The work presented in this thesis has not been submitted as part of any other degrees.

Brendon M. Lee

December 2017

Acknowledgements

I would first like to acknowledge my supervisor Associate Professor Colin Jackson for taking me into his lab, mentoring me, and allowing me to further my scientific career. I am also thankful for being patience with me in the weaker aspects of my work, especially my writing. This is best shown from your comments that started off as ‘I think Craig Marshall is right and you may be a little dyslexic’ to becoming ‘when I was reading your work, I didn’t believe you were the one that wrote it’. A compliment is a compliment.

I am very thankful to the people in the Jackson lab that helped me through this journey from helping me in the lab to becoming some of the greatest friends I have. I am particularly thankful for Hafna Ahmed for teaching me the majority of what I now know today. I am also thankful to the rest of the F_{420} crew including Elaaf Mohamed who helped with quite a few things.

To the people at CSIRO, I thank you for allowing me to use your lab but also becoming good friends in the process. My special thanks to Dr. Matt Taylor who helped me with a lot there and had a lot of patience and excitement when we discuss what was needed to be done. I am also thankful to Dr. Shoko Okada for the help you provided to a much stressed man trying to use a very new and expensive machine. To Chris Greening who has now moved on to Monash, I thank you for the help you had provided while at CSIRO, I learned a lot from you.

To Professor Gregory Cook, whose passion for life is unchallenged. I thank you for allowing me to work in your lab and allowing that great experience. I am very thankful to Kiel Hards and Liam Harold for the help you gave me while I was back in Dunedin, this project would not have been as successful without you. To the rest of the sixth floor, the banter, the friendships, and the water skiing will never be forgotten.

Outside of science I would like to thank the lads and lasses at the Uni North Owls. My passion for rugby has never been higher and the friends I have made are some that will be a lifetime. I will also thank the great athletes that are the RSC touch team, a Thursday is nothing without a touch game in 40 degree weather. To my friends at City at Night, you really helped me in a lot of ways.

To my Family, I am very thankful. Mum and Pa, although you still do not understand what I do, your support has been overwhelming. Alastair, Chris, Kerri, and Kevin, I am honoured to have you as my siblings.

Finally I would like to acknowledge the Australian Government for support through the Research Training Program Scholarship, and the Australian National University and Research School of Chemistry for support through the Alan Sargeson Merit Scholarship and the Research School of Chemistry Scholarship.

Abstract

Tuberculosis (TB) is the leading cause of death by an infectious disease, recently surpassing HIV/AIDS. The causative agent, *Mycobacterium tuberculosis*, is difficult to treat as it can survive harsh conditions and can switch between an active infection, which causes ~1.5 million deaths a year, and a latent state, which infects up to one third of the world's population. *M. tuberculosis* is also becoming more resistant to frontline drugs, making it a dangerous world epidemic. It is therefore essential that new treatments are developed to help combat TB. A new enzyme superfamily has recently been discovered that utilises the rare co-factor F_{420}, which is not produced or utilized by humans, allowing for specific drug targeting of the mostly uncharacterized enzymes that utilise it. The aim of this thesis is to better understand the roles of these enzymes in *Mycobacteria* and to investigate the mechanism by which *M. tuberculosis* might evolve resistance to a new class of prodrugs that are activated by the F_{420}-dependent enzyme deazaflavin-dependent nitroreductase (Ddn).

Prodrugs that are activated by Ddn include pretomanid and delamanid, which are effective against both an active and latent TB infection. Ddn is natively a quinone reductase, but also reacts with these drugs to reduce them, thereby releasing nitrous oxide and other breakdown products that are thought to inhibit hydroxymycolic acid dehydrogenase. Resistance against pretomanid *in vitro* has been documented in laboratory studies to occur *via* mutations to the F_{420} biosynthetic pathway, the enzyme F_{420}-dependent glucose-6-phosphate dehydrogenase that reduces F_{420}, and Ddn. However, the fitness cost of such mutations, i.e. whether they would still be virulent and transmissible, has not been studied. This important question will determine whether such genetic changes could lead to clinically relevant resistance. I explored this question with a detailed study of Ddn to establish (i) whether its activity is essential for the fitness of *M. tuberculosis* and (ii) whether any mutations could knock out the prodrug-activating activity without substantially affecting the native quinone reductase activity. I investigated this by better defining the physiological role of Ddn, showing that it can reduce menaquinone, and that this activity can enhance respiration of the cell by coupling with cytochrome *bd*. I also demonstrated that Ddn orthologues have similar quinone reductase activity as Ddn, but have no activity with pretomanid, except for the *M. marinum* orthologue that has activity with both. Through site directed mutagenesis I have identified a number of mutations to Ddn's active site that eliminate activity with pretomanid while retaining some quinone reductase activity. A clinical strain that had acquired one of the tested mutations

through neutral genetic drift/variation showed resistance to pretomanid, despite never having been exposed to the compound. Interestingly, the other nitroimidazole prodrug, delamanid, was still effective Computational modelling suggets this to be due to the way that each nitroimidazole binds Ddn.

The first step to developing a new drug to target an F_{420}-dependent enzyme, we first need to identify genes/proteins that are essential for some aspect of the life cycle of *M. tuberculsosis.* Collaborators have shown that the F_{420}-dependent enzyme Rv0121c (homologous to MSMEG_6526 in *Mycobacterium* smegmatis) from the flavin/deazaflavin oxidoreductase (FDOR) protein superfamily is essential for escape from dormancy. As a model for *M. tuberculosis* we made a MSMEG_6526 knockout in *M. smegmatis* and confirmed that it is conditionally essential. This was demonstrated by the slower growth rate of Δ6526 compared to wildtype in minimal media with several different carbon sources, and the lack of growth on acetate and pyruvate. Proteomics showed the upregulation of the methylcitrate cycle, glyoxylate cycle, and several F_{420}-dependent enzymes, including the Ddn orthologue MSMEG_2027. Proteins that were downregulated were part of the Kerbs cycle, late stage glycolysis, and several amino acid metabolomic pathways. This was complemented with metabolomics, revealing several metabolites that were affected by the MSMEG_6526 knockout. The pathway that these metabolites were involved in included the Krebs cycle and several related amino acid metabolic pathways. This suggests that MSMEG_6526 is somehow involved in amino acid metabolism. The crystal structures of Rv0121c and MSMEG_6526 in complex with F_{420} were solved, revealing homodimers of the split β-barrel fold that defines the FDOR super family. The structures revealed three extended loops, two of which made a more defined active site compared to other FDORs. The third loop was not involved with the active site and is not conserved between the two enzymes, while the active site and F_{420} binding are highly conserved. The structure was also used to identify the type of substrates that can bind these enzymes.

The other chapters presented in this thesis are collaborative projects that I had contributed towards. These include detailed characterization of the FDOR superfamily in which a number of specific sub-groups of the FDOR superfamily based on sequence similarity and structural motifs. We also identified novel F420-dependent biliverdin reductases in *M. tuberculosis* that reduce bilirubin, a known antioxidant. Finally, we expand the list of chemicals that FDORs has promiscuous activity with, including antimicrobials that we show are more

potent with F_{420} knocked out. The final chapter is a comprehensive review of F_{420}, it precursor F_o, and related enzymes in *Mycobacteria*, methanogens, and other bacteria that utilise it.

Table of Contents

Chapter 1

Introduction

1.1 *Mycobacterium tuberculosis*

In the 2016 World Health Organisation (WHO) tuberculosis report, tuberculosis was declared in the top ten causes of death, and is the leading cause of death by infectious disease, surpassing HIV/AIDS. In 2015 alone, 1.8 million people died (Fig. 1.1a), with 10.4 million people falling ill from tuberculosis. It is estimated that one third of the world's population is infected with latent *Mycobacterium tuberculosis*, the causation of tuberculosis (WHO, 2016).

The standard treatment for tuberculosis since the 1980s, is a four drug cocktail (isoniazid, rifampin, pyrazinamide, and ethambutol) over six months (Lienhardt *et al.*, 2012). This therapy was only completely effective until the 1990s, after which major issues arose, including high costs per patient, poor compliance and management, and extensive drug-drug interactions (Zumla *et al.*, 2013). Due to these problems, tuberculosis acquired extensive resistance towards these drugs and is now a major problem (Jain *et al.*, 2008). This rise in resistance reflects the biology of *M. tuberculosis*, which can transition between chronic and latent infection states allowing the ability to evade the immune system and resist drug treatment (Boshoff and Barry, 2005). In 2015, there were 480,000 new cases of multi-drug resistant tuberculosis (MDR-TB); tuberculosis that is resistant to the two most powerful anti-tuberculosis drugs (Isoniazid and Rifampicin), and 100,000 new cases of Rifampin-resistant tuberculosis (RR-TB). The majority of these cases come from China, India, and Russia (Fig. 1.1b). The proportion of MDR-TB that were extensively-drug resistant tuberculosis (XDR - TB); tuberculosis that is resistant to at least four of the front line anti-TB drugs, was 9.5 % (WHO, 2016).

The rise of tuberculosis that is resistant to frontline drugs has been increasing, and it is therefore important to develop new drugs to combat tuberculosis, including new strategies that not only target active tuberculosis, but latent tuberculosis. Unfortunately, the gap in funding for implementation of detection and treatment, and research and development is short of what is needed (WHO, 2016). Despite this, there are new drugs that are promising but the possibility and impact of resistance is not fully understood. Therefore, it is important to understand the mechanisms by which resistance to new drugs might arise, and to understand the physiology and function of potential new targets to develop novel treatments to continue the improvement of tuberculosis treatment. The overall aim of this thesis is to further understand the physiological, promiscuous, and drug related function of F_{420}-dependent enzymes in

Mycobacteria. This will allow for the improvement of the current tuberculosis drug regime, the development of new antimycobacterials, and to provide a molecular basis for enzyme engineering of F_{420}-dependent enzymes for biosynthetically useful reactions.

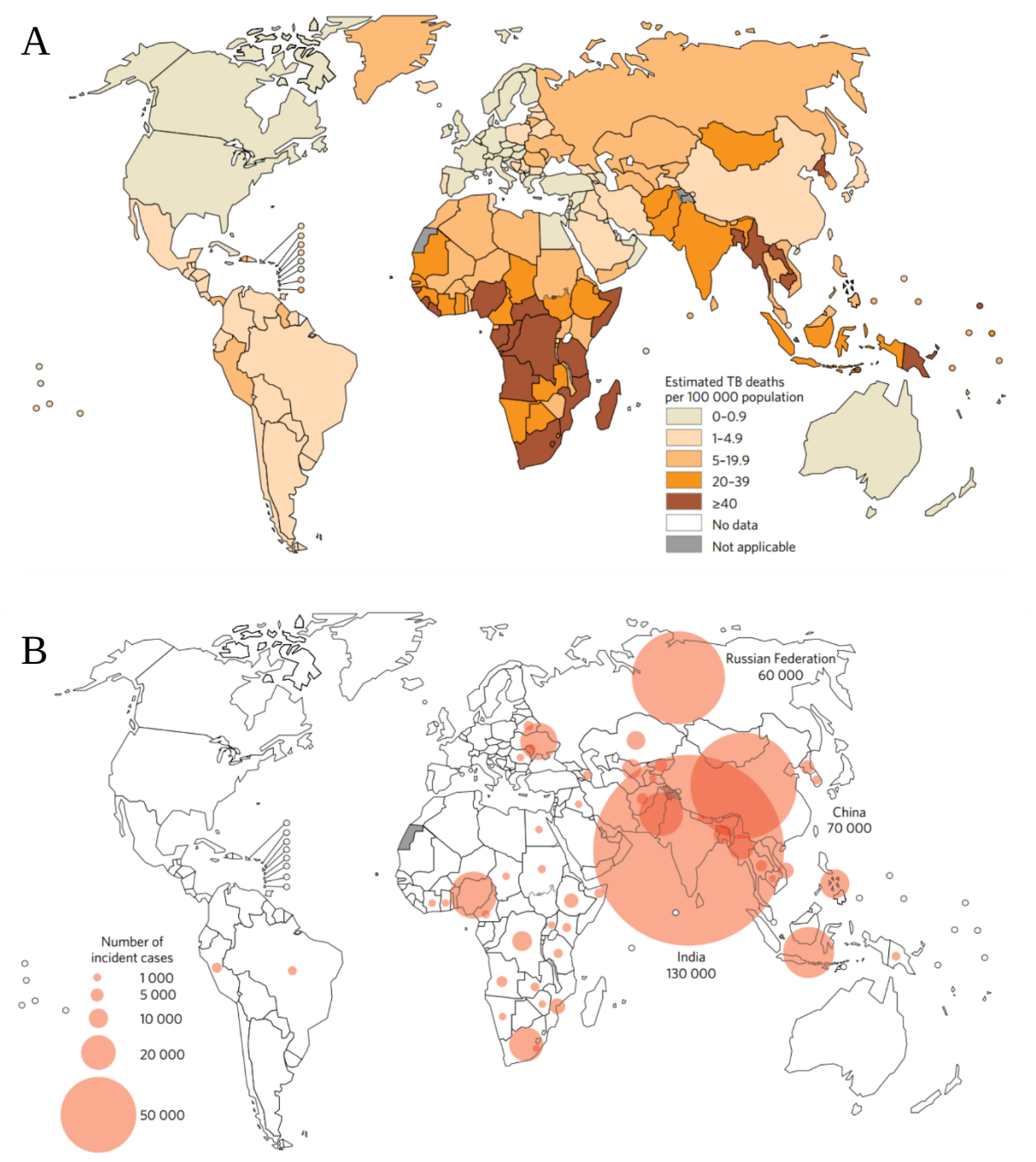

Figure 1.1. Global impact of tuberculosis. (A) Estimated TB mortality rates in HIV-negative people in 2015. (B) Estimated incidence of MDR/RR-TB in 2015, for countries with at least 1000 cases. Adapted from WHO 2016.

1.2 Next generation Anti-mycobacterials

Until recently, no new anti-tuberculosis drug had been approved in more than 40 years. In 2012 and 2014, the diarylquinoline, Bedaquiline, and the nitroimidazole, Delamanid, were conditionally approved respectively for treatment against MDR-TB (Mahajan, 2013; Ryan and Lo, 2014). These two classes of drugs are discussed in Section 1.2.1 and Section 1.2.2. Another nitroimidazole, Pretomanid, which predates Delamanid in development, is in phase III trials, in regimens that include Bedaquiline and the repurposed antibiotic, Linezolid, or with Pyrazinamide and the repurposed antibiotic, Moxifloxacin (Fig. 1.2a) (Dawson, Diacon, Everitt, Niekerk, Donald, Burger, Schall, Spigelman, Pym, Groote-bidlingmaier, Mendel, *et al.*, 2015; Tasneen *et al.*, 2016). There is a regimen of Pretomanid with Bedaquiline and pyrazinamide also in phase III trials (Diacon *et al.*, 2015). Another repurposed antibiotic, Rifapentine, is in phase III trials with Moxifloxcin to reduce the treatment time of drug-susceptible tuberculosis down from over six months to four months (Jindani *et al.*, 2014).

Between 2015 and 2016 two drugs were abandoned in clinical trials, AZD5847, due to the lack of demonstrated anti-tuberculosis activity, and a third generation nitroimidazole, TBA-354, due to toxicity found in the Phase I trial (WHO, 2016). Despite this, there are three new drugs in early clinical trials. In Phase I trials, there is the imidazopyridine amide, Q203, that targets the respiratory cytochrome bc1 complex, and the piperazine-containing benzothiazinones, PBTZ169, which inhibits decaprenylphosphoryl-beta-D-ribose 2-epimerase, an essential flavoenzyme involved in cell wall synthesis (Pethe *et al.*, 2013; Makarov *et al.*, 2014; WHO, 2016). The oxazolidinone Sutelozid, an analogue of Linezolid that inhibits protein synthesis is in phase II trials (Fig. 1.2a) (Williams *et al.*, 2009; WHO, 2016).

Vaccines against tuberculosis are limited with the Bacille-Calmette-Guérin (BCG) vaccine, a attenuated vaccine containing the strain *M. bovis* BCG, as the only available vaccine, having limited use due to its variable efficacy (Colditz *et al.*, 1994). As of 2016, there are five vaccines in phase I trials, seven in phase II trials, and one in phase III trials (Fig.1.2b). These vaccines includes recombinant BCG strains whole-cell derived vaccines, recombinant viral-vectored platforms, protein and adjuvant combinations, and mycobacterial extracts. They aim to prevent infection, prevent primary progression to disease, or the reactivation of latent tuberculosis infection (WHO, 2016).

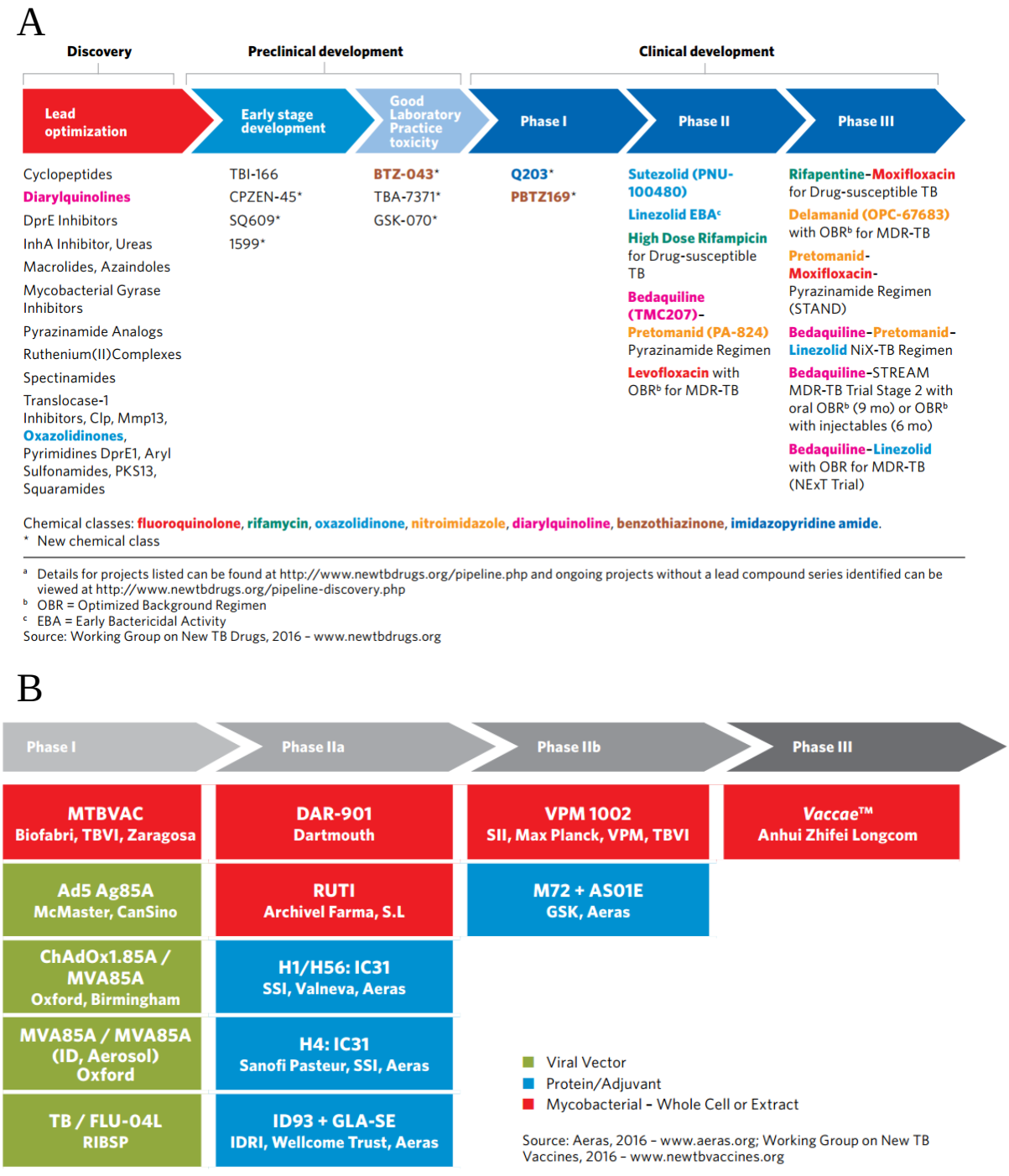

Figure 1.2 Current tuberculosis treatments in development. (A) Anti-tuberculosis drugs in development. (B) Current tuberculosis vaccines treatments in development. Adapted from WHO 2016

1.2.1 Bedaquiline

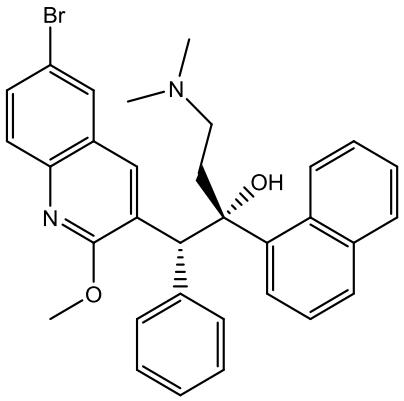

Figure 1.4 Structure of Bedaquiline.

In 2012, Bedaquiline (Fig. 1.3) was conditionally approved and was the first anti-tuberculosis drug with a novel mode of action to be approved since 1974, with the approval of Rifampicin (Deoghare, 2013; Mahajan, 2013). It is a diarylquinoline that is effective against both active and latent *M. tuberculosis*, MDR-TB, and other Mycobacteria species including, *M. ulcerans*, *M. abscessus* and *M. smegmatis* (Andries *et al.*, 2005; Koul *et al.*, 2008). Initial studies of bedaquiline showed that it binds to the c-subunit of the ATP synthase and is able to inhibit the synthesis of ATP in the cell (Andries *et al.*, 2005; de Jonge *et al.*, 2007; Koul *et al.*, 2007).

The crystal structure of the *M. phlei* ATP synthase revealed a binding pocket in the c-subunit that provides hydrogen bonding between a conserved glutamic acid and the dimethylamino moiety of bedaquiline. Mutations found in bedaquiline resistant strains have shown to directly or indirectly disrupt this hydrogen bonding (Segala *et al.*, 2012; Preiss *et al.*, 2015). Specificity of bedaquiline to *Mycobacteria* ATP synthases is due to a phenylalanine that provides a hydrophobic platform for bedaquiline to bind. This phenylalanine is highly conserved across *Mycobacterial* species but is not found throughout other bacteria and eukaryotes, (Preiss *et al.*, 2015). This interaction allows bedaquiline to bind the *Mycobacteria* ATP synthases 20,000 times more effectively than the mitochondrial ATP synthase (Haagsma *et al.*, 2009). Initial human trials showed mild to moderate side effects to bedaquiline, which was expected due to its specificity to the Mycobacterial ATPase (Diacon *et al.*, 2009). Unfortunately, further trials have raised concern over bedaquiline having a higher mortality rate when compared to the placebo and has received a black-box warning for risk of death and arrhythmias (Cox and Laessig, 2014; Diacon *et al.*, 2014). The effect of bedaquiline does not increase with higher concentrations, and studies suggests a time dependent mechanism rather than a concentration-dependent effect (Koul *et al.*, 2014). Early studies suggested bedaquiline

to be an inhibitor of ATP synthase due to the decreases in ATP (Koul *et al.*, 2008). Further studies showed that the presences of bedaquiline removes the proton gradient, eliminating the proton-motive force across the membrane, while maintaining the difference in pH, which is most likely due to another salt such as K^+. Therefore, the proposed mechanism is, bedaquiline binds to the c-subunit of the ATP synthase that forms a gap between the c-subunit and the a-

subunit that allows an uncontrolled proton leak, eliminating the proton motive force (Fig.1.4) (Hards *et al.*, 2015).

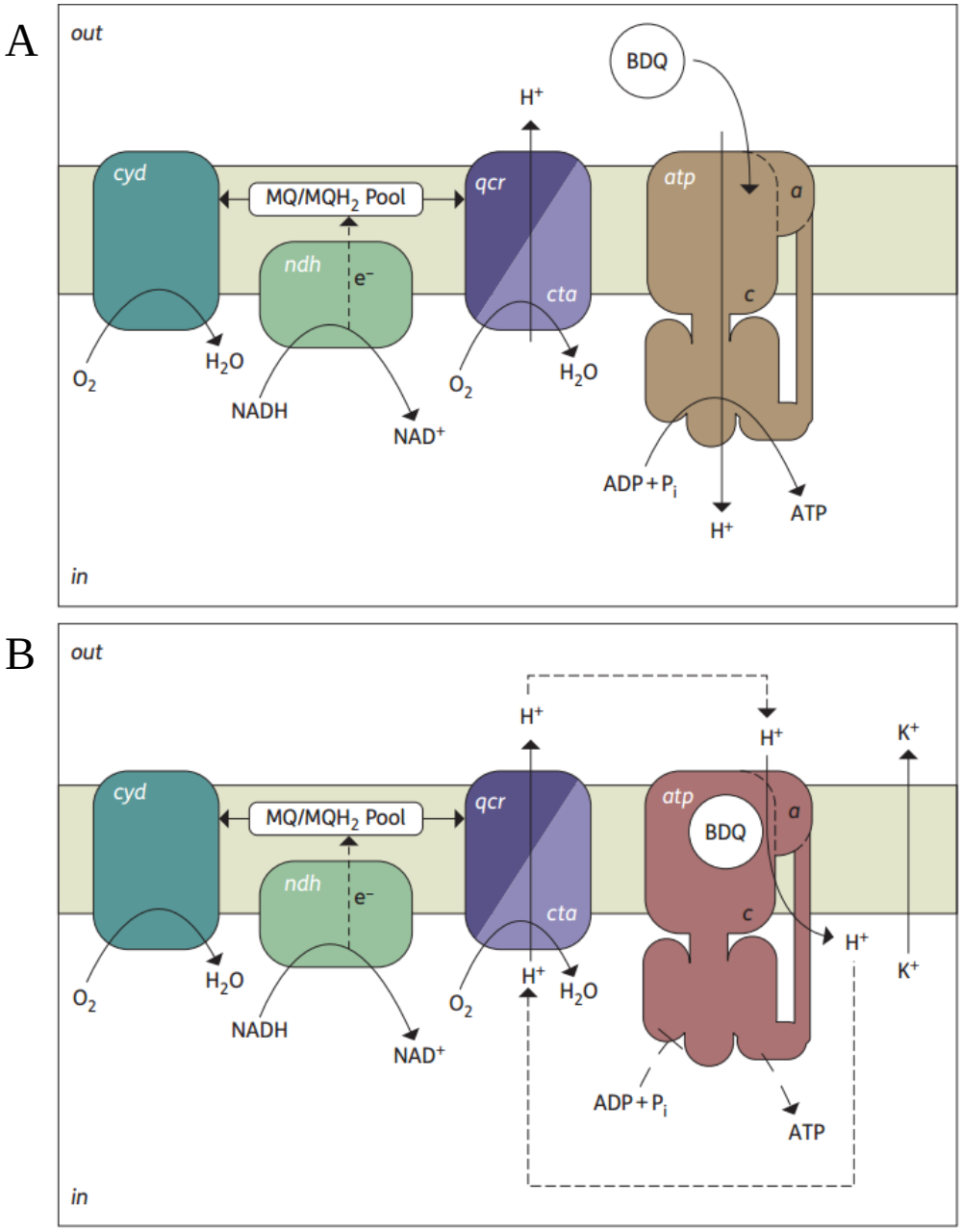

Figure 1.4 The mechanism of Bedaquiline. The majority of ATP synthesis is respiratory (a), driven by the PMF. The binding of bedaquiline (b) to the c-ring creates a gap in the a-c subunit interface, causes an uncontrolled proton leak uncoupled from ATP synthesis and resulting in a futile proton cycle. The membrane potential is most likely compensated by the exchange of other cations (i.e. K^+). BDQ, bedaquiline. Adapted from Hards *et al.* 2015

1.2.2 Nitroimidazoles, Pretomanid and Delamanid

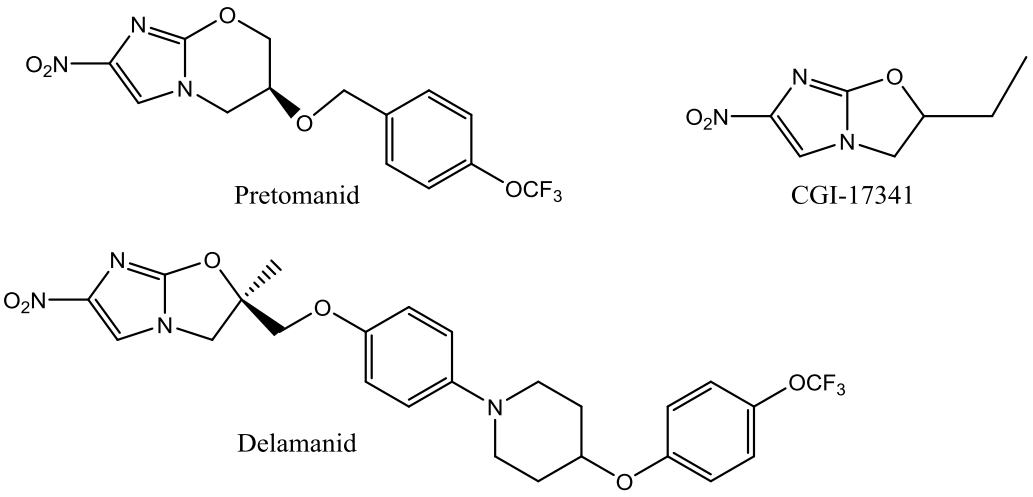

Figure 1.5 Structures of Nitroimidazole Prodrugs

Nitroimidazoles (Fig. 1.5) are a class of prodrugs that have been shown to have promising effects on both active and latent *M. tuberculosis* (Greening *et al.*, 2016; Chen *et al.*, 2017). They are activated by the enzyme deazaflavin-dependent nitroreductase (Ddn, Rv3547) through a two electron hydride transfer from $F_{420}H_2$ (Stover *et al.*, 2000; Ji *et al.*, 2006; Manjunatha *et al.*, 2006). Ddn orthologues are conserved throughout *mycobacteria* (except *M. leprae*), although related species have been shown to be resistant to pretomanid and delamanid, due to the difference in sequence identity that leads to a lack of activity with nitroimidazoles (Ji *et al.*, 2006; Manjunatha *et al.*, 2006; Cellitti *et al.*, 2012; Gurumurthy *et al.*, 2012) Resistance in *M. tuberculosis* towards nitroimidazoles has been shown to arise through mutations in the F_{420} biosynthetic pathway (see Section 1.3.2), the enzyme F_{420}-dependent glucose-6-phosphate dehydrogenase (fgd), that reduces F_{420} to $F_{420}H_2$ (see section 1.4.1), or Ddn (Feuerriegel *et al.*, 2011; Haver *et al.*, 2015). Nitroimidazoles have also been shown to be effective against visceral leishmaniasis, a diseased caused by the protozoan parasites, *Leishmania donovani*, or *L. infantum* (Patterson *et al.*, 2013; Patterson *et al.*, 2016). The activation of Nitroimidazoles in *Leishmania* is by a FMN-dependent NADH oxidoreductase (NTR2) (Wyllie *et al.*, 2016).

The first nitroimazole to be shown to be effective against *M. tuberculosis* was CGI-17341 (Ashtekar *et al.*, 1993). It is suggested to be activated by several F_{420}-dependent enzymes as well as Ddn, as it still effective when Ddn is knocked out, but loses activity when F_{420} biosynthesis is eliminated. The promiscuity of CGI-17341 is most likely due to the lack of

hydrophobic tail and phenyloxazole resides found on pretomanid and delamanid (Manjunatha *et al.*, 2006; Gurumurthy *et al.*, 2012). Unfortunately, CGI-17341 is mutagenic, which is seen with most nitroimidazoles that have a mono- or di-alkyl tail, and development has been discontinued (Stover *et al.*, 2000; Matsumoto *et al.*, 2006). Pretomanid was developed from CGI-17341 by replacing the short alkyl substitution with a longer hydrophobic tail. This made it non-mutagenic but can only activated by Ddn (Stover *et al.*, 2000; Gurumurthy *et al.*, 2012). Delamanid has a longer lipophilic tail than pretomanid that leads to a higher potency but at the cost of a poor pharmacokinetic profile (Matsumoto *et al.*, 2006; Upton *et al.*, 2015). To try and improve the solubility while maintaining high potency, TBA-354 was developed, but has been discontinued due to its toxic side effects and lack of novelty (Tasneen *et al.*, 2015; Upton *et al.*, 2015).

The reduction of nitroimidazoles leads to the decomposition into three metabolites, predominantly a des-nitro compound, and nitric oxide or nitrous oxide (Fig. 1.6) (Matsumoto *et al.*, 2006; Singh *et al.*, 2008). The activation of nitroimidazoles in Ddn is stabilised by a serine hydrogen bonding to the nitrogen group. This stabilises the transition intermediate after the initial hydride transfer from $F_{420}H_2$, allowing a second hydride transfer leading to the rearrangement of the imidazole group, releasing nitric oxide or nitrous oxide (Singh *et al.*, 2008). This reaction needs to be protected from the solvent that is provided through a hydrophobic barrier provided by three tyrosines in the active site of Ddn (Mohamed *et al.*, 2016). The reduction of nitroimidazoles has a dual bactericidal effect as a result of the products formed (Manjunatha *et al.*, 2009). The initial bactericidal effect is through the release of the reactive nitrogen species, which react with cytochromes and cytochrome c oxidase, which in turn interferes with the electron flow of the electron transport chain leading to respiratory poisoning (Singh *et al.*, 2008). The primary metabolite formed, the des-nitro compound, inhibits the oxidation of hydroxy-mycolic acid to keto-mycolic acid, a key component of the cell wall of *M. tuberculosis* that enhances it pathogenic nature, by inhibiting the enzyme F_{420}-dependent hydroxymycolic acid dehydrogenase (fHMAD) (see section 1.4.1) (Stover *et al.*, 2000; Matsumoto *et al.*, 2006; Purwantini and Mukhopadhyay, 2013)

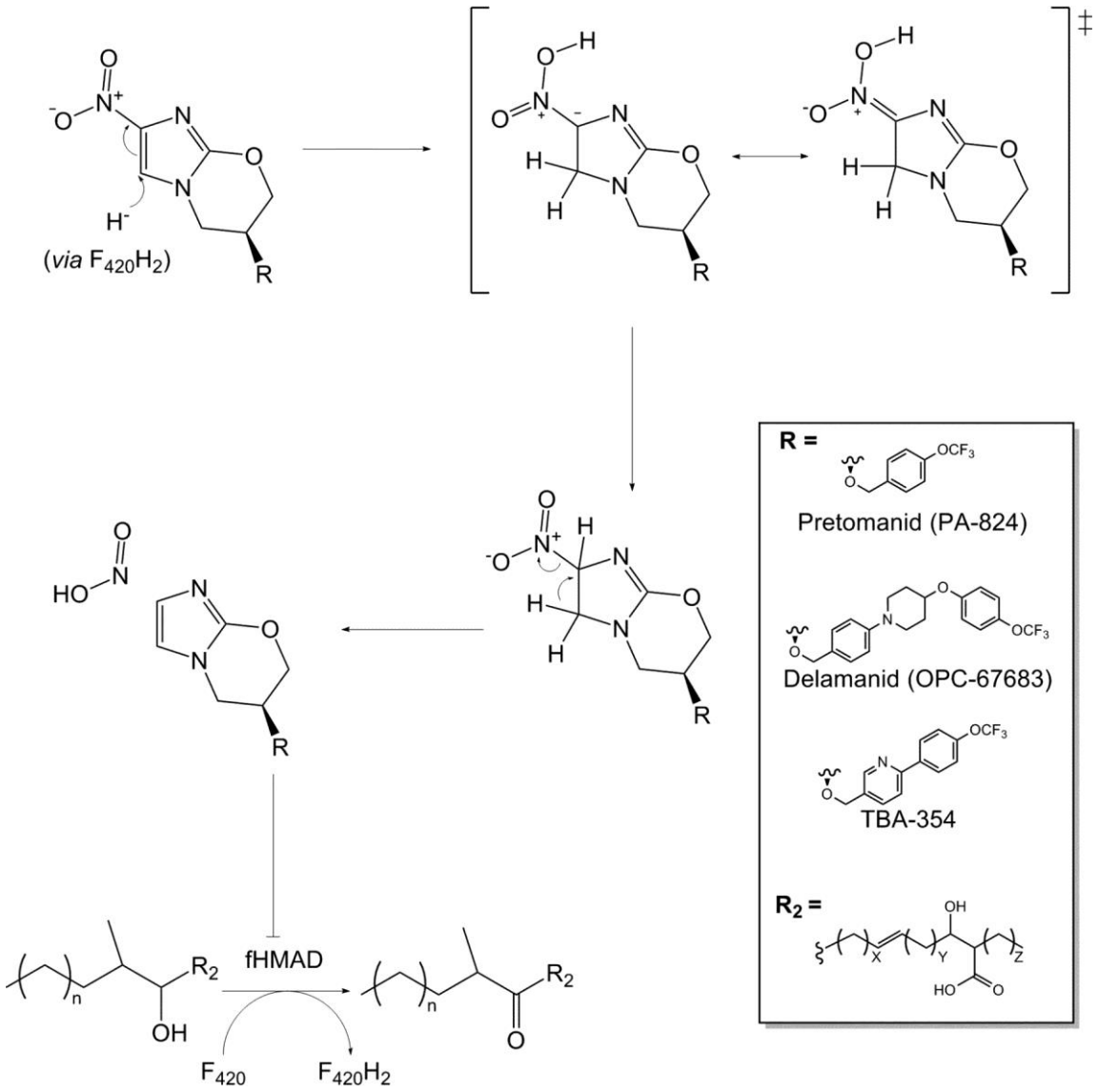

Figure 1.6 Mechanism of nitroimidazole reduction by the activation of $F_{420}H_2$. Adapted from Greening et al. 2016.

1.3 The Co-Factor F420

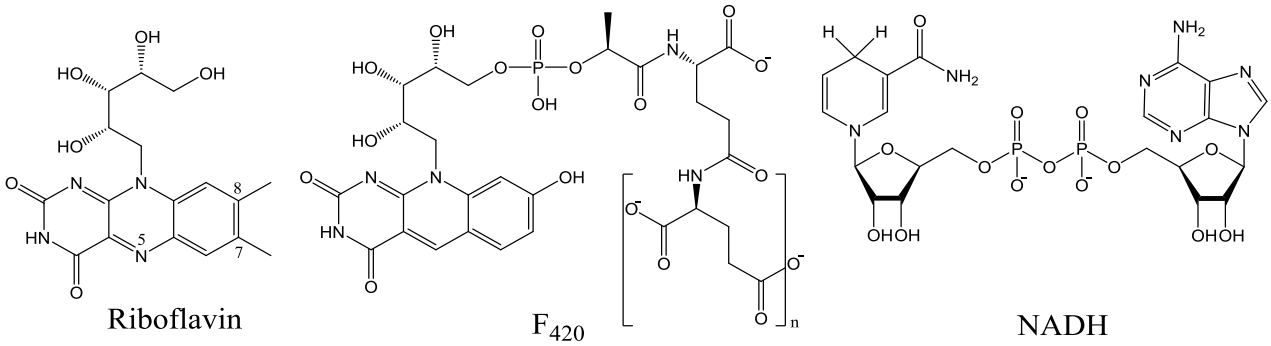

Figure 1.7 Structure of Riboflavin, F_{420}, and NADH.

The cofactor, F_{420} (Fig. 1.7), was first identified from methanogen crude lysate in 1972. The components that were identified through acid hydrolysis were glutamate, an acid-stable chromophore, phosphate, and an ether-soluble phenolic component. It was also noted that F_{420} could be reduced using either sodium dithionite or sodium borohydride (Cheeseman *et al.*, 1972). The full structure was characterised using spectroscopic analysis of its degradation products and validated by chemical synthesis (Eirich *et al.*, 1976; Ashton *et al.*, 1979; Ashton and Brown, 1980; Pol *et al.*, 1980). F_{420} is named due to its characteristic absorbance at 420 nm, giving a yellow-green colour, which disappears when reduced to $F_{420}H_2$ (Fig.1.8) (Cheeseman *et al.*, 1972).

F_{420} is structurally similar to flavins (Riboflavin, FMN, and FAD), except for a carbon atom substituted for the N-5 atom of the isoalloxazine ring, C-8 is hydroxylated, and C-7 is demethylated (Fig. 1.7). It is a obligate two-electron carrier, whereas flavins can be a one or two electron carrier (Edmondson *et al.*, 1972; Xia *et al.*, 2015). This is due to the C-5 substitute in F_{420} that does not allow it to be stabilised as a semiquinone, whereas the N-5 unpaired electrons in flavins can delocalise throughout the isoalloxazine, allowing them to be stable as a semiquinone (Fisher *et al.*, 1976). The N-5 substitution to carbon gives F_{420} a lower redox potential (-340 mV) compared to riboflavin (-210 mV), FAD (-220 mV), or FMN (-190mV). This makes F_{420} functionally more similar to NADH/NADPH (-320 mV) (Thauer *et al.*, 1977; Jacobson and Walsh, 1984; Walsh, 1986; Buckel and Thauer, 2013) Due to its low redox potential, F_{420} is capable of reducing a wide range of organic compounds that are otherwise difficult to activate and can be utilized by aerobic bacteria in hypoxic and anoxic environments, potentially substituting for NADH/NADPH (Ebert *et al.*, 1999; Lapalikar *et al.*, 2012; Greening *et al.*, 2016; Jirapanjawat *et al.*, 2016).

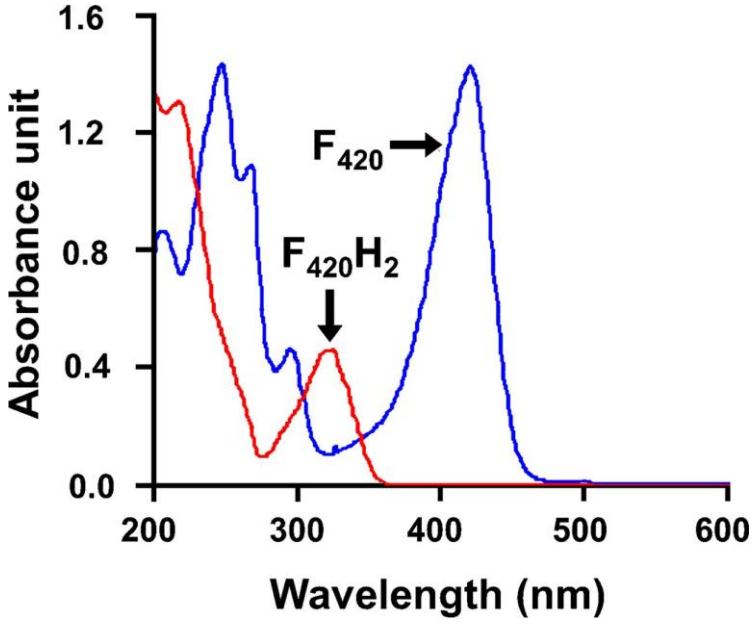

Figure 1.8 UV-visible absorption spectra of F_{420} (blue) and $F_{420}H_2$ (red). Adapted from Purwantini *et al.* 2009.

The physiological roles of F_{420} in methanogens, and certain non-methanogenic archaea, include energy metabolism, NADP reduction, oxygen detoxification, and sulfite reduction (Yamazaki *et al.*, 1980; Schauer *et al.*, 1986; Seedorf *et al.*, 2004; Johnson and Mukhopadhyay, 2005). In contrast, the physiological role of F_{420} in *Mycobacteria* is not fully understood. Current studies have shown that F_{420} may have a role in a defence against oxidative stress. This is suggested by its ability to reduce nitrogen dioxide, F_{420} knockouts are more prone to oxidative stress, and F_{420} levels are elevated when mycothiol and ergothioneine, glutathione analogues that maintain redox homeostasis, are absent (Purwantini and Mukhopadhyay, 2009; Gurumurthy *et al.*, 2013; Singh *et al.*, 2016). F_{420} is also suggested to protect the cell against xenobiotic agents, as *Mycobacteria* that cannot produce F_{420} are more susceptible to bactericidal agents (Gurumurthy *et al.*, 2013; Jirapanjawat *et al.*, 2016)

1.3.1 F_{420} Distribution

Bioinformatic analysis has revealed that the F_{420} biosynthesis genes (cofC, cofD, cofE, cofG and cofH) are present in at least 653 bacterial and 173 archaeal species. The ecosystems of these species are mostly soil and marine environments (Fig. 1.9) (Ney *et al.*, 2017). Among archaea, F_{420} is thought to be distributed in all methanogens and is proposed that F_{420} is central to the metabolism of the various anaerobic methanotrophic archaea (Cheeseman *et al.*, 1972; Eirich *et al.*, 1979; Haroon *et al.*, 2013). F_{420} has been shown to be present in many hydrogenotrophs and has been identified in several non-methanogenic euryarchaeota, including three species of the sulphate-reducing genus, *Archaeoglobus*, and seven species of the photosynthetic genera, *Halobacteria*, and *Halococcus* (Beelen *et al.*, 1983; Dolfing and Mulder, 1985; De Wit and Eker, 1987; Möller-Zinkhan *et al.*, 1989; Vornolt *et al.*, 1995). The ammonia- and cyanate-oxidizing thaumarchaeon, *Nitrososphaera gargensis*, is shown to produce high levels of F_{420} (Spang *et al.*, 2012). Comparative genomics identified the F_{420} biosynthesis genes present in *Thaumarchaeota, Aigarchaeota, Geoarchaeota, Bathyarchaeota,* and *Lokiarchaeota* (Wu *et al.*, 2009; Kozubal *et al.*, 2013; Rinke *et al.*, 2013; Evans *et al.*, 2015; Spang *et al.*, 2015). The presence of F_{420} has been reported in both *Sulfolobus* and *Thermoplasma*, but the genomes lack the known genes to synthesis it (Lin and White, 1986).

Within bacteria, F_{420} has been identified in *Mycobacteria* including the major obligate pathogens *M. tuberculosis, M. bovis,* and several opportunistic species (Purwantini *et al.*, 1997). *M. leprae,* which has undergone a genome reduction event, also produces F_{420}, suggesting the importance of F_{420} to *Mycobacteria* species (Purwantini *et al.*, 1997; Cole *et al.*, 2001). F_{420} is found in representatives of the actinobacterial genera including *Streptomyces, Nocardia,* and *Nocardioides* (Kuo *et al.*, 1989; Purwantini *et al.*, 1997; Ebert *et al.*, 1999). Comparative genomic analyses show that F_{420} biosynthesis genes are found in representatives of the *Chloroflexi*, *Alphaproteobacteria*, *Betaproteobacteria*, and *Gammaproteobacteria* (Selengut and Haft, 2010; Ahmed *et al.*, 2016). The biosynthetic pathway of F_{420} is proposed to have evolved in bacteria after acquiring from archaea the biosynthetic genes for F_o, a redox chromophore used in oxidoreductases and photocatalytic systems that contains the same isoallazine rings as F_{420} but lacks the lactate moiety and glutamate tail (Walsh, 1986; Hossain *et al.*, 2015; Ney *et al.*, 2017). Phylogenetic studies of each of the F_{420} biosynthetic genes suggest the biosynthesis of F_o was developed in an early methanogen. This pathway was acquired by actinobacteria that evolved the genes to synthesis F_{420} from F_o. Multiple gene

transfers allowed for other bacteria and archaea to acquire the ability to synthesis F_{420} (Nelson-Sathi *et al.*, 2015; Ney *et al.*, 2017).

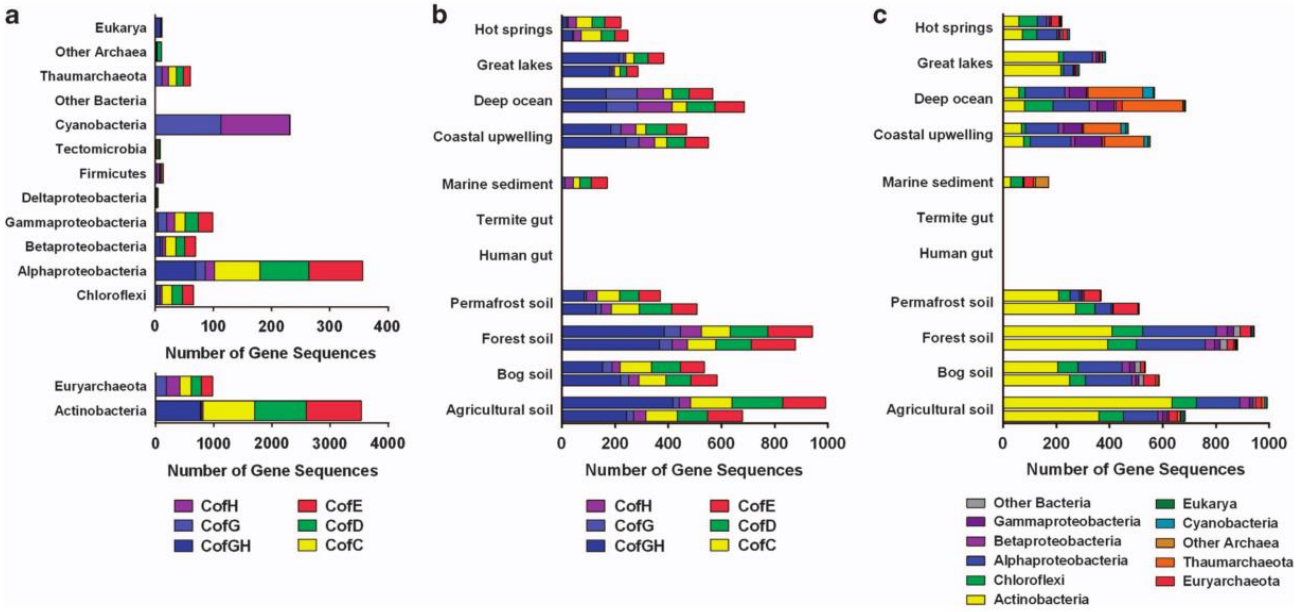

Figure 1.9 Genomic and metagenomic distribution of the cof genes that encode F420 biosynthesis enzymes. (a) Distribution of cof genes by phyla in the NCBI Reference Sequence database. (b) Distribution of cof genes in 19 publicly available metagenomes by enzyme. (c) Distribution of cof genes in 19 publicly available metagenomes by phylum of the closest BLAST hit (>60% identity). Adapted from Ney *et al.* 2016.

1.3.2 F_{420} Biosynthesis

The biosynthesis of F_{420} starts with the synthesis of its precursor F_o. This biosynthesis uses the flavin pathway which condenses pyrimidine ribityldiaminouracil (5-amino-6-ribityl-amino-2,4[1H,3H]-pyrimidinedione), derived from GTP, with 3,4-dihydroxy-2-butanone 4-phosphate to make 6,7-dimethyl-8-ribityllumazine. Two of these molecules condense to regenerate 5-amino-6-ribitylamino-2,4(1H,3H)-pyrimidinedione with concomitant production of riboflavin (Fischer and Bacher, 2011) For the biosynthesis of F_o, pyrimidine ribityl diaminouracil from the flavin pathway is condensed with tyrosine by cof G and H (Fig.1.10) (Graham *et al.*, 2003; Berteau, 2012). The formation of F_o in *Mycobacteria*, is catalysed by *fbi*C, an ezyme that contains two subunits homologous to cof G and H. (Choi *et al.*, 2001).

Mechanistic studies of *fbi*C demonstrated that the formation of the heterocycle depends on the coordinated action of two radical S-adenosylmethionine (SAM) sites contained in each domain. In the CofG domain the SAM abstracts a hydrogen atom from tyrosine that fragments to form a *p*-hydroxybenzyl radical and a glycine imine, which undergoes hydrolysis to form

glyoxylate. The *p*-hydroxybenzyl radical attacks pyrimidine ribityldiaminouracil to form an intermediate that is transferred to the cof H domain. The SAM of cofH abstracts a hydrogen from the intermediate allowing for electron rearrangement leading to the cyclisation and oxidation of the radical electron forming F_o (Berteau, 2012; Philmus *et al.*, 2015).

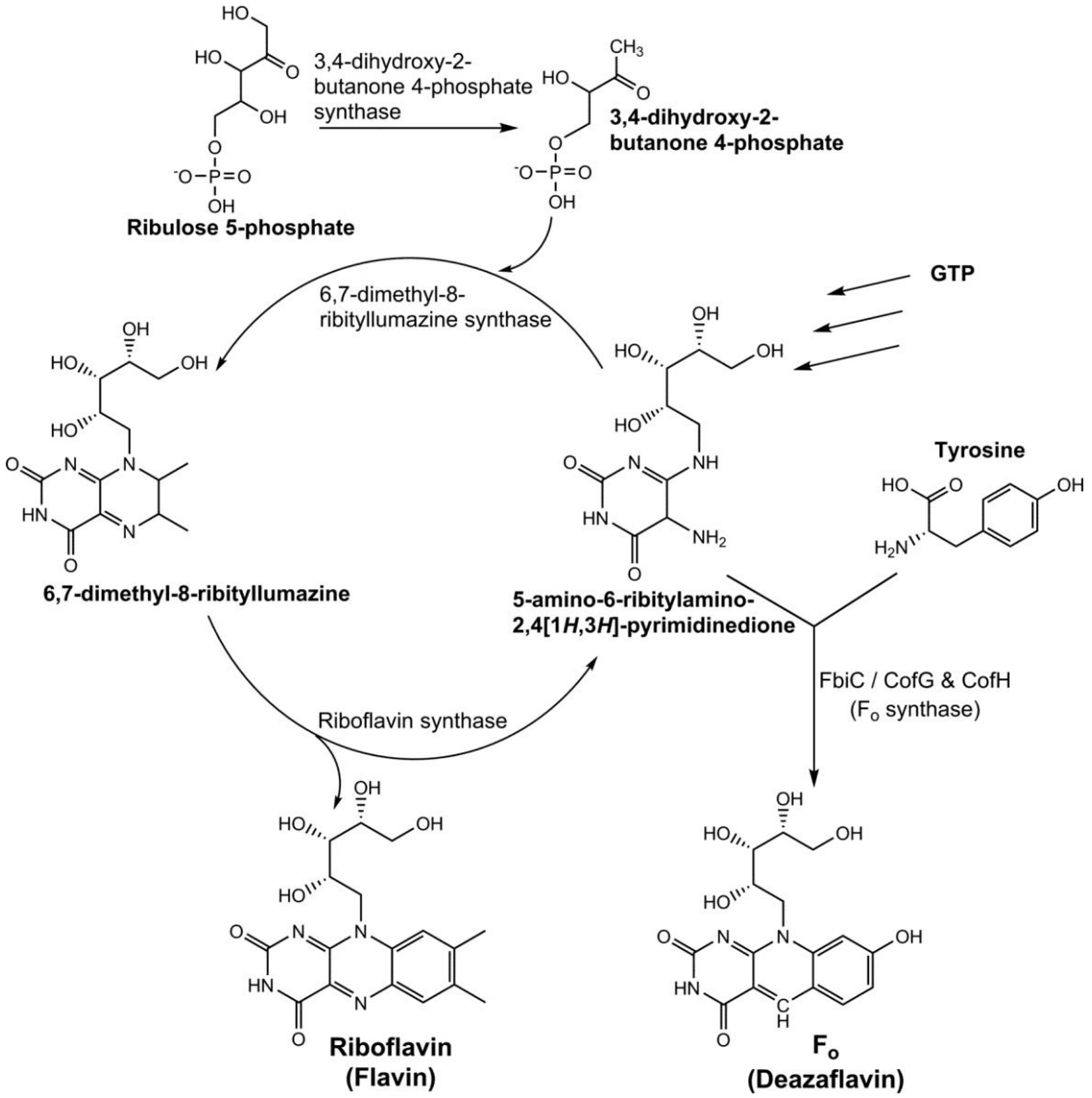

Figure 1.10 Biosynthesis of F_0 from the flavin biosynthesis pathway. Adapted from Greening *et al.* 2016.

There are two major steps in the formation of F_{420} from F_o (Fig. 1.11). The first step requires the condensation of F_o with L-lactyl-2-diphospho-5-guanosine (LPPG), synthesised from lactate, to form the phosphodiester F_{420}-0 (F_{420} containing no glutamate side chain) (Graupner and White, 2001). This reaction is catalysed by a 2-phospho-L-lactate transferase, *fbi*A in *Mycobacteria*, and CofD in archaea (Choi *et al.*, 2001; Graupner *et al.*, 2002). The crystal structure of CofD from *Methanosarcina mazei*, revealed that the deazaflavin ring of F_o interacts with a hydrophobic pocket and two water molecules, while the nucleotide moiety of LPPG is accommodated in a Rossmann fold domain with a Mg^{2+} ion. The proposed mechanism is that conformational changes in the binding pocket caused by the substrates binding puts the terminal hydroxyl group of F_o close to the β-phosphate of LPPG. After the extraction of the terminal proton from F_o by a general base, the two molecules are condensed (Forouhar *et al.*, 2008).

The pathway that produces LPPG is not fully understood. It is assumed that 2-phospho-L-Lactate, is the precursor for LPPG. The proposed pathway is from the reduction of methylglyoxal or the aldol cleavage of fuculose-1-phosphate, which is then oxidized to lactate by the NAD^+-dependent L-lactaldehyde dehydrogenase, CofA (Graupner *et al.*, 2000; Grochowski *et al.*, 2006) L-lactate is phosphorylated in a GTP-dependent manner to form 2-phospho-L-Lactate (Graupner and White, 2001). The enzyme that catalyses this reaction is yet to be discovered. The final step involves the conversion of 2-phospho-L-Lactate to LPPG by the GTP-dependent enzyme 2-phospho-L-lactate guanylyltransferase (CofC) (Graupner *et al.*, 2000; Graupner and White, 2001; Guerra-Lopez *et al.*, 2007)

The second major step in the formation of F_{420} from F_o, is the addition of the glutamate tail to F_{420}-0. The L-Glutamate residues are added in a sequential manner via γ-linkages catalysed through a GTP-dependent manner by the nonribosomal peptide synthase F_{420}:γ-L-glutamyl ligase CofE (Choi *et al.*, 2001; Li, Graupner, *et al.*, 2003; Nakano *et al.*, 2004; Bashiri *et al.*, 2016) The structure of the *Archaeoglobus fulgidus* CofE orthologue reveals a butterfly-like homodimer that accommodates GTP and Mn^{2+} at the dimer interface. The addition of glutamate is catalysed by the phosphorylation of F_{420} at the terminal hydroxyl group of the lactate moiety or the terminal glutamate. The resulting acyl-phosphate is then subject to nucleophilic attack by the amino group of the incoming glutamate residue (Nocek *et al.*, 2007). The *Mycobacterial* CofE orthologue, *fbi*B, has an N-terminus domain that is homologous with the *A. fulgidus* CofE, but the C-terminus domain is homologous to an enzyme of a FMN-dependent nitroreductase family. The N-terminus alone of *fbiB* can only produce F_{420}-1 and the

C-terminus alone cannot add any glutamate to F_{420}-0, but both domains are needed to elongate the tail by more than one glutamate. (Bashiri *et al.*, 2016). In some archaea, a terminal α-linked glutamate residue is also added by the enzyme, γ-F_{420}-2:α-L-glutamate ligase (CofF) (Graupner and White, 2003; Li, Xu, *et al.*, 2003). The number of glutamate residues on F_{420} is dependent of the species. This number can range from two or three residues in methanogens without cytochromes, four or five in methanogens with cytochromes, or five to seven in *Mycobacteria* (Gorris and Van der Drift, 1994; Bair *et al.*, 2001). The reason for the difference in glutamate chains is unknown.

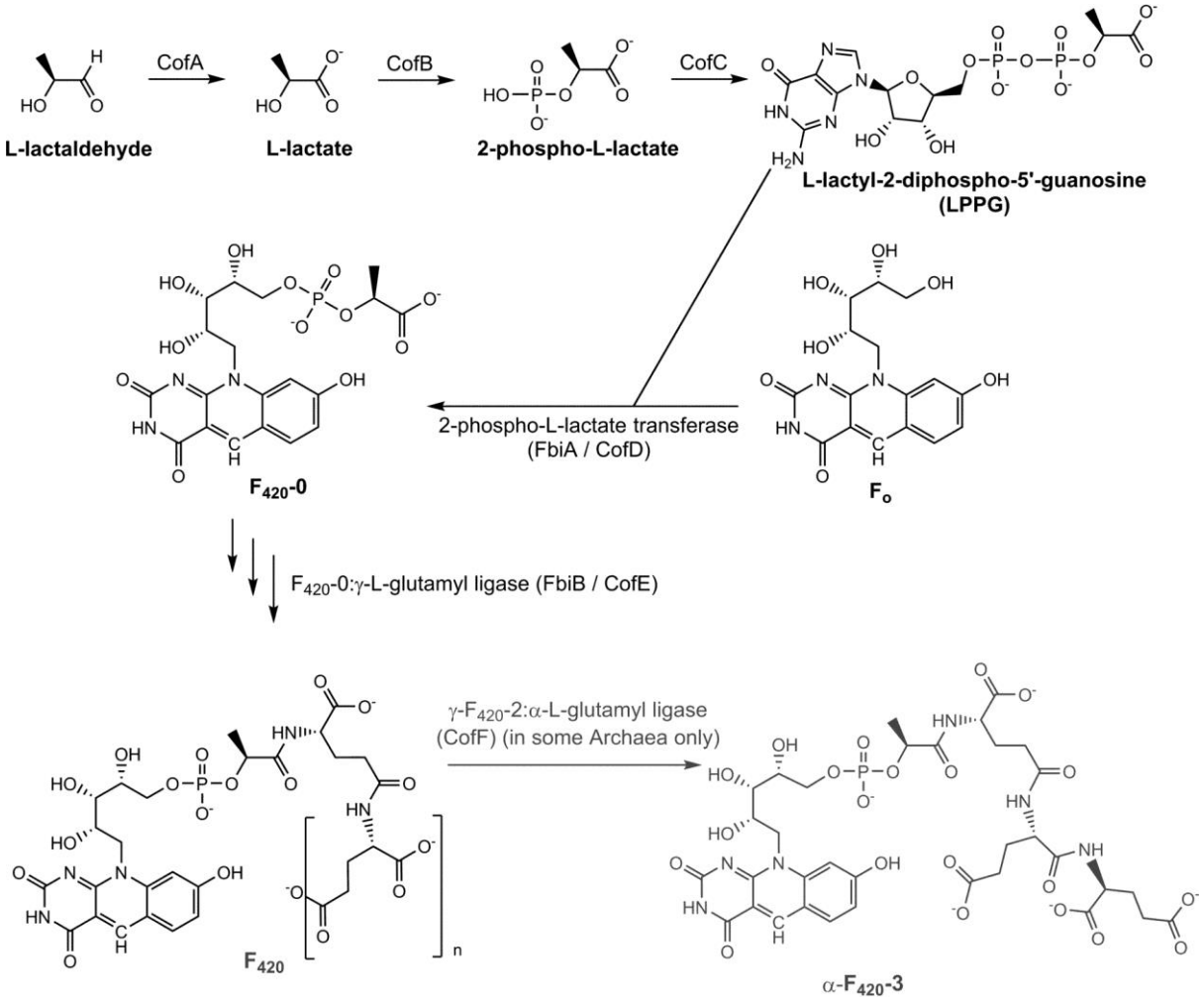

Figure 1.11 F_{420} biosynthesis pathway. Adapted from Greening *et al.* 2016.

1.4 F_{420}-dependent enzymes

F_{420}-dependent enzymes mediate a wide range of redox reactions in biological systems (Hemmerich *et al.*, 1970). The role of F_{420}-dependent enzymes is well defined in methanogenic archaea as the primary catabolic electron carrier, but the physiological role in *Mycobacteria* is not well understood (Thauer *et al.*, 2008; Greening *et al.*, 2016). Despite this, studies of these enzymes have shown that there is a great diversity within *Mycobacteria* showing two distinct super families, which also include FMN/FAD binding proteins and vary in their catalytic mechanisms (Greening *et al.*, 2016). Initial phylogenetic profiling revealed 28 F_{420}-dependent enzymes present in *M. tuberculosis*, which were separated into three groups, luciferase-like monooxygenase, pyridoxamine 5'-phosphate oxidase, and deazaflavin-dependent nitroreductase family (Selengut and Haft, 2010). Further studies revealed that the pyridoxamine 5'-phosphate oxidase, and deazaflavin-dependent nitroreductase families are part of the same flavin/deazaflavin oxioreductase super family, and the luciferase-like monooxygenases were renamed to Luciferase-like Hydride Transferases (LLHT) due to the observation that they are not oxygen dependent (Taylor *et al.*, 2010; Ahmed *et al.*, 2015; Greening *et al.*, 2016).

LLHTs can be defined by their TIM barrel fold (Fig. 1.13), and have a primary sequence of approximately 360 amino acids, and a molecular weight of approximately 38 kDa (Fisher *et al.*, 1996; Kertesz *et al.*, 1999; Chaiyen *et al.*, 2001; Bashiri *et al.*, 2008). FDORs are defined by their split β-barrel fold (Fig. 1.16), and have a primary sequence of approximately 150 amino acids, and a molecular weight of approximately 15 kDa (Ahmed *et al.*, 2015; Greening *et al.*, 2016). The FDORs have been separated into three groups based on their sequence and function. These three groups include FDOR-A, FDOR-AA, and FDOR-B and are separated into several clades within each group (Fig. 1.12) (Ahmed *et al.*, 2015). Molecular dynamics and binding studies of $F_{420}H_2$ bound to an FDOR revealed that it is in its deprotonated state and the ribityl-phospholactyl region is stable while the oligoglutamate tail is more mobile (Ahmed *et al.*, 2016; Mohamed *et al.*, 2016).

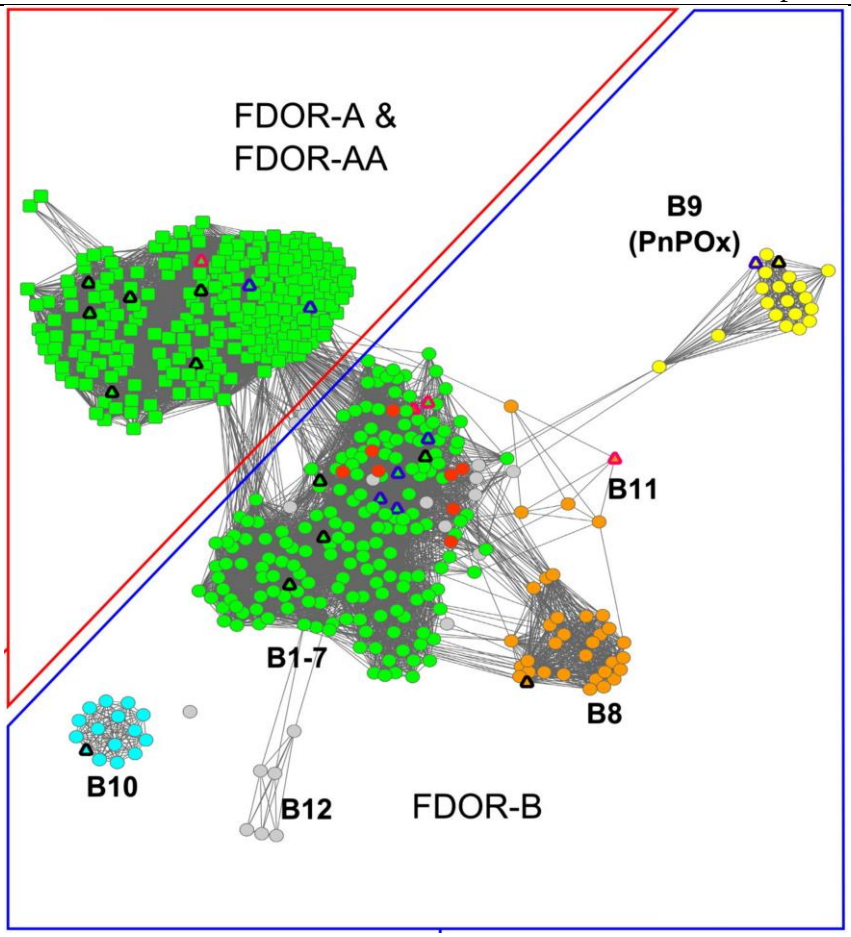

Figure 1.12 Sequence similarity network of FDOR in *Mycobacteria*. Each node represents an individual protein and edges represent E-values between proteins generated by BLAST. Proteins from *M. tuberculosis* H37Rv and *M. smegmatis* strain MC^2 155 are marked as black triangles and those structurally characterised in Ahmed *et al.*, 2015 are marked as pink triangles. Structures solved in other studies are marked as blue triangles. Nodes are coloured based on their cofactor binding, F_{420} (green), FMN (yellow), FAD (Orange), Heme (red), and cyan (unknown). Nodes within the Red box belong to the FDOR-A or AA clades and Nodes within the blue box belong to the FDOR-B clades. The node clustering represented here have a logE cutoff of −3. Adapted from Ahmed *et al.*, 2015

1.4.1 Luciferase-like Hydride Transferases

LLHT enzymes are known to bind different co-factors (Greening *et al.*, 2016). F_{420}-dependent LLHTs are defined by a conserved glycine residue, not found in other flavin-binding LLHTs, which binds the phosphate group of F_{420} without steric hindrance caused with other flavins. (Aufhammer *et al.*, 2005). Within *Mycobacteria,* 48 F_{420}-dependent LLHTs have been identified from a possible 86 LLHTs in *M. smegmatis* and 14 F_{420}-dependent LLHTs from a possible 17 LLHTs are identified in *M. tuberculosis* (Selengut and Haft, 2010). Three F_{420}-dependent LLHTs in *Mycobacteria* have been functionally characterise, Rv2951c, which codes for a F_{420}-dependent phthiodiolone ketoreductase (fPKR), Rv0132c, which codes for fHMAD,

and the most studied *Mycobacterial* LLHT, Rv0407 including the *M. smegmatis* orthologue, MSMEG_0777, which codes for FGD.

The reduction of F_{420} in most species, including Methanogens and *Streptomyces*, is achieved by the oxidation of NADPH to $NADP^+$ by the enzyme, F_{420}-dependent NADPH dehydrogenase (*fno*) (Berk and Thauer, 1997). FGD is the primary enzyme that reduces F_{420} to $F_{420}H_2$ in *Mycobacteria*, *Nocardia*, and *Rhodococcus* by the oxidation of Glucose-6-phosphate (G6P) to 6-phospogluconolactone (Purwantini and Daniels, 1996; Purwantini *et al.*, 1997; Nguyen *et al.*, 2016). The use of G6P over NADPH is thought to be due to the role of G6P as an electron store that FGD mobilises in response to oxidative stress (Hasan *et al.*, 2010). This is evident by the high levels of G6P in *Mycobacteria* compared to other bacterial species, is the preferred gluconeogenesis intermediate, and *M. smegmatis* is more sensitive to oxidative stress when FGD activity is knocked out (Hasan *et al.*, 2010).

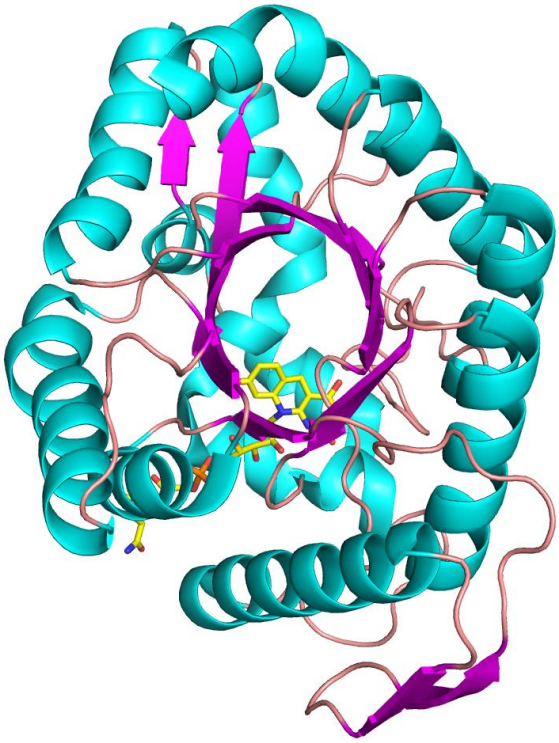

Figure 1.13 Structure of the F_{420}-dependent Luciferase-like Hydride Transferase, F_{420}-dependent glucose-6-phosphate dehydrogenase with F_{420} bound (PDB ID 3B4Y). The structure of FGD with F_{420} (yellow) bound, which exhibits the conserved TIM barrel fold that structurally defines the LLHT. Alpha helices are coloured teal and beta sheets are coloured magenta.

The crystal structure of FGD from *M. tuberculosis* revealed a homodimer, with each dimer composing an $(\alpha/\beta)_8$ TIM barrel. Although FGD shares only 20-30% amino acid sequence identity with other LLHT proteins from methanogens, this structure closely resembles the structure of F_{420}-dependent secondary alcohol dehydrogenase (ADF), which reduces F_{420} through the oxidation of secondary alcohols, and $F_{420}H_2$-dependent methylene-H_4MPT reductase (MER), which reduces CH_2=H_4MPT to CH_3-H_4MPT by oxidising $F_{420}H_2$, (Bashiri *et al.*, 2008; Greening *et al.*, 2016). The binding of F_{420} into FGD revealed by the structure shows the isoallazine ring binding adjacent to a budge in a β-strand containing a non-prolyl cis-peptide bond, and the poly-glutamate tail extending into the solvent. Binding of G6P is achieved by the sugar ring being sandwiched by a leucine and F_{420}. The phosphate moiety is accommodated by a positively charged pocket provided by two lysines and an arginine. This pocket can also facilitate the binding of citrate that is competitive inhibitor of G6P. This pocket is not conserved in LLHT orthologues that do not exhibit FGD activity (Bashiri *et al.*, 2008; Nguyen *et al.*, 2016). The reaction mechanism of FGD relies on a base, yet to be identified, to remove the hydrogen of the hydroxyl group on G6P that allows a hydride transfer onto the C5 of the F_{420} molecule and forms the carbonyl group on G6P. A conserved glutamate of FGD acts as a general acid by donating a hydrogen onto the N2 of F_{420} forming $F_{420}H_2$ (Oyugi *et al.*, 2016; Oyugi *et al.*, 2017).

fHMAD has 36 % sequence identity to FGD and was annotated as *fgd2* in *M. tuberculosis*, but does not have FGD activity (Bashiri *et al.*, 2012). Further studies revealed that the activity of fHMAD involves reducing F_{420} to oxidize hydroxyl-mycolic acid to keto-mycolic acid, which is found in the cell wall of pathogenic *Mycobacteria*, thereby enhancing pathogenicity (Dubnau *et al.*, 2000; Purwantini and Mukhopadhyay, 2013). Strains lacking oxygenated mycolic acids such as keto-mycolic acid, have altered envelope permeability, are more susceptible to antibiotics, and are attenuated in macrophages and mice (Yuan *et al.*, 1998; Sambandan *et al.*, 2013). The expression of fHMAD is controlled by the sigma factor, sigF, a transcription factor contributing to the pathogenesis of *Mycobacteria* and is upregulated when the cell is under stress and in the late stationary stage. *M. tuberculosis* is attenuated when sigF is knocked out (DeMaio *et al.*, 1996; Geiman *et al.*, 2004). The N-terminus of fHMAD contains a twin–arginine translocation (TAT) motif, and a lipobox motif that mediates lipid modifications to anchor it to the cell envelope. This motif in LLHT is highly conserved in the *M. tuberculosis* complex (*M. bovis*, *M. africanum*, *M. microti* and *M. canetti*) and other pathogenic *Mycobacteria* orthologues, but is not found in non-pathogenic *Mycobacteria*

paralogues such as *M. smegmatis* (Bashiri *et al.*, 2012). fHMAD is inhibited by des-nitro products formed from the reduction of pretomanid and delamanid (Stover *et al.*, 2000; Matsumoto *et al.*, 2006; Purwantini and Mukhopadhyay, 2013)

The biosynthesis of the cell surface lipid, phthiocerol dimycocerosates (DIM A), relies on the reduction of phthiodiolone dimycocerosates (DIM B) by the F_{420}-dependent LLHT, fPKR (Simeone *et al.*, 2007; Purwantini *et al.*, 2016). The synthesis of DIM A is a two-step process that starts with the reduction of the keto group of DIM B to an alcohol by $F_{420}H_2$ using fPKR (Fig. 1.14). This alcohol is methylated by the enzyme Rv2952, which is present in the same open reading frame (Purwantini *et al.*, 2016). Diacylated polyketides, including DIM A and B, are found in the cell wall of pathogenic *Mycobacteria* and are virulence factors in *M. tuberculosis* that protects it from the early innate immune response of an infected host (Daffé *et al.*, 1987; Guenin-Macé *et al.*, 2009; Day *et al.*, 2014). DIM A and B are only present in slow growing *Mycobacteria* (Onwueme *et al.*, 2005; Purwantini *et al.*, 2016).

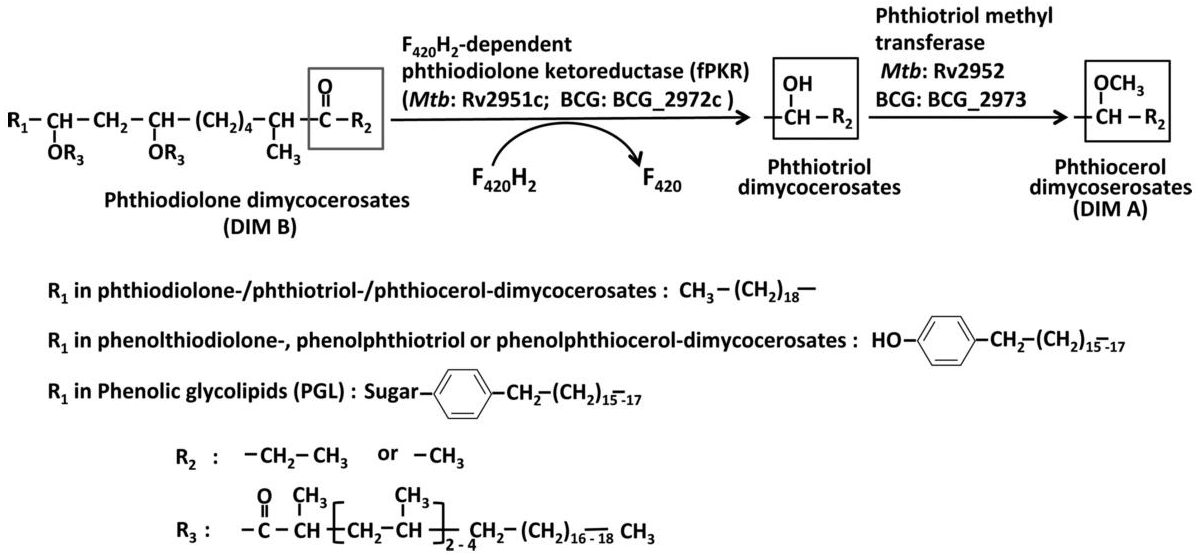

Figure 1.14 Biosynthesis of phthiodiolone dimycocerosates (DIM B) to phthiocerol dimycocerosates (DIM A) in mycobacteria using the F420-dependent LLHT, fPKR. The biosynthetic pathway that converts phthiodiolone dimycocerosates (DIM B) to phthiocerol dimycocerosates (DIM A) in mycobacteria via the intermediate formation of phthiotriol dimycocerosates by the $F_{420}H_2$-dependent phthiodiolone ketoreductase (fPKR). fPKR is encoded by the gene Rv2951c in *M. tuberculosis* and by BCG_2972c in *M. bovis* BCG. The R_1 groups represent the structures of the three classes of dimycocerosates. R_2 and R_3 represent the extend structures found in all dimycocerosates. Adapted from Purwantini et al. 2016.

1.4.2 FDOR-A Enzymes

The first identified FDOR-A, Rv3547, was renamed to deazaflavin-dependent nitroreductase (Ddn) due to its ability to reduce pretomanid in *M. tuberculosis*. It was identified by sequencing *M. tuberculosis* mutants resistant to pretomanid (Manjunatha *et al.*, 2006). Phylogenetic profiling based on F_{420} biosynthesis revealed FDOR-As are present within *M. smegmatis* and *M. tuberculosis*, with further analysis revealing that this group is present in most actinobacteria (Selengut and Haft, 2010; Ahmed *et al.*, 2015). Sequence similarity networks have categorised this subgroup into four subclades A1–A4 (Fig. 1.15), with A1, which includes Ddn, conserved in most *Mycobacteria* indicating evolutionary conservation and a significant physiological role while the A2-A3 subclades are poorly conserved throughout *Mycobacteria* (Ahmed *et al.*, 2015).

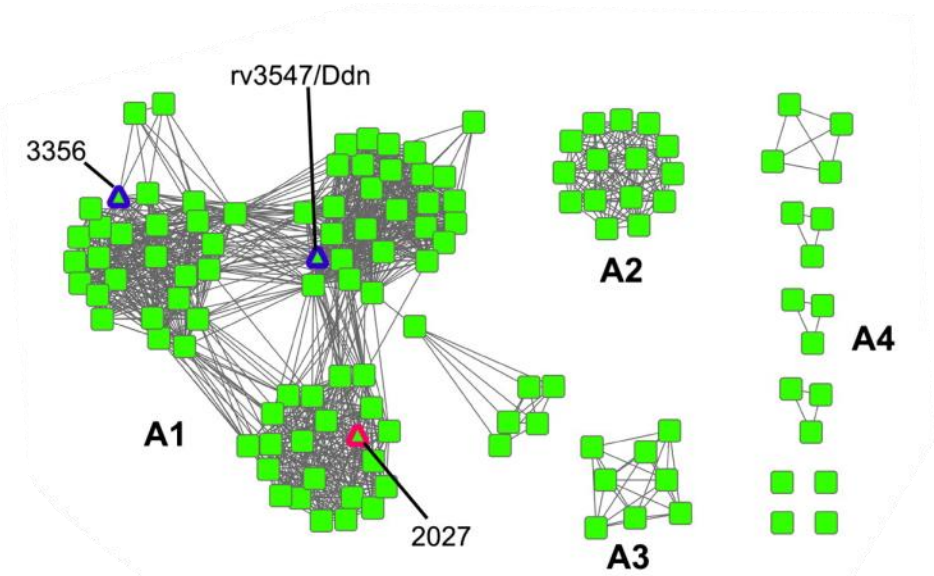

Figure 1.15 Sequence similarity network of FDOR-A in *Mycobacteria*. Each node represents an individual protein and edges represent E-values between proteins generated by BLAST. Proteins from *M. tuberculosis* H37Rv and *M. smegmatis* strain MC^2 155 are marked as black triangles and those structurally characterised in Ahmed *et al.*, 2015 are marked as pink triangles. Structures solved in other studies are marked as blue triangles. All nodes bind cofactor F_{420}. The node clustering represented here have a logE cutoff of −28. Adapted from Ahmed et al., 2015

The proposed function of FDOR-As involves the reduction of quinones (Gurumurthy *et al.*, 2013). It has been shown that they are able to reduce benzoquinone and naphthoquinone analogues, including a synthetic analogue of menaquinone, the endogenous quinone in *Mycobacteria* used in the electron transport chain, menadione (Gurumurthy *et al.*, 2013;

Ahmed *et al.*, 2015). This activity, along with knockout data shows *Mycobacteria* are more susceptible to oxidative stress (see Section 1.3), and has led to the conclusion that the role of Ddn and the FDOR-As in *Mycobacteria* protects the cell from oxidative stress by reducing the level of semiquinones (Hasan *et al.*, 2010; Gurumurthy *et al.*, 2013). Although possible, there has been no direct evidence of this, as all knockout experiments eliminated F_{420} biosynthesis and not Ddn directly. Studies have shown that this quinone reductase activity is promiscuous throughout the other FDORs, although with lower activity than the FDOR-As (Gurumurthy *et al.*, 2013; Jirapanjawat *et al.*, 2016). FDOR-As have promiscuous activity with other organic compound including aflatoxins, coumarin, furanocoumarins, and arylmethanes but Ddn is the only FDOR shown so far that can reduce pretomanid and delamanid, (Ji *et al.*, 2006; Manjunatha *et al.*, 2006; Taylor *et al.*, 2010; Gurumurthy *et al.*, 2012; Jirapanjawat *et al.*, 2016).

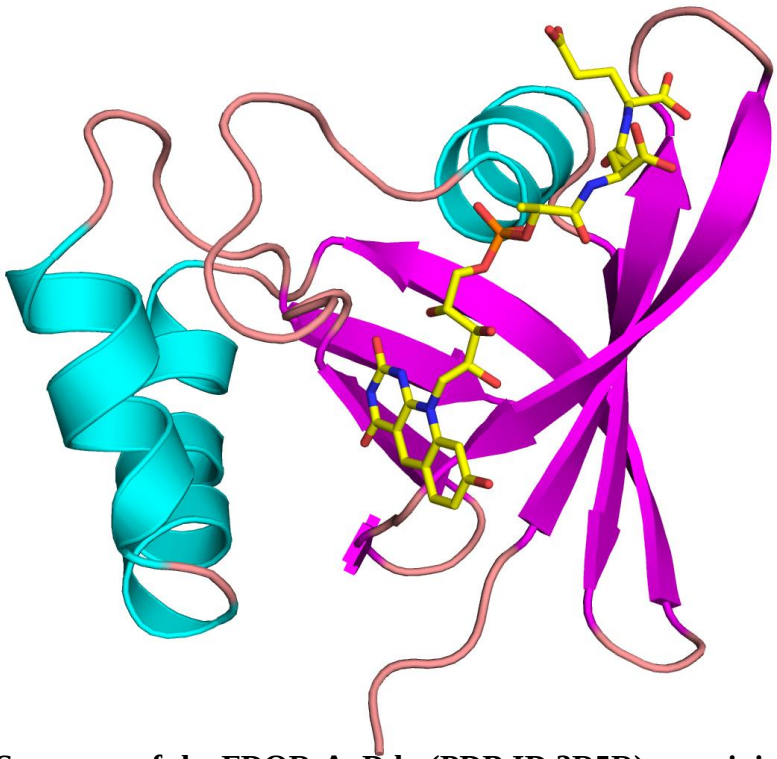

Figure 1.16 Structure of the FDOR-A, Ddn (PDB ID 3R5R) containing the conserved split beta-barrel fold with F_{420} (yellow) bound. The structure of Ddn with F_{420} (yellow) bound, which exhibits the conserved split beta-barrel fold that structurally defines the FDOR. Alpha helices are coloured teal and beta sheets are coloured magenta.

Five structures of FDOR-A have been solved, one from *M. tuberculosis* (ddn [3R5R]), two from *M. smegmatis* (MSMEG_2027 [4Y9I], and MSMEG_3356 [3H96]), and two orthologues from *Nocardia farcinica* (nfa33440 [3R5Y], and nfa18080 [3R5Z]) (Taylor *et al.*, 2010; Cellitti *et al.*, 2012; Ahmed *et al.*, 2015). All the structures solved are monomeric and contain a split β-barrel fold while having less than 50% sequence identity between them (Fig. 1.17). F_{420} is housed by a positively charged groove, that is principally formed by lysine and arginine side-chains, and the active site contains hydrophobic pocket formed by several aromatic or hydrophobic residues which differ between enzymes (Taylor *et al.*, 2010; Cellitti *et al.*, 2012; Ahmed *et al.*, 2015). The structure of Ddn lacked an N-terminus due to it causing aggregation and the full structures of nfa33440, and nfa18080 were solved in attempt to model it. The structures showed a helix packed against the core of the protein when F_{420} was bound and was disordered when F_{420} was not bound (Cellitti *et al.*, 2012). The structure of Ddn, along with mutagenic studies, computational studies, and the lack of quinone activity with truncated MSMEG_2027, implies that the N-terminus tail is important for the function of FDOR-A (Cellitti *et al.*, 2012; Ahmed *et al.*, 2015; Mohamed *et al.*, 2016).

1.4.3 FDOR-AA Enzymes

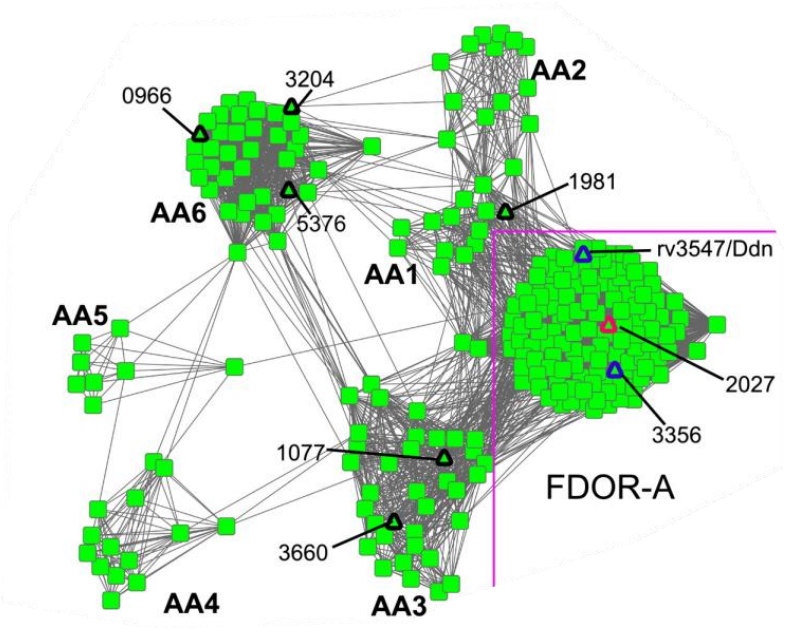

Figure 1.17 Sequence similarity network of FDOR-AA in *Mycobacteria*. Each node represents an individual protein and edges represent E-values between proteins generated by BLAST. Proteins from *M. tuberculosis* H37Rv and *M. smegmatis* strain MC^2 155 are marked as black triangles and those structurally characterised in Ahmed *et al.*, 2015 are marked as pink triangles. Structures solved in other studies are marked as blue triangles. All nodes bind cofactor F_{420}. The node clustering represented here have a logE cutoff of −7.6. Adapted from Ahmed et al., 2015

FDOR-AA were first defined as FDOR-As that had the inability to reduce aflatoxins, coumarin, and furanocoumarins. Further phylogenetic analysis revealed two distinct clades within FDOR-As (Lapalikar *et al.*, 2012). One study has shown that the FDOR-AA, MSMEG_1981, can reduce arachidonic acid (Ahmed *et al.*, 2015). Proteomic studies have revealed that these proteins in *M. tuberculosis* and *M. smegmatis* are membrane associated (Mawuenyega *et al.*, 2005; He and De Buck, 2010; de Souza *et al.*, 2011) and bioinformatics studies have predicted enzymes to be associated with proteins that are involved in lipid synthesis and metabolism, i.e. cutinases, lipoproteins, and acyl-CoA synthetases (Ahmed *et al.*, 2015). This has led to the hypothesis that FDOR-AAs are involved with lipid metabolism (Ahmed *et al.*, 2015). Microarray data has shown four FDOR-AAs (MSMEG_1981, MSMEG_1077, MSMEG_3278, and MSMEG_3204) are upregulated in the presence of bedaquiline, which upregulates the glyoxylate cycle, a cycle that hijacks the citric acid cycle to allow fatty acids to be used as an energy source when the cell cannot use other carbon sources or to maintain redox balance (Kornberg, 1966; Hards *et al.*, 2015). Sequence similarity networks have expanded the FRDOR-AA group into six clades (AA1-AA6). *M. tuberculosis* has proteins from AA2, AA4, and AA6 whereas *M. smegmatis* has proteins from AA1, AA3, AA5, and AA6 (Ahmed *et al.*, 2015). No FDOR-AA structure has been solved.

1.4.4 FDOR-B Enzymes

FDOR-Bs were first identified as FMN-dependent pyridoxine/pyridoxamine 5′-phosphate oxidases (PnPOx) due to their sequence similarity, but did not have any activity associated with PnPOx. (Selengut and Haft, 2010). Phylogenetic profiling re-classified seven PnPOxs in *M. smegmatis* and four in *M. tuberculosis* as F_{420}-dependent PnPOx-like enzymes. This group was renamed to FDOR-B as it was expanded further with the discovery of these PnPOx-like enzymes and other related F_{420}-dependent oxioreductases being able to reduce aflatoxins, but at a lower level than FDOR-A and were phylogenetically separate (Selengut and Haft, 2010; Taylor *et al.*, 2010). Sequence similarity networks divided the FDOR-B class into twelve different functional clades, B1-B12, based on sequence (Fig. 1.18), and co-factor preference was confirmed by binding studies. The co-factor preference of clades B1-6 is F_{420} while the other clades co-factor preferences include, heme (B7), FAD (B8), FMN (B9), heme and FAD (B11) and B10 and B12, which have unknown cofactors (Ahmed *et al.*, 2015).

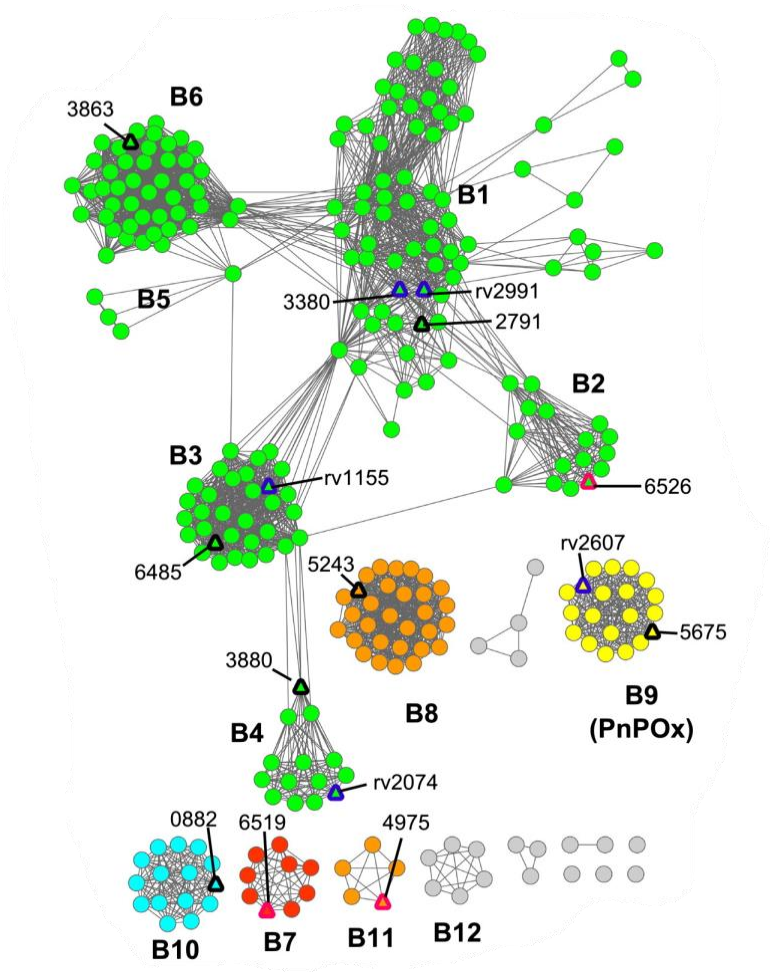

Figure 1.18 Sequence similarity network of FDOR-B in *Mycobacteria*. Each node represents an individual protein and edges represent E-values between proteins generated by BLAST. Proteins from *M. tuberculosis* H37Rv and *M. smegmatis* strain MC^2 155 are marked as black triangles and those structurally characterised in Ahmed *et al.*, 2015 are marked as pink triangles. Structures solved in other studies are marked as blue triangles. Nodes are coloured based on their cofactor binding, F_{420} (green), FMN (yellow), FAD (Orange), Heme (red), and cyan (unknown). The node clustering represented here have a logE cutoff of −7.6. Adapted from Ahmed et al., 2015.

The function and physiological role of several FDOR-B are known. In *Streptomyces*, enzymes found in the FDOR-B1 are known to be involved in the biosynthesis of the antibiotics; tetracycline, oxotetracycline, and chlortetracycline (Wang *et al.*, 2013). The function of MSMEG_3880, and RV2074, found in FDOR-B4, are F_{420}-dependent biliverdin reductases, that reduces the heme oxidation product, biliverdin to bilirubin, a known antioxidant (Ahmed *et al.*, 2016). The FDOR-B7, MSMEG_6519, was co-purified with biliverdin and when tested, MSMEG_6519 was able to oxidise heme to biliverdin (Ahmed *et al.*, 2016). MSMEG_6519 is in a clade cluster containing HugZ, a heme oxygenase from *Helicobacter pylori* (Guo *et al.*,

2008; Ahmed *et al.*, 2016). The FDOR-B9, Rv2607, is a PnPOx, that oxidises pyridoxine 5′-phosphate to pyridoxal 5′-phosphate (Mashalidis *et al.*, 2011). Despite the known function of some of the FDOR-B, they are known to have promiscuous activity. The FDOR-B3, Rv1155, is known to have biliverdin reductase activity, although at a reduced rate compared to Rv2074 and MSMEG_3880. Reduced activity and being in a different clades has led to the hypothesis that Rv1155 has evolved a different function and catalyses the reduction of an alternative molecule yet to be identified (Ahmed *et al.*, 2015; Ahmed *et al.*, 2016). Other promiscuous activities of the FDOR-Bs include the ability to reduce aflatoxins, coumarin, furanocoumarins, arylmethanes, and quinones (Taylor *et al.*, 2010; Lapalikar *et al.*, 2012; Jirapanjawat *et al.*, 2016).

Several structures of FDOR-Bs have been solved and include the FDOR-B1 proteins rv2991 (PDB ID 1RFE) and MSMEG_3380 (PDB ID 3F7E), the FDOR-B2 protein MSMEG_6526 (PDB ID 4ZKY), the FDOR-B3 protein Rv1155 (PDB ID 4QVB with F_{420}, 1W9A without F_{420}), the FDOR-B4 protein Rv2074 (PBD ID 5JAB with F_{420}, 2ASF without F_{420}), the FDOR-B7 protein MSMEG_6519 (PDB ID 5BNC), the FDOR-B9 protein Rv2607 (PDB ID 2A2J), and the FDOR-B11 protein MSMEG_4975 (PDB ID 4YBN) (Safo *et al.*, 2001; Canaan *et al.*, 2005; Biswal *et al.*, 2006; Pédelacq *et al.*, 2006; Taylor *et al.*, 2010; Mashalidis *et al.*, 2015; Ahmed *et al.*, 2016). All FDOR-B structures solved contain a split β-barrel fold similar to the FDOR-A despite having less than 30 % sequence identity and are homodimers, except Rv2991 (Fig. 1.19) (Greening *et al.*, 2016). The F_{420} binding channels and substrate binding pockets of both the FDOR-A and FDOR-B enzymes occur in homologous regions although the identities of the residues involved are not conserved between them and FDOR-B require residues from both monomers to form the binding pocket and the groove that houses F_{420} (Taylor *et al.*, 2010; Ahmed *et al.*, 2015).

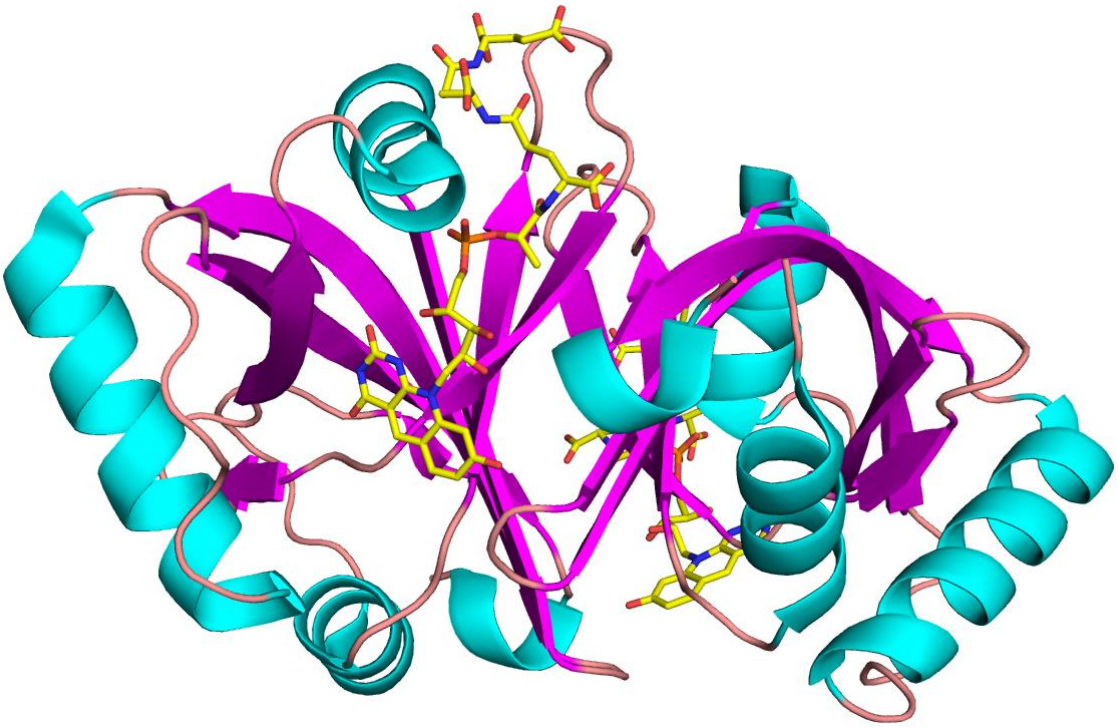

Figure 1.19 Structure of the FDOR-B, Rv2074 (PDB ID 5JAB) containing the conserved split beta-barrel fold with F_{420} (yellow) bound.

1.5 Thesis Outline

This thesis is presented as a series or published, submitted, and draft journal articles with the manuscripts presented in the chapters below.

1.5.1 Chapter outlines

Chapter 2 presents a draft manuscript discussing the possible role of the nitroimidazole activating enzyme, Ddn, and effect of point mutations on its physiological and drug activating activity. This is shown by exploring the role of Ddn and F_{420} in the respiration of *Mycobacteria* by looking at the effect on the electron transport chain. The effect of point mutations is explored with directed mutagenesis, enzyme kinetics, and resistance towards nitroimidazoles in a clinical strain was tested. The evolution of point mutations in Ddn is discussed by assessing the phylogenies of sequenced tuberculosis stains. A strain that exhibited resistance to pretomanid in clinical cases was tested to understand the effect of the mutations on the ability of tuberculosis to be transmissible. I was the primary researcher of this study.

Chapter 3 presents a draft manuscript that describes the function of the F_{420}-dependent enzyme, MSMEG_6526. The role of MSMEG_6526 in *Mycobacteria* is explored through phenotyping of a knockout strain on various carbons sources. This is followed up with proteomics,, and metabolomics data to analyse the chemical differences in the phenotypes. Kinetics were used to confirm MSMEG_6526 substrate. Crystal structures of MSMEG_6526, and the orthologue from *M. tuberculosis* Rv0121c, were solved to elaborate the catalytic mechanism. I was the primary researcher of this study.

Chapter 4 presents two publications that describes the function of select FDOR and the classification of the FDOR superfamily. The first publication uses bioinformatics, structural studies, binding assays, to further classify the three groups, FDOR-A, FDOR-AA, and FDOR-B, into different clades. The function of each group is explored with activity discovered including quinone reduction, fatty acid reduction, and biliverdin reduction. The second publication describes the structure and function of a novel F_{420}-dependent biliverdin reductase from *M. tuberculosis*, Rv2074. Kinetics and molecular dynamic simulations, using the solved structure with F_{420} bound, showed the function and the catalytic mechanism of biliverdin reduction by Rv2074.

Chapter 5 presents two publications that describe the promiscuous roles of FDOR in *M. smegmatis*. The first publication describes the role of F_{420} in detoxification, protecting *Mycobacteria* from a diverse range of antimicrobial compounds and detoxification. F_{420} and *fgd* knockout strains of *M. smegmatis* were used to show the increased effect of antimicrobials in the cell. This is further elaborated by kinetic data of a range of FDORs reducing these compounds. The second publication describes a range of compounds that FDORs from *M. smegmatis* can reduce and the common catalytic mechanism. Kinetic data of a range of FDORs reducing a range of different compounds is shown. Docking and mass spec data is used to identify the common catalytic mechanism.

Chapter 6 presents a publication of a comprehensive literature review of the cofactors F_{420} and its precursor F_o in archaea and actinobacteria, including their role, biosynthesis and associated enzymes. The sections of the literature review relevant for the purposes of this thesis are highlighted in the paper introduction.

Chapter 7 summarises the key outcomes of this thesis with a brief discussion on the role of F_{420}-dependent enzymes and the potential medical and biotechnology applications.

Chapter 2

Pretomanid Resistance, Evolution, and Susceptibility in Tuberculosis

2.1 Introduction

The nitroimidazoles pretomanid and delamanid are promising prodrugs against *M. tuberculosis* (Stover *et al.*, 2000; Matsumoto *et al.*, 2006). They have a dual mode of action with the release of nitrous oxide, which causes respiratory poisoning, and the inhibition of keto-mycolic acid biosynthesis, a key component of the mycobacterial cell wall (Singh *et al.*, 2008; Purwantini and Mukhopadhyay, 2013). The dual mode of action is achieved through the reduction of pretomanid or delamanid by the F_{420}-dependent oxidoreductase Ddn, a quinone reductase that normally protects the cell from oxidative stress (Ujjini H Manjunatha *et al.*, 2006; Gurumurthy *et al.*, 2013). *In vitro* resistance towards nitroimidazoles has been found to result from mutations in *ddn*, enzymes of the F_{420} biosynthesis pathway, and the F_{420} reducing enzyme, *fgd* (Haver *et al.*, 2015). Acquired resistance towards nitroimidazoles in clinical strains have been found. This resistance arose through mutations in *fbi*A, which is involved in F_{420} biosynthesis, and *fgd* (Bloemberg *et al.*, 2015; Hoffmann, Kohl, *et al.*, 2016). Although the mode of action of nitroimidazoles, and the mechanism by which resistance occurs is understood, mutations to Ddn and its impact on cell fitness, and how it effects transmissible resistance has not been studied. Clinical strains that have mutations in Ddn with no exposure to nitroimidazoles have not been studied for resistance towards pretomanid and delamanid.

To further understand the impact of nitroimidazole resistance through mutations to *ddn*, this chapter presents a manuscript that expands our understanding of the role of Ddn in *Mycobacteria*, and examines the cost of fitness caused by mutations in *ddn* and what effect it has on transmissible resistance. This is achieved though examining the effect of $F_{420}H_2$ and Ddn on the electron transport chain using oxygen consumption assays. Activity of Ddn and Ddn orthologues with their proposed physiological substrate, menaquinone, was determined. To examine the cost of fitness of Ddn mutants, activity with a menaquinone analogue and nitroimidazoles was measured. MIC values of pretomanid and delamanid were measured with *M. marinum*, and *M. tuberculosis* strains that were expected to be resistant to nitroimidazoles through our activity screen. Docking experiments were used to understand the difference in the MIC values between delamanid and pretomanid. This chapter also examines the natural sequence variation within *ddn* and *ddn* orthologues using phylogenetic studies of *M. tuberculosis* clinical strains that have been sequenced. The activity of Ddn mutants that were of interest from the phylogenetic studies were determined to predict drug resistance.

2.2 The evolution of nitroimidazole antibiotic resistance in *Mycobacterium tuberculosis*

The chapter contains the following paper draft:

The evolution of nitroimidazole antibiotic resistance in *Mycobacterium tuberculosis*

Brendon M. Lee, Livnat Afriat-Jurnou, Brian F. Forde, Htin Lin Aung, Kiel Hards, Sacha J. Pidot, F. Hafna Ahmed, A. Elaaf Mohamed, Matthew C. Taylor, Nicholas West, Timothy P. Stinear, Chris Greening, Scott A. Beatson, Gregory M. Cook, Colin J. Jackson

Current status of paper: Draft

Brendon Lee cloned, expressed and purified Ddn, Ddn mutants, and Ddn orthologues, performed all enzymatic assays, oxygen consumption assays, sequence alignment of Ddn orthologues, docking experiment and designed Figures 1-3, S1, and Tables 1-2, S1. Livnat Afriat-Jurnou helped design the experiments and did some initial assays. Scott Beatson and Brian Forde performed the phylogenetic analysis and created Figure 4 and Tables S2-4. Htin Lin Aung performed the MIC experiment for the *M. tuberculosis* N0008 strain with pretomanid and delamanid. Kiel Hards help design the oxygen consumption assay, supervised Brendon to perform them and helped edit Figure 1b and c. Sacha Pidot performed the MIC experiments for *M. Marinum*. Hafna Ahmed help designing the experiments and supervised Brendon performing them. Elaaf Mohammad assisted with the docking experiments. Nicholas West provided intellectual insight. Matthew Taylor, Timothy Stinear, Brian Forde, Gregory Cook, and Colin Jackson supervised students. Brendon Lee and Colin Jackson wrote the paper with input from other authors.

The evolution of nitroimidazole antibiotic resistance in *Mycobacterium tuberculosis*

Brendon M. Lee[1], Livnat Afriat-Jurnou[1,2,3], Scott A. Beatson[4], Htin Lin Aung[5], Kiel Hards[5], Sacha J. Pidot[6], F. Hafna Ahmed[1], A. Elaaf Mohamed[1], Matthew C. Taylor[7], Nicholas West[4], Timothy P. Stinear[6], Chris Greening[7,8], Brian F. Forde[4], Gregory M. Cook[5], Colin J. Jackson[1]

[1]Australian National University, Research School of Chemistry, Sullivans Creek Road, Acton, ACT 2601, Australia

[2] MIGAL, Galilee Research Institute, Kiryat Shmona 11016, Israel

[3] Faculty of Sciences and Technology, Tel-Hai Academic College, 12208 Upper Galilee, Israel

[4]The University of Queensland, School of Chemistry and Molecular Biosciences, St Lucia, QLD 4067, Australia

[5] Department of Microbiology and Immunology, University of Otago, Dunedin 9054, New Zealand

[6] Department of Microbiology and Immunology, University of Melbourne, Parkville VIC 3052, Australia

[7] The Commonwealth Scientific and Industrial Organisation, Ecosystems Science Building, Clunies Ross Street, Acton, ACT 2601, Australia

[8] Monash University, School of Biological Sciences, Clayton, VIC 3800, Australia

Abstract

The nitroimidazole prodrugs delamanid and pretomanid are in advanced clinical development to treat tuberculosis (TB). These drugs comprise one of only two new classes of antitubercular agents to be approved for use within the last 50 years and are active against resistant strains. They are administered as prodrugs, which undergo reductive activation by the deazaflavin ($F_{420}H_2$) dependent nitroreductase (Ddn). To ensure these drugs remain effective for as long as possible, it is important that we establish how resistance to these new drugs could develop after their introduction. Here, we identify mutations in Ddn that can prevent pretomanid activation without significantly affecting its physiological role, thereby potentially conferring transmissible resistance. Analysis of ~15,000 sequenced *M. tuberculosis* genomes revealed ~1.5% of *M. tuberculosis* strains have non-synonymous mutations in the *ddn* gene. Notably, several of these were shown to prevent pretomanid activation *in vitro*. We confirmed that a transmissible *M. tuberculosis* isolate from the hypervirulent Beijing family already possesses one such mutation and is resistant to pretomanid, even though it has never been exposed to pretomanid. Notably, delamanid was still effective against this strain, which is consistent with structural analysis that indicates delamanid and pretomanid bind to Ddn differently. We suggest that SNPs identified in this work be monitored for informed pretomanid treatment and to slow the emergence of resistance.

Introduction

Tuberculosis is currently the leading cause of death from infectious disease worldwide (WHO, 2016). Limitations of current treatment regimens, combined with the rapid emergence of multidrug resistant tuberculosis (MDR-TB) strains, necessitate the development of new drugs. Three new antitubercular agents are now in advanced clinical development: bedaquiline (Andries *et al.*, 2005) and delamanid (Matsumoto *et al.*, 2006), which have been approved for MDR-TB treatment (Diacon *et al.*, 2009; Gupta *et al.*, 2015), and pretomanid (Stover *et al.*, 2000), which is part of regimens in phase III trials (Dawson, Diacon, Everitt, Niekerk, Donald, Burger, Schall, Spigelman, Pym, Groote-bidlingmaier, and Mendel, 2015). The nitroimidazoles, delaminid and pretomanid, are prodrugs that are reductively activated in an $F_{420}H_2$-dependent reaction in *Mycobacterium tuberculosis* by the deazaflavin-dependent nitroreductase (Ddn) (Singh *et al.*, 2008; Cellitti *et al.*, 2012). An initial hydride transfer step from the $F_{420}H_2$ cofactor leads to their decomposition into *des*-nitro products and releases reactive nitrogen species (Singh *et al.*, 2008) that elicit a bactericidal mode-of-action linked to respiratory poisoning and inhibition of mycolic acid synthesis (Singh *et al.*, 2008; Manjunatha *et al.*, 2009; Cellitti *et al.*, 2012).

Due to pretomanid and delamanid being prodrugs that require activation, mutations that knock-out the activity of Ddn or the biosynthesis of the enzyme's cofactor (F_{420}), could confer resistance. However, the fitness cost of such knockouts would be considerable given that F_{420} has been shown to be conditionally essential to the survival of *M. tuberculosis*, being used by at least 28 different enzymes (Greening *et al.*, 2016), and playing important roles in hypoxic survival, protection against oxidative and nitrosative damage, and in allowing *M. tuberculosis* to evade the host immune system (Purwantini and Mukhopadhyay, 2009; Hasan *et al.*, 2010; Gurumurthy *et al.*, 2013). Ddn is highly conserved across almost all species of mycobacteria (except *Mycobacterium leprae*), suggesting its physiological role is under strong evolutionary selection (Ahmed *et al.*, 2015). It has been hypothesised that Ddn serves as an $F_{420}H_2$-dependent menaquinone reductase given its membrane localisation (de Souza *et al.*, 2011) and catalytic activity with the synthetic quinone analogue menadione (Gurumurthy *et al.*, 2013), although further work is required to fully define its physiological role.

Despite the recent introduction of nitroimidazoles, cases of acquired clinical resistance, i.e. resistance that occurs during the long treatment of TB infection but is not necessarily

transmissible, have already been reported (Bloemberg *et al.*, 2015; Hoffmann, Kohl, *et al.*, 2016). Acquired resistance to pretomanid and delamanid can occur through genetic changes that cause loss of function within the biosynthetic pathway for F_{420} production or in the F_{420}-dependent glucose 6-phosphate dehydrogenase (FGD) that catalyzes F_{420} reduction to $F_{420}H_2$ (Choi *et al.*, 2001; Ujjini H Manjunatha *et al.*, 2006). Laboratory studies have also shown that genetic changes that abolish Ddn activity can also confer resistance (Haver *et al.*, 2015; Hoffmann, Borroni, *et al.*, 2016). While such mutations will compromise treatments for already infected individuals, transmission of *M. tuberculosis* to healthy individuals after these genetic changes has never been documented and is unlikely given the severe fitness costs incurred by them.

In this study, we have analysed Ddn orthologs from related mycobacteria to identify natural sequence variation that can make mycobacteria resistant to pretomanid, as well as analysing the genomes of ~15,000 *M. tuberculosis* isolate to identify the spectrum of naturally occurring non-synonymous Ddn polymorphisms. Mutations were then made to Ddn at positions identified in orthologs and through analysis of non-synoymous polymorphisms to analyse their effect on the native activity (quinone reduction) and pretomanid activation. This identified several mutations that can prevent pretomanid activation; a hypervirulent strain of TB from Vietnam that contains one such mutation (and has never been exposed to pretomanid) was shown to be resistant to pretomanid. Curiously, delamanid activation was not affected, which is consistent with structural analysis that suggests it binds to the active site of Ddn in an alternative orientation.

Results

The physiological role of Ddn. To investigate the potential for mutations in Ddn to confer transmissible resistance, it was first necessary to define its physiological role in *M. tuberculosis*. A role for Ddn as a quinone reductase was suggested based on activity with the synthetic quinone analogue menadione (Gurumurthy *et al.*, 2013). Here, we show that purified Ddn catalyzes the $F_{420}H_2$-dependent reduction of menaquinone-1 *in vitro* with moderate efficiency (k_{cat}/K_M = 8.6 x 10^2 M^{-1} s^{-1}) and physiologically relevant affinity (K_M = 22.4 ± 3.8 μM) **((Figure 1A; Table S1)**; despite a lower rate constant compared to menadione, the conversion rate is likely to differ in the native environment of the *M. tuberculosis* cell where Ddn and menaquinone are co-localised at the cell membrane in higher concentrations compared

to our in vitro assays (Sinha *et al.*, 2005). Ddn orthologs encoded by *Mycobacterium smegmatis* (MSMEG_2027, MSMEG_5998) were also able to reduce menaquinone, suggesting Ddn orthologs have similar physiological roles across the genus **(Table 1)**. Indeed, Ddn and its orthologs are highly conserved and abundant throughout mycobacteria (Ahmed *et al.*, 2015).

We then investigated whether the menaquinone reductase activity of Ddn was coupled to the mycobacterial respiratory chain by comparing the rates of respiratory oxygen consumption of *M. smegmatis* in the presence and absence of a complementation vector expressing *ddn*. We observed that the addition of Glucose 6-phosphate (G6P), F420, and FGD, which catalyzes the reduction of F_{420} to $F_{420}H_2$ for use by $F_{420}H_2$-dependent enzymes such as Ddn (Oyugi *et al.*, 2016), resulted in a 1.4-fold increase in oxygen consumption by mycobacterial membranes when the membranes are activated by NADH **(Figure 1B)**. This was dependent on the presence of cytochrome *bd* oxidase, which utilizes reduced menaquinone (i.e. menaquinol) as an electron source **(Figure 1B)**. The rate of NADH oxidation was not affected by the addition of $F_{420}H_2$, which implies endogenous NADH-dependent oxidases do not contribute to the increased oxygen consumption **(Figure 1C)**. This supports the idea that mycobacteria can couple $F_{420}H_2$ oxidation to O_2 reduction through the respiratory chain *via* cytochrome *bd* oxidase, and provides the first evidence that bacteria can use $F_{420}H_2$ as a respiratory electron donor. We also observed that the extent of oxygen consumption was significantly higher in membranes purified from the *ddn* expressing strain, relative to empty vector controls **(Figure 1B)**, which suggest Ddn serves as a menaquinone reductase in the respiratory chain, with the remaining stimulation attributable to $F_{420}H_2$ oxidation by native Ddn homologs of *M. smegmatis*.

Natural sequence variation in Ddn can prevent pretomanid activation. To investigate the effect of natural sequence variation within Ddn from mycobacteria, we purified Ddn orthologs from *M. tuberculosis, M. marinum, M. smegmatis, M. vanbaalenii, M. avium* and *M. ulcerans* **(Figure 2A&B)**. All Ddn orthologs catalyzed the reduction of menadione at physiologically relevant levels, consistent with a shared physiological function under selective pressure, but only Ddn from *M. tuberculosis* and its ortholog from *M. marinum* could activate pretomanid **(Figure 2B; Table 2)**. This demonstrates that the native Ddn activity can exist in *M. smegmatis, M. vanbaalenii, M. avium and M. ulcerans* in the absence of nitroimidazole reductase activity.

Having demonstrated that sequence polymorphisms in the active site of Ddn and its orthologs can result in substantial loss of pretomanid reduction activity *in vitro,* we investigated whether

this corresponded to differences in nitroimidazole susceptibility *in vivo*. *M. tuberculosis* H37Rv and *M. marinum*, which were the only two strains that encoded Ddn orthologs with *in vitro* pretomanid activation activity, were found to be susceptible to pretomanid and delamanid treatment (**Table 3**). In contrast, species from which Ddn orthologs did not exhibit pretomanid activation activity (*M. smegmatis*, *M. ulcerans*, *M. avium*) have been shown to be naturally resistant to pretomanid (Stover *et al.*, 2000; Ji *et al.*, 2006; Upton *et al.*, 2015).

Genome sequences of *M. tuberculosis* were then searched to identify nonsynonymous sequence polymorphisms within the *ddn* gene. We found that around 1.5% (218/14,876) of *M. tuberculosis* genomes screened had a non-synonymous mutation in *ddn* (**Table S2**). Altogether, we identified 47 non-synonymous substitutions and 2 deletions in *ddn* distributed throughout the *M. tuberculosis* phylogeny. Among these mutations, a Trp88Arg mutation was previously associated with resistance in a laboratory evolution study (Haver *et al.*, 2015). Three other polymorphisms are located close to the active site of Ddn: Ser22Leu, Ser78Tyr, and Lys79Gln. Notably, the Ser78Tyr polymorphism is found in the genome of N0008 (Comas *et al.*, 2013), a clinical isolate of the hypervirulent Beijing family (Hoffmann, Kohl, *et al.*, 2016), and in two other genomes (ERR718320 and ERR751847) that are phylogenetically closely related, which indicates a shared evolutionary history (Figure 1). The effects of the Ser22Leu, Ser78Tyr, Lys79Gln and Trp88Arg mutations were tested *in vitro* (**Figure 2C; Table 2**). Ser22Leu and Lys79Gln abolished pretomanid activation with no significant loss of menadione reduction, Ser78Tyr abolished pretomanid activation with some loss of menadione reduction although there was still significant activity, while Trp88Arg abolished both activities.

We obtained the hypervirulent Beijing strain R0008 (the other strains were not available) to investigate whether the Ser78Tyr mutation in the *ddn* gene, which results in loss of pretomanid reduction *in vitro* **(Figure 2C)**, corresponded to resistance to pretomanid *in vivo*. No other genetic changes previously observed to cause nitroimidazole resistance were apparent in the genome of R0008. We observed a 64-fold increase in minimum inhibitory concentration (MIC) of R0008 (256 μg mL^{-1}) compared to H37Rv (4 μg mL^{-1}). This suggests SNPs, such as Ser78Tyr in the *ddn* gene can confer resistance to pretomanid and confirms that transmissible pretomanid-resistant populations of *M. tuberculosis* harbouring this SNP already exist.

The potential for spontaneous pretomanid resistance mutations to arise in *M. tuberculosis.* Previous studies have used laboratory evolution/engineering to assess

investigating the potential for pathogens to evolve resistance to antibiotics (Orencia *et al.*, 2001; Hart *et al.*, 2016). We took a similar approach here, using structure-guided mutagenesis to investigate the robustness of the nitroreductase activity of Ddn to mutations. We used the structure of Ddn to identify which residues are present in the binding site that would immediately effect the binding and reduction of both quinones and pretomanid. The binding site of Ddn has been defined over several studies (Cellitti *et al.*, 2012; Ahmed *et al.*, 2015; Mohamed *et al.*, 2016), identifying a number of polar amino acids within the active site that contribute to activity, particularly Tyr65, Ser78, Tyr130, Tyr133, Tyr136. Three of the active site residues are highly conserved among the Ddn orthologs tested here, while Tyr65 and Tyr133 are significantly more variable **(Fig. 2A, Fig. 3A)**. We mutated these five residues to a range of different amino acids, including those already observed in various Ddn orthologs or accessible *via* single nucleotide changes **(Fig. 2C,D).** Across the 24 mutants tested, 14 resulted in complete loss of pretomanid activation while retaining significant levels of the native activity **(Table S2)**. In other words, while the native activity was not greatly affected by sequence variation, the nitroreductase activity was extremely sensitive and could be lost relatively easily. Among the Tyr65 mutants, Tyr65Phe was neutral for both activities, but Tyr65Leu and Tyr65Cys resulted in loss of pretomanid activity. All of the tested mutations of Ser78 (Thr, Ala, Cys, Val, Tyr) resulted in loss of pretomanid activity. Mutation of Tyr130 to Trp, Cys, Ser, His, Phe, Asp or Asn did not affect pretomanid activation, relative to the menadione activity. Mutations of Tyr133 and Tyr136 behaved similarly to mutations of Tyr65, where the Tyr to Phe mutation had no effect on catalysis, but mutations to residues with less structural similarity (Leu, Met, Trp, Thr, Ser, Glu) resulted in complete loss of pretomanid reductases activity, while retaining activity towards menadione.

We used our genomic survey of *ddn* in *M. tuberculosis* to estimate the level of sequence variation in *ddn* and predict the rate at which mutations could spontaneously arise at one of the positions identified in this work. This revealed that virtually every distinct strain of *M. tuberculosis* contains SNPs in *ddn*; given the number of cells present in a typical patient (millions), and the number of infected individuals (millions), under conditions of selective pressure (the administration of pretomanid), genetic selection for mutations around the active site of Ddn that prevent pretomanid activation could occur rapidly.

The molecular basis of resistance. The effects of the mutations shown in **Fig. 2C** are generally consistent with our mechanistic understanding of Ddn from mutagenesis and computational

simulation (Cellitti *et al.*, 2012; Mohamed *et al.*, 2016). Ser78 is thought to interact with the nitro-moiety of pretomanid and to stabilize the transition state; none of the Ser78 mutants retained pretomanid activity, suggesting this interaction is particularly important. Tyr65, Tyr130, Tyr 133 and Tyr136 are known to form a hydrophobic wall in the binding site, which can move during the catalytic cycle to shield the active site from solvent and thereby facilitate pretomanid reduction (Mohamed *et al.*, 2016). This is in keeping with the observation that Tyr to Phe mutations at positions 65, 133 and 136 were essentially neutral, whereas substitution with other residues (Met, Leu, Cys, Trp, Thr, Ser, Glu) led to loss of pretomanid activation. Menadione is less susceptible to loss of activity through mutation, which is consistent with work showing native activities are substantially more robust to mutation than promiscuous activities (such as pretomanid activation) (Aharoni *et al.*, 2005), as well as the observation that menadione is more chemically labile. Trp88 is known to be involved in F_{420} binding (Cellitti *et al.*, 2012) and the Trp88Arg mutation that lead to a loss of activity with both menadione and pretomanid would be due to the inability to bind F_{420}.

Delamanid is less susceptible to resistance mutations. Surprisingly, we observed that the susceptibility of R0008 to delamanid was not affected by the Ser78Tyr sequence polymorphism. We therefore tested the *in vitro* activity of Ddn with delamanid as a substrate for both wild-type Ddn and the Ser78Tyr mutant. Owing to the low solubility of delamanid, full Michaelis-Menten kinetics could not be obtained, but we were able to measure specific activity, revealing similar substrate reduction activity for both the wild-type and mutant protein (**Fig . S1; Table 3**). To better understand the molecular basis for the insensitivity of delamanid to the Ser78Tyr mutation, we docked both pretomanid and delamanid into the crystal structure of Ddn. The *in silico* docking of both delamanid and pretomanid revealed ten different poses for each drug. For this study, we removed any pose where the drug was bound to the surface of Ddn and not bound into the binding site. To compare the binding of the two drugs we chose the poses with the bicyclic-nitroimidazole group present in the binding site with the lowest binding energy score. The binding of delamanid was revealed to be different than that of pretomanid (**Fig. 3C,D**), with the dual methyl and phenoxy-methyl substituents on the oxazole ring preventing delamanid binding to the deazaflavin ring in a ring-stacked orientation, as is seen in pretomanid, which has a singly-substituted oxazine ring in an analogous position. This results in a change in the angle at which the nitroimidazole group interacts with the cofactor, binding in a perpendicular orientation that results in an increase in the distance to Ser78. Thus,

there appears to be structural basis for the different effects of the Ser78 mutation on delamanid activity *in vitro* and *in vivo*.

Discussion

The fitness trade-off between resistance and native function. Given the conservation Ddn-like genes throughout mycobacteria, its activity with menaquinone and its role in respiration, it is likely that mutations that completely knock-out Ddn activity (such as the introduction of stop or large genetic deletions) will result in substantial loss of fitness given it is involved in both redox and energy metabolism. Loss of this function is likely to have severe consequences to bacterial fitness, given the bactericidal effects of inhibiting mycobacterial respiration (Diacon *et al.*, 2009; Cook *et al.*, 2014; Hards *et al.*, 2015; Lamprecht *et al.*, 2016). Indeed, phenotypic studies have linked Ddn to maintaining redox balance in response to hypoxia and treatment with first-line antimycobacterial drugs (Gurumurthy *et al.*, 2013).

We have investigated the likelihood that mutations to *M. tuberculosis* Ddn will result in loss of pretomanid activation activity without substantial disruption of the native activity. Extending our *in vitro* measurements to *in vivo* measurement of MICs revealed that Ddn orthologs from related species and clinical isolates of *M. tuberculosis* that harbor certain differences within the active site do not efficiently activate pretomanid, resulting in antibiotic insensitivity. These results have important implications for the management of nitroimidazole administration in order to prevent or slow the development of resistance: if pretomanid is clinically administered in regions in which the R0008 strain is endemic, natural selection will drive selective sweeps in the *ddn* gene towards Ser78Tyr variants. Moreover, the chances of spontaneous mutation of Ddn in currently sensitive strains is significant, given our observation of the number of single nucleotide mutations that can knock out pretomanid activity. Given that the clinical isolate R0008 is highly transmissible, it is likely that other Ddn variants in which pretomanid activity can be abolished without substantial loss of the native activity will also be transmissible owing to minimal loss of fitness due to the mutations. Thus, fitness-neutral Ddn mutations are likely to be the main route through which transmissible clinical pretomanid resistance spread.

Our findings have broad implications for the continued clinical development of nitroimidazole antitubercular agents. Through two phase III clinical trials, the TB Alliance are currently

evaluating combination therapies using pretomanid; a trial with the three-drug PaMZ regimen (pretomanid, moxifloxacin, pyrazinamide) is on hold and a replacement trial with the four-drug BPaMZ regimen (incorporating bedaquiline) has been initiated (Murray *et al.*, 2016). If pretomanid is clinically approved, we advise intensive monitoring of *ddn* polymorphisms to ensure informed drug administration and allow interventions that will avoid spreading of transmissible resistance. Our findings indicate that delamanid binds to Ddn in a different conformation than pretomanid does, suggesting that combination therapy of both nitroimidazoles could help prevent the evolution and spread of resistance (since the simultaneous loss of both activities will be less likely to result from single amino acid substitution). Further studies on how delamanid and pretomanid are activated in the *M. tuberculosis* cell will inform the development of improved nitroimidazole therapies and testing of a broad range of nitroimidazole analogs against a panel of Ddn variants could help to identify compounds for which resistance is less likely to evolve.

Materials and Methods

Plasmid construction and point mutation. The *E. coli* codon optimised sequences for Ddn from *M. tuberculosis,* MSMEG_5998 from *M. smegmatis*, MMAR_5035 from *M. marinum,* MVAN_5261 from *M. vanbaalenii*, MAV_0613 from *M. avium,* and MUL_4109 from *M. ulcerans* were purchased as gene strings from ThermoFisher Scientific (Massachusetts, USA) and cloned into the expression vector pMAL-c2X using Gibson assembly (Gibson *et al.*, 2009). All mutations to Ddn were made by site-directed mutagenesis using Gibson assembly (Gibson *et al.*, 2009). Construction of MSMEG_2027 and FGD has been described previously (Bashiri *et al.*, 2008; Lapalikar *et al.*, 2012) . For work in *M. smegmatis* the *E. coli* optimized genes were not used but instead the Ddn gene was amplified from *M. tuberculosis* DNA using the primers GTACTGCAGATGCCGAAATCTCCACCGCG, and GTAAAGCTTCTACGGTTCACAAACAACAATCGGAATG. The amplified DNA and pMV261 vector were cut using the Fast Digest enzymes PstI, and HindIII from ThermoFisher Scientific (Massachusetts, USA) and ligated together using T4 DNA ligase from New England Biolabs (Massachusetts, USA).

Protein expression and purification. MSMEG_2027 was expressed and purified as previously described (Ahmed *et al.*, 2015). Ddn, Ddn mutants, and Ddn orthologs were transformed into *E. coli* BL21 (DE3) cells and grown on LB agar containing 100 µg/ml

ampicillin. Single colonies were picked and inoculated in LB media with 100 µg/ml ampicillin. Starter cultures were grown overnight and diluted 1/100 and grown at 37 °C until OD = 0.4. Cultures were induced with IPTG to a final concentration of 0.3 mM, and grown for 3 h at 25 °C. Cells were harvested by centrifugation at 8,500 × *g* for 20 minutes at 4 °C and resuspended in lysis buffer (20 mM Tris-Cl, pH 7.5, 200 mM NaCl) and lysed by sonication using an Omni Sonicator Ruptor 400 (2 x 6 min. at 50% power). The soluble extract was obtained by centrifugation at 13,500 × *g* for 1 h at 4 °C. The protein was purified using amylose resin (NEB) using the provided protocol. Briefly the lysate was passed over the amylose resin and washed with 12 column volumes of lysis buffer. The protein was eluted using elution buffer (same as lysis buffer but with 10 mM maltose). Samples were frozen at -80 °C in 20 mM tris pH 7.5, 200 mM NaCl, 10 mM maltose, and 10% glycerol.

FGD was expressed and purified as described by Bashiri *et al*. (Bashiri *et al.*, 2008), with minor modifications. FGD was transformed into *E. coli* BL21 (DE3) cells and grown on LB agar containing 100 µg/ml ampicillin. Single colonies were picked and inoculated in Terrific Broth (TB) (Sambrook *et al.*, 1989) with 100 µg/ml. ampicillin. Starter cultures were grown overnight and diluted 1/100 into auto-induction media (20 g/l tryptone, 5 g/l yeast extract, 5 g/l NaCl, 6 g/l Na_2HPO_4, 3 g/l KH_2PO_4, 6 ml/l glycerol, 2 g/l lactose, 0.5 g/l glucose, 100 mg/ml ampicillin) and grown at 30 °C for 24 h. The cells were harvested by centrifugation at 8500 g for 20 min at 4 °C and resuspended in lysis buffer (20 mM $NaPO_4$ pH 8, 300 mM NaCl, 25 mM imidazole) and lysed by sonication using an Omni Sonicator Ruptor 400 (2 x 6 min at 50% power). The soluble extract was obtained by centrifugation at 13500 g for 1 h at 4 °C. The soluble fraction was filtered and loaded 5-ml HisTrap HP column (GE Healthcare) and washed with lysis buffer. The protein was eluted with elution buffer (lysis buffer with 250 mM imidazole). The purified protein was dialyzed in 50 mM Tris-Cl, pH 7, 200 mM ammonium sulphate. Samples were frozen at -80 °C in 50 mM Tris-Cl, pH 7, 200 mM ammonium sulphate, and 10% glycerol.

Membrane purification. *M. smegmatis* mc^2155 wild type (Snapper *et al.*, 1990), *M. smegmatis* mc^2155 with a kanamycin cassette disruption of the *cydA* gene (Kana *et al.*, 2001), and *M. smegmatis* mc^2155 transformed with empty vector pMV261 or pMV261-Ddn were all grown on LB agar supplemented with 0.05% (v/v) Tween 80. Single colonies were picked and grown in Hartmans–de Bont (HdeB) medium supplemented with 25 mM glycerol and 0.05% (v/v) Tween 80 until an OD of 0.4 to 0.8. Cultures were diluted to an OD of 0.005 in 500 ml

of HdeB and grown for 72 h with agitation (200 rpm) at 37 °C. Cultures were harvested by centrifugation at, 5,000 × *g* for 15 min at 4 °C and resuspended in lysis buffer (10 mM HEPES, pH 7.5, 200 mM KCl, 5 mM $MgCl_2$, 1 mM PMSF, and 1 mg DNase), homogenised on ice, and passed through a French pressure cell 3 times at 20,000 psi. Unbroken cells were removed by centrifugation at 10,000 × *g* for 10 mins at 4 °C. The membranes were isolated by ultracentrifugation at 150,000 × *g* for 45 mins at 4 °C and resuspended in working buffer (10 mM HEPES, pH 7.5, 200 mM KCl, 5 mM $MgCl_2$). The protein concentrations of the membranes were measured by BCA assay (Pierce) against BSA standards.

Enzymatic assays. F_{420} was purified from M. *smegmatis* $mc^2$4517 as described by Ahmed *et al*.(Ahmed *et al.*, 2015) F_{420} was reduced overnight with 10 µM FGD and 10 mM glucose-6-phosphate in 20 mM Tris-CL, pH 7.5 under anaerobic conditions. FGD was removed by spin filtration in a 1 mL 10 K MWCO spin filter (Millipore) and used $F_{420}H_2$ within 8 hours. Enzyme assays were performed according to Ahmed *et al.* (Ahmed *et al.*, 2015; Jirapanjawat *et al.*, 2016) in 200 mM Tris-HCl, pH 7.5, 0.1 % Triton X-100, 25 µM $F_{420}H_2$, and varying amounts of substrate at room temperature. Enzyme concentrations used were between 0.1 µM and 1 µM. Activity was monitored following the oxidation of $F_{420}H_2$ which was measured spectrophotometrically at 420 nm (ε = 41,400 M^{-1} cm^{-1}) (Purwantini *et al.*, 1992)(Purwantini et al., 1992)(Purwantini et al., 1992)(Purwantini et al., 1992)(Purwantini et al., 1992)(Purwantini et al., 1992)(Purwantini et al., 1992)(Purwantini et al., 1992)(Purwantini et al., 1992)(Purwantini et al., 1992) and a Michaelis–Menten curve of best fit was used to calculate K_M and k_{cat}. Specific enzymatic activity with delamanid was measured using fluorescence (excitation/emission: 400 nm/470 nm). Assays were prepared the same as above, using 10 µM delamanid and 10 % DMSO in the reaction to solubilize the substrate.

Measurement of oxygen consumption. To determine the rate of oxygen consumption, assays were performed as described by Pecsi *et al.* (Pecsi *et al.*, 2014) in 10 mM HEPES, pH 7.5, 200 mM KCl, and 5mM $MgCl_2$ at 37 °C with *M. smegmatis* membranes that had a protein concentration of 0.5 mg/ml, 200 µM NADH, 1 mM glucose-6-phosphate, and 25 µM F_{420} and 2.5 µM FGD where stated. The rate of oxygen consumption was measured using a model 10 Clark-type oxygen electrode (Rank Brothers Ltd., Cambridge, England) linked to a PicoLog ADC-20 data logger that was calibrated with saturated sodium dithionite.

NADH oxidation assay. The rate of NADH oxidation was determined using purified *M. smegmatis* membranes that had a protein concentration of 0.5 mg/ml in 10 mM HEPES, pH 7.5, 200 mM KCl, and 5mM $MgCl_2$, 200 µM NADH, 1 mM glucose-6-phosphate, 2.5 µM FGD, and 25 µM F_{420} where stated at 37 °C. Activity was measured following the oxidation of NADH which was measured spectrophotometrically at 340 nm (6,220 M^{-1} cm^{-1}).

Computational analysis. Sequences of Ddn and orthologs were obtained from the NCBI sequence database. Alignment of the sequences were performed using MUSCLE (Edgar, 2008) *via* the EMBL-EBI web services (Li *et al.*, 2015). Autodock Vina (Trott and Olson, 2010) was used to dock menadione and PA-824 into Ddn (PDB ID: 3R5R (Cellitti *et al.*, 2012)). The protein and ligand were prepared using in Autodock tools with default settings (Morris and Huey, 2009) and visualized using Pymol (DeLano, 2002). Substrate structures were obtained from the ZINC database (Irwin and Shoichet, 2005).

Drug susceptibility test. Minimum inhibitory concentration (MIC) testing of M. marinum was performed according to the method of Wiegand *et al*. (Wiegand *et al.*, 2008) with some minor modifications. A culture was grown on Brown and Buckle media and colonies were scraped and diluted to an OD600 of 0.2, and was used as the inoculum for the MIC assay. Plates were incubated at 30 °C in a humid environment and were read after 5 days of incubation. MICs of *M. tuberculosis* isolates were determined as described previously (Heikal *et al.*, 2016) with slight modifications. Briefly, U-bottomed 96-well microtitre plates containing Middlebrook 7H9 broth supplemented with oleic acid, albumin, dextrose and catalase were inoculated with *M. tuberculosis* H37Rv or R0008 (OD_{600} 0.02) in the presence of delamanid and pretomanid (0.015-512 µg/ml), and incubated at 37 °C for 5 days. The presence/absence of a cell pellet was checked visually. Resazurin (0.03% w/v) was then added, and plates were further incubated for 7 days. Viable cells reduce resazurin (blue) to resofurin (pink). Bedaquiline (0.015–32 µg/ml) was used as a drug susceptibility control.

Dataset. To determine the frequency of non-synonymous sequence polymorphisms in the ddn gene we assembled a collection of 5,184 publicly available complete and draft *M. tuberculosis* genomes from Genbank (Benson *et al.*, 2013) and unassembled *M. tuberculosis* sequencing data from the sequence read archive (SRA; https://www.ncbi.nlm.nih.gov/sra/) on the 7th and 28th of April 2017, respectively. Using a structured query (Illumina[Platform]) AND

"Mycobacterium tuberculosis"[orgn:__txid1773]) to search the SRA we identified 9692 unassembled *M. tuberculosis* genome datasets.

Taxonomic profiling of unassembled sequencing data. Kraken (Wood and Salzberg, 2014), an ultrafast sequence classification tool, was used to assign taxonomic labels to the unassembled *M. tuberculosis* genomes from the SRA. Sequence reads for each genome from the SRA were screened against a NCBI refseq database (https://www.ncbi.nlm.nih.gov/refseq) using Kraken version 0.10.5 to identify contaminants. Of the 243 *M. tuberculosis* genomes with sequence polymorphisms in *ddn* 67 (27.5%) were found to be contaminated with DNA from unidentified organisms or from *Mycobacterium* species other than *M. tuberculosis* (Table S2). These genomes were excluded from all further analysis.

Lineage-typing of *M. tuberculosis* genomes. Classification of M. tuberculosis phylogenetic lineages was performed using KvarQ version 0.12.3a1 and default parameters (Steiner *et al.*, 2014). Using KvarQ scan, unassembled sequencing data were screened against a database of previously defined sequence polymorphisms known to delineate the 7 major *M. tuberculosis* phylogenetic lineages (Table S1).

Characterisation of *ddn* sequence polymorphisms in *M. tuberculosis*. Using BLASTn (with default parameters) complete and draft *M. tuberculosis* genome assemblies from Genbank were queried with the *ddn* gene from *M. tuberculosis* H37Rv (Genbank accession:AL123456; (Cole *et al.*, 1998)), identifying 145 *M. tuberculosis* genomes carrying alternative *ddn* alleles (relative to H37Rv). For these 145 genomes the Ddn sequence was extracted and aligned using Clustal Omega version 1.2.4 (Sievers *et al.*, 2011) to identify non-synonymous mutation and other sequence polymorphism which could impact the function of Ddn (Table S2).
For the unassembled genomes datasets, raw sequencing reads were aligned to the reference genome *M. tuberculosis* H37Rv using Snippy version 2.9 (BWA-mem version 0.7.12 (Li, 2013))(https://github.com/tseeman/snippy). Variant calling was performed using Snippy (Freebayes version 0.9.21 (Garrison and Marth, 2012) with default parameters (minimum read coverage of 10x and 90% read concordance at the variant locus). 180 unassembled genome datasets were identified as having a mutation in *ddn*, only three of which were represented amongst the afore-mentioned 145 assembled genomes available in GenBank.

Phylogenetic reconstruction *M. tuberculosis* strains with sequencing polymorphisms in Ddn. To determine the phylogenetic distribution of *ddn* alleles in *M. tuberculosis* we carried out a phylogenomic analysis of *M. tuberculosis* strains with sequence polymorphism in *ddn*. Firstly, unassembled genomes from the SRA were assembled *de novo* using SPAdes version 3.9.0 (Bankevich *et al.*, 2012). Next all 322 complete and draft genomes (Table S4) were aligned with Parsnp version 1.2 (Treangen *et al.*, 2014) using the genome of H37Rv as a reference to produce a core genome alignment of 848,476 bp. Core genome SNPs were identified and recombinant regions removed using Gubbins version 2.2.0 (Croucher *et al.*, 2015). Finally, a maximum-likelihood phylogenetic tree was estimated using RAxML version 8.2.9 (Stamatakis, 2014) under the GTRGAMMA nucleotide substitution model.

Footnotes

The authors declare no conflict of interest.

Acknowledgements: We acknowledge Thomas Cuddihy (QFAB Bioinformatics) for assistance with genome data retrieval. SAB is supported by an NHMRC Career Development Fellowship (GNT1090456).

Figures and Tables

Figure 1. Ddn is a respiratory primary dehydrogenase that couples $F_{420}H_2$ oxidation to menaquinone reduction. **A.** Michaelis-Menten curve of the activity of purified Ddn with menaquinone-1 in the presence of $F_{420}H_2$. Rates were determined by measuring change of absorbance at 420 nm. Error bars indicate SEM (n = 3). **B.** Relative oxygen consumption of *M. smegmatis* membranes. F_{420}, NADH, and glucose 6-phosphate were present in all assays, while the availability of the F_{420}-dependent glucose 6-phosphate dehydrogenase (FGD) was varied. Membranes were purified from four different genetic backgrounds: wild-type, a transformant with the empty complementation vector pMV261, a transformant with pMV261 expressing the *ddn* gene, and a strain containing a chromosomal cytochrome *bd* oxidase deletion (Δ*cydA*). Error bars indicate SEM (n = 3). Stars above each column indicate a statistically significant difference compared to the first column. Other significant differences are shown by starred lines between columns. * = $p \leq 0.05$, ** = $p \leq 0.01$, **** = $p \leq 0.0001$ n.s = $p > 0.05$ (one-way ANOVA followed by Tukey's multiple comparison test). **C.** Rate of NADH oxidation in the presence and absence of $F_{420}H_2$. Rates were determined by following change of absorbance at 340 nm. n.s indicates $p > 0.05$, two tailed t-test, error bars indicate SEM (n = 3).

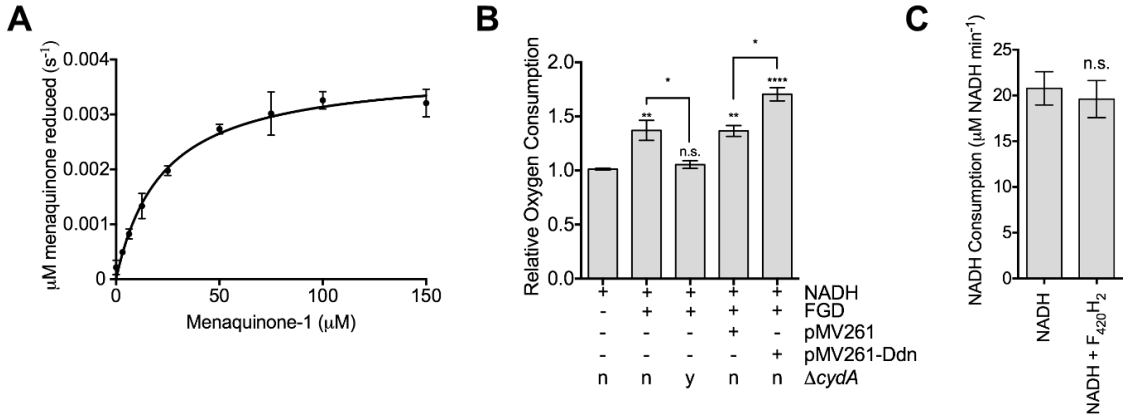

Figure 2. Mutations in Ddn prevent pretomanid activation without affecting native activity. **A.** Multiple sequence alignment of Ddn and orthologs from other mycobacterial species. Highlighted residues indicate active site residues and numbers indicate their residue position in Ddn. *Indicates enzymes tested from a previous study (Ahmed *et al.*, 2015) **B.** Comparison of the turnover rates of Ddn orthologs with menadione and pretomanid. Six orthologs were tested: Rv3547 (*M. tuberculosis* Ddn), MMAR_5035 (*M. marinum*), MSMEG_5998 (*M. smegmatis*), MVAN_5261 (*M. vanbaalaenii*), MAV_0613 (*M. avium*), and MUL_4109 (*M. ulceran*). Error bars show SEM (n = 3). **C.** Comparison of the turnover rates of Ddn mutants with menadione and pretomanid. 24 point mutations in active site were tested. Full kinetic data for panels B and C are shown in **Table S2**. **D.** Nucleotide changes to obtain the aligned amino acid mutations. Highlighted nucleotides show indicate differences from the original sequence.

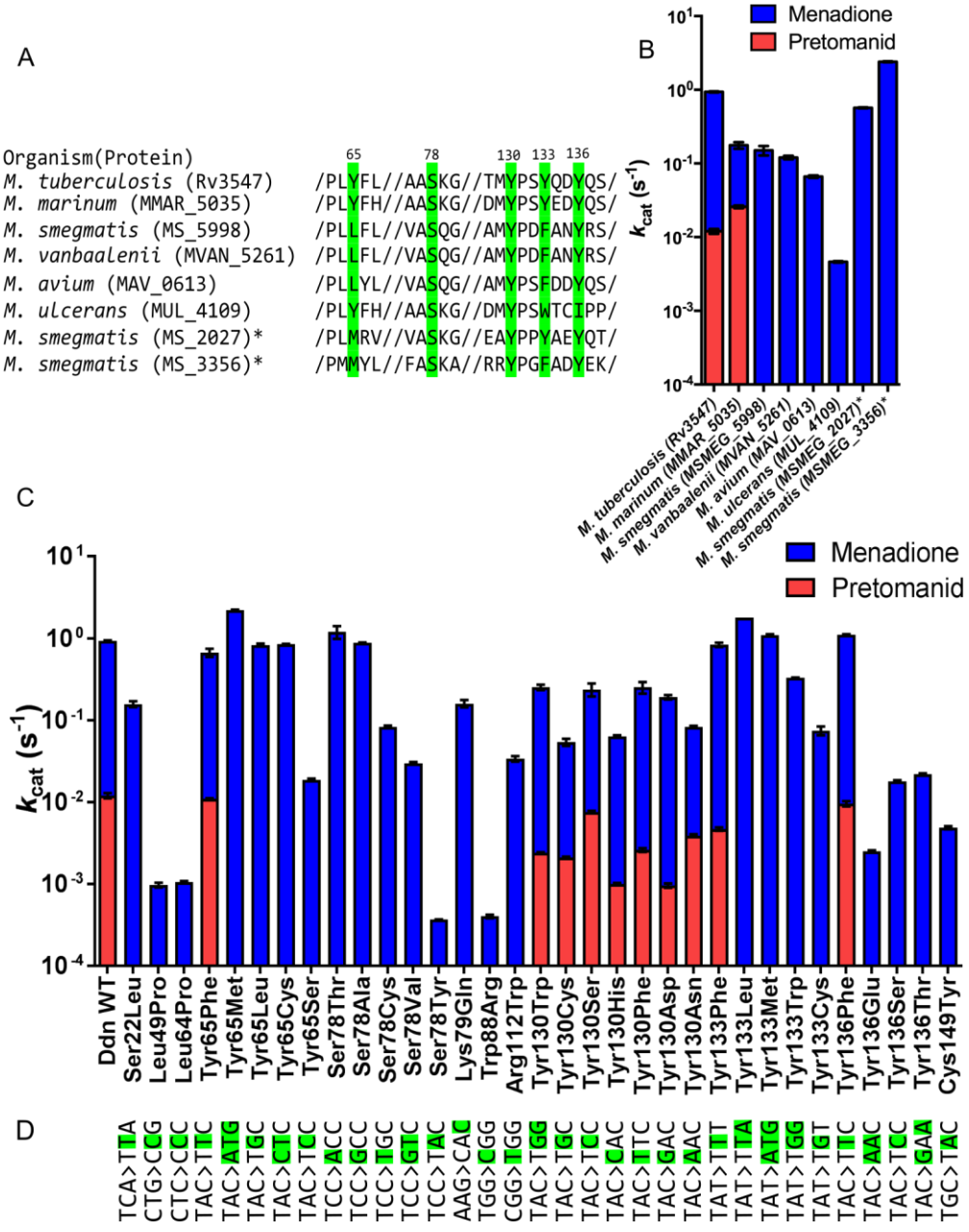

Figure 3. The substrate-binding pocket of Ddn (PDB: 3R5R[9]). **A.** The binding pocket in Ddn consists of F_{420}/$F_{420}H_2$, Tyr65, Ser78, Tyr130 and Tyr136. These residues were all mutated to investigate their effects on the native (menadione) and drug-activating (pretomanid/delamanid) activities. **B.** Menadione binds above the deazaflavin ring of $F_{420}H_2$ in a complementary pocket formed by the aromatic rings of the tyrosine residues and the hydroxyl group of Ser78. **C.** Pretomanid docked into wild type Ddn with $F_{420}H_2$ bound. The nitroimidazo-oxazine moiety can bind parallel to the deazaflavin group of F_{420}, extending the nitro- group deep into the active site, towards Ser78. **D.** Delamanid docked into wild type Ddn with $F_{420}H_2$ bound. The dual methyl/phenoxy-methyl substitution at the C6 position of the oxazole ring creates steric hindrance with the deazaflavin ring of F_{420}, causing it to bind above F_{420} in a perpendicular orientation. This results in additional distance to Ser78.

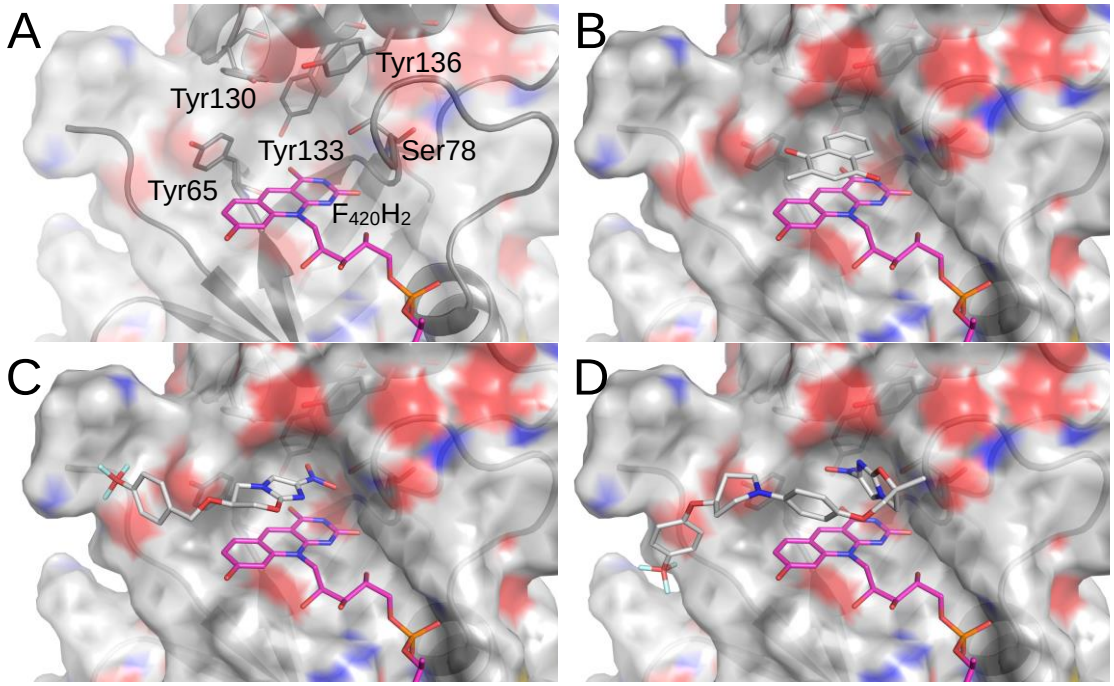

Figure 4: Phylogeny *M. tuberculosis* strains with sequencing polymorphisms in Ddn. Maximum-likelihood phylogenetic tree of 332 *M. tuberculosis* strains built using 2099 non-recombinant core genome SNPs (relative to H37Rv). The tree shows all *M. tuberculosis* strains for which public genome data is available in Genbank or the short read archive (SRA) that have either synonymous and non-synonymous mutations in Ddn (relative to H37Rv). The amino acid changes of the non-synonymous mutations are indicated on the branch tips. Blank tips represent strains with synonymous mutations in Ddn. Branches are coloured by Lineage: Lineage 1 (Indo-Oceanic), yellow; Lineage 2 (East Asian-Beijing), red; Lineage 3 (East African-Indian), purple; Lineage 4 (Euro-American), green; Lineage 5 (West African), teal. The scale bar indicates branch length in number of SNPs. Genome alignments, recombination filtering and phylogenetic reconstruction where done using Parsnp, Gubbins and RaxML, respectively. The phylogenetic tree was visualised using Figtree version 1.4.3 (https://tree.bio.ed.ac.uk/software/figtree).

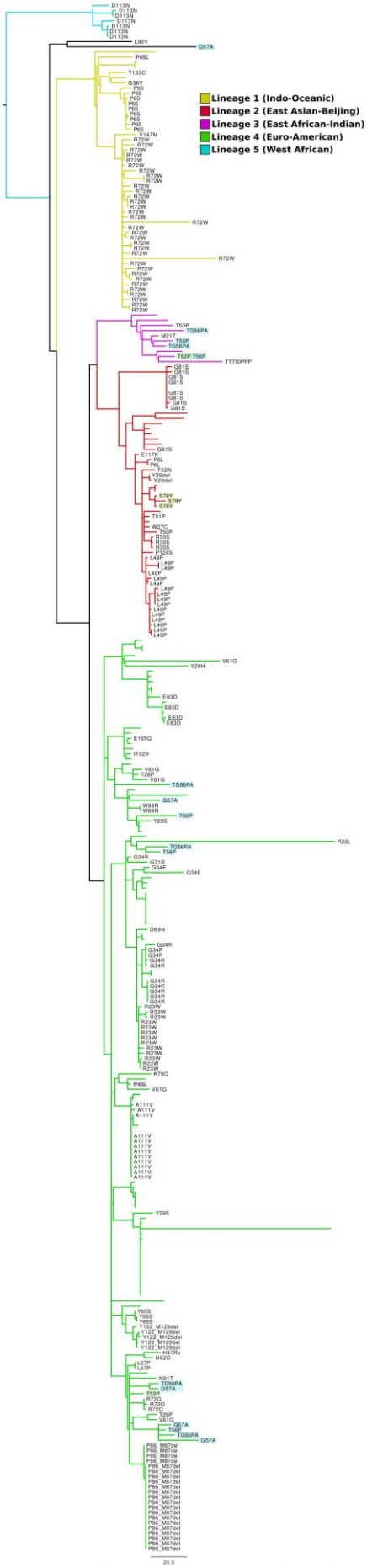
Lineage 1 (Indo-Oceanic)
Lineage 2 (East Asian-Beijing)
Lineage 3 (East African-Indian)
Lineage 4 (Euro-American)
Lineage 5 (West African)

Table 1: Kinetic parameters of native $F_{420}H_2$-dependent menaquinone reductase activities of Ddn and *M. smegmatis* homologs *in vitro* assays.

	Menaquinone		
Enzyme	k_{cat} (s^{-1})	K_M (μM)	k_{cat}/K_M (M^{-1} s^{-1})
Ddn	$1.9\times10^{-2} \pm 9.7\times10^{-4}$	22.4 ± 3.8	8.6×10^{2}
MSMEG_2027	$5\times10^{-3} \pm 1.2\times10^{-3}$	80.7 ± 34.4	6.1×10^{1}
MSMEG_5998	$1.2\times10^{-2} \pm 1.5\times10^{-3}$	97.9 ± 20.4	1.2×10^{2}

Table 2. MICs of different mycobacterial strains with pretomanid and delamanid.

	Pretomanid		**Delamanid**	
Strain	Reduction (nmol min^{-1} μmol_{enzyme}^{-1})	MIC (μg mL^{-1})	Reduction (nmol min^{-1} μmol_{enzyme}^{-1})	MIC (μg mL^{-1})
M. tuberculosis H37Rv	243 ± 8.1	4	15.8 ± 1.4	32
M. tuberculosis N0008[a]	0	256	12.4 ± 1.2	32
M. marinum M	60.3 ± 9.3	16	N/A	16
M. smegmatis mc^2155	0	>50*	N/A	>50*

[a]S78Y mutation

*MICs obtained from Upton, A. et al. (Upton *et al.*, 2015)

Table 3: Distribution of Ddn alleles in the major TB Lineages. Distribution of Ddn alleles in five major lineages of *M. tuberculosis.*

Ddn allele	#Strains	Lineage(s)
A111V	12	Lineage 4 (Euro American)
D113N	7	Lineage 5 (West Africa)
D69N	1	Lineage 4 (Euro American)
E105Q	1	Lineage 4 (Euro American)
E117K	1	Lineage 2 (East Asian-Beijing)
E83D	4	Lineage 4 (Euro American)
G34R	11	Lineage 4 (Euro American)
G34E	2	Lineage 4 (Euro American)
G36V	1	Lineage 1 (Indo-Oceanic)
G57A	5	Lineage 1(Indo-Oceanic),Animal Lineage
G71R	1	Lineage 4 (Euro American)
G81S	9	Lineage 2 (East Asian-Beijing)
I102V	1	Lineage 4 (Euro American)
K79Q	1	Lineage 4 (Euro American)
L49P	16	Lineage 2 (East Asian-Beijing)
L67P	2	Lineage 4 (Euro American)
L90V	1	Animal Lineage
M21T	1	Lineage 3(East African-Indian)
N62D	1	Lineage 4 (Euro American)
N91T	1	Lineage 4 (Euro American)
P124S	1	Lineage 2 (East Asian-Beijing)
P45L	2	Lineage 4 (Euro American),Lineage 1 (Indo-Oceanic)
P6L	2	Lineage 2 (East Asian-Beijing)
P6S	9	Lineage 1 (Indo-Oceanic)
P6T	2	Lineage 3(East African-Indian)
P86_M87del	22	Lineage 4 (Euro American)
R23L	1	Lineage 4 (Euro American)
R23W	14	Lineage 4 (Euro American)
R30S	3	Lineage 2 (East Asian-Beijing)
R72Q	3	Lineage 4 (Euro American)
R72W	34	Lineage 1 (Indo-Oceanic)
S78Y	3	Lineage 2 (East Asian-Beijing)
T140I	1	Lineage 4 (Euro American)
T26P	2	Lineage 4 (Euro American)
T50P	2	Lineage 2 (East Asian-Beijing)

T51P	1	Lineage 2 (East Asian-Beijing)
T52N	1	Lineage 2 (East Asian-Beijing)
T52P	2	Lineage 3(East African-Indian),Lineage 4 (Euro American)
T56P	5	Lineage 4 (Euro American),Lineage 3(East African-Indian)
TTT50PPP	1	East African-Indian
V147M	1	Lineage 1 (Indo-Oceanic)
V61G	5	Lineage 4 (Euro American)
W27C	1	Lineage 2 (East Asian-Beijing)
W88R	2	Lineage 4 (Euro American)
Y122_M129del	5	Lineage 4 (Euro American)
Y133C	1	Lineage 1 (Indo-Oceanic)
Y29del	2	Lineage 2 (East Asian-Beijing)
Y29H	1	Lineage 4 (Euro American)
Y29S	2	Lineage 4 (Euro American)
Y65S	3	Lineage 4 (Euro American)
TG56PA	6	Lineage 3(East African-Indian),Lineage 4 (Euro American)

References

Aharoni, A., Gaidukov, L., Khersonsky, O., Gould, S.M.Q., Roodveldt, C., and Tawfik, D.S. (2005) The'evolvability'of promiscuous protein functions. Nat Genet 37: 73–76.

Ahmed, F.H., Carr, P.D., Lee, B.M., Afriat-Jurnou, L., Mohamed, A.E., Hong, N.S., et al. (2015) Sequence-Structure-Function Classification of a Catalytically Diverse Oxidoreductase Superfamily in Mycobacteria. J Mol Biol 427: 3554–3571.

Andries, K., Verhasselt, P., Guillemont, J., Göhlmann, H.W.H., Neefs, J.-M., Winkler, H., et al. (2005) A diarylquinoline drug active on the ATP synthase of Mycobacterium tuberculosis. Science 307: 223–7.

Bankevich, A., Nurk, S., Antipov, D., Gurevich, A.A., Dvorkin, M., Kulikov, A.S., et al. (2012) SPAdes: A New Genome Assembly Algorithm and Its Applications to Single-Cell Sequencing. J Comput Biol 19: 455–477.

Bashiri, G., Squire, C.J., Moreland, N.J., and Baker, E.N. (2008) Crystal structures of F420-dependent glucose-6-phosphate dehydrogenase FGD1 involved in the activation of the anti-tuberculosis drug candidate PA-824 reveal the basis of coenzyme and substrate binding. J Biol Chem 283: 17531–17541.

Benson, D.A., Cavanaugh, M., Clark, K., Karsch-Mizrachi, I., Lipman, D.J., Ostell, J., and Sayers, E.W. (2013) GenBank. Nucleic Acids Res 41: D36–D42.

Bloemberg, G. V., Keller, P.M., Stucki, D., Trauner, A., Borrell, S., Latshang, T., et al. (2015) Acquired Resistance to Bedaquiline and Delamanid in Therapy for Tuberculosis. N Engl J Med 373: 1986–1988.

Cellitti, S.E., Shaffer, J., Jones, D.H., Mukherjee, T., Gurumurthy, M., Bursulaya, B., et al. (2012) Structure of Ddn, the deazaflavin-dependent nitroreductase from Mycobacterium tuberculosis involved in bioreductive activation of PA-824. Structure 20: 101–112.

Choi, K.P., Bair, T.B., Bae, Y.M., and Daniels, L. (2001) Use of transposon Tn5367 mutagenesis and a nitroimidazopyran-based selection system to demonstrate a requirement for fbiA and fbiB in coenzyme F420 biosynthesis by Mycobacterium bovis BCG. J Bacteriol 183: 7058–7066.

Cole, S.T., Brosch, R., Parkhill, J., Garnier, T., Churcher, C., Harris, D., et al. (1998) Deciphering the biology of Mycobacterium tuberculosis from the complete genome sequence. Nature 393: 537–544.

Comas, I., Coscolla, M., Luo, T., Borrell, S., Holt, K.E., Kato-Maeda, M., et al. (2013) Out-of-Africa migration and Neolithic coexpansion of Mycobacterium tuberculosis with modern humans. Nat Genet 45: 1176–1182.

Cook, G.M., Greening, C., Hards, K., and Berney, M. (2014) Chapter One-Energetics of Pathogenic Bacteria and Opportunities for Drug Development. Adv Microb Physiol 65: 1–62.

Croucher, N.J., Page, A.J., Connor, T.R., Delaney, A.J., Keane, J.A., Bentley, S.D., et al. (2015) Rapid phylogenetic analysis of large samples of recombinant bacterial whole genome sequences using Gubbins. Nucleic Acids Res 43: e15–e15.

Dawson, R., Diacon, A.H., Everitt, D., Niekerk, C. Van, Donald, P.R., Burger, D.A., et al. (2015) Effi ciency and safety of the combination of moxifl oxacin , pretomanid (PA-824), and pyrazinamide during the fi rst 8 weeks of antituberculosis treatment : a phase 2b , open-label , partly randomised trial in patients with drug-susceptible or drug-resi. Lancet 385: 1738–1747.

DeLano, W.L. (2002) The PyMOL molecular graphics system. http//pymol org .

Diacon, A.H., Pym, A., Grobusch, M., Patientia, R., Rustomjee, R., Page-Shipp, L., et al. (2009) The Diarylquinoline TMC207 for Multidrug-Resistant Tuberculosis. N Engl J Med 360: 2397–2405.

Edgar, R.C. (2008) MUSCLE : multiple sequence alignment with high accuracy and high throughput. Nucleic Acids Res 32: 1792–1797.

Garrison, E., and Marth, G. (2012) Haplotype-based variant detection from short-read sequencing. arXiv Prepr arXiv12073907 .

Gibson, D.G., Young, L., Chuang, R.-Y., Venter, J.C., Hutchison, C. a, Smith, H.O., et al. (2009) Enzymatic assembly of DNA molecules up to several hundred kilobases. Nat Methods 6: 343–5.

Greening, C., Ahmed, F.H., Mohamed, A.E., Lee, B.M., Pandey, G., Warden, A.C., et al. (2016) Physiology, Biochemistry, and Applications of F420 - and Fo -Dependent Redox Reactions. Microbiol Mol Biol Rev 80: 451–493.

Gupta, R., Gao, M., Cirule, A., Xiao, H., Geiter, L.J., and Wells, C.D. (2015) Delamanid for Extensively Drug-Resistant Tuberculosis. N Engl J Med 373: 291–292.

Gurumurthy, M., Rao, M., Mukherjee, T., Rao, S.P.S., Boshoff, H.I., Dick, T., et al. (2013) A novel F420-dependent anti-oxidant mechanism protects Mycobacterium tuberculosis against oxidative stress and bactericidal agents. Mol Microbiol 87: 744–755.

Hards, K., Robson, J.R., Berney, M., Shaw, L., Bald, D., Koul, A., et al. (2015) Bactericidal mode of action of bedaquiline. J Antimicrob Chemother 70: 2028–2037.

Hart, K.M., Ho, C.M.W., Dutta, S., Gross, M.L., and Bowman, G.R. (2016) Modelling proteins' hidden conformations to predict antibiotic resistance. Nat Commun 7: 12965.

Hasan, M.R., Rahman, M., Jaques, S., Purwantini, E., and Daniels, L. (2010) Glucose 6-phosphate accumulation in mycobacteria: implications for a novel F420-dependent anti-oxidant defense system. J Biol Chem 285: 19135–19144.

Haver, H., Chua, A., and Ghode, P. (2015) Mutations in genes for the F420 biosynthetic pathway and a nitroreductase enzyme are the primary resistance determinants in spontaneous in vitro-selected PA-824-. Antimicrob agents 59: 5316–5323.

Heikal, A., Hards, K., Cheung, C.Y., Menorca, A., Timmer, M.S.M., Stocker, B.L., and Cook, G.M. (2016) Activation of type II NADH dehydrogenase by Quinolinequinones mediates antitubercular cell death. J Antimicrob Chemother 71: 2840–2847.

Hoffmann, H., Borroni, E., Schena, E., Nedialkova, L., Hofmann-Thiel, S., and Cirillo, D. (2016) Delamanid susceptibility testing of Mycobacterium tuberculosis using the resazurin

microtitre assay and the BACTECTM MGITTM 960 system—authors' response. J Antimicrob Chemother 71: 3625–3625.

Hoffmann, H., Kohl, T.A., Hofmann-Thiel, S., Merker, M., Beckert, P., Jaton, K., et al. (2016) Delamanid and bedaquiline resistance in MTB ancestral Beijing genotype causing extensive drug-resistant TB in a tibetan refugee. Am J Respir Crit Care Med 193: 337–340.

Irwin, J.J., and Shoichet, B.K. (2005) ZINC − A Free Database of Commercially Available Compounds for Virtual Screening ZINC - A Free Database of Commercially Available Compounds for Virtual Screening. J Chem Inf Model 45: 177–182.

Ji, B., Lefrançois, S., Robert, J., Chauffour, A., Truffot, C., and Jarlier, V. (2006) In vitro and in vivo activities of rifampin, streptomycin, amikacin, moxifloxacin, R207910, linezolid, and PA-824 against Mycobacterium ulcerans. Antimicrob Agents Chemother 50: 1921–1926.

Jirapanjawat, T., Ney, B., Taylor, M.C., Warden, A.C., Afroze, S., Russell, R.J., et al. (2016) The redox cofactor F420 protects mycobacteria from diverse antimicrobial compounds and mediates a reductive detoxification system. Appl Environ Microbiol 82: 6810–6818.

Kana, B.D., Weinstein, E.A., Avarbock, D., Dawes, S.S., Rubin, H., and Mizrahi, V. (2001) Characterization of the cydAB -Encoded Cytochrome bd Oxidase from Mycobacterium smegmatis. J Bacteriol 183: 7076–7086.

Lamprecht, D.A., Finin, P.M., Rahman, M.A., Cumming, B.M., Russell, S.L., Jonnala, S.R., et al. (2016) Turning the respiratory flexibility of Mycobacterium tuberculosis against itself. Nat Commun 7: 12393.

Lapalikar, G. V., Taylor, M.C., Warden, A.C., Scott, C., Russell, R.J., and Oakeshott, J.G. (2012) F 420H 2-dependent degradation of aflatoxin and other furanocoumarins is widespread throughout the Actinomycetales. PLoS One 7: e30114.

Li, H. (2013) Aligning sequence reads, clone sequences and assembly contigs with BWA-MEM. arXiv Prepr arXiv13033997 .

Li, W., Cowley, A., Uludag, M., Gur, T., McWilliam, H., Squizzato, S., et al. (2015) The EMBL-EBI bioinformatics web and programmatic tools framework. Nucleic Acids Res 43: W580–W584.

Manjunatha, U., Boshoff, H.I.M., and Barry, C.E. (2009) The mechanism of action of PA-824: Novel insights from transcriptional profiling. Commun Integr Biol 2: 215–218.

Manjunatha, U.H., Boshoff, H., Dowd, C.S., Zhang, L., Albert, T.J., Norton, J.E., et al. (2006) Identification of a nitroimidazo-oxazine-specific protein involved in PA-824 resistance in Mycobacterium tuberculosis. Proc Natl Acad Sci U S A 103: 431–436.

Matsumoto, M., Hashizume, H., Tomishige, T., Kawasaki, M., Tsubouchi, H., Sasaki, H., et al. (2006) OPC-67683, a nitro-dihydro-imidazooxazole derivative with promising action against tuberculosis in vitro and in mice. PLoS Med 3: 2131–2144.

Mohamed, A.E., Condic-Jurkic, K., Ahmed, F.H., Yuan, P., O'Mara, M.L., Jackson, C.J., and Coote, M.L. (2016) Hydrophobic shielding drives catalysis of hydride transfer in a family of F420H2-dependent enzymes. Biochemistry .

Morris, G., and Huey, R. (2009) AutoDock4 and AutoDockTools4: Automated docking with selective receptor flexibility. J … 30: 2785–2791.

Murray, S., Mendel, C., and Spigelman, M. (2016) TB Alliance regimen development for multidrug-resistant tuberculosis. Int J Tuberc Lung Dis 20: 38–41.

Orencia, M.C., Yoon, J.S., Ness, J.E., Stemmer, W.P.C., and Stevens, R.C. (2001) Predicting the emergence of antibiotic resistance by directed evolution and structural analysis. Nat Struct Mol Biol 8: 238–242.

Oyugi, M.A., Bashiri, G., Baker, E.N., and Johnson-Winters, K.L. (2016) Investigating the reaction mechanism of F420-dependent glucose-6-phosphate dehydrogenase from Mycobacterium tuberculosis: kinetic analysis of the wild-type and mutant enzymes. Biochemistry.

Pecsi, I., Hards, K., Ekanayaka, N., Berney, M., Hartman, T., Jacobs, W.R., and Cook, G.M. (2014) Essentiality of succinate dehydrogenase in Mycobacterium smegmatis and its role in the generation of the membrane potential under hypoxia. MBio 5: e01093-14.

Purwantini, E., and Mukhopadhyay, B. (2009) Conversion of NO2 to NO by reduced coenzyme F420 protects mycobacteria from nitrosative damage. Proc Natl Acad Sci U S A 106: 6333–6338.

Purwantini, E., Mukhopadhyay, B., Spencer, R.W., and Daniels, L. (1992) Effect of temperature on the spectral properties of coenzyme F420 and related compounds. Anal Biochem 205: 342–350.

Sambrook, J., Fritsch, E.F., and Maniatis, T. (1989) Molecular cloning: a laboratory manual. Cold spring harbor laboratory press, .

Sievers, F., Wilm, A., Dineen, D., Gibson, T.J., Karplus, K., Li, W., et al. (2011) Fast, scalable generation of high-quality protein multiple sequence alignments using Clustal Omega. Mol Syst Biol 7.

Singh, R., Manjunatha, U., Boshoff, H.I.M., Ha, Y.H., Niyomrattanakit, P., Ledwidge, R., et al. (2008) PA-824 kills nonreplicating Mycobacterium tuberculosis by intracellular NO release. Science 322: 1392–5.

Sinha, S., Kosalai, K., Arora, S., Namane, A., Sharma, P., Gaikwad, A.N., et al. (2005) Immunogenic membrane-associated proteins of Mycobacterium tuberculosis revealed by proteomics. Microbiology 151: 2411–2419.

Snapper, S.B., Melton, R.E., Mustafa, S., Kieser, T., and WR Jr, J. (1990) Isolation and characterization of efficient plasmid transformation mutants of Mycobacterium smegmatis. Mol Microbiol 4: 1911–1919.

Souza, G.A. de, Leversen, N.A., Målen, H., and Wiker, H.G. (2011) Bacterial proteins with cleaved or uncleaved signal peptides of the general secretory pathway. J Proteomics 75: 502–510.

Stamatakis, A. (2014) RAxML version 8: a tool for phylogenetic analysis and post-analysis of large phylogenies. Bioinformatics 30: 1312–1313.

Steiner, A., Stucki, D., Coscolla, M., Borrell, S., and Gagneux, S. (2014) KvarQ: targeted and direct variant calling from fastq reads of bacterial genomes. BMC Genomics 15: 881.

Stover, C.K., Warrener, P., VanDevanter, D.R., Sherman, D.R., Arain, T.M., Langhorne, M.H., et al. (2000) A small-molecule nitroimidazopyran drug candidate for the treatment of tuberculosis. Nature 405: 962–966.

Treangen, T.J., Ondov, B.D., Koren, S., and Phillippy, A.M. (2014) The Harvest suite for rapid core-genome alignment and visualization of thousands of intraspecific microbial genomes. Genome Biol 15: 524.

Trott, O., and Olson, A.J. (2010) AutoDock Vina: Improving the Speed and Accuracy of Docking with a New Scoring Function, EfficientOptimization, and Multithreading. J Comput Chem 31: 455–61.

Upton, A.M., Cho, S., Yang, T.J., Kim, A.Y., Wang, Y., Lu, Y., et al. (2015) In vitro and in vivo activities of the nitroimidazole TBA-354 against Mycobacterium tuberculosis. Antimicrob Agents Chemother 59: 136–144.

WHO (2016) Global Tuberculosis Report 2016. Cdc 2016 214.

Wiegand, I., Hilpert, K., and Hancock, R.E.W. (2008) Agar and broth dilution methods to determine the minimal inhibitory concentration (MIC) of antimicrobial substances. Nat Protoc 3: 163–75.

Wood, D.E., and Salzberg, S.L. (2014) Kraken: ultrafast metagenomic sequence classification using exact alignments. Genome Biol 15: R46–R46.

2.3 Supplementary Materials

Figure S1: Ddn and Ddn Ser78Tyr can both reduce Delamanid. Comparison of the reduction rate of Delamanid by Ddn (15.8±1.4 nmol min^{-1} μmol^{-1} enzyme and Ddn S78Y (12.4±1.21 nmol min^{-1} μmol^{-1} enzyme).

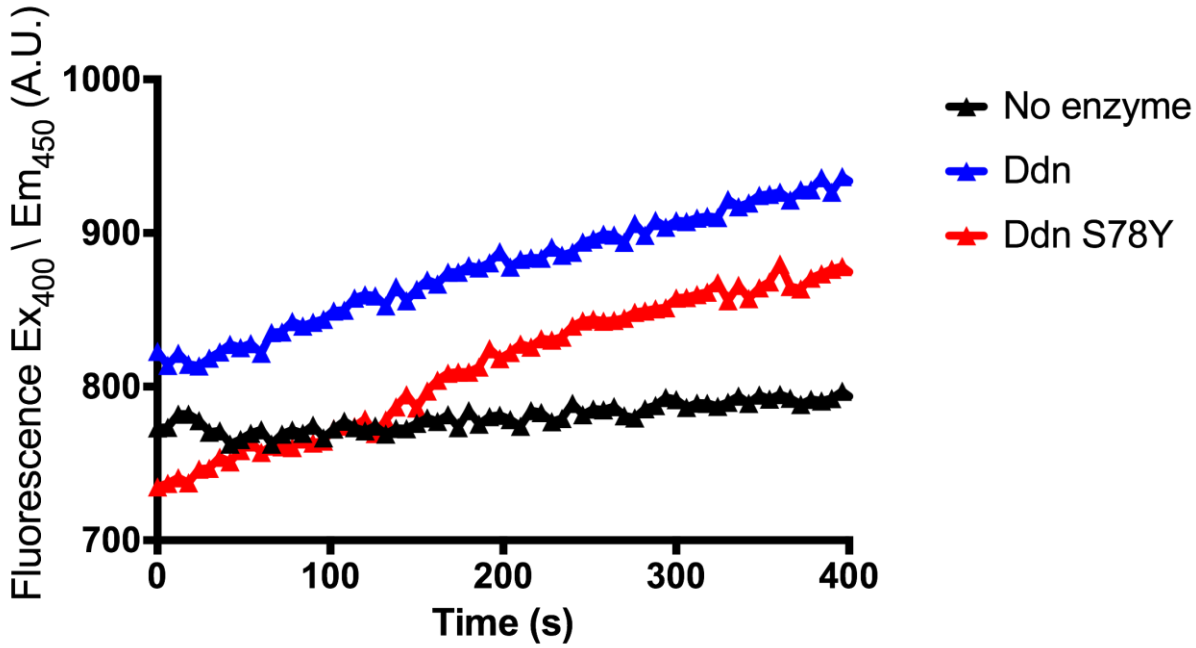

Table S1: Comparison of kinetics of $F_{420}H_2$-dependent menadione and pretomanid reduction of Ddn variants and homologs.

	Menadione			Pretomanid		
	k_{cat} (s^{-1})	K_M (μM)	k_{cat}/K_M (M^{-1} s^{-1})	k_{cat} (s^{-1})	K_M (μM)	k_{cat}/K_M (s^{-1} M^{-1})
Ddn	$9.2\times10^{-1} \pm 1.6\times10^{-2}$	3.2 ± 0.4	2.9×10^{5}	$1.2\times10^{-2} \pm 8.9\times10^{-4}$	22.3 ± 0.9	5.3×10^{2}
MMAR_5035	$1.5\times10^{-1} \pm 1.8\times10^{-2}$	2.8 ± 0.2	5.4×10^{4}	$2.58\times10^{-2} \pm 1.1\times10^{-3}$	178.0 ± 0.9	1.5×10^{2}
MSMEG_5998	$1.5\times10^{-1} \pm 2.2\times10^{-2}$	5.1 ± 0.04	3.0×10^{4}	0		
MVAN_5261	$1.2\times10^{-1} \pm 6.6\times10^{-3}$	6.0 ± 0.8	2.0×10^{4}	0		
MAV_0613	$6.6\times10^{-2} \pm 2.5\times10^{-3}$	4.1 ± 0.1	1.6×10^{4}	0		
MUL_4109	$4.6\times10^{-3} \pm 1.1\times10^{-4}$	1.5 ± 0.1	3.0×10^{3}	0		
Ddn S22L	$1.6\times10^{-1} \pm 1.3\times10^{-2}$	26.2 ± 5.5	6.0×10^{3}	0		
Ddn L49P	0			0		
Ddn L64P	0			0		
Ddn Y65F	$6.6\times10^{-1} \pm 7.7\times10^{-2}$	1.3 ± 0.2	4.9×10^{5}	$1.1\times10^{-2} \pm 1.5\times10^{-4}$	27.1 ± 3.4	4.1×10^{2}
Ddn Y65M	$2.2\times10^{0} \pm 5.4\times10^{-2}$	21.2 ± 0.9	1.0×10^{5}	0		
Ddn Y65L	$8.3\times10^{-1} \pm 3.5\times10^{-2}$	9.4 ± 0.01	8.8×10^{4}	0		

Ddn Y65C	$8.5\times10^{-1} \pm 1.1\times10^{-2}$	17.5 ± 0.1	4.8×10^{4}	0				
Ddn Y65S	$1.9\times10^{-2} \pm 6.3\times10^{-4}$	2.6 ± 0.4	7.1×10^{3}	0				
Ddn S78T	$1.2\times10^{0} \pm 2.1\times10^{-1}$	5.4 ± 0.8	2.2×10^{5}	0				
Ddn S78A	$8.8\times10^{-1} \pm 1.5\times10^{-2}$	7.9 ± 0.2	1.1×10^{5}	0				
Ddn S78C	$8.3\times10^{-2} \pm 3.0\times10^{-3}$	8.0 ± 0.2	1.0×10^{4}	0				
Ddn S78V	$3.0\times10^{-2} \pm 1.1\times10^{-3}$	12.7 ± 2.1	2.4×10^{3}	0				
Ddn S78Y	$3.7\times10^{-4} \pm 1.4\times10^{-6}$	5.3 ± 0.4	7.0×10^{1}	0				
Ddn K79Q	$1.6\times10^{-1} \pm 1.6\times10^{-2}$	12.5± 4.0	1.3×10^{4}	0				
Ddn W88R	0			0				
Ddn R112W	0			0				
Ddn Y130W	$2.5\times10^{-1} \pm 1.9\times10^{-2}$	1.6 ± 0.03	1.5×10^{5}	$2.4\times10^{-3} \pm 4.5\times10^{-5}$	12.9 ± 0.3	1.9×10^{2}		
Ddn Y130C	$5.2\times10^{-2} \pm 5.5\times10^{-3}$	0.7 ± 0.05	7.5×10^{4}	$2.1\times10^{-3} \pm 5.3\times10^{-5}$	13.8 ± 0.4	1.6×10^{2}		
Ddn Y130S	$2.3\times10^{-1} \pm 4.3\times10^{-2}$	3.1 ± 0.5	7.2×10^{4}	$7.6\times10^{-3} \pm 2.5\times10^{-4}$	32.5 ± 5.0	2.4×10^{2}		
Ddn Y130H	$6.3\times10^{-2} \pm 1.5\times10^{-3}$	1.4 ± 0.1	4.3×10^{4}	$1.0\times10^{-3} \pm 3.2\times10^{-5}$	25.0 ± 0.3	4.1×10^{1}		
Ddn Y130F	$2.5\times10^{-1} \pm 4.1\times10^{-2}$	6.3 ± 0.4	4.0×10^{4}	$2.6\times10^{-3} \pm 1.4\times10^{-4}$	36.2 ± 0.6	7.2×10^{1}		

Ddn Y130D	$1.9\times10^{-1} \pm 1.2\times10^{-2}$	7.2 ± 0.3	2.6×10^{4}	$9.6\times10^{-4} \pm 5.7\times10^{-5}$	20.3 ± 0.6	4.7×10^{1}
Ddn Y130N	$7.9\times10^{-2} \pm 3.0\times10^{-3}$	6.7 ± 0.1	1.2×10^{4}	$3.9\times10^{-3} \pm 1.5\times10^{-4}$	57.5 ± 1.2	6.7×10^{1}
Ddn Y133F	$8.3\times10^{-1} \pm 5.4\times10^{-2}$	1.6 ± 0.1	5.4×10^{5}	$4.7\times10^{-3} \pm 2.2\times10^{-4}$	26.6 ± 0.01	1.8×10^{2}
Ddn Y133L	$1.8\times10^{0} \pm 1.0\times10^{-3}$	4.0 ± 0.05	4.4×10^{5}	0		
Ddn Y133M	$1.1\times10^{0} \pm 2.9\times10^{-2}$	3.6 ± 0.01	3.0×10^{5}	0		
Ddn Y133W	$3.3\times10^{-1} \pm 3.1\times10^{-3}$	8.9 ± 1.8	3.9×10^{4}	0		
Ddn Y133C	$7.5\times10^{-2} \pm 9.2\times10^{-3}$	17.1 ± 5.7	4.4×10^{3}			
Ddn Y136F	$1.1\times10^{-0} \pm 1.5\times10^{-1}$	2.1 ± 0.3	4.9×10^{5}	$9.6\times10^{-3} \pm 6.9\times10^{-4}$	14.6 ± 2.9	6.7×10^{2}
Ddn Y136E	$2.5\times10^{-3} \pm 8.0\times10^{-5}$	4.1 ± 1.4	6.7×10^{2}	0		
Ddn Y136S	$1.8\times10^{-2} \pm 5.9\times10^{-4}$	25.2 ± 1.4	7.1×10^{2}	0		
Ddn Y136T	$2.2\times10^{-2} \pm 5.4\times10^{-4}$	21.4 ± 0.2	1.0×10^{3}	0		
Ddn C149Y	$9.2\times10^{-3} \pm 2.2\times10^{-4}$	4.6 ± 0.8	1.1×10^{3}	0		

Table S2: Characterisation of non-synonymous Ddn mutations in *M. tuberculosis*. Table showing all *M. tuberculosis* genomes with non-synonymous mutations in *ddn*, substitution type and lineage to which the strain belongs.

Strain_ID[a]	Ddn Allele	Lineage-typing (Kvarq)	Lineage
ERR1023406	W27C	lineage 2	East Asian/Beijing
ERR1034696	R72W	lineage 1	Indo-Oceanic
ERR1034824	R23W	lineage 4	Euro-American
ERR1034917	R72Q	lineage 4	Euro-American
ERR1035261	R23W	lineage 4	Euro-American
ERR1035262	G34R	lineage 4	Euro-American
ERR1035268	R23W	lineage 4	Euro-American
ERR1035277	R23W	lineage 4	Euro-American
ERR1035292	R23W	lineage 4	Euro-American
ERR1035301	R23W	lineage 4	Euro-American
ERR1035316	G34R	lineage 4	Euro-American
ERR1035334	G34R	lineage 4	Euro-American
ERR1035336	G34R	lineage 4	Euro-American
ERR1035344	R23W	lineage 4	Euro-American
ERR1035345	R23W	lineage 4	Euro-American
ERR1035350	R23W	lineage 4	Euro-American
ERR1144974	P86_M87del	lineage 4	Euro-American
ERR1144975	P86_M87del	lineage 4	Euro-American
ERR1144976	P86_M87del	lineage 4	Euro-American
ERR1144977	P86_M87del	lineage 4	Euro-American
ERR1144978	P86_M87del	lineage 4	Euro-American
ERR1144979	P86_M87del	lineage 4	Euro-American
ERR1144980	P86_M87del	lineage 4	Euro-American

ERR1144981	P86_M87del	lineage 4	Euro-American
ERR1144982	P86_M87del	lineage 4	Euro-American
ERR1144983	P86_M87del	lineage 4	Euro-American
ERR1144984	P86_M87del	lineage 4	Euro-American
ERR1144985	P86_M87del	lineage 4	Euro-American
ERR1144986	P86_M87del	lineage 4	Euro-American
ERR1144987	P86_M87del	lineage 4	Euro-American
ERR1144988	P86_M87del	lineage 4	Euro-American
ERR1144989	P86_M87del	lineage 4	Euro-American
ERR1144990	P86_M87del	lineage 4	Euro-American
ERR1144991	P86_M87del	lineage 4	Euro-American
ERR1144992	P86_M87del	lineage 4	Euro-American
ERR1144993	P86_M87del	lineage 4	Euro-American
ERR1144994	P86_M87del	lineage 4	Euro-American
ERR1144995	P86_M87del	lineage 4	Euro-American
ERR1193688	R23W	lineage 4	Euro-American
ERR1193708	R23W	lineage 4	Euro-American
ERR1193721	G71R	lineage 4	Euro-American
ERR1193737	R23W	lineage 4	Euro-American
ERR1193814	R23W	lineage 4	Euro-American
ERR1193827	G34R	lineage 4	Euro-American
ERR1199079	A94T	lineage 4	Euro-American
ERR1200607	P6T	lineage 3	East African-Indian
ERR1200648	P6T	lineage 3	East African-Indian
ERR1213864	G81S	lineage 2	East Asian/Beijing
ERR1213871	R23W	Lineage 4	Euro-American

ERR1213919	G34R	Lineage 4	Euro-American
ERR1465874	L67P	lineage 4	Euro-American
ERR1465959	N91T	lineage 4	Euro-American
ERR1465981	L67P	lineage 4	Euro-American
ERR1633788	R72Q	lineage 4	Euro-American
ERR1633884	R72Q	lineage 4	Euro-American
ERR233357	S78Y	Lineage 2	East Asian/Beijing
ERR718303	A111V	lineage 4	Euro-American
ERR718313	P6L	lineage 2	East Asian/Beijing
ERR718320	S78Y	lineage 2	East Asian/Beijing
ERR718334	P6S	lineage 1	Indo-Oceanic
ERR718464	A111V	lineage 4	Euro-American
ERR718477	A111V	lineage 4	Euro-American
ERR718488	Y122_M129del	lineage 4	Euro-American
ERR718491	P6S	lineage 1	Indo-Oceanic
ERR718512	P6S	lineage 1	Indo-Oceanic
ERR718553	P6S	lineage 1	Indo-Oceanic
ERR751801	A111V	lineage 4	Euro-American
ERR751827	A111V	lineage 4	Euro-American
ERR751827	S78Y	lineage 2	East Asian/Beijing
ERR751922	Y122_M129del	lineage 4	Euro-American
ERR751923	Y122_M129del	lineage 4	Euro-American
ERR752065	A111V	lineage 4	Euro-American
ERR752103	P6S	lineage 1	Indo-Oceanic
ERR752105	A111V	lineage 4	Euro-American
ERR752109	Y122_M129del	lineage 4	Euro-American

ERR752111	A111V	lineage 4	Euro-American
ERR752112	Y29del	lineage 2	East Asian/Beijing
ERR752117	A111V	lineage 4	Euro-American
ERR752138	P6S	lineage 1	Indo-Oceanic
ERR752147	P6L	lineage 2	East Asian/Beijing
ERR752206	A111V	lineage 4	Euro-American
ERR767965	P6S	lineage 1	Indo-Oceanic
ERR768008	P6S	lineage 1	Indo-Oceanic
ERR775776	Y122_M129del	lineage 4	Euro-American
ERR841494	D113N	lineage 5	West Africa
ERR841495	D113N	lineage 5	West Africa
ERR894427	G34R	lineage 4	Euro-American
ERR894428	G34R	lineage 4	Euro-American
ERR894429	G34R	lineage 4	Euro-American
ERR894430	G34R	lineage 4	Euro-American
ERR894431	G34R	lineage 4	Euro-American
ERR979071	N62D	lineage 4	Euro-American
GCA_000159755	D113N	Lineage 5	West African
GCA_000389945	V147M	Lineage 1	Indo-Oceanic
GCA_000653935	D69N	lineage 4	Euro-American
GCA_000654255	R72W	lineage 1	Indo-Oceanic
GCA_000654275	R72W	lineage 1	Indo-Oceanic
GCA_000654555	R72W	lineage 1	Indo-Oceanic
GCA_000654755	R72W	lineage 1	Indo-Oceanic
GCA_000654775	R72W	lineage 1	Indo-Oceanic
GCA_000654815	R72W	lineage 1	Indo-Oceanic

GCA_000654915	R72W	lineage 1	Indo-Oceanic
GCA_000654975	R72W	lineage 1	Indo-Oceanic
GCA_000655055	R72W	lineage 1	Indo-Oceanic
GCA_000655075	R72W	lineage 1	Indo-Oceanic
GCA_000657255	R30S	Lineage 2	East Asian/Beijing
GCA_000662485	R72W	lineage 1	Indo-Oceanic
GCA_000662705	R72W	lineage 1	Indo-Oceanic
GCA_000662725	R72W	lineage 1	Indo-Oceanic
GCA_000662885	R72W	lineage 1	Indo-Oceanic
GCA_000662965	R72W	lineage 1	Indo-Oceanic
GCA_000663005	R72W	lineage 1	Indo-Oceanic
GCA_000663045	R72W	lineage 1	Indo-Oceanic
GCA_000663065	R72W	lineage 1	Indo-Oceanic
GCA_000663085	R72W	lineage 1	Indo-Oceanic
GCA_000663145	R72W	lineage 1	Indo-Oceanic
GCA_000663225	R72W	lineage 1	Indo-Oceanic
GCA_000663285	R72W	lineage 1	Indo-Oceanic
GCA_000665505	R72W	lineage 1	Indo-Oceanic
GCA_000665565	R72W	lineage 1	Indo-Oceanic
GCA_000665665	R72W	lineage 1	Indo-Oceanic
GCA_000665705	R72W	lineage 1	Indo-Oceanic
GCA_000665945	D113N	lineage 5	West Africa
GCA_000671135	W88R	lineage 4	Euro-American
GCA_000671155	W88R	lineage 4	Euro-American
GCA_000706145	R72W	lineage 1	Indo-Oceanic
GCA_000797435	G34E	lineage 4	Euro-American

GCA_001110005	V61G	lineage 4	Euro-American
GCA_001173265	R23L	lineage 4	Euro-American
GCA_001193195	K79Q	lineage 4	Euro-American
GCA_001200495	V61G	lineage 4	Euro-American
GCA_001322025	R30S	Lineage 2	East Asian/Beijing
GCA_001324745	R30S	Lineage 2	East Asian/Beijing
GCA_001325465	T51P	Lineage 2	East Asian/Beijing
GCA_001327995	T56P	lineage 4	Euro-American
GCA_001328055	V61G	lineage 4	Euro-American
GCA_001328255	T50P	Lineage 3	East African-Indian
GCA_001328375	TG56PA	lineage 4	Euro-American
GCA_001345295	Y29S	lineage 4	Euro-American
GCA_001387175	G34E	lineage 4	Euro-American
GCA_001389755	T50P	Lineage 2	East Asian/Beijing
GCA_001390435	T52P	lineage 4	Euro-American
GCA_001392215	V61G	lineage 4	Euro-American
GCA_001392375	G57A	lineage 4	Euro-American
GCA_001392915	T26P	lineage 4	Euro-American
GCA_001393335	V61G	lineage 4	Euro-American
GCA_001394175	G57A	Animal Lineage	
GCA_001394455	T26P	lineage 4	Euro-American
GCA_001394515	D113N	lineage 5	West Africa
GCA_001395635	Y29S	lineage 4	Euro-American
GCA_001395735	D113N	lineage 5	West Africa
GCA_001396455	Y29H	lineage 4	Euro-American
GCA_001396575	TG56PA	lineage 4	Euro-American

GCA_001396655	T56P	lineage 4	Euro-American
GCA_001396975	T52P,T56P	Lineage 3	East African-Indian
GCA_001397075	T56P	Lineage 3	East African-Indian
GCA_001397115	TG56PA	Lineage 3	East African-Indian
GCA_001397335	G57A	lineage 4	Euro-American
GCA_001397515	G57A	lineage 4	Euro-American
GCA_001397555	T56P	lineage 4	Euro-American
GCA_001397575	TG56PA	lineage 4	Euro-American
GCA_001397595	TTT50PPP	Lineage 3	East African-Indian
GCA_001397695	TG56PA	lineage 4	Euro-American
GCA_001397875	G57A	lineage 4	Euro-American
GCA_001397935	TG56PA	Lineage 3	East African-Indian
GCA_001997495	L49P	Lineage 2	East Asian/Beijing
GCA_002000965	L49P	Lineage 2	East Asian/Beijing
GCA_900120615	P124S	Lineage 2	East Asian/Beijing
GCA_900120745	P45L	lineage 4	Euro-American
SRR2467264	A111V	lineage 4	Euro-American
SRR2467268	R72W	lineage 1	Indo-Oceanic
SRR3085307	R72W	lineage 1	Indo-Oceanic
SRR3085317	E83D	lineage 4	Euro-American
SRR3085514	R72W	lineage 1	Indo-Oceanic
SRR3086377	R72W	lineage 1	Indo-Oceanic
SRR3205958	G81S	lineage 2	East Asian/Beijing
SRR3205959	G81S	lineage 2	East Asian/Beijing
SRR3675493	D113N	lineage 5	West Africa
SRR3724667	T140I	lineage 4	Euro-American

SRR3724678	M21T	lineage 3	East African-Indian
SRR3724766	A111V	lineage 4	Euro-American
SRR3725356	Y29del	lineage 2	East Asian/Beijing
SRR5007159	L90V	Animal Lineage	
SRR5065311	L49P	lineage 2	East Asian/Beijing
SRR5065432	P6S	lineage 1	Indo-Oceanic
SRR5065491	G36V	lineage 1	Indo-Oceanic
SRR5065629	I102V	lineage 4	Euro-American
SRR5065636	Y65S	lineage 4	Euro-American
SRR5065639	Y65S	lineage 4	Euro-American
SRR5065695	Y133C	lineage 1	Indo-Oceanic
SRR5067277	L49P	lineage 2	East Asian/Beijing
SRR5067302	L49P	lineage 2	East Asian/Beijing
SRR5067338	L49P	lineage 2	East Asian/Beijing
SRR5067366	L49P	lineage 2	East Asian/Beijing
SRR5067368	L49P	lineage 2	East Asian/Beijing
SRR5067434	L49P	lineage 2	East Asian/Beijing
SRR5067441	L49P	lineage 2	East Asian/Beijing
SRR5067504	L49P	lineage 2	East Asian/Beijing
SRR5067527	L49P	lineage 2	East Asian/Beijing
SRR5067533	L49P	lineage 2	East Asian/Beijing
SRR5067543	L49P	lineage 2	East Asian/Beijing
SRR5067612	L49P	lineage 2	East Asian/Beijing
SRR5067699	L49P	lineage 2	East Asian/Beijing
SRR5073572	Y65S	lineage 4	Euro-American
SRR5073681	T52N	lineage 2	East Asian/Beijing

SRR5073688	E105Q	lineage 4	Euro-American
SRR5073730	E117K	lineage 2	East Asian/Beijing
SRR5074079	P45L	lineage 1	Indo-Oceanic
SRR5114017	G81S	lineage 2	East Asian/Beijing
SRR5114018	G81S	lineage 2	East Asian/Beijing
SRR5114019	G81S	lineage 2	East Asian/Beijing
SRR5114020	G81S	lineage 2	East Asian/Beijing
SRR5114021	G81S	lineage 2	East Asian/Beijing
SRR5114022	G81S	lineage 2	East Asian/Beijing
SRR5153219	E83D	lineage 4	Euro-American
SRR5153316	E83D	lineage 4	Euro-American
SRR5153811	E83D	lineage 4	Euro-American
SRR5314267	R72W	lineage 1	Indo-Oceanic
SRR5314270	R72W	lineage 1	Indo-Oceanic

[a]Only strains with non-synonymous mutations in Ddn are shown

Table S3: Taxonomic classification of M. tuberculosis strains downloaded from the sequence read archive. Table showing the taxonomic classification of all sequencing reads belonging to M. tuberculosis strains from the SRA database. Strains where the majority of reads could not be classified or where the majority of reads were found to belong to Mycobacterium species other than M. tuberculosis are highlighted in red. These strains were removed from all subsequent analysis.

Strain ID	Read classified (%)	# reads identified as M. tuberculosis complex	Total no. reads classified As genus Mycobacterium	Mycobacterium_kansasii	Mycobacterium_leprae	Mycobacterium_smegmatis	Mycobacterium_marinum	Mycobacterium_chubuense	Mycobacterium_gilvum	Mycobacterium_ulcerans	Mycobacterium_rhodesiae	Mycobacterium_bovis	Mycobacterium_tuberculosis	Mycobacterium_africanum	Mycobacterium_canettii	Mycobacterium_vanbaalenii	Mycobacterium_avium	Mycobacterium_intracellulare	Mycobacterium_indicus_pranii	Mycobacterium_yongonense	Mycobacterium_sp_MCS	Mycobacterium_sp_JLS	Mycobacterium_sp_KMS	Mycobacterium_liflandii	Mycobacterium_abscessus	Mycobacterium_sinense	Mycobacterium_sp_MOTT36Y
ERR1023325	99.99	97.45	2383286	22	10	6	2	8	2	0	3	28	18198	19	401	7	12	1	0	1	0	0	0	5	2	8	1
ERR1023347	99.99	97.46	1933037	30	11	7	3	2	6	0	5	21	15092	20	304	4	12	0	0	1	0	1	0	3	0	8	0
ERR1023406	99.99	97.42	2913711	43	12	8	6	9	7	0	5	12	29451	4	396	5	27	1	0	20	0	3	0	3	3	8	1
ERR1034576	99.17	96.36	20355390	601	140	173	154	77	81	0	69	294	122745	1122	8638	73	378	41	16	37	0	19	0	57	56	126	16
ERR1034652	30.31	3.19	1239901	469118	12428	24141	17559	14162	16797	0	11322	361	1241	21	46255	14458	69809	6391	3697	6312	0	1909	0	10358	7451	18657	2545
ERR1034696	99.64	94.57	1076855	21	7	3	0	0	3	0	2	79	6208	147	776	10	3	3	1	2	0	0	0	1	1	3	1
ERR1034824	99.98	97.39	3357058	55	17	12	3	4	5	0	8	35	31053	20	566	6	30	2	2	1	0	3	0	5	1	10	1
ERR1034917	94.08	91.36	3927715	323	60	98	43	49	49	0	40	69	32235	72	3683	36	243	22	6	27	0	11	0	29	19	79	14
ERR1035162	93.5	0.05	2202913	2148415	9	279	34	69	2902	0	105	1	4	0	264	31	33	4581	3	37	0	508	27	4	158	32	1
ERR1035202	99.96	97.39	2582111	30	18	11	11	4	0	0	3	10	25596	6	387	3	26	2	2	1	0	2	0	6	3	8	2
ERR1035242	99.92	97.28	4171110	73	21	23	7	12	14	0	8	15	41304	5	597	10	48	5	2	5	0	2	0	5	5	17	1
ERR1035261	99.97	97.46	3283813	51	12	9	27	11	2	0	8	42	30471	32	643	5	30	5	1	3	0	1	0	17	7	6	1
ERR1035262	99.95	97.46	3274766	44	15	11	9	7	5	0	6	19	30676	11	609	8	21	4	1	4	0	2	0	3	3	12	1
ERR1035268	99.88	97.27	3480326	47	12	30	11	8	7	0	11	38	32770	20	729	8	123	6	2	3	0	5	0	11	15	19	3
ERR1035277	99.96	97.44	3729464	53	15	14	5	7	6	0	6	41	34604	10	729	6	30	3	0	7	0	0	0	2	3	12	1
ERR1035292	99.97	97.44	3651113	57	14	15	199	13	6	0	10	104	35026	24	721	3	85	1	1	2	0	1	0	122	5	11	0
ERR1035301	99.66	94.01	5506580	80	32	19	117	10	10	0	9	47	49612	27	1173	8	180	6	2	13	0	4	0	61	10	23	2
ERR1035316	98.28	91.09	2736335	80	32	25	200	19	15	0	6	42	25124	16	875	14	285	2	1	7	0	2	0	133	32	21	4
ERR1035334	99.96	97.38	1590111	12	2	10	5	0	1	0	4	6	14059	0	157	2	5	2	1	2	0	0	0	1	3	2	0
ERR1035336	99.73	97.19	1514559	27	4	10	5	4	3	0	2	13	14088	9	350	3	6	1	1	1	0	1	0	6	0	4	2
ERR1035344	99.9	97.25	2467834	36	25	7	197	7	10	0	8	46	22978	16	492	5	23	2	2	3	0	1	0	91	5	8	1
ERR1035345	99.85	97.3	1525324	26	13	7	58	4	4	0	3	25	14265	6	351	3	15	1	0	1	0	0	0	34	2	3	0
ERR1035350	99.94	97.41	2234170	42	8	12	5	2	2	0	3	26	20812	21	386	6	16	0	0	0	0	2	0	2	3	5	1
ERR1063856	29.99	1.82	1147726	91432	9770	95005	7810	38541	34545	0	39584	259	350	28	25418	34422	150933	9827	4218	13902	0	11221	0	6534	15336	76512	5234
ERR1063857	38.75	0.62	1748530	38574	2867	317362	2648	137031	131617	0	200600	18	195	6	8992	137220	94410	8580	2237	6636	2	17569	179	1788	17230	64607	4283
ERR1144974	97.25	94.04	18146639	191	20	26	36	8	12	0	6	39	148509	63	1971	9	55	4	2	9	0	0	0	22	75	22	1
ERR1144975	98.93	95.95	11441854	173	6	14	19	4	6	0	2	20	91823	25	1237	9	25	2	2	3	0	0	0	5	41	11	2
ERR1144976	97.72	94.59	9335661	108	8	5	27	3	1	0	4	21	75731	15	1099	4	14	4	4	3	0	0	0	6	41	22	0
ERR1144977	98.84	95.9	11738187	153	9	6	27	8	11	0	7	21	94344	38	1241	7	22	4	2	2	0	2	0	4	28	20	1
ERR1144978	99.04	95.97	10914955	162	6	4	40	1	4	0	11	28	87758	30	1228	7	37	8	0	2	0	5	0	5	50	17	0
ERR1144979	93.39	83.17	6392823	80	14	7	20	5	3	0	3	20	51462	13	755	3	19	1	3	1	0	0	0	5	27	13	1
ERR1144980	95.76	90.52	17898845	206	10	19	37	9	9	0	4	20	145453	39	1801	6	30	8	2	1	0	0	0	18	81	31	4
ERR1144981	96.68	89.06	7205121	99	10	18	28	6	8	0	3	24	60315	23	1129	5	33	6	1	4	0	1	0	14	38	16	2
ERR1144982	91.13	82.64	16711431	200	7	7	40	6	7	0	10	24	135786	34	1612	8	24	2	2	6	0	2	0	10	82	27	5
ERR1144983	98.23	94.27	8421874	119	14	24	24	6	14	0	9	20	67749	37	1308	4	32	3	1	5	0	4	0	13	50	19	2

ERR1144984	99.03	95.92	11133592	198	27	25	32	10	4	0	9	36	90225	39	1664	10	44	3	4	8	0	3	0	14	46	33	4
ERR1144985	90.94	71.28	13048689	175	6	10	17	8	8	0	5	21	105427	28	1250	5	23	2	1	1	0	0	0	7	70	24	0
ERR1144986	96.56	91.63	8163435	162	21	23	46	9	10	0	8	30	66735	32	1745	11	45	7	5	1	0	4	0	6	36	20	1
ERR1144987	97.54	91.77	7219610	129	19	16	32	7	12	0	3	26	60893	25	1194	10	31	3	3	4	0	1	0	10	28	13	2
ERR1144988	98.43	95.43	10628247	173	17	22	36	5	9	0	3	34	89540	31	1472	6	46	5	2	1	0	5	0	14	63	21	4
ERR1144989	46.2	24.21	3322917	66	5	8	10	1	3	0	2	5	27239	15	556	1	14	0	2	0	0	1	0	9	24	3	3
ERR1144990	96.23	70.51	7367301	110	13	17	22	11	9	0	4	16	59566	42	1123	4	22	7	3	5	0	0	0	6	34	11	3
ERR1144991	89.7	79.83	12428230	134	12	15	23	6	5	0	3	26	101384	38	1402	8	30	3	3	1	0	0	0	11	62	14	2
ERR1144992	97.31	92.19	15979667	174	14	18	27	6	8	0	2	37	132933	38	1715	5	35	7	2	5	0	7	0	14	81	19	6
ERR1144993	97.63	92.24	8240113	149	23	22	34	13	12	0	9	29	66778	42	1488	6	57	4	3	6	0	1	0	18	39	16	1
ERR1144994	95.64	90.36	7277269	109	14	16	29	12	14	0	7	27	59925	34	1254	8	39	4	1	1	0	6	0	13	35	11	0
ERR1144995	98.69	95.53	9903054	166	17	28	32	16	12	0	9	25	82717	40	1661	12	37	8	3	10	0	2	0	12	37	24	0
ERR1193688	99.86	97.08	499239	16	2	2	0	0	4	0	1	0	4553	3	168	6	6	4	1	1	0	1	0	0	2	4	1
ERR1193708	98.91	95.95	460097	57	6	8	12	6	3	0	4	19	4601	11	621	4	18	6	2	0	0	0	0	7	10	9	2
ERR1193721	99.92	97.1	641900	11	4	3	4	0	2	0	1	17	5769	5	213	1	17	2	0	0	0	1	0	3	0	4	0
ERR1193737	99.78	96.92	1164390	55	13	9	4	10	5	0	7	19	10515	17	692	7	41	9	2	2	0	1	0	3	5	20	1
ERR1193793	99.96	97.3	1040084	21	16	7	3	6	0	0	2	11	6366	5	317	1	8	2	0	0	0	1	0	2	1	9	2
ERR1193814	99.99	97.42	1854673	24	7	9	0	5	5	0	5	18	17092	7	443	6	19	5	2	2	0	0	0	2	1	9	0
ERR1193827	99.97	97.41	3708914	66	22	23	10	8	11	0	13	14	34932	22	1346	10	38	3	1	3	0	0	0	9	3	23	1
ERR1199093	95.26	92.54	453437	63	18	19	10	8	10	0	13	30	3576	12	730	10	51	6	1	3	0	3	0	6	12	25	0
ERR1199099	99.69	96.96	1715953	39	12	11	4	5	7	0	4	45	12985	16	542	8	29	2	0	2	0	1	0	2	13	12	1
ERR1199106	99.8	97.05	1782856	34	8	10	7	5	7	0	2	17	13416	16	532	6	23	4	0	2	0	2	0	1	4	15	0
ERR1199108	99.74	97.03	2009333	32	18	9	9	6	5	0	6	21	14902	18	560	8	19	5	0	5	0	1	0	2	6	9	2
ERR1199109	99.48	96.78	2411248	78	22	25	10	9	9	0	12	64	18354	23	850	16	31	7	4	8	0	4	0	4	5	22	0
ERR1199115	99.79	97.06	2619374	56	9	22	5	4	7	0	3	28	19643	17	666	5	36	3	2	2	0	0	0	5	3	14	4
ERR1199127	99.74	97.06	3589231	65	12	17	8	14	7	0	7	52	27003	40	870	5	41	3	2	8	0	2	0	2	9	21	3
ERR1199153	99.4	96.82	3058595	128	25	35	18	24	19	0	15	71	24114	43	1818	12	71	10	1	5	0	5	0	6	13	35	4
ERR1213864	99.68	97.06	4378183	145	26	130	28	50	20	0	97	108	36309	130	1209	47	309	7	1	6	0	5	0	4	1831	28	3
ERR1213871	98.56	94.08	994976	160	11	24	49	15	51	0	16	20	9109	13	545	207	9610	11	195	6	0	6	0	26	53	14	9
ERR1213919	98.24	94.38	1371435	74	18	409	1501	99	94	0	81	18	12622	13	666	155	2929	13	3	22	0	28	0	674	90	85	5
ERR1367635	99.37	96.72	3119454	112	24	33	8	34	18	0	17	55	23881	43	1517	23	74	5	2	9	0	6	0	8	10	27	4
ERR1367655	99.84	97.2	4676378	100	22	49	9	37	10	0	16	45	34387	102	1487	14	51	8	2	3	0	1	0	6	14	33	2
ERR1367666	99.52	96.91	3884614	155	27	37	10	41	13	0	15	50	28784	79	1669	21	85	9	1	8	0	4	0	8	8	41	4
ERR1367687	99.63	97.07	5455632	152	33	45	18	57	27	0	20	87	41328	170	2387	27	117	10	6	7	0	2	0	10	11	52	6
ERR1413483	99.96	97.34	1317119	18	2	6	1	0	1	0	0	15	9884	13	321	3	13	0	1	1	0	0	0	1	2	5	0
ERR1465769	99.37	96.72	4348258	145	43	48	14	34	23	0	22	39	40147	28	1733	21	113	12	3	12	0	5	0	15	19	47	3
ERR1465874	99.98	97.39	3970291	53	13	16	6	7	5	0	2	20	33388	14	780	7	27	1	1	4	0	1	0	3	2	15	0
ERR1465885	99.96	97.34	1083769	30	5	11	4	2	6	0	3	11	8724	7	368	6	16	1	0	0	0	1	0	1	35	7	1
ERR1465959	99.55	96.92	4901247	159	45	47	27	21	18	0	25	86	41457	51	1953	19	103	8	9	12	0	5	0	9	12	56	4
ERR1465981	99.98	97.4	1225405	14	5	3	1	3	4	0	0	8	10335	5	237	2	6	0	0	0	0	0	0	0	2	5	1
ERR1633788	99.98	97.38	2071080	44	13	14	6	8	3	0	7	11	17866	19	517	4	33	0	0	5	0	0	0	1	6	9	2
ERR1633884	99.87	97.25	2295983	33	8	6	6	18	7	0	4	12	19438	16	438	6	22	4	1	10	0	1	0	6	5	9	0
ERR1679643	98.83	96.22	662688	7	2	3	1	4	5	0	2	5	3439	9	156	1	4	4	0	1	0	0	0	1	2	3	0
ERR1873393	88.38	0.54	2149716	888	29	3123	134	1552	3895	0	1045	0	84	0	2676	1067	1869983	29491	194	1382	0	4473	264	1819	1145	992	576
ERR718303	99.97	97.42	2023441	38	7	10	6	4	4	0	4	15	14579	14	385	3	13	2	2	0	0	1	0	4	6	8	0
ERR718313	99.96	97.42	2025695	24	11	8	0	1	4	0	6	40	18005	55	415	1	14	0	1	0	0	1	0	1	3	5	1
ERR718320	99.96	97.42	1996561	36	11	13	3	3	2	0	2	12	19660	6	337	4	9	5	1	3	0	4	0	1	2	4	1
ERR718334	99.96	97.39	1966297	31	21	6	5	8	5	0	6	252	7808	247	1246	9	17	3	1	0	0	2	0	2	5	2	1

ERR718464	99.96	97.44	2339117	48	9	11	4	9	5	0	7	20	17691	17	445	8	28	3	0	1	0	0	0	5	3	12	3
ERR718477	99.96	97.44	2150901	32	6	11	6	1	3	0	5	18	16095	4	399	4	19	4	1	2	0	1	0	0	1	3	0
ERR718488	99.97	97.4	2165274	44	9	9	5	3	7	0	7	19	15771	7	355	6	17	3	1	0	0	0	0	3	4	20	1
ERR718491	99.94	97.39	2091862	46	14	7	6	4	6	0	2	283	8531	240	1321	19	22	1	1	0	0	0	0	1	6	8	2
ERR718512	99.96	97.42	1839169	52	9	10	3	1	2	0	3	250	7370	199	1115	13	13	1	0	0	0	1	0	3	3	2	0
ERR718553	99.97	97.43	2004595	61	13	14	3	0	1	0	4	240	7865	204	1211	26	26	2	0	4	0	0	0	5	0	8	0
ERR736835	38.66	2.23	859647	63878	6285	35585	4434	17079	15008	0	12748	126	234	51	15539	15964	191512	13235	4580	16016	0	2036	0	2873	5386	24696	6155
ERR736863	79.2	0.64	2302118	18599	1926	15025	1959	8039	6481	0	7373	21	102	19	4936	6245	196786	81872	30506	122922	0	1046	0	1164	2810	9347	53121
ERR736867	68.63	0.11	1956294	1116	151	1165	101	523	447	0	322	1	28	0	247	295	10788	54602	14597	162728	0	32	0	155	119	390	68527
ERR736871	94.68	0.13	2822634	1436	153	1240	154	463	569	0	353	0	37	0	375	487	13361	69933	17011	243441	0	105	0	29	127	507	104148
ERR736874	94.32	0.12	2345277	1240	20	1665	75	720	4579	0	151	1	17	0	637	287	2130	28035	4043	83188	0	2	0	108	257	209	154446
ERR751801	99.95	97.43	2017425	64	8	16	11	3	6	0	4	23	14699	11	603	5	29	4	1	3	0	0	0	4	4	18	0
ERR751827	99.91	97.48	2814536	77	20	21	19	7	6	0	5	30	23811	15	893	7	49	7	2	1	0	0	0	5	5	18	0
ERR751847	99.95	97.43	2862414	74	15	19	12	7	8	0	5	21	29688	25	805	12	42	3	0	3	0	3	0	7	4	19	1
ERR751922	99.74	97.31	2427726	151	14	26	19	12	10	0	13	50	21202	20	886	6	42	1	0	2	0	1	0	6	7	33	2
ERR751923	99.87	97.4	2557733	100	21	23	27	6	2	0	12	40	21408	8	822	12	33	4	6	3	0	1	0	7	8	20	1
ERR752065	99.91	97.44	2825302	64	17	19	15	7	2	0	7	29	22535	15	813	5	40	2	0	8	0	2	0	5	8	11	3
ERR752103	99.94	97.39	3263258	96	50	21	12	13	12	0	5	531	13025	351	2315	17	51	7	3	5	0	1	0	4	7	20	0
ERR752105	99.93	97.4	3503644	76	18	23	17	9	13	0	9	30	26602	18	925	11	51	9	0	3	0	2	0	4	14	13	3
ERR752109	99.94	97.4	3620669	146	17	19	18	14	12	0	6	63	27371	13	889	12	59	8	1	4	0	2	0	7	5	38	3
ERR752111	99.93	97.41	2722446	72	22	9	6	6	10	0	7	30	21100	15	666	11	52	7	1	1	0	1	0	3	4	12	1
ERR752112	99.92	97.4	3185011	75	20	17	9	10	9	0	5	21	33623	11	706	6	41	6	4	3	0	4	0	5	7	21	0
ERR752117	99.93	97.4	3511899	92	16	23	9	11	15	0	7	36	26405	16	889	8	60	2	3	4	0	3	0	8	8	24	1
ERR752118	99.94	97.39	3819228	124	21	27	26	12	14	0	7	471	14975	233	1966	26	67	2	3	1	0	0	0	12	4	24	3
ERR752138	99.92	97.42	2441780	84	16	18	16	11	5	0	4	368	9503	211	1730	33	38	3	1	1	0	1	0	2	4	7	4
ERR752147	99.93	97.44	2092575	45	11	11	16	2	5	0	3	43	20273	22	543	10	22	1	0	3	0	3	0	5	4	4	1
ERR752206	99.91	97.4	2987022	85	16	11	5	10	4	0	6	41	22242	13	738	11	30	2	0	0	0	0	0	3	5	13	4
ERR760820	99.94	96.91	4094224	67	15	19	11	5	10	0	5	27	38336	12	826	12	54	2	4	5	0	1	0	6	11	14	1
ERR767965	99.9	97.46	2779677	87	16	12	15	13	11	0	8	562	10321	282	1928	30	38	8	3	2	0	0	0	7	3	16	1
ERR768008	99.77	97.28	2668292	91	18	22	7	6	3	0	2	582	10666	322	2017	23	28	3	0	1	0	0	0	5	6	17	0
ERR775776	99.93	97.3	2949607	110	11	12	10	6	9	0	4	31	22041	12	656	5	21	2	1	3	0	1	0	4	7	26	1
ERR775780	99.86	97.3	2771175	47	12	17	22	10	2	0	8	375	10742	221	1354	18	34	6	0	2	0	2	0	6	1	8	3
ERR841494	99.68	97.07	5967036	407	87	83	28	61	30	0	36	361	17176	664	6939	51	255	15	10	18	0	12	0	23	38	71	6
ERR841495	99.74	97.13	5966249	460	82	136	30	46	45	0	35	427	17565	625	7301	56	245	24	10	15	0	9	0	15	26	82	12
ERR894427	99.82	97.16	11619808	178	41	57	21	20	27	0	23	56	114197	32	2050	31	88	10	4	11	0	3	0	8	28	50	7
ERR894428	99.77	96.83	13202182	193	44	62	18	24	30	0	32	62	126578	25	2393	36	124	10	6	11	0	11	0	14	30	48	9
ERR894429	99.85	96.97	16941512	235	62	80	31	33	45	0	35	88	163221	187	3153	33	147	15	3	13	0	8	0	20	33	70	3
ERR894430	99.79	96.94	13446652	171	47	77	18	42	30	0	35	85	122159	33	2681	35	124	16	8	13	0	10	0	18	24	56	11
ERR894431	99.89	97.16	16594156	186	51	57	12	30	30	0	28	62	156124	29	2481	31	139	18	5	8	0	8	0	8	19	43	5
ERR979071	99.99	97.37	2798047	22	8	10	3	0	5	0	2	24	23972	3	246	4	14	3	0	1	0	0	0	1	2	6	0
SRR2467264	98.06	95.53	8242640	146	40	37	10	13	17	0	16	90	60152	18	1762	20	102	6	6	5	0	5	0	13	22	23	1
SRR2467268	98.93	96.4	7833567	379	100	99	59	45	58	0	61	829	48748	1084	8780	74	193	15	7	19	0	13	0	30	32	98	9
SRR3085285	99.75	97.08	3641909	61	16	14	13	6	4	0	1	22	36002	8	747	9	66	12	3	4	0	2	0	4	6	18	1
SRR3085288	99.62	96.9	3950904	60	8	18	11	7	6	0	11	23	39416	22	753	9	60	149	7	11	0	3	1	3	5	11	6
SRR3085289	98.31	95.46	3126962	57	5	28	6	13	14	0	7	20	31088	8	610	15	2824	11	1	5	0	1	0	6	7	16	2
SRR3085307	99.84	97.09	1265755	27	9	3	3	3	1	0	4	178	7800	123	1191	5	12	0	0	1	0	0	0	3	1	3	1
SRR3085317	99.47	96.66	498399	15	3	18	2	3	4	0	8	7	3578	3	177	2	10	0	1	5	0	10	0	3	2	3	0
SRR3085514	99.93	97.33	3954540	135	38	37	17	17	25	0	20	386	24336	497	3674	32	59	6	3	3	0	4	0	10	13	36	5

SRR3086364	98.31	95.46	3126962	57	5	28	6	13	14	0	7	20	31088	8	610	15	2824	11	1	5	0	1	0	6	7	16	2
SRR3086377	99.84	97.09	1265755	27	9	3	3	3	1	0	4	178	7800	123	1191	5	12	0	0	1	0	0	0	3	1	3	1
SRR3105735	99.31	96.55	9183247	294	75	100	25	60	47	0	36	135	73131	123	3315	41	157	30	4	14	0	11	0	35	334	63	5
SRR3205958	99.99	97.36	531566	3	2	3	0	0	0	0	0	2	3359	9	108	1	2	0	0	0	0	0	0	0	1	0	0
SRR3205959	99.99	97.53	544133	11	2	5	1	4	0	0	1	2	3752	13	136	1	3	0	0	0	0	1	0	1	2	1	0
SRR3675214	74.92	1.39	992562	21963	94	1399	692	1732	2799	0	1135	1	155	1	733	750	6700	19614	19458	67721	0	428	51	322	4991	441	32588
SRR3675216	94.9	0.13	1996435	288	50	313	69	187	220	0	794	1	19	0	65	175	11988	113711	37479	8551	0	28	0	48	708	211	7482
SRR3675221	87.05	0.18	701989	17516	54	766	490	929	1303	0	813	0	7	1	495	523	4693	13392	16188	49713	0	125	29	256	3785	217	23031
SRR3675231	36.21	2.52	397525	32761	3952	27848	2765	18461	11103	0	10768	113	75	0	12721	14644	44866	10972	1407	4389	0	2314	1	1658	16149	20927	2196
SRR3675234	48.27	4.13	296967	27992	3983	8216	2003	4401	4191	0	3410	21	160	58	7751	4329	63353	4341	2148	4894	0	420	18	1090	3242	6442	1582
SRR3675243	92.76	0.04	550835	885	39	216	145	290	330	0	96	0	2	0	33	61	503588	135	13	1129	6	78	6	4	112	150	192
SRR3675248	78.84	0.78	641555	4903	397	3317	891	2324	2038	0	2696	1	56	0	1524	3194	46028	66422	19005	21184	8	317	0	446	1244	2366	10961
SRR3675267	39.34	2.15	380692	55002	3011	21439	5997	11367	13654	0	10073	21	173	7	10452	13727	42400	3805	1574	3979	0	1533	15	2453	4964	12896	1745
SRR3675280	40.36	2.37	73697	9773	664	4915	494	2436	1864	0	1802	11	9	0	2360	2601	7962	562	299	765	0	412	0	289	2751	3652	410
SRR3675311	84.26	3.38	984530	33952	57	1402	728	1353	3042	0	1214	2	265	6	1041	909	6352	16687	25558	66093	0	414	8	394	9440	385	31415
SRR3675320	98.27	1.07	1107020	217	18	122	745	54	331	0	80	2	68	0	110	111	1009916	184	88	86	5	2	1	10	889	43	884
SRR3675322	95.71	0.71	1677244	498	28	2407	368	38	736	0	259	0	95	1	640	1680	1518067	10581	1093	573	0	3195	24	29	4792	177	579
SRR3675383	96.21	1.98	711766	128	5	190	3	45	100	0	31	77	26	0	175	18	633008	665	11	336	0	31	3	50	55	107	40
SRR3675385	33.33	2.44	282363	33669	2307	15392	6291	9542	10012	0	9323	19	140	4	7277	7539	33155	2741	1193	2812	17	1066	118	1751	3223	10034	1462
SRR3675390	99.19	0.08	792296	771728	33	59	18	17	77	0	78	0	11	0	104	48	296	19	22	23	0	3	0	3	2542	38	1
SRR3675441	32.61	4.12	271324	26303	1838	13666	6791	7166	8428	0	5876	75	844	34	6145	6755	30365	2433	1021	2457	2	2009	6	1449	3960	8391	812
SRR3675444	92.11	1.17	833847	291	10	699	32	266	759	0	242	0	92	0	401	215	737627	8242	539	359	0	1565	0	201	1831	207	215
SRR3675446	99.53	0.12	590209	574396	21	44	18	18	61	0	55	0	5	0	96	40	260	8	6	18	0	2	0	7	1785	29	0
SRR3675450	87.55	0.6	2035491	5426	94	2227	4672	6172	4054	0	2077	1	90	0	1441	9456	1762178	2800	6955	3258	0	130	0	1759	16715	1201	8713
SRR3675456	36.93	2.54	191142	15718	1820	13160	1236	6429	5189	0	5105	40	16	0	6284	6734	21974	5244	791	2451	0	1111	0	806	4286	10342	1052
SRR3675457	89.57	0.26	310120	4193	25	434	188	322	524	0	272	0	5	0	201	203	2580	5974	5008	22266	0	111	0	81	1336	111	10637
SRR3675464	91.91	5.56	1441602	31470	32	2404	1291	1452	2447	0	720	1	846	1	746	5362	1152645	2912	18451	1077	0	51	17	66	8038	2451	194
SRR3675465	81.78	0.16	1990587	82223	125	3129	1514	2918	6070	0	2170	0	7	0	1746	1835	13066	36427	49287	140294	0	848	0	651	2947	803	65147
SRR3675467	84.64	0.46	1486135	1927	132	2773	1137	1842	3173	0	2591	0	50	0	983	1195	16487	49972	8944	112642	0	1205	0	333	3665	577	52356
SRR3675481	98.61	0.14	1042422	52	2	113	0	94	40	0	32	0	14	0	44	50	948033	4893	11	88	1	0	18	11	32	20	61
SRR3675482	95.82	1.98	816136	244	6	119	14	226	390	0	434	2	134	0	33	178	727692	281	20	770	0	62	20	107	12083	678	54
SRR3675486	94.68	1.53	2575559	1006	56	3693	559	618	1150	0	356	1	321	0	491	305	2273366	20329	141	1434	47	698	50	503	3558	340	518
SRR3675487	96.12	0.17	442451	4371	25	503	238	283	511	0	127	0	7	0	175	199	394990	200	2369	330	0	8	0	18	1251	343	57
SRR3675488	28.68	2.77	413983	45404	3039	19329	8136	10833	15234	0	9432	128	1415	91	12341	8889	38309	3719	2563	3564	89	1473	147	2993	15158	12868	1841
SRR3675490	89.47	0.54	1580384	22125	136	1868	913	1461	2044	0	1275	0	69	0	1007	744	12265	31824	31358	108940	0	400	0	475	8210	788	52181
SRR3675492	32.13	3.44	200550	21769	1479	8787	7808	6439	7696	0	8038	70	449	20	5902	4630	18417	2429	1052	1857	0	615	61	1341	6160	5671	1157
SRR3675493	75.68	70.04	467076	19	1	1	1	1	3	0	1	17	1286	30	243	1	33	0	0	1	0	0	0	0	5	2	0
SRR3675494	88.2	0.19	245468	2657	8	764	135	239	562	0	284	0	3	0	131	1855	211077	913	2538	793	0	52	1	72	901	149	122
SRR3675495	33.52	3.2	307627	33250	2947	20002	3178	10878	7760	0	8378	90	129	0	11695	11126	32755	8548	1112	3658	0	1751	1	1145	5432	14881	2016
SRR3675502	74.87	2.73	400856	370639	28	97	93	29	90	0	33	1	93	1	120	47	205	74	11	20	0	6	0	5	3215	67	14
SRR3675506	90.43	0.84	1215239	14680	49	851	1098	465	1569	0	399	0	79	0	508	1108	1063595	1261	3774	864	0	52	61	270	11862	1121	654
SRR3675507	89.15	3.9	585264	3360	46	1147	149	765	2349	0	753	0	174	0	516	658	475556	5429	620	1069	0	1428	67	46	2908	509	582
SRR3675508	87.39	0.81	1626748	11706	79	4501	465	1364	8771	0	3194	0	100	0	362	9829	735844	47327	63317	16770	0	507	1532	418	20463	507	6899
SRR3675510	44.78	3.65	328910	15893	1201	13994	1581	7869	7458	0	5007	33	235	36	3559	6576	70601	5309	1858	5013	0	1274	46	796	3248	8687	2263
SRR3675515	85.57	0.08	877001	11649	32	7900	525	1128	2220	0	688	0	6	0	258	9740	731096	5883	18494	737	1	34	2	486	4564	710	342
SRR3675517	92.02	0.05	3337128	1368	85	1451	7572	1253	1220	0	1394	0	51	0	329	1105	6656	35511	11295	103758	68	228	45	33	1555218	1447	74978
SRR3675518	91.07	0.17	2409761	1321	78	3981	2736	1057	4039	0	2477	0	28	0	1353	3845	2140380	18943	2957	520	0	4427	325	1061	1785	663	3408
SRR3675520	41.49	2.36	1147087	90448	8030	94354	7056	40160	36392	0	36771	175	342	35	26085	37466	165174	10176	5172	10073	0	6362	1	3921	14074	79732	4972

SRR3675524	81.19	1.52	2037575	58626	132	2777	1861	3044	5946	1	2816	1	254	0	1750	1783	13195	37799	45824	139759	1	518	83	871	27018	709	66130		
SRR3675529	86.38	0.5	1392566	36527	161	2087	2278	5664	4829	1	3256	1	28	0	1758	1298	10193	30686	9528	102488	0	524	0	1189	3516	1728	47775		
SRR3675539	41.01	2.16	453739	35795	4267	29592	4093	17373	10793	0	12587	109	153	3	16184	16025	50934	14512	1666	5074	0	2391	2	1613	26429	22055	3279		
SRR3675545	95.87	0.36	1277191	2101	67	1005	2018	513	1139	0	922	5	10	0	391	4889	1134553	1303	3239	1767	0	17	0	940	3311	778	5364		
SRR3675550	99.48	0.59	788086	761611	25	79	31	44	97	0	125	0	32	0	143	41	391	37	40	119	0	3	0	5	2894	30	55		
SRR3675554	96.73	0.96	4901124	6180	114	1449	373	1429	2110	0	4129	9	452	1	1100	53442	4388299	21286	391	8465	5	18	4	104	538	1212	1393		
SRR3675555	36.83	2.73	448367	36554	4447	30955	2954	15321	11887	1	12066	117	69	1	14805	16970	50848	3651	1823	5140	0	2719	1	1865	16279	23685	2468		
SRR3675561	96.93	0.39	1138552	128	22	172	352	73	86	0	64	0	28	0	47	115	1050631	183	66	228	6	4	12	18	171	243	490		
SRR3675568	90.18	0.62	2499872	50103	86	6619	1116	1805	2714	0	1333	3	110	1	961	884	2126108	4711	49604	2280	27	73	10	635	12860	1865	1078		
SRR3675571	37.76	2.45	1189997	92113	11824	52834	9851	27090	28052	0	27795	9	209	0	25449	30172	196565	18063	7904	24719	0	2666	8	5091	26606	31671	10330		
SRR3675574	73.59	1.44	1056256	9784	924	6009	2176	5198	3941	0	4744	1	118	1	2544	2888	80662	61145	24405	38236	0	1238	0	717	1856	3726	17890		
SRR3675581	83.47	0.8	1677652	43115	127	2368	1211	2583	4378	0	2289	0	96	0	1542	1338	11361	30527	41143	115170	1	566	99	660	29407	632	53854		
SRR3675582	52.71	1.92	166297	11761	1327	9386	1145	4792	3808	0	3731	43	170	3	5123	5242	15309	1125	746	1975	0	671	6	633	13558	7305	975		
SRR3675586	99.42	0.49	607537	589199	31	44	18	12	75	0	50	0	20	0	75	37	235	12	6	22	0	2	0	0	1725	23	7		
SRR3724659	95.08	90.98	2590288	135	28	25	18	22	16	0	12	51	22295	33	1801	12	54	16	0	9	0	4	0	10	17	45	3		
SRR3724667	91.19	86.05	3221257	87	16	27	27	23	11	0	24	43	30065	26	1405	12	54	12	2	5	0	2	0	13	12	54	3		
SRR3724678	98.24	95.43	5207007	268	72	68	44	36	40	0	38	117	32287	244	4504	26	154	25	4	10	0	7	0	35	21	116	9		
SRR3724755	98.77	95.04	4791449	470	75	53	80	33	37	0	23	137	41440	200	4425	32	180	41	1	23	0	5	0	41	47	89	16		
SRR3724766	98.59	95.59	2487733	107	22	24	23	18	5	0	12	63	19456	32	1408	14	74	13	1	6	0	1	0	6	12	29	3		
SRR3725356	99.08	96.17	2968128	102	16	23	28	13	7	0	10	60	30879	39	1610	7	59	14	0	4	0	7	0	13	13	25	3		
SRR3725711	97.29	94.45	7857302	966	124	195	158	135	89	0	74	309	62998	468	10382	82	431	58	19	49	0	15	0	91	101	231	26		
SRR5007159	91.03	87.24	1592580	229	27	103	8	38	37	0	34	288	3500	185	802	44	4271	245	155	76	0	8	1	5	46	51	53		
SRR5007175	98.58	94.48	1275987	30	2	13	5	14	14	0	7	19	8952	16	377	4	1378	664	35	69	0	1	0	8	2050	14	16		
SRR5065311	99.9	97.35	1333355	27	6	13	2	1	4	0	2	13	13860	6	306	10	10	2	1	1	0	1	0	2	2	6	1		
SRR5065432	99.9	97.22	1258574	27	15	5	2	0	3	0	2	111	5635	158	883	10	15	0	0	0	0	1	0	1	2	8	0		
SRR5065491	99.92	97.34	1962777	39	17	14	10	4	1	0	7	201	8756	301	1470	4	37	7	0	2	0	1	0	2	2	10	0		
SRR5065629	99.94	97.3	1746651	24	2	6	4	2	5	0	1	6	15367	11	322	4	22	2	1	2	0	2	0	1	2	16	1		
SRR5065636	99.56	96.91	2027100	22	8	5	6	6	2	0	2	4	14638	2	400	4	17	1	0	1	0	1	0	1	2	21	0		
SRR5065639	99.93	97.28	1220031	18	5	1	0	1	5	0	0	6	8801	4	276	2	14	2	0	0	0	2	0	1	0	7	0		
SRR5065673	99.84	97.17	1402938	19	17	8	7	2	3	0	2	138	6147	184	1049	2	21	0	0	1	0	0	0	0	1	8	0		
SRR5065695	99.94	97.31	1794383	52	17	18	7	6	5	0	4	157	7850	224	1185	1	20	5	1	1	0	0	0	4	4	6	0		
SRR5067277	99.92	97.31	2044352	24	2	6	2	3	4	0	6	8	20455	9	321	6	21	6	0	3	0	0	0	2	7	7	0		
SRR5067302	99.66	97	1599905	30	5	5	5	4	8	0	3	5	16258	2	301	9	15	0	1	0	0	1	0	3	3	8	1		
SRR5067338	99.87	97.18	1533115	24	5	8	3	2	2	0	2	14	15760	4	276	8	14	3	0	2	0	0	0	0	286	12	0		
SRR5067366	99.92	97.27	1320813	20	3	5	1	2	0	0	1	1	13163	2	221	12	8	3	0	0	0	0	0	1	8	3	1		
SRR5067368	99.4	96.52	1621583	13	9	9	7	0	1	0	2	13	16255	4	265	5	18	1	0	1	0	2	0	3	1	6	0		
SRR5067415	99.94	97.29	1292137	15	5	10	2	3	1	0	2	8	9386	2	244	7	8	1	0	0	0	0	0	4	432	14	0		
SRR5067434	99.89	97.24	1775417	24	6	4	5	8	5	0	2	8	17849	4	315	4	19	3	1	1	0	1	0	2	4	7	0		
SRR5067441	99.9	97.27	1557835	18	5	3	1	4	1	0	3	9	15802	7	302	13	22	1	0	0	0	0	0	0	1	3	2		
SRR5067504	99.88	97.14	1211395	20	3	2	1	0	3	0	5	9	11987	1	245	9	5	1	0	0	0	0	0	2	1	6	1		
SRR5067527	99.93	97.32	912422	12	3	8	2	3	0	0	4	3	9087	10	180	0	8	0	0	1	0	2	0	1	1	7	1		
SRR5067533	99.93	97.33	1348732	19	7	5	4	4	2	0	3	5	13599	2	257	1	9	2	0	3	0	1	0	0	3	2	0		
SRR5067543	99.81	97.17	1807547	26	4	6	1	7	2	0	4	12	18489	5	344	11	18	0	2	0	0	1	0	1	3	5	1		
SRR5067612	99.93	97.33	1672567	23	4	5	2	6	6	0	4	7	16904	3	238	15	13	3	0	1	0	1	0	2	11	13	0		
SRR5067670	99.93	97.34	1388293	26	4	5	2	2	0	0	10	19	13750	5	245	1	17	0	0	1	0	0	0	4	0	5	1		
SRR5067699	99.93	97.31	1546061	27	6	8	2	3	1	0	5	10	15587	16	287	5	15	0	1	0	0	1	0	3	4	3	0		
SRR5067714	99.93	97.3	1422938	20	4	4	1	4	3	0	12	21	13943	7	243	2	9	3	0	2	0	0	0	0	6	11	1		
SRR5073572	99.94	97.34	1057373	16	3	4	3	0	1	0	5	8	7556	5	255	1	10	4	0	0	0	0	0	0	2	11	1		

Table S4: *M. tuberculosis* strains analysed in this study. List of *M. tuberculosis* strains identified in this study as having synonymous or non-synonymous mutations in *ddn*.

ERR1023325	ERR1193827	ERR752118	GCA_000663045
ERR1023347	ERR1199093	ERR752138	GCA_000663065
ERR1023406	ERR1199099	ERR752147	GCA_000663085
ERR1034576	ERR1199106	ERR752206	GCA_000663145
ERR1034696	ERR1199108	ERR760820	GCA_000663225
ERR1034824	ERR1199109	ERR767965	GCA_000663285
ERR1034917	ERR1199115	ERR768008	GCA_000665505
ERR1035202	ERR1199127	ERR775776	GCA_000665565
ERR1035242	ERR1199153	ERR775780	GCA_000665645
ERR1035261	ERR1213864	ERR841494	GCA_000665665
ERR1035262	ERR1213871	ERR841495	GCA_000665705
ERR1035268	ERR1213919	ERR894427	GCA_000665945
ERR1035277	ERR1367635	ERR894428	GCA_000671135
ERR1035292	ERR1367655	ERR894429	GCA_000671155
ERR1035301	ERR1367666	ERR894430	GCA_000672115
ERR1035316	ERR1367687	ERR894431	GCA_000672135
ERR1035334	ERR1413483	ERR979071	GCA_000673635
ERR1035336	ERR1465769	GCA_000159755	GCA_000674095
ERR1035344	ERR1465874	GCA_000220415	GCA_000674375
ERR1035345	ERR1465885	GCA_000220435	GCA_000674515
ERR1035350	ERR1465959	GCA_000220455	GCA_000677155
ERR1144974	ERR1465981	GCA_000364945	GCA_000677335
ERR1144975	ERR1633788	GCA_000389905	GCA_000681155
ERR1144976	ERR1633884	GCA_000389945	GCA_000706145
ERR1144977	ERR1679643	GCA_000526115	GCA_000738445
ERR1144978	ERR233357	GCA_000652855	GCA_000738475
ERR1144979	ERR718303	GCA_000653935	GCA_000797435
ERR1144980	ERR718313	GCA_000654255	GCA_000804025
ERR1144981	ERR718320	GCA_000654275	GCA_000805885
ERR1144982	ERR718334	GCA_000654555	GCA_001086825
ERR1144983	ERR718464	GCA_000654755	GCA_001086845
ERR1144984	ERR718477	GCA_000654775	GCA_001108845
ERR1144985	ERR718488	GCA_000654815	GCA_001110005
ERR1144986	ERR718491	GCA_000654915	GCA_001112325
ERR1144987	ERR718512	GCA_000654975	GCA_001123765
ERR1144988	ERR718553	GCA_000655055	GCA_001144025
ERR1144990	ERR751801	GCA_000655075	GCA_001145965
ERR1144991	ERR751827	GCA_000656795	GCA_001160225
ERR1144992	ERR751847	GCA_000657255	GCA_001173265
ERR1144993	ERR751922	GCA_000659445	GCA_001193195
ERR1144994	ERR751923	GCA_000659765	GCA_001197475
ERR1144995	ERR752065	GCA_000659785	GCA_001199055
ERR1193688	ERR752103	GCA_000662485	GCA_001199935
ERR1193708	ERR752105	GCA_000662705	GCA_001200395
ERR1193721	ERR752109	GCA_000662725	GCA_001200495
ERR1193737	ERR752111	GCA_000662885	GCA_001204615
ERR1193793	ERR752112	GCA_000662965	GCA_001206715
ERR1193814	ERR752117	GCA_000663005	GCA_001207015
GCA_001208505	GCA_001397075	SRR5065695	
GCA_001318065	GCA_001397115	SRR5067277	
GCA_001318165	GCA_001397335	SRR5067302	

GCA_001318425
GCA_001318445
GCA_001318645
GCA_001318805
GCA_001318905
GCA_001322025
GCA_001322085
GCA_001323185
GCA_001323285
GCA_001324045
GCA_001324745
GCA_001325465
GCA_001327755
GCA_001327995
GCA_001328055
GCA_001328255
GCA_001328375
GCA_001345295
GCA_001375835
GCA_001378175
GCA_001379715
GCA_001381215
GCA_001386495
GCA_001387175
GCA_001389315
GCA_001389755
GCA_001390435
GCA_001392215
GCA_001392375
GCA_001392915
GCA_001393335
GCA_001393835
GCA_001393915
GCA_001394175
GCA_001394195
GCA_001394215
GCA_001394455
GCA_001394515
GCA_001395635
GCA_001395735
GCA_001396455
GCA_001396575
GCA_001396655
GCA_001396915
GCA_001396975
GCA_001397515
GCA_001397555
GCA_001397575
GCA_001397595
GCA_001397695
GCA_001397875
GCA_001397935
GCA_001847205
GCA_001849965
GCA_001997425
GCA_001997495
GCA_002000965
GCA_900120615
GCA_900120745
GCA_900127285
SRR2467264
SRR2467268
SRR3085285
SRR3085288
SRR3085289
SRR3085307
SRR3085317
SRR3085514
SRR3086364
SRR3086377
SRR3105735
SRR3205958
SRR3205959
SRR3675493
SRR3724659
SRR3724667
SRR3724678
SRR3724755
SRR3724766
SRR3725356
SRR3725711
SRR5007159
SRR5007175
SRR5065311
SRR5065432
SRR5065491
SRR5065629
SRR5065636
SRR5065639
SRR5065673
SRR5067338
SRR5067366
SRR5067368
SRR5067415
SRR5067434
SRR5067441
SRR5067504
SRR5067527
SRR5067533
SRR5067543
SRR5067612
SRR5067670
SRR5067699
SRR5067714
SRR5073572
SRR5073681
SRR5073688
SRR5073730
SRR5073748
SRR5074079
SRR5114017
SRR5114018
SRR5114019
SRR5114020
SRR5114021
SRR5114022
SRR5153219
SRR5153316
SRR5153811
SRR5153830
SRR5314267
SRR5314270

Chapter 3

The role of MSMEG_6526 in *Mycobacteria*

3.1 Introduction

Tuberculosis (TB) is one of the top ten causes of death worldwide and in the last five years it is the highest cause of death by an infectious disease, surpassing HIV/AIDS (WHO, 2016). *Mycobacterium tuberculosis*, the causative agent of TB, is difficult to combat as it has the ability to switch between active and latent infections (Boshoff and Barry, 2005), and can resist harsh conditions including hypoxia, nitrosative stress, and oxidative stress (Rohde *et al.*, 2007; Rustad *et al.*, 2008). *M. tuberculosis* is becoming increasingly resilient to most drug treatments, as the current treatment for tuberculosis is expensive, has poor compliance and management, and extensive drug-drug interactions (Zumla *et al.*, 2013). Drug development for tuberculosis is slow and has been largely unsuccessful (Zuniga *et al.*, 2015). Recently two new drugs, Bedaquiline (Deoghare, 2013) and Delamanid (Ryan and Lo, 2014), have been conditionally approved for multi-resistant tuberculosis, and are the first drugs to be approved for tuberculosis in 40 years (Mahajan, 2013). Bedaquiline targets the mycobacterial ATP synthase and disrupts the membrane thereby decoupling and, subsequently, inhibiting ATP production (Hards *et al.*, 2015; Preiss *et al.*, 2015). Delamanid is a prodrug that when reduced by the F_{420}-dependent enzyme, Deazaflavin-dependent nitroreductase (Ddn), releases a des-nitro product that inhibits ketomycolic acid biosynthesis, and nitrous oxide causing respiratory poisoning to the cell (Stover *et al.*, 2000; Singh *et al.*, 2008).

Enzymes in mycobacteria that utilise the co-factor F_{420} are hypothesised to be potential drug targets against tuberculosis (Selengut and Haft, 2010). F_{420} is structurally similar to flavins but because of its low reducing potential, it is more functionally similar to NADH/NADPH (Walsh, 1986). It is found in a wide range of aerobic bacteria throughout soil and aquatic ecosystems, but its absence in humans and other Mammalia allowing highly specific targeting of these enzymes (Ney *et al.*, 2017). Studies have shown that F_{420} is conditionally essential in mycobacteria (Gurumurthy *et al.*, 2013). The absence of F_{420} make mycobacteria more susceptible to hypoxia, nitrosative and oxidative stress (Purwantini and Mukhopadhyay, 2009; Hasan *et al.*, 2010; Gurumurthy *et al.*, 2013). Within mycobacteria, F_{420} is utilised by at least 28 enzymes, some of which can break down a range of bactericidal agents (Selengut and Haft, 2010; Taylor *et al.*, 2010; Greening *et al.*, 2016; Jirapanjawat *et al.*, 2016). F_{420} is utilised by two super families in mycobacteria, the luciferase-like hydride transferase (LLHT) and the Flavin/Deazaflavin OxidoReductase (FDOR) super families (Greening *et al.*, 2016).

The structures of several FDORs have been solved (Greening *et al.*, 2016), allowing them to be used for structure-based drug design. However, it must first be established that their physiological roles are essential or conditionally essential, i.e. it must be established that inhibiting these enzymes would actually be deleterious to the organism. The FDORs are divided into three groups: FDOR-A, FDOR-AA, and FDOR-B (Taylor *et al.*, 2010; Ahmed *et al.*, 2015). The FDOR-As are quinone reductases that are predicted to have a role in oxidative stress protection (Gurumurthy *et al.*, 2013; Ahmed *et al.*, 2015) and in enhancing the respiration in the cell (see Chapter 2). The roles of FDOR-AAs are unknown but may be involved in fatty acid metabolism (Ahmed *et al.*, 2015). The FDOR-Bs are the most diverse group and can be separated into 12 distinct clades that are predicted to have evolved separate physiological roles (Ahmed *et al.*, 2015). Several FDOR-Bs have been functionally annotated, including FDOR-B4, which reduces biliverdin to bilirubin, a known antioxidant (Ahmed *et al.*, 2015; Ahmed *et al.*, 2016). The FDORs can reduce a range of organic compounds including aflatoxins and coumarins, but this activity is most likely promiscuous and unlikely to be related to their physiological role (Taylor *et al.*, 2010; Lapalikar *et al.*, 2012; Jirapanjawat *et al.*, 2016; Greening *et al.*, 2017).

Understanding the physiological roles of these enzymes will help in the development of novel treatments for tuberculosis and further our understanding of the biology of mycobacteria. In this study we reveal the physiological role of the FDOR-B2 clade by investigating the enzymes MSMEG_6526 from *M. smegmatis*, and its orthologue Rv0121c from *M. tuberculosis*. Knockout studies were used to identify phenotypes of partially and completely inhibited growth in defined growth conditions, making these enzymes conditionally essential. These phenotypes were shown to have an accumulative effect instead of a toxic effect. Proteomics and metabolomics revealed that pathways related to central metabolism and amino acid metabolism were affected by the knockout. Crystal structures of each protein were solved to examine the structure features of the protein revealing structure similarities to other FDOR-Bs but with an active site that is distinct than other FDORs due to a large dynamic loop.

3.2 Materials and Methods

3.2.1 Mycobacterial strains, media, and growth conditions

In this study, the mycobacterial strains used were *M. smegmatis* mc^2155 WT (Snapper *et al.*, 1990) or *M. smegmatis* MSMEG_6526 knock out (this study). Strains were grown on LB agar plates supplemented with 0.05% (w/v) Tween80 (LBT) and inoculated into Hartmans de Bont (HdB) minimal medium supplemented with 25 mM glycerol (Berney *et al.*, 2012) and grown at 37 °C with agitation (180 rpm) for starter cultures. For growth experiments, starter cultures at mid-logarithmic phase (OD_{600} 0.2–0.8) were inoculated in HdB containing 25 mM of a specified carbon sources and grown either aerobically (30 ml medium in a 125 ml flask) or microaerobically (30 ml medium in 120 ml sealed serum vials, butyl rubber stoppered, O_2 impermeable) at 37 °C with agitation (180 rpm). Optical densities to assess growth were measured at 600 nm in a WPA CO 8000 Cell Density Meter.

3.2.2 Construction of M. smegmatis Δ6526 mutant

The MSMEG_6526 markerless knockout was created by amplifying a 1041 bp fragment flanking *MSMEG_6526* on the left using the primers GTCCTGCCGTGACGGCTCAGAATTCGGCCATGGCCCCAGGG and GTACACTAGTCAATCCGGTGGCAGCGCAATCAC and a 1068 bp fragment flanking *MSMEG_6526* on the right with the primers GTACATAGTCAGGATTCCGCACAGGTTGAACGTG and CTGGGGCCATGGCCGAATTCTGAGCCGTCACGGCAGGACG. The two products were fused by PCR-overlap extension (Ho *et al.*, 1989). The PCR product and the vector pX33 (Gebhard *et al.*, 2006) were digested with SpeI from New England Biolab (Massachusetts, USA) and ligated together using T4 DNA ligase from New England Biolabs (Massachusetts, USA). Deletion of *MSMEG_6526* was carried out using the two-step method for integration and excision of the plasmid as described previously (Tran and Cook, 2005). Briefly the vector was transformed into *M. smegmatis* mc^2155 and grown on LBT plates supplemented with 5 μg/ml gentamycin (LBTG) and grown at 28 °C until colonies were visible. Colonies were picked and grown in LBTG liquid medium at 28 °C until they reached an OD_{600} of 0.5-1.0. The culture was plated on LBTG plates and incubated at 40 °C until colonies were present. The

colonies were exposed to 250 mM catechol and colonies that turned yellow were picked and streaked on a LBTG plate and incubated at 40 °C until colonies were visible. Colonies were picked an inoculated into LBTG liquid media and grown until OD reached 0.5-1.0 and plated onto low salt LBT sucrose plates containing no antibiotics (yeast extract 5 g/L, tryptone 10 g/L, NaCl 2g/L, sucrose 100 g/L, agar 15 g/L) until colonies were visible. Colonies were exposed to 250 mM catechol and colonies that remain white were picked and streaked on a LBT plate. Knockouts were confirmed by sequencing.

3.2.3 Proteomic preparation and analysis

Cultures for proteomics were grown at 37 ºC in 30 ml HdB containing 25 mM Glycerol in sealed 120 ml serum vials in biological triplicate for both wild type and Δ6526. 5 ml samples were harvested at OD 0.5 and 1.0 into 60 % methanol at -20 °C and pelleted by centrifugation at 10,000 × *g* for 10 mins at – 10 °C. Samples were washed 3 times in 40 % methanol (-20 °C) three times and stored at -80 °C. Cells were suspended in 50 mM triethylammonium bicarbornate and 1 % (w/v) sodium deoxycholate and boiled for 5 min. Samples were cooled down to room temperature and incubated with benzonase nuclease (Sigma Aldrich, Missouri, USA). Total protein concentration was measured using a Direct Detect® Infrared Spectrometer (Merck, Darmstadt, Germany) and sample were normalised to the lowest concentration. Samples were incubated with DTT (10 mM final concentration) at room temperature for 5 mins before incubating with iodoacetamide (20 mM final concentration) for 5 mins at room temperature. Samples were digested with 1:50 w/w protein ratio of sequencing grade modified trypsin (Promega, Wisconsin, United States) at 37 °C for 16 h. The tryptic digest was stopped by adding formic acid (1% v/v final concentration) and the soluble extract was obtained by centrifugation at 18,000 ×g for 5 min. samples were dried using a miVac Sample Concentrators (SP Scientific, New York, USA) and resuspended in 2 % acetonitrile and 0.1 % formic acid and filtered through 0.22 μM filters.

The samples were chromatographically separated on a Nanomate 3000 (ThermoFisher) nano LC system directly coupled to an Orbitrap Fusion Tribrid Mass Spectrometer. The peptides were desalted for 5 min on an Acclaim PepMap C18 (300 Å, 5 mm x 300 μm) trap column at a flow rate of 10 μL/min with loading solvent, and separated on an Acclaim PepMap C18 (100 Å, 150 mm × 0.075 mm) column at a flow rate of 0.3 μL/min at 35 °C. A linear gradient from 5% to 40% solvent B over 60 min was employed followed by a wash and re-

equilibrate 40−99% B over 5 min, a 5 min hold at 99% B, return to 5% B over 6 min, and held for 7 min. The solvents used were: (A) 0.1% formic acid, 99.9% water; (B) 0.08% formic acid, 80% acetonitrile, 19.92% water. The nano-LC was directly coupled to the Nanospray Flex Ion source of the Orbitrap Fusion MS. The ion spray voltage was set to 2400 V, the sweep gas was set to 1 Arb, and the ion transfer tube temperature was set to 300 °C. Data were acquired in data-dependent acquisition mode consisting of a Orbitap-MS survey scan followed by parallel acquisition of a high resolution Orbitrap scan at 120 000 resolution and multiple MS/MS events in the linear ion trap, over a 3 second period. First stage MS analysis was performed in positive ion mode over the mass range of m/z 400−1500 with an AGC target of 4×10^5 and a maximum injection time of 50 ms. Tandem mass spectra were acquired in the ion trap on precursor ions that exceeded an intensity threshold of 1000 counts with charge state 2−7. Spectra were acquired using quadrupole isolation with a 1.6 m/z isolation window and (Higher energy Collisional Dissociation) HCD set at 28% based on the size and charge of the precursor ion for optimum peptide fragmentation. Ion trap scan rate was set to rapid with an AGC target of 4×10^3 and a maximum injection time of 300 ms, the instrument was set to utilise the maximum parallelizable time for injecting ions into the trap during a 3 second window whilst the Orbitrap was collecting high resolution MS spectra. Dynamic exclusion was set to exclude precursor ions after one occurrence with a 15 sec interval and a mass tolerance of 10 ppm.

Protein identification was conducted using the Sequest algorithm in Proteome Discoverer v2.1 (ThermoFisher). Carbamidomethyl was selected as the alkylating agent and trypsin, was selected as the digestion enzyme, dynamic modifications for oxidation on H, M, W and deamidated N and Q were selected, with a maximum of three modifications. Tandem mass spectrometry data were searched against the *M. smegmatis* annotated database from UniProt. The database search results were manually curated to yield the protein identifications using a 1% global false discovery rate (FDR) determined by using the in-built FDR tool, Proteome Discoverer decoy database search feature, within Proteome Discoverer software.

3.2.4 Metabolomic preparation and analysis

Cultures for metabolomics were grown at 37 ºC in HdB media containing 25 mM Glycerol in biological triplicate to OD_{600} ~0.8. Cultures were pelleted and washed three times in HdB media containing no carbon source and then resuspended in HdB media containing 25 mM Sodium Acetate and grown at 37 ºC. 5 ml samples were harvested before being pelleted and 3

h after the carbon source was changed to Acetate. Samples were added to 60 % methanol (-20 °C) and pelleted by centrifugation at 10,000 × *g* for 10 mins at – 10 °C in pre-weighed tubes and then washed 3 times in 40 % methanol (-20 °C) three times and stored at -80 °C. Samples were dried down by freeze drying and then weighed. 100 µl of Methanol containing 8.8 ng/ml ribitol (-20 °C) were added to 1 mg of dried cell weight. Cells were lysed by bead beating at 30 Hz for 5 Mins twice using a Tissue lyser (Qiagen, Hilden, Germany) and the supernatant was recovered by centrifugation at 20,000 ×g for 10 mins at -10 °C. Chloroform (-20 °C) was added at a 3:1 (methanol:chloroform) ratio, vortexed and incubated on ice for 10 mins. Ice cold Deionised water was added at a 3:3:1 (methanol:water:chloroform) ratio, vortexed, and centrifuged at 10,000 ×g for 5 mins. The aqueous layer was obtained from the organic layer and dried down by miVac Sample Concentrators (SP Scientific, New York, USA). Dried down samples were derivatised using an automated method on a PAL3 (CTC Analytics, Switzerland) autosampler, as previously published (Carroll *et al.*, 2015). Briefly, samples were resuspended with 10 µl of 20 mg/ml methoxamine in pyridine and incubated at 37 °C for 90 mins. 15 µl of BSTFA was added to the sample and incubated at 37 °C for 30 mins then 5 µl of pyridine was added and incubated at 37 °C for 60 mins, all incubation steps were conducted with incubation at 750 rpm. 1 µl of derivatised samples were loaded onto a GCMS-TQ8050 (Shimadzu, Kyoto, Japan) with a DB-5 Column (30 m × 0.25 mm, 1 µm) (Agilent, California, USA) with a starting temperature of 100 °C for 4 mins then ramped to 320 °C at 10 °C/min and held for 11 mins and a 1:1 split. The Shimadzu Smart Metabolites Database was used for both MS source and MRM conditions for the detection of metabolites. The retention time was corrected with the Automatic Adjustment of Retention Time (AART) function of the GCMS solutions software using a standard of alkanes (C7 to C33), as per the manufacturer's instructions. All peaks were automatically integrated and manually checked for correct retention time and qualifier ion ratio. Data manipulation and statistical analysis was conducted using base R in RStudio and the tidyverse packages (Wickham, 2016)

3.2.5 Protein expression and purification

The gene used for MSMEG_6526 in vector pETMCSIII was cloned previous work (Ahmed *et al.*, 2015). MSMEG_6526 was transformed into *E. coli* BL21 (DE3) cells and grown on LB agar containing 100 µg/ml ampicillin. Single colonies were picked and inoculated in LB media with 100 µg/ml ampicillin. Starter cultures were grown overnight at 37 °C and diluted 1/100

in auto-induction media (Ahmed *et al.*, 2015) and grown for 24 h at 30 °C. Cells were harvested by centrifugation at 8,500 × *g* for 20 minutes at 4 °C and resuspended in lysis buffer (50 mM $NaPO_4$, pH 8, 300 mM NaCl, 25 mM imidazole) and lysed by sonication using an Omni Sonicator Ruptor 400 (2 x 6 min. at 50% power). The soluble extract was obtained by centrifugation at 13,500 ×*g* for 1 h at 4 °C and passed through a 5 mL HisTrap FF column (GE Healthcare), washed with lysis buffer and eluted with elution buffer (50 mM $NaPO_4$, pH 8, 300 mM NaCl, 250 mM imidazole). Purified protein was passed through a GE HiPrep 26/10 desalting column for buffer exchange into TEV buffer (50 mM Tris pH 8 and 150 mM NaCl 0.5 mM EDTA, 1 mM DTT) and the histidine-tag was cleaved by adding TEV protease at a 1:10 ratio and left overnight at room temperature. Tag-free protein was purified from by passing the TEV reaction over a 5 mL HisTrap FF column and the flow through was collected. The collected protein was incubated with 1.5-fold excess F_{420} overnight at 4 °C, followed by size exclusion chromatography on a GE Hiload 16/ 600 Superdex 75 pg column in buffer containing 20 mM HEPES pH 7.5 and 150 mM NaCl. Fractions that were yellow and contained protein were pooled and used for crystallography after the sample diluted was in 20 mM HEPES pH 7.5 to a final solution of in 20 mM HEPES pH 7.5 and 50 mM NaCl and concentrated to 20 mg/ mL and stored at 4 °C.

Rv0121c was ordered as a gene string from Invitrogen and cloned into the *M. smegmatis* expression vector pYUB28b (Bashiri *et al.*, 2010) using Gibson assembly (Gibson *et al.*, 2009). Rv0121c was transformed into *M. smegmatis* $mc^2$4517 cells (Wang *et al.*, 2010) and grown on LB agar containing 0.05% Tween 80 and 50 µg/ml kanamycin and hygromycin. Single colonies were picked and inoculated in LB media with 0.05% Tween 80 and 50 µg/ml kanamycin and hygromycin. Starter cultures were grown for 3 days at 37 °C and diluted 1/100 in auto-induction media (Ahmed *et al.*, 2015) and grown for 5 days at 37 °C. Cells were harvested by centrifugation at 8,500 × *g* for 20 minutes at 4 °C and resuspended in lysis buffer (50 mM $NaPO_4$, pH 8, 300 mM NaCl, 25 mM imidazole) and lysed by homogenisation using a M-110P electric benchtop homogeniser (Microfluidics, Massachusetts, USA). The soluble extract was obtained by centrifugation at 13,500 ×*g* for 1 h at 4 °C. Rv0121c was purified from the soluble extract as described for MSMEG_6526 above but was concentrted to 12 mg/ml.

3.2.6 Protein crystallography

The MSMEG_6526:F_{420} and Rv0121c:F_{420} complexes were screened for crystallisation conditions using SG1 (Molecular Dimensions, Newmarket, Suffolk, UK), Index HT, Peg/Ion

HT, and Crystal screen HT (Hampton Research, California, USA) high-throughput 96-well crystallization screens, set up by hand.

The best crystal for MSMEG_6526 that was used for data collection was grown in 100 mM sodium acetate pH 4.6, 20 mM calcium chloride, and 28% MPD and was flash-cooled under a stream of nitrogen gas at 100 K. X-ray diffraction data was collected at the Australian Synchrotron beamline MX1 with an ADSC Q315 detector and Blu-Ice software (McPhillips *et al.*, 2002). Diffraction data were integrated using XDS (Kabsch, 2010), and scaled using AIMLESS (Evans *et al.*, 2013), in the CCP4 suite (Winn *et al.*, 2011). Molecular replacement was performed with the previously solved apo-structure of MSMEG_6526 (PDB ID: 4ZKY) (Ahmed *et al.*, 2015) using Phaser (McCoy, 2007) with F_{420} modelled manually into the difference density (mFo–DFc) at the binding site using COOT (Emsley *et al.*, 2010). Model building was performed using Buccaneer (Cowtan, 2006) followed by manual loop building in Coot (Emsley *et al.*, 2010). Refinement was performed using REFMAC (Murshudov *et al.*, 2011)

The best crystal for Rv0121c that was used for data collection was grown in 0.1 M Sodium Acetate pH 4.6, 1.5 M sodium formate with seeding from initial screens. The cryobuffer used was the same as the crystallization conditions, with the addition of a 35% glycerol. The crystal was flash-cooled under a stream of nitrogen gas at 100 K and X-ray diffraction data was collected using the MX2 beamline at the Australian Synchrotron. Diffraction data were integrated using XDS (Kabsch, 2010), and scaled using AIMLESS (Evans *et al.*, 2013), in the CCP4 suite (Winn *et al.*, 2011). Molecular replacement was performed with the MSMEG_6526:F_{420} structure solved in this study (PDB ID: 5JV4) using Molrep (Vagin and Teplyakov, 1997) and residues were replaced to the correct sequence using chainsaw (Stein, 2008). Model building was performed using auto-build from PHENIX (Chen *et al.*, 2010) followed by manual loop building in COOT (Emsley *et al.*, 2010). Refinement was performed using REFMAC (Murshudov *et al.*, 2011) and PHENIX (Chen *et al.*, 2010).

3.2.7 Computational substrate docking

MSMEG_6526 (PDB ID: 5JV4) was prepared using Protein Preparation Wizard (Sastry *et al.*, 2013) from the Schrödinger biological suite (Schrödinger, 2017) to identify the likely protonation state at pH 7.4 The KEGG database was obtained from the Zinc15 repository (Sterling and Irwin, 2015), prepared using Ligprep (Schrödinger Release, 2016) and docked in the active site of the protein using Glide with default settings (Friesner *et al.*, 2004). The top 1000 compounds successfully docked and ranked by docking score were used for selection of potential substrates. Of these, approximately two thirds were synthetic chemicals (650). Of the remaining naturally occurring chemicals, the largest chemical classes were aromatic amino acid, and closely related metabolites, and metabolites involved nucleic acid metabolism.

3.3 Results

3.3.1 Growth of Δ6526 on Primary Carbon Sources

Personal communication from Dr. Nicholas West of the University of Queensland revealed that *M. tuberculosis* strains that have the *rv0121c* interrupted *via* transposon mutagenesis cannot survive latent infection within mice. Therefore, we investigated the function and physiological role of Rv0121c to understand why it is essential. We used *M. smegmatis* as a non-pathogenic model of *M. tuberculosis,* and created a knockout of MSMEG_6526 (Δ6526), an Rv0121c orthologue, to identify phenotypes. The knockout was grown in different growth media to observed differences in growth rate compared to wild type. We observed that in a nutrient rich media (Lysogeny broth) there is no difference in the growth rates between wildtype and Δ6526 (Fig 3.1a). However, there is a slight difference in final cell density when the stationary phase is reached. We observed that the wildtype reached a maximum OD_{600} reading of 4.1 ± 0.15 and Δ6526 reached a maximum OD_{600} reading of 3.6 ± 0.1. This difference may be due to carbon and oxygen limitation that occurs when the cell reaches the stationary phase (Smeulders *et al.*, 1999) and MSMEG_6526 is needed to these conditions.

To further the investigation of the effect of Δ6526 on *M. smegmatis*, we compared the growth of wildtype and Δ6526 in minimal media with different major carbon sources; glucose (carbohydrate), glycerol (polyol), and butyrate (lipid). Between carbon sources there was a difference in growth rate for the wild-type strain. This has been previously observed (Hasan *et al.*, 2010) and the differences between the various media are most likely due to how the cells uptake and metabolise the various carbon sources. Despite this, the Δ6526 strain had a slower growth rate and lower maximum OD_{600} reading compared to the wildtype in all minimal media conditions tested. When grown on glucose (Fig 3.1b), Δ6526 had a 32% decrease in growth rate compared to wildtype and had a maximum OD_{600} reading of 1.9 ± 0.1 compared to maximum OD_{600} reading of the wildtype with 2.5 ± 0.1. The Δ6526 strain had a similar reduction in growth rate of 39% and a maximum OD_{600} reading of 1.93 ± 0.06 compare to wildtype type with 2.37 ± 0.11 when using glycerol, which metabolism uses part of the glycolysis pathway, as a carbon source (Fig 3.1b). When butyrate is used as the carbon source, which is metabolised differently from glucose and glycerol, Δ6526 still has a 14% slower growth rate and a lower maximum OD_{600} reading of 0.53 ± 0.06 compared to the wildtype of 0.9 ± 0.01 (Fig 3.1c).

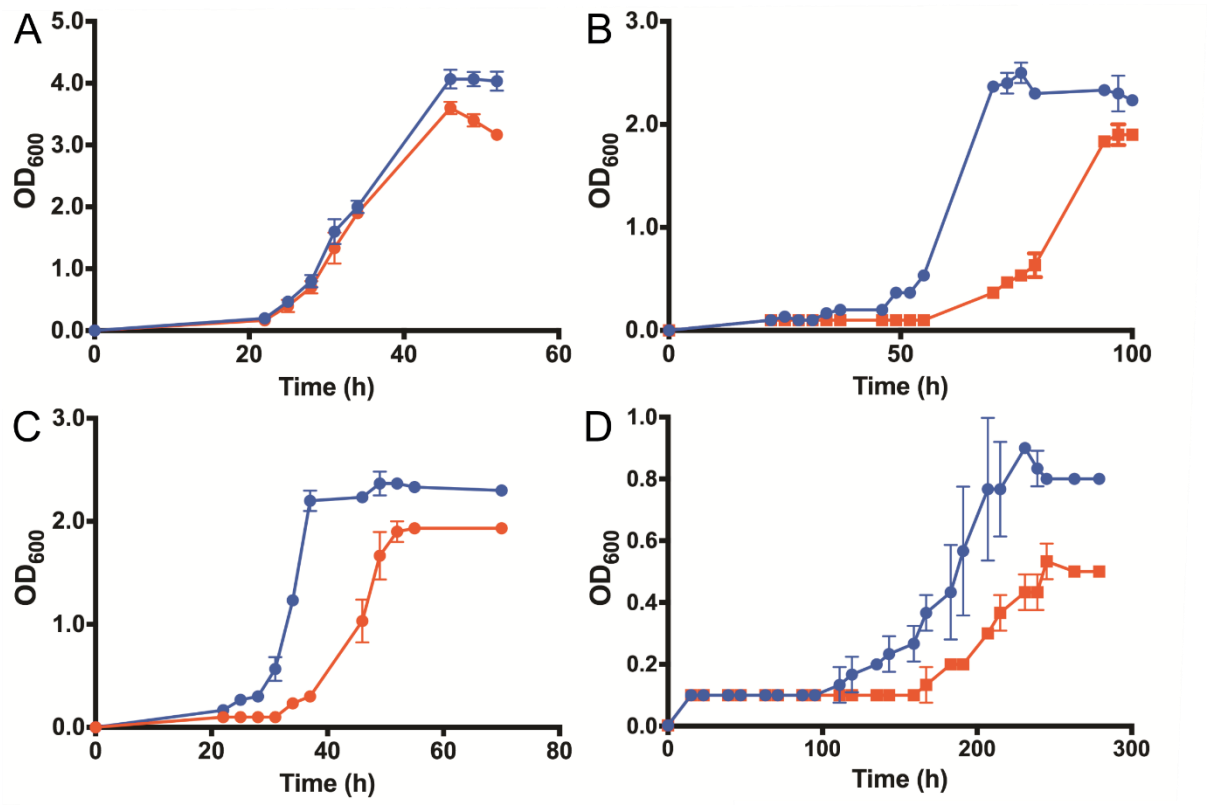

Figure 3.1 Growth rates of wildtype and Δ6526 *M. smegmatis* on major carbon sources. The measured optical densities of wildtype (blue) and Δ6526 (red) at the given time points when grown in LBT (a) or in HdB minimal media containing 25 mM Glucose (b), Glycerol (c), or butyrate (d). All conditions contained 0.05% (w/v) tyloxapol to avoid clumping. Error bars represent standard deviations from three biological replicates.

3.3.2 The Changes in Protein Expression in Δ6526

After identifying the phenotypes of Δ6526, we wanted to understand how the biochemical processes were affected by the knockout. To investigate this, we compared the protein expression levels of wildtype *M. smegmatis* verses Δ6526 in the exponential phase of cell growth at OD_{600} 0.5 and OD_{600} 1.0 when both strains were grown on glycerol as the sole carbon source. Only a few proteins were seen to be upregulated at both growth points, including isocitrate lyase, one of the key enzymes of the glyoxylate pathway, and methylcitrate dehydratase, a key enzyme in the methylcitrate cycle (Table 3.1). Isocitrate lyase in mycobacteria is known to be the enzyme that converts methylisocitrate to succinate and pyruvate in the last step of the methyl citrate cycle instead of a separate enzyme like in other species (Gould *et al.*, 2006; Upton and McKinney, 2007). Therefore, isocitrate lyase is most likely being upregulated for the methylcitrate cycle as well. The upregulation of these cycles

seems to indicate that the Krebs cycle is not being fully utilised, as these cycles allow the cell to assimilate metabolites that cannot be produced by the Krebs cycle, such as odd chain fatty acids (Muñoz-Elías *et al.*, 2006).

Proteins involved in the Krebs cycle were downregulated in Δ6526, including succinate dehydrogenase, which is downregulated in both growth points (Table 3.3), and citrate synthase, and 2-ketoglutarate ferredoxin oxidoreductase that were downregulated in the OD_{600} 0.5 growth point. Late stage glycolysis that feeds into the Krebs cycle seemed to be downregulated as the concurrent enzymes, pyruvate kinase, and pyruvate flavodoxin /ferredoxin oxidoreductase, were downregulated as well as L-lactate dehydrogenase. Amino acid metabolism that utilises metabolites from the Krebs cycle were downregulated in Δ6526. This included glutamate metabolism with glutamate decarboxylase, ferredoxin-dependent glutamate synthase, NADPH-glutamate synthase, and glutamate dehydrogenase all being downregulated. The first two enzymes in aspartate metabolism, aspartokinase and aspartate-semialdehyde dehydrogenase, were downregulated. This pathway is also involved in arginine, and methionine biosynthesis, where two key enzymes arginine biosynthesis bifunctional protein, and methionine synthase were downregulated. The first step of the branched amino acid biosynthesis from pyruvate, acetolactate synthase, was also downregulated. The electron transport chain was affected with the downregulation of NADH dehydrogenase A, suggesting a decrease in cell respiration that correlates with the slower growth seen by Δ6526. Despite being grown in glycerol, two enzymes that degrade it in different pathways, glycerol dehydratase and the co-enzyme B12-dependent glycerol dehydrogenase, were downregulated at the OD 0.5 growth point. The downregulation of all these proteins seem to show that several pathways were affected by the loss of MSMEG_6526, although there seems to be a correlation with central metabolism (Krebs cycle), and amino acid metabolism which have highly related pathways.

Interestingly, we identified three F_{420}-dependent enzymes that were upregulated in both growth points. Firstly, the FDOR MSMEG_2027, which is found in the FDOR-A clade, is proposed to be involved in cell respiration (see Chapter 2). As the enzymes that have altered regulation in Δ6526 are related to metabolism, this can be seen as further evidence for the role of FDOR-As in the cells energetics. The other two F_{420}-dependent enzymes, MSMEG_4879 and MSMEG_5732, are LLHT enzymes with unknown function (Greening *et al.*, 2016). Although blast searches of these enzymes show homology to $F_{420}H_2$-dependent methylene-H_4MPT reductase (Mer), which are involved in the CO_2-reducing pathway in methanogenesis

by reducing CH_2=H_4MPT to CH_3-H_4MPT (Aufhammer *et al.*, 2005). The function of these enzyme will need to be tested to confirm function but it is unlikely that they retain Mer function as mycobacteria are unknown to perform methanogenesis. The only known activity of LLHTs in mycobacteria other than Fgd, are involved with cell surface lipids biosynthesis (Purwantini and Mukhopadhyay, 2013; Purwantini *et al.*, 2016).

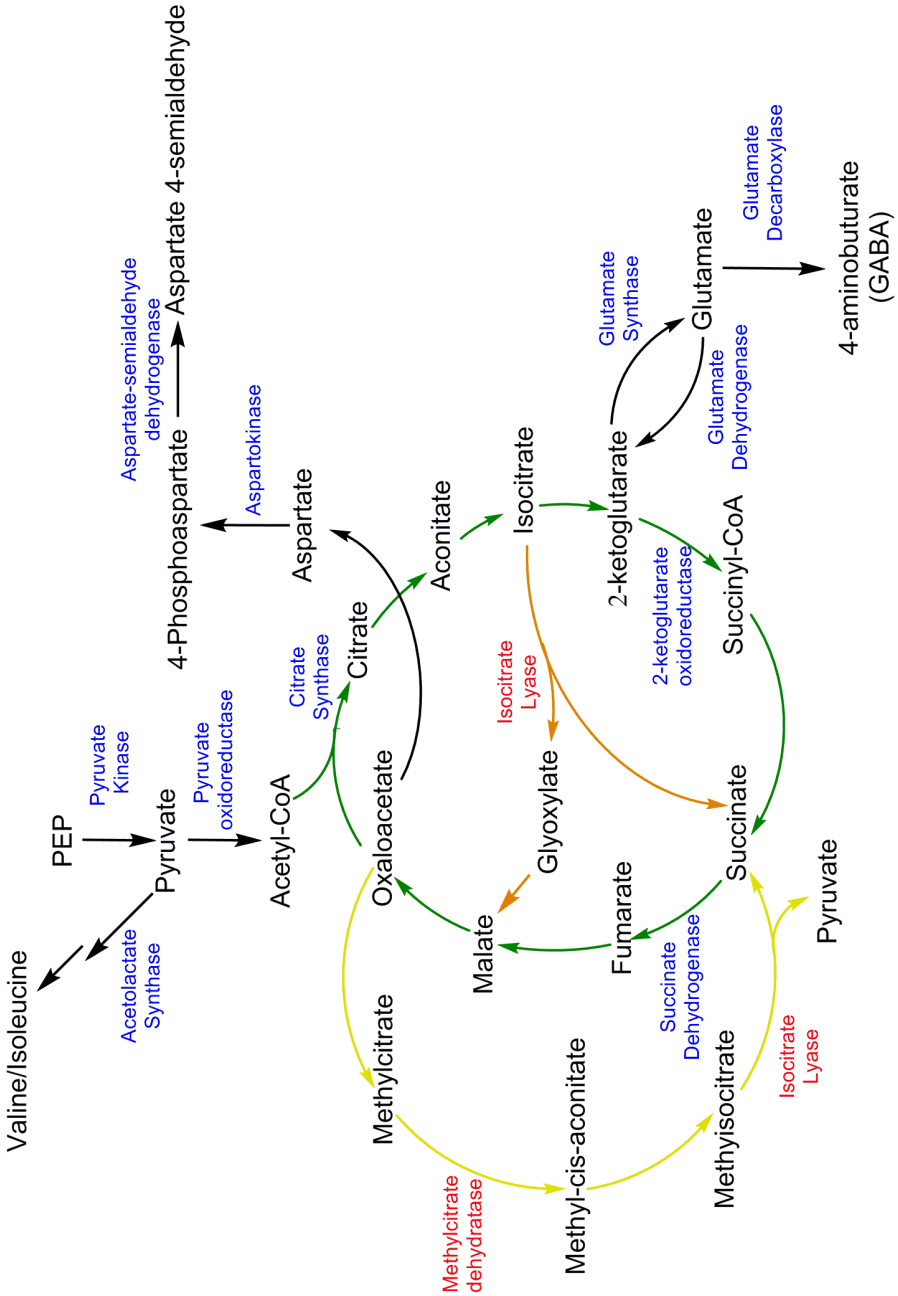

Figure 3.2 Summary of the Proteomics. Diagram of the pathways affected by the Δ6526 strain. Proteins upregulated in the Δ6526 strain are presented in red, and proteins downregulated proteins in the Δ6526 strain are represented in blue. The Krebs cycle is represented in green arrows, glyoxylate cycle is represented in orange arrows, and the methylcitrate cycle is represented in yellow arrows.

Table 3.1: Upregulated proteins of interest in MSMEG_6526 Knockout

Protein	Description	OD_{600}	Fold change[a]	*P* value[b]
MSMEG_0911	Isocitrate lyase	0.5/1.0	6.465/11.636	0.0113/0.0465
MSMEG_0912	3-hydroxybutyryl-CoA dehydrogenase	0.5	1.471	0.0431
MSMEG_1946	NADH pyrophosphatase	1.0	5.497	0.0199
MSMEG_3816	UvrABC system protein B	1.0	1.451	0.0473
MSMEG_5243	FAD-binding FDOR	1.0	4.783	0.039
MSMEG_6307	Glutamine transport system permease protein	1.0	2.625	0.0263
MSMEG_6387	Indolylacetylinositol arabinosyltransferase EmbC	1.0	3.03	0.0174
MSMEG5136	PPM-dependent Mannosyltransferase	1.0	8.424	0.0357

Table 3.2: Proteins absent in MSMEG_6526 Knockout but present in Wild Type

Protein	Description	OD_{600}	PSM[a]	*Sum Peptide score*
MSMEG_0194	Cutinase Cut1	1.0	14	20.238
MSMEG_0225	MmpL4	0.5	9	12.447
MSMEG_0389	Glycosyltransferase gtf1	0.5	7	8.247
MSMEG_0422	PEP phosphonomutase	0.5	5	10.803
MSMEG_0645	Beta-1,3-glucanase	0.5	7	16.72
MSMEG_0766	Phosphoribosylglycinamide formyltransferase 2	0.5	5	16.482
MSMEG_1114	Short chain dehydrogenase	0.5	7	6.807
MSMEG_1255	DNA helicase	0.5	5	16.662
MSMEG_1703	N-acyl-L-amino acid amidohydrolase AmiA1	1.0	6	17.023
MSMEG_1878	Ribosome hibernation promoting factor/RaiA	1.0	13	30.253
MSMEG_2023	CAIB/BAIF CoA-transferase family protein	0.5/1.0	20/13	35.799/34.087
MSMEG_2027	Quinone reductase (Ddn orthologue)	0.5/1.0	15/4	26.672/8.122
MSMEG_2131	Fatty acyl AMP-ligase, FadD33	0.5	7	12.072
MSMEG_2274	Hydrogenase assembly chaperone HypC/HupF	1.0	5	8.564
MSMEG_2275	Hydrogenase expression/formation protein HypD	1.0	7	10.472
MSMEG_2276	Hydrogenase expression/formation protein HypE	1.0	9	26.488
MSMEG_2349	Glycoside hydrolase	1.0	4	12.218
MSMEG_2611	Mycothione reductase	0.5	5	21.468
MSMEG_3042	Uracil phosphoribosyltransferase, PyrR	1.0	4	7.479
MSMEG_3066	Ribulose-phosphate 3-epimerase	0.5	6	13.976
MSMEG_3192	Maltooligosyltrehalose synthase	0.5	7	12.028
MSMEG_4269	Asparagine synthase (glutamine-hydrolyzing)	1.0	5	10.641
MSMEG_4464	Modulator of DNA gyrase	0.5	6	9.928
MSMEG_4511	Linear gramicidin synthetase subunit B, MbtE	0.5	26	62.151
MSMEG_4713	HpcH/HpaI aldolase/citrate lyase family protein	1.0	3	13.565
MSMEG_4716	Acetyl-/propionyl-coenzyme A carboxylase alpha chain	1.0	3	15.422

MSMEG_4879	F420-dependent LLHT	0.5/1.0	29/17	58.189/40.333
MSMEG_4911	Nicotinate phosphoribosyltransferase	1.0	5	7.601
MSMEG_5244	DevR family transcriptional regulator	1.0	6	13.694
MSMEG_5732	F420-dependent LLHT	0.5/1.0	29/17	58.189/40.333
MSMEG_6389	Integral membrane indolylacetylinositol arabinosyltransferase EmbB	0.5	3	9.64
MSMEG_6645	2-methylcitrate dehydratase	0.5/1.0	29/11	62.789/34.864
MSMEG_6907	MmcI protein	0.5	9	16.938

[a]peptide-spectrum match

Table 3.3: Downregulated proteins of interest in MSMEG_6526 Knockout

Protein	Description	OD_{600}	Fold change[a]	*P* value[b]
MSMEG_0002	6-phosphogluconate dehydrogenase	0.5	0.623	0.0346
MSMEG_0109	NAD(P) transhydrogenase subunit beta	0.5	0.641	0.0492
MSMEG_0239	O-acetylhomoserine/O-acetylserine sulfhydrylase	0.5	0.472	0.0405
MSMEG_0406	Acyl-CoA dehydrogenase	0.5	0.295	0.0122
MSMEG_0599	Fatty-acid-CoA ligase FadD2	0.5	0.619	0.0291
MSMEG_0603	Acyl-CoA dehydrogenase, FadE6	0.5/1	0.253/0.575	0.017/0.0282
MSMEG_0826	Phosphomethylpyrimidine synthase	0.5	0.532	0.0208
MSMEG_0859	Transcriptional regulator, TetR family	0.5	0.377	0.0201
MSMEG_0889	Aldehyde dehydrogenase	0.5/1.0	0.462/0.657	0.0201/0.0444
MSMEG_0954	Uroporphyrinogen-III synthase	0.5	0.608	0.024
MSMEG_1038	GTP cyclohydrolase II	1.0	0.474	0.0354
MSMEG_1185	AsnC-family transcriptional regulator	0.5	0.181	0.0388
MSMEG_1392	Alcohol dehydrogenase, class IV	0.5	0.703	0.0298
MSMEG_1424	FMN-dependent L-lactate dehydrogenase	0.5	0.511	0.007
MSMEG_1528	Cutinase	0.5	0.648	0.0387
MSMEG_1543	EPTC-inducible aldehyde dehydrogenase	0.5	0.633	0.0373
MSMEG_1546	Coenzyme B12-dependent glycerol dehydrogenase small subunit	0.5	0.175	9.00E-04
MSMEG_1547	Glycerol dehydratase large subunit	0.5	0.448	0.0064
MSMEG_1574	Glutamate decarboxylase	0.5	0.259	0.005
MSMEG_1604	Cholesterol oxidase chod	0.5	0.464	0.0059
MSMEG_1665	Betaine-aldehyde dehydrogenase	0.5	0.56	0.0078
MSMEG_1775	Cytochrome P450	0.5	0.6	0.0457
MSMEG_1807	Acetyl-/propionyl-coenzyme A carboxylase alpha chain	0.5	0.573	0.0187
MSMEG_1809	Thiosulfate/3-mercaptopyruvate sulfurtransferase	0.5	0.723	0.0339
MSMEG_1813	Propionyl-CoA carboxylase beta chain	0.5	0.669	0.0379
MSMEG_2007	Fumarylacetoacetate (FAA) hydrolase	0.5	0.409	0.0124

MSMEG_2092	D-aminopeptidase	0.5	0.573	0.0241
MSMEG_2122	Dihydroxyacetone kinase, L subunit	0.5	0.306	0.0061
MSMEG_2123	Dihydroxyacetone kinase, DhaK subunit	0.5	0.562	0.0362
MSMEG_2372	Acetolactate synthase	0.5	0.365	0.0106
MSMEG_2387	3-isopropylmalate dehydratase large subunit	0.5	0.548	0.0209
MSMEG_2421	OsmC family protein	0.5	0.567	0.0024
MSMEG_2580	4-hydroxy-3-methylbut-2-en-1-yl diphosphate synthase (flavodoxin)	0.5	0.399	0.0059
MSMEG_2684	4-hydroxy-tetrahydrodipicolinate synthase	0.5	0.582	0.047
MSMEG_3072	Riboflavin biosynthesis protein, ribBA	0.5	0.61	0.0376
MSMEG_3199	Quinolinate synthase	0.5	0.428	0.0156
MSMEG_3227	Pyruvate kinase	0.5	0.6	0.0223
MSMEG_3580	Diacylglycerol O-acyltransferase / trehalose O-mycolyltransferase	0.5	0.245	0.007
MSMEG_3621	Membrane NADH dehydrogenase ndhA	0.5	0.583	0.0409
MSMEG_3775	Arginine biosynthesis bifunctional protein argJ	0.5	0.641	0.043
MSMEG_4108	NAD(P) transhydrogenase subunit beta	0.5	0.622	0.0461
MSMEG_4185	Methionine synthase	0.5	0.364	0.011
MSMEG_4270	Adenosine kinase	0.5	0.419	0.0185
MSMEG_4327	3-oxoacyl-(acyl-carrier-protein) synthase 1, KasA	0.5	0.525	0.0097
MSMEG_4367	Formamidase	0.5	0.434	0.0385
MSMEG_4645	2-ketoglutarate ferredoxin oxidoreductase, beta subunit	0.5	0.395	0.0426
MSMEG_4646	Pyruvate flavodoxin/ferredoxin oxidoreductase	0.5	0.608	0.0224
MSMEG_4684	Ribose 5-phosphate isomerase	0.5	0.617	0.0424
MSMEG_4934	ATP:cob(I)alamin adenosyltransferase	0.5	0.317	0.0129
MSMEG_5199	Acetyl-CoA acetyltransferase	0.5	0.442	0.0188
MSMEG_5258	Steroid delta-isomerase	0.5	0.475	0.0241
MSMEG_5265	Cystathionine gamma-synthase	0.5	0.517	0.0225
MSMEG_5270	Cystathionine beta-synthase	0.5	0.563	0.0065
MSMEG_5427	Ribose-phosphate pyrophosphokinase	0.5	0.732	0.0448
MSMEG_5428	Arsenate reductase	0.5	0.432	0.0069
MSMEG_5442	Glutamate dehydrogenase	0.5	0.524	0.0239

MSMEG_5477	2-hydroxy-3-oxopropionate reductase	0.5/1.0	0.459	0.0213
MSMEG_5664	Peptidyl-prolyl cis-trans isomerase	0.5	0.28	0.0084
MSMEG_5672	Citrate synthase	0.5	0.419	0.0219
MSMEG_5721	Acetyl-CoA acetyltransferase	0.5	0.411	0.0175
MSMEG_5832	Phosphoribosylformylglycinamidine synthase subunit PurS	0.5	0.387	0.035
MSMEG_5866	Alcohol dehydrogenase B	0.5	0.354	0.0039
MSMEG_6036	Biphenyl-2,3-diol 1,2-dioxygenase	1.0	0.446	0.0217
MSMEG_6038	Acyl-CoA dehydrogenase, type 2, C-terminal domain protein	0.5	0.505	0.0303
MSMEG_6114	Inorganic pyrophosphatase	0.5	0.62	0.0175
MSMEG_6242	Formaldehyde dismutase / methanol dehydrogenase	0.5	0.465	0.0103
MSMEG_6256	Aspartate-semialdehyde dehydrogenase	0.5	0.573	0.0482
MSMEG_6257	Aspartokinase	0.5	0.578	0.0136
MSMEG_6271	2-isopropylmalate synthase	1.0	0.613	0.0446
MSMEG_6284	Cyclopropane fatty-acyl-phospholipid synthase	0.5	0.565	0.0004
MSMEG_6291	D-amino acid dehydrogenase	0.5	0.652	0.0338
MSMEG_6293	Transcriptional regulator, TetR family	0.5/1.0	0.493/0.555	0.0253/0.046
MSMEG_6391	Propionyl-CoA carboxylase beta chain	0.5	0.52	0.0359
MSMEG_6392	Polyketide synthase	0.5	0.55	0.0287
MSMEG_6393	Acyl-CoA synthase	0.5	0.537	0.0314
MSMEG_6398	Diacylglycerol O-acyltransferase / trehalose O-mycolyltransferase	0.5	0.33	0.0165
MSMEG_6458	Glutamate synthase, NADH/NADPH, small subunit	0.5	0.474	0.0273
MSMEG_6459	Ferredoxin-dependent glutamate synthase 1	0.5	0.523	0.0313
MSMEG_6511	Acyl-CoA dehydrogenase	0.5	0.396	0.0099
MSMEG_6512	Acyl-CoA dehydrogenase	0.5	0.521	0.0041
MSMEG_6532	Transcriptional regulator, TetR family	0.5/1.0	0.225/0.193	0.006/0.0461
MSMEG_6585	Acyl-CoA dehydrogenase	0.5	0.332	0.0149
MSMEG_6636	Superoxide dismutase	0.5	0.401	0.0072
MSMEG_6740	1-aminocyclopropane-1-carboxylate deaminase	0.5	0.292	0.0164

Table 3.4: Proteins absent in MSMEG_6526 Knockout but present in Wild Type

Protein	Description	OD_{600}	PSM[a]	*Sum Peptide score*
MSMEG_0069	Translation initiation factor IF-2 protein	1.0	6	8.695
MSMEG_0085	PTS system, Fru family protein, IIABC components	0.5	9	12.603
MSMEG_0158	Formyl-CoA:oxalate CoA-transferase	1.0	6	12.799
MSMEG_0270	Aminoglycoside phosphotransferase	0.5	5	6.164
MSMEG_0409	Acyltransferase, PapA3	0.5	11	21.974
MSMEG_0417	Succinate dehydrogenase iron-sulfur subunit	1.0	9	14.586
MSMEG_0418	Succinate dehydrogenase flavoprotein subunit	0.5/1.0	5/5	6.932/14.493
MSMEG_0422	PEP phosphonomutase	1.0	5	10.81
MSMEG_0833	Transcriptional regulator, Fis family	0.5	7	11.277
MSMEG_0909	Acyl-ACP thioesterase	0.5/1.0	7/5	12.068/18.359
MSMEG_0924	Nitrilase/cyanide hydratase and apolipoprotein N-acyltransferase	0.5	5	12.329
MSMEG_1350	Cyclopropane-fatty-acyl-phospholipid synthase 1	1.0	6	9.793
MSMEG_1621	Pyrimidine-specific ribonucleoside hydrolase rihA	1.0	3	7.392
MSMEG_1679	AmiB	0.5	7	9.653
MSMEG_1819	N5-carboxyaminoimidazole ribonucleotide synthase	0.5	5	9.826
MSMEG_2271	Hydrogenase accessory protein, HypB	0.5	6	7.46
MSMEG_2357	Cysteine desulfurase	1.0	6	8.222
MSMEG_2529	Glyoxylate reductase	0.5	3	11.342
MSMEG_2900	2-hydroxy-6-oxo-6-phenylhexa-2,4-dienoate hydrolase	1.0	4	6.034
MSMEG_2959	4-aminobutyrate aminotransferase	1.0	6	8.876
MSMEG_3094	Galactitol-1-phosphate 5-dehydrogenase	1.0	6	12.658
MSMEG_3201	Nicotinate-nucleotide pyrophosphorylase, NadC	0.5/1.0	4/4	5.772/8.369
MSMEG_3225	Ferredoxin-dependent glutamate synthase 1	0.5	5	7.986
MSMEG_3226	Glutamate synthase, NADH/NADPH, small subunit	0.5	6	9.384
MSMEG_3422	D-lactate dehydrogenase, NAD-binding protein	1.0	3	6.932
MSMEG_3602	D-ribose ABC transporter ATP-binding protein	1.0	4	10.634

MSMEG_3626	Urease subunit beta	0.5	9	8.123
MSMEG_3738	GTPase, Der	0.5	3	8.991
MSMEG_3873	Cobalamin biosynthesis protein cobIJ	1.0	6	14.431
MSMEG_4117	2-deoxy-D-gluconate 3-dehydrogenase	1.0	3	1.265
MSMEG_4231	UDP-N-acetylmuramoyl-tripeptide--D-alanyl-D-alanine ligase	0.5	6	14.355
MSMEG_4232	UDP-N-acetylmuramoyl-L-alanyl-D-glutamate--2,6-diaminopimelate ligase	1.0	4	11.327
MSMEG_4320	Alkyl hydroperoxide reductase	1.0	4	7.777
MSMEG_4471	MarR-family protein transcriptional regulator	0.5/1.0	5/7	8.818/10.457
MSMEG_4932	UDP-N-acetylglucosamine 1-carboxyvinyltransferase	0.5/1.0	6/9	6.386/11.08
MSMEG_4977	3'(2'),5'-bisphosphate nucleotidase	0.5	6	10.147
MSMEG_5243	FAD-binding FDOR	0.5	4	2.77
MSMEG_5413	Exopolyphosphatase	0.5	4	8.247
MSMEG_5423	Transcription-repair-coupling factor, Mfd	0.5	4	4.628
MSMEG_5477	2-hydroxy-3-oxopropionate reductase	1.0	8	10.439
MSMEG_6024	Acetoacetyl-CoA synthase	0.5	9	15.301
MSMEG_6387	Indolylacetylinositol arabinosyltransferase, EmbC	0.5	5	7.803
MSMEG_6686	Acyl CoA dehydrogenase	0.5	4	8.68
MSMEG_6903	Transcriptional regulator, PadR family protein	0.5	7	10.763

[a]peptide-spectrum match

3.3.3 Growth Curves of Δ6526 on Central Metabolism Intermediates

To further investigate the effect of Δ6526 on the central metabolic pathways we compared the growth of wildtype *M. smegmatis* to the Δ6526 strain on compounds related to the Krebs, glyoxylate, and methylcitrate cycles (Fig 3.3). We observed that wildtype *M. smegmatis* was able to grow on all selected carbon sources, but Δ6526 was not able to grow on pyruvate or acetate (Fig 3.3a, b), precursors to the Krebs cycle and several amino acid metabolomic pathways. This suggests that MSMEG_6526 is conditionally essential to *M. smegmatis*. The Δ6526 strain was able grow on propionate, a precursor to the methylcitrate cycle, although had a 25% slower growth rate compared to the wildtype and a lower maximum OD_{600} reading of 0.93 ± 0.06 compared to the wild type with 1.17 ± 0.06 (Fig 3.3c). The Δ6526 strain was also able to grow on succinate, a key metabolite involved in the Krebs, glyoxylate, and methylcitrate cycle, but with a 33% slower growth rate compared to wildtype (Fig 3.3d). A difference in final cell density was observed when grown on succinate with the Δ6526 strain having a lower maximum OD_{600} reading of 1.36 ± 0.06 compared to the wildtype maximum OD_{600} reading of 1.83 ± 0.15. These growths are similar to the previous growth curves above (glucose, glycerol, and butyrate). This suggests that these compounds as carbon sources can use an alternative pathway whereas pyruvate and acetate cannot.

The Δ6526 strain can recover growth when glycerol is added to the culture that has been incubated with acetate or pyruvate as the sole carbon source. As the Δ6526 strain cannot grow on acetate or pyruvate, we wanted to investigate if this is due to cell's inability to utilise a pathway that relies on these compounds, or if there was an accumulation of a toxic compound due to the loss of MSMEG_6526. To investigate this, we grew the Δ6526 strain for 100 h and then added glycerol to examine any effect (Fig 3.4). We also grew wildtype strain on acetate as a positive control. Both the wildtype and the Δ6526 strain grew as previously shown (Fig 3.3a), while the addition of glycerol to the Δ6526 strain allowed growth to recover. We also observe a higher growth reading for the Δ6526 with glycerol than the wildtype strain on acetate as different carbon sources dictate different growth rates and cell density as seen in figure 3.1. The recovery of growth by the Δ6526 strain incubated on acetate implies that the lack of growth is not due to cell death by the accumulation of a toxic compound, as we would expect no growth recovery due to the death of cells if that was the case. We therefore predict that the inability to grow is due to the inhibition of a pathway by the lack of MSMEG_6526 that utilises acetate. This pathway seems to be bypassed if a carbon source earlier in the pathway is available, such as glycerol.

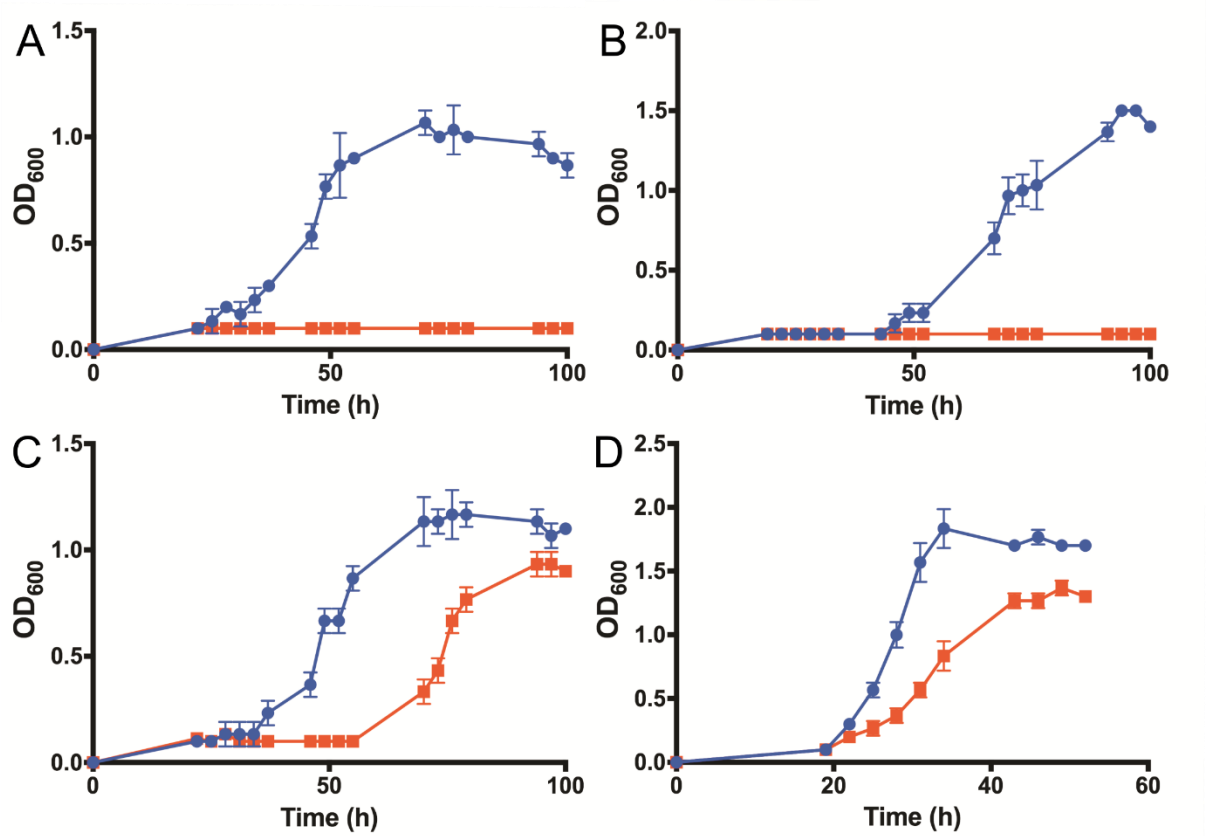

Figure 3.3 Growth rates of wildtype and Δ6526 *M. smegmatis* on different carbon sources. The measured optical densities of wildtype (blue) and Δ6526 (red) at the given timepoints when grown in HdB minimal media containing 25 mM acetate (a) pyruvate (b), proprionate (c), or succinate (d). All conditions contained 0.05% (w/v) tyloxapol to avoid clumping. Error bars represent standard deviations from three biological replicates.

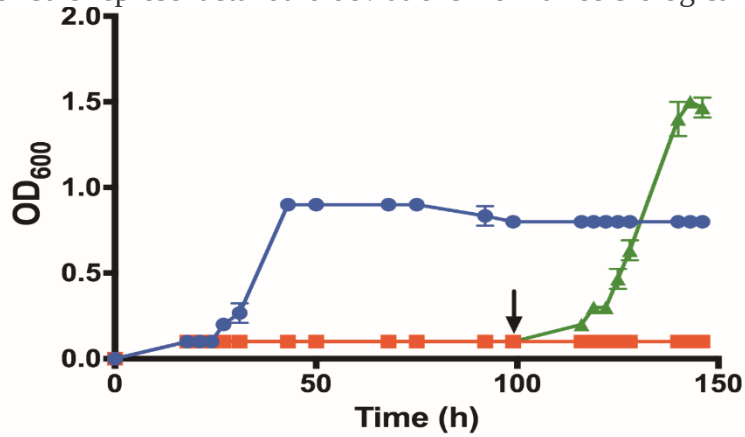

Figure 3.4 Growth of Δ6526 on acetate can be restored by other carbon source. The measured optical densities of wildtype (blue), Δ6526 (red), Δ6526 with 0.2% Glycerol at 100 h (green) at the given timepoints when grown in HdB minimal media containing 25 mM Acetate. The black arrow indicates when glycerol to a final concentration of 0.2% was added. All conditions contained 0.05% (w/v) tyloxapol to avoid clumping. Error bars represent standard deviations from three biological replicates.

3.3.4 The Change in the Metabolome of Δ6526

To investigate the changes to the metabolome when grown on acetate, we grew both wildtype and Δ6526 on glycerol until the exponential growth phase and switched the carbon source to acetate and analysed the change in the metabolome (Table 3.5). We first analysed changes that were observed in both strains as that would suggest effects caused by the carbon source change to acetate. This included the accumulation of several metabolites directly involved in the Krebs cycle including citrate, aconitate, and fumarate. Arginine and tyrosine, amino acid precursors to fumarate, were also accumulated in both stains. The accumulation of these metabolites seen in both strains would suggest that when grown on acetate the Krebs cycle is limited, as seen in our proteomics. This may also explain the slower growth rate on acetate compared to glycerol (Fig 3.1, 3.2). The ability to synthesis pyruvate may also effect the energetics of the cell grown on acetate as homoserine, threonine, glycine, and serine, which all form one pathway that synthesises pyruvate, and are accumulated in both strains.

In the Δ6526 strain, the glutamate metabolomic pathway was affected with the accumulation of the key metabolites 2-ketoglutaric acid, 4-aminobutyric acid (GABA), and glutamate. This complements our proteomics, as we saw this entire pathway downregulated in Δ6526. We observed several pathways that were related to glutamate metabolism being affected by Δ6526. This included the metabolism of lysine, which was accumulated in Δ6526, where one of the two biosynthetic pathway has 2-ketoglutarate as a precursor. Aspartate was also accumulated in Δ6526, and is involved in serval other amino acid pathway but is also a metabolite involved in lysine's second biosynthesis pathway. Proteins involved in aspartate metabolism, aspartokinase and aspartate-semialdehyde dehydrogenase were also downregulated in Δ6526. We also observed the accumulation of the lysine degradation product, N^6-acetyllysine, which was not detected in the wildtype at all and was not detected in Δ6526 when grown on glycerol. 2-ketoglutarate can be reduced to 2-hydroxylglutarate to feed into butanoate metabolism. We observed that in the wildtype strain that this compound was accumulated but was not affected in Δ6526 suggesting the knockout could be affecting the butyrate metabolism as well amino acid metabolism. Interestingly, as Δ6526 was also not able to grown on pyruvate, we observe accumulation of the valine, and isoleucine. These amino acids have pyruvate as a precursor and degradation product.

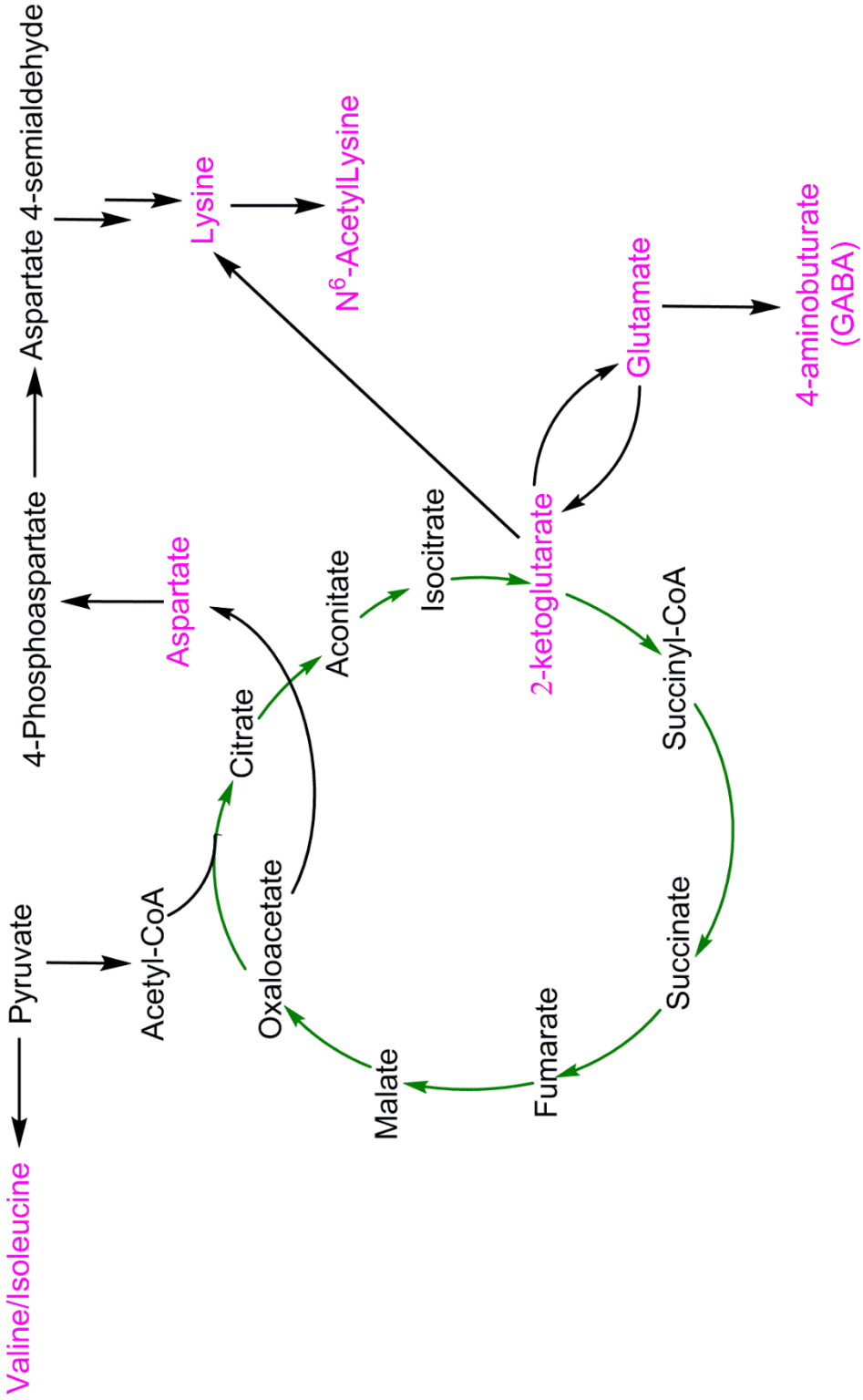

Figure 3.5 Summary of the Metabolomics. Diagram of the pathways affected by the Δ6526 strain. Metabolites that were accumulated in just the Δ6526 strain when grown on acetate are presented in pink. The Krebs cycle is represented in green arrows.

Table 3.5: Change in metabolome when grown in acetate

Metabolite	Strain	Fold Change[a]	*P* value[b]
2-Aminoethanol	Δ6526	1.428	0.0296
2-Aminopimelate	Wt/Δ6526	23.895/7.223	0.0327/0.0022
2-Hydroxyglutarate	Wt	1.562	0.0399
2-Ketoglutarate	Δ6526	4.831	0.0004
3-Aminoglutarate	Δ6526	1.594	0.0001
3-Aminopropanoate	Wt/Δ6526	0.142/0.569	0.026/0.0367
3-Methylglutarate	Wt	0.583	0.0406
4-Aminobutyrate	Δ6526	2.274	0.0004
4-Hydroxyproline	Δ6526	1.538	0.0008
5-Hydroxymethyl-2-furoate	Δ6526	0.882	0.0463
Aconitate	Wt/Δ6526	Upregulated/5.011	na/0.0023
Adenine	Δ6526	1.695	0.0094
Adenosine	Δ6526	3.078	0.0034
Arginine	Wt/Δ6526	2.539/11.937	0.0272/<0.0001
Aspartate	Δ6526	1.595	0.0001
Benzoate	Δ6526	0.786	0.0072
Citrate	Wt/Δ6526	22.984/7.405	0.0286/0.0024
Cystathionine	Δ6526	2.576	0.0075
Cytosine	Δ6526	1.417	0.0284
Decanoate	Wt	0.591	0.0389
Dihydroxyacetone phosphate	Δ6526	2.117	0.0022
Erythrulose	Δ6526	14.029	<0.0001
Fumarate	Wt/Δ6526	2.753/3.431	<0.0001
Glucono-1,5-lactone	Δ6526	2.014	0.0002
Glutamate	Δ6526	1.582	0.0012
Glutamine	Δ6526	3.422	0.0202
Glycerol 2-phosphate	Δ6526	1.705	0.0038
Glycerol 3-phosphate	Δ6526	2.126	0.0021
Glycine	Wt/Δ6526	8.47/3.744	0.0043/0.0014
Guanine	Δ6526	1.711	0.0082
Homocysteine	Δ6526	2.498	0.0030
Homoserine	Wt/Δ6526	9.581/21.61	0.0069/0.0014
Hydroquinone	Δ6526	1.221	0.0365
Isoleucine	Δ6526	2.14	0.0047
Lysine	Δ6526	8.951	0.0010
Maleate	Wt/Δ6526	2.066/2.941	0.0123/<0.0001
Mesaconate	Wt	2.854	0.0262
Methionine	Δ6526	2.016	0.0017

N^6-Acetyllysine	Δ6526	Upregulated	na
N-Acetylaspartate	Wt/Δ6526	23.642/17.886	0.0095/0.0006
Niacinamide	Δ6526	1.865	0.0213
Nicotinate	Δ6526	1.689	0.0356
Nonanoate	Δ6526	0.752	0.0126
Norvaline	Wt/Δ6526	2.316/11.342	0.006/0.0002
Octanoate	Wt/Δ6526	0.53/0.633	0.045/0.0022
Ornithine	Δ6526	12.914	0.0002
Proline	Wt/Δ6526	3.994/4.211	0.0097/0.0003
Protocatechuate	Wt	1.921	0.0203
Serine	Wt/Δ6526	3.71/3.372	0.0134/0.0017
Threonine	Wt/Δ6526	7.735/9.712	0.0029/<0.0001
Thymine	Wt	0.338	0.0405
Tryptophan	Δ6526	2.326	0.0011
Tyramine	Δ6526	8.598	0.0011
Tyrosine	Wt/Δ6526	2.967/3.375	0.0196/0.0002
Valine	Δ6526	2.746	0.0008

[a] upregulated is defined as only being present in the samples when switched to acetate as a carbon source

[b] na = *P* value cannot be calculated for upregulation due to lack of compound present in the reference sample

3.3.5 The Structures of MSMEG_6526 and Rv0121c

The apo structure of MSMEG_6526 has been previously solved and published with little comment (Ahmed *et al.*, 2015). To expand our understanding of the structural aspects of MSMEG_6526, we solved the structure with F_{420} bound at a resolution of 1.7 Å. As expected the structure revealed a split β-barrel fold homodimer. The asymmetric unit contained 3 homodimers with F_{420} bound with only one molecule of F_{420} having electron density past the phosphate group, containing two well-resolved glutamate moieties. F_{420} in mycobacteria typically has a chain lengths of five to eight glutamates (Bair *et al.*, 2001). The lack of electron density for the full molecule of F_{420} can be explained by the flexibility of the glutamate chain (Ahmed *et al.*, 2016). We also solved the structure of the *M. tuberculosis* orthologue, Rv0121c at a resolution of 2.99 Å, to compare structural aspects and to enable us to be able to perform structure based drug design. The structure revealed a split β-barrel fold monomer, although the native homodimer can be generated by crystal symmetry. Residues 41 to 47 and 58 to 67 had no discernible electron density, which is most likely due to disorder in the crystal. This may also explain why density corresponding to F_{420} was not clearly visible in the structure. It is also possible that $F_{420}H_2$ would be the preferred bound co-factor, as it is the form that is used when reducing substrates but since F_{420} is present in the MSMEG_6526 structure. Despite this, $F_{420}H_2$ would be difficult to get in a crystal structure as it will oxidise too quickly before obtaining crystal and would have to be done in an anaerobic or harsh reducing conditions. F_{420} is also present in other FDOR structures (Ahmed *et al.*, 2015) and therefore it may be possible to get a structure of Rv0121c with F_{420} by improving the crystal used to diffract.

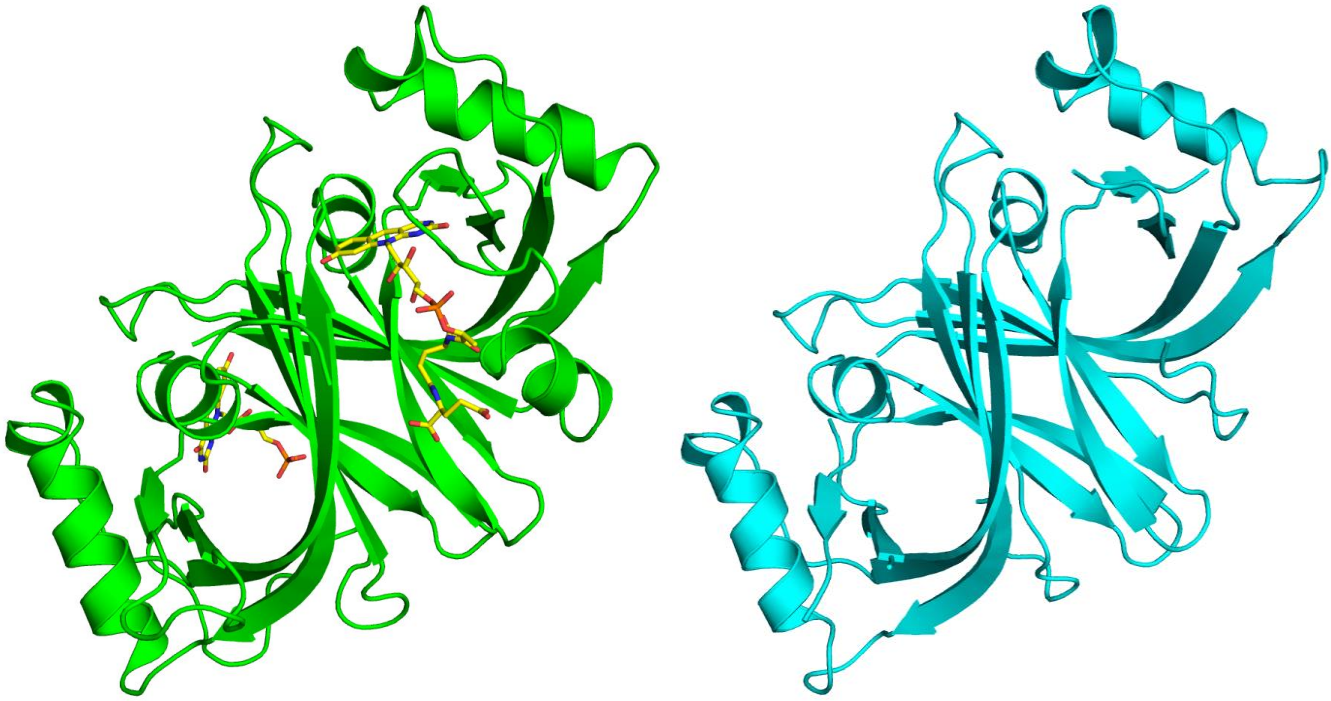

Figure 3.6 Structures of MSMEG_6526 and Rv0121c. Structure of MSMEG_6526 (green) with bound F_{420} (yellow) at 1.7 Å resolution and structure of Rv0121c (cyan) at 2.99 Å resolution.

Crystal	**MSMEG_6526**	**Rv0121c**
PDB ID	**5JV4**	**To be submitted**
Data collection		
Space group	C 1 2 1	H 3 2
Unit-cell parameters		
a, b, c (Å)	139.95, 82.24, 75.98	98.74, 98.74, 76.41
α, β, γ (°)	90, 90.85, 90	90, 90, 120
Wavelength (Å)	0.9501	0.953735
Resolution range (Å) [a]	75.97- 1.7 (1.74-1.7)	37.31-2.99 (3.17– 2.99)
Total reflections [a]	360146 (17700)	43353 (7408)
Unique reflections [a]	96899 (6750)	3004 (475)
Completeness (%)[a]	99.9 (99.9)	100 (100)
Multiplicity [a]	3.7 (3.7)	14.4 (15.6)
R_{merge} [a]	0.122 (0.803)	0.525 (2.985)
R_{pim} [a]	0.075 (0.482)	0.144 (0.778)
Mean $\langle I/\sigma(I)\rangle$ [a]	6.6 (1.7)	4.3 (0.9)
$CC_{1/2}$ [a]	0.986 (0.626)	0.994 (0.445)
Refinement		
R_{work} / R_{free}	0.189/0.231	0.2242/0.3264
No. of Macro molecules	6	1
Number of atoms (all)	7362	973
Protein	6544	962
Water molecules	542	11
Ligands	276	0
B-factor (Å^2)		
Main chains	26.30	72.9
Water molecules	28.00	71.7
Ligands	27.30	0
RMSD		
Bond Lengths (Å)	0.018	0.011
Bond Angles (°)	1.831	2.05
Ramachandran plot regions (%)		
Favored	98	88.7
Allowed	2	10.43
Outliers	0	0.87

[a]Values in parentheses are for the highest-resolution shell.

The structure of MSMEG_6526 contained three enlarged loops that seem to be unique to these proteins as highlighted in Figure 3.5a. We have designated these loops as I (residues 38 to 46), II (residue 52 to 62), and III (residue 81 to 88). Loop I is not involved in the active site and seems to have no involvement in the catalytic reaction based on placement. This loop most likely has no structural importance as the residues between MSMEG_6526 and Rv0121c are not conserved (Fig 3.5c). Loop II and III flank both sides of the active site and create a more define and smaller active site compared to other FDORs (Fig. 3.5a). Loop II creates a hinge that has an open and closed conformation over the active site when F_{420} binds, and loop III flanks the opposite side of the active site with no notable conformational changes (Fig 3.5b). Both of these loops are conserved between MSMEG_6526 and Rv0121c. Aligning Rv0121c to MSMEG_6526 shows the active site is highly conserved (Fig 3.7D). Except for aspartate 53 and lysine 55, which seem to have different conformations between the two structures. This will probably be due to the position of loop II as we observed these two residues are in different conformations in the active site depending if loop II is in the closed or open state. The position of lysine 55 when the loop is in the closed conformation is siting over the F_{420} and therefore most likely in a different conformation when a substrate is bound.

To investigate the substrate that can be utilised by these enzymes, we performed high throughput *in silico* docking of MSMEG_6526:F_{420} with the KEGG database. From the top 1000 hits, we observed two pathways that contain a high level of hits within the top substrates docked, aromatic amino acid biosynthesis and nucleic acid metabolism. The docking of both these pathways as demonstrated by 3-dehydroshikimate (Fig 3.8a), a key precursor in aromatic amino acid biosynthesis, and guanine (Fig 3.8b), are shown to involve aromatic rings that allow for pi stacking between F_{420} and Trp85. The docking also revealed that the residues Tyr120 and Asp53 are important in binding these substrates. Tyr120 interacts with the hydroxyl groups of 3-dehydroshikimate while this residue interacts with the carbonyl group of guanine and the Asp53 interacts with the nitrogen groups. Unfortunately, binding assays of tyrosine, tryptophan, phenylalanine, shikimate, and 3-dehydroshikimate with MSMEG_6526 and F_{420} revealed no binding, and activity assays did not reveal any activity (data not shown). Several of nucleotide metabolism substrates have been shown to have no activity with MSMEG_6526 including all the dNTPs, xanthine, hypoxanthine, caffeine and adenosine (Greening *et al.*, 2017). Interestingly, in the crystal structure of MSMEG_6526 we found the crystallisation agent 2-Mehtyl-2,4-pentadiol (MPD) present in all the active sites with open conformations (Fig 3.8c). This revealed that despite the bias towards compounds containing aromatic rings

found in our *in silico* docking, MSMEG_6526 can bind aliphatic substrates. This could allow it to bind other aliphatic compounds, such as carboxylic acids found in the Krebs cycle.

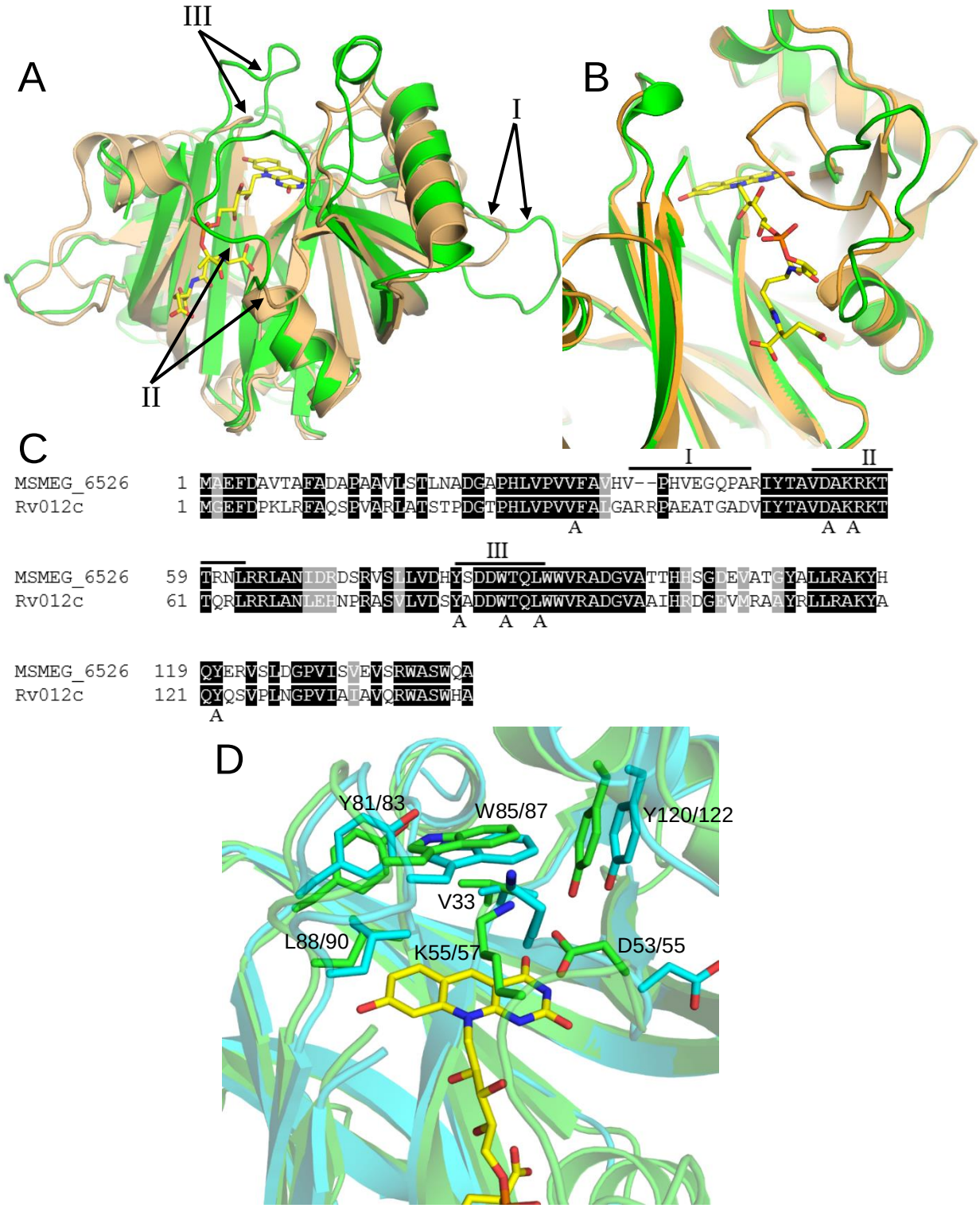

Figure 3.7 Structural aspects and comparisons of MSMEG_6526 and Rv0121c. (a) Structural comparison of MSMEG_6526 (green) with F_{420} (yellow) and Rv2074 (PDB ID: 5JAB) (orange) highlighting difference in loop size as indicated by arrows. (b) Comparison of MSEG_6526 with F_{420} (yellow) in a closed (orange) and open state. (c) Sequence alignment of MSMEG_6526 and Rv0121c shaded black for identical residues, and grey for similar residues. Lines above sequence indicate the region relating to the loop indicated, active site residues are indicated by A below the sequence. (d) Comparison of the active site residues of MSMEG_6526 (green) with F_{420} (yellow) and Rv012c (cyan)

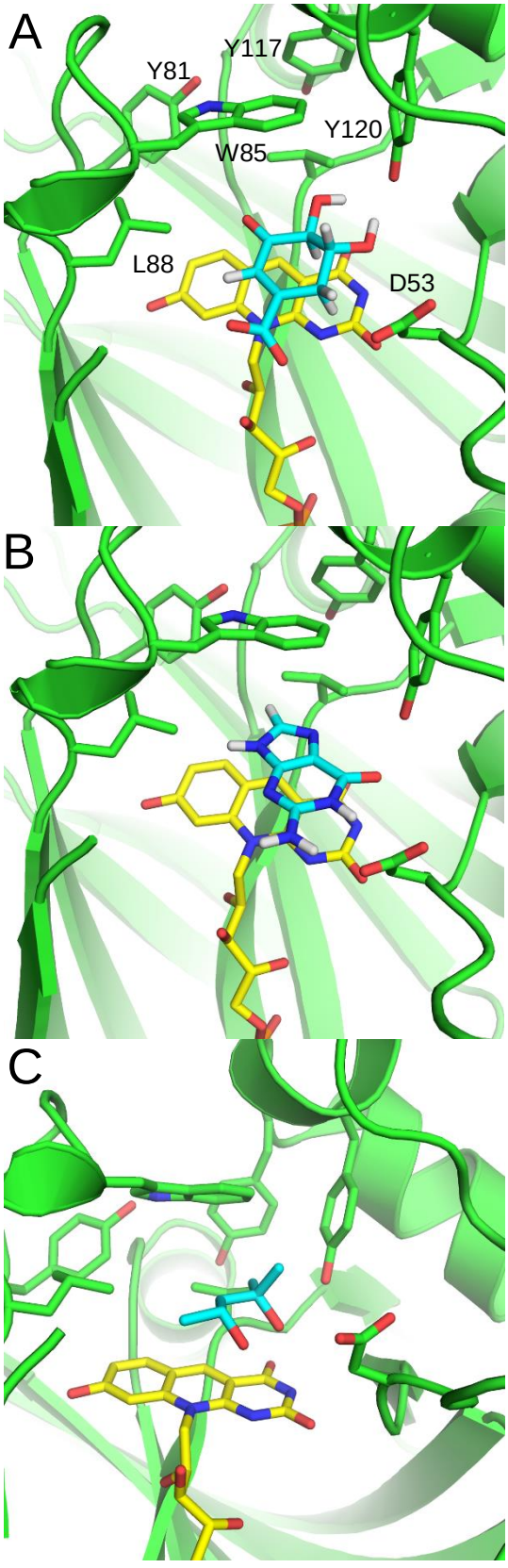

Figure 3.8 Binding of substrates in MSMEG_6526 active site. *In silico* docking of 3-dehydroshikimate (A) and guanine (B) into the active site of MSMEG_6526 with F_{420} bound. The binding of 2-Mehtyl-2,4-pentadiol (C) into the active site of MSMEG_6526 with F_{420} bound as found in the crystal structure.

3.4 Discussion

In this study we explored the role of MSMEG_6526 in *M. smegmatis* as a model to understand the role of Rv0121c in *M. tuberculosis*. We showed that that MSMEG_6526 was conditionally essential as the MSMEG_6526 knockout was not able to grow on acetate or pyruvate and had a slower growth rate compared to the wildtype when grown on other carbon sources. Due to this, it is probable that MSMEG_6526 is involved in a conditionally important metabolomic pathway (such as would be required for emergence from dormancy) and the cell can use an alternative pathway if the carbon source supplied, such as glycerol or glucose, can utilise the alternative pathway. These data reveal that the pathway, which we are yet to fully identify, does not have an alternative if pyruvate or acetate are the only source of carbon. The data from Dr. Nick West showed that Rv0121c is essential in latent tuberculosis, therefore the pathway MSMEG_6526 is involved with is only used when the cell is in latency and does not have access to the other pathway. The effect of MSMEG_6526/Rv0121c should therefore be further explored for understanding the metabolism of mycobacterial is latency.

Proteomics and metabolomics were used to understand the underlying biochemical processes that happen in the Δ6526 phenotype and are summarised in Figure 3.6. Comparison of the proteome in wildtype and Δ6526 revealed that the central metabolism was highly affected with proteins displaying upregulation generally belonging to either the glyoxylate cycle or the methylcitrate cycle being upregulated. These cycles both allow the cell to utilised other substrates to be used for energy and synthesis of carbohydrates and amino acids when glucose is not available (Lorenz and Fink, 2002; Wang *et al.*, 2003; Upton and McKinney, 2007). This was complemented with the downregulation of several enzymes in the Krebs cycle showing that it was underutilised in the cell. Although this does not imply the that MSMEG_6526 is directly involved in the Krebs cycle as *M. smegmatis* has all the functioning enzymes needed for the Krebs cycle (Tian *et al.*, 2005) and previous studies have shown similar growth defects including lack of growth on acetate with the knockout of gluconeogenesis (Marrero *et al.*, 2010), suggesting that MSMEG_6526 is involved indirectly with the Krebs cycle. Interesting we saw the downregulation of citrate synthase, the first step in both the Krebs cycle and glyoxylate cycle, but as isocitrate lyase is also used in the methylcitrate cycle in mycobacteria, this suggest that the glyoxylate cycle is not being used and is being used primary in the methyl citrate cycle.

We complemented this by examining the metabolome of Δ6526 in acetate to identify the changes that stop it from growing. We observed the same pathways were affected as we observed in proteomics. Some of these changes happen in both strains and although these changes are not a direct effect of the Δ6526 strain, it helps understand the differences between carbons sources and why the knockout cannot grown on acetate while still being able to grow other carbon sources. As a result of acetate, we see the Krebs cycle is affected suggesting that acetate is not an effective energy source. This may explain why we see the wildtype grow slower on it compared to other carbon sources. As there seems to be lower energetics with acetate, the effect that Δ6526 causes may amplify this defect this making it too hard for the cell to grow. Within the Δ6526 strain we saw the glutamate pathway being affected which was also downregulated in the proteomics. Glutamate is important for many functions of the cell as it feeds into the Krebs cycle, but also feeds into other pathway including lysine biosynthesis that also seemed to be affected by the knockout. The first two steps into aspartate catabolism were downregulated in proteomics and aspartate itself was affected by Δ6526. Aspartate also feed into a separate pathway for lysine biosynthesis. Interestingly a degradation product of lysine, N^6-acetyllysine was only detected on Δ6526 when it had been grown on acetate suggesting that lysine metabolism may play a role in the function of MSMEG_6526.

The structures of both MSMEG_6526 and Rv0121c revealed the split β-barrel fold that defines the FDORs (Ahmed *et al.*, 2015). These structures also revealed three extended loops, two of which make a more defined active site compared to the structures of other FDORs that reveal less define, open active sites (Taylor *et al.*, 2010; Ahmed *et al.*, 2016). There is no immediate evidence for the function of the third loop that is not involved in the active site. It is possible it could be involved in other interaction, such as protein-protein interactions but as the loop is not conserved, it may not be important to the enzyme or the loop sequence is specific to the species. Since the active site of both enzymes are the same, it will allow the use of MSMEG_6526 to be used as a model for Rv0121c for further studies. These structures will allow for structure-based drug design, although the position of the loop when a substrate is bound will need to be further investigated to identify the position of the key lysine and aspartate in loop II. High throughput *in silico* docking revealed the binding of compounds containing aromatic rings and included substrates involved in the aromatic amino acid biosynthesis pathway and nucleic acid metabolism. Binding and activity assays showed that MSMEG_6526 is not associated with these compounds. Although the docking did not reveal the physiological substrate, the data from the docking study may help for a starting point of identifying potential

inhibitors once activity is found. However, the position of loop II will need to be identified to account for all of the interactions of residues in the active site. Despite this, the crystal structure revealed the binding of MPD, an aliphatic compound that is structurally similar to compounds related to the Krebs cycle. This reveals that despite our omics data not containing pathways that contain aromatic substrates, it is feasible for MSMEG_6526 to bind compounds found in our omics data.

Our findings have implications in the understanding of the metabolism of mycobacteria that can allow for the development of a new novel treatment against tuberculosis. As the burden of TB is becoming more apparent with the rise of drug resistance, there is a need for new novel treatments. The distribution of F_{420}-dependent enzymes can allow for very specific targeting, and with our data revealing the importance of MSMEG_6526/Rv0121c to mycobacteria, we have reveal a new potential target. The WHO has announced as part of their End TB strategy that eliminating latent tuberculosis, especially in areas where HIV/AIDS is prevalent, is a key step (WHO, 2016). Since Rv0121c is essential to tuberculosis in latency, this research can be helpful in the development of new treatments to preventing more active infections arising from those already affected. Future studies to discover the role and function of MSMEG_6526/Rv0121c in mycobacteria will allow for the understanding of its unique biology in latency. This will allow us to set up system that can test new compounds and have a true understanding of the treatment that this will allow us to develop.

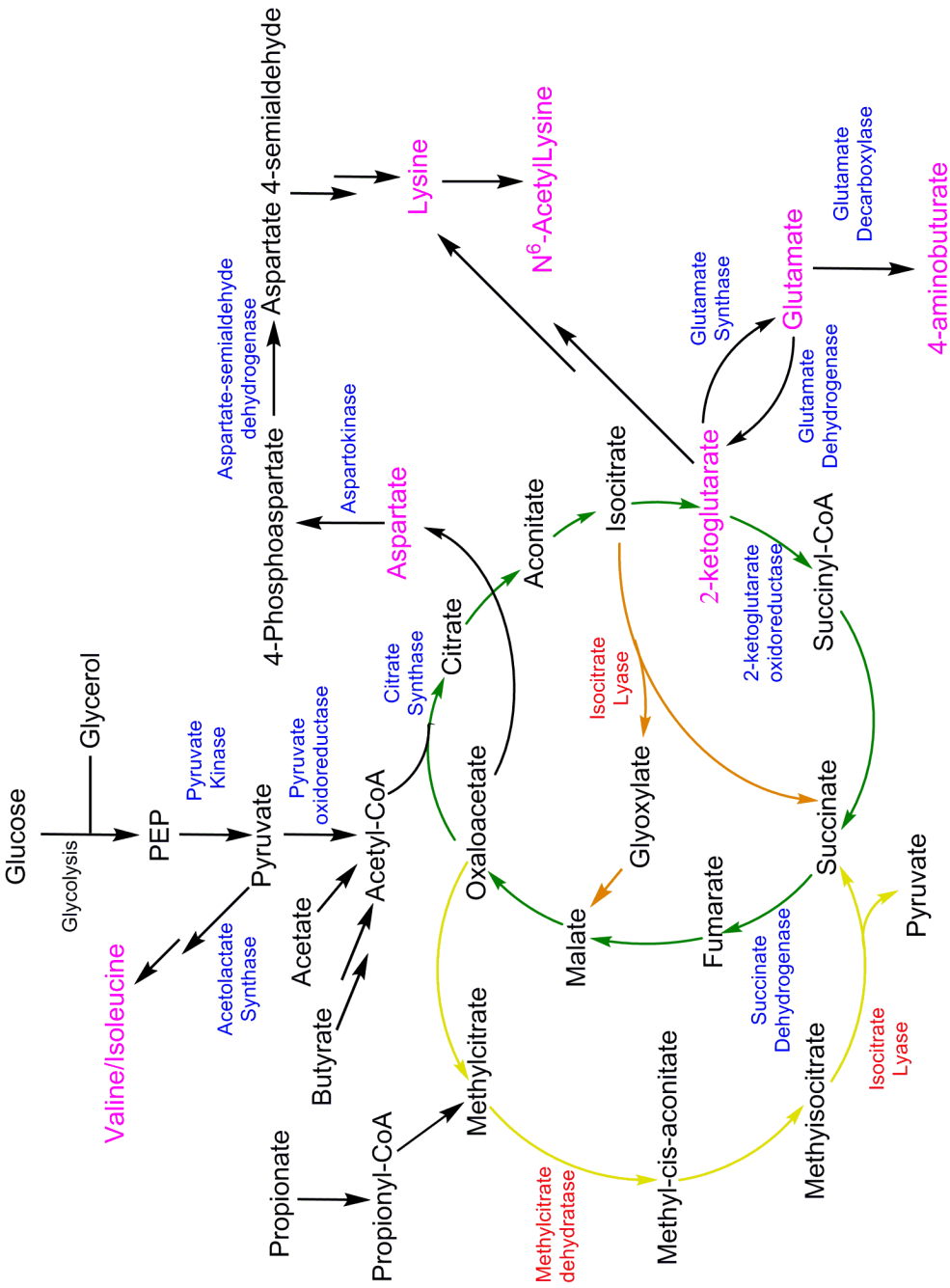

Figure 3.9 Summary of the Proteomics and Metabolomics. Diagram of the pathways affected by the Δ6526 strain. Upregulated proteins are presented in red, Downregulated proteins are represented in blue. Metabolites that were accumulated in Δ6526 strain when grown on acetate are represented in pink. The Krebs cycle is represented in green arrows, glyoxylate cycle is represented in orange arrows, and the methylcitrate cycle is represented in yellow arrows.

Chapter 4

Structure and Function Classification of Flavin/Deazaflavin Oxidoreductases

4.1 Introduction

The flavin/deazaflavin oxidoreductase (FDOR) superfamily in *Mycobacteria* has a large number of enzymes separated into three groups: FDOR-A, FDOR-AA, and FDOR-B (Taylor *et al.*, 2010; Lapalikar *et al.*, 2012). Ddn (Rv3547) was the first described FDOR and was discovered because it is responsible for activating the prodrug pretomanid (Ujjini H Manjunatha *et al.*, 2006). After the discovery of Ddn, 28 proteins that utilised F_{420} in *M. tuberculosis*, including FDORs, were identified using phylogenetic profiling and were separated into the following three families: the luciferase-like monooxygenase (LLM) family, the pyridoxamine 5'-phosphate oxidase (PNPOx) family, and the Ddn family (Selengut and Haft, 2010). During the same time Taylor *et al.* identified 30 Ddn and PNPOx homologues in *M. smegmatis* that were able to degrade aflatoxins using $F_{420}H_2$. Phylogenetic analysis divided the enzymes into two clades: FDOR-A (Ddn family), and FDOR-B (PNPOx family) (Taylor *et al.*, 2010). The FDOR-A clade was further divided into two groups, FDOR-A, and FDOR-AA, based on their ability to reduce aflatoxins (Lapalikar *et al.*, 2012). As well as phylogenetic profiling, several structures of FDOR-Bs have been solved including: Rv1155 (1W9A), Rv2074 (2ASF), Rv2991 (1RFE), and MSMEG_3380 (3F7E) (Canaan *et al.*, 2005; Biswal *et al.*, 2006; Taylor *et al.*, 2010). These structures have revealed that FDOR-Bs are dimers and contain a conserved split β-barrel fold despite sequence identify of less than 30%. Two structures of FDOR-As have been solved, MSMEG_3356 (3H96), and Ddn (3R5R) (Taylor *et al.*, 2010; Cellitti *et al.*, 2012). These structures show that FDOR-As contain the spilt β-barrel fold but are monomeric.

Despite the initial profiling of the FDORs, the physiological roles of these enzymes are generally unknown and there has been no systematic classification of FDORs that includes the potential cofactors FMN, FAD and heme. The only proposed physiological role for a FDOR is Ddn, which has been shown to reduce quinones and is proposed to protect the cell from oxidative stress (Gurumurthy *et al.*, 2013). To further the structure classification of FDORs, this chapter presents two published papers. The first paper classifies the sub-groups of FDOR-A, FDOR-AA, and FDOR-B by sequence, structure, function and co-factor preference. This is achieved using experimental spectroscopic assays, enzymatic assays, phylogenetic analysis, and structural comparison and analysis. The preliminary functions of several groups were

identified including $F_{420}H_2$-dependent fatty acid reductases, $F_{420}H_2$-dependent biliverdin reductases, heme oxygenases and potential electron transfer proteins.

The second paper reveals the physiological role of the *M. tuberculosis* FDOR-B Rv2074. This is achieved using enzymatic assays to identify activity and confirmed using NMR, and spectrum scanning to identity the product. The structure of Rv2074 with F_{420} bound was solved and *in silico* docking, molecular dynamics, and mutagenic studies were used to identify the binding mode of F_{420} and biliverdin, and catalytic mechanism was proposed. Using bioinformatics the abundance and distribution of F_{420}-dependent biliverdin reductases was identified.

4.2 Sequence–Structure–Function Classification of a Catalytically Diverse Oxidoreductase Superfamily in Mycobacteria

The following paper is presented in this chapter.

Sequence–Structure–Function Classification of a Catalytically Diverse Oxidoreductase Superfamily in Mycobacteria

F. Hafna Ahmed, Paul D. Carr , Brendon M. Lee, Livnat Afriat-Jurnou, A. Elaaf Mohamed, Nan-Sook Hong, Jack Flanagan, Matthew C. Taylor, Chris Greening and Colin J. Jackson

Journal of Molecular Biology 2015, 427(22): 3554-3571

Current status of paper: Published

Hafna Ahmed performed the majority of the experiments including all bioinformatics analysis, *in silico* substrate docking, and the majority of protein purification, crystallography, and assays. Paul Carr collected the crystallography data and helped with refinement. I analysed the *in silico* docking results from the high throughput screen performed by Jack Flanagan, I purified Rv1155, MSMEG_1981, and MSMEG_6526, and solved and refined the structure of MSMEG_6526. I designed and performed the biliverdin reduction assays with Rv1155 and MSMEG_3380 and performed the arachidonic acid binding and reduction assay with MSMEG_1981. Livnat Afriat-Jurnou helped with the initial FDOR classification and the development of experimental methods. Elaaf Mohamed purified the F_{420} used in the experiments and helped with the development of experimental methods. Nan-Sook Hong performed the binding assay for MSMEG_3880. Matthew Taylor assisted with the preparation and purification of F_{420}. Hafna Ahmed and Colin Jackson wrote the paper with input from all authors.

Article

Sequence–Structure–Function Classification of a Catalytically Diverse Oxidoreductase Superfamily in Mycobacteria

F. Hafna Ahmed [1], Paul D. Carr [1], Brendon M. Lee [1], Livnat Afriat-Jurnou [1], A. Elaaf Mohamed [1], Nan-Sook Hong [1], Jack Flanagan [2], Matthew C. Taylor [3], Chris Greening [3] and Colin J. Jackson [1]

*1 - **Australian National University Research School of Chemistry,** Sullivans Creek Road, Acton, ACT 2601, Australia*
*2 - **University of Auckland Faculty of Medical and Health Sciences,** 85 Park Road, Grafton, Auckland 2013, New Zealand*
*3 - **Commonwealth Scientific and Industrial Research Organisation Land and Water Flagship,** Clunies Ross Street, Acton, ACT 2060, Australia*

Correspondence to Colin J. Jackson: *colin.jackson@anu.edu.au*
http://dx.doi.org/10.1016/j.jmb.2015.09.021
Edited by M. Guss

Abstract

The deazaflavin cofactor F_{420} enhances the persistence of mycobacteria during hypoxia, oxidative stress, and antibiotic treatment. However, the identities and functions of the mycobacterial enzymes that utilize F_{420} under these conditions have yet to be resolved. In this work, we used sequence similarity networks to analyze the distribution of the largest F_{420}-dependent protein family in mycobacteria. We show that these enzymes are part of a larger split β-barrel enzyme superfamily (flavin/deazaflavin oxidoreductases, FDORs) that include previously characterized pyridoxamine/pyridoxine-5′-phosphate oxidases and heme oxygenases. We show that these proteins variously utilize F_{420}, flavin mononucleotide, flavin adenine dinucleotide, and heme cofactors. Functional annotation using phylogenetic, structural, and spectroscopic methods revealed their involvement in heme degradation, biliverdin reduction, fatty acid modification, and quinone reduction. Four novel crystal structures show that plasticity in substrate binding pockets and modifications to cofactor binding motifs enabled FDORs to carry out a variety of functions. This systematic classification and analysis provides a framework for further functional analysis of the roles of FDORs in mycobacterial pathogenesis and persistence.

Introduction

Flavin- and deazaflavin-dependent enzymes mediate a wide range of redox reactions in biological systems [1]. Flavin mononucleotide (FMN) and flavin adenine dinucleotide (FAD) are the most common flavins and are ubiquitous in all kingdoms. In addition to FMN and FAD, some bacteria and archaea synthesize and utilize a deazaflavin cofactor called F_{420} (Fig. 1) [2,3]. While these three compounds are structurally similar, they have markedly different redox properties: F_{420} has a lower reducing potential (−360 mV) than FMN and FAD (−210 mV) and is an obligate two-electron carrier [4]. The role of F_{420} is well defined in methanogenic archaea, where it is the primary catabolic electron carrier [5], but much less is understood about why certain aerobic actinobacteria synthesize and utilize this cofactor. In this phylum, F_{420} is synthesized from a riboflavin precursor by specific maturases (FbiA, FbiB, FbiC) [6] and is reduced by an F_{420}-dependent glucose-6-phosphate dehydrogenase (Fgd) [7]. In turn, $F_{420}H_2$-dependent reductases couple the re-oxidation of $F_{420}H_2$ to the reduction of a range of unsaturated organic compounds [8–10]. F_{420}-dependent processes appear to be particularly abundant in mycobacteria [8,9,11], including both pathogenic species such as *Mycobacterium tuberculosis* and environmental saprophytes such as *Mycobacterium smegmatis* [11]. Studies on *M. smegmatis* and *M. tuberculosis* have implicated F_{420} in mycobacterial persistence: the cofactor is required to combat reactive oxygen and nitrogen species [10,12–14] and plays a role in mycobacterial resuscitation after

0022-2836/

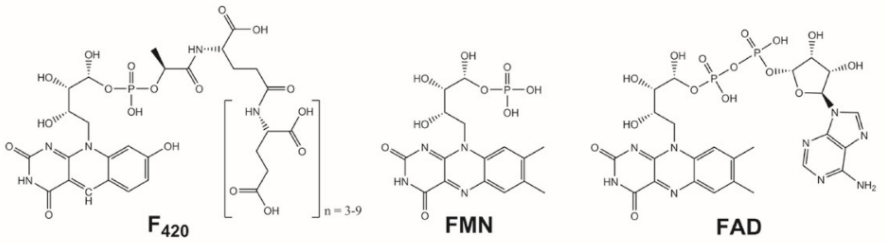

Fig. 1. Structures of F_{420}, FMN, and FAD. F_{420} is a deazaflavin while FMN and FAD are riboflavin based. All cofactors contain a ribityl moiety, which is followed by a phosphate in FMN, as well as adenosine diphosphate group in FAD and a phospholactate polyglutamate tail in F_{420}.

hypoxia-induced dormancy [10]. However, much is still to be understood about the physiological role of F_{420}-dependent proteins in mycobacterial metabolism.

Our previous work identified an enzyme superfamily, herein defined as the flavin/deazaflavin oxidoreductases (FDORs) (previously $F_{420}H_2$-dependent reductases; FDRs [8]), that bind F_{420} in mycobacteria [8,9,15]. For reasons still unclear, over 30 different FDOR homologs can be present in a single mycobacterial species [8,11,15]. As the largest known F_{420}-dependent protein family, it is assumed that the FDORs carry out the majority of the physiological roles of F_{420} in mycobacteria. These small, single-domain proteins adopt a split β-barrel fold, consisting of a cofactor binding channel and a substrate binding pocket [8,16,17]. The enzymes can be divided into FDOR-A and FDOR-B families, which have ~30% sequence identity but share the same structural fold [8]. Proteins from the FDOR-A family not only have been shown to reduce a wide range of quinones, suggesting a possible physiological role as menaquinone reductases [10], but also have been shown to promiscuously reduce coumarin derivatives (e.g., aflatoxins) in *M. smegmatis* [8,9] and activate bicyclic 4′-nitroimidazole antibiotics (e.g., PA-824/pretomanid) in *M. tuberculosis* [18,19]. A subgroup of proteins from the FDOR-A family, classified as FDOR-AAs, have no known activity [9]. As for proteins belonging to the more diverse FDOR-B family, there has been no functional annotation beyond the observation of very low promiscuous activity with aflatoxins [8,9]. While FDOR-As appear to be taxonomically restricted to mostly actinobacteria [11], enzymes homologous to FDOR-B proteins are found in many organisms, including those that do not synthesize F_{420}. They include the conserved FMN-dependent pyridoxine/pyridoxamine 5′-phosphate oxidases (PnPOx) involved in vitamin B_6 biosynthesis [20–22] and heme oxygenases (HugZ) that degrade heme to biliverdin [23,24]. The subsequent reduction of biliverdin to bilirubin (a potent antioxidant [25,26]) by biliverdin reductases can enhance mammalian and bacterial cell survival during oxidative stress [27–29] but has not been reported in mycobacteria or *via* an F_{420}-mediated process. These few characterized FDORs highlight the broad functional roles of split β-barrel proteins as oxidases (PnPOx), reductases (FDOR-A), and oxygenases (HugZ), as well as their diversity in their cofactor specificity (FMN, F_{420}, and heme).

Despite their potentially important physiological functions, there has been no systematic classification and functional annotation of the FDORs to date. In this work, we present an experimental and computational analysis of the FDORs present in mycobacteria, providing the first functional classification and annotation of this diverse protein family. To aid this, we have adopted the growing trend of using sequence similarity networks (SSN) to highlight structure–function relationships within protein families [30–34]. On this basis, we propose the expansion of the FDOR superfamily to include all split β-barrel oxidoreductases, including $F_{420}H_2$-dependent reductases, PnPOxs, heme oxygenases, and multiple uncharacterized clades. Since the chemistry underlying the catalytic functions of members of this superfamily will be determined by cofactor specificity [15], we have tested the cofactor preference of representatives of all subgroups, identifying specific clades with preferences for F_{420}, FMN, FAD, and heme. Functional annotation was performed through the use of high-throughput *in silico* substrate docking and the analysis of their conservation in various mycobacteria, genomic context, and cellular locations. This provided a basis for further characterization, leading us to identify fatty acid reductases within the FDOR-AAs and a novel class of biliverdin reductases within the FDOR-Bs through enzymatic and spectroscopic methods. In addition, we resolved the basis of differences in the cofactor and substrate specificities by solving four novel crystal structures of diverse members of this superfamily. In combination, these results have allowed us to describe a functional expansion of the flavin/deazaflavin oxidoreductase superfamily that may be essential in allowing mycobacteria to persist in otherwise hostile environments.

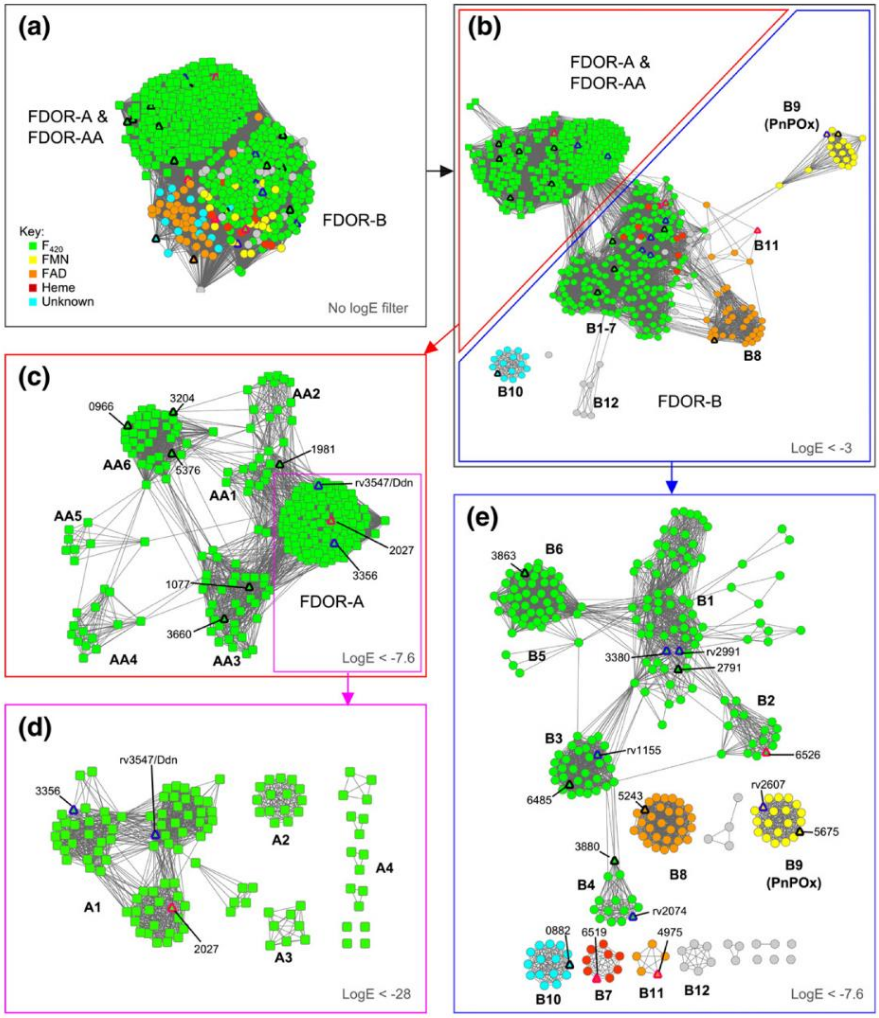

Fig. 2. SSN of mycobacterial FDORs. Each node represents an individual protein and edges represent *E*-values between proteins generated by BLAST [39]. Proteins from *M. tuberculosis H37Rv* (rv) and *M. smegmatis strain MC2 155* (numbers) expressed and purified in this study are annotated and marked as black triangles and those structurally characterised in this study are marked as pink triangles. Structures solved in previous studies are marked as blue triangles. Nodes are colored based on known cofactor specificities confirmed for homologous proteins in this study or previously. (a) SSN of FDORs including all relationships between proteins, showing the distribution of sequences to FDOR-As and FDOR-Bs. (b) Node clustering at a log*E* cutoff of −3, showing that FMN, FAD, and non-flavin-specific proteins are distantly related to the F_{420} binding proteins that form two large clusters. (c) Node clustering observed for FDOR-AAs at a log*E* filter of −7.6, showing the presence of five subgroups (AA1–AA6), as well as the conserved FDOR-A group. (d) Expansion of the FDOR-As where only relationships with log less than −28 are considered, showing the clustering of the FDOR-As into four subgroups (A1–A4) where the A1 subgroup comprises three main homologous clades and A4 includes proteins that do not cluster with any other subgroup. (e) Expansion of the FDOR-Bs where only relationships at a log*E* filter of −7.6 are considered, showing their division into 12 subgroups where the F_{420} binding subgroups B1–B6 are more closely related to each other and proteins with other cofactor specificities form individual clusters.

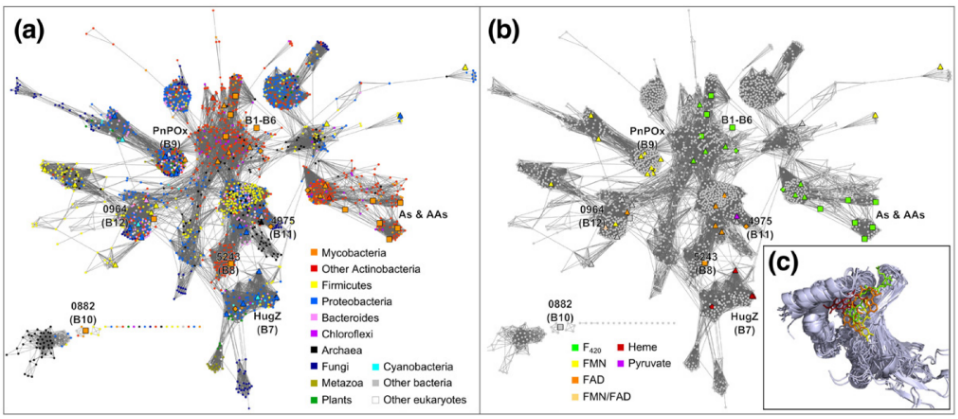

Fig. 3. Abundance of FDORs in different organisms (a) and cofactor preferences of characterised proteins (b). Clusters with associated functional characterization are identified, as well as subgroups from mycobacterial proteins identified in Fig. 2 (key proteins of unknown function from *M. smegmatis* are identified as numbers). Structurally solved proteins from previous work are marked as triangles, structures solved in this study are marked as diamonds, and the rest of the proteins characterised in this study are marked as squares. (c) Overlay of available PDB IDs of FDORs showing their conserved split β-barrel fold for cofactor binding. F_{420} molecule shown in green is from the structure of rv3547 (PDB ID: 3R5W) [16], FAD in orange is from MSMEG_4975, FMN in yellow is from the PnPOx of *E. coli* [46] (PDB ID: 1WV4), and heme in red is from HugZ [23] (PDB ID: 3GAS). Generated using the MUSTANG-MR Web server [47] at a sieving level of 2.0 Å, using the following PDB IDs: 1CI0, 1FLM [48], 1NRG [22], 1RFE, 1T9M [41], 1VL7, 1W3O [49], 1W9A [50], 1WV4 [46], 2A2J [51], 2ARZ, 2ASF [40], 2FG9, 2FHQ, 2FUR, 2HHZ, 2HQ9, 2HTD, 2HTI, 2I02, 2I51, 2IAB, 2IG6, 2OU5, 2RE7, 3BA3, 3DB0, 3DNH, 3EC6, 3F7E, 3GAS [23], 3H96 [8], 3IN6, 3R5L [16], 3R5Z [16], 3SWJ [24], 3TGV [52], 3U0I, 3U34 [53], 4HMW [43], and 4Y91 and 4YBN from this work.

Results

There are 22 FDOR subgroups in mycobacteria

In order to explore the roles of FDORs in mycobacteria, we retrieved and curated all sequences belonging to the split β-barrel superfamily from 18 mycobacterial species. A maximum-likelihood phylogenetic tree shows that all enzymes can be divided into two previously established major clades [8], namely the FDOR-As and FDOR-Bs (Fig. S1). However, in situations such as these, where there has been rapid evolutionary expansion, gene duplication, and horizontal gene transfer within a protein superfamily, phylogenetic trees lack robustness [35–37]. Indeed, we found that bootstrap support for the ancestral nodes was extremely low. We therefore used SSN to predict sequence–structure–function relationships in this large and divergent protein family without the phylogenetic evolutionary inference [31,33]. An SSN, in which edges represent all-*versus*-all BLAST *E*-values [38], supported the broad relationships identified by the phylogenetic analysis while providing detailed information about the relationships about subgroups (Fig. 2). We observed that, with no log*E* value filter, the FDOR-A and FDOR-AA groups immediately separate from the more diverse FDOR-B group (Fig. 2a). These broad groups separate into at least 22 different subclades: FDORs A1–A4, AA1–AA6, and B1–B12 (Fig. S2) when only close relationships between proteins (edges with log$E < -28$) were considered. Sequence identity within clusters was generally greater than 50%, although identity between clusters was as low as 30%, which is indicative of the great sequence divergence between homologs.

The FDOR-A proteins separate from the FDOR-AA proteins at a log*E* value of −7.6. The FDOR-As are closely related to each other and separate out at a log*E* filter of −28 to four smaller subgroups (A1–A4), which have less than 50% sequence identity between them (Fig. 2c and d). Consistent with a conserved physiological role, the A1 subgroup is present in almost all mycobacteria with up to three unique sequences per species, whereas the A2, A3, and A4 are more sparsely distributed (Fig. 2d and Fig. S2). Within the A1 subgroup, we see separation into three primary clusters that are closely related. While the FDOR-As form one tight cluster with four subgroups, their FDOR-AA homologs [9] separate into six clusters (AA1–AA6) when only edges with log*E* values less than −7.6 are considered (Fig. 2c). These clusters are just as distantly related to each other as to the FDOR-As. It is therefore possible that each of the FDOR-AA clusters has distinct physiological roles and potentially different substrates.

Table 1. Affinity (K_d) of mycobacterial FDORs for flavin cofactors

Group	Protein	K_d F_{420} (μM)	K_d FMN (μM)	K_d FAD (μM)	Specificity[a]
A1	MSMEG_2027	0.5 ± 0.1	26.1 ± 0.9	40.9 ± 3.9	0.02
AA1	MSMEG_1981	8.4 ± 2.2	40.0 ± 1.5	37.5 ± 6.2	0.22
AA3	MSMEG_1077	3.2 ± 0.4	30.9 ± 0.7	28.0 ± 5.1	0.11
	MSMEG_3660	8.7 ± 0.3	35.9 ± 1.0	27.7 ± 0.1	0.31
AA6	MSMEG_0966	7.3 ± 1.0	53.7 ± 9.2	42.8 ± 7.0	0.17
	MSMEG_5376	7.7 ± 1.9	39.0 ± 3.5	30.9 ± 5.1	0.25
	MSMEG_3204	8.4 ± 0.3	32.3 ± 5.3	37.1 ± 7.7	0.26
B1	rv2991	7.8 ± 0.9	27.9 ± 4.3	26.4 ± 1.4	0.30
	MSMEG_2791	12.0 ± 0.1	43.4 ± 4.9	39.5 ± 0.4	0.30
	MSMEG_3380	0.13[b]	24.9 ± 5.1	37.5 ± 0.6	0.01
B2	MSMEG_6526	1.8 ± 0.1	25.5 ± 3.8	32.4 ± 0.1	0.07
B3	rv1155	2.4 ± 0.4	28.1 ± 1.6	57.4 ± 0.8	0.09
	MSMEG_6485	10.8 ± 0.1	42.3 ± 1.6	48.3 ± 4.3	0.25
B4	MSMEG_3880	4.0 ± 1.3	32.7 ± 1.2	33.9 ± 11.4	0.12
B6	MSMEG_3863	4.4 ± 1.0	25.2 ± 4.6	23.1 ± 0.6	0.19
B8	MSMEG_5243	16.9 ± 1.2	27.7 ± 3.8	3.6 ± 0.2	0.21
B9 (PnPOx)	MSMEG_5675	15.9 ± 1.2	3.6 ± 0.6	42.9 ± 4.4	0.23
B10	MSMEG_0882	17.1 ± 2.5	39.4 ± 1.8	38.0 ± 2.3	**0.45**

K_d values were determined by measuring the quenching of intrinsic tryptophan fluorescence of the protein upon titration with increasing ligand concentrations.
[a] Specificity = K_d [primary]/K_d [secondary].
[b] From Taylor *et al.* [9].

Our results show that the FDOR-B group is even more diverse and that, at a low log*E* value of −3, the evolutionary conserved PnPOx family (B9), as well as four other uncharacterized subgroups (B8, B10, B11, B12), separates from a more tightly clustered central group containing the B1–B7 subgroups. When the log*E* value is increased to −7.6, we observed further separation into 12 subgroups (B1–B12) that are likely to have distinct functional roles (Fig. 2e). The largest subgroup is B1, which consists of many loosely related clusters, while the other groups form more tightly related clusters. These include the PnPOx (B9) and heme oxygenase (B7) clusters, given that they are clearly phylogenetically and structurally [23,40] related to the other members of the FDOR-Bs.

Having established the diversity of FDORs in mycobacteria, we also investigated the taxonomic distribution of FDORs beyond mycobacteria. To analyze the abundance and summarize our current knowledge of the FDOR protein family across different organisms, we generated an SSN of 2148 sequences from all available genomes from the Pfam database [41] using all-*versus*-all BLAST *E*-values (Fig. 3). The network consists of over 15 major clusters. It is immediately noticeable that several of these clusters are dominated by sequences from a minority of bacterial phyla. In particular, the FDOR-As, FDOR-AAs, FDOR-B1-B6s, and FDOR-B8 clusters are dominated by sequences from actinobacteria (including mycobacteria) and chloroflexi. Several clusters, notably the PnPOx family (B7), are distributed in the majority of bacterial phyla [42,43]. The heme oxygenases [44,45] are abundant in proteobacterial sequences but are only sporadically represented by sequences from other organisms, such as MSMEG_6519 from *M. smegmatis*. There are also several smaller conserved clusters dominated by fungal, metazoal, and archaeal sequences. This result highlights the potentially unique role that many of these FDORs play in mycobacterial physiology.

The FDOR superfamily includes F_{420}, FAD, FMN, and heme binding proteins

To gain insight into the functional basis of this diversity, we expressed and purified 16 previously uncharacterized FDORs from *M. smegmatis* across the FDOR-A/AA (MSMEG loci 2027, 1981, 1077, 3660, 0966, 5376, and 3204) and FDOR-B (MSMEG loci 2791, 3380, 6526, 6485, 3380, 3863, 6519, 0882, 5243, and 5675) families, including the putative PnPOx from *M. smegmatis* (MSMEG_5675). In addition, we also purified the FDOR-B proteins rv1155 (PDB ID: 4QVB [17]) and rv2991 (PDB ID: 2RFE) from *M. tuberculosis*, which have been structurally characterized but have no known enzymatic activity. The relative F_{420}, FMN, and FAD binding affinities of all proteins were measured (Table 1 and Figs. 2 and 3). These results revealed that, despite some degree of promiscuous binding with other flavins, the proteins are generally specialized to bind specific cofactors with high affinities.

All FDOR-A and FDOR-AAs subgroups are F_{420} specific, with K_d values for the cofactor between 0.5 and 12 μM (generally 5- to 10-fold lower than with FMN or FAD). In contrast, FDOR-Bs are more diverse and include F_{420}, FAD, FMN, and heme

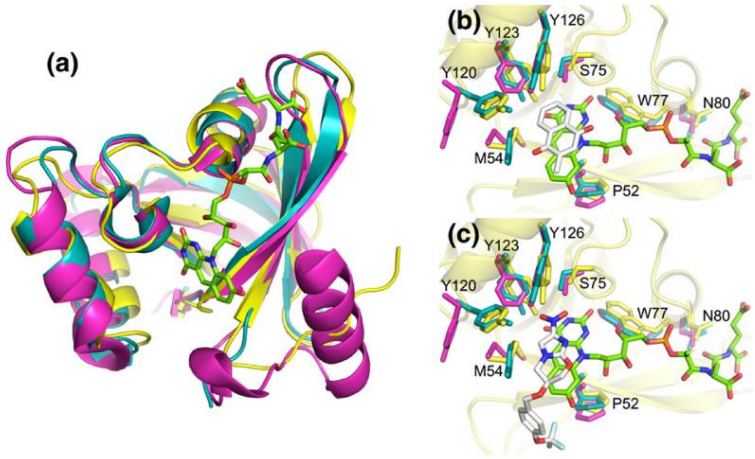

Fig. 4. Structural conservation in the FDOR-A1 subgroup. (a) Overlayed structures of MSMEG_2027 at 1.5 Å resolution (Δ26 at N-terminus, yellow), MSMEG_3356 (PDB ID: 3H96 [8], pink), and the complex of rv3547 with F_{420} (PDB ID: 3R5R [16], teal). (band c) Conserved residues at the cofactor and substrate binding site of the FDOR-As with menadione and PA-824 (respectively) computationally docked.

binding proteins (Fig. 2B and Fig. S3). The PnPOx MSMEG_5675 was specific for FMN (K_d = 3.6 μM) as expected, whereas MSMEG_5243 (B8) had a higher affinity for FAD (K_d = 3.6 μM) than other ligands. Reflecting its homology with heme oxygenases that catalyze heme degradation to biliverdin, MSMEG_6519 (B7) binds and coordinates heme (K_d = 13.2 ± 2.0 μM) and has less affinity for flavin or deazaflavin cofactors (Fig. S3 and Table 1). The accumulation of excess biliverdin in the MSMEG_6519 expression media and cell pellet produced a distinctive green color as previously reported for heme oxygenases [44,54]. Additionally, although it binds to heme with high affinity, the MSMEG_6519 co-purified with biliverdin (Fig. S3), consistent with heme being a substrate for this enzyme. MSMEG_4975 (B11) was also exceptional as it co-purified simultaneously bound both FAD and heme (Fig. S3). In contrast to MSMEG_6519, the heme molecule co-purified intact, suggesting that heme is more likely to be a cofactor than a substrate. MSMEG_0882 from subgroup B10 was an outlier; it did not have high specificity for any of the flavins nor heme tested and instead may bind a different, still unknown, ligand. Notably, it is also the most divergent of all the FDOR-B subgroups (Figs. 2 and 3). Based on these data, it is probable that homologous (>50% sequence) proteins that cluster with representative proteins from each FDOR subgroup in the SSN share the same cofactor preference: As, AAs, and B1-B6s bind F_{420}; B7s bind heme; B8s bind FAD; B9s bind FMN; B10s bind an unknown ligand; and B11s bind both heme and FAD.

FDOR-As

We subsequently elucidated potential substrate classes that various FDORs could function with in order to carry out functional annotation of this superfamily. Of the F_{420}-dependent split β-barrel proteins from mycobacteria, only the FDOR-A group has a proposed physiological role, as quinone reductases [8–10]. Whereas the A2, A3, and A4 subgroups are poorly conserved across mycobacteria, the largest subgroup A1 is present in almost all mycobacteria, indicating evolutionary conservation and a significant physiological role (Fig. 2D and Fig. S2). The A1 enzymes could be separated out into three clusters at a log*E* filter of −28 that can be represented by the pro-drug activating rv3547 from *M. tuberculosis* [10], MSMEG_2027, and MSMEG_3356 [8] (Fig. 2d and Fig. S2). We showed that all three representatives of this class can reduce the napthoquinone derivative menadione to menadiol in a $F_{420}H_2$-dependent manner with a high degree of catalytic efficiency (Table S4), as previously observed for the *M. tuberculosis* homologs [10]. The rates and affinities of each FDOR-A for menadione reduction differed (Table S4), which is similar to the quantitative differences in their activities against non-physiological coumarin substrates [8,9]. Only rv3547 showed any activity with the nitroimidazole pro-drug PA-824 (Table S4).

To gain more insight into the enzymes from the A1 subclusters, we compared the previously solved crystal structures of rv3547 [16] and MSMEG_3356 [8] with a 1.5-Å-resolution structure of MSMEG_2027 (Fig. 4a and Table S5). Comparison

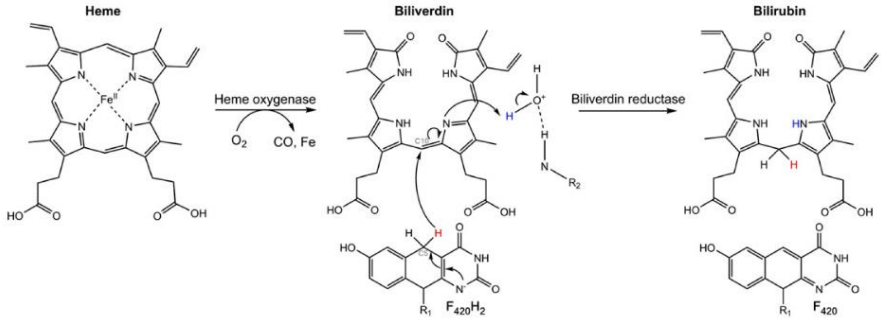

Fig. 5. Scheme for heme degradation to biliverdin and bilirubin. $F_{420}H_2$-dependent biliverdin reduction to bilirubin is based on the mechanism proposed by Smith *et al.* [66]. R_1 = ribityl, phospholactate, and polyglutamate chain; R_2 = amino acid.

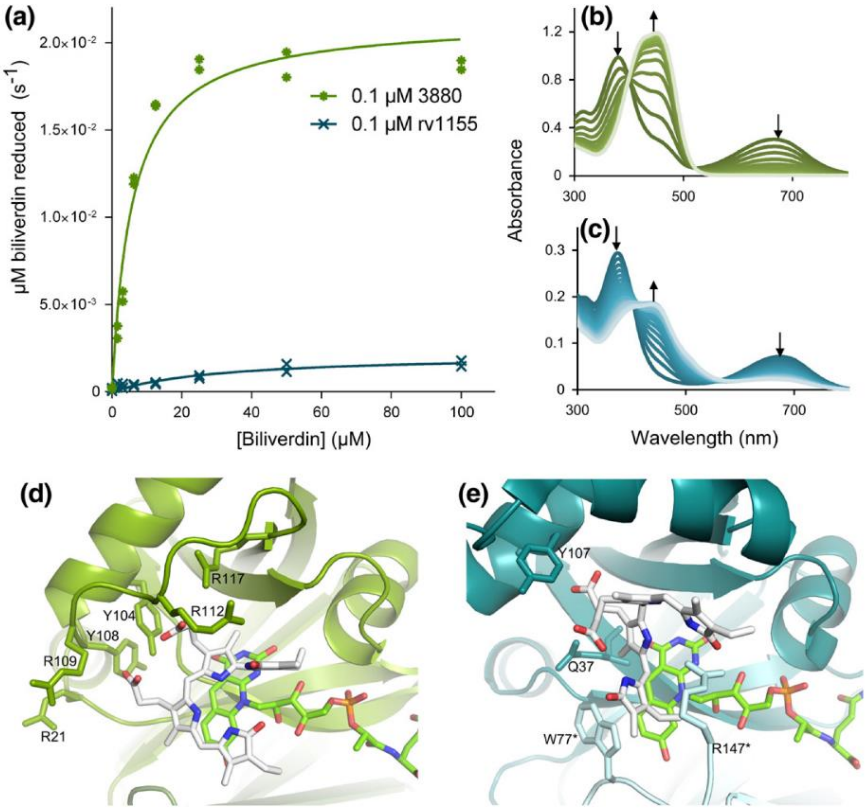

Fig. 6. Biliverdin reduction by the FDOR-Bs MSMEG_3380 and rv1155. (a) Biliverdin reductase activity by MSMEG_3880 (K_m = 5.7 ± 0.2 μM, K_{cat} = 2.1 × 10^{-1} ± 1.3 × 10^{-3} s^{-1}, andK_{cat}/K_m = 3.8 × 10^4 M^{-1} s^{-1}) and rv1155 (K_m = 33 ± 11 μM, K_{cat} = 2.2 × 10^{-2} ± 4.8 × 10^{-3} s^{-1}, andK_{cat}/K_m = 6.6 × 10^2 M^{-1} s^{-1}). Data presented are from two independent experiments. (b) Absorbance spectra over time (every 1 min for 15 min) showing biliverdin (25 μM) reduction by 50 nM MSMEG_3880. (c) Absorbance spectra over time (every 5 min for 3 h) showing biliverdin (6.25 μM) reduction by 10 μM rv1155. (d and e) Computational docking of biliverdin to the F_{420} complexes of rv2074 [40] (homolog of MSMEG_3880) and rv1155 [17], respectively. Residues labeled with asterisks (*) represent those from the secondary chain.

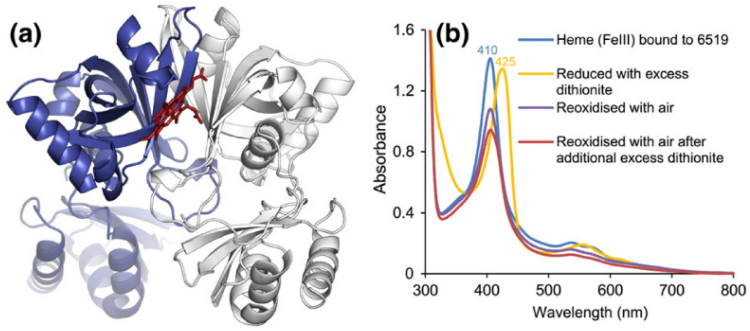

Fig. 7. Structural and functional characterization of the heme binding protein MSMEG_6519. (a) Structure of the heme binding protein MSMEG_6519 with heme computationally docked into the active site. (b) Degradation of heme bound to MSMEG_6519 after reduction with sodium dithionite followed by air oxidation.

of these structures shows that the overall protein fold is highly conserved (Fig. 4a), where the positions of the split β-barrel and substrate binding helices are almost identical, despite less than 50% sequence identity. The key residues involved in F_{420} stabilization including P52, W77, and N80 are structurally conserved, as are residues in the substrate binding pocket such as Y120 and Y126 that have been shown to be important for PA-824 activity in rv3547 [16] (Fig. 4b and c). A structural explanation for the non-overlapping PA-824 activity is evident in a comparison between the structures. MSMEG_3356 has a phenylalanine residue at position 123 in place of a tyrosine in rv3547; previous work has shown that this mutation knocked out PA-824 activity in rv3547 [16]. Additionally, both MSMEG_2027 and MSMEG_3356 have methionine residues at position 54 in place of a tyrosine residue in rv3547; again, mutations at this position (Y65L and Y65A) completely knocked out PA-824 activity [16]. The significance of these tyrosine residues for catalytic activity with PA-824 is currently unclear, but it is possible that they are involved in stabilizing the nitro moiety that is not present in menadione.

FDOR-AAs

Despite their discovery in 2010 and subsequent study [8,9], no activity has ever been reported for enzymes of the FDOR-AA family. Proteomic studies in *M. tuberculosis* and *M. smegmatis* have shown that these proteins are membrane associated [55–57]. Our analysis of their genomic context and co-occurrence, using STRING [58], revealed that proteins in the AA1–AA3 subgroups are predicted to be associated with cutinases, lipoproteins, and acyl-CoA synthetases (Table S6) that are generally involved in lipid synthesis and metabolism. In addition, the AA2 homolog from *Mycobacterium avium* is implicated in the invasion of host cell membranes for pathogenesis [59]. Together, these findings suggest that these enzymes possibly interact with lipids, which led us to perform an initial screen for their ability to bind fatty acids using arachidonic acid, a pro-inflammatory molecule secreted by macrophages in response to mycobacterial infection [60]. Our results show that MSMEG_1981 (AA1), which is located just upstream of a predicted acyl-CoA synthetase (MSMEG_1982), has detectable reductase activity with this substrate (K_m = 113 ± 21 μM, K_{cat} = $5.4 \times 10^{-4} \pm 2.0 \times 10^{-5}$ s^{-1}, K_{cat}/K_m = 4.8 M^{-1} s^{-1}; Fig. S7). All other FDOR-AAs that were tested also bind this lipid with high affinity (K_d = 4–12 μM), but no activity was detected (Fig. S7). As the first activity observed for any FDOR-AA, we predict that this class of enzymes (AA1) could function as fatty acid reductases. However, further metabolic profiling of these enzymes and testing of genetic knockouts will be required to characterize their exact substrate range and specificity.

FDOR-Bs

Similar to the FDOR-AAs, despite substantial effort, the FDOR-B family in mycobacteria remains almost entirely uncharacterized, with the sole exception of the PnPOx from *M. tuberculosis* [20]. In this work, we have investigated the F_{420}-dependent B1–B6 clusters, the heme-dependent B7 cluster, and the FAD-dependent B8 and B11 clusters.

Although the first structure of an F_{420}-dependent FDOR-B (i.e., B1–B6) was solved 10 years ago [61], no physiological role has been identified for these enzymes [8,9]. To identify potential substrates for the F_{420}-dependent FDOR-B clusters, we performed a high-throughput *in silico* docking experiment, similar

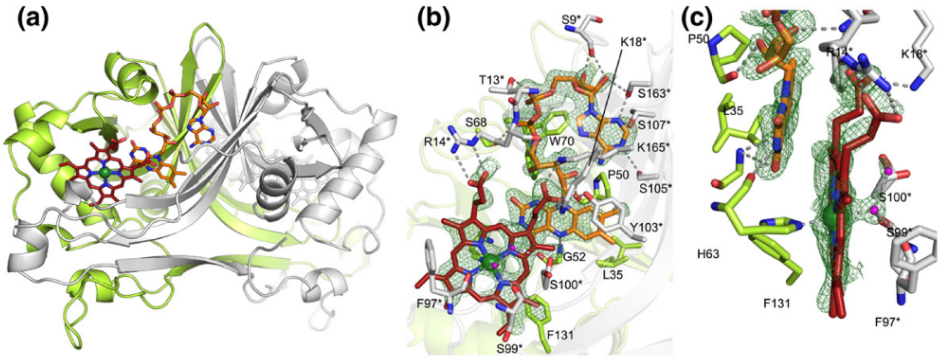

Fig. 8. Structures of FAD and heme binding protein MSMEG_4975. (a) Structure of MSMEG_4975 solved at 1.9 Å resolution. (b) Residues involved in cofactor (FAD) binding and (c) heme binding in MSMEG_4975. Electron density represents difference ($mF_o - dF_c$) omit maps contoured at 2 σ and residues labeled with asterisks (*) represent those from the secondary chain.

to several previous studies that led to the characterization of novel enzyme functions [62–64]. A series of heme degradation products were identified among the top hits, including biliverdin, which is produced by the degradation of heme by heme oxygenases (such as FDOR-B7) to liberate iron and carbon monoxide (Fig. 5) [65]. We tested representatives from the F_{420}-binding FDOR-B families (B1–B6) for $F_{420}H_2$-dependent reduction of biliverdin-IXα and found activity with representatives from the B3 (rv1155) and B4 (MSMEG_3880) families (Fig. 6a). The efficiency of the biliverdin reductase activity of MSMEG_3880 was 50-fold higher than that observed for rv1155, although both activities were significant. Docking of biliverdin to the published structure of rv2074 [40] (a B4 homolog of MSMEG_3880 with 85% sequence similarity) shows that the active site is highly complementary to biliverdin, which is mostly bound *via* interactions between the propionate side chains and highly conserved arginine residues (Fig. 6d). Hydride transfer from C5 of $F_{420}H_2$ to C10 in biliverdin then yields bilirubin (Fig. 5), with its characteristic absorption peak at 455 nm for both enzymes (Fig. 6b and c). In comparison, biliverdin docks in a different, less complementary, conformation in rv1155 (B3) (Fig. 6e), which is consistent with the 50-fold lower activity observed in assays.

We also found that the FDOR-B7 representative from *M. smegmatis* clusters with the previously characterized heme oxygenase from *Helicobacter pylori* HugZ (Fig. 3) [44]. However, the domain arrangement of the protein is reversed and the sequence identity is low (30%). To investigate the function of this protein in more detail, we have solved the crystal structure of MSMEG_6519 (Fig. 7a). As expected from sequence analysis, MSMEG_6519 contains a secondary domain to the central FDOR-like domain, although it is located at the C-terminus rather than at the N-terminus as in HugZ [23]. It is unusual that the two domains are conserved yet arranged in opposite orientation. MSMEG_6519 was observed to bind and coordinate heme (Fig. 7b and Fig. S3), and its co-purification with the product of heme oxygenation, biliverdin (Fig. S3), suggests that it is catalytically active using an endogenous electron donor/reductase present in the *Escherichia coli* (BL21DE3) cells used for protein expression. It also degraded heme in the presence of dithionite with air re-oxidation (Fig. 7b), which was not observed for the other heme-coordinating FDOR studied in this work, MSMEG_4975 (Fig. S3). Further work will be required to identify the exact biliverdin isomer produced and the physiologically relevant electron donor/redox partner for this protein in *M. smegmatis*.

Finally, we investigated the uncharacterized FDOR-B11 family. The crystal structure of MSMEG_4975 at 1.9 Å resolution, solved from purified protein without reconstitution, revealed the presence of two FAD molecules bound at either side of the dimer interface (Fig. 8a). A heme molecule is also present within each canonical substrate binding site of the FDORs, which is facilitated by the extended β-sheets in this region (Fig. 8a and b). It is a *b*-type heme protein, coordinated with a proximal histidine from the main chain (H63) and an axial water molecule (Fig. 8c). The heme is stabilized in place by interactions of the propionate side chains with positively charged and polar residues from the secondary chain (R14*, K18*, Y103*, and K165*), as well as hydrophobic interactions of the vinyl groups with residues such as F97* and F101* from the extended β-sheets from the secondary chain at the substrate binding site (Fig. 8b and c). The buried

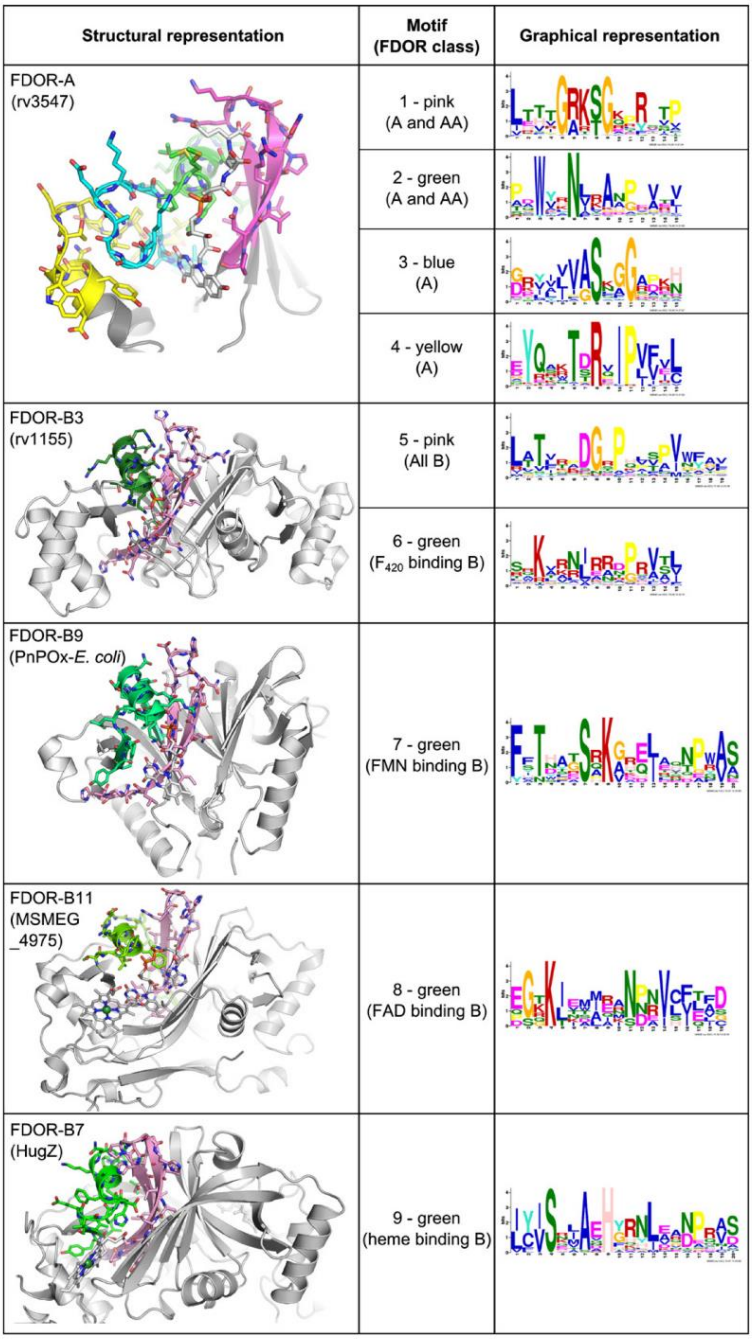

Fig. 9. Conserved motifs for identification between FDORs of different cofactor specificities. Motifs were found using the MEME Web server [68] and their text representation is provided in Table S8.

nature of the heme along with the inability of MSMEG_4975 to degrade it in the presence of dithionite implies that the heme molecule is more likely to be a secondary cofactor instead of a substrate for the protein, even though it is bound at the pocket that accommodates the substrate in other FDORs. Instead, the reversible reduction of the ferric ion with excess dithionite suggests that it is redox active (Fig. S3) and the structure reveals solvent accessibility at the axial binding site on the heme, with two serine residues (S99* and S100*) nearby, which could serve as the substrate binding site for this protein. (Fig. 8c).

Conserved motifs differentiate F_{420}-, FMN-, FAD-, and heme-binding FDORs

One of the most difficult aspects of characterizing proteins of unknown function, such as those described here, is that of determining cofactor preference on the basis of very similar protein sequences. In addition to the structures of MSMEG_2027 (A1), MSMEG_4975 (B11), and MSMEG_6519 (B7) discussed above, we have solved the structure of MSMEG_6526 from the FDOR-B2 family, which was previously not structurally characterized (Table S5). These structures, along with the previously solved structures of MSMEG_3380 (B1), rv2991 (B1), rv1155 (B3), rv2074 (B4), and rv2607 (B9) now provide a large structural dataset that we have used to define unique sequence and structural elements that can be used to predict their cofactor preference and family. We have used MEME to identify conserved motifs within each subgroup [67]. This demonstrated that, while the cofactor binding regions are highly conserved (Fig. 3c), the substrate binding regions are extremely variable among different subgroups, consistent with varying functions.

FDOR-As and FDOR-AAs can be easily identified by motifs 1 and 2 (Fig. 9). Motif 1 is primarily involved in stabilizing the ribityl and polyglutamate chain of F_{420} [16], as defined by the conserved P52 in the MSMEG_2027 structure involved in binding the ribityl moiety (Figs. 9 and 4b). Similarly, motif 2 contains a highly conserved WxxN region, with residues W77 and N80 in MSMEG_2027 involved in stabilizing the ribityl phosphate and polyglutamate tail, respectively (Figs. 9 and 4b). Although the cofactor binding regions of the FDOR-AAs are conserved, they lack motif 3 present in FDOR-As, which has a highly conserved serine residue (S75 in MSMEG_2027) and forms a distinct loop. This region is involved in binding both cofactor and substrate and is essential for catalysis [16]. Its absence in the FDOR-AAs may be partly responsible for the functional discrepancy between FDOR-As and FDOR-AAs. In addition, FDOR-AAs also lack motif 4, including the Y126 from MSMEG_2027, which is involved in substrate binding (Fig. 4b). This supports the notion that these proteins are likely to have different substrate specificities from the FDOR-As.

The FDOR-As and the F_{420}-specific FDOR-Bs (B1–B6) do not share any conserved motifs despite their structural similarity (Fig. 9). Instead, the F_{420}-binding FDOR-Bs share sequence homology in the cofactor binding region with the FMN, FAD, and heme binding proteins, which is reflected in the SSN (Fig. 2a). They all harbor motif 5, which forms the β-sheets involved in binding the ribityl and flavin groups that are common structural features for F_{420}, FAD, and FMN (Fig. 9) [17,51]. The FDOR-Bs also have a highly conserved lysine residue that binds the phosphate and ribityl moieties of flavin cofactors [17,51]. This region is conserved as motif 6 in the F_{420} binding subgroups (B1–B6), which contains several basic residues that facilitate the binding of the negatively charged polyglutamate tail of F_{420} [8,17]. This motif is not conserved in the FAD and FMN binding proteins. Instead, motif 7, which is specific to FAD-binding FDOR-Bs has more hydrophobic residues and is located at the adenine binding pocket, can be used to identify proteins of the B8 and B11 families. Likewise, motif 8 of FMN-binding FDOR-Bs (B9) contains an additional serine residue for additional hydrogen binding to the phosphate [51,69]. In the heme-binding FDOR-Bs, the phosphate binding lysine is replaced by a highly conserved histidine residue (motif 9), which binds a propionate side chain of the heme molecule [23].

Discussion

In this work, we investigated the FDORs in mycobacteria, defining a superfamily of at least 22 subgroups of split β-barrel proteins that facilitate electron transfer between a cofactor binding site and a substrate binding site in diverse biological redox reactions. By analyzing the relationships between these enzymes, we propose classification of this superfamily into A and B families, with several distinct subgroups within each family. These sequence- and structure-based groupings are likely to reflect the functional differentiation of these enzymes. We demonstrate that these enzymes have a significantly wider cofactor range than previously thought. In addition to including $F_{420}H_2$, FMN, and heme binding proteins, this superfamily includes distinct groups of FAD binding proteins as well. This diverse cofactor specificity has enabled FDORs to evolve diverse roles, ranging from FMN-dependent PnPOxs (FDOR-B9) [46] and heme oxygenases (FDOR-B7) [23] to $F_{420}H_2$-dependent enzymes specialized to reduce biliverdin (FDOR-B3/B4), fatty acids (FDOR-AA1), and, in support of previous work, quinones (FDOR-A1). In addition, their structures show clear functional adaptation, where the architecture of the substrate binding pocket is

extremely variable and can accommodate extra structural domains (FDOR-B7) or be extended to incorporate a secondary cofactor (FDOR-B11). Our analysis unifies these functionally disparate proteins into a wider superfamily of FDORs on the basis of common evolutionary origin and structural homology.

The SSN networks presented in this work emphasize that FDORs have undergone extreme functional diversification and expansion in mycobacteria (Fig. 2), with up to 30 sequences present in some species. While several FDOR groups are widely distributed (e.g., the PnPOxs), the majority of the clades are exclusive to the phyla actinobacteria and chloroflexi, that is, FDOR-As, FDOR-AAs, FDOR-B1-B6s, and FDOR-B8. The striking overrepresentation of such families in these phyla, and especially the genus mycobacteria, indicates that they have been strongly selected for roles specific to these taxa. It is notable that the majority of these exclusive clusters (B1–B6, A1–A4, AA1–AA6) are all F_{420} dependent. Why would an aerobic bacterium make such extensive use of a cofactor that is only otherwise seen in anaerobic methanogens [11]? Our data along with previous work show that many of these functions appear to be consistent with physiological roles in persistence. It is already known that, by deleting the F_{420} biosynthesis enzymes, pathogenic mycobacteria become sensitive to reactive oxygen and nitrogen species [10,12–14] and are unable to recover after hypoxia-induced dormancy [10]. Similarly, persistence is also important for soil-dwelling bacteria [70,71]; environmental mycobacteria are likely to predominantly exist in a persistent dormant state [72], allowing them to survive adverse environmental conditions such as hypoxia [73] and resource limitation [74]. However, the mechanisms by which F_{420} is involved in persistence was unclear, although its importance is evident in the observation that, despite its high metabolic cost, the genes for F_{420} production have been retained even in the greatly reduced genome of *Mycobacterium leprae* [75,76].

In terms of persistence-related strategies, this work clearly implicates the FDORs in the heme catabolism of mycobacteria. We observed that *M. smegmatis* produces a heme oxygenase (FDOR-B7) and that two families of F_{420}-dependent FDORs (B3s and B4s) can reduce the breakdown product of heme, biliverdin, to bilirubin. Biliverdin reductases can generate a potent antioxidant mechanism, with cycling between bilirubin and biliverdin able to compensate for a 10,000-fold excess in hydrogen peroxide radicals [27,28]. To the best of our knowledge, the FDOR-B3 and B4 proteins are the second family of biliverdin reductases to be characterized from bacteria and the first $F_{420}H_2$-dependent proteins with this function. The previously characterized mammalian [77] and cyanobacterial [78] biliverdin reductases utilize NADPH or NADH instead.

Recent work has shown that biliverdin production is increased in macrophages infected with *Mycobacterium abscessus* due to upregulation of host heme oxygenases [29]. This in turn was shown to enhance the survival of the invading bacterium, possibly due to the antioxidant effect of biliverdin–bilirubin cycling [29]. Whether these highly conserved FDORs (B3s and B4s) play a role in this process is intriguing. Both proteins have been shown to be membrane associated [57,79] and F_{420} is transported outside the cytosol to the lipid-rich outer membrane of mycobacteria [80], suggesting that they could be involved in reducing host generated biliverdin to bilirubin. Interestingly, *M. tuberculosis* is only known to produce a conserved unique heme oxygenase (MhuD) [81,82], which produces the closely related mycobilins instead of biliverdin. The relative lack of conservation of the mycobacterial heme oxygenases from this study (B7s) among other mycobacterial species is consistent with the functional replacement of this protein by MhuD in *M. tuberculosis* and other mycobacterial species [81,82]. Whether these FDORs can also use mycobilins as substrates for an antioxidant mechanism such as the biliverdin–bilirubin system remains to be investigated.

In this work, we also implicated FDORs in energetics and fatty acid modification. We observed that three FDOR-As efficiently reduced quinones; these enzymes may serve as $F_{420}H_2$-menaquinone oxidoreductases that input electrons into the respiratory chain and generate proton-motive force through a redox-loop mechanism [83]. The FDOR-AA family is located in the cell wall proteome and has been implicated for virulence in *M. avium* complex [59]. We have shown that these enzymes are able to modify lipids, including arachidonic acid, which is produced by human macrophages [60]. Given the importance of fatty acid modification in mycobacterial persistence—for instance, *M. tuberculosis* is able to accumulate host fatty acids from infected macrophages for utilization as an energy source when entering and resuscitating from dormancy [84]—this preliminary functional annotation provides new directions for research into F_{420}-dependent host fatty acid modification. Finally, the FAD binding protein MSMEG_5243 that belongs to the only non-F_{420}-dependent family that is specific for actinobacteria (and chloroflexi) has recently been shown to be regulated by DosR in response to the redox and oxygenation state [73]. However, further work is required to identify any specific roles of these proteins.

In conclusion, this work has redefined and expanded the FDOR superfamily in mycobacteria and related species. FDORs are diverse in their cofactor preference, substrate specificity, and

enzymatic function. Through extensive kinetic and spectroscopic studies, we have distinguished between the F_{420}-, FMN-, FAD- and heme-binding FDORs found in mycobacteria, and we have identified the preferred substrate classes of several families. Our structural analysis shows that the functional differentiation of these proteins is due to the plasticity of their structures: regions of the protein sequence involved in cofactor binding are more conserved and suggestive of their common evolutionary origin while the substrate binding region is extremely variable between homologs, allowing for their functional discrepancy. Considering the conservation of some of these proteins in *M. tuberculosis* and other pathogens, we predict that the quinone reductase, fatty acid reductase, and biliverdin reductase activities of FDORs may be relevant for mycobacterial pathogenesis and persistence. This provides a new framework for the future resolution of the variety of physiological roles of FDORs in mycobacteria.

Materials and Methods

Sequence analysis

Conserved motifs for proteins were found using MEME [68], proteins with known and predicted interactions with the FDOR-AAs were found using the STRING online database [58], and the conservation of FDORs was inferred from the TB Database [85]. For phylogenetic tree construction, FDOR protein sequences from mycobacteria were aligned based on the structural alignment of all available crystal structures from this family using PROMAS3D [86] and curated to remove poorly aligned or highly similar sequences. The final tree was then produced using the LG with frequencies evolutionary model with five distinct gamma categories on MEGA 6.0 [87].

Sequences belonging to the FMN binding split barrel superfamily (except the "Flavin_Reduct" family, which is only loosely related to the rest of the subfamilies) were obtained from the Pfam database [41] and CD-HIT [88] was used to curate and remove sequences with more than 50% sequence identity. A PSI-BLAST search with MSMEG_3380 was used to find all structures solved from this superfamily and these sequences (once duplicates were removed using CD-HIT), along with all proteins characterized in this study, were pooled to obtain a final set of 2148 sequences. SSNs were created as previously described [33], where the sequences were subjected to an all-*versus*-all BLAST and the BLAST *E*-values were used as edges to represent the similarity between proteins that are represented as individual nodes. Any self and duplicate edges were removed and the nodes were visualized using the organic layout on Cytoscape 3.1 [89]. Different log*E*-value cutoffs were set to control the degree of separation between nodes, which was based on visual observation of the clustering of characterized proteins with known cofactor specificities.

For the mycobacterial SSN, a total of 532 sequences from 18 *Mycobacteria sp.* were used for analysis: *M. smegmatis MC2 155*; *M. tuberculosis H37Rv*; *Mycobacterium ulcerans Agy99*; *M. leprae TN*; *M. avium 104*; *M. abscessus 6G-1108*; *Mycobacterium marinum M*, *JDM601*; *Mycobacterium thermoresistibile ATCC 19527*; *Mycobacterium sp. MCS*; *Mycobacterium gilvum Spyr1*; *Mycobacterium vanbaalenii* DSM 7251; *Mycobacterium rhodesiae JS60*; *Mycobacterium tusciae JS617*; *Mycobacterium parascrofulaceum ATCC BAA-614*; *Mycobacteriumintracellulare ATCC 13950*; *Mycobacterium colombiense 10B*; and *Mycobacterium massiliense CCUG 48898*. Initially, separate PSI-BLAST searches were performed using the FDOR-A rv3547 and FDOR-B MSMEG_3380 until no further sequences were found, and the sequences were pooled and any duplicates were deleted. The SSN was created as described above, and a high threshold at −28 was initially set to identify closely related proteins with more than 50% sequence homology, where clades were separated until no major change in clustering was observed with large increases in cutoff value. Next, the threshold was decreased until a log*E* filter of −7.6, where at least one edge was present between all previously found clusters for the FDOR-AAs and this same cutoff was used for the FDOR-Bs as well, where clusters with cofactor preferences other than F_{420} were identified. Finally, a cutoff of −3 was chosen to visually clusters based on cofactor preference.

Protein expression, purification, and crystallography (detailed in Text S9)

All sequences for the FDOR-B-related proteins were ordered as Gene Strings from Invitrogen and cloned into the expression vector pETMCSIII using Gibson assembly [90]. The genes used for MSMEG_2027, MSMEG_3356, and the FDOR-AAs in the expression vector pDEST17 were from previous work [9] and the truncated MSMEG_2027 was also cloned into petMCSIII. The FDOR-AAs and MSMEG_3863 were purified as previously published [9] and the rest were expressed in *E. coli* (BL21DE3) grown in modified auto-induction media [91]. Proteins were purified using nickel affinity and size-exclusion chromatography and co-purified flavin was stripped by partial on-column protein refolding [92]. High-throughput screens from Hampton Research were used to identify initial crystal forming conditions that were refined and data were collected in-house or at the Australian Synchrotron. Diffraction data were integrated using XDS [93], and the CCP4 suite [94] was used for scaling using AIMLESS [95], followed by molecular replacement using Phaser [96]. Model building was performed using Buccaneer [97] and ARP/wARP [98] followed by manual loop building in Coot [99]. Interspersed refinements were performed using REFMAC [100] and PHENIX [101].

Computational substrate docking

Prior to the high-throughput molecular docking with rv1155, the likely protonation state of the rv1155-FMN complex (PDB ID: 1Y30 [50]) at pH 7.4 was predicted using PROPKA3 [102]. The KEGG database was obtained from the ZINC repository [103] and docked into a 12-Å cavity centered on the FMN O4 atom using GOLD v5.1 [104]. The ChemPLP scoring function was used with a

search efficiency of 100%, the number of Genetic Algorithm runs set at 5, automatic atom typing was used for both ligand and protein atoms, and 5 poses per ligand were kept, with an RMSD of 2 Å between poses. All solutions were rescored with ChemPLP after minimization using the protocol implemented within GOLD. The top 5% of compounds (972 compounds) successfully docked and ranked by fitness score were used for selection of potential substrates. Of these, approximately half were synthetic chemicals (472). Of the remaining naturally occurring chemicals, the largest chemical classes were arachidonic acid and metabolites, linoleic acid and metabolites, heme breakdown products, flavonoids, and quinones.

AutoDock Vina [105] was used to dock PA-824, menadione, and biliverdin-IXα for the figures, where both protein and ligand were prepared using AutoDockTools [106] with default settings. Menadione and PA-824 were modeled into the active site of rv3547 with F_{420} (PDB ID: 3R5R [16]). F_{420} (rigid) from the structure of the solved F_{420}-rv1155 complex [17] was docked into the structure of rv2074 [40] with flexible residues at the cofactor binding pocket. Biliverdin-IXα was then docked into the substrate binding region of the modeled F_{420}-rv2074 and F_{420}-rv1155 complex (PDB ID: 4QVB [17]).

Ligand and substrate binding assays

F_{420} was extracted and purified from *M. smegmatis* cultures grown following the methods outlined in Bashiri *et al.* [107] and Isabelle *et al.* [108]. FMN, FAD, and arachidonic acid were purchased from Sigma-Aldrich. Cofactor binding assays were performed using 1 μM protein titrated against increasing concentrations of cofactor or substrate in an opaque 96-well plate (200 μL reactions in 50 mM Tris, pH 7.5). The samples were left to equilibrate by shaking at 25 °C for 20–30 min, excited at 260 nm, and the emission spectra were measured at 330 nm to observe ligand associated changes in intrinsic tryptophan fluorescence. K_d was obtained by assuming a simple bimolecular binding reaction, where the fractional occupancy of protein is [ligand]/(K_d + [ligand]).

To check the ability of MSMEG_6519 to coordinate heme, we initially added excess heme (Sigma-Aldrich) to protein and incubated it by shaking for half an hour at room temperature. Unbound heme was removed by passing the sample through a PD-10 desalting column and the absorbance spectrum of the elution was measured. For the dithionite-mediated heme reduction of MSMEG_6519 and MSMEG_4975, excess sodium dithionite was added to a final concentration of 50 mM and the absorbance spectra were measured before re-oxidation by bubbling air into the solution.

Enzyme activity assays

For the FDOR-A and MSMEG_1981 activity assays, F_{420} was reduced overnight with 10–50 μM F_{420}-dependent glucose-6-phosphate dehydrogenase (Fgd, purified according to previous methods [7]) and excess glucose-6-phosphate under anaerobic conditions in 200 mM Tris (pH 7.5). The Fgd was removed by spin filtration and $F_{420}H_2$ produced was used on the same day. The activity assays were based on previously reported methods [10], where reactions contained 200 mM Tris at pH 7.5, 0.1% triton-X100, 100 μL of 25 μM $F_{420}H_2$, and increasing concentrations of substrate at room temperature. Enzyme concentrations used were 0.1 μM for the FDOR-As and 1 μM for MSMEG_1981. The oxidization of F_{420} upon substrate reduction was monitored at an absorbance of 420 nm (ε = 41,400 M^{-1} cm^{-1} [109]) and a Michaelis–Menten curve of best fit was used to calculate K_m and V_{max}.

Biliverdin reductase activity was monitored following the decrease of the absorbance peak at 650 nm of biliverdin (ε = 25,000 M^{-1} cm^{-1} [110]) upon bilirubin production in reactions containing 1 μM F_{420}, 1 μM Fgd, 2.5 mM G6P, 0.1 μM FDOR-B, and increasing concentration of biliverdin-IXα. To observe the change in biliverdin spectra over time, we prepared 1 mL reactions with the same concentrations of reactants with 25 μM and 6.25 μM biliverdin for MSMEG_3880 (50 nm) and rv1155 (10 μM), respectively.

Accession numbers

Coordinates and structure factors have been deposited in the Protein Data Bank with PDB IDs 4Y9I (MSMEG_2027), 4YBN (MSMEG_4975), 4ZKY (MSMEG_6526), and 5BNC (MSMEG_6519).

Supplementary data to this article can be found online at http://dx.doi.org/10.1016/j.jmb.2015.09.021.

Acknowledgements

This work was supported by Australian Research Council research grants (DE120102673 and DP130102144) awarded to C.J.J., Commonwealth Scientific and Industrial Research Organisation Office of the Chief Executive Postdoctoral Fellowship awarded to C.G., and Australian National University Higher Degree by Research PhD scholarships awarded to F.H.A., B.M.L., and A.E.M. C.J.J. and P.D.C. thank the Australian Synchrotron for beamtime.

Received 28 July 2015;
Received in revised form 23 September 2015;
Accepted 24 September 2015
Available online 3 October 2015

Keywords:
F_{420};
mycobacteria;
flavin/deazaflavin oxidoreductase (FDOR);
pyridoxamine/pyridoxine-5-phosphate oxidase (PnPOx);
biliverdin reductase

Abbreviations used:
FDOR flavin/deazaflavin oxidoreductases; FMN flavin mononucleotide; FAD flavin adenine dinucleotide; PnPOx pyridoxine/pyridoxamine 5′-phosphate oxidase; SSN sequence similarity networks.

References

[1] P. Hemmerich, G. Nagelschneider, C. Veeger, Chemistry and molecular biology of flavins and flavoproteins, FEBS Lett. 8 (1970) 69–83.

[2] L. Daniels, N. Bakhiet, K. Harmon, Widespread Distribution of a 5-deazaflavin Cofactor in Actinomyces and Related Bacteria, Syst. Appl. Microbiol. 6 (1985) 12–17.

[3] P. Cheeseman, A. Toms-Wood, R.S. Wolfe, Isolation and Properties of a Fluorescent Compound, Factor420, from Methanobacterium Strain M.o.H, J. Bacteriol. 112 (1972) 527–531.

[4] C. Walsh, Naturally occurring 5-deazaflavin coenzymes: biological redox roles, Acc. Chem. Res. 19 (1986) 216–221.

[5] R.K. Thauer, A.K. Kaster, H. Seedorf, W. Buckel, R. Hedderich, Methanogenic archaea: ecologically relevant differences in energy conservation, Nat. Rev. Microbiol. 6 (2008) 579–591.

[6] D.E. Graham, H. Xu, R.H. White, Identification of the 7,8-didemethyl-8-hydroxy-5-deazariboflavin synthase required for coenzyme F_{420} biosynthesis, Arch. Microbiol. 180 (2003) 455–464.

[7] G. Bashiri, C.J. Squire, N.J. Moreland, E.N. Baker, Crystal structures of F_{420}-dependent glucose-6-phosphate dehydrogenase FGD1 involved in the activation of the anti-tuberculosis drug candidate PA-824 reveal the basis of coenzyme and substrate binding, J. Biol. Chem. 283 (2008) 17531–17541.

[8] M.C. Taylor, C.J. Jackson, D.B. Tattersall, N. French, T.S. Peat, J. Newman, L.J. Briggs, G.V. Lapalikar, P.M. Campbell, C. Scott, R.J. Russell, J.G. Oakeshott, Identification and characterization of two families of $F4_{20}H_2$-dependent reductases from Mycobacteria that catalyse aflatoxin degradation, Mol. Microbiol. 78 (2010) 561–575.

[9] G.V. Lapalikar, M.C. Taylor, A.C. Warden, C. Scott, R.J. Russell, J.G. Oakeshott, F_{420}-H_2-Dependent Degradation of Aflatoxin and other Furanocoumarins Is Widespread throughout the Actinomycetales, PLoS One 7 (2012) e30114.

[10] M. Gurumurthy, M. Rao, T. Mukherjee, S.P.S. Rao, H.I. Boshoff, T. Dick, C.E. Barry, U.H. Manjunatha, A novel F_{420}-dependent anti-oxidant mechanism protects Mycobacterium tuberculosis against oxidative stress and bactericidal agents, Mol. Microbiol. 8 (2013) 744–755.

[11] J.D. Selengut, D.H. Haft, Unexpected Abundance of Coenzyme F_{420}-Dependent Enzymes in Mycobacterium tuberculosis and Other Actinobacteria, J. Bacteriol. 192 (2010) 5788–5798.

[12] M.R. Hasan, M. Rahman, S. Jaques, E. Purwantini, L. Daniels, Glucose 6-Phosphate Accumulation in Mycobacteria, J. Biol. Chem. 285 (2010) 19135–19144.

[13] D. Guerra-Lopez, L. Daniels, M. Rawat, Mycobacterium smegmatis mc2 155 fbiC and MSMEG_2392 are involved in triphenylmethane dye decolorization and coenzyme F_{420} biosynthesis, Microbiology 153 (2007) 2724–2732.

[14] E. Purwantini, B. Mukhopadhyay, Conversion of NO_2 to NO by reduced coenzyme F_{420} protects mycobacteria from nitrosative damage, Proc. Natl. Acad. Sci. U. S. A. 106 (2009) 6333–6338.

[15] G.V. Lapalikar, M.C. Taylor, A.C. Warden, H. Onagi, J.E. Hennessy, R.J. Mulder, C. Scott, S.E. Brown, R.J. Russell, C.J. Easton, J.G. Oakeshott, Cofactor promiscuity among F_{420}-dependent reductases enables them to catalyse both oxidation and reduction of the same substrate, Catal. Sci. Technol. 2 (2012) 1560–1567.

[16] S.E. Cellitti, J. Shaffer, D.H. Jones, T. Mukherjee, M. Gurumurthy, B. Bursulaya, H.I. Boshoff, I. Choi, A. Nayyar, Y.S. Lee, J. Cherian, P. Niyomrattanakit, T. Dick, U.H. Manjunatha, C.E. Barry III, G. Spraggon, B.H. Geierstanger, Structure of Ddn, the Deazaflavin-Dependent Nitroreductase from Mycobacterium tuberculosis Involved in Bioreductive Activation of PA-824, Structure 20 (2012) 101–112.

[17] E.H. Mashalidis, A.G. Gittis, A. Tomczak, C. Abell, C.E. Barry, D.N. Garboczi, Molecular insights into the binding of coenzyme F_{420} to the conserved protein Rv1155 from Mycobacterium tuberculosis, Protein Sci. 24 (2015) 729–740.

[18] R. Singh, U. Manjunatha, H.I.M. Boshoff, Y.H. Ha, P. Niyomrattanakit, R. Ledwidge, C.S. Dowd, I.Y. Lee, P. Kim, L. Zhang, S. Kang, T.H. Keller, J. Jiricek, C.E. Barry, PA-824 Kills Nonreplicating Mycobacterium tuberculosis by Intracellular NO Release, Science 322 (2008) 1392–1395.

[19] M. Gurumurthy, T. Mukherjee, C.S. Dowd, R. Singh, P. Niyomrattanakit, J.A. Tay, A. Nayyar, Y.S. Lee, J. Cherian, H.I. Boshoff, T. Dick, C.E. Barry, U.H. Manjunatha, Substrate specificity of the deazaflavin-dependent nitroreductase from Mycobacterium tuberculosis responsible for the bioreductive activation of bicyclic nitroimidazoles, FEBS J. 279 (2012) 113–125.

[20] E.H. Mashalidis, T. Mukherjee, P. Śledź, D. Matak-Vinković, H. Boshoff, C. Abell, C.E. Barry III, Rv2607 from Mycobacterium tuberculosis Is a Pyridoxine 5′-Phosphate Oxidase with Unusual Substrate Specificity, PLoS One 6 (2011) e27643.

[21] M.L. Salvo, M.K. Safo, F.N. Musayev, F. Bossa, V. Schirch, Structure and mechanism of Escherichia coli pyridoxine 5′-phosphate oxidase, Biochim. Biophys. Acta 1647 (2003) 76–82.

[22] F.N. Musayev, M.L. Di Salvo, T.-P. Ko, V. Schirch, M.K. Safo, Structure and properties of recombinant human pyridoxine 5′-phosphate oxidase, Protein Sci. 12 (2003) 1455–1463.

[23] Y. Hu, F. Jiang, Y. Guo, X. Shen, Y. Zhang, R. Zhang, G. Guo, X. Mao, Q. Zou, D.-C. Wang, Crystal Structure of HugZ, a Novel Heme Oxygenase from Helicobacter pylori, J. Biol. Chem. 286 (2011) 1537–1544.

[24] R. Zhang, J. Zhang, G. Guo, X. Mao, W. Tong, Y. Zhang, D.-C. Wang, Y. Hu, Q. Zou, Crystal structure of Campylobacter jejuni ChuZ: A split-barrel family heme oxygenase with a novel heme-binding mode, Biochem. Biophys. Res. Commun. 415 (2011) 82–87.

[25] R. Stocker, Y. Yamamoto, A. McDonagh, A. Glazer, B. Ames, Bilirubin is an antioxidant of possible physiological importance, Science 235 (1987) 1043–1046.

[26] L.C. Mireles, M.A. Lum, P.A. Dennery, Antioxidant and Cytotoxic Effects of Bilirubin on Neonatal Erythrocytes, Pediatr. Res. 45 (1999) 355–362.

[27] D.E. Barañano, M. Rao, C.D. Ferris, S.H. Snyder, Biliverdin reductase: A major physiologic cytoprotectant, Proc. Natl. Acad. Sci. U. S. A. 99 (2002) 16093–16098.

[28] T. Jansen, A. Daiber, Direct antioxidant properties of bilirubin and biliverdin. Is there a role for biliverdin reductase? Front. Pharmacol. 3 (2012) 30.

[29] M.Y. Abdalla, I.M. Ahmad, B. Switzer, B.E. Britigan, Induction of heme oxygenase-1 contributes to survival of Mycobacterium abscessus in human macrophages-like THP-1 cells, Redox Biol. 4 (2015) 328–339.

[30] S.T. Mashiyama, M.M. Malabanan, E. Akiva, R. Bhosle, M.C. Branch, B. Hillerich, K. Jagessar, J. Kim, Y. Patskovsky, R.D. Seidel, M. Stead, R. Toro, M.W. Vetting, S.C. Almo, R.N. Armstrong, P.C. Babbitt, Large-Scale Determination of Sequence, Structure, and Function Relationships in Cytosolic Glutathione Transferases across the Biosphere, PLoS Biol. 12 (2014) e1001843.

[31] R. Uberto, E.W. Moomaw, Protein Similarity Networks Reveal Relationships among Sequence, Structure, and Function within the Cupin Superfamily, PLoS One 8 (2013) e74477.

[32] S.D. Brown, P.C. Babbitt, New Insights about Enzyme Evolution from Large Scale Studies of Sequence and Structure Relationships, J. Biol. Chem. 289 (2014) 30221–30228.

[33] H.J. Atkinson, J.H. Morris, T.E. Ferrin, P.C. Babbitt, Using Sequence Similarity Networks for Visualization of Relationships Across Diverse Protein Superfamilies, PLoS One 4 (2009) e4345.

[34] A.J.M. Martin, I. Walsh, T.D. Domenico, I. Mičetić, S.C.E. Tosatto, PANADA: Protein Association Network Annotation, Determination and Analysis, PLoS One 8 (2013) e78383.

[35] M.J. Sanderson, A.C. Driskell, The challenge of constructing large phylogenetic trees, Trends Plant Sci. 8 (2003) 374–379.

[36] W.P. Maddison, Gene Trees in Species Trees, Syst. Biol. 46 (1997) 523–536.

[37] A. Som, Causes, consequences and solutions of phylogenetic incongruence, Brief. Bioinform. 16 (2015) 536–548.

[38] S.F. Altschul, W. Gish, W. Miller, E.W. Myers, D.J. Lipman, Basic local alignment search tool, J. Mol. Biol. 215 (1990) 403–410.

[39] S.F. Altschul, T.L. Madden, A.A. Schäffer, J. Zhang, Z. Zhang, W. Miller, D.J. Lipman, Gapped BLAST and PSI-BLAST: a new generation of protein database search programs, Nucleic Acids Res. 25 (1997) 3389–3402.

[40] B.K. Biswal, K. Au, M.M. Cherney, C. Garen, M.N.G. James, The molecular structure of Rv2074, a probable pyridoxine 5'-phosphate oxidase from Mycobacterium tuberculosis, at 1.6 A resolution, Acta Crystallogr. Sect. F: Struct. Biol. Cryst. Commun. 62 (2006) 735–742.

[41] R.D. Finn, A. Bateman, J. Clements, P. Coggill, R.Y. Eberhardt, S.R. Eddy, A. Heger, K. Hetherington, L. Holm, J. Mistry, E.L.L. Sonnhammer, J. Tate, M. Punta, Pfam: the protein families database, Nucleic Acids Res. 42 (2014) D222–D230.

[42] J.F. Parsons, K. Calabrese, E. Eisenstein, J.E. Ladner, Structure of the phenazine biosynthesis enzyme PhzG, Acta Crystallogr. D Biol. Crystallogr. 60 (2004) 2110–2113.

[43] N. Xu, E.G. Ahuja, P. Janning, D.V. Mavrodi, L.S. Thomashow, W. Blankenfeldt, Trapped intermediates in crystals of the FMN-dependent oxidase PhzG provide insight into the final steps of phenazine biosynthesis, Acta Crystallogr. D Biol. Crystallogr. 69 (2013) 1403–1413.

[44] Y. Guo, G. Guo, X. Mao, W. Zhang, J. Xiao, W. Tong, T. Liu, B. Xiao, X. Liu, Y. Feng, Q. Zou, Functional identification of HugZ, a heme oxygenase from Helicobacter pylori, BMC Microbiol. 8 (2008) 226.

[45] A.L. Oldham, T.A. Wood, D.P. Henderson, Plesiomonas shigelloides hugZ encodes an iron-regulated heme binding protein required for heme iron utilization, Can. J. Microbiol. 54 (2008) 97–102.

[46] M.K. Safo, I. Mathews, F.N. Musayev, M.L. di Salvo, D.J. Thiel, D.J. Abraham, V. Schirch, X-ray structure of Escherichia coli pyridoxine 5′-phosphate oxidase complexed with FMN at 1.8 Å resolution, Structure 8 (2000) 751–762.

[47] A.S. Konagurthu, C.F. Reboul, J.W. Schmidberger, J.A. Irving, A.M. Lesk, P.J. Stuckey, J.C. Whisstock, A.M. Buckle, MUSTANG-MR Structural Sieving Server: Applications in Protein Structural Analysis and Crystallography, PLoS One 5 (2010) e10048.

[48] K. Suto, K. Kawagoe, N. Shibata, Y. Morimoto, Y. Higuchi, M. Kitamura, T. Nakaya, N. Yasuoka, How do the X-ray structure and the NMR structure of FMN-binding protein differ? Acta Crystallogr. D Biol. Crystallogr. 56 (2000) 368–371.

[49] H.-K.S. Leiros, S. Kozielski-Stuhrmann, U. Kapp, L. Terradot, G.A. Leonard, S.M. McSweeney, Structural Basis of 5-Nitroimidazole Antibiotic Resistance: The crystal structure of NimA from Deinococcus radiodurans, J. Biol. Chem. 279 (2004) 55840–55849.

[50] S. Canaan, G. Sulzenbacher, V. Roig-Zamboni, L. Scappuccini-Calvo, F. Frassinetti, D. Maurin, C. Cambillau, Y. Bourne, Crystal structure of the conserved hypothetical protein Rv1155 from Mycobacterium tuberculosis, FEBS Lett. 579 (2005) 215–221.

[51] J.-D. Pédelacq, B.-S. Rho, C.-Y. Kim, G.S. Waldo, T.P. Lekin, B.W. Segelke, B. Rupp, L.-W. Hung, S.-I. Kim, T.C. Terwilliger, Crystal structure of a putative pyridoxine 5′-phosphate oxidase (Rv2607) from Mycobacterium tuberculosis, Proteins 62 (2006) 563–569.

[52] X. Liu, J. Gong, T. Wei, Z. Wang, Q. Du, D. Zhu, Y. Huang, S. Xu, L. Gu, Crystal structure of HutZ, a heme storage protein from Vibrio cholerae: A structural mismatch observed in the region of high sequence conservation, BMC Struct. Biol. 12 (2012) 23.

[53] E. Hilario, Y. Li, D. Niks, L. Fan, The structure of a Xanthomonas general stress protein involved in citrus canker reveals its flavin-binding property, Acta Crystallogr. D Biol. Crystallogr. 68 (2012) 846–853.

[54] A. Wilks, M.P. Schmitt, Expression and Characterization of a Heme Oxygenase (Hmu O) from Corynebacterium diphtheriae : iron acquisition requires oxidative cleavage of the heme macrocycle, J. Biol. Chem. 273 (1998) 837–841.

[55] H. Zhiguo, J.D. Buck, Cell wall proteome analysis of Mycobacterium smegmatis strain MC2 155, BMC Microbiol. 10 (2010) 121.

[56] K.G. Mawuenyega, C.V. Forst, K.M. Dobos, J.T. Belisle, J. Chen, E.M. Bradbury, A.R.M. Bradbury, X. Chen, Mycobacterium tuberculosis Functional Network Analysis by Global Subcellular Protein Profiling, Mol. Biol. Cell 16 (2005) 396–404.

[57] G.A. De Souza, N.A. Leversen, H. Målen, H.G. Wiker, Bacterial proteins with cleaved or uncleaved signal peptides of the general secretory pathway, J. Proteome 75 (2011) 502–510.

[58] A. Franceschini, D. Szklarczyk, S. Frankild, M. Kuhn, M. Simonovic, A. Roth, J. Lin, P. Minguez, P. Bork, C. von Mering, L.J. Jensen, STRING v9.1: protein-protein interaction networks, with increased coverage and integration, Nucleic Acids Res. 41 (2013) D808–D815.

[59] J.A. McGarvey, L.E. Bermudez, Phenotypic and Genomic Analyses of the Mycobacterium avium Complex Reveal Differences in Gastrointestinal Invasion and Genomic Composition, Infect. Immun. 69 (2001) 7242–7249.

[60] S.M. Behar, M. Divangahi, H.G. Remold, Evasion of innate immunity by Mycobacterium tuberculosis: is death an exit strategy? Nat. Rev. Microbiol. 8 (2010) 668–674.

[61] B.K. Biswal, M.M. Cherney, M. Wang, C. Garen, M.N.G. James, Structures of Mycobacterium tuberculosis pyridoxine 5′-phosphate oxidase and its complexes with flavin mononucleotide and pyridoxal 5′-phosphate, Acta Crystallogr. D Biol. Crystallogr. 61 (2005) 1492–1499.
[62] D.F. Xiang, P. Kolb, A.A. Fedorov, C. Xu, E.V. Fedorov, T. Narindoshivili, H.J. Williams, B.K. Shoichet, S.C. Almo, F.M. Raushel, Structure-Based Function Discovery of an Enzyme for the Hydrolysis of Phosphorylated Sugar Lactones, Biochemistry 51 (2012) 1762–1773.
[63] G.Q. Dong, S. Calhoun, H. Fan, C. Kalyanaraman, M.C. Branch, S.T. Mashiyama, N. London, M.P. Jacobson, P.C. Babbitt, B.K. Shoichet, R.N. Armstrong, A. Sali, Prediction of Substrates for Glutathione Transferases by Covalent Docking, J. Chem. Inf. Model. 54 (2014) 1687–1699.
[64] J.C. Hermann, E. Ghanem, Y. Li, F.M. Raushel, J.J. Irwin, B.K. Shoichet, Predicting Substrates by Docking High-Energy Intermediates to Enzyme Structures, J. Am. Chem. Soc. 128 (2006) 15882–15891.
[65] M. Unno, T. Matsui, M. Ikeda-Saito, Structure and catalytic mechanism of heme oxygenase, Nat. Prod. Rep. 24 (2007) 553–570.
[66] Liam J. Smith, S. Browne, Adrian J. Mulholland, Timothy J. Mantle, Computational and experimental studies on the catalytic mechanism of biliverdin-IXβ reductase, 411 (2008) 475–484.
[67] T.L. Bailey, C. Elkan, Fitting a mixture model by expectation maximization to discover motifs in biopolymers, Proceedings of the Second International Conference on Intelligent Systems for Molecular BiologyAAAI Press, Menlo Park, CA 1994, pp. 28–36.
[68] T.L. Bailey, M. Boden, F.A. Buske, M. Frith, C.E. Grant, L. Clementi, J. Ren, W.W. Li, W.S. Noble, MEME Suite: tools for motif discovery and searching, Nucleic Acids Res. 37 (2009) W202–W208.
[69] M.K. Safo, F.N. Musayev, M.L. di Salvo, V. Schirch, X-ray structure of Escherichia coli pyridoxine 5′-phosphate oxidase complexed with pyridoxal 5′-phosphate at 2.0 Å resolution, J. Mol. Biol. 310 (2001) 817–826.
[70] J.T. Lennon, S.E. Jones, Microbial seed banks: the ecological and evolutionary implications of dormancy, Nat. Rev. Microbiol. 9 (2011) 119–130.
[71] M.S. Rappé, S.J. Giovannoni, The Uncultured Microbial Majority, Annu. Rev. Microbiol. 57 (2003) 369–394.
[72] R.J. Whittington, D.J. Marshall, P.J. Nicholls, I.B. Marsh, L.A. Reddacliff, Survival and Dormancy of Mycobacterium avium subsp. paratuberculosis in the Environment, Appl. Environ. Microbiol. 70 (2004) 2989–3004.
[73] M. Berney, C. Greening, R. Conrad, W.R. Jacobs, G.M. Cook, An obligately aerobic soil bacterium activates fermentative hydrogen production to survive reductive stress during hypoxia, Proc. Natl. Acad. Sci. U. S. A. 111 (2014) 11479–11484.
[74] M.J. Smeulders, J. Keer, R.A. Speight, H.D. Williams, Adaptation of Mycobacterium smegmatis to Stationary Phase, J. Bacteriol. 181 (1999) 270–283.
[75] E. Purwantini, L. Daniels, Purification of a novel coenzyme F420-dependent glucose-6-phosphate dehydrogenase from Mycobacterium smegmatis, J. Bacteriol. 178 (1996) 2861–2866.
[76] S.T. Cole, K. Eiglmeier, J. Parkhill, K.D. James, N.R. Thomson, P.R. Wheeler, N. Honore, T. Garnier, C. Churcher, D. Harris, K. Mungall, D. Basham, D. Brown, T. Chillingworth, R. Connor, R.M. Davies, K. Devlin, S. Duthoy, T. Feltwell, A. Fraser, N. Hamlin, S. Holroyd, T. Hornsby, K. Jagels, C. Lacroix, J. Maclean, S. Moule, L. Murphy, K. Oliver, M.A. Quail, M.A. Rajandream, K.M. Rutherford, S. Rutter, K. Seeger, S. Simon, M. Simmonds, J. Skelton, R. Squares, S. Squares, K. Stevens, K. Taylor, S. Whitehead, J.R. Woodward, B.G. Barrell, Massive gene decay in the leprosy bacillus, Nature 409 (2001) 1007–1011.
[77] T. Yamaguchi, Y. Komoda, H. Nakajima, Biliverdin-IX alpha reductase and biliverdin-IX beta reductase from human liver Purification and characterization, J. Biol. Chem. 269 (1994) 24343–24348.
[78] W.M. Schluchter, A.N. Glazer, Biliverdin Reductase: conversion of biliverdin to bilirubin is important for normal phycobiliprotein biosynthesis, J. Biol. Chem. 272 (1997) 13562–13569.
[79] H. Målen, F.S. Berven, K.E. Fladmark, H.G. Wiker, Comprehensive analysis of exported proteins from Mycobacterium tuberculosis H37Rv, Proteomics 7 (2007) 1702–1718.
[80] G. Bashiri, E.F. Perkowski, A.P. Turner, M.E. Feltcher, M. Braunstein, E.N. Baker, Tat–Dependent Translocation of an F(420)–Binding Protein of Mycobacterium tuberculosis, PLoS One 7 (2012) e45003.
[81] S. Nambu, T. Matsui, C.W. Goulding, S. Takahashi, M. Ikeda-Saito, A new way to degrade heme: the mycobacterium tuberculosis enzyme mhud catalyzes heme degradation without generating CO, J. Biol. Chem. 288 (2013) 10101–10109.
[82] A.B. Graves, R.P. Morse, A. Chao, A. Iniguez, C.W. Goulding, M.D. Liptak, Crystallographic and Spectroscopic Insights into Heme Degradation by Mycobacterium tuberculosis MhuD, Inorg. Chem. 53 (2014) 5931–5940.
[83] G.M. Cook, C. Greening, K. Hards, M. Berney, Chapter One - Energetics of Pathogenic Bacteria and Opportunities for Drug Development, in: K.P. Robert (Ed.) Adv. Microb. Physiol., 65, Academic Press 2014, pp. 1–62.
[84] J. Daniel, H. Maamar, C. Deb, T.D. Sirakova, P.E. Kolattukudy, Mycobacterium tuberculosis uses host triacylglycerol to accumulate lipid droplets and acquires a dormancy-like phenotype in lipid-loaded macrophages, PLoS Pathog. 7 (2011) e1002093.
[85] J.E. Galagan, P. Sisk, C. Stolte, B. Weiner, M. Koehrsen, F. Wymore, T.B.K. Reddy, J.D. Zucker, R. Engels, M. Gellesch, J. Hubble, H. Jin, L. Larson, M. Mao, M. Nitzberg, J. White, Z.K. Zachariah, G. Sherlock, C.A. Ball, G.K. Schoolnik, TB database 2010: Overview and update, Tuberculosis 90 (2010) 225–235.
[86] J. Pei, B.-H. Kim, N.V. Grishin, PROMALS3D: a tool for multiple protein sequence and structure alignments, Nucleic Acids Res. 36 (2008) 2295–2300.
[87] K. Tamura, G. Stecher, D. Peterson, A. Filipski, S. Kumar, MEGA6: Molecular Evolutionary Genetics Analysis version 6.0, Mol. Biol. Evol. 30 (2013) 2725–2729.
[88] L. Fu, B. Niu, Z. Zhu, S. Wu, W. Li, CD-HIT: accelerated for clustering the next-generation sequencing data, Bioinformatics 28 (2012) 3150–3152.
[89] P. Shannon, A. Markiel, O. Ozier, N.S. Baliga, J.T. Wang, D. Ramage, N. Amin, B. Schwikowski, T. Ideker, Cytoscape: A Software Environment for Integrated Models of Biomolecular Interaction Networks, Genome Res. 13 (2003) 2498–2504.
[90] D.G. Gibson, L. Young, R.-Y. Chuang, J.C. Venter, C.A. Hutchison, H.O. Smith, Enzymatic assembly of DNA molecules up to several hundred kilobases, Nat. Methods 6 (2009) 343–345.

[91] K.D. Tartof, C.A. Hobbs, Improved media for growing plasmid and cosmid clones, Focus 9 (1987) 12.
[92] M.H. Hefti, F.J. Milder, S. Boeren, J. Vervoort, W.J.H. van Berkel, A His-tag based immobilization method for the preparation and reconstitution of apoflavoproteins, Biochimi. Biophys. Acta 1619 (2003) 139–143.
[93] W. Kabsch, XDS. *Acta Crystallogr.* D Biol. Crystallogr. 66 (2010) 125–132.
[94] N. Collaborative Computational Project, The CCP4 Suite: Programs for Protein Crystallography, Acta Crystallogr. D Biol. Crystallogr. 50 (1994) 760–763.
[95] P.R. Evans, G.N. Murshudov, How good are my data and what is the resolution? Acta Crystallogr. D Biol. Crystallogr. 69 (2013) 1204–1214.
[96] A.J. McCoy, R.W. Grosse-Kunstleve, P.D. Adams, M.D. Winn, L.C. Storoni, R.J. Read, Phaser crystallographic software, J. Appl. Crystallogr. 40 (2007) 658–674.
[97] K. Cowtan, Fitting molecular fragments into electron density, Acta Crystallogr. D Biol. Crystallogr. 64 (2008) 83–89.
[98] C.G. Carolan, V.S. Lamzin, Automated identification of crystallographic ligands using sparse-density representations, Acta Crystallogr. D Biol. Crystallogr. 70 (2014) 1844–1853.
[99] P. Emsley, B. Lohkamp, W.G. Scott, K. Cowtan, Features and development of Coot, Acta Crystallogr. D Biol. Crystallogr. 66 (2010) 486–501.
[100] G.N. Murshudov, P. Skubak, A.A. Lebedev, N.S. Pannu, R.A. Steiner, R.A. Nicholls, M.D. Winn, F. Long, A.A. Vagin, REFMAC5 for the refinement of macromolecular crystal structures, Acta Crystallogr. D Biol. Crystallogr. 67 (2011) 355–367.
[101] P.D. Adams, P.V. Afonine, G. Bunkoczi, V.B. Chen, I.W. Davis, N. Echols, J.J. Headd, L.-W. Hung, G.J. Kapral, R.W. Grosse-Kunstleve, A.J. McCoy, N.W. Moriarty, R. Oeffner, R.J. Read, D.C. Richardson, J.S. Richardson, T.C. Terwilliger, P.H. Zwart, PHENIX: a comprehensive Python-based system for macromolecular structure solution, Acta Crystallogr. D Biol. Crystallogr. 66 (2010) 213–221.
[102] M.H.M. Olsson, C.R. Søndergaard, M. Rostkowski, J.H. Jensen, PROPKA3: Consistent Treatment of Internal and Surface Residues in Empirical pKa Predictions, J. Chem. Theory Comput. 7 (2011) 525–537.
[103] J.J. Irwin, T. Sterling, M.M. Mysinger, E.S. Bolstad, R.G. Coleman, ZINC: A Free Tool to Discover Chemistry for Biology, J. Chem. Inf. Model. 52 (2012) 1757–1768.
[104] M.L. Verdonk, J.C. Cole, M.J. Hartshorn, C.W. Murray, R.D. Taylor, Improved protein–ligand docking using GOLD, Proteins 52 (2003) 609–623.
[105] O. Trott, A.J. Olson, AutoDock Vina: Improving the speed and accuracy of docking with a new scoring function, efficient optimization, and multithreading, J. Comput. Chem. 31 (2010) 455–461.
[106] G.M. Morris, R. Huey, W. Lindstrom, M.F. Sanner, R.K. Belew, D.S. Goodsell, A.J. Olson, AutoDock4 and AutoDockTools4: Automated docking with selective receptor flexibility, J. Comput. Chem. 30 (2009) 2785–2791.
[107] G. Bashiri, A.M. Rehan, D.R. Greenwood, J.M. Dickson, E.N. Baker, Metabolic engineering of cofactor F_{420} production in Mycobacterium smegmatis, PLoS One 5 (2010) e15803.
[108] D. Isabelle, D.R. Simpson, L. Daniels, Large-scale production of coenzyme F_{420}-5,6 by using Mycobacterium smegmatis, Appl. Environ. Microbiol. 68 (2002) 5750–5755.
[109] E. Purwantini, B. Mukhopadhyay, R.W. Spencer, L. Daniels, Effect of temperature on the spectral properties of coenzyme F_{420} and related compounds, Anal. Biochem. 205 (1992) 342–350.
[110] D.B. Chen, D. Jason, Y. Kawasaki, J. Bommer, J.Y. Takemoto, Scalable production of biliverdin IXα by Escherichia coli, BMC Biochem. 12 (2012) 89.

4.3 Supplementary Material

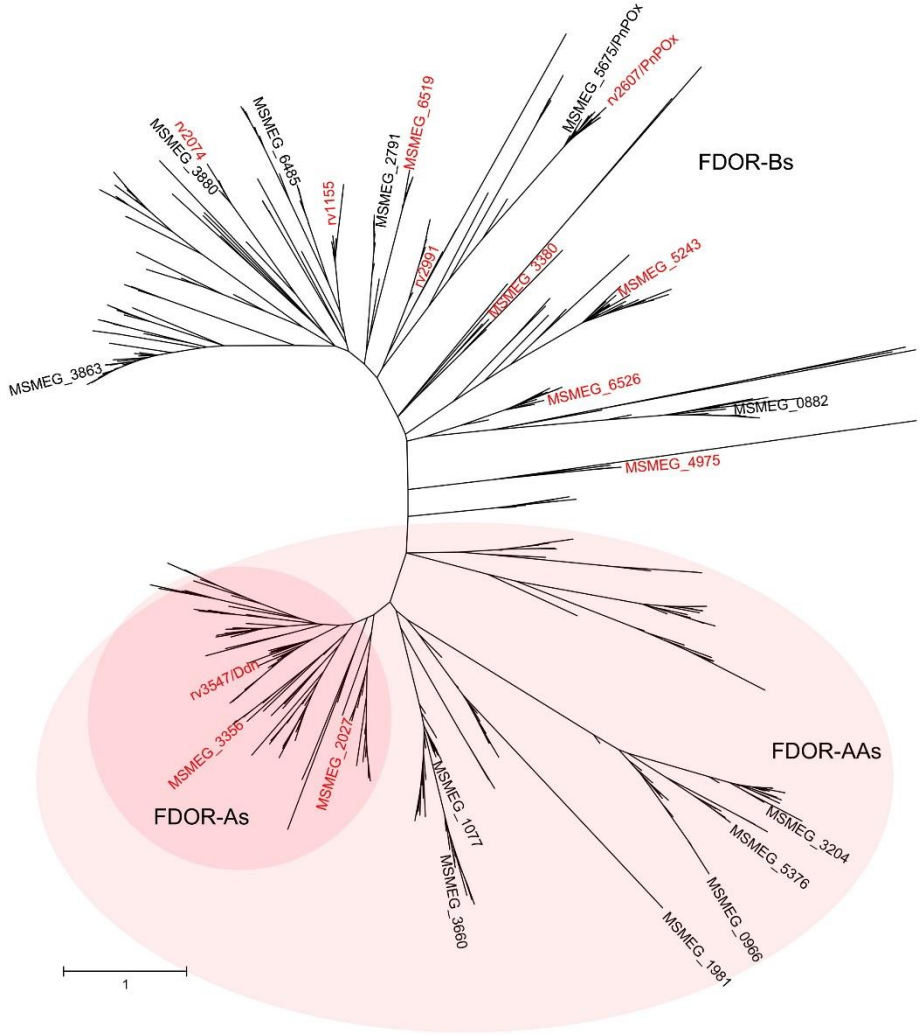

Fig. S1. Phylogenetic tree of the FDORs from *Mycobacteria*. All proteins characterised in this work from *M. smegmatis* (MSMEG_) and *M. tuberculosis* (rv) are annotated, where the solved crystal structures (in this work and previously) are annotated in red.

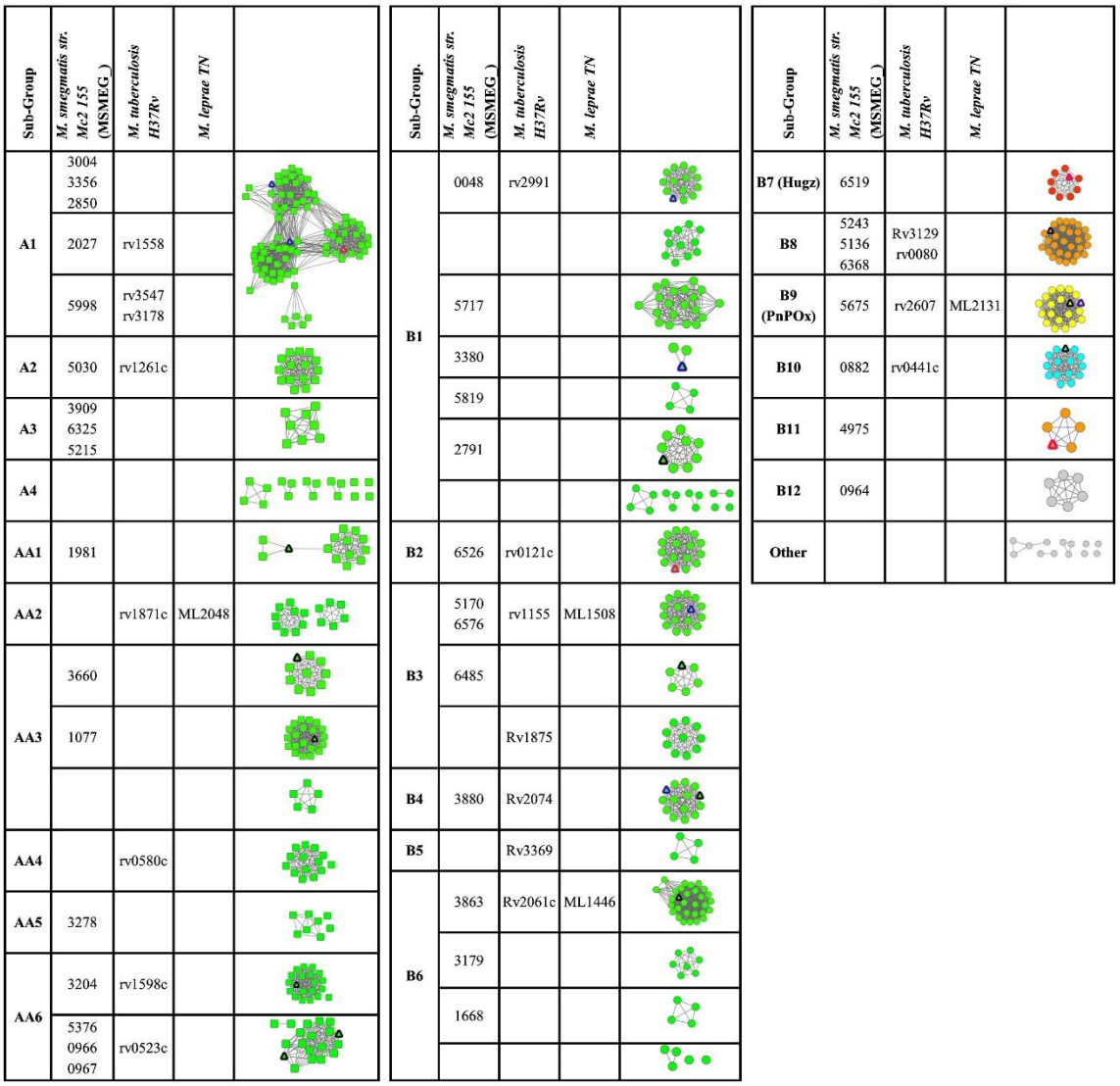

Fig. S2. Abundance and conservation of FDORs in mycobacteria. Nodes from the SSN (Fig. 2) were separated for cofactor specificity (FMN,yellow; FAD,orange; heme,red; non-specific,blue; not tested, gray) at a log*E* cutoff of − 7.6. The F_{420}-dependent proteins (green) were further separated at a log*E* cutoff of − 28, where each cluster represents proteins with ~ 50% sequence identity. Black and pink triangles represent proteins characterized and structures solved in this study, respectively. Blue triangles represent previously published structures

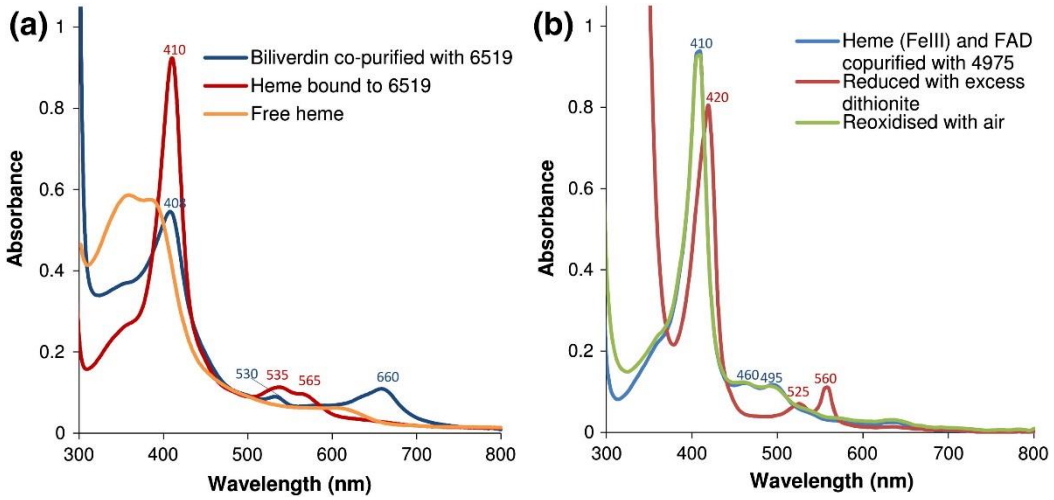

Fig. S3. Ligand-bound absorbance spectra of MSMEG_6519 and MSMEG_4975. (a) Heme coordination to MSMEG_6519 and spectra of co-purified biliverdin. (b) FAD and heme binding protein MSMEG_4975 and its reduction with sodium dithionite.

S4 Table. Comparison of $F_{420}H_2$ dependent reductase activity by proteins in the FDOR-A1 sub-group

substrate	**enzyme**	**K_m (µM)**	**K_{cat} (s^{-1})**	**K_{cat}/K_m (s^{-1} M^{-1})**
Menadione	2027	23.4 ± 2.56	0.567 ± 0.009	2.42×10^4
	3356	8.67 ± 1.09	2.39 ± 0.04	2.76×10^5
	rv3547*	3.44 ± 1.27	0.295 ± 0.002	8.58×10^4
PA-824	2027	nd	nd	nd
	3356	nd	nd	nd
	rv3547*	28.6 ± 3.55	0.078 ± 0.004	2.74×10^3

***** data from Gurumurthy et al. [1]

Data are averaged from two independent experiments ± standard error from the mean

nd, no detected activity

[1] Gurumurthy, M., Rao, M., Mukherjee, T., Rao, S. P., Boshoff, H. I., Dick, T., Barry, C. E., 3rd & Manjunatha, U. H. (2013). A novel F(420) -dependent anti-oxidant mechanism protects Mycobacterium tuberculosis against oxidative stress and bactericidal agents. *Mol Microbiol* **87**, 744-55.

S5 Table. Data collection and refinement statistics for crystallography.

Crystal	**MSMEG_2027**	**MSMEG_4975**	**MSMEG_6526**	**MSMEG_6519**
PDB ID	**4Y9I**	**4YBN**	**4ZKY**	**5BNC**
Data collection				
Space group	I1 2 1	C1 2 1	P 21 21 21	P 61
Unit-cell parameters				
a (Å)	37.49	84.72	56.7	62.10
b (Å)	36.85	59.88	59.42	62.10
c (Å)	77.59	89.66	95.99	301.41
α, β, γ (°)	90, 96.59, 90	90, 93.83, 90	90, 90, 90	90, 90, 120
Wavelength (Å)	1.5418	0.9655	0.9537	0.9537
Resolution range (Å)*	26.19-1.50 (1.52-1.50)	44.73-1.90 (1.94-1.90)	19.81-1.65 (1.67-1.65)	43.77-2.25 (2.32-2.25)
Unique reflections	16332	35306	39312	31095
Completeness (%)*	95.6 (92.1)	99.6 (99.2)	98.3 (76.8)	99.9 (99.2)
Multiplicity*	2.7 (2.7)	7.5 (7.6)	7.0 (3.9)	5.2 (3.2)
R_{merge} *#	0.062 (0.514)	0.101 (1.109)	0.057 (0.901)	0.097 (0.637)
R_{pim} *^	0.044 (0.369)	0.039 (0.428)	0.031 (0.667)	0.046 (0.417)
Mean $\langle I/\sigma(I)\rangle$*	13.0 (2.1)	13.0 (2.1)	21.3 (1.4)	14.1 (1.9)
$CC_{1/2}$ *†	0.997 (0.699)	0.998 (0.760)	0.999 (.467)	0.996 (0.516)
Molecules per asymmetric unit	1	2	2	2
solvent content (%, v/v)	41	45	51	56
Refinement				
Reflections used	16330	33553	39257	29399
Resolution range (Å)*	26.2-1.50 (1.54-1.50)	43.6-1.90 (1.95-1.90)	19.4-1.65 (1.68 -1.65)	43.8-2.25 (2.31-2.25)
R_{work} / R_{free} *‡	0.155/0.199 (0.267/0.334)	0.176/0.223 (0.274/0.313)	0.222/0.259 (0.324/0.362)	0.185/0.230 (0.282/0.332)
Number of atoms (all)	1170	3805	2398	3989
Water molecules	188	326	165	250
Average B-factor (Å²)				
Main chains	10.3	30.2	29.7	31.4
Side chains	13.6	36.5	33.0	35.7
Water molecules	26.2	41.5	32.2	36.0
FAD molecules	-	39.9	-	-
Heme molecules	-	35.1	-	-
R.M.S Deviations				
Bond Lengths (Å)	0.02	0.02	0.01	0.01
Bond Angles (°)	1.91	1.90	1.11	1.77
Chain A to B (Å)	-	0.51	1.1	1.4
Ramachandran plot regions (%)				
Favored	99.1	99.0	97.8	98.0
Allowed	0.9	1.0	1.8	1.8
Outliers	0	0	0.4	0.2

*Values in parenthesis are for the highest-resolution shell

#$R_{merge} = (\Sigma_{\mathbf{h}} \Sigma_i |I_{\mathbf{h}i} - \langle I_{\mathbf{h}}\rangle|) / (\Sigma_{\mathbf{h}} \Sigma_i \langle I_{\mathbf{h}}\rangle)$ where $\langle I_{\mathbf{h}}\rangle$ is the average intensity of *i* symmetry-related observations of the unique refection **h**.

^$R_{pim} = (\Sigma_{\mathbf{h}} \Sigma_i (1/(n_{\mathbf{h}} - 1))^{1/2} |I_{\mathbf{h}i} - \langle I_{\mathbf{h}}\rangle|) / (\Sigma_{\mathbf{h}} \Sigma_i \langle I_{\mathbf{h}}\rangle)$

†$CC_{1/2}$ = linear correlation coefficient between intensities from random half-datasets

‡$R_{work} = \Sigma_{\mathbf{h}} |F_{(obs)} - F_{(calc)}| / \Sigma_{\mathbf{h}} |F_{(obs)}|$ and 5% of the data that were excluded from the refinement were used to calculate R_{free}.

S6 Table. Genomic context and co-occurrence analysis of AA1-AA3 subgroups

Group	Protein	Associated protein	Biological role/process of associated protein	STRING score
AA1	MSMEG_1981	MSMEG_1982 (acyl coA synthetase)	Fatty acid biosynthesis	0.520
AA2	Rv1871c	Rv0593 (lipoprotein LprL)	Found when searching for genes that are present in *M. avium* that may help invade intestinal mucosa [47]. LprL and LprK are membrane bound lipoproteins.	0.860
		Rv0173 (lipoprotein LprK)		0.760
AA3	MUL2188	Cut5 (cutinase)	Cutin (fatty acid) hydrolysis, facilitates pathogenesis	0.601
		Cut1 (cutinase)		0.488
		Cut4 (cutinase)		0.469
		Lppx (lipoprotein)	Lipoprotein	0.561
		MUL_3253 (lipid A biosynthesis lauroyl acyltransferase)	Lipopolysaccharide synthesis for outer cell membrane	0.475
AA3	MSMEG_1077	MSMEG_1528 (cutinase)	Cutin (fatty acid) hydrolysis, facilitates pathogenesis	0.530
		Cut3 (cutinase)		0.515
		MSMEG_1526 (cutinase)		0.485
		MSMEG_4465 (cutinase)		0.439

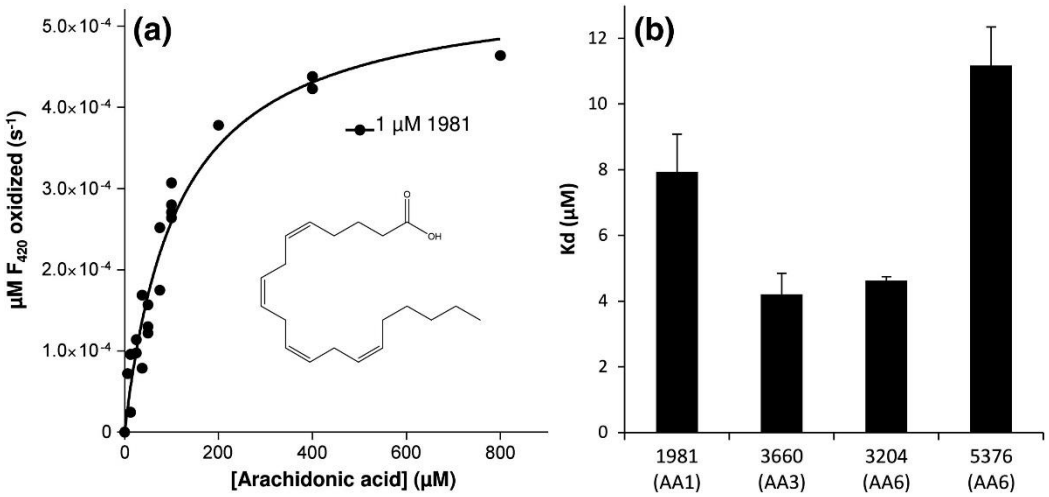

Fig. S7. Preliminary functional characterization of the FDOR-AAs. (a) Arachidonic reductase activity by MSMEG_1981 in the presence of 25 µM $F_{420}H_2$ (K_m = 113 ± 21 µM, $K_{cat} = 5.4 \times 10^{-4} \pm 2.0 \times 10^{-5}$ s^{-1}, andK_{cat}/K_m = 4.8 M^{-1} s^{-1}). (b) Affinity for arachidonic acid by FDOR-AAs

S8 Table. Text representation of conserved motifs in FDORs

No.	Motif (regular expression)	Role	Group
1	LT[TH]T**G**[RA]K[ST]**G**[KQ]PRxTP	F_{420} binding	All As and AAs
2	P[DA]**W**[YV]R**N**[LV][RK]A[NA][PG]x[VA][TE][VLI]	F_{420} binding	All As and AAs
3	[GD]R[YV][IV][VIL]V[AG]**S**[KN]G**G**[AR][PD]K[HN]	F_{420} and substrate binding	All As
4	E**Y**QA[KR]**T**[DS]**R**[VQ]**IP**[VL][FV][VEI][LC]	Substrate binding	All As
	V[TR]ARE[LAV]TG[DEA]ER[DA][RE]L[WL]		All As AA1, AA2
5	L[AT]T[VLF][RT][PA]**DG**R**P**[HQ][LV][SVT]P[VI]W[FY]AV	Cofactor binding	All Bs
6	SR**K**[VA]R[NR][IL]R[RA]DPR[VA][TSA][LVI]	F_{420} binding	B1-B6
7	F[FS]T[HDN]A[GT]**S**[RAQ]**K**[GAV][RH][EQ][IL][AE][HQ][NT]P[WR][AV][SA]	FMN binding	B9
8	EG[KT]**K**[IL]EM[AIM][ER]AN[PDN][NR]V[CL][FIV][ELT][AF]D	FAD binding	B8, B11
9	[IL][YC][IV]Sx[IL]AE**H**[GY]RNL[EA]A[ND]PR[AV][SD]	heme binding	B7
	G[RW][YW][VL]S[VA][ED]G[TR]A[ET][VIL]xxD[PG][AD]AV		B1-B4, B6, B8

S9 Text. Materials and Methods

Cloning, expression and purification of proteins. All sequences for the FDOR-B related proteins were ordered as Gene Strings from Invitrogen, with additional 50 base pair flanking regions at each end, homologous to the multiple cloning site (Nde1 – EcoR1) of the target cloning vector pETMCSIII. The sequence at the 5' end introduced a TEV protease cleavage site (GAGAACCTGTATTTTCAGGGT) between the His-tag and the N-terminus of the protein as well. These genes were amplified (forward primer: GTTTAATCGGATCCTAAGGAGGTTAATATTATG, reverse primer: GTTAGCAGCCG-GATCTATCGATGCATGCCATGGTAC) and cloned into pETMCSIII using Gibson assembly [1]. The genes for MSMEG_2027, MSMEG_3356 and the FDRAAs in the expression vector pDEST17 were generously provided by CSIRO [2]. Truncated MSMEG_2027 (Δ26 amino acids at the N-terminus) for protein crystallography was also cloned into petMCSIII using the Nde1 and EcoR1 restriction sites. (forward primer: CAAATAGTCATATGGTGCACGTGCTGGACCG, reverse primer: CAAGAATTCCT-ATTCGACGATGAACACGGGGATC).

The FDRAAs and MSMEG_3863 were purified using previously published methods [2]. For the rest of the proteins, *Escherichia coli* strain BL21DE3 cells were transformed and starter cultures were grown in TB media containing 0.5% glucose at 37 °C. After 6 hours, the starter cultures were transferred to and grown overnight at 25-30 °C in 1 L of modified auto-induction TB media [3], containing 5 g yeast extract, 20 g tryptone, 85.5 mM NaCl, 22 mM KH_2PO_4, 42 mM Na_2HPO_4, 0.6% glycerol, 0.05% glucose, 0.2% lactose and 100 µg/ml Ampicillin. Cell pellets were harvested by centrifugation at 5000 × g for 15 min at 4 °C, resuspended in 30 mL of lysis buffer (50 mM NaH_2PO_4, 300 mM NaCl, 25 mM imidazole, pH 8) and lysed by sonication using an Omni Sonicator Ruptor 400 (3 × 3 min at 60% power). The soluble fraction was separated by further centrifugation at 13000 × g for 1 hr at 4 °C and the lysate was passed onto a Qiagen or GE NiNTA column, where the purified protein was eluted with the same buffer containing an additional 250 mM imidazole.

An additional step was performed before elution for the MSMEG_5243 and MSMEG_5675 prepared for cofactor binding assays. The flavin co-purified with the protein was stripped by partial on-column protein refolding [4], which involved washing with buffer containing 50 mM NaH_2PO_4, 300 mM NaCl, 2 M urea and 2 M KBr at pH 6.5. The eluted samples were dialyzed into 50 mM Tris-HCl, 200 mM NaCl, pH 8 and stored at 4°C. Proteins used for crystallography were further purified by cleaving off the His-tag with TEV protease (expressed and purified in-house) and removing it by a second pass through the NiNTA column. They were then further purified by size exclusion chromatography using a GE Hiload 16/600 Superdex 75 pg column, and the final sample was concentrated to 1.3 mM (~30 mg/mL) in buffer containing 20 mM HEPES, 50 mM NaCl, pH 7.5.

Protein crystallography. High-throughput screens from Hampton Research were used to identify initial crystal forming conditions for MSMEG_2027, MSMEG_6526, MSMEG_6519 as well as cofactor-bound MSMEG_4975. Truncated MSMEG_2027 (NΔ26) was used since the full-length protein failed to crystallize, similar to what was observed for the closely related protein rv3547 [5]. Refined conditions for the crystals used for data collection were as follows: MSMEG_2027 = 20% PEGMME5000, 0.05 M imidazole pH 6.7; MSMEG_4975 = 25 % PEG4000, 0.2 M ammonium sulfate, 0.1 M sodium acetate pH 4.6; MSMEG_6526 = 0.2 M sodium iodide, 22% PEG3350; and MSMEG_6519 = 0.2 M magnesium acetate, 0.1M HEPES pH 7.5 and 23% PEG3350.

Data for MSMEG_2027 was collected in house (Xenocs GeniX 3D Cu HF microbeam X-ray generator, MAR345 plate detector) and MSMEG_4975, MSMEG_6526 and MSMEG_6519 were collected at the Australian Synchrotron (beamline MX1 and detector ADSC Q210r for MSMEG_6519, beamline MX2 and detector ADSC Q315r for MSMEG_4975 and MSMEG_6526). Crystals were cryo-cooled under a stream of 100K nitrogen gas in the following cryobuffers: MSMEG_2027 - 35% PEGMME5000, 0.05 M imidazole pH 6.7, 500 µM FMN; MSMEG_4975 - 35 % PEG4000, 0.2 M ammonium sulfate, 0.1 M sodium acetate pH 4.6; MSMEG_6526 - 0.2 M sodium iodide, 22% PEG3350, 13% ethylene glycol; MSMEG_6519 - 0.2 M magnesium acetate, 0.1M HEPES pH 7.5 and 24% PEG3350, 11% ethylene glycol. Diffraction data were integrated using XDS [6], and the CCP4 suite [7] was used for scaling using AIMLESS [8], followed by molecular replacement using Phaser [9]. The structures 3R5Z [5] 3FHK,2FUR, 4QVB [10] and 2ARZ were obtain phases for MSMEG_2027, MSMEG_5243, MSMEG_4975, MSMEG_6526 and MSMEG_6519 respectively. Model building was performed using Buccaneer [11] and ARP/wARP [12] followed by manual loop building in Coot [13]. Interspersed refinements were done using Refmac [14] and PHENIX [15]. Local non-crystallographic symmetry restraints were used for the refinement of MSMEG_4975, MSMEG_6519 and MSMEG_6526. A difference (mF_o – dF_c) omit map for FAD and heme in MSMEG_4975 was generated by refining the structure with the ligands removed (restrained refinement with no prior phase information using Refmac [14]).

1. Gibson, D. G., Young, L., Chuang, R.-Y., Venter, J. C., Hutchison, C. A. & Smith, H. O. (2009). Enzymatic assembly of DNA molecules up to several hundred kilobases. *Nat Meth* **6**, 343-345.
2. Lapalikar, G. V., Taylor, M. C., Warden, A. C., Scott, C., Russell, R. J. & Oakeshott, J. G. (2012). F420-H2-Dependent Degradation of Aflatoxin and other Furanocoumarins Is Widespread throughout the Actinomycetales. *PLoS One* **7**, e30114.
3. Tartof, K. D. & Hobbs, C. A. (1987). Improved media for growing plasmid and cosmid clones. *Focus* **9**.
4. Hefti, M. H., Milder, F. J., Boeren, S., Vervoort, J. & van Berkel, W. J. H. (2003). A His-tag based immobilization method for the preparation and reconstitution of

apoflavoproteins. *Biochimica et Biophysica Acta (BBA) - General Subjects* **1619**, 139-143.

5. Cellitti, Susan E., Shaffer, J., Jones, David H., Mukherjee, T., Gurumurthy, M., Bursulaya, B., Boshoff, Helena I., Choi, I., Nayyar, A., Lee, Yong S., Cherian, J., Niyomrattanakit, P., Dick, T., Manjunatha, Ujjini H., Barry Iii, Clifton E., Spraggon, G. & Geierstanger, Bernhard H. (2012). Structure of Ddn, the Deazaflavin-Dependent Nitroreductase from Mycobacterium tuberculosis Involved in Bioreductive Activation of PA-824. *Structure* **20**, 101-112.
6. Kabsch, W. (2010). XDS. *Acta Crystallographica Section D* **66**, 125-132.
7. Collaborative Computational Project, N. (1994). The CCP4 Suite: Programs for Protein Crystallography. *Acta Crystallogr.* **D50**, 760-763.
8. Evans, P. R. & Murshudov, G. N. (2013). How good are my data and what is the resolution? *Acta Crystallographica Section D* **69**, 1204-1214.
9. McCoy, A. J., Grosse-Kunstleve, R. W., Adams, P. D., Winn, M. D., Storoni, L. C. & Read, R. J. (2007). Phaser crystallographic software. *J. Appl. Crystallogr.* **40**, 658-674.
10. Mashalidis, E. H., Gittis, A. G., Tomczak, A., Abell, C., Barry, C. E. & Garboczi, D. N. (2015). Molecular insights into the binding of coenzyme F420 to the conserved protein Rv1155 from Mycobacterium tuberculosis. *Protein Sci.* **24**, 792-740.
11. Cowtan, K. (2008). Fitting molecular fragments into electron density. *Acta Crystallographica Section D* **64**, 83-89.
12. Carolan, C. G. & Lamzin, V. S. (2014). Automated identification of crystallographic ligands using sparse-density representations. *Acta Crystallographica Section D* **70**, 1844-1853.
13. Emsley, P., Lohkamp, B., Scott, W. G. & Cowtan, K. (2010). Features and development of Coot. *Acta Crystallographica Section D* **66**, 486-501.
14. Murshudov, G. N., Skubak, P., Lebedev, A. A., Pannu, N. S., Steiner, R. A., Nicholls, R. A., Winn, M. D., Long, F. & Vagin, A. A. (2011). REFMAC5 for the refinement of macromolecular crystal structures. *Acta Crystallographica Section D* **67**, 355-367.
15. Adams, P. D., Afonine, P. V., Bunkoczi, G., Chen, V. B., Davis, I. W., Echols, N., Headd, J. J., Hung, L.-W., Kapral, G. J., Grosse-Kunstleve, R. W., McCoy, A. J., Moriarty, N. W., Oeffner, R., Read, R. J., Richardson, D. C., Richardson, J. S., Terwilliger, T. C. & Zwart, P. H. (2010). PHENIX: a comprehensive Python-based system for macromolecular structure solution. *Acta Crystallographica Section D* **66**, 213-221.

4.4 Rv2074 is a novel $F_{420}H_2$-dependent biliverdin reductase in *Mycobacterium tuberculosis*

The following paper is presented in this chapter

Rv2074 is a novel $F_{420}H_2$-dependent biliverdin reductase in *Mycobacterium tuberculosis*

F. Hafna Ahmed, A. Elaaf Mohamed, Paul D. Carr, Brendon M. Lee, Karmen Condic-Jurkic, Megan L. O'Mara, and Colin J. Jackson

Protein Science, 25(9), 1692-1709.

Current status of paper: Published

Hafna Ahmed performed most of the experiments including enzyme assays, NMR, bioinformatics, protein purification and crystallography. Elaaf Mohamed performed and analysed all the computational simulations assisted by Karmen Condic-Jurkic and Megan O'Mara. Paul Carr collected the crystallography data and helped with structure refinement. I prepared and purified F420 for the experiments and developed the enzyme assay. Hafna Ahmed, Elaaf Mohamed, and Colin Jackson wrote the paper with input from all authors.

THE PROTEIN SOCIETY

Rv2074 is a novel $F_{420}H_2$-dependent biliverdin reductase in *Mycobacterium tuberculosis*

F. Hafna Ahmed, A. Elaaf Mohamed, Paul D. Carr, Brendon M. Lee, Karmen Condic-Jurkic, Megan L. O'Mara, and Colin J. Jackson*

Research School of Chemistry, The Australian National University, Canberra, ACT 2601, Australia

Received 11 May 2016; Accepted 29 June 2016
DOI: 10.1002/pro.2975
Published online 1 July 2016 proteinscience.org

Abstract: Bilirubin is a potent antioxidant that is produced from the reduction of the heme degradation product biliverdin. In mammalian cells and Cyanobacteria, NADH/NADPH-dependent biliverdin reductases (BVRs) of the Rossmann-fold have been shown to catalyze this reaction. Here, we describe the characterization of Rv2074 from *Mycobacterium tuberculosis*, which belongs to a structurally and mechanistically distinct family of $F_{420}H_2$-dependent BVRs (F-BVRs) that are exclusively found in Actinobacteria. We have solved the crystal structure of Rv2074 bound to its cofactor, F_{420}, and used this alongside molecular dynamics simulations, site-directed mutagenesis and NMR spectroscopy to elucidate its catalytic mechanism. The production of bilirubin by Rv2074 could exploit the anti-oxidative properties of bilirubin and contribute to the range of immunoevasive mechanisms that have evolved in *M. tuberculosis* to allow persistent infection.

Keywords: F420; biliverdin reductase; biliverdin; bilirubin; *Mycobacterium tuberculosis*; mycobacteria; enzyme catalysis; flavin/deazaflavin oxidoreductase

Abbreviations: BVR, biliverdin reductase; ESI-MS, electrospray ionization mass spectrometry; F_{420}, factor 420; F-BVR, $F_{420}H_2$-dependent biliverdin reductase; FDOR, flavin/deazaflavin oxidoreductase; Fgd, F420-dependent glucose-6-phopshate dehydrogenase; G6P, glucose-6-phosphate; HO, heme oxygenase; MD, molecular dynamics; NO, nitric oxide; RMSD, root mean square deviation; RMSF, root mean square fluctuation; WT, wild type

Statement: Rv2074 from *Mycobacterium tuberculosis*, the causative agent of Tuberculosis, belongs to a novel class of $F_{420}H_2$-dependent biliverdin reductases found in Actinobacteria. It reduces biliverdin-IXα to bilirubin-IXα, a potent antioxidant. As biliverdin-IXα is produced in high amounts in macrophages infected with *M. tuberculosis*, its reduction by Rv2074 could play a role in protecting mycobacteria against oxidative stress, aiding the persistence of *M. tuberculosis* infection.

Grant sponsor: The Australian Research Council; Grant numbers: DE120102673, DP130102144; Grant sponsor: CJJ, Australian Research Council; Grant numbers: DE120101550, National Health and Medical Research Council, APP1049685, MLO and the Australian National University PhD scholarships awarded to FHA and AEM.

*Correspondence to: Colin J. Jackson, Research School of Chemistry, The Australian National University, ACT 2601, Australia. E-mail: colin.jackson@anu.edu.au

Introduction

Biliverdin is a naturally occurring linear tetrapyrrole produced from the oxidative degradation of heme by heme oxygenases (HOs) (Fig. 1).[1] It is used for a variety of purposes, for instance as the precursor to light harvesting phycobilins in Cyanobacteria and green algae,[2] and as pigmentation in birds, amphibians and reptiles.[3] In mammals, biliverdin is reduced to bilirubin by biliverdin reductases (BVRs).[4] Bilirubin is toxic in high concentrations and mostly excreted after solubilization by conjugation with glucuronic acid.[4] However, it is also a strong antioxidant and lipophilic radical scavenger,[5] capable of compensating for a 10,000-fold increase in reactive oxygen species and quenching reactive nitrogen species like nitric oxide (NO) to protect against cellular oxidative damage.[6–9]

Two BVR isoforms have been identified from mammalian cells, BVR-A and BVR-B.[6,10–12] BVR-A reduces biliverdin-IXα (formed by the cleavage of heme at the α-meso position) to bilirubin-IXα (Fig. 1).[10,12] It is the predominant isoform found in

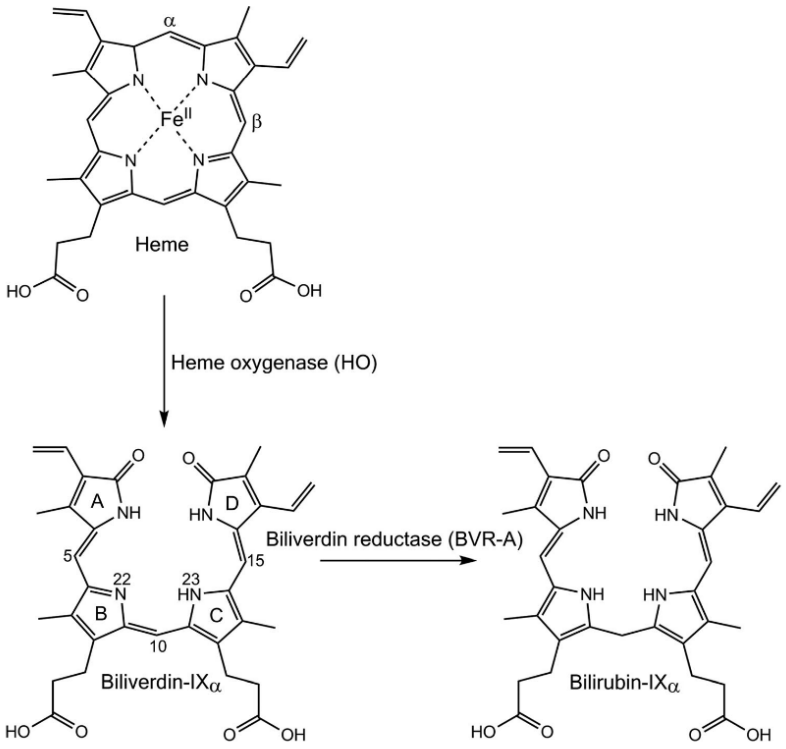

Figure 1. Structures of the heme degradation products biliverdin-IXα and bilirubin IXα. Pyrrole rings (A–D) and atom positions discussed in the text are labeled on biliverdin-IXα.

adult mammalian tissue,[13] with the highest expression levels found in the brain, lungs and pancreas.[12,14] BVR-B is highly expressed in fetal tissue and reduces biliverdin-IXβ (heme cleaved at the β-meso position) to bilirubin-IXβ.[12] In adults, bilirubin-IXβ constitutes just 3–5% of total bilirubin in bile while 95–97% is bilirubin-IXα.[15] Both mammalian BVR isoforms utilize a nicotinamide cofactor (NADH or NADPH) as an electron donor and have catalytic domains similar to short-chain alcohol dehydrogenases with a core α/β dinucleotide binding motif (a "Rossmann" fold).[16,17] BVR-A also contains an additional C-terminal domain that forms a six stranded β-sheet, containing additional motifs for regulatory serine/threonine kinase activity and DNA and transcription factor binding sites that allows participation in cellular signaling.[11,17] In mammals, BVR-A expression is induced in response to stress resulting from reactive oxygen species, endotoxins and heavy metals,[10,18] and has been shown to confer resistance towards oxidative stress.[19,20] This is partly because of its involvement in signaling during inflammation,[11,21] for instance in the induction of anti-inflammatory cytokines,[22] modulation of downstream cytokine responses,[23] and upregulation of oxidative stress response proteins like HO.[24] However, the oxidative stress resistance conferred by BVR-A can also be attributed to the antioxidative and cytoprotective nature of the bilirubin produced.[6–9]

Although the antioxidative and anti-inflammatory roles of BVR and bilirubin in mammalian cells have been widely described and studied,[21] only one other BVR has been characterized; an NADH/NADPH-dependent enzyme from the cyanobacterium *Synechocystis* sp. PCC 6803.[25] *In vivo* production of bilirubin has been detected in *Salmonella enterica serovar Typhimurium*,[26] but the protein that was responsible for this transformation was not identified. Although there has been relatively little focus on prokaryotic BVRs, bilirubin can have a similar antioxidative effect on bacterial cells.[27] Recent work has shown that infection of macrophages by *Mycobacterium tuberculosis*, *Mycobacterium avium*, and *Mycobacterium abscessus* induces HO production,[27–29] which produces biliverdin and subsequently bilirubin, and that these molecules have a protective effect on the bacteria during early infection.[27] Bilirubin has also been shown to downregulate the production of inducible nitric oxide

synthases,[30,31] that generate microbicidal NO in human and murine macrophages infected with *M. tuberculosis*.[32,33]

The many strategies used by *M. tuberculosis* to evade the host immune response, including the involvement of BVRs, are not well understood, but are of critical importance because they allow the pathogen to persist within macrophages, leading to latent infection.[34] Over a third of the world's population is infected by latent *M. tuberculosis*, which can convert to active tuberculosis (TB), especially in immune-compromised patients, resulting in approximately 10 million cases of TB and 1.5 million deaths in 2015.[35] Our recent functional assignment of a flavin/deazaflavin oxidoreductase (FDOR) superfamily in Actinobacteria,[36] showed that the *M. tuberculosis* protein Rv2074 had significant sequence similarity to a novel BVR from *Mycobacterium smegmatis* (MSMEG_3880) that is structurally and mechanistically distinct to the previously described NADH/NADPH-dependent BVRs, relying on the deazaflavin cofactor $F_{420}H_2$.[36] The crystal structure of Rv2074 was first solved as an apo-protein 10 years ago,[37] and annotated as an FMN-dependent pyridoxine 5′-phosphate oxidase. To better understand the function and physiological roles of $F_{420}H_2$-dependent biliverdin reductases (F-BVRs) in TB, we have performed a detailed mechanistic analysis of Rv2074, solving its X-ray crystal structure in complex with F_{420} for the first time, and elucidating its catalytic mechanism using site-directed mutagenesis, molecular dynamics simulations and NMR spectroscopy. We also show that this family of BVRs is exclusive to Actinobacteria and is abundant in pathogenic and commensal mycobacteria, where they are likely to produce bilirubin during infection as an antioxidant and cytoprotectant.

Results

Rv2074 reduces biliverdin-IXα to bilirubin-IXα

To further investigate the predictions from our bioinformatics analysis,[36] specifically that the *M. tuberculosis* FDORs Rv2074 and Rv1155 are biliverdin reductases,[36] we tested the ability of these enzymes to catalyze the reduction of biliverdin-IXα to bilirubin-IXα *in vitro* using purified, recombinant proteins. In the absence of either enzyme, no increase in absorbance was observed in the broad peak at 450 nm that is characteristic of bilirubin-IXα production [Fig. 2(A)]. Similarly, the reaction did not proceed in the absence of glucose-6-phosphate (G6P) or F_{420}-dependent G6P dehydrogenase (Fgd) required for $F_{420}H_2$ production. In contrast, when Rv2074 and Rv1155 were included in the reaction, we observed a rapid change in the UV/Vis spectrum of the reaction, with a reduction in the absorbance of the peaks characteristic of biliverdin-IXα at 390 nm and 690 nm. Bilirubin-IXα formation is indicated by the increase in absorbance at 450 nm that includes a shoulder at 510 nm due to its low solubility in aqueous solutions at pH 7.5.[38] The characteristic spectroscopic peaks of these compounds allowed us to monitor the reaction continuously and obtain kinetic parameters for the enzyme-catalyzed reactions [Fig. 2(B), Table I]. Rv2074 exhibited kinetic efficiency that is consistent with a native substrate, with a low K_M value of 8.0 ± 1.0 μM and a k_{cat}/K_M of 9×10^3 M^{-1} s^{-1} that is comparable to other FDORs with their proposed native substrates like the menaquinone analogue menadione for the $F_{420}H_2$-dependent quinone reductase Rv3547 (K_M value of 3.4 ± 1.3 μM and k_{cat}/K_M of 9×10^4 M^{-1} s^{-1}).[39] It is also comparable to its homolog from *M. smegmatis* MSMEG_3880 (K_M of 5.7 ± 0.2 and k_{cat}/K_M of 4×10^4 M^{-1} s^{-1}) that has 85% amino acid identity with Rv2074.[36] Mammalian and cyanobacterial BVR-As have similar K_M values ranging from 1 to 7 μM, and a range of specific activities reported at the maximum observed reaction rate (0.2–8 μmol min^{-1} mg^{-1})[40–43] that are comparable to Rv2074 (0.18 μmol min^{-1} mg^{-1}). In contrast to Rv2074, the k_{cat}/K_M of Rv1155 for biliverdin-IXα was 30-fold lower (3×10^2 M^{-1} s^{-1}), and the K_M for the substrate was 10-fold higher, at 82 ± 13 μM, which suggests biliverdin-IXα is unlikely to be the native substrate of Rv1155, and that it is likely to have evolved to catalyze the reduction of an alternative molecule.

Our previous preliminary assignment of biliverdin reductase activity to this family of mycobacterial proteins was based on spectroscopic analysis, but did not explore the reaction mechanism in detail.[36] To confirm whether reduction was taking place, and to identify the nature of the reaction, we performed mass spectrometry on the purified reaction products [Fig. 2(C)]. Electrospray ionization mass spectrometry (ESI-MS) was used to confirm loss of a compound with an equivalent mass to biliverdin-IXα (582.2 Da; observed $[M-H]^- m/z = 581.4$) and accumulation of a product with an equivalent mass to bilirubin-IXα (584.3 Da; $[M-H]^- m/z = 583.4$). This was followed by proton NMR-spectroscopy to identify the position at which biliverdin-IXα was reduced [Fig. 2(D)]. The proton NMR spectra for the products (assigned as previously described)[44] showed that the reaction products from the Rv2074 and Rv1155-catalyzed reactions were essentially identical and displayed clear singlets at 4.09, 6.15 and 6.22 ppm corresponding to a methylene bridge at the C10 position and methine moieties at the C15 and C5 positions of bilirubin, respectively, thus confirming the specific reduction of biliverdin at the C10 position.

The structure of Rv2074 with its native cofactor, F_{420}

The apo-enzyme structure of Rv2074 has been reported previously,[37] and was initially suggested to

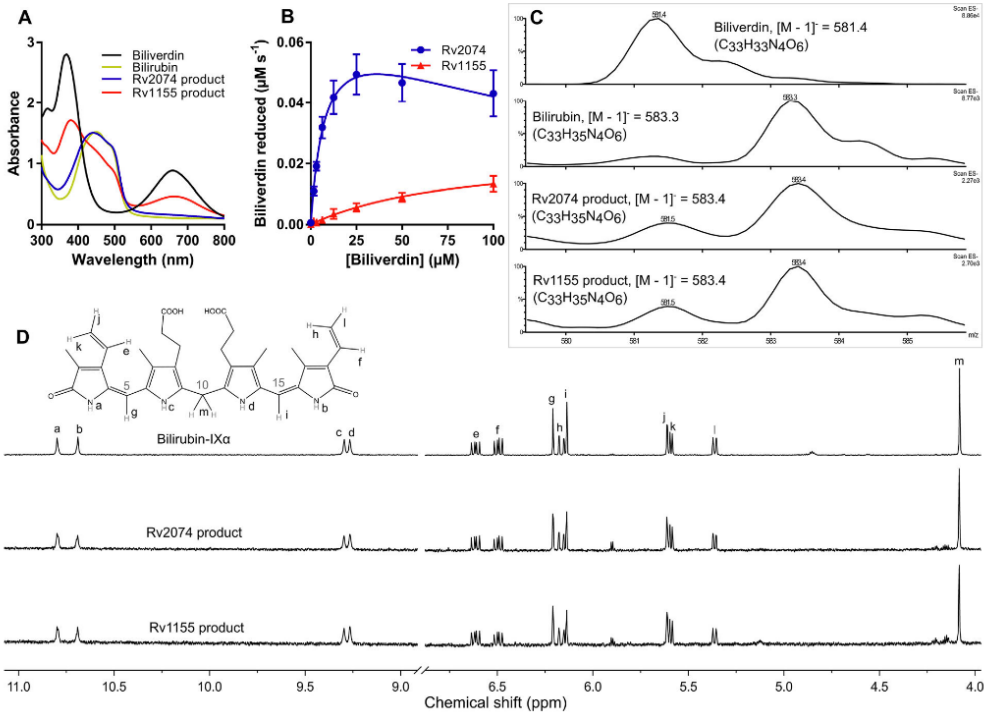

Figure 2. Characterization of F-BVRs from *M. tuberculosis* and the reaction product formed. **A.** Absorbance spectra in aqueous solution of the reaction products formed by Rv2074 and Rv1155 in comparison to biliverdin-IXα and bilirubin-IXα. Differences between the Rv2074 and Rv1155 products to pure bilirubin-IXα can be attributed to remaining unreacted biliverdin-IXα. **B.** Activity of Rv2074 and Rv1155 (1 μM) with biliverdin-IXα in the presence of reduced $F_{420}H_2$. For Rv2074, $K_M = 8.0 \pm 1.0$ μM, $k_{cat} = 7.5 \times 10^{-2} \pm 4.5 \times 10^{-3}$ s^{-1} and $k_{cat}/K_M = 8.9 \times 10^3$ M^{-1} s^{-1}. For Rv1155, $K_M = 82.8 \pm 12.7$ μM, $k_{cat} = 2.4 \times 10^{-2} \pm 2.1 \times 10^{-3}$ s^{-1}, and $k_{cat}/K_M = 2.9 \times 10^2$ M^{-1} s^{-1}. **C.** Low resolution (ESI negative) mass spectra of the reaction products compared to biliverdin-IXα and bilirubin-IXα. **D.** Proton NMR spectra of the products formed compared with bilirubin-IXα. Chemical shifts were assigned as previously reported,[44] and peaks for the methyl and propionate substituents are not shown for clarity.

be an FMN-dependent enzyme based on homology to the human and *Escherichia coli* pyridoxamine 5′-phosphate oxidases.[45,46] However, our bioinformatics analysis suggested that it might instead function with F_{420} as a cofactor.[36] The results presented in Figure 2 are the first demonstration of any catalytic activity with Rv2074, and notably occur in an $F_{420}H_2$ dependent-fashion, suggesting that it is indeed an $F_{420}H_2$ dependent oxidoreductase. In order to better understand the catalytic mechanism involved in biliverdin-IXα reduction, we have solved the structure of Rv2074 in complex with F_{420} at a resolution of 1.65 Å (Table II). Omit electron density corresponding to one molecule of F_{420} with an oligo-glutamate tail consisting of three residues is observed in the cofactor binding site of each of the

Table I. In vitro *Activity of Rv2074, Rv1155, and Rv2074 Mutants with Biliverdin IXα*

Protein	k_{cat} (s^{-1})	K_M (μM)	k_{cat}/K_M (M^{-1} s^{-1})
Rv2074	$7.2 \times 10^{-2} \pm 4.5 \times 10^{-3}$	8.0 ± 1.0	8.9×10^3
Rv1155	$2.4 \times 10^{-2} \pm 2.1 \times 10^{-3}$	82.8 ± 12.7	2.9×10^2
R21A	$5.1 \times 10^{-2} \pm 5.5 \times 10^{-3}$	15.4 ± 3.0	3.3×10^3
R109A	$4.0 \times 10^{-2} \pm 2.3 \times 10^{-3}$	21.2 ± 3.3	1.9×10^3
R112A	$4.7 \times 10^{-2} \pm 3.3 \times 10^{-3}$	13.8 ± 1.7	3.4×10^3
R117A	$2.0 \times 10^{-2} \pm 1.4 \times 10^{-3}$	19.7 ± 3.7	1.0×10^3
Y104A	$0.7 \times 10^{-2} \pm 6.8 \times 10^{-3}$	12.8 ± 3.9	0.5×10^3
Y104F	$1.4 \times 10^{-2} \pm 1.4 \times 10^{-3}$	14.8 ± 2.5	1.0×10^3
Y108A	$0.4 \times 10^{-2} \pm 6.9 \times 10^{-3}$	19.0 ± 8.4	0.2×10^3
Y108F	$2.0 \times 10^{-2} \pm 5.6 \times 10^{-3}$	7.6 ± 0.7	2.7×10^3

Table II. *Data Collection and Refinement Statistics for Crystallography*

Data collection	
Space group	P 2 21 21
Unit-cell parameters	
a, b, c (Å)	61.76, 88.62, 98.62
α, β, γ (°)	90, 90, 90
Wavelength (Å)	0.9537
Resolution range (Å)[a]	65.9–1.65 (1.68–1.65)
Unique reflections[a]	65830 (3221)
Completeness (%)[a]	100 (99.6)
Multiplicity[a]	7.1 (6.7)
R_{merge}[a,b]	0.181 (1.261)
R_{pim}[a,c]	0.073 (0.527)
Mean $<I/\sigma(I)>$[a]	9.3 (1.7)
$CC_{1/2}$[a,d]	0.994 (0.581)
Molecules per asymmetric unit	4
Solvent content (%, v/v)	43.8
Refinement	
Reflections used	62534
Resolution range (Å)[a]	65.92–1.65 (1.69–1.65)
R_{work}/R_{free}[a,e]	0.178/0.217 (0.295/0.375)
Number of atoms (all)	5032
Water molecules	654
Average B-factor (Å²)	
Main chains	17.9
Side chains	22.3
Water molecules	30.5
F_{420} molecules	22.9
R.M.S. deviations	
Bond lengths (Å)	0.019
Bond angles (°)	1.962
Ramachandran plot regions (%)	
Favored	98.6
Allowed	1.4
Outliers	0
PDB ID	**5JAB**

[a] Values in parenthesis are for the highest-resolution shell.
[b] $R_{merge} = (\Sigma_{\mathbf{h}} \Sigma_i |I_{\mathbf{h}i} - \langle I_{\mathbf{h}} \rangle|)/(\Sigma_{\mathbf{h}} \Sigma_i \langle I_{\mathbf{h}} \rangle)$, where $\langle I_{\mathbf{h}} \rangle$ is the average intensity of i symmetry-related observations of the unique refection **h**.
[c] $R_{pim} = (\Sigma_{\mathbf{h}} \Sigma_i (1/(n_{\mathbf{h}} - 1))^{1/2} |I_{\mathbf{h}i} - \langle I_{\mathbf{h}} \rangle|)/(\Sigma_{\mathbf{h}} \Sigma_i \langle I_{\mathbf{h}} \rangle)$.
[d] $CC_{1/2}$ = linear correlation coefficient between intensities from random half-datasets.
[e] $R_{work} = \Sigma_{\mathbf{h}} |F_{(obs)} - F_{(calc)}|/\Sigma_{\mathbf{h}} |F_{(obs)}|$ and 5% of the data that were excluded from the refinement were used to calculate R_{free}.

four protein chains in the asymmetric unit. Each monomer adopts the conserved split β-barrel protein fold characteristic of the FDORs, as previously described,[36,47–49] and the proteins are arranged as homodimers, which is supported by analysis from the Proteins, Interfaces, Structures and Assemblies (PISA) server [Fig. 3(A)].[50] The F_{420} binding site is located at the dimer interface as observed in the Rv1155-F_{420} complex,[49] and also in complexes of FDORs with other flavin cofactors, including the FMN binding pyridoxamine-5-phosphate oxidases and the FAD binding MSMEG_4975 from *M. smegmatis*.[36,45,46] In many respects, the binding of F_{420} to Rv2074 is similar to that observed in Rv1155 [Fig. 3(B)],[49] particularly at the phosphate group, which is coordinated by a highly conserved lysine residue (Lys-61) that is present in all members of the FDOR-B superfamily.[36] However, whereas the deazaflavin moiety in Rv1155 was observed to be present in a bent "butterfly" conformation, it is planar in Rv2074.

Each F_{420} molecule is coordinated through an extensive network of intermolecular interactions [Fig. 3(C)]. Hydrogen bonds between the nitrogen and carboxyl groups of the deazaflavin moiety of F_{420} and residues from Chain A of the homodimer include the main chain amide group of Gly-41 and the side chains of Thr-55, Thr-56, and Tyr-104. In addition, the carbonyl group of Gly-78 of Chain B hydrogen bonds to the hydroxyl group of the deazaflavin. Hydrophobic interactions from Leu-23, Ala-39, and Val-40 in Chain A and Val-76 in Chain B provide additional stabilization to the aromatic rings. The highly conserved base Lys-61 from Chain A stabilizes the ribityl moiety and forms a salt bridge to the negatively charged phosphate group, along with His-36. Trp-81 from Chain B also hydrogen bonds with the ribityl moiety. Val-38 of Chain A and Leu-128 of Chain B form hydrophobic interactions with the methyl group of the lactyl moiety. A series of positively charged residues form salt bridges with the negatively charged glutamate side chains of the oligoglutamate tail (His-36, Gln-60, Arg-67 of Chain A and Arg-126 of Chain B).

In comparison with the apo-enzyme,[37] the overall topology of the F_{420} bound protein remains mostly unchanged, except that residues at the cofactor binding site undergo conformational change to optimize its interaction with F_{420} [Fig. 3(D)]. These include Lys-61, Arg-67, Gln-60, and His-36 from Chain A and Arg-126 from Chain B that interact with the oligoglutamate chain of F_{420} and Leu-23 from Chain A that has moved further away due to hydrophobic interactions with the deazaflavin moiety. In addition, Chain B of the F_{420} bound complex moves closer to Chain A, due to the association of Val-76, Gly-78, Ala-79, Trp-81, and Leu-128 of Chain B with the cofactor at the dimer interface [Fig. 3(D)].

To investigate the contribution of the different regions of the protein to F_{420} binding, we performed molecular dynamics (MD) simulations with the cofactor bound homodimer for a total of 100 ns. These results show that the ribityl-phospholactyl region maintains salt bridge interactions with Lys-61 and His-36 during the simulations, anchoring $F_{420}H_2$ in the binding pocket. The oligoglutamate tail and, to some extent, the deazaflavin group seem to be more mobile [Fig. 3(E)], consistent with the decreasing electron density and increasing temperature factors observed in this region of the oligoglutamate chain [Fig. 3(A,F)].

Biliverdin binding and reduction by Rv2074

Extensive co-crystallization and crystal-soaking experiments with Rv2074 and biliverdin-IXα

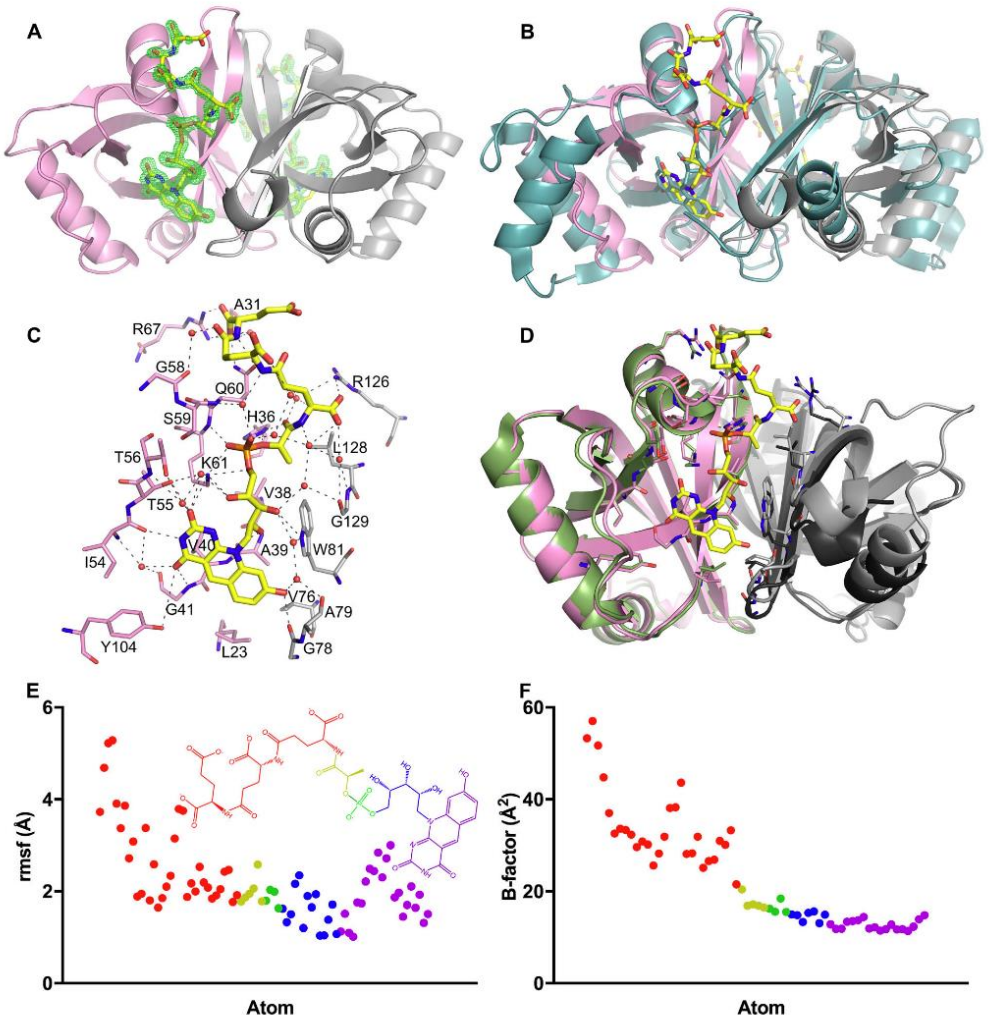

Figure 3. Structure of Rv2074 complexed with F_{420}. **A.** Overall structure of the Rv2074:F_{420} complex at 1.65 Å resolution (chain A in pink and B in grey). Difference (mF_o–DF_c) density at 3 σ for the F_{420} molecules at each chain are shown in green. Clear density showed the placement of the alloxazine, ribityl and phospholactate moieties in all four monomers in the asymmetric unit, although the clarity of the density for the polyglutamate chain was variable. **B.** Structure shown in **A** overlaid with the homodimeric Rv1155:F_{420} complex in cyan (PDB ID: 4QVB).[49] **C.** Residues involved in interacting with F_{420} in Rv2074. Pink and grey residues represent those from Chain A and Chain B of the homodimer, respectively. **D.** Comparison of the Rv2074:F_{420} complex in **A** with the structure of the apo-protein (PDB ID: 2ASF).[37] Chain A is shown in green and its crystallographic symmetry mate is in black, where key residues involved in F_{420} binding in **C** are shown as sticks. **E.** Plot of the RMSF values for the atoms of $F_{420}H_2$ showing the larger deviation of the oligo-glutamate chain compared with the rest of the molecule over the course of the MD simulation. The atoms are color coded by group as represented in the inset structure. **F.** Plot of the temperature (*B*) factors in the crystal structure for the atoms in the F_{420} molecule in **E**, showing a similar trend.

resulted in weak, ambiguous electron density within the active site that was not sufficient for accurate modeling of the substrate. To further investigate the mode of substrate coordination and the likely catalytic mechanism, we have used a combination of *in silico* docking and MD simulations to predict the most likely conformation of biliverdin in the active site of Rv2074 [Fig. 4(A)]. Using AUTODOCK VINA,[51] we obtained initial binding poses that showed biliverdin with the pyrrole rings B and C on either side of the reactive C10 atom stacked on to the deazaflavin moiety with the propionate chains

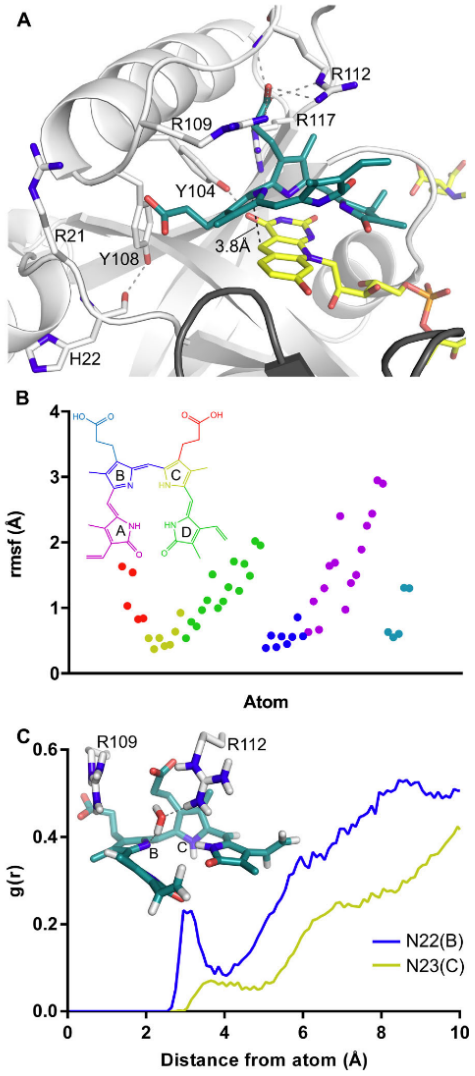

Figure 4. Biliverdin binding mode of Rv2074. **A.** Dominant biliverdin binding conformation simulated by MD, representing 59% of the structures at a cutoff of 2 Å. Residues chosen for mutagenesis are shown as sticks and dotted lines in grey represent hydrogen bonding interactions. **B.** Plot of the RMSF values for biliverdin demonstrating the mobility of the propionate groups and pyrrole rings A and D compared to pyrrole rings B and C. The atoms are color-coded by group as represented in the inset structure. **C.** Radial distribution function *g*(*r*) of water plotted by distance from reference nitrogen atoms N22 on pyrrole ring B or N23 on pyrrole ring C to oxygen of water. The inset figure shows one of the frames from the simulation where a water molecule is hydrogen bonding to N22(B) and to R112 within sufficient distance for proton transfer.

and the distal pyrrole rings A and D in variable positions. Through manual inspection and analysis of the docking scores, the most plausible binding orientation, with the propionate chains stabilized by arginine residues in the active site (Arg-21, Arg-109, Arg-112 and Arg-117) and the distal pyrrole rings A and D oriented such that biliverdin is in a porphyrin-like conformation, was then subjected to two independent sets of 50 ns MD simulations for a combined total 100 ns [Fig. 4(A)]. These results show that the substrate is stable in this conformation for the length of the simulation and is stabilized by hydrogen bonding of the propionate side chains with Arg-109 and Arg-112, with intermittent binding contributions from Arg-21 also being observed during the simulation. In addition, Arg-117 forms cation–π interactions with pyrrole ring C and pyrrole ring B forms aromatic interactions with the deazaflavin of F_{420}. The propionate side chains of rings B and C show significant flexibility [Fig. 4(B)], which is consistent with the flexibility of the multiple arginine residues (Arg-21, Arg-109, and Arg-112) that interact with them. In contrast, the pyrrole rings B and C are less mobile, especially in comparison to the terminal pyrrole rings A and D, which are extremely flexible in the large open active site [Fig. 4(B)], with no specific interactions with the protein [Fig. 4(A)]. These observations suggest that the hydride transfer from $F_{420}H_2$ to biliverdin-IXα relies upon correct alignment and stable binding of the B and C pyrrole groups that determine the position of the reactive C10 of biliverdin with respect to the cofactor.

The MD simulation results were analyzed to identify the most populated conformations of the active site in the presence of substrate using cluster analysis (see Methods). The analysis was performed on the subset of atoms that included the substrate and the surrounding active site residues Arg-21, Tyr-104, Tyr-108, Arg-109, Arg-112, and Arg-117. Structures from the individual frames of the simulation were clustered together if their RMSD was lower than the cutoff value, which was set to 2.0 Å. The most populated cluster consisted of 59% of the structures at an RMSD cutoff of 2.0 Å and the representative conformation of substrate and the residues is shown in Figure 4(A). The C–C distance between F_{420} and substrate in the representative conformation is 3.8 Å, but the average value of this distance measured during simulations is 3.9 ± 0.3 Å. In previously solved ternary structures of F_{420} binding proteins with their substrates this distance was 2.7 Å and 3.1 Å,[52,53] This is consistent with typical Michaelis complex structures that precede the formation a transition state, which is characterized with donor–acceptor distance of ~2.7 Å for hydride transfer.[54] The flexibility of the deazaflavin ring of $F_{420}H_2$ and the C10 and pyrrole rings B and C of

biliverdin, as evident from the RMSF plots which show fluctuations of 0.5 Å and 2 Å, respectively [Figs. 3(D) and 4(B)], can allow for the donor–acceptor distance to reach optimum values for successful hydride transfer.

To identify the residues within the active site that are directly involved in biliverdin reduction, we generated eight point mutants of Rv2074: Arg-21-Ala, Arg-109-Ala, Arg-112-Ala, Arg-117-Ala, Tyr-104-Ala, Tyr-104-Phe, Tyr-108-Ala, and Tyr-108-Phe [Fig. 4(C), Table I]. These residues were chosen as they are located in active site pocket and are highly conserved among the putative F-BVR family [Figs. 4(A) and 5(A)], suggesting that they are under evolutionary selection and are likely to have a functional role. All of these mutations led to some reduction in the catalytic efficiency, particularly the mutations of the active site tyrosine residues. Tyr-104 hydrogen bonds to the carbonyl group on the pyrimidine ring of $F_{420}H_2$ and mutation of this amino acid to either alanine or phenylalanine reduces both biliverdin affinity (increased K_M) and catalytic rate (k_{cat}), suggesting that a stabilized F_{420} molecule is important for the reaction [Figs. 3(C) and 4(A)]. Although Tyr-108 is located on the same loop as Arg-109 that bind the propionate side chains of biliverdin, it is directed away from both the substrate and cofactor, with minimal fluctuation over the course of the simulation. However, the Tyr-108-Ala mutant shows almost complete loss of catalytic activity (k_{cat}), while the Tyr-108-Phe mutant retains 30% activity compared to wild-type Rv2074. In the wild type protein, the hydroxyl group of Tyr-108 hydrogen bonds to the carbonyl group of the His-22 backbone. This hydrogen bond is important to hold the loop containing the important arginine residue Arg-21 within the correct vicinity. In addition to this, the aromatic group of Tyr-108 and the Tyr-108-Phe mutant could also provide a secondary effect towards the catalytic activity by desolvation of the $F_{420}H_2$-biliverdin interaction region. Although the immediate area above biliverdin was solvent accessible in the MD simulations, the area immediately below where the hydride transfer takes place was devoid of water molecules. The catalytic advantages for desolvated protein cages have been highlighted,[55] where charge transfer occurs between reactant and product as the desolvated microenvironment can aid charge reorganization through stabilization of charged transition states such as those found in our system.

All four arginine residues are involved in biliverdin binding by association with the propionate side chains (Arg-21, Arg-109, Arg-112) and cation–π interactions with the pyrrole ring C (Arg-117), and mutations of any of these residues to alanine negatively affects both k_{cat} and K_M (Table I). Arg-21 associates with biliverdin by hydrogen bonding with the propionate side chain of pyrrole ring B, although this was a transient interaction throughout the simulation, occurring intermittently when the biliverdin substrate drifted away from the proper cofactor alignment. Meanwhile Arg-117 was consistently observed to form cation–π interactions with pyrrole ring C [Fig. 4(A)]. The Arg-117-Ala mutation has the highest influence on reaction rate, lowering the k_{cat} to just 25% of the wild type, suggesting that the stabilization of pyrrole ring C by this residue is important in maintaining the correct biliverdin orientation for hydride transfer.

Since biliverdin features electronic delocalization across pyrrole rings B and C, either ring could be protonated at any one time. Both these protonated conformations were investigated in the MD simulations by manually protonating either N22 on ring B or N23 on ring C of biliverdin in separate simulations with otherwise identical parameters. The previously mentioned MD results were all performed with the N23 atom protonated since in the alternate conformation with N22 atom protonated, the enzyme-substrate complex was observed to be unstable and the cofactor and substrate moved out of alignment for the length of the simulation. This further highlights the importance of the cation–π interactions involving Arg-117, since it requires proper aromatic configuration of the biliverdin substrate to bind in a stable conformation. The very high sequence conservation of arginine at position 117 also lends credence to this as arginine residues are more often involved in cation–π bonding than other charged residues such as lysine [Fig. 5(A)].[56] The complete reduction of biliverdin to bilirubin requires proton transfer to one of the pyrrole nitrogens in addition to hydride transfer to C10. In this study we have mutated every ionizable residue that forms significant interactions with the substrate near C10 to non-ionizable residues, such as alanine or phenylalanine (Table I). None of these mutations led to complete loss of activity, suggesting that the protein is unlikely to be the proton donor in the reaction. Computational analysis of biliverdin reduction by the human BVRs has suggested that the primary proton donor is likely to be a hydroxonium ion, generated via hydrogen bonding of a water molecule with a basic residue such as histidine or arginine.[57,58] Therefore, using MD simulations we investigated the permeability of solvent within the active site and the hydrogen bonding behavior near the pyrrole nitrogens of interest, N22 on ring B and N23 on ring C [Fig. 4(C)]. In statistical mechanics, the radial distribution function $g(r)$ can be used to define the density distribution or the probability of finding particles as a function of a distance r from a central reference particle. Thus, in our case, the radial distribution function $g(r)$ can be used to determine the probability of finding water molecules with respect to a distance r from the proton accepting nitrogen

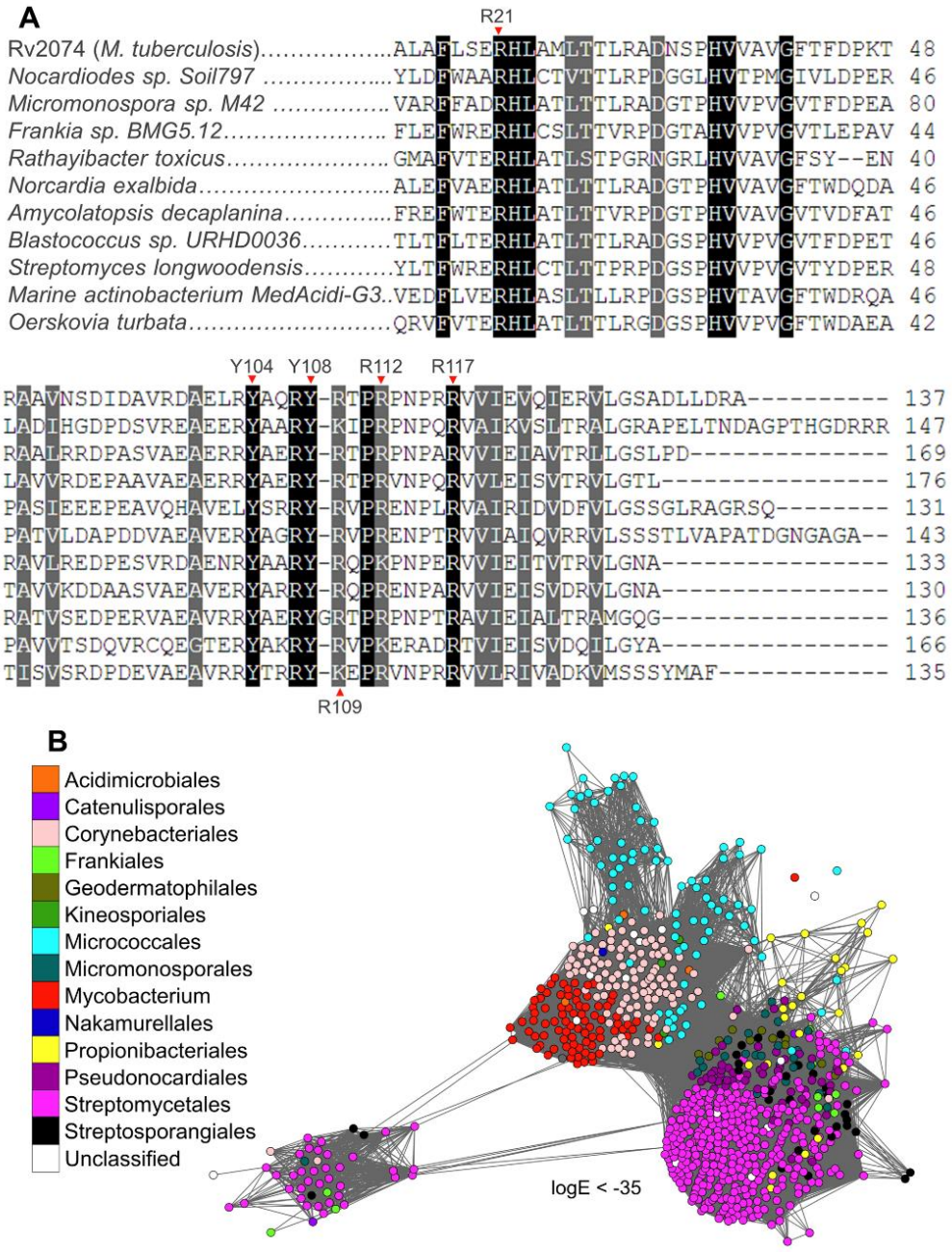

Figure 5. A. Sequence alignment of Rv2074 homologs from various Actinobacteria with ~50% amino acid identity between them, showing conservation of active site residues chosen for site-directed mutagenesis. **B.** SSN of all available F-BVR homologs retrieved from the NCBI non-redundant protein database using BLAST,[59] showing their exclusive presence in species belonging to actinobacterial orders. Each node represents an individual protein, which are colored according to the taxonomic order of the originating organism, except for the genus *Mycobacterium*. Only edges with BLAST log *E*-values less than −35 are shown.

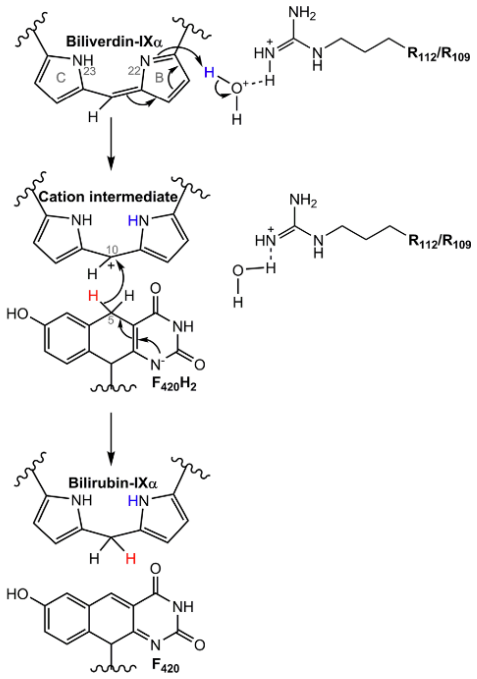

Figure 6. Proposed mechanism for biliverdin reduction by Rv2074. Proton donation to N22 on pyrrole ring B of biliverdin-IXα by a hydroxonium ion generated by a nearby arginine residue occurs first, creating a cationic intermediate. This is then followed by hydride transfer from C5 of $F_{420}H_2$ to C10 of the intermediate, resulting in the formation of bilirubin-IXα.

atoms which are used as our references. Water molecules were found to associate with N22, which was deprotonated in the simulation, with a clear peak in the probability distribution at a distance of 3.0 Å (from pyrrole nitrogen to the oxygen atom of water) before gradually extending into the bulk solvent, providing a sufficient window for hydrogen bonding. In contrast, the distribution with N23 (protonated) as a reference shows a much smaller probability peak at a longer distance of 3.6 Å suggesting that proton transfer to N22 during the reaction is more favorable in this biliverdin conformation due to easier solvent access. Furthermore, the presence of Arg-109 and Arg-112 in this vicinity [Fig. 4(C)], and the reduction of catalytic activity without these residues (Table I), suggests that they could assist in generating a hydroxonium ion for this reaction (Fig. 6).

Abundance and distribution of F-BVRs

Finally, we investigated the taxonomic distribution of the F-BVR family, especially within pathogenic mycobacteria, and its presence in other Actinobacteria. We retrieved all sequences with more than 50% sequence identity to Rv2074 from the NCBI non-redundant protein database using BLAST,[59] and found that these proteins are exclusively found in Actinobacteria and are particularly abundant in mycobacteria (Fig. 5(B)]. In addition to *M. tuberculosis*, homologs were also identified from opportunistic human pathogens including the more commonly reported species *Mycobacterium ulcerans*, *avium*, *marinum*, *intracellulare*, *abscessus*, *simiae*, *kansasii*, *haemophilum*, *xenopi*, *genavense*, *fortuitum*, and *chelonae* (Table III).[60–62] It is absent from the genome of *Mycobacterium leprae*, which has undergone significant reductive evolution,[63] and from the genome of the attenuated *Mycobacterium bovis* used for vaccination against *M. tuberculosis*.[64] The presence of these proteins appears more common in obligate and opportunistic pathogens (86% of genomes) rather than in species that are not known to cause infection of which only 60% of the analyzed genomes encode an F-BVR (Table III). All other orders of Actinobacteria identified are predominantly soil bacteria and have previously been suggested to produce F_{420}.[65]

Discussion

The catalytic mechanism of F-BVRs

Proton NMR-spectroscopy confirmed that Rv2074 catalyzes the reduction of biliverdin-IXα at the C10 position in an $F_{420}H_2$-dependent reaction. The crystal structure of the F_{420}:Rv2074 complex allowed us to simulate biliverdin binding at the active site. Along with the site-directed mutagenesis of key catalytic residues, we can now propose a plausible mechanism for this enzyme. Previous analysis of human BVR-A and BVR-B suggests that, in these enzymes, biliverdin reduction involves the use of NADPH as a cofactor and proceeds in two steps: (i) proton donation by a hydroxonium ion to a pyrrole nitrogen atom adjacent to C10 of biliverdin to make a cationic intermediate, followed by (ii) hydride transfer from NADPH to C10 to form bilirubin.[57,58] Based on our results, we also propose that a similar two-step mechanism is plausible with $F_{420}H_2$ as the hydride donor (Fig. 6). This is also consistent with our recent work showing that F_{420} most likely exists in its deprotonated state when bound to FDORs,[66] requiring the need for an alternate proton source during the reaction.

For the initial proton donation step, the most likely donor is a hydroxonium ion, as proposed for BVR-A and BVR-B,[57,58] considering the accessibility of the active site to water and the presence of Arg-109 and Arg-112 in the vicinity to generate the proton donating hydroxonium ion. The aromatic nature and steric bulk of the Tyr-108 side chain most likely plays a role in desolvating the hydride transfer site and forming a nonpolar environment which helps enhance catalytic activity through strengthening polar interactions and stabilization of the charged

Table III. *Conservation of F-BVRs in Mycobacteria*

Mycobacterium genome	Rv2074 homolog	common reservoir/ isolation source[59–61]	Genome accession
Pathogenic			
Mycobacterium tuberculosis	Yes	Human infection	NC_000962.3
Mycobacterium bovis	Yes	Human/animal infection	NZ_JKAL00000000.1
Mycobacterium africanum	Yes	Human infection	NZ_JLAN00000000.1
Mycobacterium canettii	Yes	Human infection	NC_019951.1
Mycobacterium leprae	—	Human infection	NC_002677.1
Opportunistic/commensal			
Mycobacterium abscessus	Yes	Soil, water, infection	NC_010397.1
Mycobacterium avium	Yes	Water, soil, infection	NC_002944.2
Mycobacterium intracellulare	Yes	Water, soil, infection	NC_016946.1
Mycobacterium marinum	Yes	Water, soil, infection	NC_010612.1
Mycobacterium kansasii	Yes	Human infection	NC_022663.1
Mycobacterium fortuitum	Yes	Soil, water, infection	NZ_CP011269.1
Mycobacterium xenopi	Yes	Soil, water, infection	NZ_AJFI00000000.1
Mycobacterium neoaurum	Yes	Soil, infection	NC_023036.2
Mycobacterium ulcerans	Yes	Water, soil, infection	CP000325.1
Mycobacterium chelonae	Yes	Water, soil, infection	NZ_CP010946.1
Mycobacterium genavense	Yes	Human infection	NZ_JAGZ00000000.1
Mycobacterium iranicum	Yes	Human infection	NZ_AUWT00000000.1
Mycobacterium yongonense	Yes	Human infection	NC_021715.1
Mycobacterium simiae	Yes	Rhesus monkey	NZ_CBMJ000000000.2
Mycobacterium haemophilum	Yes	Human infection	NZ_CP011883.2
Mycobacterium lepromatosis	—	Human infection	NZ_LAWX00000000.1
Mycobacterium setense	Yes	Human infection	NZ_JTJW00000000.1
Mycobacterium kyorinense	—	Human infection	NZ_BBKA00000000.1
Mycobacterium vulneris	Yes	Human infection	NZ_CCBG000000000.1
Mycobacterium celatum	—	Human infection	NZ_BBUN00000000.1
Rarely pathogenic/commensal			
Mycobacterium phlei	Yes	Soil	NZ_AJFJ00000000.1
Mycobacterium smegmatis	yes	Soil	NC_008596.1
Mycobacterium rhodesiae	Yes	Soil	NC_016604.1
Non-pathogenic			
Mycobacterium rutilum	—	Soil	BBHF00000000.1
Mycobacterium pallens	—	Soil	BBHE00000000.1
Mycobacterium crocinum	—	Soil	BBHD00000000.1
Mycobacterium rufum	Yes	Soil	NZ_JROA00000000.1
Mycobacterium aromaticivorans	Yes	Soil	NZ_JALN00000000.2
Mycobacterium indicus pranii	Yes	Soil	NC_018612.1
Mycobacterium bovis (BCG vaccine)	—	Laboratory	NZ_JNAF00000000.1
Mycobacterium vanbaalenii	Yes	Mineral oil, soil	NC_008726.1
Mycobacterium gilvum	Yes	Water, soil	NC_014814.1
Mycobacterium chubuense	Yes	Soil	NC_018027.1

transition state.[55] This is corroborated by the MD simulations that show the Tyr-108 residue does not form a direct association with either the cofactor or substrate, and instead has its hydroxyl group hydrogen bonded to the backbone carbonyl group of His-22. This interaction helps align this loop within the correct distance for the neighboring Arg-21 residue to interact with biliverdin. The alignment and distance between biliverdin and $F_{420}H_2$, which requires the presence of Arg-21, Arg-109, Arg-112, and Arg-117 for substrate stabilization, is essential for optimal hydride transfer to take place from C5 of $F_{420}H_2$ to C10 of biliverdin.

A physiological role for F-BVRs

Of the two proteins with F-BVR activity in *M. tuberculosis*, only Rv2074 appears to be functionally specialized in terms of its affinity for biliverdin IXα reduction and its catalytic efficiency. In contrast, Rv1155 does not bind biliverdin-IXα with high affinity, suggesting that its biliverdin reductase activity is a promiscuous, and probably not physiologically relevant, function. Such substrate promiscuity appears to be common in the $F_{420}H_2$-dependent FDORs, probably as a result of their common evolutionary origin.[36] While homologs of Rv2074 are present in a number of pathogenic mycobacteria, we did not observe any closely related homolog (>50% amino acid identity) in the greatly reduced genome of *M. leprae*.[63] However, *M. leprae* does have a homologue of Rv1155 (88% amino acid identity),[36] that could at least in part compensate for the loss of the Rv2074 homolog through its promiscuous F-BVR activity.

The abundance and conservation of F-BVRs in Actinobacteria suggests that they are under evolutionary selection for an important physiological role.

Heme is universally used as a prosthetic group in many proteins and, although it is synthesized in Actinobacteria,[67] its acquisition from the environment and subsequent degradation by heme oxygenase (HO) liberates iron that is essential for bacterial growth and produces biliverdin.[68] Little is known about the heme homeostasis and degradation process in Actinobacteria and it is likely that F-BVRs contribute to this *via* metabolism and removal of the biliverdin produced by HO while simultaneously producing bilirubin. Recently, new classes of bacterial HOs have been discovered,[69] which includes the mycobacterial MhuD that produces the biliverdin analogue mycobilin.[70] Mycobilin differs from biliverdin by the presence of a ketone group instead of a carboxyl group at either of the terminal pyrrole rings A or D.[70] The active site of Rv2074, which does not seem to have specific interactions for pyrrole rings A and D, could allow the reduction of mycobilin as well, which could have similar anti-oxidative properties as bilirubin.

The over-representation of F-BVRs in pathogenic mycobacteria is notable, but consistent with the observation that their substrate, biliverdin-IXα, is produced by mammalian cells. It has been observed that biliverdin-IXα reduction produces a potent anti-oxidant system,[6] making it possible that bilirubin-IXα production by F-BVRs could contribute to protecting pathogenic mycobacteria against oxidative stress. Proteomics studies have shown that Rv2074 is found in the membrane of *M. tuberculosis*,[71,72] and is also secreted.[73] F_{420} is also known to be exported to the outer mycobacterial membrane.[74] Therefore, it is likely that Rv2074 reduces the excess biliverdin produced in macrophages upon mycobacterial infection due to HO upregulation,[27–29] producing bilirubin for its antioxidant activity.[6–9] HO upregulation has already been shown to promote *M. tuberculosis* and *M. abscessus* proliferation inside macrophages during early infection.[27,29] where bilirubin itself can also have a similar protective effect on intracellular *M. abscessus*.[27] The bilirubin produced by F-BVRs could form an "anti-oxidative pocket" around the bacterial cell that can quench lethal nitrosative species like NO produced by the engulfing macrophage.[8] NO production controls active mycobacterial infection inside macrophages,[32,33] and has multiple targets in *M. tuberculosis*.[75,76] It has already been shown that mutant *M. tuberculosis* strains lacking enzymes required for F_{420} biosynthesis are hypersusceptible to reactive nitrogen and oxygen species,[39,77] and bilirubin production through the activity of the F-BVRs could be one of the contributing mechanisms through which F_{420} protects *M. tuberculosis* against oxidative stress. The potential involvement of bilirubin production by F-BVRs in mycobacterial pathogenesis is further supported by comparative genomics indicating that Rv2074 is encoded in one of the regions of difference in the *M. tuberculosis* genome that are absent in the closely related attenuated *M. bovis* strains used for TB vaccination.[64]

Bilirubin produced by the F-BVRs could also be involved in cell signaling as it can inhibit inducible nitric oxide synthase production,[30,31] which is required for the generation of NO in *M. tuberculosis* infected macrophages.[32,33] It is unlikely that the F-BVRs with their different protein fold are able to mimic the direct regulatory functions of BVR-A since mammalian BVR-A contains an additional regulatory C-terminal domain that comprises of multiple motifs involved in cellular signaling mechanisms which are absent in BVR-B that has not yet been observed to have a similar regulatory role.[11,17] However, increased presence of biliverdin-IXα has been shown to have anti-inflammatory effects like the inhibition of pro-inflammatory cytokine production,[78,79] and inhibition of antigen specific immune responses,[80] that could be attributed to its fast conversion to bilirubin-IXα by a BVR.[21] Further work is required to confirm the exact physiological importance of F-BVRs as part of an immune evasive strategy employed by mycobacteria to mediate oxidative stress and inflammation inside macrophages.

Summary

In this work, we describe the first comprehensive characterization of bacterial $F_{420}H_2$-dependent biliverdin reductases, focusing on Rv2074 from *M. tuberculsosis*.[36] Prior to this, biliverdin reductases had largely been studied from mammalian hosts. We have demonstrated that the F-BVR family of BVRs is abundant in Actinobacteria, especially in mycobacterial pathogens, and characterized the mechanism by which Rv2074 from *M. tuberculosis* catalyzes the reduction of biliverdin-IXα (the principle isomer produced in mammalian cells)[13] to produce bilirubin-IXα in an $F_{420}H_2$-dependent manner, performing the same catalytic function as human BVR-A. As previous work has already demonstrated the increased production of biliverdin by mycobacteria infected macrophages,[27–29] anti-oxidative properties of bilirubin,[6–9] and the presence of excreted Rv2074 in the extracellular medium,[73] we suggests that Rv2074 may be involved in the pathogenesis of *M. tuberculosis* by conferring protection against oxidative and nitrosative species.

Materials and Methods

Materials

Biliverdin-IXα, bilirubin-IXα and G6P were purchased from Sigma-Aldrich (Missouri, U. S. A.). The codon optimized sequences for *rv2074* and *rv1155* from *M. tuberculosis* (H37Rv) were purchased as GeneStrings from ThermoFisher Scientific

(Massachusetts, U. S. A) and cloned into the expression vector pETMCSIII using Gibson assembly,[81] as previously described for other FDORs.[36] The *rv2074* mutants were generated by Dr Ruhu Qi from the ANU Mutagenesis and Cloning service and validated by Sanger sequencing from the ANU Biomolecular Resource Facility. The plasmids used for F_{420} and Fgd overexpression (pYUBDuet-*fbiABC* and pDEST17-*fgd*, respectively) have been previously described.[47,82,83] General molecular biology reagents and chemicals were purchased from Sigma-Aldrich or Astral Scientific.

F_{420} purification

F_{420} was overexpressed and purified from *M. smegmatis* using a modified protocol based on previously published methods.[83,84] Briefly, *M. smegmatis* ($mc^2$4517) cells were transformed with pYUBDuet-*fbiABC* by electroporation, plated on LB tween80 agar plates containing 50 μg/mL each of hygromycin B and kanamycin, and grown for 3 days at 37°C. Individual colonies were used to grow starter cultures for 5 days at 37°C in LB media containing 0.05% tween 80, 50 μg/mL hygromycin B and 50 μg/mL kanamycin C. This was then diluted into 500 mL of the same media and grown for a further 5 days at 37°C. Cells were harvested by centrifugation at 10,000*g* and resuspended in 20 mM tris(hydroxymethyl)aminomethane, pH 7.5, before being autoclaved at 121°C for 20 min. The insoluble fraction was removed by further centrifugation at 20,000*g* for 1 h. F_{420} was purified from the filtered lysate using a 60 mL Macro-prep High-Q ion-exchange column (Bio-Rad, California, U. S. A.). Fractions containing F_{420} (identified by the presence of an absorption peak at 420 nm) were further purified using a high-capacity C-18 Reversed-Phase Extract-Clean column (Alltech, Kentucky, U. S. A.). Fractions containing F_{420} (eluted using a methanol gradient from 0% to 100%) were freeze dried for storage at −80°C.

Protein expression and purification

Fgd for $F_{420}H_2$ generation was expressed and purified as described previously.[82] Expression vectors for *rv2074*, its mutants and *rv1155* were transformed into *E. coli* (BL21(DE3) from New England Biolabs, Massachusetts, U. S. A.) and grown overnight at 37°C on LB agar containing 100 μg/mL ampicillin and 0.5% glucose. Starter cultures were grown the following morning in Terrific Broth (TB) containing 100 μg/mL ampicillin and 0.5% glucose at 37°C for 5 h and transferred to 500 mL (or 1L for Rv2074 grown for protein crystallization) of modified auto-induction media,[36] for overnight growth at 30°C. Cells were harvested by centrifugation at 5000*g* for 15 min at 4°C, resuspended in lysis buffer (50 mM $NaPO_4$, 300 mM NaCl, 25 mM imidazole at pH 8) and lysed by sonication using an Omni Sonicator Ruptor 400 (3 × 3 min at 60% power). The soluble fraction obtained from centrifugation at 13,000*g* for 1 hr at 4°C was passed over a gravity column containing 500 μL Ni-NTA resin (Qiagen, Hilden, Germany). Columns were washed with 4 mL of lysis buffer followed by 4 mL of the same buffer containing 50 mM imidazole. Samples were eluted with 4 mL of elution buffer (same as lysis buffer but with 250 mM imidazole), dialyzed overnight and stored at −80°C in 50 mM Tris, 300 mM NaCl and 10% glycerol at pH 7.5 until further use.

For protein crystallization, Rv2074 was purified using a 5 mL GE HisTrap FF column using the same protocol as above but with 25 mL wash and elution steps instead. Purified protein was passed through a GE HiPrep 26/10 desalting column for buffer exchange into 50 mM Tris and 150 mM NaCl at pH 8.0. The histidine-tag was then cleaved using TEV protease as described for other FDORs.[36] The tag-free protein was concentrated to ~1 mM and incubated at 4°C overnight with a 1.5-fold excess of F_{420}, followed by size exclusion chromatography to remove excess unbound ligand on a GE Hiload 16/600 Superdex 75 pg column in buffer containing 20 mM HEPES and 150 mM NaCl at pH 7.5. The final sample was concentrated to 1.4 mM (21 mg/mL) and stored at 4°C in 20 mM HEPES and 50 mM NaCl at pH 7.5.

Enzyme activity assays and reaction product analysis

1 μM enzyme was added to reactions of 1 μM F_{420}, 1 μM Fgd, 2.5 mM G6P, and 0–100 μM biliverdin in 100 μL buffer containing 50 mM Tris at pH 7.5. Enzyme activity was measured in 96-well plates (path-length 0.25 cm) by following the decrease in absorbance at 650 nm ($\epsilon = 25{,}000\ M^{-1}\ cm^{-1}$)[85] on an Epoch Microplate Spectrophotometer (BioTek, Vermont, U. S. A.). Average K_M and V_{max} values for three independent experiments were calculated from substrate inhibition curves of best fit ($y = V_{max} \cdot x/K_M + x \cdot (1 + x)/K_i$) on GraphPad Prism. The specific activity of Rv2074, calculated for comparison with previously characterized BVRs was measured at a concentration of 25 μM biliverdin IXα, which gave the highest reaction rate.

For the purification and analysis of reaction products, 5 mL reactions containing 100 μM biliverdin, 5 mM G6P, 1 μM Fgd, 1 μM F_{420}, and 10 μM Rv2074 or Rv1155 were left incubating at room temperature for 2 h in 50 mM Tris at pH 7.5. A control reaction without enzyme, and another with 100 μM bilirubin instead of biliverdin were also set. Reaction products were purified in a similar manner to other studies of heme degradation products.[86] Reactions were terminated with 1 mL each of 3M HCl and glacial acetic acid and the porphyrin products were

extracted into 1 mL of chloroform. The aqueous layer was discarded; the chloroform layer was washed twice with 1 mL water and finally evaporated under a stream of nitrogen. For proton NMR, samples were resuspended in 500 μL deuterated chloroform and data were collected on a Bruker Ascend 700 MHz NMR spectrometer. For mass spectrometry, samples were resuspended in 500 μL methanol and spectra were collected on a Micromass ZMD mass spectrometer in the ESI negative mode.

Protein crystallization, data collection, and structure determination

The saturated Rv2074:F_{420} complex used was at a concentration of 1.4 mM (21 mg/mL) in 20 mM HEPES and 50 mM NaCl at pH 7.5, and was obtained after incubation of the pure protein with a 1.5-fold excess of F_{420} followed by gel purification. SG1 (Molecular Dimensions, Newmarket, Suffolk, U. K.) and Index (Hampton Research, California, U. S. A.) high-throughput crystallization screens were set to identify initial crystallization conditions for the Rv2074:F_{420} complex. The final crystal that was used for data collection was grown in 27% PEG-3350, 0.2M $MgCl_2$ and 0.1 M BisTris at pH 5.5. The cryobuffer used was the same as the crystallization conditions, with the addition of an additional 8% ethylene glycol. The crystal was flash-cooled under a stream of nitrogen gas at 100 K. X-ray diffraction data were collected at the Australian Synchrotron beamline MX2 with an ADSC Q315 detector and Blu-Ice software.[87] Diffraction data were integrated using XDS,[88] and scaled using AIMLESS,[89] in the CCP4 suite.[90] Molecular replacement was performed with the previously solved apo-structure of Rv2074 (PDB ID: 2ASF)[37] using Phaser,[91] and F_{420} was manually modeled into the difference density (mF_o–DF_c) at the binding site using COOT.[92] Interspersed structural refinement was performed using Refmac and PHENIX,[93,94] with local non-crystallographic symmetry restraints, and the final submitted structure was refined using Refmac.[93] The Proteins, Interfaces, Structures and Assemblies server (http://www.ebi.ac.uk/pdbe/pisa/)[50] that compares the interface between protein chains was used to analyze the most probable multimeric state of Rv2074 in solution.

Substrate docking and molecular dynamics simulations

Biliverdin-IXα was docked to chain D of the Rv2074:F_{420} complex using Autodock Vina.[51] Both protein and ligand were prepared using AutodockTools using default settings,[95] where R21, Y104, Y108, R109, R112, and R117 were flexible. The MD simulations on the dimeric structure was performed with the GROMACS 4.6.5 suite,[96] using the most plausible biliverdin conformation that was chosen based on the predicted free energy scores of binding and recurrence during manual inspection. Since there are delocalized electrons in the two central pyrrole rings, conformations with either ring protonated were used for separate simulations to investigate any preference in the binding modes and stability. The second chain in the homodimer included $F_{420}H_2$, but not biliverdin, to allow analysis of the cofactor stability in the enzyme complex. $F_{420}H_2$ and biliverdin were parameterized for simulation using the Automated Topology Builder (MolIDs: $F_{420}H_2$ for both chains; 29471 and 29452, Biliverdin N23-protonated; 29436 and Biliverdin N22-protonated; 29350) and the GROMOS 54A7 force field,[96,97]. The simulations were performed under periodic boundary conditions with the system coordinates in a cubic box with 1.4 nm distance between the protein and the box wall. The van der Waals and Coulombic interactions were evaluated using a 1.4 nm cut-off scheme for both. A dielectric constant of $\varepsilon_r = 78.5$ was used to apply a corrective reaction-field for long-range electrostatic interactions beyond the cut-off. Bond lengths were constrained with a time step of 2 fs using the LINCS algorithm.[98] The simulations were performed at reference pressure and temperature of 1 bar and 300 K, respectively, which was achieved with the Berendsen weak coupling method,[99] with time constants of 0.4 ps and 0.1 ps. VMD was used to visualize the simulation results.[100]

The dimeric structure in the box was solvated using SPC water.[101] To ensure the overall charge neutrality of the complex, 14 Na^+ ions were added to the solvent to counter the −14 *e* charge on the protein complex. The resulting system was minimized *via* steepest descent, followed by gradual relaxation in series of 4 simulations with position restraints placed on the protein-cofactor-substrate complex. Each simulation was 2 ns long and the force constants used were set to 1000 kJ mol^{-1} nm^{-1}, 500 kJ mol^{-1} nm^{-1}, 200 kJ mol^{-1} nm^{-1}, and 50 kJ mol^{-1} nm^{-1}, respectively. After the equilibration, two independent unrestrained runs of 50 ns were performed. The flexibility and motion of the substrate and cofactor in the active site were analyzed by calculating the root mean square fluctuation (RMSF) of their atoms, which were then grouped based on the chemical structure of the compounds. To investigate the accessibility of the solvent to the active site and probability of water molecules within sufficient distance to facilitate possible proton transfer, radial distribution function was calculated and graphed with the nitrogen atoms of interest as reference particles. The two trajectories were concatenated prior to cluster analysis, which was performed using the method by Daura et al.[102] Briefly, all frames of the concatenated trajectory were aligned with respect to the reference (initial) structure by fitting the backbone root mean

square deviation (RMSD). Cluster analysis was performed on the subset of atoms consisting of the substrate and active side residues Arg-21, Tyr-104, Tyr-108, Arg-109, Arg-112, and Arg-117. Conformations were considered to fall within the same cluster when their RMSD was less than the specified cutoff value of 2.0 Å.

Sequence similarity networks (SSNs)

Sequences of proteins homologous to Rv2074 were retrieved from the NCBI non-redundant protein database using BLAST to an *E*-value cut-off of 1,[103] and curated with CD-hit,[104] removing species level duplicates with more than 98% sequence identity. The SSN was generated using the Enzyme Function Initiative Enzyme Similarity Tool,[105] where each node represents an individual protein and edges represent the BLAST log*E*-value.[59] A log*E*-value cut-off of −20 was used to identify the cluster of Rv2074 homologs of >50% amino acid identity (FDOR-B4)[36] from other distantly related proteins. The presence of F-BVRs in pathogenic and non-pathogenic mycobacteria were compared using 38 mycobacterial genomes from species that are documented to either cause infection or are only in the environment.[60–62]

Acknowledgments

We thank the ANU Cloning and Mutagenesis Facility and Dr Ruhu Qi for generating the Rv2074 mutants. We also thank Dr Matt Taylor at the Commonwealth Scientific and Industrial Research Organisation (CSIRO) for providing the facilities for F_{420} purification. We also thank Dr Stephen Watt and Anithahini Jeyasingham at the Australian National University Mass Spectrometry facility and Chris Blake at the Australian National University Nuclear Magnetic Resonance Centre for data collection on the purified biliverdin degradation products. This research was undertaken on the MX2 beamline at the Australian Synchrotron, Victoria, Australia.

Conflict of interest

The authors declare that they have no conflicts of interest with the contents of this article.

Author contributions

FHA performed most of the experiments. AEM proposed the catalytic mechanism and performed the molecular dynamics simulations with assistance from KCJ and MLO. PDC acquired crystallography data and finalized structural refinement. BML purified F_{420}. FHA and CJJ designed the project and FHA, AEM, and CJJ wrote the paper.

References

1. Tenhunen R, Marver HS, Schmid R (1968) The enzymatic conversion of heme to bilirubin by microsomal heme oxygenase. Proc Natl Acad Sci USA 61:748–755.
2. Beale SI, Cornejo J (1983) Biosynthesis of phycocyanobilin from exogenous labeled biliverdin in *Cyanidium caldarium*. Arch Biochem Biophys 227:279–286.
3. Cornelius CE (1991) Bile pigments in fishes: a review. Vet Clin Pathol 20:106–115.
4. Mantle TJ (2002) Haem degradation in animals and plants. Biochem Soc Trans 30:630–633.
5. Stocker R, Yamamoto Y, McDonagh AF, Glazer AN, Ames BN (1987) Bilirubin is an antioxidant of possible physiological importance. Science 235:1043–1046.
6. Barañano DE, Rao M, Ferris CD, Snyder SH (2002) Biliverdin reductase: a major physiologic cytoprotectant. Proc Natl Acad Sci USA 99:16093–16098.
7. Jansen T, Daiber A (2012) Direct antioxidant properties of bilirubin and biliverdin. Is there a role for biliverdin reductase? Front Pharmacol 3:30. doi: 10.3389/fphar.2012.00030
8. Kaur H, Hughes MN, Green CJ, Naughton P, Foresti R, Motterlini R (2003) Interaction of bilirubin and biliverdin with reactive nitrogen species. FEBS Lett 543:113–119.
9. Minetti M, Mallozzi C, Di Stasi AM, Pietraforte D (1998) Bilirubin is an effective antioxidant of peroxynitrite-mediated protein oxidation in human blood plasma. Arch Biochem Biophys 352:165–174.
10. Maines MD (2005) New insights into biliverdin reductase functions: linking heme metabolism to cell signaling. Physiology 20:382–389.
11. Kapitulnik J, Maines MD (2009) Pleiotropic functions of biliverdin reductase: cellular signaling and generation of cytoprotective and cytotoxic bilirubin. Trends Pharmacol Sci 30:129–137.
12. Yamaguchi T, Komoda Y, Nakajima H (1994) Biliverdin-IX alpha reductase and biliverdin-IX beta reductase from human liver. Purification and characterization. J Biol Chem 269:24343–24348.
13. Maines MD (1988) Heme oxygenase: function, multiplicity, regulatory mechanisms, and clinical applications. FASEB J 2:2557–2568.
14. Komuro A, Tobe T, Nakano Y, Yamaguchi T, Tomita M (1996) Cloning and characterization of the cDNA encoding human biliverdin-IXα reductase. Biochim Biophys Acta 1309:89–99.
15. Yamaguchi T, Yamaguchi N, Komoda Y, Nakajima H, Ishikawa M (1979) Studies on bilirubin metabolism. Proc Jpn Acad Ser B Phys Biol Sci 55:84–88.
16. Pereira PJ, Macedo-Ribeiro S, Párraga A, Pérez-Luque R, Cunningham O, Darcy K, Mantle TJ, Coll M (2001) Structure of human biliverdin IXbeta reductase, an early fetal bilirubin IXbeta producing enzyme. Nat Struct Biol 8:215–220.
17. Whitby FG, Phillips JD, Hill CP, McCoubrey W, Maines MD (2002) Crystal structure of a biliverdin IXalpha reductase enzyme–cofactor complex. J Mol Biol 319:1199–1210.
18. Maines MD, Ewing JF, Huang TJ, Panahian N (2001) Nuclear localization of biliverdin reductase in the rat kidney: response to nephrotoxins that induce heme oxygenase-1. J Pharmacol Exp Ther 296:1091–1097.
19. Young SC, Storm MV, Speed JS, Kelsen S, Tiller CV, Vera T, Drummond HA, Stec DE (2009) Inhibition of biliverdin reductase increases ANG II-dependent superoxide levels in cultured renal tubular epithelial cells. Am J Physiol Regul Integr Comp Physiol 297:R1546–R1553.

20. Sedlak TW, Saleh M, Higginson DS, Paul BD, Juluri KR, Snyder SH (2009) Bilirubin and glutathione have complementary antioxidant and cytoprotective roles. Proc Natl Acad Sci USA 106:5171–5176.
21. Wegiel B, Otterbein LE (2012) Go green: the anti-inflammatory effects of biliverdin reductase. Front Pharmacol 3:47. doi: 10.3389/fphar.2012.00047
22. Hu Z, Pei G, Wang P, Yang J, Zhu F, Guo Y, Wang M, Yao Y, Zeng R, Liao W, Xu G. (2015) Biliverdin reductase A (BVRA) mediates macrophage expression of interleukin-10 in injured kidney. Int J Mol Sci 16: 22621–22635.
23. Lerner-Marmarosh N, Miralem T, Gibbs PEM, Maines MD (2007) Regulation of TNF-alpha-activated PKC-zeta signaling by the human biliverdin reductase: identification of activating and inhibitory domains of the reductase. FASEB J 21:3949–3962.
24. Tudor C, Lerner-Marmarosh N, Engelborghs Y, Gibbs PEM, Maines MD (2008) Biliverdin reductase is a transporter of haem into the nucleus and is essential for regulation of HO-1 gene expression by haematin. Biochem J 413:405–416.
25. Schluchter WM, Glazer AN (1997) Characterization of cyanobacterial biliverdin reductase. Conversion of biliverdin to bilirubin is important for normal phycobiliprotein biosynthesis. J Biol Chem 272:13562–13569.
26. Mölzer C, Huber H, Diem K, Wallner M, Bulmer AC, Wagner K-H (2013) Extracellular and intracellular anti-mutagenic effects of bile pigments in the *Salmonella typhimurium* reverse mutation assay. Toxicol In Vitro 27:433–437.
27. Abdalla MY, Ahmad IM, Switzer B, Britigan BE (2015) Induction of heme oxygenase-1 contributes to survival of *Mycobacterium abscessus* in human macrophages-like THP-1 cells. Redox Biol 4:328–339.
28. Silva-Gomes S, Appelberg R, Larsen R, Soares MP, Gomes MS (2013) Heme catabolism by heme oxygenase-1 confers host resistance to *Mycobacterium* infection. Infect Immun 81:2536–2545.
29. Scharn CR, Collins AC, Nair VR, Stamm CE, Marciano DK, Graviss EA, Shiloh MU (2016) Heme oxygenase-1 regulates inflammation and mycobacterial survival in human macrophages during *Mycobacterium tuberculosis* infection. J Immunol 196:4641–4649.
30. Wang WW, Smith DLH, Zucker SD (2004) Bilirubin inhibits iNOS expression and NO production in response to endotoxin in rats. Hepatology 40:424–433.
31. Lanone S, Bloc S, Foresti R, Almolki A, Taillé C, Callebert J, Conti M, Goven D, Aubier M, Dureuil B, El-Benna J, Motterlini R, Boczkowski J. (2005) Bilirubin decreases nos2 expression via inhibition of NAD(P)H oxidase: implications for protection against endotoxic shock in rats. Faseb J 19:1890–1892.
32. Chan J, Xing Y, Magliozzo RS, Bloom BR (1992) Killing of virulent *Mycobacterium tuberculosis* by reactive nitrogen intermediates produced by activated murine macrophages. J Exp Med 175:1111–1122.
33. Kröncke K-D, Fehsel K, Kolb-Bachofen V (1998) Inducible nitric oxide synthase in human diseases. Clin Exp Immunol 113:147–156.
34. Gengenbacher M, Kaufmann SHE (2012) *Mycobacterium tuberculosis*: success through dormancy. FEMS Microbiol Rev 36:514–532.
35. World Heath Organization (2015) Global tuberculosis report. WHO Press, Geneva.
36. Ahmed FH, Carr PD, Lee BM, Afriat-Jurnou L, Mohamed AE, Hong N-S, Flanagan J, Taylor MC, Greening C, Jackson CJ (2015) Sequence-structure-function classification of a catalytically diverse oxidoreductase superfamily in mycobacteria. J Mol Biol 427:3554–3571.
37. Biswal BK, Au K, Cherney MM, Garen C, James MNG (2006) The molecular structure of Rv2074, a probable pyridoxine 5′-phosphate oxidase from *Mycobacterium tuberculosis*, at 1.6 A resolution. Acta Crystallogr 62: 735–742.
38. Lee KS, Gartner LM (1976) Spectrophotometric characteristics of bilirubin. Pediatr Res 10:782–788.
39. Gurumurthy M, Rao M, Mukherjee T, Rao SPS, Boshoff HI, Dick T, Barry CE, Manjunatha UH (2013) A novel F_{420}-dependent anti-oxidant mechanism protects *Mycobacterium tuberculosis* against oxidative stress and bactericidal agents. Mol Microbiol 8:744–755.
40. Phillips O, Mantle TJ (1981) Some kinetic and physical properties of biliverdin reductase. Biochem Soc Trans 9:275–278.
41. Kutty RK, Maines MD (1981) Purification and characterization of biliverdin reductase from rat liver. J Biol Chem 256:3956–3962.
42. Cunningham O (2000) Studies on the specificity of the tetrapyrrole substrate for human biliverdin-IXalpha reductase and biliverdin-IXbeta reductase. Structure–activity relationships define models for both active sites. J Biol Chem 275:19009–19017.
43. Hayes JM, Mantle TJ (2009) The effect of pH on the initial rate kinetics of the dimeric biliverdin-IXalpha reductase from the *Cyanobacterium synechocystis* PCC6803. FEBS J 276:4414–4425.
44. Kaplan D, Navon G (1981) Nuclear magnetic resonance studies of the conformation of bilirubin and its derivatives in solution. J Chem Soc Perkin Trans 2:1374–1383.
45. Safo MK, Mathews I, Musayev FN, di Salvo ML, Thiel DJ, Abraham DJ, Schirch V (2000) X-ray structure of *Escherichia coli* pyridoxine 5′-phosphate oxidase complexed with FMN at 1.8 Å resolution. Structure 8:751–762.
46. Musayev FN, Di Salvo ML, Ko T-P, Schirch V, Safo MK (2003) Structure and properties of recombinant human pyridoxine 5′-phosphate oxidase. Protein Sci 12:1455–1463.
47. Taylor MC, Jackson CJ, Tattersall DB, French N, Peat TS, Newman J, Briggs LJ, Lapalikar GV, Campbell PM, Scott C, Russell RJ, Oakeshott JG. (2010) Identification and characterization of two families of $F_{420}H_2$-dependent reductases from mycobacteria that catalyse aflatoxin degradation. Mol Microbiol 78:561–575.
48. Cellitti SE, Shaffer J, Jones DH, Mukherjee T, Gurumurthy M, Bursulaya B, Boshoff HI, Choi I, Nayyar A, Lee YS, Cherian J, Niyomrattanakit P, Dick T, Manjunatha UH, Barry CE 3rd, Spraggon G, Geierstanger BH. (2012) Structure of Ddn, the deazaflavin-dependent nitroreductase from *Mycobacterium tuberculosis* involved in bioreductive activation of PA-824. Structure 20:101–112.
49. Mashalidis EH, Gittis AG, Tomczak A, Abell C, Barry CE, Garboczi DN (2015) Molecular insights into the binding of coenzyme F_{420} to the conserved protein Rv1155 from *Mycobacterium tuberculosis*. Protein Sci 24: 279–240.
50. Krissinel E, Henrick K (2007) Inference of macromolecular assemblies from crystalline state. J Mol Biol 372: 774–797.
51. Trott O, Olson AJ (2010) AutoDock Vina: improving the speed and accuracy of docking with a new scoring function, efficient optimization, and multithreading. J Comput Chem 31:455–461.

52. Warkentin E, Mamat B, Sordel-Klippert M, Wicke M, Thauer RK, Iwata M, Iwata S, Ermler U, Shima S (2001) Structures of $F_{420}H_2$:$NADP^+$ oxidoreductase with and without its substrates bound. EMBO J 20: 6561–6569.
53. Ceh K, Demmer U, Warkentin E, Moll J, Thauer RK, Shima S, Ermler U (2009) Structural basis of the hydride transfer mechanism in F_{420}-dependent methylenetetrahydromethanopterin dehydrogenase. Biochemistry 48:10098–10105.
54. Hammes-Schiffer S, Watney JB (2006) Hydride transfer catalysed by *Escherichia coli* and *Bacillus subtilis* dihydrofolate reductase: coupled motions and distal mutations. Philos Trans R Soc Lond B Biol Sci 361: 1365–1373.
55. Richard JP, Amyes TL, Goryanova B, Zhai X (2014) Enzyme architecture: on the importance of being in a protein cage. Curr Opin Chem Biol 21:1–10.
56. Gallivan JP, Dougherty DA (1999) Cation–pi interactions in structural biology. Proc Natl Acad Sci USA 96: 9459–9464.
57. Smith LJ, Browne S, Mulholland AJ, Mantle TJ (2008) Computational and experimental studies on the catalytic mechanism of biliverdin-IXβ reductase. Biochem J 411:475–484.
58. Fu G, Liu H, Doerksen RJ (2012) Molecular modeling to provide insight into the substrate binding and catalytic mechanism of human biliverdin-IXα reductase. J Phys Chem B 116:9580–9594.
59. Altschul SF, Madden TL, Schäffer AA, Zhang J, Zhang Z, Miller W, Lipman DJ (1997) Gapped BLAST and PSI-BLAST: a new generation of protein database search programs. Nucleic Acids Res 25:3389–3402.
60. Rastogi N, Legrand E, Sola C (2001) The mycobacteria: an introduction to nomenclature and pathogenesis. Rev Sci Tech 20:21–54.
61. Tortoli E (2014) Microbiological features and clinical relevance of new species of the genus *Mycobacterium*. Clin Microbiol Rev 27:727–752.
62. van Ingen J, Boeree MJ, Dekhuijzen PNR, van Soolingen D (2009) Environmental sources of rapid growing nontuberculous mycobacteria causing disease in humans. Clin Microbiol Infect 15:888–893.
63. Cole ST, Eiglmeier K, Parkhill J, James KD, Thomson NR, Wheeler PR, Honore N, Garnier T, Churcher C, Harris D, Mungall K, Basham D, Brown D, Chillingworth T, Connor R, Davies RM, Devlin K, Duthoy S, Feltwell T, Fraser A, Hamlin N, Holroyd S, Hornsby T, Jagels K, Lacroix C, Maclean J, Moule S, Murphy L, Oliver K, Quail MA, Rajandream MA, Rutherford KM, Rutter S, Seeger K, Simon S, Simmonds M, Skelton J, Squares R, Squares S, Stevens K, Taylor K, Whitehead S, Woodward JR, Barrell BG. (2001) Massive gene decay in the leprosy bacillus. Nature 409:1007–1011.
64. Behr MA, Wilson MA, Gill WP, Salamon H, Schoolnik GK, Rane S, Small PM (1999) Comparative genomics of BCG vaccines by whole-genome DNA microarray. Science 284:1520–1523.
65. Selengut JD, Haft DH (2010) Unexpected abundance of coenzyme F_{420}-dependent enzymes in *Mycobacterium tuberculosis* and other actinobacteria. J Bacteriol 192: 5788–5798.
66. Mohamed AE, Ahmed FH, Arulmozhiraja S, Lin CY, Taylor MC, Krausz ER, Jackson CJ, Coote ML (2016) Protonation state of F420H2 in the prodrug-activating deazaflavin dependent nitroreductase (Ddn) from *Mycobacterium tuberculosis*. Mol Biosyst 12:1110–1113.
67. Dailey HA, Gerdes S, Dailey TA, Burch JS, Phillips JD (2015) Noncanonical coproporphyrin-dependent bacterial heme biosynthesis pathway that does not use protoporphyrin. Proc Natl Acad Sci USA 112:2210–2215.
68. Li C, Stocker R (2009) Heme oxygenase and iron: from bacteria to humans. Redox Rep 14:95–101.
69. Wilks A, Ikeda-Saito M (2014) Heme utilization by pathogenic bacteria: not all pathways lead to biliverdin. Acc Chem Res 47:2291–2298.
70. Nambu S, Matsui T, Goulding CW, Takahashi S, Ikeda-Saito M (2013) A new way to degrade heme: the mycobacterium tuberculosis enzyme MhuD catalyzes heme degradation without generating CO. J Biol Chem 288: 10101–10109.
71. Målen H, Pathak S, Søfteland T, de Souza GA, Wiker HG (2010) Definition of novel cell envelope associated proteins in Triton X-114 extracts of *Mycobacterium tuberculosis* H37Rv. BMC Microbiol 10:132. DOI: 10.1186/1471-2180-10-132
72. De Souza GA, Leversen NA, Målen H, Wiker HG (2011) Bacterial proteins with cleaved or uncleaved signal peptides of the general secretory pathway. J Proteomics 75:502–510.
73. Målen H, Berven FS, Fladmark KE, Wiker HG (2007) Comprehensive analysis of exported proteins from *Mycobacterium tuberculosis* H37Rv. Proteomics 7:1702–1718.
74. Bashiri G, Perkowski EF, Turner AP, Feltcher ME, Braunstein M, Baker EN (2012) Tat–dependent translocation of an F(420)-binding protein of *Mycobacterium tuberculosis*. PLoS One 7:e45003.
75. Rhee KY, Erdjument-Bromage H, Tempst P, Nathan CF (2005) S-nitroso proteome of *Mycobacterium tuberculosis*: enzymes of intermediary metabolism and antioxidant defense. Proc Natl Acad Sci USA 102:467–472.
76. Buck ZH, De J (2010) Cell wall proteome analysis of *Mycobacterium smegmatis* strain MC2 155. BMC Microbiol 10:121. doi: 10.1186/1471-2180-10-121.
77. Greening C, Ahmed FH, Mohamed AE, Lee BM, Pandey G, Warden AC, Scott C, Oakeshott JG, Taylor MC, Jackson CJ (2016) F_{420}- and F_o-dependent redox reactions: physiology, biochemistry, and applications. Microbiol Mol Biol Rev 80:451–493.
78. Bellner L, Wolstein J, Patil KA, Dunn MW, Laniado-Schwartzman M (2011) Biliverdin rescues the HO-2 null mouse phenotype of unresolved chronic inflammation following corneal epithelial injury. Invest Ophthalmol Vis Sci 52:3246–3253.
79. Bisht K, Wegiel B, Tampe J, Neubauer O, Wagner K-H, Otterbein LE, Bulmer AC (2014) Biliverdin modulates the expression of C5aR in response to endotoxin in part via mTOR signaling. Biochem Biophys Res Commun 449:94–99.
80. Yamashita K, McDaid J, Ollinger R, Tsui T-Y, Berberat PO, Usheva A, Csizmadia E, Smith RN, Soares MP, Bach FH (2004) Biliverdin, a natural product of heme catabolism, induces tolerance to cardiac allografts. FASEB J 18:765–767.
81. Gibson DG, Young L, Chuang R-Y, Venter JC, Hutchison CA, Smith HO (2009) Enzymatic assembly of DNA molecules up to several hundred kilobases. Nat Meth 6:343–345.
82. Bashiri G, Squire CJ, Moreland NJ, Baker EN (2008) Crystal structures of F_{420}-dependent glucose-6-phosphate dehydrogenase FGD1 involved in the activation of the anti-tuberculosis drug candidate PA-824 reveal the basis of coenzyme and substrate binding. J Biol Chem 283:17531–17541.
83. Bashiri G, Rehan AM, Greenwood DR, Dickson JMJ, Baker EN (2010) Metabolic engineering of cofactor F_{420}

production in *Mycobacterium smegmatis*. PLoS One 5: e15803.
84. Isabelle D, Simpson DR, Daniels L (2002) Large-scale production of coenzyme F_{420}−5,6 by using *Mycobacterium smegmatis*. Appl Environ Microbiol 68:5750–5755.
85. Chen Jason DDB, Kawasaki Y, Bommer J, Takemoto JY (2012) Scalable production of biliverdin IXα by *Escherichia coli*. BMC Biochem 12:89. DOI: 10.1186/1472-6750-12-89
86. Zhu W, Wilks A, Stojiljkovic I (2000) Degradation of heme in Gram-negative bacteria: the product of the HemO gene of *Neisseriae* is a heme oxygenase. J Bacteriol 182:6783–6790.
87. McPhillips TM, McPhillips SE, Chiu H-J, Cohen AE, Deacon AM, Ellis PJ, Garman E, Gonzalez A, Sauter NK, Phizackerley RP, Soltis SM, Kuhn P. (2002) Blu-Ice and the distributed control system: software for data acquisition and instrument control at macromolecular crystallography beamlines. J Synchrotron Radiat 9:401–406.
88. Kabsch W (2010) XDS. Acta Crystallogr D66:125–132.
89. Evans PR, Murshudov GN (2013) How good are my data and what is the resolution? Acta Crystallogr D69: 1204–1214.
90. Collaborative Computational Project N 4 (1994) The CCP4 suite: programs for protein crystallography. Acta Crystallogr D50:760–763.
91. McCoy AJ, Grosse-Kunstleve RW, Adams PD, Winn MD, Storoni LC, Read RJ (2007) Phaser crystallographic software. J Appl Crystallogr 40:658–674.
92. Emsley P, Lohkamp B, Scott WG, Cowtan K (2010) Features and development of Coot. Acta Crystallogr 66:486–501. D
93. Murshudov GN, Skubak P, Lebedev AA, Pannu NS, Steiner RA, Nicholls RA, Winn MD, Long F, Vagin AA (2011) REFMAC5 for the refinement of macromolecular crystal structures. Acta Crystallogr D67:355–367.
94. Adams PD, Afonine PV, Bunkoczi G, Chen VB, Davis IW, Echols N, Headd JJ, Hung L-W, Kapral GJ, Grosse-Kunstleve RW, McCoy AJ, Moriarty NW, Oeffner R, Read RJ, Richardson DC, Richardson JS, Terwilliger TC, Zwart PH. (2010) PHENIX: a comprehensive Python-based system for macromolecular structure solution. Acta Crystallogr D66:213–221.
95. Morris GM, Huey R, Lindstrom W, Sanner MF, Belew RK, Goodsell DS, Olson AJ (2009) AutoDock4 and AutoDockTools4: automated docking with selective receptor flexibility. J Comput Chem 30:2785–2791.
96. Hess B, Kutzner C, van der Spoel D, Lindahl E (2008) GROMACS 4: algorithms for highly efficient, load-balanced, and scalable molecular simulation. J Chem Theory Comput 4:435–447.
97. Koziara KB, Stroet M, Malde AK, Mark AE (2014) Testing and validation of the Automated Topology Builder (ATB) version 2.0: prediction of hydration free enthalpies. J Comput Aided Mol Des 28:221–233.
98. Hess B, Bekker H, Berendsen HJC, Fraaije JGEM (1997) LINCS: a linear constraint solver for molecular simulations. J Comput Chem 18:1463–1472.
99. Berendsen HJC, Postma JPM, van Gunsteren WF, DiNola A, Haak JR (1984) Molecular dynamics with coupling to an external bath. J Chem Phys 81:3684–3690.
100. Humphrey W, Dalke A, Schulten K (1996) VMD – visual molecular dynamics. J Mol Graph 14:33–38.
101. Smith PE, van Gunsteren WF (1993) The viscosity of SPC and SPC/E water at 277 and 300 K. Chem Phys Lett 215:315–318.
102. Daura X, Gademann K, Jaun B, Seebach D, van Gunsteren WF, Mark AE (1999) Peptide folding: when simulation meets experiment. Angew Chem Int Ed 38:236–240.
103. Altschul SF, Gish W, Miller W, Myers EW, Lipman DJ (1990) Basic local alignment search tool. J Mol Biol 215:403–410.
104. Fu L, Niu B, Zhu Z, Wu S, Li W (2012) CD-HIT: accelerated for clustering the next-generation sequencing data. Bioinformatics 28:3150–3152.
105. Gerlt JA, Bouvier JT, Davidson DB, Imker HJ, Sadkhin B, Slater DR, Whalen KL (2015) Enzyme Function Initiative-Enzyme Similarity Tool (EFI-EST): a web tool for generating protein sequence similarity networks. Biochim Biophys Acta 1854:1019–1037.

Chapter 5

The Promiscuous Mechanism of F_{420}-Dependent Enzymes in Detoxification by *Mycobacteria*

5.1 Introduction

The FDOR superfamily have a range of promiscuous activities that allow *Mycobacteria* to be resilient against several conditions including hypoxia, oxidative stress, and resistance to bactericidal agents (Gurumurthy *et al.*, 2013). The range of activities that the FDORs exhibit includes the degradation of toxic compounds such as aflatoxins, furanocoumarins, triarylmethane dyes, and a range of quinones (Guerra-Lopez *et al.*, 2007; Taylor *et al.*, 2010; Lapalikar *et al.*, 2012; Gurumurthy *et al.*, 2013; Greening *et al.*, 2017). This promiscuity extends to the activation of nitroimidazole drugs including pretomanid, delamanid, and cgi-17341, a nitroimidazole activated by a range of FDORs (Gurumurthy *et al.*, 2012). Due to this, F_{420} in *Mycobacteria* and the enzymes that utilise it are attractive targets for anti-mycobactericial development and enzyme engineering for biocatalysis (Williams and Duncan, 2007; Taylor *et al.*, 2013). Although interesting, the extent of these promiscuous activities and their involvement in cell protection and potential biotechnological applications has not been fully explored. This includes understanding how effective F_{420} is for protecting the cell against known bactericidal agents, and the range of compounds that can be reduced by FDOR and by which mechanism.

To further explore the potential and effect of the various promiscuous activities of FDORs, this chapter presents two published papers. The first paper presented identifies compounds that can be reduced by FDORs and are known to have bactericidal effects. This is achieved through enzymatic assays of these compounds with FDORs from *M. smegmatis* and confirmed using mass spectrometry to identify the product. A time course using LC-MS analysis is used to show the degradation of these compounds by *M. smegmatis* and fgd and *fbi*C knockouts are used to show the loss of this activity. MIC values were determined of wildtype *M. smegmatis*, and fgd and *fbi*C knockouts against the assayed compounds to show the effect of F_{420} loss on *Mycobacteria* detoxification.

The second paper presented reveals a range of compounds, ranging from synthetic building blocks to more complex polycyclic compounds, which contain activated alkene groups and can be reduced by a range of FDORs from *M. smegmatis*. This was achieved using enzymatic assays to identify activity. Using substrate docking to determine the binding mode and donor-acceptor distance, and LC-MS and GC-MS to identify the products of the enzyme

assays including modified compounds. A common mechanism of the promiscuous activities of the FDORs is proposed.

5.2 The redox cofactor F420 protects mycobacteria from diverse antimicrobial compounds and mediates a reductive detoxification system

This section contains the following paper

The Redox Cofactor F_{420} Protects *Mycobacteria* from Diverse Antimicrobial Compounds and Mediates a Reductive Detoxification System

Thanavit Jirapanjawat, Blair Ney, Matthew C. Taylor, Andrew C. Warden, Shahana Afroze, Robyn J. Russell, Brendon M. Lee, Colin J. Jackson, John G. Oakeshott, Gunjan Pandey, Chris Greening

Applied and Environmental Microbiology, 82(23), 6810-6818.

Current status of paper: Published

Thanavit Jirapanjawat expressed and purified the enzymes and F_{420}, and performed the enzymatic assays. Blair Ney performed the whole-cell consumption analysis and LC-MS analysis. Chris Greening performed the phenotyping analysis including MIC and CFU analysis. I designed the enzymatic assays and supervised Thanavit Jirapanjawat performing assays and data analysis, and created Figures 3b and S4. Colin Jackson, Matt Taylor, and Chris Greening supervised students. Thanavit, Blair, and Chris designed the figures and wrote the paper with input from all authors.

AMERICAN SOCIETY FOR MICROBIOLOGY | Applied and Environmental Microbiology

The Redox Cofactor F_{420} Protects Mycobacteria from Diverse Antimicrobial Compounds and Mediates a Reductive Detoxification System

Thanavit Jirapanjawat,[a,b] Blair Ney,[a,b] Matthew C. Taylor,[a] Andrew C. Warden,[a] Shahana Afroze,[a,b] Robyn J. Russell,[a] Brendon M. Lee,[b] Colin J. Jackson,[b] John G. Oakeshott,[a] Gunjan Pandey,[a] Chris Greening[a*]

The Commonwealth Scientific and Industrial Research Organisation, Land and Water, Acton, ACT, Australia[a]; Australian National University, Research School of Chemistry, Acton, ACT, Australia[b]

ABSTRACT

A defining feature of mycobacterial redox metabolism is the use of an unusual deazaflavin cofactor, F_{420}. This cofactor enhances the persistence of environmental and pathogenic mycobacteria, including after antimicrobial treatment, although the molecular basis for this remains to be understood. In this work, we explored our hypothesis that F_{420} enhances persistence by serving as a cofactor in antimicrobial-detoxifying enzymes. To test this, we performed a series of phenotypic, biochemical, and analytical chemistry studies in relation to the model soil bacterium *Mycobacterium smegmatis*. Mutant strains unable to synthesize or reduce F_{420} were found to be more susceptible to a wide range of antibiotic and xenobiotic compounds. Compounds from three classes of antimicrobial compounds traditionally resisted by mycobacteria inhibited the growth of F_{420} mutant strains at subnanomolar concentrations, namely, furanocoumarins (e.g., methoxsalen), arylmethanes (e.g., malachite green), and quinone analogues (e.g., menadione). We demonstrated that promiscuous $F_{420}H_2$-dependent reductases directly reduce these compounds by a mechanism consistent with hydride transfer. Moreover, *M. smegmatis* strains unable to make $F_{420}H_2$ lost the capacity to reduce and detoxify representatives of the furanocoumarin and arylmethane compound classes in whole-cell assays. In contrast, mutant strains were only slightly more susceptible to clinical antimycobacterials, and this appeared to be due to indirect effects of F_{420} loss of function (e.g., redox imbalance) rather than loss of a detoxification system. Together, these data show that F_{420} enhances antimicrobial resistance in mycobacteria and suggest that one function of the $F_{420}H_2$-dependent reductases is to broaden the range of natural products that mycobacteria and possibly other environmental actinobacteria can reductively detoxify.

IMPORTANCE

This study reveals that a unique microbial cofactor, F_{420}, is critical for antimicrobial resistance in the environmental actinobacterium *Mycobacterium smegmatis*. We show that a superfamily of redox enzymes, the $F_{420}H_2$-dependent reductases, can reduce diverse antimicrobials *in vitro* and *in vivo*. *M. smegmatis* strains unable to make or reduce F_{420} become sensitive to inhibition by these antimicrobial compounds. This suggests that mycobacteria have harnessed the unique properties of F_{420} to reduce structurally diverse antimicrobials as part of the antibiotic arms race. The $F_{420}H_2$-dependent reductases that facilitate this process represent a new class of antimicrobial-detoxifying enzymes with potential applications in bioremediation and biocatalysis.

The redox cofactor F_{420} [7,8-didemethyl-8-hydroxy-5-deazariboflavin-5′-phosphoryllactyl(glutamyl)$_n$ glutamate] is unique to bacteria and archaea. This deazaflavin is structurally similar to flavin adenine dinucleotide (FAD) and flavin mononucleotide (FMN) but behaves more similarly electrochemically to the nicotinamides NAD and NADP (1). An obligate two-electron carrier, F_{420} mediates hydride transfer to or from a wide range of organic carbon compounds. Its low standard redox potential of −340 mV enables it to catalyze otherwise challenging reduction reactions, for example, those of enone, imine, enamine, and nitro groups (2–5). Due to these unique properties, F_{420} has been harnessed by bacteria and archaea in a wide range of metabolic pathways. The cofactor is best known for its role in methanogens, where it serves as the main catabolic cofactor (6). However, we have shown it is also synthesized by aerobic bacteria from at least three phyla, the *Actinobacteria*, *Chloroflexi*, and *Proteobacteria* (7). While the cofactor is of secondary importance to nicotinamides in bacteria, an increasing number of redox reactions in central and secondary metabolic pathways have been shown to depend on it (1). These include the biodegradation of aflatoxins and nitrophenols (2, 4), the biosynthesis of tetracycline and lincosamide antibiotics (8, 9),

Received 30 August 2016 **Accepted** 6 September 2016

Accepted manuscript posted online 16 September 2016

Citation Jirapanjawat T, Ney B, Taylor MC, Warden AC, Afroze S, Russell RJ, Lee BM, Jackson CJ, Oakeshott JG, Pandey G, Greening C. 2016. The redox cofactor F_{420} protects mycobacteria from diverse antimicrobial compounds and mediates a reductive detoxification system. Appl Environ Microbiol 82:6810–6818. doi:10.1128/AEM.02500-16.

Editor: H. Atomi, Kyoto University

Address correspondence to Chris Greening, chris.greening@monash.edu, or Gunjan Pandey, gunjan.pandey@csiro.au.

* Present address: Chris Greening, Monash University, School of Biological Sciences, Clayton, Victoria, Australia.

T.J. and B.N. contributed equally to this work.

Supplemental material for this article may be found at http://dx.doi.org/10.1128/AEM.02500-16.

and the reduction of biliverdin, quinones, and mycolic acids (5, 10, 11). In turn, it was recently recognized that F_{420} may have a significant role in shaping the biological and chemical compositions of soil ecosystems (7).

In recent years, F_{420} has inspired interest for its role in the redox metabolism of mycobacteria, an actinobacterial genus of environmental and medical significance. Most of these studies have focused on the soil saprophyte *Mycobacterium smegmatis* and the human pathogen *Mycobacterium tuberculosis*. These studies have shown that F_{420} is dispensable for growth but essential for the survival of antibiotic stress, oxidative stress, and hypoxia, for reasons still incompletely understood (10, 12, 13). In this genus, the cofactor is synthesized by four known enzymes (FbiC, CofC, CofD, and CofE) and is reduced by the F_{420}-dependent glucose 6-phosphate dehydrogenase (Fgd) (14). The physiological roles of the cofactor are elicited by $F_{420}H_2$-dependent reductases that couple the reoxidation of $F_{420}H_2$ to the reduction of organic compounds (1, 5, 11, 15). Genomic and biochemical studies have shown that mycobacteria synthesize a multiplicity of $F_{420}H_2$-dependent reductases from two superfamilies, the flavin/deazaflavin oxidoreductases (FDORs) and the luciferase-like hydride transferases (LLHTs). The soil organism *M. smegmatis* encodes some 31 FDORs and 45 LLHTs that are predicted to bind F_{420} (1, 5, 15). A smaller number of these proteins are encoded in the reduced genomes of the human pathogens *M. tuberculosis* and *Mycobacterium leprae* (5, 15).

The recently discovered FDOR superfamily is of particular interest because of its physiological and pharmacological roles in mycobacteria (1, 5). This diverse family is subdivided into 16 subgroups (A1 to A4, AA1 to AA6, and B1 to B6), with genes encoding the A1 and B1 subgroups in multiple copies in individual mycobacterial genomes (2, 5, 16, 17). To date, the physiological role of just one mycobacterial FDOR has been fully defined, a biliverdin reductase from the B3 subfamily that reduces the heme oxygenation product biliverdin to the potent antioxidant bilirubin (5, 18). Other subgroups have been implicated in quinone and fatty acid metabolism (5, 10). Several FDORs of the manifold A1 and B1 subgroups are also known for their ability to reduce several medically important exogenous compounds, including furanocoumarin natural products (e.g., aflatoxins) (2, 16) and clinical nitroimidazole prodrugs (i.e., delamanid and pretomanid) (19–21). Our previous structural studies have shown that the $F_{420}H_2$ moiety binds at an amphiphilic conserved F_{420}-binding domain, whereas the substrate binds in a more variable substrate-binding pocket (1, 2, 5). The promiscuous FDORs of the A1 subgroups are able to accommodate a range of substrates in wide pockets through a combination of hydrophobic and hydrophilic interactions involving conserved aromatic residues. Hydride transfer occurs directly between C-5 of $F_{420}H_2$ to the proximal electrophilic alkene or imine groups of the substrate (2, 5, 18, 22).

Despite the progress in understanding its biochemical basis, it remains unclear whether substrate promiscuity in the FDOR superfamily is physiologically significant and, if so, how this promiscuity has been shaped by natural selection. We recently proposed that mycobacteria evolved a multiplicity of promiscuous $F_{420}H_2$-dependent reductases in order to enhance the range of substrates which they may biodegrade (1, 5). These enzymes may use electrons derived from the cytosolic reservoir of glucose 6-phosphate (12) to reductively transform exogenous compounds, leading to their detoxification and/or biomineralization. To explore this hypothesis, this paper investigates the role of $F_{420}H_2$-dependent reductases in the metabolism of a range of antibiotics and xenobiotics. By combining cellular physiology, protein biochemistry, and analytical chemistry approaches, we resolved that F_{420} is crucial for the ability of mycobacteria to resist a range of antimicrobial compounds and demonstrated that $F_{420}H_2$-dependent FDORs can likely reductively detoxify some of these compounds.

MATERIALS AND METHODS

Bacterial strains and growth conditions. This study employed *Mycobacterium smegmatis* mc^2155 (23) and two derivative strains containing disruptions in the genes *fgd* and *fbiC* with kanamycin resistance cassettes (2). The strains were grown on LBT (lysogeny broth containing 0.05% Tween 80) and maintained on LBT agar. Kanamycin at 20 $\mu g \cdot ml^{-1}$ was used to propagate the mutant strains. For all physiological experiments, liquid cultures (30 ml) were grown to mid-exponential phase (optical density at 600 nm [OD_{600}], ≈0.5) in 125-ml aerated conical flasks in a rotary incubator (200 rpm, 37°C).

Phenotypic experiments. Twenty antimicrobial compounds were sourced from Sigma-Aldrich and dissolved into 1 M working stocks in dimethyl sulfoxide (DMSO). The structures of the compounds tested are shown in Table S1 in the supplemental material. Phenotypic experiments studied the effect of these compounds on the growth and survival of *M. smegmatis* and derivative strains. MICs were determined by a standard protocol (24) by serially diluting the compounds in 96-well plates and measuring growth inhibition by OD_{600} following incubation (400 rpm, 37°C, 12 h). Strain viability following challenge with antimicrobial agents was measured by challenging mid-exponential-phase cultures with the compound of interest at a concentration of 5 times the MIC of the wild-type strain. At regular time intervals, 1-ml cultures were centrifuged (16,000 × *g*, 1 min) and resuspended in 1 ml of HBTP (Hartmans de Bont minimal medium supplemented with 0.05% tyloxapol) (25) two times to remove the compounds. CFU · ml^{-1} were subsequently counted by spot-plating serially diluted cultures, as previously described (26). No CFU or MIC differences were observed for DMSO-only controls. To test the capacity of strains to grow on compounds as a sole source of carbon, exponential-phase cultures were inoculated to a starting OD_{600} of 0.005 into HBTP medium (25) supplemented with either 1 mM or 10 mM the compounds of interest, and growth was determined by the OD_{600} following incubation (200 rpm, 37°C, 24 h). Eight compounds were tested: coumarin, methoxsalen, imperatorin, menadione, azure B, malachite green, crystal violet, and phenol red.

Protein expression and purification. Six $F_{420}H_2$-dependent reductases of the flavin/deazaflavin oxidoreductase (FDOR) superfamily (MSMEG_5998, MSMEG_2027, MSMEG_6325, MSMEG_3380, MSMEG_0048, and MSMEG_5170 loci) and the F_{420}-reducing glucose 6-phosphate dehydrogenase (Fgd) were recombinantly overexpressed in *Escherichia coli* BL21(DE3) and purified by nickel-nitrilotriacetic acid (Ni-NTA) affinity chromatography, as previously described (2, 5). F_{420} was extracted, purified, and concentrated from a recombinant F_{420} overexpression strain of *M. smegmatis* mc^24517 (27) by a combination of anion-exchange chromatography, hydrophobic interaction chromatography, and rotary evaporation, as previously described (28).

Enzymatic assays. Two assays were optimized to monitor $F_{420}H_2$-coupled substrate reduction. A high-performance liquid chromatography (HPLC)-based method monitored the reduction of substrates by measuring changes in their absorbance at λ_{max} (maximum absorbance wavelength) or their fluorescence at $\lambda_{em\ max}$ (maximum emission wavelength) in aerobic vials containing the FDOR of interest, F_{420}, Fgd, and glucose 6-phosphate. The second method monitored the reoxidation of $F_{420}H_2$ by the absorbance at 420 nm in anoxic mixtures containing prereduced $F_{420}H_2$ and one of the FDORs. The rates obtained for the two methods were similar (see Table S2 in the supplemental material), demonstrating that rates of $F_{420}H_2$ reoxidation are proportional to those with substrate reduction. However, the second method proved more reliable and sys-

tematic, in part because it better discriminated between enzyme-dependent and enzyme-independent $F_{420}H_2$-mediated substrate reduction. Using this method, we assayed the specific activities of the six purified FDORs for 20 compounds. All assays were prepared in a nitrogen glove box and used buffers that were degassed by sonication. F_{420} was enzymatically reduced overnight with 1 μM Fgd and purified by spin filtration using previously reported methods (5). All reaction mixtures contained degassed Tris buffer (200 mM Tris, 0.1% [wt/vol] Triton X-100 [pH 8.0]) sequentially supplemented with 50 μM substrate, 25 μM $F_{420}H_2$, and, depending on reactivity, between 100 nM and 1 μM the FDOR. Reaction rates were monitored by recording the initial linear increase in absorbance at 420 nm using an Epoch 2 microplate spectrophotometer (BioTek). Specific activities were calculated by subtracting rates of no-enzyme controls and expressed in nmol · min^{-1} · μmol $enzyme^{-1}$, as previously described (2).

LC-MS analysis. For liquid chromatography-mass spectrometry (LC-MS) analysis of the FDOR-mediated reactions, 100 μM standards of malachite green and methoxsalen were prepared in 20 mM Tris buffer (pH 8.0). The mass spectra of their FDOR reaction products were measured after the addition of 100 μM glucose 6-phosphate, 10 μM F_{420}, 1 μM Fgd, and 1 μM MSMEG_2027, followed by incubation at 37°C for 1 h. An Agilent 1100 series binary LC equipped with a diode array detector and in-line time of flight mass spectrometer (LC-MSD TOF) were used, with mass data obtained by electrospray ionization (ESI) in positive ion mode. Samples were separated on an Agilent Poroshell 120 EC-C_{18} column (2.7 μm, 2.1 by 100 mm), utilizing a gradient protocol composed of buffer A, with ammonium formate plus 0.1% formic acid; and buffer B, with acetonitrile plus 0.1% formic acid. The applied gradient was as follows: 10% buffer B from 0.5 min to 60% buffer B at 6.50 min, and then increased to 90% buffer B at 7 min, at a flow rate of 0.4 ml · min^{-1}. The Agilent MassHunter quantitative analysis software was used to analyze product formation.

Whole-cell consumption assays. Whole-cell assays measured the consumption of the antimicrobial compounds malachite green and methoxsalen. Mid-exponential-phase cells grown in LBT were centrifuged (16,000 × *g*, 10 min) and resuspended in a buffer containing 50 mM MOPS (pH 7.4), 25 mM NaCl, and 25 mM KCl. The antimicrobial compound of interest was then added to a final concentration of 1/2 the MIC of the *fbiC* mutant strain. At regular intervals, samples of 200 μl were centrifuged to remove cells (16,000 × *g*, 5 min), and supernatants were analyzed via a high-performance liquid chromatography–diode array detection (HPLC-DAD) protocol. The analysis was carried out on an Agilent 1200 series system equipped with autosampler and a Poroshell 120 EC-C_{18} 2.7-μm, 2.1 by 100-mm column. A gradient consisting of buffer A (ultrapure water plus 0.1% formic acid) and buffer B (acetonitrile plus 0.1% formic acid) was applied as follows: 0 to 1 min 10% buffer B, 1 to 5 min 90% buffer B, 5 to 10 min 10% buffer B, 10 to 12 min 10% buffer B. Degradation of malachite green (retention time, 7.2 min) and methoxsalen (retention time, 6.9 min) was measured by tracking the loss of absorbance at 615 nm and 310 nm, respectively. Concentration was calculated by integrating the area of the absorbance peaks and calibrating with standards of known concentration.

RESULTS

F_{420}-deficient mutants are hypersusceptible to growth inhibition by antimicrobial compounds. We compared the susceptibility of wild-type and F_{420}-deficient mutant strains to growth inhibition by 20 antimicrobial agents. Two mutant strains were employed: one unable to synthesize F_{420} (*fbiC*::*kan* mutant) due to disruption of the gene encoding the first enzyme in the F_{420} biosynthesis pathway (FbiC), the other unable to reduce F_{420} (*fgd*::*kan* mutant) due to disruption of the gene encoding F_{420}-dependent glucose 6-phosphate dehydrogenase (Fgd). Six of the compounds were first- and second-line clinical antimycobacterial agents. The remainders were aminocoumarins/furanocoumarins, quinolones/fluoroquinolones, quinone analogues, and arylmethane compounds containing enone, lactone, or imine functionalities known to be catalytically compatible with $F_{420}H_2$-dependent reductases (2, 5, 10, 16).

The MICs for the *fgd* and *fbiC* mutants were lower than those of the wild type for 18 of the 20 compounds (Table 1). The mutant strains showed greatly increased susceptibility to four compound classes usually resisted by mycobacteria: furanocoumarins, quinone analogues, arylmethane dyes, and quinolones. Whereas wild-type strains were only compromised by high concentrations of these compounds, the mutants were susceptible even at subnanomolar levels. In addition, the mutants exhibited small but reproducible increases in susceptibility to growth inhibition to the five first-line clinical antimycobacterials tested. Similar MICs were observed for the *fgd* and *fbiC* mutants, which is consistent with FbiC being essential for F_{420} biosynthesis and Fgd being the main route for F_{420} reduction in *M. smegmatis* (1, 14). The slight increase in susceptibility of the *fbiC* mutant over the *fgd* mutant for three of the compounds suggests that some residual functions of F_{420} can be maintained in the absence of Fgd.

CFU measurements confirmed that loss of function of F_{420} reduces the capacity of *M. smegmatis* to survive treatment with representative antimicrobial compounds (Fig. 1). Whereas malachite green proved bacteriostatic to the wild-type strain at high concentrations, the dye rapidly killed F_{420} mutant strains. Likewise, the bactericidal agent menadione killed the *fbiC* mutant and, to a lesser extent, the *fgd* mutant strains at higher rates than for the wild-type strain. At 24 h following administration, we observed reductions in the survival of the *fbiC* mutant strain versus the wild type of 10,000-fold for malachite green and 100-fold for menadione ($P < 0.001$). Despite inhibiting growth of the *fbiC* mutant at subnanomolar concentrations (Table 1), the furanocoumarin methoxsalen proved bacteriostatic to all three strains even at a high concentration (640 μg · ml^{-1}). CFU and OD measurements confirmed that wild-type cells resumed growth on LBT medium following initial growth inhibition (Fig. 1). This suggests that the strain detoxified the furanocoumarin to sub-MIC levels. The mutant strains also exhibited a modest acceleration in killing following administration of the clinical antimycobacterial agent rifampin (see Fig. S1 in the supplemental material).

$F_{420}H_2$-dependent reductases directly reduce antimicrobial compounds. We hypothesized that the increased susceptibility of the mutant strains to many of the compounds tested was due to their inability to detoxify the compounds using $F_{420}H_2$-dependent reductases. To test this, we recombinantly expressed and purified six $F_{420}H_2$-dependent FDORs (see Fig. S2 in the supplemental material) from *M. smegmatis*. Enzymes were selected to cover a range of FDOR subgroups while focusing on A1 and B1 enzymes that have previously been shown to display the greatest substrate promiscuity (2, 5, 16). We spectroscopically measured the rates of $F_{420}H_2$-dependent reduction of the compounds, employing anaerobic conditions to prevent low-level spontaneous $F_{420}H_2$ reoxidation. These enzymes catalyzed the $F_{420}H_2$-dependent reduction of 10 of the 20 compounds tested (Fig. 2). Consistent with previous observations on the reactivity of $F_{420}H_2$ (11), several compounds were additionally reduced by $F_{420}H_2$ in an enzyme-independent manner (see Fig. S3 in the supplemental material).

FDORs transformed quinone analogues at high rates (>100,000 nmol · min^{-1} · μmol $enzyme^{-1}$) and furanocoumarins at low rates (>1,000 nmol · min^{-1} · μmol $enzyme^{-1}$). In

TABLE 1 Antibiotic susceptibility of F_{420}-deficient mycobacteria[a]

Substrate	MIC ($\mu g \cdot ml^{-1}$)			MIC ratio (WT/mutant)[b]
	WT	*fgd*::*kan*	*fbiC*::*kan*	
Quinone analogues				
Menadione	32	2	2	16
1,4-Naphthoquinone	32	1	1	32
1,2-Naphthoquinone	32	2	2	16
Furanocoumarins and aminocoumarins				
Methoxsalen	64	1	1	64
Angelicin	128	1	1	128
Imperatorin	32	0.5	0.5	64
Novobiocin	0.5	0.5	0.5	1
Arylmethane dyes				
Malachite green	64	1	0.5	64, 128
Crystal violet	16	1	0.5	16, 32
Phenol red	8	0.5	0.5	16
Azure B	16	2	2	8
Quinolones and fluoroquinolones				
Oxolinic acid	16	0.125	0.125	128
Nalidixic acid	128	1	1	128
Ciprofloxacin	0.25	3.1×10^{-2}	7.8×10^{-3}	8
Moxifloxacin	6.3×10^{-2}	6.3×10^{-2}	3.1×10^{-2}	1, 2
Clinical antimycobacterials				
Rifampin	4	2	2	2
Ethambutol	0.5	0.13	0.13	4
Isoniazid	32	16	16	2
Pyrazinamide	512	256	256	2
Clofazimine	8	4	4	2

[a] MICs are shown for exponential-phase wild-type (WT), *fgd* mutant, and *fbiC* mutant cultures. MICs were determined by serially diluting antibiotic stocks in 96-well plates and measuring growth inhibition by the OD_{600}. Five first-line antimycobacterials (rifampin, ethambutol, isoniazid, pyrazinamide, and clofazimine) and 1 second-line antimycobacterial (moxifloxacin) were tested.

[b] Cells with two values are the ratios for the *fgd*::*kan* mutant and *fbiC*::*kan* mutant, respectively.

addition, all four arylmethane compounds were also reduced by $F_{420}H_2$ through both FDOR-facilitated (malachite green and crystal violet) (Fig. 2) and nonenzymatic (azure B, phenol red, and malachite green) activities (see Fig. S3 in the supplemental material). While it is well established that mycobacteria reductively decolorize malachite green in an F_{420}-dependent manner (29), the enzymatic determinants of this process have remained elusive until now. Two of the six clinical antimycobacterials, namely, rifampin and clofazimine, were also reduced, although at very low rates of below 100 and 600 nmol $\cdot$ min^{-1} $\cdot$ μmol $enzyme^{-1}$, respectively. All six FDORs tested had some degree of promiscuity, although they varied significantly in their substrate ranges and reaction rates. The A1 enzymes (MSMEG_5998 and MSMEG_2027) exhibited the widest substrate range and generally the highest rates of the enzymes, with MSMEG_2027 having detectable activity with all 10 compounds for which FDOR activity

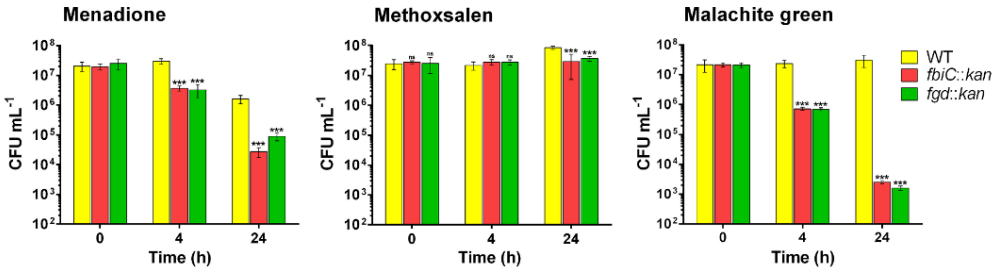

FIG 1 F_{420}-dependent survival of *M. smegmatis* following antimicrobial challenge. The wild-type (WT), *fgd* mutant, and *fbiC* mutant strains were challenged with three antimicrobials (menadione, methoxsalen, and malachite green) during mid-exponential growth. The survival of the strains, as determined by CFU, is shown following administration of antimicrobials at 5 times the MIC of the wild-type strain. Error bars represent standard deviations from the results from three biological replicates. *P* values were calculated by comparing CFU counts between wild-type and mutant strains. ***, $P < 0.001$; ns, not significant.

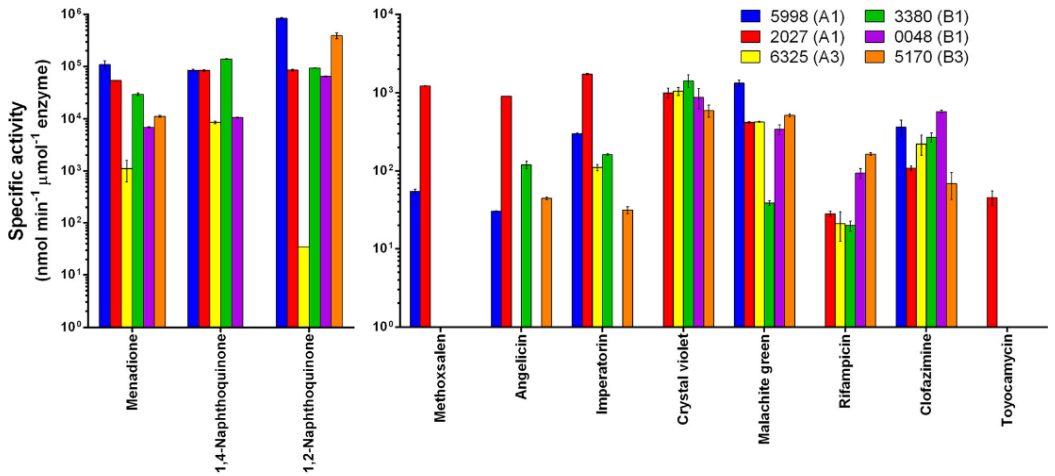

FIG 2 Reduction of antimicrobials by $F_{420}H_2$-dependent reductases from *Mycobacterium smegmatis*. Six characterized $F_{420}H_2$-dependent reductases (MSMEG_5998, MSMEG_2027, MSMEG_6325, MSMEG_3380, MSMEG_0048, and MSMEG_5170) were recombinantly expressed and purified from *E. coli*. The specific activity for each substrate was determined by recording the rate of $F_{420}H_2$ reoxidation by absorbance at 420 nm. Error bars show standard deviations from the results from three independent replicates. No $F_{420}H_2$-dependent reduction of ethambutol, isoniazid, pyrazinamide, oxolinic acid, novobiocin, nalidixic acid, ciprofloxacin, or moxifloxacin was observed. Significant rates of enzyme-independent $F_{420}H_2$ reoxidation were observed for phenol red and azure B (see Fig. S3 in the supplemental material).

was observed. Members of the B1 subgroup (MSMEG_0048 and MSMEG_3380) had high activities against quinones and arylmethanes but not furanocoumarins, whereas representatives of the A3 (MSMEG_6325) and B3 (MSMEG_5170) subgroups generally catalyzed reactions at fractional rates compared to the other FDORs. This is consistent with our previous studies showing most FDOR-A and FDOR-B enzymes can reduce aflatoxins, but at rates varying by four orders of magnitude (2, 16).

HPLC experiments with selected compounds validated that substrates were reduced by $F_{420}H_2$-dependent reductases. This occurred at rates similar to that of $F_{420}H_2$ reoxidation, suggesting an equimolar reaction (see Table S2 in the supplemental material). LC-MS analysis of two of the compounds, methoxsalen and malachite green, demonstrated the emergence of reduced forms of the compounds, with [M+H] ions corresponding to a 2-Da increase in the reaction product spectrum (Fig. 3A and B). This is consistent with direct hydride transfer occurring from the C-5 atom of $F_{420}H_2$ to the electrophilic double bonds of the substrates (Fig. 3C and D), coupled with addition of a proton from either solvent or a proximate residue, as observed for other FDOR-dependent reactions (2, 5, 17, 18, 30). Our previous structural studies provide a basis for understanding how these substrates can be accommodated into the substrate-binding sites of FDORs through both hydrophilic and hydrophobic interactions (1, 2, 5, 18). All other compounds reduced by $F_{420}H_2$ also contain functional groups known to be reduced by FDORs (1), namely, enones (quinone analogues), lactones (furanocoumarins), and imines (arylmethane dyes, clofazimine, and rifampin). On this basis, we propose probable reaction mechanisms for their reductions in Fig. S4 in the supplemental material. Two interesting exceptions are the quinolones (oxolinic acid and nalidixic acid), which were not reduced by FDORs despite containing enone moieties and inhibiting the growth of F_{420} mutant strains. It is possible that these compounds are instead substrates for other $F_{420}H_2$-dependent enzymes, such as the luciferase-like hydride transferases (LLHTs).

F_{420} is required for detoxification of antimicrobial compounds. With the exception of the quinolones, all compounds that strongly inhibited growth of F_{420} mutant strains were reduced by FDORs (see Fig. S5 in the supplemental material). The correlation between the phenotypic and biochemical data suggests that $F_{420}H_2$-dependent reductases directly detoxify many of these compounds, and the loss of these activities results in enhanced growth inhibition. It is impossible to test this hypothesis with targeted FDOR knockouts, as *M. smegmatis* encodes multiple $F_{420}H_2$-dependent reductases with overlapping substrate specificities, including five enzymes each from the promiscuous fast-acting A1 and B1 subgroups. Instead, we substantiated this hypothesis by comparing the abilities of the wild-type and mutant strains to detoxify model antimicrobial compounds from two distinct chemical classes that were reduced *in vitro* by FDORs. The furanocoumarin methoxsalen and the arylmethane malachite green were selected on the basis that their reduction can be sensitively monitored via diode array detection when supplemented in cultures at sub-MIC levels.

The wild-type strain transformed the two antimicrobial compounds tested. All the malachite green added was consumed to below-detectable limits within 40 min, while methoxsalen was more slowly degraded over 120 h (Fig. 3E and F). In contrast, the concentrations of the two compounds in the mutant cultures remained similar to those in the no-culture controls (although, in accordance with previous reports [31], significant culture-independent decolorization of malachite green was also observed). The rates of biotransformation observed suggest that the wild-type strain may survive malachite green treatment and recover from methoxsalen-induced growth inhibition (Fig. 1) by reductively detoxifying these compounds. Malachite green may have

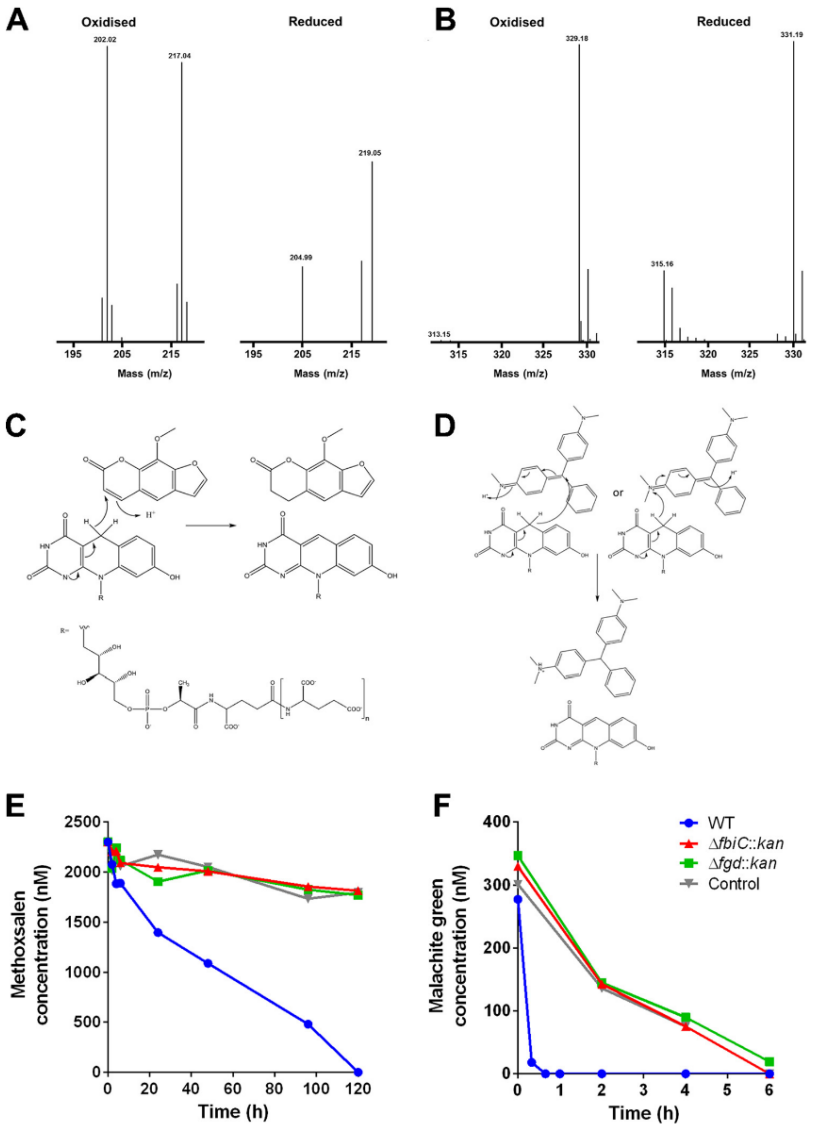

FIG 3 F_{420}-dependent antimicrobial detoxification *in vitro* and *in vivo*. (A and B) Mass spectra of methoxsalen (A) and malachite green (B) before and after reduction with the FDOR MSMEG_2027. Major peaks corresponding to oxidized (*m/z* 217) and reduced (*m/z* 219) methoxsalen and oxidized (*m/z* 329) and reduced (*m/z* 331) malachite green were observed. For both compounds, there are also ionization fragments corresponding to the demethylated compounds. (C and D) Plausible mechanisms for FDOR mediated hydride transfer from $F_{420}H_2$ to methoxsalen (C) and malachite green (D) are shown based on the mass spectra. (E and F) F_{420}-dependent reduction of methoxsalen (E) and malachite green (F) in resting cells of *Mycobacterium smegmatis*. The concentration of the antimicrobial following administration at 1/2 the MIC of the *fbiC* mutant strain is shown over time for the wild-type strain, *fbiC* mutant, *fgd* mutant, and a no-culture control.

been transformed more rapidly than methoxsalen *in vivo* because FDORs able to reduce the compound are more numerous and faster acting (Fig. 2). In combination, these results show that phenotypic resistance (Fig. 1), *in vitro* reactivity (Fig. 2), and *in vivo* reactivity (Fig. 3) to methoxsalen and malachite green are strongly correlated and F_{420} dependent.

We previously predicted that $F_{420}H_2$-dependent reductases might also support growth of mycobacteria by reductively activating exogenous compounds for use as sources of carbon and energy (1, 2, 16). However, we confirmed *in vivo* that neither wild-type nor mutant strains could grow when inoculated with minimal salts medium supplemented with any one of eight known FDOR

substrates as the sole carbon or energy source. This is again consistent with our hypothesis that mycobacteria employ $F_{420}H_2$-dependent reductases to support detoxification rather than growth.

DISCUSSION

To summarize, this study makes three interrelated findings. First, the cofactor F_{420} is critical for resistance of mycobacteria to antimicrobial compounds. Strains unable to synthesize or reduce this cofactor were hypersusceptible to most antimicrobial compounds tested, resulting in logarithmic increases in susceptibility for three compound classes (quinone analogues, furanocoumarins, and arylmethanes). Second, at least six $F_{420}H_2$-dependent reductases are capable of reducing antimicrobial compounds, including representatives of the three above-mentioned compound classes. Third, strains unable to utilize $F_{420}H_2$ were unable to reduce representatives of these compounds and exhibited accelerated death. On this basis, we propose that mycobacteria employ some $F_{420}H_2$-dependent reductases to reductively detoxify various antimicrobial compounds.

Environmental and pathogenic mycobacteria alike are renowned for their intrinsic resistance to antimicrobial compounds. Contributing to this capacity are their impermeable cell walls, abundance of efflux pumps, and diversity of chemical detoxification mechanisms (32). Mycobacteria produce a wide range of characterized enzymes capable of degrading antimicrobial compounds, including beta-lactamases (33), cytochrome P450 oxidases (34), arylamine *N*-acetyltransferases (35), and nitroreductases (36). We propose that $F_{420}H_2$-dependent reductases of the FDOR superfamily enhance this arsenal by reductively activating organic compounds otherwise recalcitrant to biodegradation. Such enzymes can reduce a wide range of functional groups (e.g., lactones, enones, and imines) in structurally diverse monocyclic and polycyclic organic compounds by hydride transfer. It is possible to rationalize why some FDOR-reduced substrates are less toxic to the cell based on the mode-of-action of the compounds: reduction of quinones will prevent spontaneous formation of semiquinone species that induce the production of reactive oxygen species (ROS) (10, 37); reduction of the central carbon of arylmethanes will produce nonplanar molecules unable to intercalate DNA (38); and reduction of furanocoumarins stimulates hydrolytic ring opening that prevents binding to topoisomerase I (16, 39). As with cytochrome P450 oxidases, however, the cellular consequences of $F_{420}H_2$-dependent transformations will depend on the compound reduced. While these enzymes will detoxify antimicrobial compounds if the reduced compounds are less toxic to the cell, as appears to be case for the furanocoumarins, quinones, and arylmethanes tested, their effects will be null if oxidized and reduced forms of the antimicrobial compound have similar efficacy, as may be the case for clofazimine and rifampin. Furthermore, some $F_{420}H_2$-dependent reductases activate certain prodrugs, as reflected by the transformation of the clinical nitroimidazoles delamanid and pretomanid by the FDOR-A1 enzyme Rv3547 (20, 30).

Natural selection for enzymatic strategies to reductively detoxify a wide range of antimicrobial natural products may explain the number, diversity, and promiscuity of $F_{420}H_2$-dependent reductases found in mycobacteria. While the genus *Mycobacterium* is renowned for its pathogens, the majority of its species are saprophytic soil organisms, including its deepest-branching members (40). We have demonstrated that FDORs can degrade fungal aflatoxins (2) and plant furanocoumarins, as well as quinone groups, which serve as building blocks for various streptomycete antibiotics. Based on their chemical structures, other substrates potentially compatible with FDORs include numerous natural products of plant (e.g., flavonoids), bacterial (e.g., germicidins and mitomycins), and fungal (e.g., ochratoxins and patulin) origin. Our recent evolutionary and structural analyses of the FDOR superfamily support the contention that the most numerous subclasses of this family are also its most promiscuous. Whereas some phylogenetically clustered subgroups of this family appear to be functionally constrained (e.g., B2 and B4 subgroups), the A1 and B1 enzymes have multiplied and diversified in function over the course of mycobacterial evolution (5). Our structural analyses have shown that enzymes from these subgroups have evolved wide substrate-binding pockets, particularly the recently solved MSMEG_2027 structure, which allow them to accommodate substrates as structurally diverse as menadione, malachite green, and methoxsalen (1, 2, 5). Docking studies have suggested that these enzymes bind quinone and coumarin compounds through multiple hydrophobic interactions with their phenyl rings and stabilizing Tyr-mediated hydrogen-bonding interactions with their ketone groups (2, 5). Thus, by encoding multiple reductases with broad specificities, mycobacteria increase the range of compounds they can reductively detoxify.

In addition to facilitating direct detoxification mechanisms, it is possible that F_{420} also enhances the capacity of mycobacteria to resist antimicrobial agents through mechanisms independent of detoxification. We found that the mutant strains unable to make $F_{420}H_2$ were significantly more susceptible to quinolones and first-line clinical antimycobacterials, even though they were not substrates for the FDORs we tested. Other groups have similarly shown that *M. tuberculosis* mutants unable to synthesize F_{420} are hypersusceptible to isoniazid and moxifloxacin (10). It cannot be ruled out that the numerous other $F_{420}H_2$-dependent reductases of the FDOR and LLHT superfamilies metabolize such compounds; this is possible in the cases of oxolinic acid and nalidixic acid, which harbor compatible enone functionalities and cause major growth inhibition. For the antimycobacterials, for which more mild phenotypes were observed, it is more likely that more general loss of functionality of F_{420}-dependent oxidoreductases results in pleiotropic effects on mycobacterial physiology that hypersensitize cells to antimicrobial stress. While the roles of this cofactor in mycobacterial physiology remain incompletely defined, F_{420} has been linked to maintaining redox homeostasis (10), maintaining cell wall structure (11), and generating antioxidants (5). Disruption of any of these processes could result in broad increases in antimicrobial susceptibility.

The findings from this work have wider environmental, medical, and industrial significance. $F_{420}H_2$-dependent reductases appear to contribute to the antibiotic arms race through dual roles in actinobacteria: whereas streptomycetes use such enzymes to synthesize antibiotics (1, 8), mycobacteria harness them for detoxification. This supports our recent hypothesis that F_{420} may significantly shape the biological and chemical composition of soil ecosystems (7). The results also have obvious clinical significance given that FDORs have been retained in pathogenic mycobacteria (1), and previous studies have shown that F_{420} is critical to antimicrobial resistance of *M. tuberculosis* (1, 10, 13). However, there is currently no evidence that $F_{420}H_2$-dependent reductases directly contribute to the detoxification of clinical antimycobacte-

rial compounds. As recently reviewed (1), the substrate promiscuity of the $F_{420}H_2$-dependent reductase superfamily also opens up potential applications for these enzymes in bioremediation and industrial biocatalysis; for example, FDORs may be used to decolorize environmental toxins, such as malachite green (31), or catalyze stereospecific imine reductions in asymmetric synthesis (41). There is now need for further biochemical studies to fully understand the basis and range of substrate promiscuity of $F_{420}H_2$-dependent reductases, as well as targeted phenotypic studies of individual FDORs to better define their physiological and pharmacological roles in mycobacteria.

ACKNOWLEDGMENTS

We thank Chris Coppin (CSIRO) for assistance with figure preparation, Ghader Bashiri (University of Auckland) for providing the *fbiABC* overexpression plasmid, and William Jacobs, Jr. (Albert Einstein College of Medicine) for supplying *Mycobacterium smegmatis* mc^24517.

This work was supported by a CSIRO Office of the Chief Executive Postdoctoral Fellowship awarded to C.G., a CSIRO Office of the Chief Executive Ph.D. Scholarship awarded to S.A., and Australian Research Council grants (DE120102673 and DP130102144) awarded to C.J.J.

C.G., G.P., J.G.O., M.C.T., A.C.W., B.N., S.A., T.J., R.J.R., C.J.J., and B.M.L. designed the experiments. T.J., B.N., C.G., S.A., G.P., and M.C.T. performed the experiments. C.G., C.J.J., M.C.T., J.G.O., G.P., A.C.W., B.M.L., and R.J.R. supervised students. C.G., J.G.O., M.C.T., T.J., B.N., A.C.W., C.J.J., G.P., S.A., and B.M.L. analyzed the data. C.G., J.G.O., B.N., and T.J. wrote the paper.

FUNDING INFORMATION

This work, including the efforts of Colin Jackson, was funded by Australian Research Council (ARC) (DE120102673 and DP130102144).

REFERENCES

1. Greening C, Ahmed FH, Mohamed AE, Lee BM, Pandey G, Warden AC, Scott C, Oakeshott JG, Taylor MC, Jackson CJ. 2016. Physiology, biochemistry, and applications of F_{420}- and F_o-dependent redox reactions. Microbiol Mol Biol Rev 80:451–493. http://dx.doi.org/10.1128/MMBR.00070-15.
2. Taylor MC, Jackson CJ, Tattersall DB, French N, Peat TS, Newman J, Briggs LJ, Lapalikar GV, Campbell PM, Scott C, Russell RJ, Oakeshott JG. 2010. Identification and characterization of two families of $F_{420}H_2$-dependent reductases from mycobacteria that catalyse aflatoxin degradation. Mol Microbiol 78:561–575. http://dx.doi.org/10.1111/j.1365-2958.2010.07356.x.
3. Li W, Khullar A, Chou S, Sacramo A, Gerratana B. 2009. Biosynthesis of sibiromycin, a potent antitumor antibiotic. Appl Environ Microbiol 75:2869–2878. http://dx.doi.org/10.1128/AEM.02326-08.
4. Ebert S, Rieger P-G, Knackmuss H-J. 1999. Function of coenzyme F_{420} in aerobic catabolism of 2,4,6-trinitrophenol and 2,4-dinitrophenol by *Nocardioides simplex* FJ2-1A. J Bacteriol 181:2669–2674.
5. Ahmed FH, Carr PD, Lee BM, Afriat-Jurnou L, Mohamed AE, Hong N-S, Flanagan J, Taylor MC, Greening C, Jackson CJ. 2015. Sequence-structure-function classification of a catalytically diverse oxidoreductase superfamily in mycobacteria. J Mol Biol 427:3554–3571. http://dx.doi.org/10.1016/j.jmb.2015.09.021.
6. Thauer RK, Kaster A-K, Seedorf H, Buckel W, Hedderich R. 2008. Methanogenic archaea: ecologically relevant differences in energy conservation. Nat Rev Microbiol 6:579–591. http://dx.doi.org/10.1038/nrmicro1931.
7. Ney B, Ahmed FH, Carere CR, Biswas A, Warden AC, Morales SE, Pandey G, Watt SJ, Oakeshott JG, Taylor MC, Stott MB, Jackson CJ, Greening C. 9 August 2016. The methanogenic redox cofactor F_{420} is widely synthesized by aerobic soil bacteria. ISME J http://dx.doi.org/10.1038/ismej.2016.100.
8. Wang P, Bashiri G, Gao X, Sawaya MR, Tang Y. 2013. Uncovering the enzymes that catalyze the final steps in oxytetracycline biosynthesis. J Am Chem Soc 135:7138–7141. http://dx.doi.org/10.1021/ja403516u.
9. Peschke U, Schmidt H, Zhang H-Z, Piepersberg W. 1995. Molecular characterization of the lincomycin-production gene cluster of *Streptomyces lincolnensis* 78-11. Mol Microbiol 16:1137–1156. http://dx.doi.org/10.1111/j.1365-2958.1995.tb02338.x.
10. Gurumurthy M, Rao M, Mukherjee T, Rao SPS, Boshoff HI, Dick T, Barry CE, Manjunatha UH. 2013. A novel F_{420}-dependent anti-oxidant mechanism protects *Mycobacterium tuberculosis* against oxidative stress and bactericidal agents. Mol Microbiol 87:744–755. http://dx.doi.org/10.1111/mmi.12127.
11. Purwantini E, Mukhopadhyay B. 2013. Rv0132c of *Mycobacterium tuberculosis* encodes a coenzyme F420-dependent hydroxymycolic acid dehydrogenase. PLoS One 8:e81985. http://dx.doi.org/10.1371/journal.pone.0081985.
12. Hasan MR, Rahman M, Jaques S, Purwantini E, Daniels L. 2010. Glucose 6-phosphate accumulation in mycobacteria: implications for a novel F_{420}-dependent anti-oxidant defense system. J Biol Chem 285:19135–19144. http://dx.doi.org/10.1074/jbc.M109.074310.
13. Purwantini E, Mukhopadhyay B. 2009. Conversion of NO_2 to NO by reduced coenzyme F_{420} protects mycobacteria from nitrosative damage. Proc Natl Acad Sci U S A 106:6333–6338. http://dx.doi.org/10.1073/pnas.0812883106.
14. Bashiri G, Squire CJ, Moreland NJ, Baker EN. 2008. Crystal structures of F_{420}-dependent glucose-6-phosphate dehydrogenase FGD1 involved in the activation of the anti-tuberculosis drug candidate PA-824 reveal the basis of coenzyme and substrate binding. J Biol Chem 283:17531–17541. http://dx.doi.org/10.1074/jbc.M801854200.
15. Selengut JD, Haft DH. 2010. Unexpected abundance of coenzyme F_{420}-dependent enzymes in *Mycobacterium tuberculosis* and other actinobacteria. J Bacteriol 192:5788–5798. http://dx.doi.org/10.1128/JB.00425-10.
16. Lapalikar GV, Taylor MC, Warden AC, Scott C, Russell RJ, Oakeshott JG. 2012. $F_{420}H_2$-dependent degradation of aflatoxin and other furanocoumarins is widespread throughout the Actinomycetales. PLoS One 7:e30114. http://dx.doi.org/10.1371/journal.pone.0030114.
17. Lapalikar GV, Taylor MC, Warden AC, Onagi H, Hennessy JE, Mulder RJ, Scott C, Brown SE, Russell RJ, Easton CJ, Oakeshott JG. 2012. Cofactor promiscuity among F_{420}-dependent reductases enables them to catalyse both oxidation and reduction of the same substrate. Catal Sci Technol 2:1560–1567. http://dx.doi.org/10.1039/c2cy20129a.
18. Ahmed FH, Mohamed AE, Carr PD, Lee BM, Condic-Jurkic K, O'Mara ML, Jackson CJ. 2016. Rv2074 is a novel $F_{420}H_2$-dependent biliverdin reductase in Mycobacterium tuberculosis. Protein Sci 25:1692–1709. http://dx.doi.org/10.1002/pro.2975.
19. Gurumurthy M, Mukherjee T, Dowd CS, Singh R, Niyomrattanakit P, Tay JA, Nayyar A, Lee YS, Cherian J, Boshoff HI, Dick T, Barry CE, III, Manjunatha UH. 2012. Substrate specificity of the deazaflavin-dependent nitroreductase from *Mycobacterium tuberculosis* responsible for the bioreductive activation of bicyclic nitroimidazoles. FEBS J 279:113–125. http://dx.doi.org/10.1111/j.1742-4658.2011.08404.x.
20. Singh R, Manjunatha U, Boshoff HIM, Ha YH, Niyomrattanakit P, Ledwidge R, Dowd CS, Lee IY, Kim P, Zhang L, Kang S, Keller TH, Jiricek J, Barry CE, III. 2008. PA-824 kills nonreplicating *Mycobacterium tuberculosis* by intracellular NO release. Science 322:1392–1395. http://dx.doi.org/10.1126/science.1164571.
21. Mohamed AE, Ahmed FH, Arulmozhiraja S, Lin CY, Taylor MC, Krausz ER, Jackson CJ, Coote ML. 2016. Protonation state of $F_{420}H_2$ in the prodrug-activating deazaflavin dependent nitroreductase (Ddn) from Mycobacterium tuberculosis. Mol Biosyst 12:1110–1113. http://dx.doi.org/10.1039/C6MB00033A.
22. Cellitti SE, Shaffer J, Jones DH, Mukherjee T, Gurumurthy M, Bursulaya B, Boshoff HI, Choi I, Nayyar A, Lee YS, Cherian J, Niyomrattanakit P, Dick T, Manjunatha UH, Barry CE, III, Spraggon G, Geierstanger BH. 2012. Structure of Ddn, the deazaflavin-dependent nitroreductase from *Mycobacterium tuberculosis* involved in bioreductive activation of PA-824. Structure 20:101–112. http://dx.doi.org/10.1016/j.str.2011.11.001.
23. Snapper SB, Melton RE, Mustafa S, Kieser T, Jacobs WR, Jr. 1990. Isolation and characterization of efficient plasmid transformation mutants of *Mycobacterium smegmatis*. Mol Microbiol 4:1911–1919. http://dx.doi.org/10.1111/j.1365-2958.1990.tb02040.x.
24. Blanco-Ruano D, Roberts DM, Gonzalez-Del-Rio R, Alvarez D, Rebollo MJ, Perez-Herran E, Mendoza A. 2015. Antimicrobial susceptibility testing for *Mycobacterium* sp. Methods Mol Biol 1285:257–268. http://dx.doi.org/10.1007/978-1-4939-2450-9_15.
25. Greening C, Berney M, Hards K, Cook GM, Conrad R. 2014. A soil

actinobacterium scavenges atmospheric H_2 using two membrane-associated, oxygen-dependent [NiFe] hydrogenases. Proc Natl Acad Sci U S A 111:4257–4261. http://dx.doi.org/10.1073/pnas.1320586111.
26. Berney M, Greening C, Conrad R, Jacobs WR, Cook GM. 2014. An obligately aerobic soil bacterium activates fermentative hydrogen production to survive reductive stress during hypoxia. Proc Natl Acad Sci U S A 111:11479–11484. http://dx.doi.org/10.1073/pnas.1407034111.
27. Bashiri G, Rehan AM, Greenwood DR, Dickson JMJ, Baker EN. 2010. Metabolic engineering of cofactor F_{420} production in *Mycobacterium smegmatis*. PLoS One 5:e15803. http://dx.doi.org/10.1371/journal.pone.0015803.
28. Isabelle D, Simpson DR, Daniels L. 2002. Large-scale production of coenzyme F_{420}-5,6 by using *Mycobacterium smegmatis*. Appl Environ Microbiol 68:5750–5755. http://dx.doi.org/10.1128/AEM.68.11.5750-5755.2002.
29. Guerra-Lopez D, Daniels L, Rawat M. 2007. *Mycobacterium smegmatis* mc^2 155 *fbiC* and MSMEG_2392 are involved in triphenylmethane dye decolorization and coenzyme F_{420} biosynthesis. Microbiology 153:2724–2732. http://dx.doi.org/10.1099/mic.0.2006/009241-0.
30. Manjunatha UH, Boshoff H, Dowd CS, Zhang L, Albert TJ, Norton JE, Daniels L, Dick T, Pang SS, Barry CE, III. 2006. Identification of a nitroimidazo-oxazine-specific protein involved in PA-824 resistance in *Mycobacterium tuberculosis*. Proc Natl Acad Sci U S A 103:431–436. http://dx.doi.org/10.1073/pnas.0508392103.
31. Jones JJ, Falkinham JO, III. 2003. Decolorization of malachite green and crystal violet by waterborne pathogenic mycobacteria. Antimicrob Agents Chemother 47:2323–2326. http://dx.doi.org/10.1128/AAC.47.7.2323-2326.2003.
32. Almeida Da Silva PE, Palomino JC. 2011. Molecular basis and mechanisms of drug resistance in *Mycobacterium tuberculosis*: classical and new drugs. J Antimicrob Chemother 66:1417–1430. http://dx.doi.org/10.1093/jac/dkr173.
33. Flores AR, Parsons LM, Pavelka MS, Jr. 2005. Genetic analysis of the beta-lactamases of *Mycobacterium tuberculosis* and *Mycobacterium smegmatis* and susceptibility to beta-lactam antibiotics. Microbiology 151:521–532. http://dx.doi.org/10.1099/mic.0.27629-0.
34. Ouellet H, Johnston JB, Ortiz de Montellano PR. 2010. The *Mycobacterium tuberculosis* cytochrome P450 system. Arch Biochem Biophys 493:82–95. http://dx.doi.org/10.1016/j.abb.2009.07.011.
35. Sim E, Sandy J, Evangelopoulos D, Fullam E, Bhakta S, Westwood I, Krylova A, Lack N, Noble M. 2008. Arylamine *N*-acetyltransferases in mycobacteria. Curr Drug Metab 9:510–519. http://dx.doi.org/10.2174/138920008784892100.
36. Manina G, Bellinzoni M, Pasca MR, Neres J, Milano A, Ribeiro ALDJL, Buroni S, Skovierova H, Dianiskova P, Mikusova K, Marak J, Makarov V, Giganti D, Haouz A, Lucarelli AP, Degiacomi G, Piazza A, Chiarelli LR, De Rossi E, Salina E, Cole ST, Alzari PM, Riccardi G. 2010. Biological and structural characterization of the *Mycobacterium smegmatis* nitroreductase NfnB, and its role in benzothiazinone resistance. Mol Microbiol 77:1172–1185. http://dx.doi.org/10.1111/j.1365-2958.2010.07277.x.
37. Winterbourn CC. 2008. Reconciling the chemistry and biology of reactive oxygen species. Nat Chem Biol 4:278–286. http://dx.doi.org/10.1038/nchembio.85.
38. Srivastava S, Sinha R, Roy D. 2004. Toxicological effects of malachite green. Aquat Toxicol 66:319–329. http://dx.doi.org/10.1016/j.aquatox.2003.09.008.
39. Diwan R, Malpathak N. 2009. Furanocoumarins: novel topoisomerase I inhibitors from *Ruta graveolens* L. Bioorg Med Chem 17:7052–7055. http://dx.doi.org/10.1016/j.bmc.2009.04.023.
40. Hartmans S, de Bont JM, Stackebrandt E. 2006. The genus *Mycobacterium*–nonmedical, p 889–918. *In* Dworkin M, Falkow S, Rosenberg E, Schleifer K-H, Stackebrandt E (ed), The prokaryotes. Springer, New York, NY.
41. Schrittwieser JH, Velikogne S, Kroutil W. 2015. Biocatalytic imine reduction and reductive amination of ketones. Adv Synth Catal 357:1655–1685. http://dx.doi.org/10.1002/adsc.201500213.

5.3 Supplementary Material

Supporting Information

Table S1. Chemical structures of the 20 compounds studied.

Family	Substrates	Structures
Quinones	Menadione (172.18 Da)	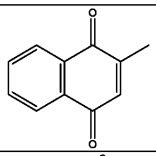
	1,4-naphthoquinone (158.15 Da)	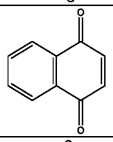
	1,2-naphthoquinone (158.15 Da)	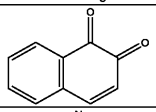
Triphenyls	Azure B (270.38 Da)	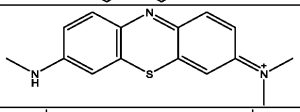
	Crystal violet (372.53 Da)	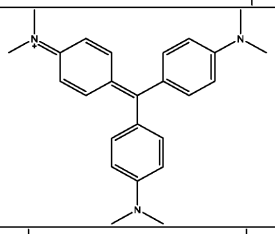
	Malachite green (329.46 Da)	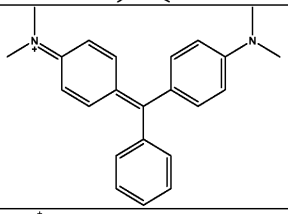
	Phenol red (354.38 Da)	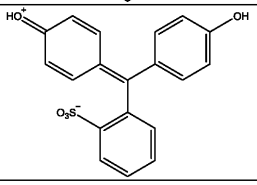

First-line antimycobacterials	Rifampicin (822.94 Da)	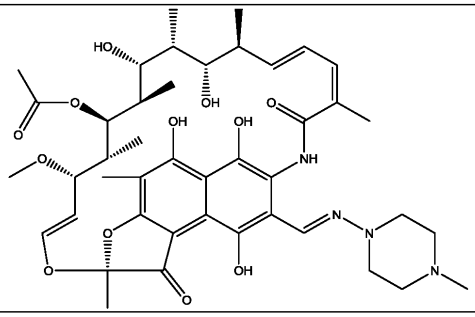
	Ethambutol (204.31Da)	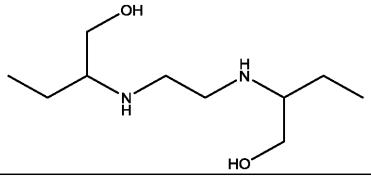
	Isoniazid (137.14 Da)	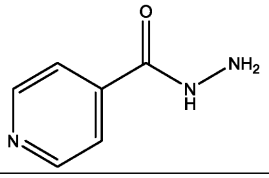
	Pyrazinamide (123.11 Da)	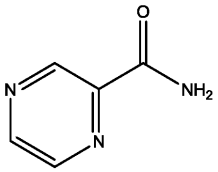
	Clofazimine (473.40 Da)	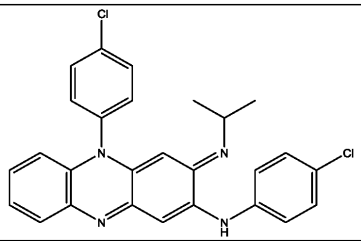
Furanocoumarins and aminocoumarins	Methoxsalen (216.19 Da)	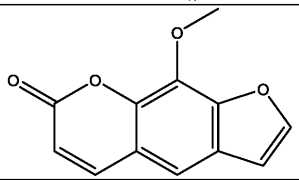
	Angelicin (186.17 Da)	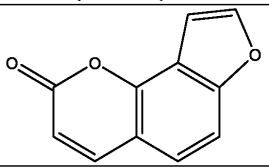

	Imperatorin (270.28 Da)	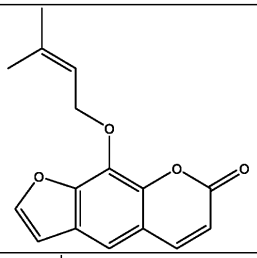
	Novobiocin (612.12 Da)	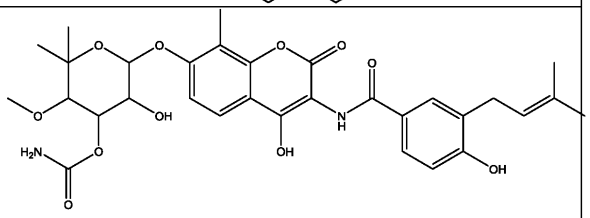
Quinolones and fluoroquinolones	Oxolinic acid (261.23 Da)	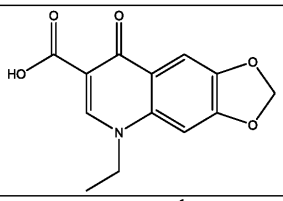
	Nalidixic acid (232.24 Da)	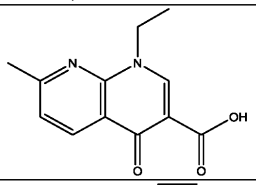
	Ciprofloxacin (331.35 Da)	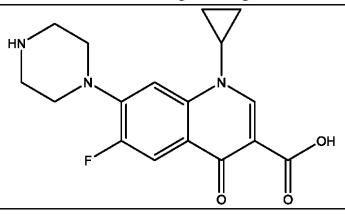
	Moxifloxacin (401.43 Da)	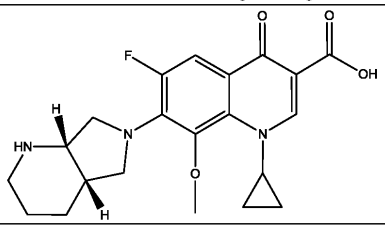

Table S2. Comparison of specific activities of $F_{420}H_2$ reoxidation and substrate reduction for selected compounds in the presence of the FDOR-A1 enzyme MSMEG_2027. $F_{420}H_2$ reoxidation was measured by absorbance at 420 nm, whereas substrate reduction was measured by the size of elution peaks on HPLC. Specific activities are expressed in nmol min^{-1} μmol^{-1} enzyme.

Substrate	Rate of cofactor oxidation	Rate of substrate reduction
1,2-napthoquinone	85200 ± 3100	108000 ± 6100
Methoxsalen	1230 ± 20	1700 ± 250
Imperatorin	1710 ± 30	1400 ± 210
Malachite green	420 ± 10	900 ± 400
Rifampicin	28.2 ± 2.0	21.8 ± 9.1

Figure S1. F_{420}-dependent survival of *M. smegmatis* following challenge with rifampicin at 5 × MIC of the wild-type strain. The survival of three strains, the wild-type, *fgd* mutant, and *fbiC* mutant, was determined by colony forming units Error bars represent standard deviations from three biological replicates. *p*-values were calculated by comparing CFU counts between wild-type and mutant strains, where * = $p < 0.05$, ** = $p < 0.01$, *** = $p < 0.001$, and ns = not significant.

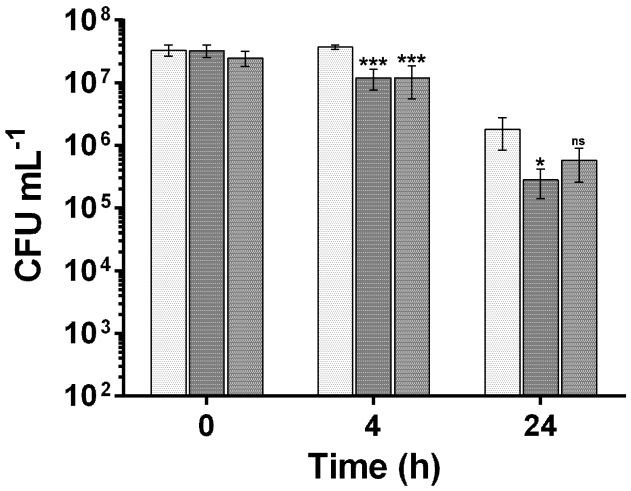

Figure S2. SDS-PAGE gels showing recombinant expression and purification of six $F_{420}H_2$-dependent FDORs and Fgd from *Mycobacterium smegmatis*. From left to right, the gels shown are MSMEG_5998 (A1), MSMEG_2027 (A1), MSMEG_6325 (A3), MSMEG_0048 (B1), MSMEG_3380 (B1), MSMEG_5170 (B1), and Fgd. Bands corresponding to the dimeric and tetrameric forms of the FDORs are visible. Legend: M = standard protein marker, WC = whole-cell lysate, S = soluble fraction, FT = flow-through, E1 to E8 = eluted protein fractions 1 to 8.

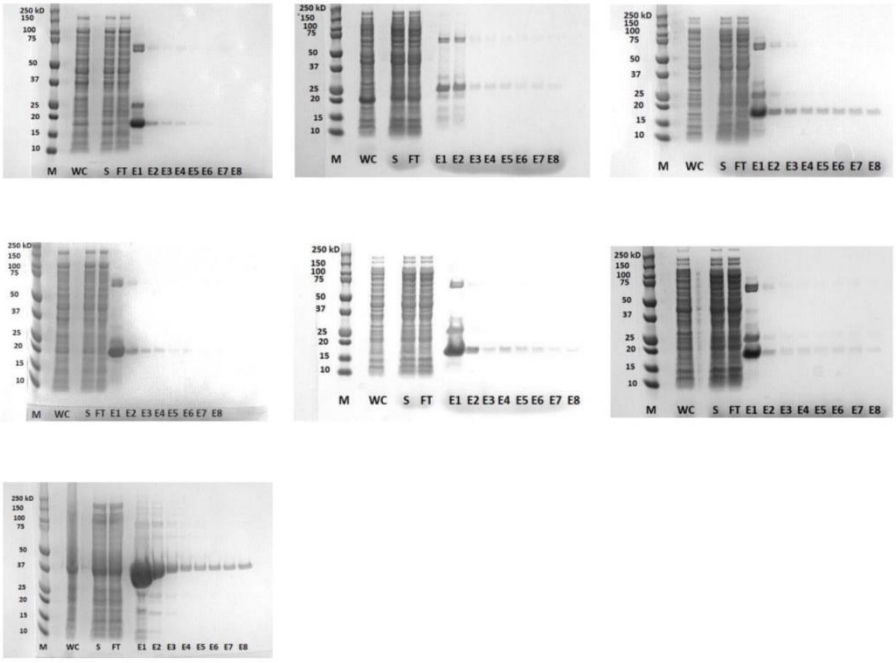

Figure S3. Rate of $F_{420}H_2$-dependent, enzyme-independent substrate reduction. The five substrates with significant reduction rates are shown.

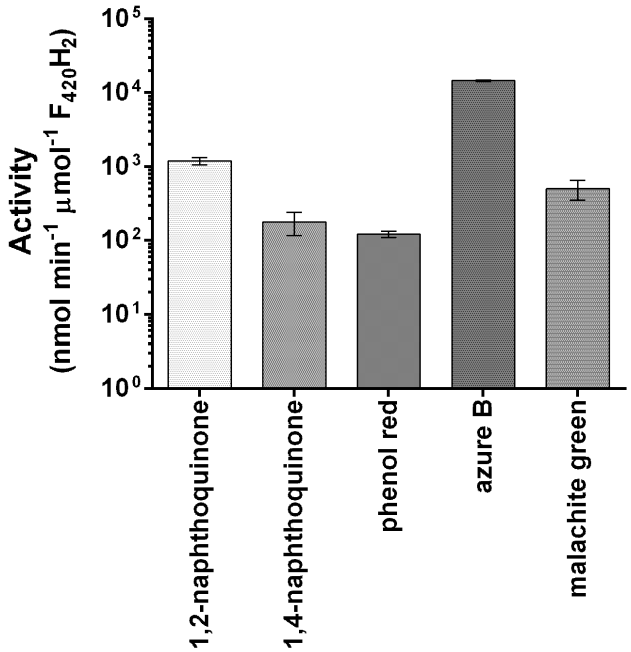

Figure S4. Proposed reaction mechanisms for the $F_{420}H_2$-dependent reduction of representative compounds from each compound class. The mechanisms for menadione (quinone analog), rifampicin, and clofazimine are shown here. The mechanisms for methoxsalen (furanocoumarin), malachite green (arylmethane dye) are shown in **Figure 3.**

Menadione:

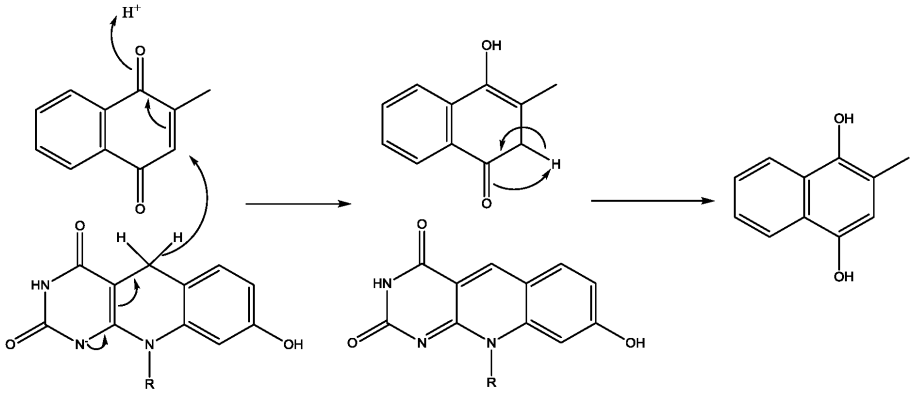

Rifampicin:

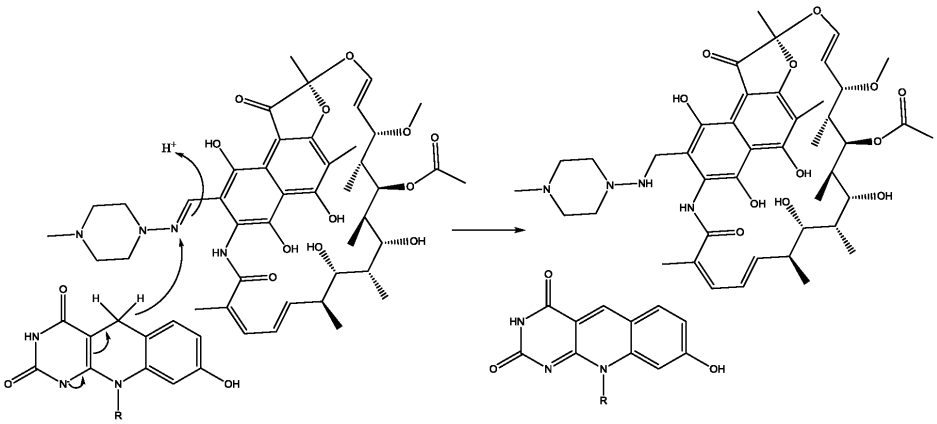

Clofazimine:

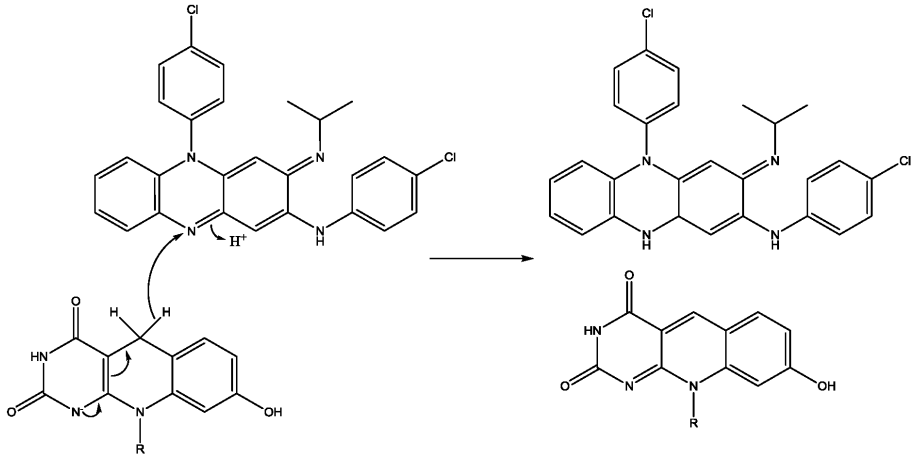

Figure S5. Correlation between FDOR activities and MIC ratios. The *y*-axis shows the maximum specific activity of the FDORs for the 20 compounds tested. The *x*-axis shows the ratio of the MIC of the wild-type and *fbiC*:*kan* mutant strains of *M. smegmatis* for the 20 compounds.

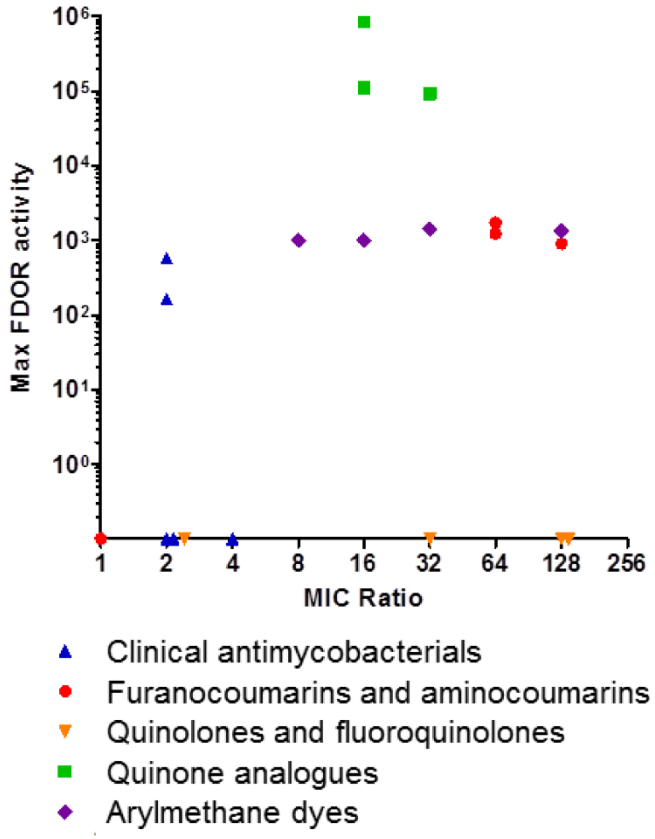

5.4 Mycobacterial $F_{420}H_2$-dependent reductases promiscuously reduce diverse compounds through a common mechanism

This section contains the following paper:

Mycobacterial $F_{420}H_2$-dependent reductases promiscuously reduce diverse compounds through a common mechanism

Chris Greening, Thanavit Jirapanjawat, Shahana Afroze, Blair Ney, Colin Scott, Gunjan Pandey, Brendon M. Lee, Robyn J. Russell, Colin J. Jackson, John G. Oakeshott, Matthew C. Taylor, Andrew C. Warden,

Frontiers in Microbiology 8 (2017)

Current status of paper: Published

Thanavit Jirapanjawat expressed and purified the enzymes and F_{420}, and performed the enzymatic assays. Shahana Afroze performed the LC-MS assay. Blair Ney performed the GC-MS analysis. Andrew Walden performed the substrate docking. I designed the kinetic assays and supervised Thanavit Jirapanjawat performing assays and data analysis and created Figure 4. Colin Jackson, Matt Taylor, John Oakeshott, Robyn Russell, Colin Scott, Gunjan Pandey and Chris Greening supervised students. Thanavit, Blair, and Chris designed the figures and wrote the paper. All Authors contributed to the editing of the manuscript.

frontiers in Microbiology

ORIGINAL RESEARCH
published: 31 May 2017
doi: 10.3389/fmicb.2017.01000

Mycobacterial $F_{420}H_2$-Dependent Reductases Promiscuously Reduce Diverse Compounds through a Common Mechanism

Chris Greening[1,2†], Thanavit Jirapanjawat[1,2,3†], Shahana Afroze[1,3†], Blair Ney[1,2,3], Colin Scott[1], Gunjan Pandey[1], Brendon M. Lee[1,3], Robyn J. Russell[1], Colin J. Jackson[3], John G. Oakeshott[1], Matthew C. Taylor[1] and Andrew C. Warden[1*]*

[1] *Land and Water Flagship, The Commonwealth Scientific and Industrial Research Organisation, Acton, ACT, Australia,* [2] *School of Biological Sciences, Monash University, Clayton, VIC, Australia,* [3] *Research School of Chemistry, Australian National University, Acton, ACT, Australia*

OPEN ACCESS

Edited by:
Dirk Tischler, Freiberg University of Mining and Technology, Germany

Reviewed by:
David E. Graham, Oak Ridge National Laboratory (DOE), United States
Alberto A. Iglesias, National University of the Littoral, Argentina

***Correspondence:**
Chris Greening
chris.greening@monash.edu
Andrew C. Warden
andrew.warden@csiro.au

† *These authors have contributed equally to this work.*

Specialty section:
This article was submitted to Microbial Physiology and Metabolism, a section of the journal Frontiers in Microbiology

Received: *31 March 2017*
Accepted: *18 May 2017*
Published: *31 May 2017*

Citation:
Greening C, Jirapanjawat T, Afroze S, Ney B, Scott C, Pandey G, Lee BM, Russell RJ, Jackson CJ, Oakeshott JG, Taylor MC and Warden AC (2017) Mycobacterial $F_{420}H_2$-Dependent Reductases Promiscuously Reduce Diverse Compounds through a Common Mechanism. Front. Microbiol. 8:1000. doi: 10.3389/fmicb.2017.01000

An unusual aspect of actinobacterial metabolism is the use of the redox cofactor F_{420}. Studies have shown that actinobacterial $F_{420}H_2$-dependent reductases promiscuously hydrogenate diverse organic compounds in biodegradative and biosynthetic processes. These enzymes therefore represent promising candidates for next-generation industrial biocatalysts. In this work, we undertook the first broad survey of these enzymes as potential industrial biocatalysts by exploring the extent, as well as mechanistic and structural bases, of their substrate promiscuity. We expressed and purified 11 enzymes from seven subgroups of the flavin/deazaflavin oxidoreductase (FDOR) superfamily (A1, A2, A3, B1, B2, B3, B4) from the model soil actinobacterium *Mycobacterium smegmatis*. These enzymes reduced compounds from six chemical classes, including fundamental monocycles such as a cyclohexenone, a dihydropyran, and pyrones, as well as more complex quinone, coumarin, and arylmethane compounds. Substrate range and reduction rates varied between the enzymes, with the A1, A3, and B1 groups exhibiting greatest promiscuity. Molecular docking studies suggested that structurally diverse compounds are accommodated in the large substrate-binding pocket of the most promiscuous FDOR through hydrophobic interactions with conserved aromatic residues and the isoalloxazine headgroup of $F_{420}H_2$. Liquid chromatography-mass spectrometry (LC/MS) and gas chromatography-mass spectrometry (GC/MS) analysis of derivatized reaction products showed reduction occurred through a common mechanism involving hydride transfer from $F_{420}H^-$ to the electron-deficient alkene groups of substrates. Reduction occurs when the hydride donor (C5 of $F_{420}H^-$) is proximal to the acceptor (electrophilic alkene of the substrate). These findings suggest that engineered actinobacterial $F_{420}H_2$-dependent reductases are promising novel biocatalysts for the facile transformation of a wide range of α,β-unsaturated compounds.

Keywords: F_{420}, redox, biocatalysis, promiscuity, biodegradation, *Mycobacterium*, Actinobacteria

INTRODUCTION

Industrial biocatalysts are making a substantial impact in the selective synthesis of pharmaceuticals and other specialist chemicals (Nestl et al., 2011; Clouthier and Pelletier, 2012). Enzymes that mediate selective alkene reduction are in particular demand (Stuermer et al., 2007). The most widely investigated of these enzymes are the "old yellow enzyme" family of NAD(P)H-dependent flavoproteins. These often-promiscuous enzymes have been shown to catalyze hydride addition to activated alkene groups of diverse substrates of both natural (e.g., quinones) and synthetic (e.g., cyclohexenones) origin (Williams and Bruce, 2002; Stuermer et al., 2007; Amato and Stewart, 2015). Their catalytic cycle proceeds by hydride transfer from bound $FMNH_2$ to the substrate, protonation of the reduced substrate by a conserved tyrosine, and reduction of the cofactor by the external hydride donor NAD(P)H (Fox and Karplus, 1994). Such enzymes are in development as *in vitro* biocatalysts and are critical in several industrial fermentation processes (e.g., levodione synthesis; Stuermer et al., 2007; Amato and Stewart, 2015). Despite these successes, there is still demand for the discovery of novel reductive biocatalysts to provide more flexible platforms for development of specific *in vitro* and *in vivo* syntheses.

Actinobacteria represent a particularly promising source of novel biocatalysts. This phylum includes genera reputed for their biodegradative capacity, notably *Mycobacterium* and *Rhodococcus*, as well as *Streptomyces* strains that are vital sources of natural products (Barka et al., 2016). One reason these organisms are so metabolically versatile is that they synthesize the unusual redox cofactor F_{420} (Greening et al., 2016; Ney et al., 2017). The low standard redox potential ($E^{\circ\prime} = -340$ mV) and obligate two-electron chemistry of $F_{420}H_2$ means that it can reduce compounds otherwise recalcitrant to activation (Walsh, 1986; Greening et al., 2016). Actinobacteria reduce F_{420} using either the F_{420}-dependent glucose-6-phosphate dehydrogenase (Fgd) (Bashiri et al., 2008; Nguyen et al., 2017) or the F_{420}-NADP oxidoreductase (Fno) (Eker et al., 1989; Ebert et al., 1999). They subsequently couple the reoxidation of $F_{420}H_2$ to the hydrogenation of diverse organic compounds. This depends on a suite of $F_{420}H_2$-dependent reductases from two different superfamilies, the luciferase-like hydride transferases (LLHT superfamily; Ebert et al., 1999; Heiss et al., 2003; Ikeno et al., 2006) and the flavin/deazaflavin oxidoreductases (FDOR superfamily; Taylor et al., 2010; Gurumurthy et al., 2013; Ahmed et al., 2015; Greening et al., 2016). The enzymatic activities and industrial potential of these enzymes have remained largely unexplored.

$F_{420}H_2$-dependent reductases of the FDOR superfamily have been advocated as particularly promising reductive biocatalysts (Ahmed et al., 2015; Greening et al., 2016). These reductases are abundant in mycobacteria and other Actinobacteria, where they have diverged into at least 14 distinct subgroups (A1–A3, B1–B6, AA1–AA5; Ahmed et al., 2015). While several native functions have been proposed, e.g., menaquinone and biliverdin reduction (Gurumurthy et al., 2013; Ahmed et al., 2015, 2016), the enzymes also mediate promiscuous activities, such as nitroimidazole prodrug activation (Cellitti et al., 2012; Mohamed et al., 2016a,b), biodegradation of furanocoumarins (Taylor et al., 2010; Lapalikar et al., 2012b; Jirapanjawat et al., 2016), and decolorization of triarylmethane dyes (Guerra-Lopez et al., 2007; Jirapanjawat et al., 2016). The findings that these enzymes can reduce such structurally and chemically diverse compounds suggests that they may also have the latent capacity to act upon industrially relevant non-natural chemicals. Mechanistic studies focused on mycobacteria indicate that these enzymes adopt a distinct mechanism from old yellow enzymes that may be relevant for selective synthesis (Greening et al., 2016; Mohamed et al., 2016b). For example, the reduced cofactor is thought to bind the enzyme from the solvent phase and directly mediate hydride addition to the substrate (Mohamed et al., 2016a,b); The cofactor can then be re-reduced *in vitro* and *in vivo* by Fgd (Purwantini and Daniels, 1996; Bashiri et al., 2008). In addition, the proton donor for reduced substrates is a solvent-accessible hydroxonium ion rather than a tyrosine residue (Mohamed et al., 2016b).

In this study, we explored the substrate promiscuity across multiple subgroups of the $F_{420}H_2$-dependent FDORs to determine their potential value as next-generation biocatalysts. To do this, we tested 11 of these enzymes from the model laboratory organism *Mycobacterium smegmatis* against 47 different substrates, ranging from synthetic building blocks to more complex polycyclic compounds. This revealed that, in common with old yellow enzymes, several of these enzymes can promiscuously reduce diverse cyclic and polycyclic compounds harboring activated alkene groups. Subsequent structural modeling and mechanistic studies suggested that these enzymes reduced these diverse substrates through a common mechanism: regioselective hydride transfer from $F_{420}H^-$ to the proximal electrophilic alkene group. The considerable promiscuity of these enzymes suggests they are promising candidate biocatalysts, but engineering will be required to optimize their rates in industrial processes.

MATERIALS AND METHODS

Recombinant Protein Expression and Purification

Eleven $F_{420}H_2$-dependent reductases of the FDOR superfamily (MSMEG loci 5998, 2850, 2027, 5030, 6325, 3380, 0048, 6848, 6526, 5170, 3880; Supplementary Table S1) and the F_{420}-reducing glucose-6-phosphate dehydrogenase (Fgd) were recombinantly overexpressed in *E. coli* BL21(DE3). MSMEG_6325, MSMEG_6526, MSMEG_3880 and *fgd* were expressed overnight in modified auto-induction TB2.0 media at 28°C (200 rpm) as previously described (Taylor et al., 2010; Lapalikar et al., 2012b). For the remaining proteins, cells were grown in lysogeny broth (LB) at 37°C (200 rpm) and induced at OD_{600} 0.6 with 0.2% L-arabinose for 2 h. Cells were harvested by centrifugation (10,000 × *g*, 20 min, 4°C), resuspended in lysis buffer (50 mM NaI_2PO4, 300 mM NaCl, 10 mM imidazole, pH 8.0), and lysed in a EmulsiFlex-C3 homogenizer (ATA Scientific, Australia). The enzymes

were purified from soluble extracts by Ni-nitrilotriacetic acid (NTA) affinity chromatography using gravity columns as previously described (Taylor et al., 2010; Ahmed et al., 2015) and stored in elution buffer (50 mM NaH_2PO_4 300 mM NaCl, 250 mM imidazole, pH 8.0) until use in enzymatic assays. The high purity of the proteins was confirmed by running the fractions on NuPAGE Novex 10% Bis-Tris gels (Invitrogen, Australia) at 200 V and staining with Coomassie Brilliant Blue. Protein concentration was determined by measuring absorbance at 280 nm using a NanoDrop ND1000 (NanoDrop Technologies) and calculating concentration with the Beer–Lambert equation. Molar absorption coefficients were calculated for each protein based on amino acid sequences (Supplementary Table S1). F_{420} was extracted, purified, and concentrated from a recombinant F_{420} overexpression strain of *M. smegmatis* $mc^2$4517 (Bashiri et al., 2010) as previously described (Isabelle et al., 2002).

Enzyme Activity Assays

Forty-seven different compounds were sourced from Sigma-Aldrich and dissolved into 1 M working stocks in dimethyl sulfoxide, except hypoxanthine and guanine that were dissolved in 1 M NaOH solution. The structures of the compounds tested are shown in Supplementary Tables S2, S3. Enzymatic assays were performed by spectroscopically monitoring the reoxidation of pre-reduced $F_{420}H_2$ in the presence of FDOR and substrate. F_{420} was enzymatically reduced to $F_{420}H_2$ by overnight incubation with 1 μM Fgd and 12 mM glucose 6-phosphate as described (Ahmed et al., 2015). The enzyme was subsequently repurified as described (Ahmed et al., 2015). All reaction mixtures contained degassed Tris buffer [200 mM Tris, 0.1% (w/v) Triton X-100, pH 8.0] sequentially supplemented with 50 μM substrate, 25 μM $F_{420}H_2$, and 1 μM of the FDOR. Enzyme concentration was decreased to 10 nM for substrates observed to be rapidly reduced, i.e., quinone compounds. Reaction rates were monitored by recording the initial linear increase in 420 nm absorbance using an Epoch 2 Microplate Spectrophotometer (BioTek). All assays were performed at room temperature (approximately 25°C). We only detected significant levels of enzyme-independent, substrate-dependent $F_{420}H_2$ reoxidation for quinone and arylmethane substrates, at rates that we previously reported (Jirapanjawat et al., 2016). We observed no enzyme-dependent, substrate-independent or spontaneous $F_{420}H_2$ reoxidation in the timeframe of our assays. Specific activities were calculated after subtracting rates of enzyme-independent $F_{420}H_2$ reoxidation and were expressed in nmol s^{-1} μmol^{-1} enzyme as previously described (Taylor et al., 2010). The rate of reduction of three of these compounds, namely 1,4-naphthoquinone, 3-cyanocoumarin, and 5,6-dihydro-2*H*-pyran-2-one, was also measured in cofactor-recycling assays. Assays used 100 μM substrate, 0.1 μM enzyme, 10 μM F_{420}, 2.5 mM glucose-6-phosphate, and 0.45 μM Fgd. Time course high performance liquid chromatography (HPLC) assays, performed according to published methodologies (Lapalikar et al., 2012b), measured loss of absorbance (at λ_{max}) of the substrates at regular time intervals.

Molecular Docking

Substrates were docked into the previously solved X-ray crystal structures of MSMEG_2027 (1.5 Å resolution; PDB: 4Y9I; Ahmed et al., 2015) and MSMEG_6526 (1.7 Å resolution; PDB: 4KZY; Ahmed et al., 2015). F_{420} was docked into the cofactor-binding pockets based on the cofactor-bound structures of Rv3547 (PDB: 3R5R; Cellitti et al., 2012) and Rv2074 (PDB: 5JAB; Ahmed et al., 2016) respectively. AutoDock Vina was used to computationally dock the substrates into their corresponding enzymes, with enzymes and ligands prepared using AutoDockTools operating with default settings (Morris et al., 2009). The docking results were visualized and analyzed in UCSF Chimera (Pettersen et al., 2004).

Substrate Reduction and Derivatization

The chemical standards and reaction products of menadione, 3-cyanocoumarin, and 2-cyclohexen-1-one were detected by mass spectrometry. These compounds were reduced by incubating them with the promiscuous $F_{420}H_2$-dependent reductase MSMEG_2027 for 2 h at 37°C. The assay mixture comprised 100 μM substrate, 10 μM F_{420}, 1 μM Fgd, 1 μM MSMEG_2027, and excess G-6-P in either 20 mM Tris buffer, pH 8.0 (for menadione and 2-cyclohexen-1-one) or 50 mM ammonium acetate buffer, pH 7.5 (for 3-cyanocoumarin). For menadione, the standard and reaction products were derivatized with methoxyamine. Specifically, the standard and products were dried by rotary evaporation, resuspended in 20 μl pyridine containing 20 mg mL^{-1} methoxyamine hydrochloride, and incubated at 37°C for 1.5 h. To this solution, 20 μl of *N*-methyl-*N*-(trimethylsilyl)trifluoroacetamide (MSTFA) was added and the solution was incubated at 37°C for 1 h. For cyclohexenone, the standard and reaction products were derivatized by spiking the solution with 1 mM 2,4-dinitrophenylhydrazine and incubating the solution at 30°C for 2 h.

LC/MS and GC/MS

The standard and reaction products of 3-cyanocoumarin were measured on an Agilent 6100 Series Single Quadrupole liquid chromatography-mass spectrometry (LC/MS) with diode array detector. Samples were separated on an Agilent Poroshell 120 EC-C18 column (2.7 μm, 2.1 × 100 mm). A gradient of two buffers, buffer A (0.1% formic acid in H_2O) and buffer B (0.1% formic acid in acetonitrile), was applied as follows: 0–0.5 min, held at 10% B; 0.5–6.5 min, 10–60% B; 6.5–7 min, held at 90% B. A positive mode electron ionisation (EI) scan was undertaken, and in these conditions the molecular ion could not be detected as the loss of the cyano (CN) group was universal. The derivatized cyclohexenone standard and reactions products were determined on an Agilent 1290 Infinity/6550 quadrupole time-of-flight (Q-TOF) LC/MS system equipped with an Agilent Poroshell 120 EC-C18 2.1 × 50 mm 2.7 μm column. A gradient comprising two buffers, buffer A (20 mM ammonium acetate, pH 7.0) and buffer B (100% acetonitrile), was applied as follows: 0–1 min, held at 10% B; 1–10 min, 10–90% B. Positive mode electrospray ionisation (ESI) was utilized, and a scan from 50 to 300 *m/z* was conducted. The menadione standard, its reaction

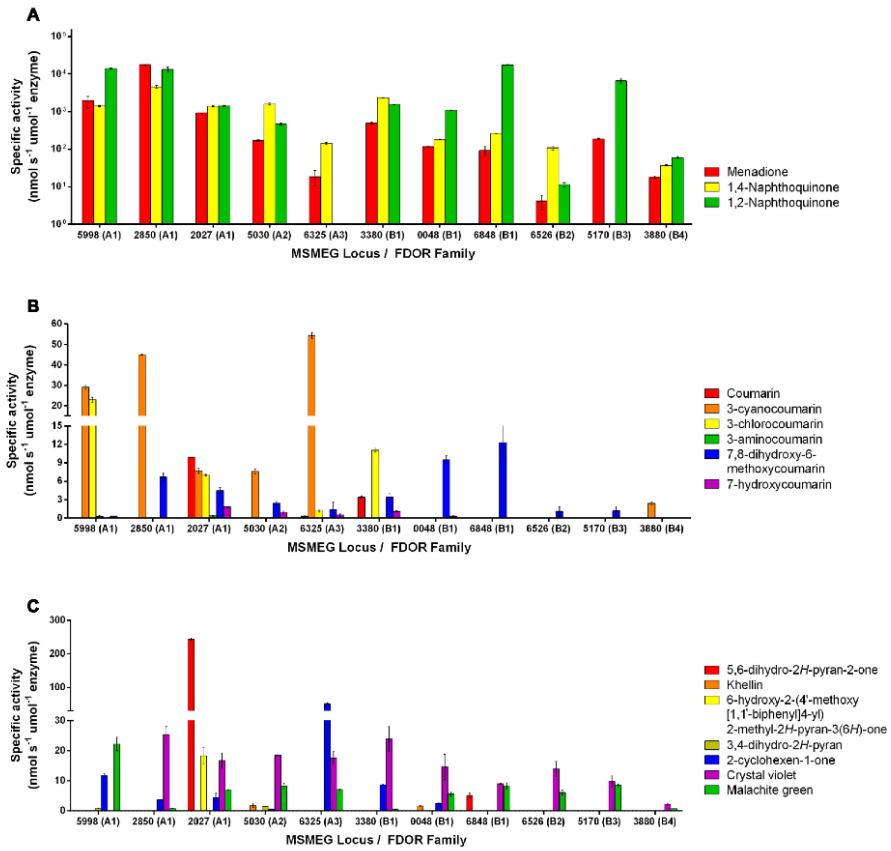

FIGURE 1 | Substrate range of the $F_{420}H_2$-dependent reductases. The results show the specific activities of five FDOR-A and six FDOR-B enzymes with 16 organic compounds. Specific activities are shown with **(A)** quinones, **(B)** coumarins, and **(C)** pyrones, pyrans, cyclohexenones, and triarylmethanes. Error bars show standard deviations from three independent replicates. The reactivity of six of the enzymes with quinone and triarylmethane compounds was previously reported (Jirapanjawat et al., 2016). The structures of the substrates are shown in Supplementary Table S2. The 32 compounds tested that were not compatible with the FDORs are listed in Supplementary Table S3.

product, and their methoxime derivatives were detected on an Agilent 7010 gas chromatography-mass spectrometry (GC/MS) triple quadrupole system. Samples were separated on an Agilent 19091S 30 m × 250 μm × 0.25 μm HP-5 ms column over a gradient of 60–320°C at a rate of 7°C min^{-1}, and a positive EI scan at 70 eV was conducted.

RESULTS

$F_{420}H_2$-Dependent Reductases Reduce Structurally Diverse Cyclic and Polycyclic Compounds

Eleven $F_{420}H_2$-dependent FDORs from *M. smegmatis* were expressed recombinantly and purified (Supplementary Table S1). We purified enzymes spanning multiple phylogenetically distinct subgroups, namely three enzymes each from the well-described FDOR-A1 and FDOR-B1 subgroups (Taylor et al., 2010; Lapalikar et al., 2012b; Ahmed et al., 2015), as well as representatives from five other subgroups (A2, A3, B1, B2, B3, B4; Ahmed et al., 2015). On the basis of previously reported data (Lapalikar et al., 2012b; Gurumurthy et al., 2013; Jirapanjawat et al., 2016), we determined the specific activities of the purified enzymes with 47 organic compounds following addition of the pre-reduced cofactor $F_{420}H_2$ (Supplementary Tables S2, S3). Of these, 16 compounds were enzymatically transformed. These compounds included fundamental monocyclic compounds, such as 3,4-dihydro-*2H*-pyran, 2-cyclohexen-1-one, and 5,6-dihydro-2*H*-pyran-2-one, as well as aromatic bicyclic and tricyclic compounds from the quinone, coumarin, and arylmethane chemical classes (Supplementary Table S2). Specific activities for the 16 substrates ranged from very low if reproducible

for some compounds (e.g., <1 nmol s^{-1} μmol $enzyme^{-1}$ for the pyran compound) to high for the quinones (e.g., >10^4 nmol s^{-1} μmol $enzyme^{-1}$ for 1,2-naphthoquinone) (**Figure 1**). Enzymes purified from the A1, A3, and B1 classes had the broadest and highest activities, with MSMEG_2027 (A1) proving catalytically compatible with all but two of the 16 substrates, whereas enzymes from the A2, B2, B3, and B4 classes had low activities with all non-quinone substrates.

Comparisons across the compounds tested for activity suggest that the presence of an electrophilic alkene is necessary for reduction to occur and implicates this group as the hydride acceptor. For example, activity was observed with pyrones that were α-substituted (e.g., 5,6-dihydro-*2H*-pyran-2-one; **Figure 1C**) but not γ-substituted (e.g., chelidonic acid; Supplementary Table S3). This is also supported by the finding that, whereas malachite green and crystal violet can be reduced, azure B cannot; while all three compounds contain triphenyl and *N,N*-dimethyliminium moieties, azure B lacks the central delocalized alkene group (Supplementary Tables S2, S3). Consistent with the proposal that the activated alkene is the hydride acceptor of $F_{420}H_2$-dependent reductases, enzymatic activity with coumarin derivatives was modulated by the nature of aromatic directing groups at the C3 position (**Figure 1**); moderate activities were observed with electron-withdrawing cyano and chloro groups, very low activities with an electron-donating amino group, and no activity with 3-hydroxycoumarin (**Figure 1B**). This suggests that electron-withdrawing groups render these compounds susceptible to nucleophilic attack by removing electron density from the π system. It is possible that differential interactions of these substrates with the substrate-binding pockets also contribute to the differences in the rates of reduction both between substrates and between enzymes.

For three of the compounds, we also measured specific activities with another independent assay that measured substrate reduction by HPLC in a cofactor-recycling system containing the Fgd (Supplementary Figure S1). While the relative activities between enzymes were comparable, initial reduction rates were generally higher in the cofactor-recycling systems and resulted in substrate conversions exceeding 90%.

$F_{420}H_2$-Dependent Reductases Selectively Reduce Electrophilic Alkene Groups

We subsequently sought to understand the structural basis of how FDORs could reduce such diverse substrates. To do this, we used automated substrate docking to compare the binding of representative substrates to the high-resolution crystal structures of the highly promiscuous MSMEG_2720 (Ahmed et al., 2015) (A1) and the more specific MSMEG_6526 (Ahmed et al., 2015) (B2) enzyme. Compounds representing four major substrate classes were tested, namely menadione (quinone class), 3-cyanocoumarin (coumarin class), 2-cyclohexen-1-one (monocyclic compounds), and malachite green (arylmethane class). Consistent with the results of the activity assays (**Figure 1**), all substrates were predicted to be structurally compatible with MSMEG_2027, whereas only menadione and malachite green were predicted to specifically bind MSMEG_6526 (Supplementary Figure S2 and Table S4).

In the MSMEG_2027 models, substrates are accommodated in the large substrate-binding pocket adjacent to the cofactor-binding site (**Figure 2**). All four substrates are predicted to make extensive hydrophobic interactions with aromatic residues in the active site, including a triad of tyrosine residues (Tyr120, Tyr123, Tyr126) that have previously been shown to facilitate hydrophobic shielding during nitroimidazole activation (Mohamed et al., 2016b). There was also evidence of hydrophobic interactions between substrate and cofactor, including different degrees of π-stacking interactions with the isoalloxazine ring (**Figure 2**). Few polar interactions were predicted, except hydrogen bonds between the cyano group of 3-cyanocoumarin and the carbonyl oxygen of 2-cyclohexen-1-one with the hydroxyl group of Tyr123. The orientation of the substrates is likely to be realistic. For example, the binding poise of menadione suggests that menaquinone (the proposed physiological substrate of FDOR-A1 enzymes (Gurumurthy et al., 2013; Ahmed et al., 2015), which comprises a menadione headgroup and a polyisoprene tail) can be accommodated in the active site, given the polyisoprene tail at the C2 position is predicted to be oriented away from the active site.

The docking results indicate that hydride transfer can occur directly between cofactor and substrate within the hydrophobic environment of the MSMEG_2027 active site. Menadione, 3-cyanocoumarin, and 2-cyclohexen-1-one are predicted to be oriented such that their activated alkene groups are within 5 Å of the nucleophilic C5 center of $F_{420}H^-$ (**Figures 2A–C**). This suggests that, in line with the activity assays (**Figure 1**) and previously proposed mechanisms (Taylor et al., 2010; Lapalikar et al., 2012b; Ahmed et al., 2015; Mohamed et al., 2016b), catalysis will occur through nucleophilic attack of the C5 hydride to the electrophilic alkene. In the case of malachite green, the alkene moiety (C1 position) of the substrate is 4.2 Å away from C5 of the cofactor, whereas the *N,N*-dimethylamine and *N,N*-dimethyliminium moieties point toward the solvent phase (**Figure 2D**). Binding modes in which the *N,N*-dimethyliminium moiety was proximal to the cofactor caused steric occlusion. This again suggests that the alkene rather than imine moiety serves as the initial site of hydride transfer from $F_{420}H^-$. In comparison, docking with the less promiscuous MSMEG_6526 enzyme suggested that menadione and malachite green are only accommodated at orientations where the distance between the hydride donor and acceptor exceeds 7 Å, which will be suboptimal for catalysis (Supplementary Table S4). This reflects that MSMEG_6526 has a smaller binding pocket than MSMEG_2027 due to its larger flanking loops (Ahmed et al., 2015).

$F_{420}H_2$-Dependent Reductases Mediate Substrate Reduction by Direct Hydride Transfer

We determined the mechanistic basis of substrate promiscuity among the $F_{420}H_2$-dependent reductases. To do so, we used

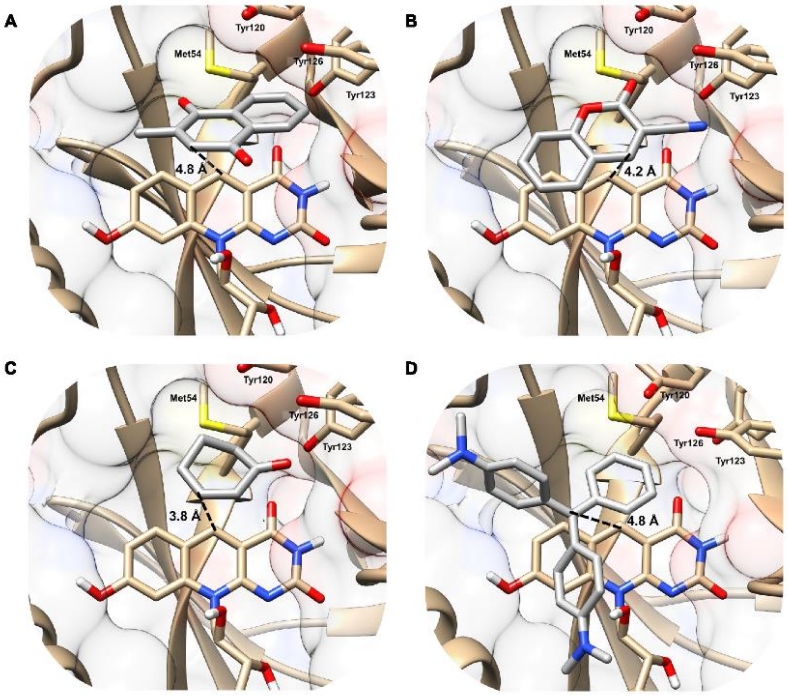

FIGURE 2 | Structural basis of substrate activation by $F_{420}H_2$-dependent reductases. The secondary structure and surface rendering of the cofactor- and substrate-binding site of MSMEG_2027 are shown based on the 1.5 Å resolution crystal structure (PDB: 4Y9I) (Ahmed et al., 2015) of the enzyme. The structures are computationally docked with **(A)** menadione, **(B)** 3-cyanocoumarin, **(C)** 2-cyclohexen-1-one, and **(D)** malachite green. The distance between the proposed hydride donor (C5 of $F_{420}H^-$) and hydride acceptor (electrophilic carbon of the substrate) are shown. Residues within 5 Å of the substrate are shown. Docking results with the more specific $F_{420}H_2$-dependent reductase MSMEG_6526 are shown in Supplementary Figure S2 and are compared with MSMEG_2027 in Supplementary Table S4.

mass spectrometry to determine the products formed by the reduction of three representative substrates. LC/MS and GC/MS studies demonstrated that, following incubation of menadione, 3-cyanocoumarin, and 2-cyclohexen-1-one with MSMEG_2027, each substrate peak increased by 2 *m/z* (**Figure 3**). This suggests that this enzyme catalyses the reduction of menadione (172 Da) to either menadiol or 2,3-dihydromenadione (both 174 Da) (Supplementary Figure S3), 3-cyanocoumarin (171 Da) to 3-cyanochroman-2-one (173 Da) (**Figures 3C,D**), and 2-cyclohexen-1-one (96 Da) to either 2-cyclohexen-1-ol or cyclohexanone (both 98 Da) (**Figures 3E,F**). This is consistent with previous observations that $F_{420}H_2$-dependent reductases mediate hydride transfer and subsequent protonation of their substrates (Taylor et al., 2010; Lapalikar et al., 2012b; Ahmed et al., 2015; Jirapanjawat et al., 2016; Mohamed et al., 2016b). In previous LC/MS studies, we demonstrated that malachite green (329 Da) was transformed by MSMEG_2027 to produce a decolorized product likely to be the protonated form of leucomalachite green (331 Da) (Jirapanjawat et al., 2016).

While these findings suggest $F_{420}H_2$-dependent reductases mediate hydride transfer from $F_{420}H_2$ to substrate, they do not resolve whether the site of attack is the alkene or carbonyl groups of the compounds. To resolve this, we derivatized the standard and reaction products of menadione with methoxyamine hydrochloride (carbonyl-specific) and MSTFA (alcohol-specific). GC/MS analysis of the reaction products revealed that reduction of menadione occurred exclusively *via* the alkene group (**Figures 3A,B**). Single and double methoxime derivatives of reduced menadione could be detected, indicating 2,3-dihydromenadione was formed as the major reaction product. No trimethylsilyl ester derivatives were formed under these conditions, underlining the absence of menadiol and other quinol products. Menadiol is nevertheless likely to form under physiological conditions through keto–enol tautomerism. In the case of cyclohexenone, the standard and reaction products were derivatized with 2,4-dinitrophenylhydrazine (carbonyl-specific), and analyzed by LC/MS. Analysis of product formation revealed the emergence of the hydrazone derivative of cyclohexanone, again indicating that reduction was mediated through the alkene (**Figures 3E,F**). Previous studies have inferred that coumarin reduction also occurs through the activated alkene group (Taylor et al., 2010; Lapalikar et al., 2012a,b).

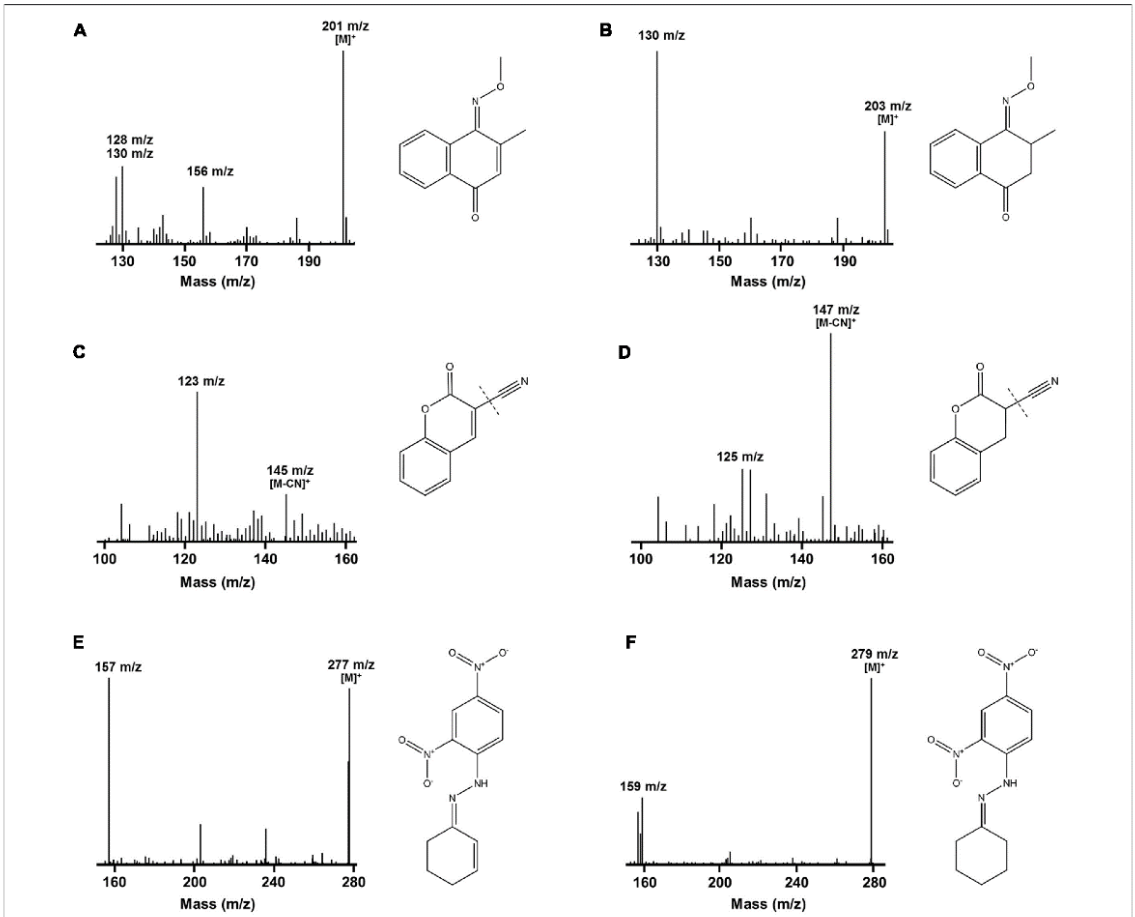

FIGURE 3 | Mass spectra infer that $F_{420}H_2$-dependent reductases mediate hydrogenation of substrates. The spectra show the detection of substrate standards and reaction products following reduction with MSMEG_2027. GC/MS spectra of the single methoxime derivatives of the **(A)** menadione standard and **(B)** 2,3-dihydromenadione product. Mass spectra of the underivatized compounds are shown in Supplementary Figure S3. Keto–enol tautomerization is likely to result in menadiol formation under physiological conditions. LC/MS spectra of the **(C)** 3-cyanocoumarin standard and **(D)** 3-cyanochroman-2-one product. The cyano groups were ionized by in-source fragmentation. LC/MS spectra of the dinitrophenylhydrazone derivatives of the **(E)** 2-cyclohexen-1-one standard and **(F)** cyclohexanone product. A mass spectrum of the underivatized product could not be obtained. In all cases, corresponding compounds are shown to the right of the spectra. A mass spectrum showing the reduction of malachite green to leucomalachite green was previously published (Jirapanjawat et al., 2016).

DISCUSSION

In this study, we explored the potential of actinobacterial $F_{420}H_2$-dependent reductases as industrial biocatalysts. We show that mycobacterial FDORs use the electron donor $F_{420}H_2$ to hydrogenate diverse organic compounds at a wide range of rates. On the basis of these findings, we propose in **Figure 4** that all FDOR substrates studied can be reduced through a common hydrogenation mechanism: The cofactor binds the FDOR in its deprotonated state ($F_{420}H^-$; Mohamed et al., 2016a) and the substrate thereafter binds the adjacent pocket through hydrophobic interactions with aromatic residues and the cofactor. Alignment of the nucleophilic C5 center of $F_{420}H^-$ with the electrophilic alkene group of the substrate will promote direct hydride transfer. Subsequent steps will result in delocalization of electron charge and protonation of the substrate by a solvent-accessible hydroxonium ion (Mohamed et al., 2016b). The FDORs promote this mechanism in multiple ways: binding the substrate and cofactor in proximal sites; generating a hydrophobic environment that promotes hydride transfer; and facilitating protonation by binding hydroxonium ions through conserved tyrosine residues (Mohamed et al., 2016b). The overall mechanism of these enzymes is therefore equivalent to the old yellow enzymes

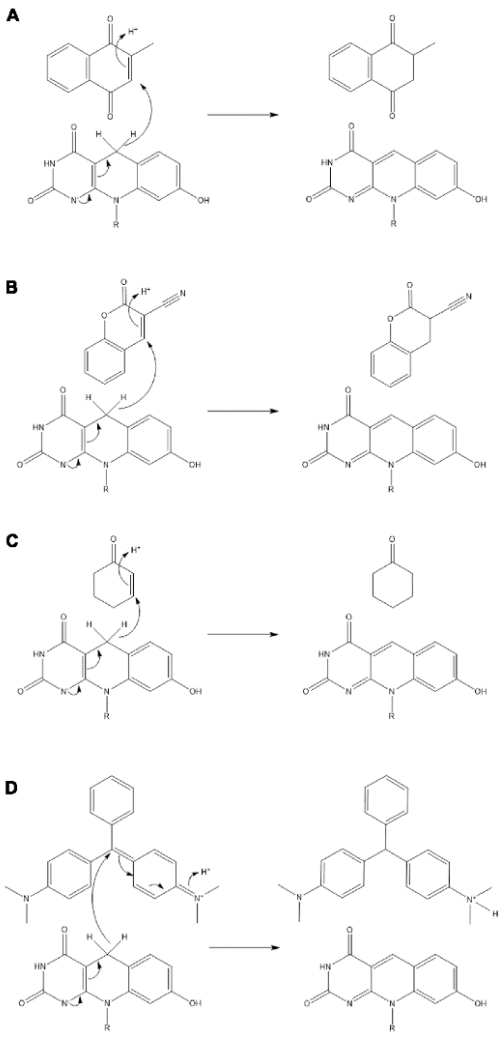

FIGURE 4 | Unifying mechanism for the hydrogenation of representative substrates by $F_{420}H_2$-dependent reductases. Reaction mechanisms are proposed for **(A)** menadione, **(B)** 3-cyanocoumarin, **(C)** 2-cyclohexen-1-one, and **(D)** malachite green. On the basis of previous studies, it is predicted that the cofactor binds in its deprotonated state ($F_{420}H^-$) (Mohamed et al., 2016a) and that a hydroxonium ion serves as the proton donor for the substrate (Mohamed et al., 2016b).

(Stuermer et al., 2007), though the hydride and proton donors are distinct.

The hydrogenation mechanism proposed here is supported by our studies exploring the observed substrate range of the FDORs (**Figure 1**). We showed that, in line with findings about the substrate range of old yellow enzymes (Stuermer et al., 2007), the presence of an electrophilic alkene group was a prerequisite for reduction to occur and that rates were enhanced in electron-withdrawing conjugated systems. The outlined mechanism is also consistent with the results of the structural modeling (**Figure 2**) and mechanistic studies (**Figure 3** and Supplementary Figure S3) that identified the probable sites of hydride attack and inferred hydrogenated reaction products using four model substrates, menadione, 3-cyanocoumarin, 2-cyclohexen-1-one, and malachite green. Similar mechanisms have been proposed for other important reactions known to be mediated by $F_{420}H_2$-dependent reductases of the FDOR superfamily, namely activation of nitroimidazole prodrugs (Mohamed et al., 2016a,b), reduction of biliverdin to bilirubin (Ahmed et al., 2015, 2016), and the terminal step in the biosynthesis of tetracyclines (Wang et al., 2013). Our mass spectral analysis suggests that these mechanisms are regioselective, with hydride transfer only favorable to electrophilic alkene groups proximal to the nucleophilic C5 center. It will be necessary to extend studies to substrates that will produce prochiral products to determine whether this process also occurs stereoselectively, i.e., through *cis* or *trans* hydrogenation. The observation that substrate reduction is faster in the cofactor-recycling assays is also of interest, and suggests that there is a mechanism that enhances cofactor exchange between FDORs and Fgd (e.g., complex formation).

Our findings warrant the further exploration of $F_{420}H_2$-dependent FDORs in *in vitro* and *in vivo* biocatalytic processes. Their inherent substrate range, combined with their ease of heterologous overexpression and the presence of a viable cofactor-recycling system, suggests that these enzymes have promise in *in vitro* systems. There may be particular value in exploring the use of these enzymes for hydrogenating substrates incompatible with inorganic catalysts or old yellow enzymes (Stuermer et al., 2007; Clouthier and Pelletier, 2012). Particularly promising are the findings that enzymes in the FDOR superfamily mediate critical steps in the biosynthesis of tetracycline antibiotics (Wang et al., 2013) and the preliminary results that the membrane-bound FDOR-AA family can saturate linear fatty acid chains (Ahmed et al., 2015). However, at least two major innovations are needed if $F_{420}H_2$-dependent reductases are to be more widely developed: Firstly, given the observation that most substrates were reduced at low rates, the directed evolution of promising FDORs (e.g., MSMEG_2027) will be required to enhance their activities with desirable substrates. Secondly, new processes must be developed if F_{420} is to be cheaply and conveniently produced (Greening et al., 2016). It may be possible to engineer the production of this cofactor in recombinant systems, but this depends on the resolution of the complete F_{420} biosynthesis pathway. Alternatively, it is plausible to synthesize deazaflavin analogs that are catalytically compatible with $F_{420}H_2$-dependent reductases, which have previously been shown to exhibit cofactor promiscuity (Lapalikar et al., 2012a). There is more immediate promise in using these enzymes within actinobacterial hosts and recombinant systems to produce natural products or bioremediate contaminants. With the vast majority of F_{420}-dependent oxidoreductases remaining functionally unannotated, it is expected that further study of these enzymes will reveal novel reactions of potential industrial and pharmaceutical relevance.

AUTHOR CONTRIBUTIONS

CG, AW, JO, MT, BN, CJ, TJ, CS, GP, RR, and BL designed experiments. TJ, CG, SA, BN, AW, MT, and BL performed experiments. CG, JO, CJ, AW, MT, RR, CS, GP, and BL supervised students. CG, AW, JO, BN, TJ, MT, CJ, and SA analyzed data. CG, TJ, AW, BN, and JO wrote the paper. Specific authors were responsible for the specific activity assays (TJ, CG, SA, BL, AW, MT, JO, CJ), substrate-docking experiments (CG, TJ, CJ), and analytical chemistry assays (BN, CG, TJ, AW).

FUNDING

This work was supported by a CSIRO Office of the Chief Executive Postdoctoral Fellowship and an ARC DECRA Fellowship (DE170100310) awarded to CG, a CSIRO Office of the Chief Executive PhD Scholarship awarded to SA, and Australian Research Council grants (DE120102673, DP130102144) awarded to CJ.

ACKNOWLEDGMENTS

We thank the two reviewers for their helpful feedback.

SUPPLEMENTARY MATERIAL

The Supplementary Material for this article can be found online at: http://journal.frontiersin.org/article/10.3389/fmicb.2017.01000/full#supplementary-material

REFERENCES

Ahmed, F. H., Carr, P. D., Lee, B. M., Afriat-Jurnou, L., Mohamed, A. E., Hong, N.-S., et al. (2015). Sequence-structure-function classification of a catalytically diverse oxidoreductase superfamily in mycobacteria. *J. Mol. Biol.* 427, 3554–3571. doi: 10.1016/j.jmb.2015.09.021

Ahmed, F. H., Mohamed, A. E., Carr, P. D., Lee, B. M., Condic-Jurkic, K., O'Mara, M. L., et al. (2016). Rv2074 is a novel F420H2-dependent biliverdin reductase in *Mycobacterium tuberculosis*. *Protein Sci.* 25, 1692–1709. doi: 10.1002/pro.2975

Amato, E. D., and Stewart, J. D. (2015). Applications of protein engineering to members of the old yellow enzyme family. *Biotechnol. Adv.* 33, 624–631. doi: 10.1016/j.biotechadv.2015.04.011

Barka, E. A., Vatsa, P., Sanchez, L., Gaveau-Vaillant, N., Jacquard, C., Klenk, H.-P., et al. (2016). Taxonomy, physiology, and natural products of Actinobacteria. *Microbiol. Mol. Biol. Rev.* 80, 1–43. doi: 10.1128/MMBR.00019-15

Bashiri, G., Rehan, A. M., Greenwood, D. R., Dickson, J. M. J., and Baker, E. N. (2010). Metabolic engineering of cofactor F420 production in *Mycobacterium smegmatis*. *PLoS ONE* 5:e15803. doi: 10.1371/journal.pone.0015803

Bashiri, G., Squire, C. J., Moreland, N. J., and Baker, E. N. (2008). Crystal structures of F420-dependent glucose-6-phosphate dehydrogenase FGD1 involved in the activation of the anti-tuberculosis drug candidate PA-824 reveal the basis of coenzyme and substrate binding. *J. Biol. Chem.* 283, 17531–17541. doi: 10.1074/jbc.M801854200

Cellitti, S. E., Shaffer, J., Jones, D. H., Mukherjee, T., Gurumurthy, M., Bursulaya, B., et al. (2012). Structure of Ddn, the deazaflavin-dependent nitroreductase from *Mycobacterium tuberculosis* involved in bioreductive activation of PA-824. *Structure* 20, 101–112. doi: 10.1016/j.str.2011.11.001

Clouthier, C. M., and Pelletier, J. N. (2012). Expanding the organic toolbox: a guide to integrating biocatalysis in synthesis. *Chem. Soc. Rev.* 41, 1585–1605. doi: 10.1039/c2cs15286j

Ebert, S., Rieger, P.-G., and Knackmuss, H.-J. (1999). Function of coenzyme F420 in aerobic catabolism of 2,4,6-trinitrophenol and 2,4-dinitrophenol by Nocardioides simplex FJ2-1A. *J. Bacteriol.* 181, 2669–2674.

Eker, A. P., Hessels, J. K., and Meerwaldt, R. (1989). Characterization of an 8-hydroxy-5-deazaflavin:NADPH oxidoreductase from Streptomyces griseus. *Biochim. Biophys. Acta* 990, 80–86. doi: 10.1016/S0304-4165(89)80015-7

Fox, K. M., and Karplus, P. A. (1994). Old yellow enzyme at 2 Å resolution: overall structure, ligand binding, and comparison with related flavoproteins. *Structure* 2, 1089–1105. doi: 10.1016/S0969-2126(94)00111-1

Greening, C., Ahmed, F. H., Mohamed, A. E., Lee, B. M., Pandey, G., Warden, A. C., et al. (2016). Physiology, biochemistry, and applications of F420- and Fo-dependent redox reactions. *Microbiol. Mol. Biol. Rev.* 80, 451–493. doi: 10.1128/MMBR.00070-15

Guerra-Lopez, D., Daniels, L., and Rawat, M. (2007). *Mycobacterium smegmatis* mc2155 fbiC and MSMEG_2392 are involved in triphenylmethane dye decolorization and coenzyme F420 biosynthesis. *Microbiology* 153, 2724–2732. doi: 10.1099/mic.0.2006/009241-0

Gurumurthy, M., Rao, M., Mukherjee, T., Rao, S. P. S., Boshoff, H. I., Dick, T., et al. (2013). A novel F420-dependent anti-oxidant mechanism protects *Mycobacterium tuberculosis* against oxidative stress and bactericidal agents. *Mol. Microbiol.* 87, 744–755. doi: 10.1111/mmi.12127

Heiss, G., Trachtmann, N., Abe, Y., Takeo, M., and Knackmuss, H.-J. (2003). Homologous npdGI genes in 2,4-dinitrophenol- and 4-nitrophenol-degrading *Rhodococcus* spp. *Appl. Environ. Microbiol.* 69, 2748–2754. doi: 10.1128/AEM.69.5.2748-2754.2003

Ikeno, S., Aoki, D., Hamada, M., Hori, M., and Tsuchiya, K. S. (2006). DNA sequencing and transcriptional analysis of the kasugamycin biosynthetic gene cluster from *Streptomyces kasugaensis* M338-M1. *J. Antibiot. (Tokyo)* 59, 18–28. doi: 10.1038/ja.2006.4

Isabelle, D., Simpson, D. R., and Daniels, L. (2002). Large-scale production of coenzyme F420-5,6 by using *Mycobacterium smegmatis*. *Appl. Environ. Microbiol.* 68, 5750–5755. doi: 10.1128/AEM.68.11.5750-5755.2002

Jirapanjawat, T., Ney, B., Taylor, M. C., Warden, A. C., Afroze, S., Russell, R. J., et al. (2016). The redox cofactor F420 protects mycobacteria from diverse antimicrobial compounds and mediates a reductive detoxification system. *Appl. Environ. Microbiol.* 82, 6810–6818. doi: 10.1128/AEM.02500-16

Lapalikar, G. V., Taylor, M. C., Warden, A. C., Onagi, H., Hennessy, J. E., Mulder, R. J., et al. (2012a). Cofactor promiscuity among F420-dependent reductases enables them to catalyse both oxidation and reduction of the same substrate. *Catal. Sci. Technol.* 2, 1560–1567. doi: 10.1039/c2cy20129a

Lapalikar, G. V., Taylor, M. C., Warden, A. C., Scott, C., Russell, R. J., and Oakeshott, J. G. (2012b). F420H2-dependent degradation of aflatoxin and other furanocoumarins is widespread throughout the Actinomycetales. *PLoS ONE* 7:e30114. doi: 10.1371/journal.pone.0030114

Mohamed, A. E., Ahmed, F. H., Arulmozhiraja, S., Lin, C. Y., Taylor, M. C., Krausz, E. R., et al. (2016a). Protonation state of F420H2 in the prodrug-activating deazaflavin dependent nitroreductase (Ddn) from *Mycobacterium tuberculosis*. *Mol. Biosyst.* 12, 1110–1113. doi: 10.1039/c6mb00033a

Mohamed, A. E., Condic-Jurkic, K., Ahmed, F. H., Yuan, P., O'Mara, M. L., Jackson, C. J., et al. (2016b). Hydrophobic shielding drives catalysis of hydride transfer in a family of F420H2-dependent enzymes. *Biochemistry* 55, 6908–6918.

Morris, G. M., Huey, R., Lindstrom, W., Sanner, M. F., Belew, R. K., Goodsell, D. S., et al. (2009). AutoDock4 and AutoDockTools4: automated docking with selective receptor flexibility. *J. Comput. Chem.* 30, 2785–2791. doi: 10.1002/jcc.21256

Nestl, B. M., Nebel, B. A., and Hauer, B. (2011). Recent progress in industrial biocatalysis. *Curr. Opin. Chem. Biol.* 15, 187–193. doi: 10.1016/j.cbpa.2010.11.019

Ney, B., Ahmed, F. H., Carere, C. R., Biswas, A., Warden, A. C., Morales, S. E., et al. (2017). The methanogenic redox cofactor F420 is widely synthesized by aerobic soil bacteria. *ISME J.* 11, 125–137. doi: 10.1038/ismej.2016.100

Nguyen, Q.-T., Trinco, G., Binda, C., Mattevi, A., and Fraaije, M. W. (2017). Discovery and characterization of an F420-dependent glucose-6-phosphate

dehydrogenase (Rh-FGD1) from *Rhodococcus jostii* RHA1. *Appl. Microbiol. Biotechnol.* 101, 2831–2842. doi: 10.1007/s00253-016-8038-y

Pettersen, E. F., Goddard, T. D., Huang, C. C., Couch, G. S., Greenblatt, D. M., Meng, E. C., et al. (2004). UCSF Chimera—a visualization system for exploratory research and analysis. *J. Comput. Chem.* 25, 1605–1612. doi: 10.1002/jcc.20084

Purwantini, E., and Daniels, L. (1996). Purification of a novel coenzyme F420-dependent glucose-6-phosphate dehydrogenase from *Mycobacterium smegmatis*. *J. Bacteriol.* 178, 2861–2866. doi: 10.1128/jb.178.10.2861-2866.1996

Stuermer, R., Hauer, B., Hall, M., and Faber, K. (2007). Asymmetric bioreduction of activated C=C bonds using enoate reductases from the old yellow enzyme family. *Curr. Opin. Chem. Biol.* 11, 203–213. doi: 10.1016/j.cbpa.2007.02.025

Taylor, M. C., Jackson, C. J., Tattersall, D. B., French, N., Peat, T. S., Newman, J., et al. (2010). Identification and characterization of two families of F420H2-dependent reductases from Mycobacteria that catalyse aflatoxin degradation. *Mol. Microbiol.* 78, 561–575. doi: 10.1111/j.1365-2958.2010.07356.x

Walsh, C. (1986). Naturally occurring 5-deazaflavin coenzymes: biological redox roles. *Acc. Chem. Res.* 19, 216–221. doi: 10.1021/ar00127a004

Wang, P., Bashiri, G., Gao, X., Sawaya, M. R., and Tang, Y. (2013). Uncovering the enzymes that catalyze the final steps in oxytetracycline biosynthesis. *J. Am. Chem. Soc.* 135, 7138–7141. doi: 10.1021/ja403516u

Williams, R. E., and Bruce, N. C. (2002). "New uses for an old enzyme"–the old yellow enzyme family of flavoenzymes. *Microbiology* 148, 1607–1614. doi: 10.1099/00221287-148-6-1607

Conflict of Interest Statement: The authors declare that the research was conducted in the absence of any commercial or financial relationships that could be construed as a potential conflict of interest.

5.5 Supplementary Material

Table S1. Enzyme subgroups, molar absorption coefficients, and amino acid sequences of the eleven $F_{420}H_2$-dependent reductases tested from *Mycobacterium smegmatis*.

Enzyme locus	Enzyme subgroup	Coefficient (M^{-1} cm^{-1})	Protein sequence
MSMEG_5998	FDOR-A1	23950	MADTSRPLNAKQLERLNAKSTGTLIKWMSRFQTFLFKTTNGKLGN KFLRGTEVGILTTIGRKSGEPRDTPLLFLQEGRRIVLVASQGGRA TNPMWYLNLKANPKVTFQTRSEKLALVAREATDAERDEYWPKLDA MYPDFANYRSYTDRKIPIVICDPA
MSMEG_2850	FDOR-A1	16960	MTDAELSPTDWVREQTERILEQGTTDGVHVLDRPIVLFTTTGAKS GKKRYVPLMRVEENGKYAMVASKGGDPKHPSWYFNVKANPTVSVQ DGDKVLPDRTARELEGEEREHWWKLAVEAYPPYAEYQTKTDRLIP VFIVE
MSMEG_2027	FDOR-A1	30940	MTDAELSPTDWVREQTERILEQGTTDGVHVLDRPIVLFTTTGAKS GKKRYVPLMRVEENGKYAMVASKGGDPKHPSWYFNVKANPTVSVQ DGDKVLPDRTARELEGEEREHWWKLAVEAYPPYAEYQTKTDRLIP VFIVE
MSMEG_5030	FDOR-A2	32430	MPWWERYIGLPLLLLHDKVYKATDGRIGHRIPGGPATLILHTVGA KTGQHRASSLAYARDGDDYLVVASKGGEPKAPGWYHNLKADPNVE INVGPKRLRATARAVFPDDPDFPRLWEIVNNMPGNKDRYIGYQKR TTRQIPVIVLTPVS
MSMEG_6325	FDOR-A3	44920	MDDKLHGIPRVDLETRPRWKRDLAWWFGGKVLATARASAIWRKIA MPYEVPLIKATGGRARLSVGIPIAVLTSTGARSGKTRQTALAYFT DGDDVVLIASNYGQARHPGWYHNLRAHPECELYVGRRGGRFVARE VDGPQRDRLYALAASRLYPGWVAYEKRAEGVRRIPVLRLTPADP
MSMEG_3380	FDOR-B1	21430	MVAVPEGYESLLERPLYGHLATVRPDGTPQVNAMWFAWDGEVLRF THTTKRQKYRNIKANPAVAMSVIDPDNPYRYLEVRGLVEDIVPDP TGAFYLKLNDRYDGPLTEPPADKADRVIIVVRPTAFSKQ

MSMEG_0048	FDOR-B1	29450	MGKNERTKIVMSDEEIAEFVERSRTATMATVLPDGRPHLVAMWYAVVDGEIWFETKAKSQKAVNLRRDPTVTVLIEDGHTYDTLRGVSIDGTAEIVDDPETLLRVGISVWERYTGPYTDEMRPFVDQMMNNRIAVRVVPGRTRSWDHRKLGMPAMPLGGSTAQYLNS
MSMEG_6848	FDOR-B1	27515	MGVSPARLRQVLDAPVFGTVATIDPDGAPQQSVVWVGRDGDDVLFAVATGSRKERNLRRDPRVSILLSPPDEPYTYAVIHGKATLHTEGGHQLRDALAVKYTGKTYAEGNADAAARYGDVAMTVVRVTPERTVGRL
MSMEG_6526	FDOR-B2	34950	MAEFDAVTAFADAPAAVLSTLNADGAPHLVPVVFAVHVPHVEGQPARIYTAVDAKRKTTRNLRRLANIDRDSRVSLLVDHYSDDWTQLWWVRADGVATTHHSGDEVATGYALLRAKYHQYERVSLDGPVISVEVSRWASWQA
MSMEG_5170	FDOR-B3	16960	MGRQVFDDKLLALICNNSLGVLATIKQDGRPQLSNVSYHFDPRAQTFQVSITEPRAKTRNLRRDPRASIHVSSDDGWAYAVAEGDAILTPPAASTHDDTVEGLIALYRNISGEHPDWDEFRQAMVDDRRVLMTLPITHVYGMPPGMR
MSMEG_3880	FDOR-B4	8480	MAASRGKATTRLTTDALAFLTERHLAMLTTLRSDGSPHVVAVGFTFDPKTHIARVITTGGSQKAVNAQERGVAVLSQVDGARWLSLEGKSTVSSDPDAVRDAELRYAQRYRTPRVNPRRVVIEVRIERVLGSSELLDRS

Table S2. Chemical structures of the 16 compounds tested that were reduced by $F_{420}H_2$-dependent FDORs.

Compound	Compound class	Structure
Menadione	Quinones	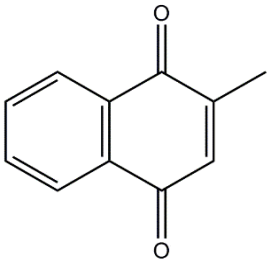
1,4-napthoquinone	Quinones	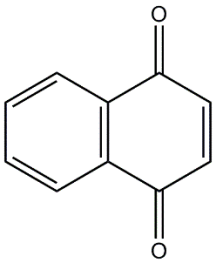
1,2-napthoquinone	Quinones	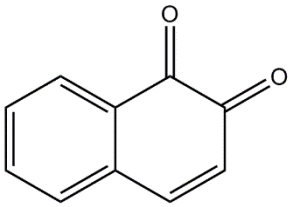
Coumarin	Coumarins	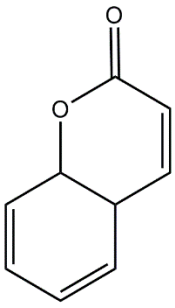
3-cyanocoumarin	Coumarins	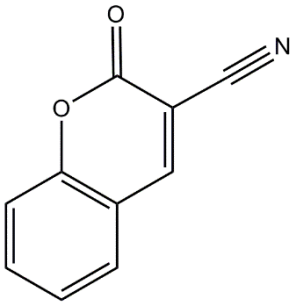

3-chlorocoumarin	Coumarins	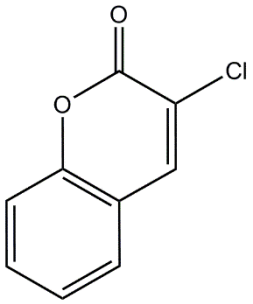
3-aminocoumarin	Coumarins	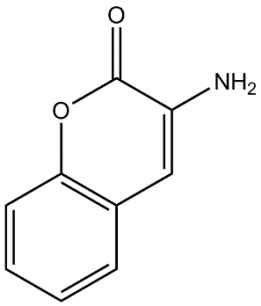
7,8-dihydroxy-6-methoxycoumarin	Coumarins	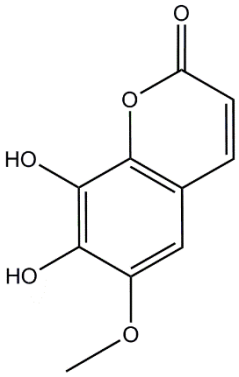
7-hydroxycoumarin	Coumarins	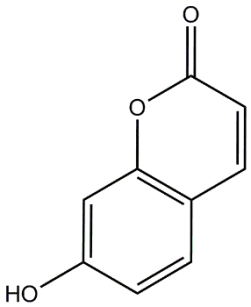
5,6-dihydro-2H-pyran-2-one	Pyrones	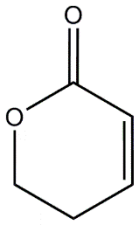

Khellin	Pyrones	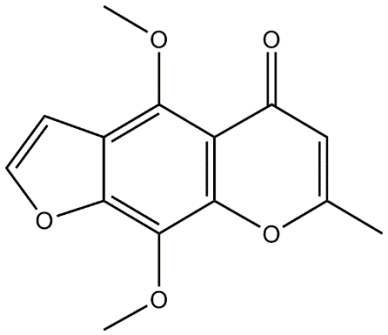
6-hydroxy-2-(4'-methoxy[1,1'-biphenyl]4-yl)-2-methyl-2*H*-pyran-3(6*H*)-one	Pyrones	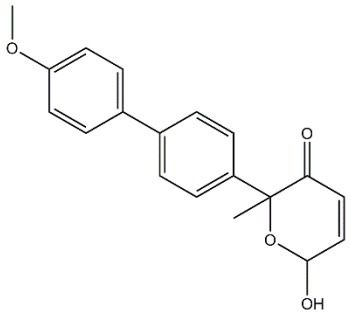
3,4-dihydro-2*H*-pyran	Pyrans	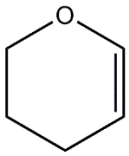
2-cyclohexen-1-one	Cyclohexenones	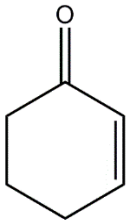
Crystal violet	Arylmethanes	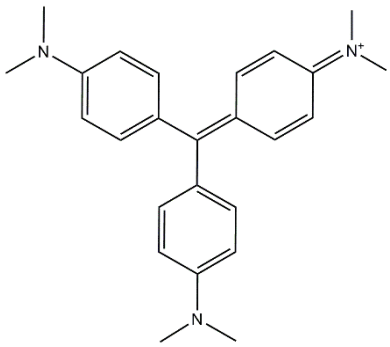

Malachite green	Arylmethanes	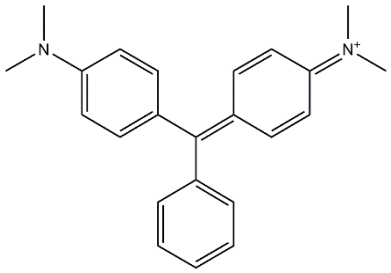

Table S3. Chemical structures of the 31 compounds tested that were catalytically incompatible with $F_{420}H_2$-dependent FDORs.

Compound	Compound class	Structure
Anthraquinone	Quinones	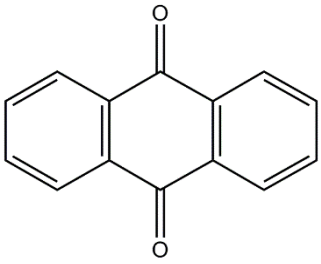
1,4-benzoquinone	Quinones	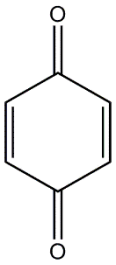
3-hydroxycoumarin	Coumarins	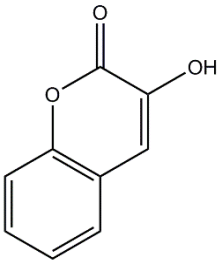
4-hydroxycoumarin	Coumarins	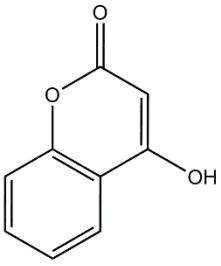
4-methoxy-6-methyl-2H-pyran-2-one	Pyrones	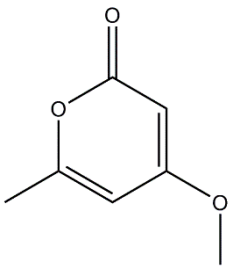

3-hydroxy-2,6-bis(hydroxymethyl)-4H-pyran-4-one	Pyrones	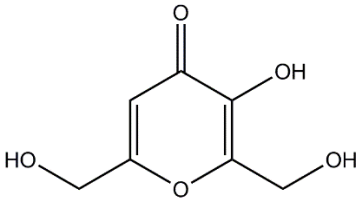
EHT 1864	Pyrones	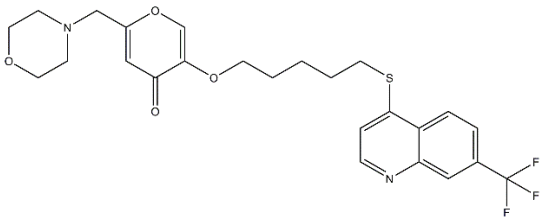
Chelidonic acid	Pyrones	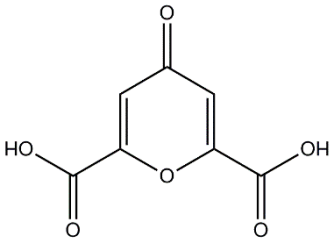
Phenol red	Triarylmethanes	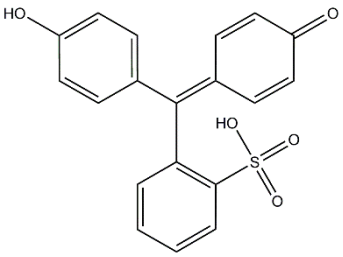
Benzonitrile	Benzene derivatives	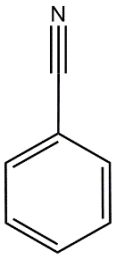
2-aminobenzonitrile	Benzene derivatives	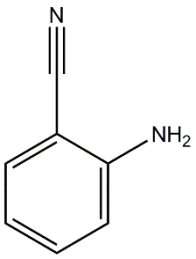

2,4-difluorobenzonitrile	Benzene derivatives	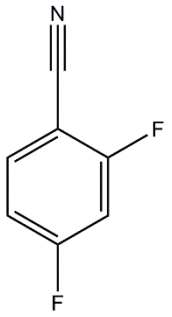
Cinnamic acid	Benzene derivatives	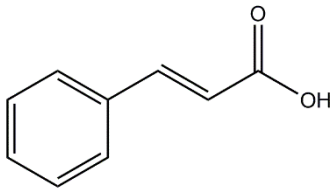
3-phenoxybenzaldehyde	Benzene derivatives	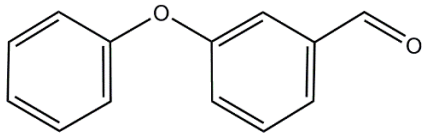
Terephthalic acid	Benzene derivatives	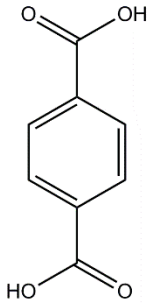
Indole-3-carboxylate	Indoles	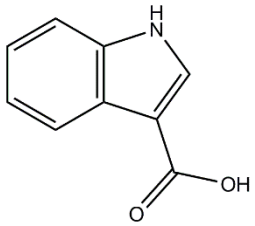
Potassium indole-6-trifluoroborate	Indoles	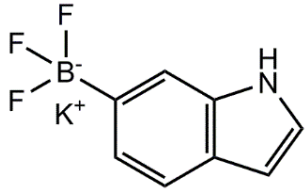

Cytosine	Pyridines	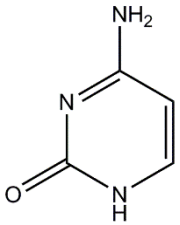
Thymine	Pyridines	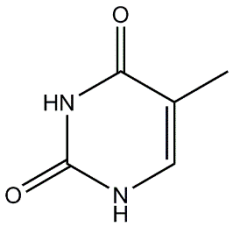
Guanine	Purines	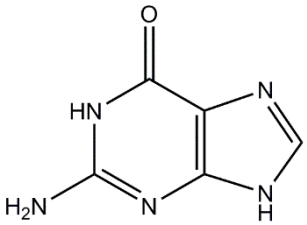
Adenine	Purines	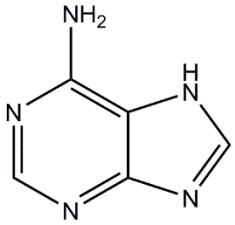
Xanthine	Purines	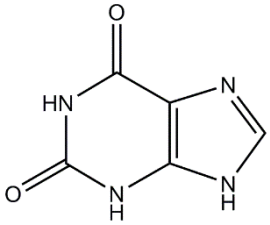
Hypoxanthine	Purines	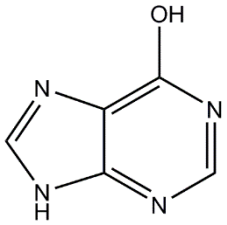

Caffeine	Purines	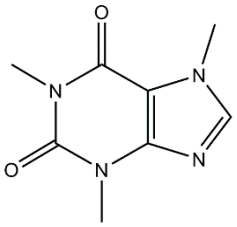
Adenosine	Purines	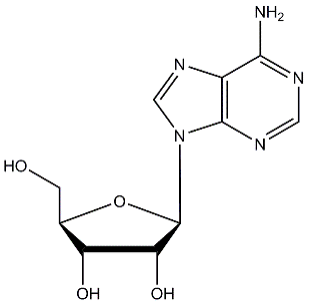
5-nitroimidazole	Imidazoles	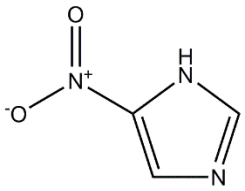
Benzimidazole	Imidazoles	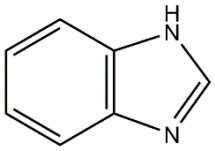
2-aminobenzimidazole	Imidazoles	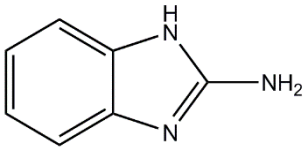
Paraquat dichloride	Other	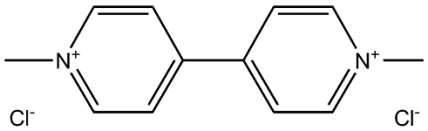
Azure B	Other	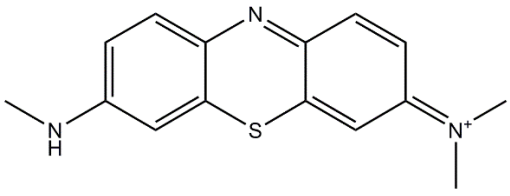

Thiamine	Other	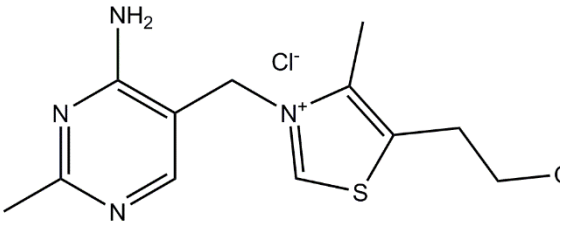

Table S4. Comparison of the donor-acceptor distances inferred from molecular docking studies and specific activities calculated from enzyme assays.

	Donor-acceptor distance (Å)	**Specific activity (nmol min^{-1} (µmol enzyme)$^{-1}$)**
MSMEG_2027 (A1)		
Menadione	4.8	917 ± 10
3-cyanocoumarin	4.2	7.7 ± 0.4
2-cyclohexen-1-one	3.8	4.6 ± 1.5
Malachite green	4.8	7.0 ± 0.2
MSMEG_6526 (B2)		
Menadione	7.5	4.1 ± 1.8
3-cyanocoumarin	N/A	0
2-cyclohexen-1-one	N/A	0
Malachite green	6.9	6.1 ± 0.8

Figure S1. Comparison of the in rates of $F_{420}H_2$-dependent reductase activity observed in two different assay setups. The specific activities are shown for (a) 1,4-napthoquinone, (b) 3-cyanocoumarin, and (c) 5,6-dihydro-2*H*-pyran-2-one based on initial reduction rates. Yellow bars show reduction rates with pre-reduced $F_{420}H_2$, whereas red bars show rates in a cofactor-recycling system containing F_{420} and Fgd. Error bars show standard deviations from three independent replicates.

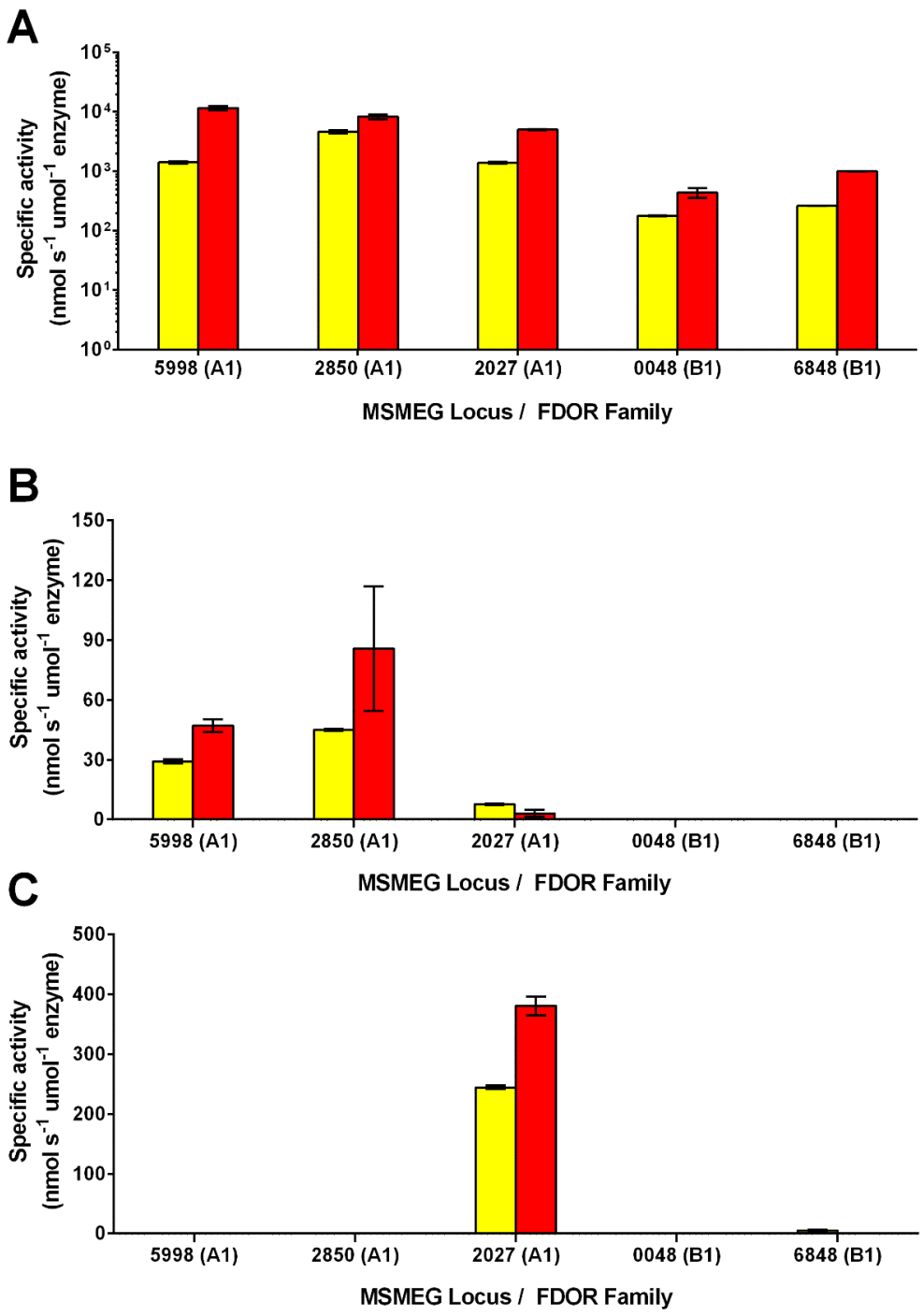

Figure S2. Structural basis of substrate activation by MSMEG_6526. The secondary structure and surface rendering of the cofactor- and substrate-binding site of MSMEG_6526 are shown based on the 1.7 Å resolution crystal structure (PDB: 4ZKY) of the enzyme (Ahmed *et al.*, 2015). The structures are computationally docked with (a) menadione and (b) malachite green. The distance between the proposed hydride donor (C5 of $F_{420}H^-$) and hydride acceptor (electrophilic carbon of the substrate) are shown. Residues within 5 Å of the substrate are shown. Computational docking suggested that 3-cyanocoumarin and 2-cyclohexen-1-one cannot specifically bind to this enzyme.

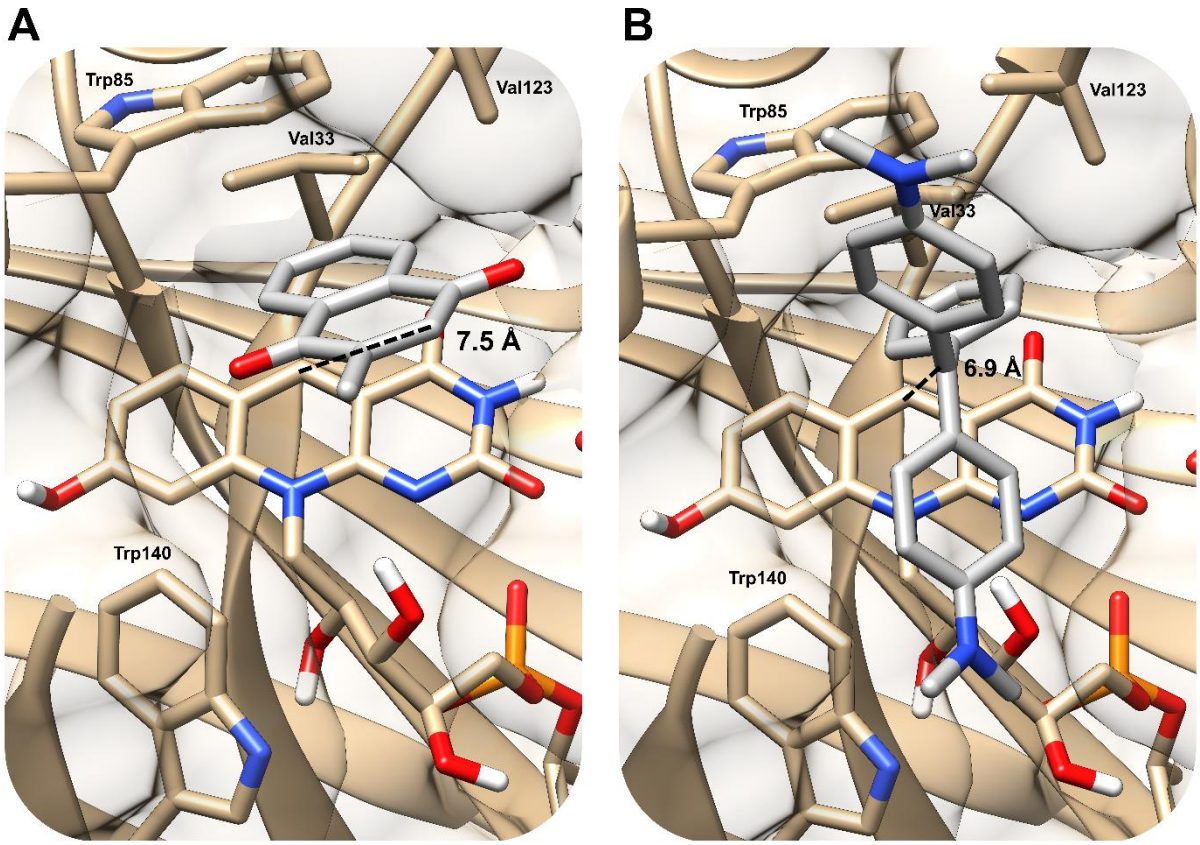

Figure S3. GC/MS detection of menadione, reaction products, and their methoxime derivatives. The mass spectra shown are of (a) menadione standard, (b) 2,3-dihydromenadione reaction product, (c) single methoxime derivative of menadione, (d) single methoxime derivative of 2,3-dihydromenadione, and (e) double methoxime derivative of 2,3-dihydromenadione. The corresponding compounds are shown to the right of the spectra. It is likely that 2,3-dihydromenadione will be converted to menadiol under physiological conditions through keto-enol tautomerism.

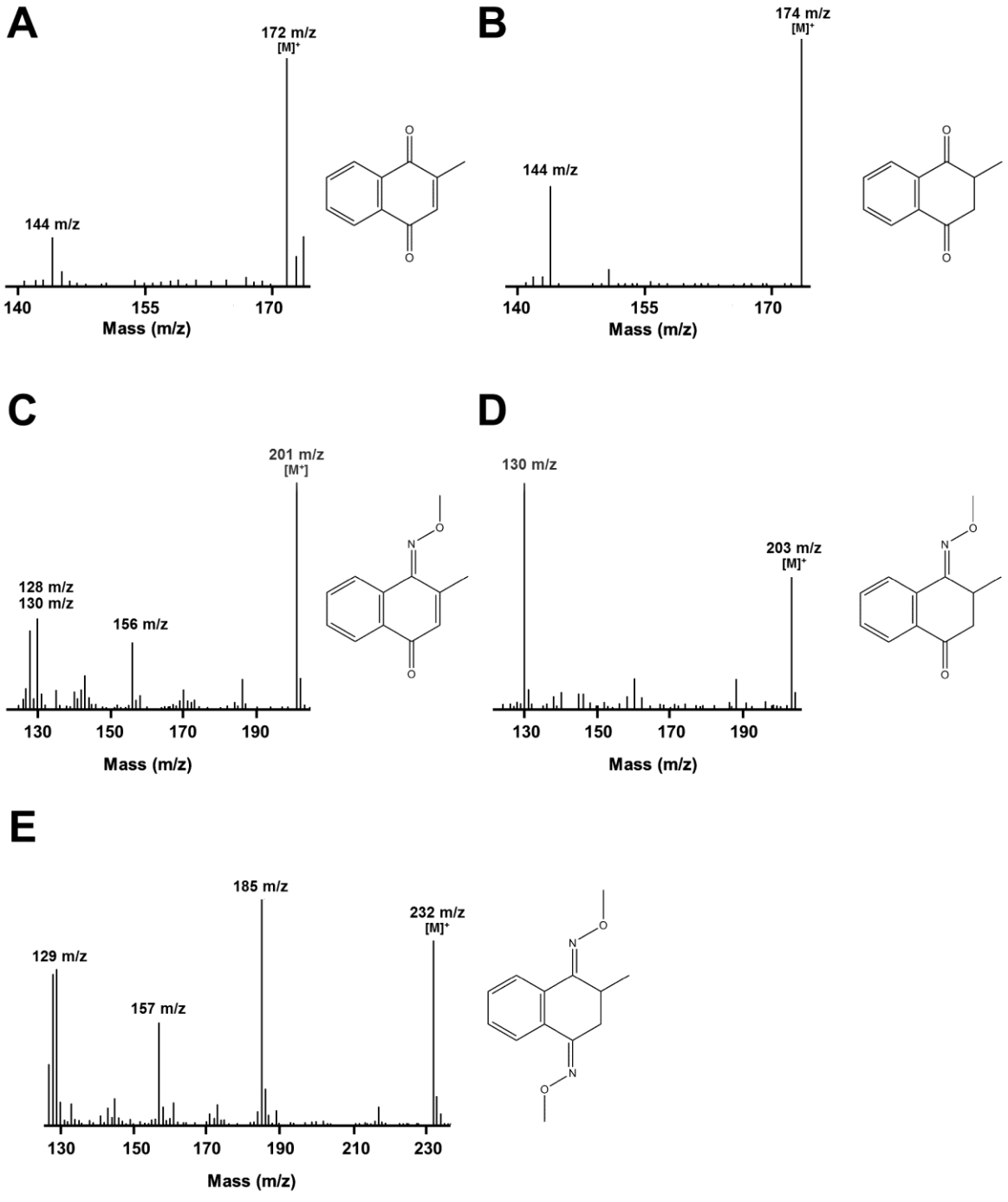

Chapter 6

Literature Review of F_o and F_{420}

6.1 Introduction

The deazaflavins F_{420} and F_o are found in a large number of bacteria and Archaea including *Mycobacteri*a and methanogens. Organisms that contain F_{420} are found in numerous environments but are absent in humans (Ney *et al.*, 2017). F_{420} and F_o are structurally similar to flavin adenine dinucleotide (FAD), and flavin mononucleotide (FMN) but are functionally similar to nicotinamide adenine dinucleotide (NAD) and nicotinamide adenine dinucleotide phosphate (NADP) by having a low redox potential (Eirich *et al.*, 1976; Jacobson and Walsh, 1984; Walsh, 1986). F_{420} is utilised by a range of enzymes for different roles in various organisms. Within methanogens, F_{420}-dependent enzymes are known to be important for central metabolism, which includes the oxidation of H_2 and formate as energy sources, and the reduction of cofactors including NADP, and tetrahydromethanopterin (Tzeng *et al.*, 1975; Tzing *et al.*, 1975; Hartzell *et al.*, 1985). There are two superfamilies of F_{420}-dependent enzymes in *Mycobacteria*, the LLHT superfamily, and the FDOR super family (Selengut and Haft, 2010; Ahmed *et al.*, 2015). The roles of these enzymes are predicted to include cell protection, especially from oxidative stress, and virulence (Gurumurthy *et al.*, 2013; Purwantini and Mukhopadhyay, 2013; Purwantini *et al.*, 2016). The large range of enzymes that utilise F_{420}, and their absence in humans, has made F_{420}-dependent enzymes potential targets for drug therapies against *M. tuberculosis*, such as Ddn, which activates the prodrugs Pretomanid, and Delamanid (Stover *et al.*, 2000; Matsumoto *et al.*, 2006). The low redox potential of F_{420} allows F_{420}-dependent enzymes from *Mycobacteria* to be able to break down a range of compounds including aflatoxins highlighting its potential in bioremediation (Taylor *et al.*, 2010; Lapalikar *et al.*, 2012). They are also seen as a potential tool in biocatalysis and biotechnology (Taylor *et al.*, 2013).

The majority of the research on F_{420} and F_{420}-dependent enzymes has been done in methanogens and sulphur-reducing Archaea (Berk and Thauer, 1997). However, there has been increasing interest in F_{420}-dependent enzymes in *Mycobacteria* due to the recent discovery of the FDOR superfamily and the discovery of Ddn and its ability to reduce pretomanid (Ujjini H Manjunatha *et al.*, 2006; Selengut and Haft, 2010; Taylor *et al.*, 2010; Ahmed *et al.*, 2015). This chapter presents a published review of the current literature on F_{420} and F_o. It provides details on the physiological properties, biochemistry, distribution, and biosynthesis of both compounds. There is an in-depth description on the role of F_{420} in Archaea with an emphasis

on methanogens and an in-depth description on the role of F_{420} in *Mycobacteria*. The implications and applications of F_{420} and related enzymes from current understandings are discussed. The sections of this review that are most relevant to this thesis address the role of F_{420} in *Mycobacteria* and the development of anti-tubercular drugs, which are found in sections 2, 4, and 5, respectively.

6.2 Physiology, Biochemistry, and Applications of F_{420}-and F_o-Dependent Redox Reactions

The chapter contains the following paper:

Physiology, Biochemistry, and Applications of F_{420}-and F_o-Dependent Redox Reactions

Chris Greening, F. Hafna Ahmed, A. Elaaf Mohamed, Brendon M. Lee, Gunjan Pandey, Andrew C. Warden, Colin Scott, John G. Oakeshott, Matthew C. Taylor, Colin J. Jackson

Microbiology and Molecular Biology Reviews 2016 80(2): 451-493

Current status of paper: Published

Chris Greening was mostly responsible for writing review. Hafna Ahmed designed Figures 1-3, 5-14, 16-21, and contributed to the sections on enzyme structure and catalysis, F_o and F_{420} biosynthesis, and mycobacterial enzymes. Elaaf Mohamed designed Figures 4, and 20 and contributed to the sections on the properties of Fo and F_{420}, the photoactivation reaction of Fo, and the activation of nitroimidazoles. I designed Figure 15 and edited Figure 20 with the addition of fHMAD inhibition, and contributed to the section on tuberculosis treatment. Gunjan Pandey, Andrew Warden, Colin Scott, John Oakeshott and Matthew Taylor contributed to the sections on biomitigation and industrial biocatalysis. Colin Jackson co-wrote the whole manuscript. All authors helped to edit the manuscript.

AMERICAN SOCIETY FOR MICROBIOLOGY | Microbiology and Molecular Biology Reviews

Physiology, Biochemistry, and Applications of F_{420}- and F_o-Dependent Redox Reactions

Chris Greening,[a]* F. Hafna Ahmed,[b] A. Elaaf Mohamed,[b] Brendon M. Lee,[b] Gunjan Pandey,[a] Andrew C. Warden,[a] Colin Scott,[a] John G. Oakeshott,[a] Matthew C. Taylor,[a] Colin J. Jackson[b]

The Commonwealth Scientific and Industrial Research Organisation, Land & Water Flagship, Acton, Australian Capital Territory, Australia[a]; Australian National University, Research School of Chemistry, Acton, Australian Capital Territory, Australia[b]

(continued)

Published 27 April 2016

Citation Greening C, Ahmed FH, Mohamed AE, Lee BM, Pandey G, Warden AC, Scott C, Oakeshott JG, Taylor MC, Jackson CJ. 2016. Physiology, biochemistry, and applications of F_{420}- and F_o-dependent redox reactions. Microbiol Mol Biol Rev 80:451–493. doi:10.1128/MMBR.00070-15.

Address correspondence to Chris Greening, chris.greening@monash.edu, or Colin J. Jackson, colin.jackson@anu.edu.au.

*Present address: Chris Greening, Monash University, School of Biological Sciences, Clayton, Victoria, Australia.

C.G. and F.H.A. contributed equally to this work.

SUMMARY

5-Deazaflavin cofactors enhance the metabolic flexibility of microorganisms by catalyzing a wide range of challenging enzymatic redox reactions. While structurally similar to riboflavin, 5-deazaflavins have distinctive and biologically useful electrochemical and photochemical properties as a result of the substitution of N-5 of the isoalloxazine ring for a carbon. 8-Hydroxy-5-deazaflavin (F_o) appears to be used for a single function: as a light-harvesting chromophore for DNA photolyases across the three domains of life. In contrast, its oligoglutamyl derivative F_{420} is a taxonomically restricted but functionally versatile cofactor that facilitates many low-potential two-electron redox reactions. It serves as an essential catabolic cofactor in methanogenic, sulfate-reducing, and likely methanotrophic archaea. It also transforms a wide range of exogenous substrates and endogenous metabolites in aerobic actinobacteria, for example mycobacteria and streptomycetes. In this review, we discuss the physiological roles of F_{420} in microorganisms and the biochemistry of the various oxidoreductases that mediate these roles. Particular focus is placed on the central roles of F_{420} in methanogenic archaea in processes such as substrate oxidation, C_1 pathways, respiration, and oxygen detoxification. We also describe how two F_{420}-dependent oxidoreductase superfamilies mediate many environmentally and medically important reactions in bacteria, including biosynthesis of tetracycline and pyrrolobenzodiazepine antibiotics by streptomycetes, activation of the prodrugs pretomanid and delamanid by *Mycobacterium tuberculosis*, and degradation of environmental contaminants such as picrate, aflatoxin, and malachite green. The biosynthesis pathways of F_o and F_{420} are also detailed. We conclude by considering opportunities to exploit deazaflavin-dependent processes in tuberculosis treatment, methane mitigation, bioremediation, and industrial biocatalysis.

1. INTRODUCTION

Flavin- and deazaflavin-dependent enzymes mediate a wide range of redox reactions in biological systems (1, 2). Flavin adenine dinucleotide (FAD) and flavin mononucleotide (FMN) are versatile flavin cofactors that are central to metabolism across the three domains of life. Some organisms also synthesize and utilize 5-deazaflavin compounds (3, 4), in which a carbon atom substitutes for the N-5 atom of the isoalloxazine ring. Two such compounds are relevant to biological systems, namely, 7,8-didemethyl-8-hydroxy-5-deazariboflavin (F_o) and its lactyl oligoglutamate phosphodiester derivative (F_{420}) (Fig. 1) (5, 6). While structurally similar to flavins, these compounds have markedly different physicochemical properties (6–9): they serve as obligate two-electron hydride carriers, have low standard redox potentials (−340 mV), and have blue-shifted intrinsic fluorescence. As elaborated upon in section 2, the chemical properties and biological functions of F_{420} are in fact more similar to nicotinamides (i.e., NAD, NADP) than flavins, leading to its description as a "nicotinamide in a flavin's clothing" (7, 10).

F_o and F_{420} have entirely distinct physiological roles. F_o is distributed across the three domains of life (*Bacteria*, *Archaea*, and *Eukarya*), but it appears to serve only one function: as a light-harvesting antenna in some DNA photolyases that repair pyrimidine dimers following exposure to UV light. As a result, F_o can be considered a chromophore rather than a cofactor; while it can substitute for F_{420} *in vitro* (11–13), it does not appear to have any redox roles in living cells. The biosynthesis, distribution, and photochemistry of this chromophore are covered in section 2. In contrast to F_o, F_{420} has a very limited taxonomic distribution and has been chemically identified in only two phyla thus far (*Euryarchaeota* and *Actinobacteria*). However, this cofactor has diverse catalytic roles in such organisms and mediates many of the challenging redox transformations necessary for their catabolic, detoxification, and biosynthetic pathways. F_{420} appears to have been selected for such processes due to its unique electrochemical properties compared to other flavins, namely, its two-electron reactivity and low redox potential. By maintaining a pool of hydride transfer redox cofactors separate from NAD(P), cells may also be able to better control the flux of specific redox reactions. The roles and enzymology of the reactions catalyzed by F_{420} are discussed in sections 3 and 4 of this review.

Nine years after the discovery of methanogenesis (14), Cheeseman et al. formally identified F_{420} in 1972 (5) in Wolfe's laboratory. They demonstrated that the compound was responsible for the characteristic 420-nm absorbance and blue-green fluorescence of oxidized lysates of *Methanobacterium bryantii* (5). The compound, thereafter named factor 420 (abbreviated F_{420}; sometimes called coenzyme F_{420} or cofactor F_{420}), was shown to be a redox-active 5-deazaflavin derivative (6) that is present at levels up to 400 mg/kg in methanogens (15). It was demonstrated that F_{420} facilitated multiple central metabolic redox reactions in methanogens, including oxidation of energy sources (H_2 and formate) (16, 17) and reduction of cofactors (NADP and tetrahydromethanopterin) (16, 18). Later, it was realized that F_{420} is also synthesized by sulfate-reducing archaea (19), halophilic archaea (20), and likely methanotrophic archaea (21). As a result of more than 5 decades of study, scientists developed a rich understanding of the physiology and biochemistry of F_{420} in the methanogenic and sulfate-reducing archaea (22), as summarized in section 3.

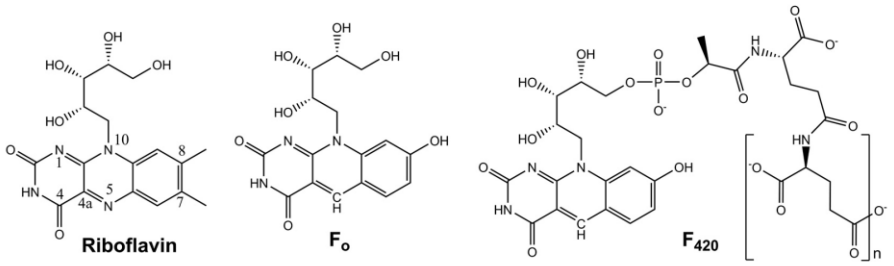

FIG 1 Structures of riboflavin, F_o, and F_{420}.

However, our understanding of the roles of F_{420} in bacteria remains in its infancy. While cofactors with properties corresponding to F_{420} were isolated in mycobacteria and streptomycetes in 1960 (23, 24), it was not until decades later that the cofactor was formally identified in these genera (25–27). As discussed throughout section 4, F_{420} is implicated in the catabolic, biosynthetic, and detoxification pathways of both saprophytic actinobacteria (28–30) and their pathogenic descendants (e.g., *Mycobacterium tuberculosis*) (31, 32). Interest in F_{420} metabolism has surged following the discovery that the recently clinically approved antimycobacterial prodrug delamanid is activated by a specific $F_{420}H_2$-dependent reductase (33–36). However, the physiological and pharmacological roles of F_{420} are still poorly understood in actinobacteria, and the majority of the predicted F_{420}-dependent enzymes in such organisms remain functionally unannotated (30, 37). There is also genomic evidence that F_{420} might be more widely distributed than previously thought, with potential roles in *Chloroflexi*, *Alphaproteobacteria*, and *Betaproteobacteria* inhabiting aerated soil ecosystems (30, 37). This review concludes by considering the diverse implications and potential environmental, medical, and industrial applications of deazaflavin compounds (section 5).

2. 5-DEAZAFLAVIN COMPOUNDS

2.1. Properties

The structure of F_o (7,8-didemethyl-8-hydroxy-5-deazariboflavin; also sometimes referred to as 8-HDF, F_0, and FO) is similar to that of riboflavin (Fig. 1). However, its physical and chemical properties are modulated by three substitutions in its isoalloxazine rings (38): N-5 is substituted for a carbon, C-7 and C-8 are demethylated, and C-7 is hydroxylated (6). F_{420} is a derivative of F_o; the rib ityl side chain forms a phosphoester bond, with a lactate moiety forming the phosphodiester and linking to an oligoglutamate chain (6). While the substitutions that distinguish 5-deazaflavins from flavins may seem superficial, pioneering work by Walsh has shown that they profoundly influence the physicochemical properties of these molecules (7, 8, 39, 43). Several years prior to their discovery in biology, chemically synthesized 5-deazaflavins (3, 4, 39) were used as probes to study the flavin-dependent reactions (40–43), revealing distinct electrochemical and photochemical properties from their flavin counterparts (44). Upon the discovery of 5-deazaflavins in biological systems (5, 6), it was realized that the electrochemical properties of these compounds are central to the role of F_{420} as a redox cofactor (6), while the photochemical properties are exploited by F_o as an antenna chromophore for DNA photolyases (45). Three features define the roles of 5-deazaflavins in biology.

(i) Two-electron carrier. Whereas flavins can serve as one or two electron carriers, 5-deazaflavins are obligate two-electron (hydride) carriers (44, 46). This is because flavins are stable as semiquinones (both neutral and anionic), whereas 5-deazaflavins are not. The nitrogen atom in position 5 is required for an unpaired electron to efficiently delocalize through the isoalloxazine ring; indeed, radicals of pyrazine groups (of flavins) are much lower energy than those of pyridine groups (of 5-deazaflavins) (7, 43). Reflecting this reactivity, F_{420}-dependent enzymes mediate diverse hydride transfer reactions that transform C=C and C≡C bonds (28, 29, 47, 48), alcohol and imine groups (49, 50), and certain inorganic compounds (51, 52). Furthermore, due to the substitution, 5-deazaflavins do not readily undergo single-electron reactions. Thus, unlike flavins, reduced 5-deazaflavins are relatively stable against air oxidation with a half-life on the order of hours instead of seconds for flavins (39, 44). This autooxidation in air has also been reported to be influenced by other factors such as stimulation from ambient light (8, 44) and, in the case of F_{420} and F_o, the addition of the 8-hydroxy group that results in the formation of a delocalized paraquinoid anion upon deprotonation of the oxidized species at pH above 6 (8). The low electrophilic reactivity of this anion results in a slower disproportionation/self-exchange reaction between F_{420} and $F_{420}H_2$ (8). Similarly, 5-deazaflavins also exhibit reduced reactivity with reducing agents that act primarily as single-electron donors (e.g., dithionite) (6, 8, 39).

(ii) Strong reductant. As a result of the substitution of N-5 to C-5, 5-deazariboflavin has a much lower standard redox potential (−310 mV) than riboflavin (−210 mV), FAD (−220 mV), or FMN (−190 mV) (7, 53). Due to the electron-withdrawing groups added to the isoalloxazine ring, F_o and F_{420} are even stronger reductants (−340 mV) than 5-deazariboflavin and thus some of the lowest-potential redox cofactors in biology (8, 9). This redox potential may be modulated under physiological conditions; for example, it will be −380 mV at standard temperature in hydrogenotrophic methanogens that maintain a 10:1 ratio of oxidized to reduced F_{420} (9). This redox potential places F_{420} at the center of the redox biology of methanogens (Table 1); the compound is capable of being reduced by exogenous fuels (H_2 and formate) and reoxidized by key cofactors (NADP and tetrahydromethanopterin derivatives) in an energetically efficient manner (7, 8, 53). Bacteria likewise appear to tightly couple substrate oxidation (glucose-6-phosphate and NADPH) to F_{420} reduction, presumably to en-

TABLE 1 List of standard redox potentials for key F_{420}-linked redox reactions[a]

Substrate[b]	Reaction	E_o' (mV)	Reference
Ferredoxin	$Fd + 2\,e^- \rightarrow Fd^{2-}$	−500 to −400	487
CO_2/formate	$CO_2 + 2\,e^- + H^+ \rightarrow HCO_2^-$	−420	487
H^+/H_2	$2\,H^+ + 2\,e^- \rightarrow H_2$	−410	487
Methenyl/methylene H_4MPT	$CH{\equiv}H_4MPT + 2\,e^- + H^+ \rightarrow CH_2{=}H_4MPT$	−390	301
F_{420}	$F_{420} + 2\,e^- + 2\,H^+ \rightarrow F_{420}H_2$	−340	8
6PGL/G6P	6-Phosphogluconolactone + $2\,e^- + 2\,H^+ \rightarrow$ Glucose-6-phosphate	−330	488
Methylene/methyl H_4MPT	$CH_2{=}H_4MPT + 2\,e^- + H^+ \rightarrow CH_3\text{-}H_4MPT$	−320	301
$NAD(P)^+$	$NAD(P)^+ + 2\,e^- + H^+ \rightarrow F_{420}H_2$	−320	487
Acetone/propan-2-ol	Acetone + $2\,e^- + 2\,H^+ \rightarrow$ Propan-2-ol	−290	53
FAD	$FAD + 2\,e^- + 2\,H^+ \rightarrow FADH_2$	−220	53
Riboflavin	$Riboflavin_{ox} + 2\,e^- + 2\,H^+ \rightarrow Riboflavin_{red}$	−210	53
FMN	$FMN + 2\,e^- + 2\,H^+ \rightarrow FMNH_2$	−190	53
Methanophenazine	$Mphen_{ox} + 2\,e^- + 2\,H^+ \rightarrow Mphen_{red}$	−170	489
Heterodisulfide	CoM-S-S-CoB + $2\,e^- + 2\,H^+ \rightarrow$ CoM-SH + CoB-SH	−140	487
Sulfite/sulfide	$SO_3^- + 6\,H^+ + 6\,e^- \rightarrow S^- + 3\,H_2O$	−120	490
Menaquinone	Menaquinone + $2\,e^- + 2\,H^+ \rightarrow$ Menaquinol	−70	53
O_2/H_2O	$O_2 + 4\,H^+ + 4\,e^- \rightarrow 2\,H_2O$	+820	53

[a] This list of standard redox potentials (E_o') demonstrates that the electrochemical properties of F_{420} enable the cofactor to mediate a wide range of oxidation and reduction reactions in biological systems, especially methanogenic archaea. In whole cells, physiological redox potentials can differ considerably due to the mass action ratios of substrates/products and differences in physical conditions (487). Potentials were determined under standard conditions (25°C, 1 atm, pH 7.0) against the standard hydrogen electrode.
[b] 6PGL, 6-phosphogluconolactone; $Mphen_{ox}$ and $Mphen_{red}$, oxidized and reduced methanophenazine, respectively.

hance catalytic efficiency (Table 1). Partly due to its low redox potential, the $F_{420}H_2$ produced is capable of reducing a wide range of organic compounds otherwise recalcitrant to activation as discussed in section 4 (28, 54, 55). Recent work also indicates that F_{420} may be utilized in aerobic bacteria in hypoxic and anoxic environments, potentially substituting for high-potential nicotinamide cofactors (NAD and NADP) (−320 mV) (30, 32, 56).

(iii) Intrinsic fluorophore. Like flavins, 5-deazaflavins are intrinsically fluorescent compounds. The delocalized charge on the isoalloxazine ring undergoes $\pi \rightarrow \pi^*$ transitions upon exposure to UV-visible light. In its oxidized state, the absorbance spectrum of F_{420} peaks at 420 nm, and the emission spectrum peaks at 470 nm (6) (Fig. 2). These peaks are pH dependent with a shift in the absorbance peak to 375 nm at lower pH along with reduced intensity (6). The reduced species $F_{420}H_2$ loses the absorbance peak at 420 nm for a new peak at 320 nm with a lower molar absorption coefficient (6) (Fig. 2). Due to the substitution of C-5 to N-5, the visible absorption spectra and fluorescence emission spectra of 5-deazaflavins are blue-shifted by about 50 nm compared to flavins (6, 44). As a result, light captured by 5-deazaflavins can be efficiently transferred to flavins through Förster resonance energy transfer (FRET). As elaborated below, this is central to the mechanism of the F_o-utilizing DNA photolyases (57, 58). The autofluorescence of F_{420} has also been used for detecting methanogens (59–66) and mycobacteria (67, 68).

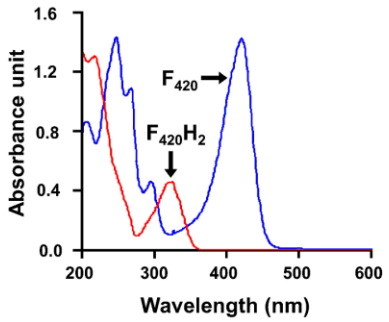

FIG 2 UV-visible absorption spectra of F_{420} (blue) and $F_{420}H_2$ (red). Adapted from reference 31.

2.2. Chromophore F_o

2.2.1. Biosynthesis

Despite its structural similarity to riboflavin, the biosynthetic pathway for F_o and other 5-deazaflavins diverges at an early step in the pathways leading to the synthesis of flavin cofactors (Fig. 3). The deazaflavin and flavin biosynthetic pathways both proceed from the pyrimidine ribityldiaminouracil (5-amino-6-ribitylamino-2,4[1*H*,3*H*]-pyrimidinedione). In the flavin pathway, this substrate is condensed with 3,4-dihydroxy-2-butanone 4-phosphate to make a lumazine derivative (6,7-dimethyl-8-ribityllumazine) (69); two of these molecules subsequently condense to regenerate 5-amino-6-ribitylamino-2,4(1*H*,3*H*)-pyrimidinedione with concomitant production of riboflavin (69). In the deazaflavin pathway, ribityldiaminouracil is instead condensed with the amino acid tyrosine (not 4-hydroxyphenylpyruvate as previously proposed [70]) leading to formation of F_o (71). The enzyme responsible for this condensation step, F_o synthase, is encoded by two polypeptides in archaea (CofG and CofH) (70) and a two-domain fusion protein (FbiC) in bacteria and eukaryotes (72). Each subunit/domain contains a radical *S*-adenosylmethionine (radical SAM) catalytic site (71, 73). A recent mechanistic study demonstrated that formation of the complex heterocycle depends on the coordinated action of the two radical SAM active sites, each of which abstract a hydrogen atom from the tyrosine (73).

2.2.2. Distribution

F_o serves as an antennal chromophore in DNA photolyases in a range of organisms across the three domains of life. Auxiliary to

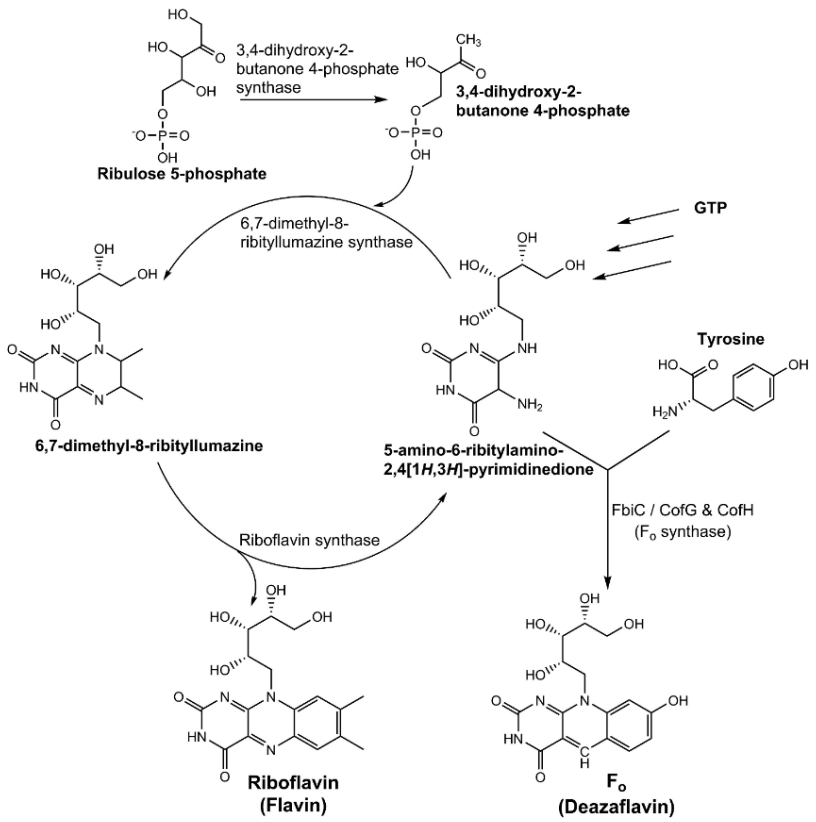

FIG 3 Summary of flavin and deazaflavin biosynthesis pathways.

the catalytic chromophore $FADH^-$, F_o captures light more effectively than $FADH^-$ owing to its longer wavelength absorption maximum and higher molar absorption coefficient (74). This is particularly important under low-light conditions, during which F_o enhances the efficiency of DNA repair by orders of magnitude (75). F_o-utilizing photolyases have been identified in multiple bacteria (e.g., *Synechococcus elongatus*, *Streptomyces griseus*) (76–80), archaea (e.g., *Methanothermobacter marburgensis*, *Methanosarcina mazei*, *Halobacterium halobium*) (81–83), and unicellular eukaryotes (e.g., *Acutodesmus obliquus*, *Chlamydomonas reinhardtii*, *Ostreococcus tauri*) (84–86). Genes encoding probable F_o synthases (CofG/CofH or FbiC) are consistently present in the genomes of such microorganisms. The question of whether F_o is utilized in higher eukaryotes is more controversial. Structural and chemical studies have demonstrated that F_o binds tightly to, and enhances the efficiency of, the two photolyases of the higher eukaryote *Drosophila melanogaster* (85, 87). Catalytically active and nucleus-targeted F_o-utilizing DNA photolyases are also known to be produced by insect baculoviruses (88–93). However, it is perplexing how such photolyases could utilize F_o *in vivo*, given that the genomes of higher eukaryotes lack F_o synthase-encoding genes (94). One explanation is that the dispensable F_o-binding domain of such enzymes is an evolutionary remnant, although it is also plausible that these organisms carry genes that encode components of a novel F_o biosynthesis pathway or acquire F_o from microbial endosymbionts and baculoviruses (85); in contrast to the highly anionic cofactors F_{420}, FMN, and FAD, F_o is uncharged and hence can readily diffuse through cell membranes (95–97). While F_o-utilizing DNA photolyases are widespread, they are hardly universal: photolyases of many species use different antennal chromophores or lack them altogether (75, 98), while eutherian lineages appear to have lost the capacity for light-driven DNA repair (99).

2.2.3. Enzymology

Enzymes of the DNA photolyase superfamily use the energy of blue light (350 to 450 nm) to facilitate the reductive cleavage of DNA pyrimidine dimers formed by far UV irradiation (200 to 300 nm). Distinct, but related, photolyases cleave cyclobutane pyrimidine dimers (CPD photolyases) and pyrimidine-pyrimidone photoproducts (6-4 photolyases) (75, 98). All DNA photolyases use the twice-reduced flavin $FADH^-$ as the catalytic chromophore. Most photolyases also use an antennal chromophore to optimize light capture, namely, methenyltetrahydrofolate or the flavin/deazaflavin compounds F_o, FMN, or FAD (100–103). Crystal structures reveal that the F_o-utilizing CPD photolyase (76, 77)

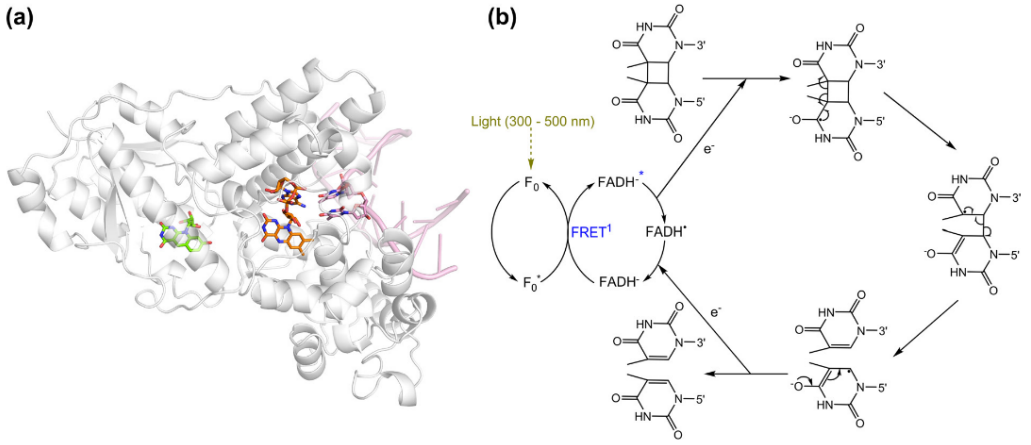

FIG 4 Structure and function of the F_o utilizing DNA photolyases. (a) Crystal structure of the F_o utilizing CPD photolyase of *Synechococcus elongatus* (PDB ID 1TEZ) (106). (b) Catalytic cycle of the enzyme. FRET is an acronym for Förster resonance energy transfer. The blue asterisk after $FADH^-$ indicates that the molecule is in the excited state.

from *Synechococcus elongatus* (Protein Data Bank [PDB] identifiers [IDs] 1QNF, 1TEZ, and 1OWL) (57, 104–106) is a single-subunit enzyme containing an N-terminal α/β domain and a C-terminal α-helical domain. Both chromophores are deeply buried, with F_o located in a cleft between the domains and $FADH^-$ embedded in the α-helical domain (Fig. 4) (57, 106). The ~17-Å distance between the chromophores enables efficient FRET while potentially preventing competitive electron transfer reactions between the cofactors (74).

The catalytic cycle of F_o-utilizing CPD photolyases has been elucidated through extensive spectroscopic and structural studies on the *S. elongatus* photolyase (Fig. 4). In the light-independent initial reaction, the enzyme recognizes and binds to damaged duplex DNA on the basis of its bent orientation (106). The antennal chromophore F_o thereafter captures a photon of blue light with an absorbance peak at 437 nm (red-shifted due to the strong interaction of the chromophore with the protein) (77). Femtosecond-scale spectroscopic studies show that F_o then transfers the energy to $FADH^-$ through FRET (107). The excited catalytic chromophore ($FADH^{-*}$) thereafter transfers an electron to the pyrimidine dimer, leading to its cleavage, and back-electron transfer restores the catalytic chromophore to an active form ready for a second catalytic cycle (108, 109). As reviewed in detail elsewhere (75, 110), similar reaction cycles facilitate light capture by other antennal chromophores and cleavage of pyrimidine-pyrimidone dimers. F_o-dependent photolyases are generally more efficient than methenyltetrahydrofolate-dependent ones, and the quantum yields of the energy transfer and electron transfer steps have been shown to be at near-unity (58, 107).

2.3. Cofactor F_{420}

2.3.1. Biosynthesis

The chemical structure of F_{420}, a lactyloligoglutamyl phosphodiester of F_o, was inferred from spectroscopic analysis of its degradation products (6) and validated by chemical synthesis (111–113) (Fig. 1). Reflecting its modular molecular structure, F_{420} is synthesized from several precursors: F_o, lactate, the amino acid glutamate, and the nucleotide GTP (97, 114, 115). Through a combination of biochemical and genetic studies in methanogens and mycobacteria, the majority of the steps in the F_{420} biosynthetic pathway have been resolved (Fig. 5).

There are two major steps in the conversion of F_o to F_{420}. In the first, the lactate-derived intermediate L-lactyl-2-diphospho-5′-guanosine (LPPG) is condensed with F_o (116) to form the phosphodiester F_{420}-0 (i.e., F_{420} containing no glutamate side chain). This reaction is catalyzed by a 2-phospho-L-lactate transferase (named CofD in archaea and FbiA in actinobacteria) (117, 118). The structure of this enzyme (PDB ID 3C3D) demonstrates that the deazaflavin ring of F_o interacts with a hydrophobic pocket and two water molecules, while the nucleotide moiety of LPPG is accommodated in a Rossmann fold domain with a Mg^{2+} ion. It is proposed that, following conformational changes initiated by substrate binding, the condensation proceeds following the abstraction of a proton from the terminal hydroxyl group of F_o by the β-phosphate of LPPG (119).

Thereafter, the nonribosomal peptide synthase F_{420}:γ-L-glutamyl ligase (CofE/FbiB) catalyzes the GTP-dependent addition of an oligoglutamate tail (118, 120–122). L-Glutamate residues are added via γ-linkages to F_{420}-0 (F_{420}-0 + glutamate + GTP → F_{420}-1 + GDP + P_i) and glutamated derivatives thereof (F_{420}-*n* + glutamate + GTP → F_{420}-*n* + 1 + GDP + P_i) in a sequential manner. The X-ray crystallographic structure of the enzyme from *Archaeoglobus fulgidus* (PDB ID 2PHN) demonstrates that it forms a butterfly-like homodimer that accommodates GTP and Mn^{2+} at the dimer interface. It is proposed that the cofactor is activated by phosphorylation (at the terminal hydroxyl group of the lactate moiety of F_{420} and the terminal glutamate of F_{420}-*n* derivatives), and the resultant acyl-phosphate is subject to nucleophilic attack by the amino group of the incoming glutamate residue (123). The number of glutamate residues on F_{420} is highly species specific, ranging from two or three in methanogens without cytochromes (124), four or five in methano-

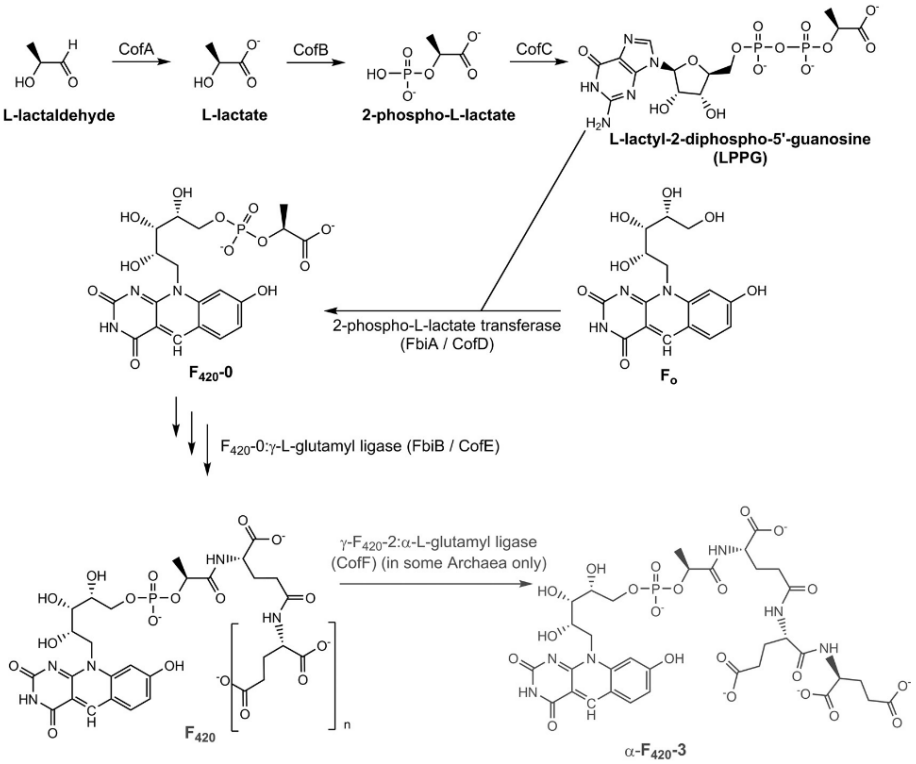

FIG 5 Summary of the F_{420} biosynthesis pathway from F_o.

gens with cytochromes (124), and five to seven in mycobacteria (125). The physiological significance and biochemical basis for these differences is not yet understood. In some archaea, a terminal α-linked glutamate residue (126, 127) is also added by γ-F_{420}-2:α-L-glutamate ligase (CofF) (128), an enzyme of the ATP-grasp superfamily.

The pathway that leads to the production of LPPG from the precursor L-lactate has only been partially resolved. Detailed studies on *Methanocaldococcus jannaschii* indicate that lactate is exclusively synthesized from L-lactaldehyde (129, 130); lactaldehyde is generated from the reduction of methylglyoxal or the aldol cleavage of fuculose-1-phosphate and is in turn oxidized to lactate by the NAD^+-dependent L-lactaldehyde dehydrogenase (CofA) (130). Though unconfirmed, it is assumed that lactate (synthesized from glycolytic pyruvate by L-lactate dehydrogenase) is also the precursor for LPPG in bacteria. It has been shown in methanogens that lactate can be phosphorylated to form 2-phospho-L-lactate in a GTP-dependent manner (116); however, the enzyme responsible (to be named CofB) has remained elusive in the 15 years since the reaction was discovered. Finally, the 2-phospho-L-lactate is converted to LPPG by the GTP-dependent enzyme 2-phospho-L-lactate guanylyltransferase (CofC) (PDB ID 2I5E) (116, 131). Homologous enzymes are required for F_{420} production in mycobacteria (132).

2.3.2. Distribution

F_{420} has a more restricted taxonomic distribution than F_o and the ubiquitous redox cofactors FAD, FMN, and NAD(P). The cofactor has been identified in a single phylum each of bacteria and archaea using analytical chemistry methods. Among the archaea, F_{420} is thought to be distributed in all methanogens, a group of strictly anaerobic methane-producing archaea (5, 15). In these organisms, F_{420} serves as a central catabolic cofactor and is also central to two of the three main methanogenesis pathways. While present in low levels in some methanogens (e.g., *Methanosarcinales*), it is present at concentrations between 100 to 400 mg per kg in many hydrogenotrophs (15, 61, 62). F_{420} has also been identified in several nonmethanogenic euryarchaeota, including three species of the sulfate-reducing genus *Archaeoglobus* (19, 133–135) and seven species of the photosynthetic genera *Halobacteria* and *Halococcus* (20, 136). The cofactor is also proposed to be central to the metabolism of the various lineages of the anaerobic methanotrophic archaea (ANME) (21, 137). Comparative genomics indicate that the genes required for F_{420} biosynthesis are also distributed in the *Thaumarchaeota*, *Aigarchaeota*, *Geoarchaeota*, *Bathyarchaeota*, and *Lokiarchaeota* (138–142). The absorbance spectra of single cells of the ammonia- and cyanate-oxidizing thaumarchaeon *Nitrososphaera gargensis* are also consistent with the presence of F_{420} (143, 144). It is unclear whether F_{420} is pro-

TABLE 2 Activity, role, and distribution of F_{420}-dependent oxidoreductases[a]

Oxidoreductase and domain	Physiological role[b]	Taxonomic distribution[c]	Description	EC no.	PDB ID	Reference(s)
F_{420}-reducing dehydrogenases						
Archaea						
Frh: F_{420}-reducing hydrogenase	Hydrogenotrophic methanogenesis. Couples oxidation of H_2 to reduction of F_{420}. May be physiologically reversible.	All orders of methanogens	Section 3.2.1	1.12.98.1	4OMF, 4CI0, 3ZFS	11, 16, 150, 219, 224, 227
Ffd: F_{420}-reducing formate dehydrogenase	Formatotrophic methanogenesis. Couples oxidation of formate to reduction of F_{420}. May be part of the electron-bifurcating complex.	*Methanobacteriales*, *Methanococcales*, *Methanopyrales*, *Methanomicrobiales*, *Methanocellales*	Section 3.2.2	1.2.99.9		17, 185, 190, 242, 259
Adf: F_{420}-reducing secondary alcohol dehydrogenase	Growth on secondary alcohols. Couples oxidation of secondary alcohols (e.g., isopropanol) to reduction of F_{420}.	*Methanomicrobiales*, *Methanocellales*	Section 3.2.3	1.1.98.5	1RHC	49, 271, 272
Bacteria						
Fno: F_{420}-reducing NADPH dehydrogenase	Exchanges electrons between NADP and F_{420}. F_{420} reduction important in bacteria, as F_{420} is the secondary cofactor.	Many *Actinomycetes* (e.g., *Streptomyces*, *Rhodococcus*, *Nocardia*, *Nocardioides*), *Alpha-* or *Betaproteobacteria*?	Section 4.2.1	1.5.1.40		12, 155
Fgd: F_{420}-reducing glucose 6 phosphate dehydrogenase	Heterotrophic growth. Couples oxidation of glucose 6 phosphate to reduction of F_{420} via the pentose phosphate pathway.	Many *Actinomycetes* (e.g., *Mycobacterium*, *Actinoplanes*, *Micrabacterium*, *Amycolatopsis*), *Chloroflexi*?	Section 4.2.2	1.1.98.2	3B4Y	163
fHMAD: F_{420}-reducing hydroxymycolic acid dehydrogenase	Cell wall biosynthesis. Catalyzes F_{420}-dependent oxidation of hydroxymycolic acids to ketomycolic acids.	Few *Mycobacterium* (primarily pathogenic species)	Section 4.2.3			364, 365
$F_{420}H_2$-dependent reductases						
Archaea						
Mtd: F_{420}-reducing methylene-H_4MPT dehydrogenase	Reduces $CH{\equiv}H_4MPT$ to $CH_2{=}H_4MPT$ with $F_{420}H_2$ in methanogenesis. Reaction physiologically reversible.	All orders of methanogens, *Archaeoglobales*, ANME	Section 3.3.1	1.5.98.1	1QV9, 1U6I, 3IQF, 3IQE	18, 47, 166, 275, 284, 285
Mer: $F_{420}H_2$-dependent methylene-H_4MPT reductase	Reduces $CH_2{=}H_4MPT$ to $CH_3{-}H_4MPT$ with $F_{420}H_2$ in methanogenesis. Reaction physiologically reversible.	All orders of methanogens, *Archaeoglobales*, ANME, *Halobacteriales*	Section 3.3.1	1.5.98.2	1F07, 1EZW, 1Z69	48, 159, 166, 284
Fpo: $F_{420}H_2$-dependent methanophenazine reductase	Proton-translocating primary dehydrogenase in respiratory chain transferring electrons from $F_{420}H_2$ to heterodisulfide	*Methanosarcinales*	Section 3.3.2	1.1.98.4		162, 304–306, 327
Fqo: $F_{420}H_2$-dependent quinone reductase	Proton-translocating primary dehydrogenase in respiratory chain transferring electrons from $F_{420}H_2$ to sulfate	*Archaeoglobales*, ANME	Section 3.3.2	1.1.98.4		21, 198–200
Fpr: $F_{420}H_2$-dependent oxidase	Detoxifies O_2 by mediating the four-electron reduction of O_2 to H_2O with $F_{420}H_2$	*Methanobacteriales*, *Methanococcales*, *Methanomicrobiales*, *Methanocellales*	Section 3.3.3	1.5.3.22	2OHH, 2OHI, 2OHJ	161, 192
Fsr: $F_{420}H_2$-dependent sulfite reductase	Detoxifies sulfite by mediating the six-electron reduction of sulfite to sulfide with $F_{420}H_2$. Also enables use of sulfite as an S source.	*Methanobacteriales*, *Methanococcales*	Section 3.3.4	1.8.98.3		51, 191

Fno: $F_{420}H_2$-dependent NADP reductase	Exchanges electrons between NADP and F_{420}. NADP reduction important in archaea, as NADP is the secondary cofactor.	All orders of methanogens, *Archaeoglobales*, ANME	Section 3.3.5	1.5.1.40	1JAY, 1JAX	16, 22, 160, 201
Bacteria						
Ddn: $F_{420}H_2$-dependent nitroreductases	May serve to detoxify redox cycling agents and other exogenous compounds. Also catalyze nitroimidazole activation.	Most *Actinomycetes* (e.g., *Mycobacterium*, *Streptomyces*, *Rhodococcus*), *Chloroflexi*?, *Methanosarcinales*?	Section 4.3.1		3H96, 4Y9I, 3R5R, 3R57	28, 30, 32, 164
Fbr: $F_{420}H_2$-dependent biliverdin reductases	Reduce the heme degradation product biliverdin to bilirubin. May also reduce mycobilins. FDOR-B3 and -B4 family.	Most *Actinomycetes* (e.g., *Mycobacterium*, *Streptomyces*, *Rhodococcus*), *Chloroflexi*?, *Halobacteriales*?	Section 4.3.1		2ASF, 4QVB, 1W9A	30, 165, 418, 419
Fts: $F_{420}H_2$-dependent tetracycline synthases	Reduce dehydrotetracyclines during streptomycete antibiotic synthesis. Role in mycobacteria unknown. FDOR-B1 family.	Most *Actinomycetes* (e.g., *Mycobacterium*, *Streptomyces*, *Rhodococcus*), *Chloroflexi*?, *Halobacteriales*?	Section 4.3.1		3I7E, 1RFE	28–30
Other $F_{420}H_2$-dependent flavin/deazaflavin oxidoreductases	Activities of A2-A4, B1, B2, B5, B6, AA1-AA5 families unknown. AA1s may be fatty acid saturases.	Most *Actinomycetes* (e.g., *Mycobacterium*, *Streptomyces*, *Rhodococcus*), *Chloroflexi*?, *Halobacteriales*?	Section 4.3.1		4ZKY	30, 55
Fht: $F_{420}H_2$-dependent picrate reductases	Reduces 2,4,6-trinitrophenol (picrate) for use as a C and N source through hydride transfer to the nitroaromatic ring	Few *Actinomycetes* (*Rhodococcus*, *Nocardia*, *Nocardioides*)	Section 4.3.2			54, 155
Fps: $F_{420}H_2$ dependent tetrahydropyrrole synthases	Reduces 4 propylidene 3,4 dihydropyrrole-2-carboxylate during biosynthesis of pyrrolobenzodiazepines antibiotics	Few *Actinomycetes* (*Streptomyces*, *Streptosporangium*)	Section 4.3.2			50, 389
Other $F_{420}H_2$-dependent luciferase-like hydride transferases	Unknown. Likely to have diverse roles in endogenous and exogenous redox metabolism of organic compounds.	Most *Actinomycetes* (e.g., *Mycobacterium*, *Streptomyces*, *Rhodococcus*)	Section 4.3.2			

[a] For more information about the enzymes, see the sections in the text where the enzymes are described, Enzyme Commission (EC) entries, Protein Data Bank structures, and key primary references.

[b] Note that several of F_{420}-dependent reactions are physiologically reversible, including those catalyzed by Fno, Mtd, Mer, and possibly Frh. Fno is primarily an $F_{420}H_2$-dependent NADP reductase in methanogens and a F_{420}-reducing NADPH dehydrogenase in bacteria; the enzyme appears to be similar in archaea and bacteria but is used in a different physiological context.

[c] *Euryarchaeota* are listed by order, namely, six methanogenic orders (*Methanobacteriales*, *Methanococcales*, *Methanopyrales*, *Methanomicrobiales*, *Methanocellales*, and *Methanosarcinales*) and two nonmethanogenic orders (*Archaeoglobales* and *Halobacteriales*). The various lineages of the uncultured anaerobic methanotrophic archaea are denoted as ANME. Actinobacteria are listed by genus (*Mycobacterium*, *Streptomyces*, *Rhodococcus*, *Nocardia*, *Nocardioides*, *Streptosporangium*, *Microbacterium*, *Actinoplanes*, and *Amycolatopsis*).

duced by *Crenarchaeota*; while the cofactor was reported to be present at low levels in representatives of the *Sulfolobus* and *Thermoplasma* (20), the genomes of these organisms suggest that in fact they lack the capacity to synthesize this deazaflavin by any currently understood biosynthetic mechanism.

It is assumed that F_{420} has a more restricted distribution among bacteria. The cofactor has been identified in representatives of the actinobacterial genera *Mycobacterium* (23, 27, 125, 145), *Streptomyces* (25, 27, 29, 146), *Nocardia* (27, 145), and *Nocardioides* (54). Most of these representatives are saprophytic soil bacteria that adopt a heterotrophic, aerobic lifestyle. The cofactor has also been reported in several mycobacterial pathogens, namely, the major obligate pathogens *Mycobacterium tuberculosis*, *Mycobacterium bovis*, and *Mycobacterium leprae*, as well as several opportunistic species (145). Comparative genomic analyses show that the genes involved in F_{420} biosynthesis and utilization are also found in representatives of the *Chloroflexi*, *Alphaproteobacteria*, *Betaproteobacteria*, and *Gammaproteobacteria* (30, 37), which constitute some of the most dominant taxa in aerated soil ecosystems (147). The occasional references to F_{420}-dependent processes in *Cyanobacteria* are erroneous; these have emerged from authors misattributing F_o-dependent processes to F_{420} (72, 148) or relying on incorrect automated sequence predictions (149). Indeed, F_{420} has yet to be chemically identified in any species outside the phyla *Euryarchaeota* and *Actinobacteria*.

2.3.3. Enzymology

In most archaea and some actinobacteria, F_{420} is reduced through coupled steps in central catabolic pathways (Table 2). Methanogens are able to oxidize their substrates for growth using F_{420}, i.e., H_2 (via the F_{420}-reducing hydrogenase [Frh]) (150), formate (via the F_{420}-reducing formate dehydrogenase [Ffd]) (17), or secondary alcohols (via the F_{420}-reducing secondary alcohol dehydrogenase [Adf]) (49). This facilitates the entry of electrons into the CO_2-reducing pathway of methanogenesis and generates $F_{420}H_2$ to drive cellular redox reactions (151). Note that, contrary to historical reports (152, 153), carbon monoxide dehydrogenase, pyruvate dehydrogenase, and α-ketoglutarate dehydrogenase of methanogens are not F_{420} dependent in methanogens (151, 154). Mycobacteria also reduce F_{420} via their central catabolic pathways by using the F_{420}-reducing glucose-6-phosphate dehydrogenase (Fgd), one of two entry points to the reductive pentose phosphate pathway. However, pathways also exist to reduce F_{420} using other redox cofactors depending on external and internal redox states, i.e., NADP (via the F_{420}-NADP oxidoreductase [Fno]) in many actinomycetes (12, 155) and tetrahydromethanopterin (via methylene tetrahydromethanopterin dehydrogenase [methylene-H_4MPT dehydrogenase {Mtd} and methylene-H_4MPT reductase {Mer}]) in methylotrophic methanogens (156, 157). As emphasized by the central placement of F_{420} in the redox ladder of Table 1, many of these reactions are physiologically reversible. The physiology and biochemistry of the F_{420}-reducing dehydrogenases is discussed in detail in sections 3.2 and 4.2.

The physiological roles of F_{420} are primarily elicited by the coupling of the oxidation of $F_{420}H_2$ to the reduction of other compounds (Table 2). In methanogens, $F_{420}H_2$ oxidation sustains a wide range of processes. $F_{420}H_2$ is used to reduce one-carbon units bound to tetrahydromethanopterin, the central one-carbon carrier in methanogenesis pathways (158), and NADP, the central cofactor for anabolic processes (16). This depends on the aforementioned reactions catalyzed by Mtd (47), Mer (159), and Fno (160). The cofactor can additionally be used to detoxify O_2 (via $F_{420}H_2$-dependent oxidase [Fpr]) (161), mobilize sulfite (via $F_{420}H_2$-dependent sulfite reductase [Fsr]) (51), and in methanogens with cytochromes, reduce methanophenazine for respiratory energy conservation (via $F_{420}H_2$-dependent methanophenazine reductase [Fpo]) (162). $F_{420}H_2$ can be used to reduce diverse organic compounds in actinomycetes, including endogenous metabolites (e.g., quinones, porphyrins, fatty acids) (30, 32) and exogenous compounds (e.g., tetracyclines, picrate, aflatoxins) (28, 29, 54). These activities depend on two diverse superfamilies distinguished by their split β-barrel (flavin/deazaflavin oxidoreductases [FDORs]) (30, 37) or TIM barrel (luciferase-like hydride transferases [LLHTs]) protein folds (Fig. 6) (37). The $F_{420}H_2$-dependent reductase enzymes are discussed in more detail in sections 3.3 and 4.3.

The majority of F_{420}- and $F_{420}H_2$-binding proteins bind the cofactor within either TIM barrel (Adf, Mer, F_{420}-reducing hydroxymycolic acid dehydrogenase [fHMAD], Fgd, and other LLHTs) (48, 49, 163), FrhB-like (Frh, Fpo, Ffd, and Fsr) (150), or split β-barrel (FDORs) (28, 30, 164, 165) folds (Fig. 6). Exceptions to this are the structures of Mtd (novel Mtd-like fold) (166), Fno (Rossmann fold) (160), and Fpr (interface of β-lactamase and flavodoxin folds) (52). Of these known F_{420} binding architectures, the F_{420}-binding TIM barrel and split β-barrel proteins share structural homology with related FMN- and FAD-binding proteins (30, 48). In contrast, the Mtd-like and FrhB-like folds have been found only in F_{420}- or $F_{420}H_2$-dependent proteins (150, 166). All of the proteins carry out hydride transfer on the *Si*-face of F_{420} (48, 49, 150, 160, 163, 166, 167), with the exception of the FDORs that catalyze the reaction on the *Re*-face (28, 165). These proteins are adapted for F_{420} binding by the presence of a positively charged channel or region that associates with the phospholactate and polyglutamate chain. In FDORs, LLHTs, Mtd, and Fno, hydrogen bonding interactions at the pyrimidine and hydroxyl of the deazaflavin moiety anchor the cofactor, along with hydrophobic interactions to the *Re*-face (*Si*-face for FDORs) that is not involved in the enzyme reaction (28, 48, 49, 150, 160, 161, 163–166). In FrhB, Fno, and Fpr, stability is also provided by aromatic interactions with the enzyme-bound FAD, NADP, or FMN (52, 150, 160).

3. F_{420} IN METHANOGENS AND OTHER ARCHAEA

3.1. Physiological Roles

3.1.1. Methanogens

F_{420} is a catabolic redox cofactor in both methanogenic and nonmethanogenic archaea. Methanogens are microorganisms that produce methane as the end product of their anaerobic pathways of energy generation (168). These organisms encompass at least six phylogenetically distinct, metabolically diverse orders of the archaeal phylum *Euryarchaeota*: *Methanobacteriales*, *Methanococcales*, *Methanopyrales*, *Methanomicrobiales*, *Methanocellales*, and *Methanosarcinales* (169–173). F_{420} is synthesized in all of these orders, where it serves as a redox cofactor in both methanogenesis pathways and wider cellular processes (5, 15). In fact, the characteristic fluorescence of many methanogens is due to the presence of this cofactor (5, 59, 60).

Methanogens can generate methane through three major routes, the CO_2-reducing, methylotrophic, and aceticlastic path-

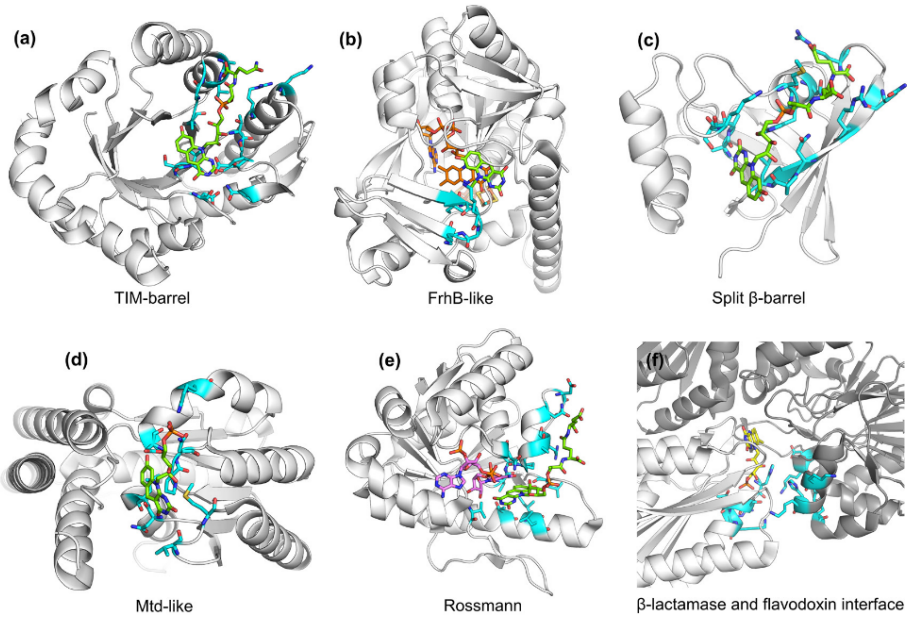

FIG 6 Structures of F_{420}-binding protein domains. (a) TIM barrel fold of Fgd (PDB ID 3B4Y [163]), (b) structure of Frh subunit B (PDB IDs 4OMF [150] and 3ZFS [167]), (c) split β-barrel fold of Ddn (PDB ID 3R5R [164]), (d) novel protein fold of Mtd (PDB ID 3IQE [166]), (e) Rossmann fold of Fno (PDB ID 1JAY [160]) and (f) the interface between β-lactamase and flavodoxin folds in Fpr (PDB ID 2OHJ [161]). Where available, the F_{420} molecule is shown in green, and key residues at the F_{420}-binding site are highlighted in cyan. In panels b, d, and f, the positions of the FAD (orange), NADP (purple), and FMN (yellow) molecules required for F_{420} binding are also shown.

ways (174–177) (Fig. 7). In the CO_2-reducing pathway, CO_2 is progressively reduced to methane using exogenously derived electrons (151, 168, 178). This pathway sustains hydrogenotrophic growth using H_2-derived electrons (16), formatotrophic growth using formate-derived electrons (17), and in some organisms, growth on secondary alcohols (179). In the methylotrophic pathway, the methyl groups of methanol, methylated amines, and methylated sulfides are converted into CH_4 (reductive route) and CO_2 (oxidative route), with the oxidative reactions occurring through a reverse arm of the CO_2-reducing pathway (157, 175, 180). In the aceticlastic pathway, acetate is fermented to methane (through reduction of the methyl group) and CO_2 (through oxidation of the carboxy group) (175, 180, 181). Most methanogens are capable of hydrogenotrophic growth, with cytochrome-containing methanogens (i.e., the *Methanosarcinales*) primarily respiring H_2 and the other five orders conserving energy through electron-bifurcating pathways (182, 183). Formatotrophic growth is also widespread (17, 184, 185), but it does not occur in the *Methanosarcinales* (186). In contrast, only a few taxa are capable of methylotrophic growth (the family *Methanosarcinaceae* and genus *Methanosphaera*) (176, 187) and aceticlastic growth (the families *Methanosarcinaceae* and *Methanosaetaceae*) (176, 188). These pathways are nevertheless quantitatively important, with the aceticlastic pathway responsible for up to two-thirds of global net methane production. The biochemistry, physiology, and ecology of methanogenesis will be discussed further only in the context of F_{420} metabolism; readers requiring further background on this topic are referred to several excellent reviews (151, 154, 168, 178, 182, 189).

F_{420} is central to the CO_2-reducing and methylotrophic pathways of methanogenesis. Dedicated F_{420}-dependent hydrogenases/dehydrogenases oxidize H_2 (Frh) (17, 150), formate (Ffd) (17, 190), and secondary alcohols (Adf) (49, 179) for entry into the CO_2-reducing pathway. F_{420} also serves as the redox cofactor for the Mtd and Mer reactions, which mediate the fourth and fifth steps of the CO_2-reducing pathway, reducing methenyl-tetrahydromethanopterin (methenyl-H_4MPT) to methyl-H_4MPT with $F_{420}H_2$ (47, 159). They operate in the reverse direction in the methylotrophic pathway, oxidizing methyl-H_4MPT to methenyl-H_4MPT. However, F_{420} is not involved in the aceticlastic pathway, which depends on a largely distinct set of enzymes (175, 181). In addition to mediating methanogenesis, dedicated F_{420}-dependent enzymes mediate a wide array of other cellular reactions in methanogens, including reduction of NADP for biosynthetic pathways (Fno) (22), mobilization of sulfite as a sulfur source (Fsr) (51, 191), and detoxification of atmospheric O_2 (Fpr) (161, 192). Methanogens with cytochromes can use $F_{420}H_2$ generated through the methylotrophic pathway as an input to the respiratory chain using the proton-translocating $F_{420}H_2$-reducing methanophenazine reductase (Fpo) (162, 193). Interestingly, F_{420} is still present in acetate-grown *Methanosarcina* (194) and the obligately aceticlastic genus *Methanosaeta* (195, 196), reinforcing the idea that the cofactor has been selected for roles well beyond methanogenesis. On the basis of metagenomic studies, it was recently reported that members of the newly defined phylum *Bathyarchaeota* may also be F_{420}-dependent methylotrophic methanogens (141).

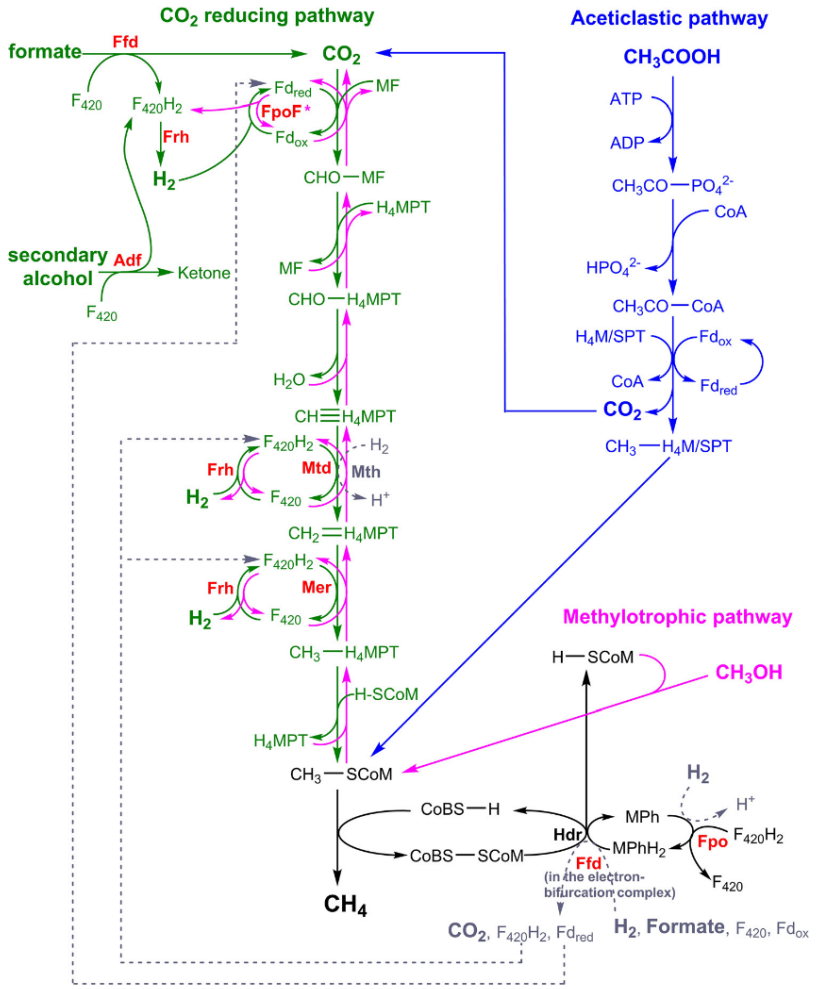

FIG 7 CO_2-reducing (green), methylotrophic (pink), and aceticlastic (blue) pathways of methanogenesis. The routes for energy generation from H_2/CO_2, formate, secondary alcohols, methanol, and acetate are shown. Processes common to all pathways are shown in black, and dashed arrows in gray show alternative pathways. F_{420}-dependent oxidoreductases are highlighted in red and catalyze both forward and reverse reactions, except for FpoF which is known to catalyze only $F_{420}H_2$ reoxidation. Abbreviations: $Fd_{red/ox}$, reduced/oxidized ferredoxin; MF, methanofuran; H_4MPT, tetrahydromethanopterin; H_4SPT, tetrahydrosarcinapterin; H-SCoM, 2-mercaptoethanesulfonate (reduced coenzyme M); CoBS-H, N-7-mercaptoheptanoylthreonine phosphate (reduced coenzyme B); MPh/$MPhH_2$, reduced/oxidized methanophenazine.

3.1.2. Sulfate-reducing archaea

F_{420} is also known to be synthesized by two orders of nonmethanogenic archaea, the *Archaeoglobales* and *Halobacteriales* (20, 136). *Archaeoglobi* are primarily heterotrophic, sulfate-reducing thermophiles that inhabit deep-sea vents (19), whereas *Halobacteria* are primarily phototrophic, facultatively aerobic halophiles that dominate hypersaline waters (197). While the two orders have very different metabolisms, both to methanogens and to each other, they are closely phylogenetically related to the *Methanomicrobiales*, *Methanosarcinales*, and *Methanocellales* (169, 171, 172). It is likely that F_{420} was synthesized in the common ancestor of each of these five orders prior to their metabolic divergence. While little is known about the role of F_{420} in *Halobacteria* (20, 136), a range of biochemical studies indicate that $F_{420}H_2$ is a central catabolic electron donor in *Archaeoglobus fulgidus* (133). $F_{420}H_2$ donates electrons to the sulfate-reducing respiratory chain via the proton-translocating $F_{420}H_2$-dependent quinonereductase (Fqo) (198–200). Additionally, the $F_{420}H_2$-dependent NADP reductase (Fno) is proposed to generate NADPH for various biosynthetic pathways (160, 201). F_{420} appears to be reduced through distinct routes depending on whether the growth substrate is H_2/CO_2 or lactate. It is well-established that, during the anaerobic oxidation of lactate to CO_2, F_{420} can be reduced by Mtd and Mer (133, 200, 202). Given that the organism lacks Frh, it

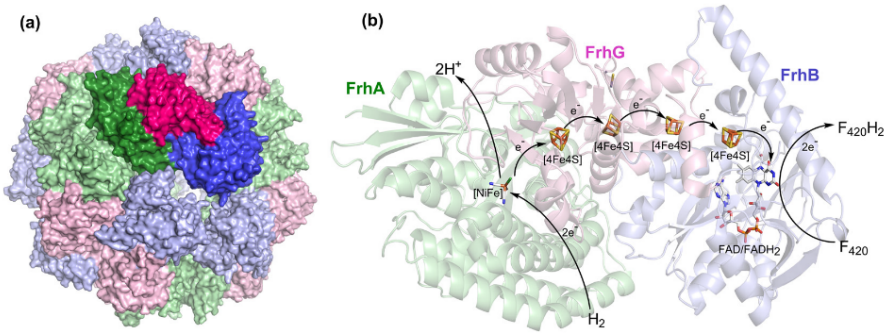

FIG 8 (a) Structure of the dodecameric complex of Frh (PDB ID 4OMF [150]), where a single protomer (identified with darker shades) contains three subunits: FrhA (green), FrhB (blue), and FrhG (pink). (b) Electron transfer route from H_2 to F_{420} within the Frh subunits during hydrogenotrophic methanogenesis.

remains to be resolved how *A. fulgidus* generates $F_{420}H_2$ during hydrogenotrophic growth (203); possible routes include electron transfer from reduced ferredoxin (Fd_{red}) (via a hypothetical complex), quinols (via reverse electron transfer), or NADPH (via Npo) (135, 200).

3.1.3. Methanotrophic archaea

There is strong evidence that F_{420} is also central to the metabolism of anaerobic methanotrophic archaea (ANME). In contrast to methanogens, these archaea consume, rather than produce, methane and use the electrons liberated from methane to drive sulfate- and nitrate-reducing respiratory chains (204–207). While these organisms have yet to be successfully cultured, they are of enormous ecological and geochemical significance; it is predicted that 90% of the methane produced by methanogens in marine sediments is immediately recycled by ANME (189, 208, 209). Extensive studies of microbial ecology have demonstrated that these organisms are closely related to two orders of methanogens (*Methanosarcinales* and *Methanomicrobiales*), and form at least three major phylogenetic clades (ANME-1, ANME-2, and ANME-3) (210, 211). A range of genomic and biochemical evidence suggests that these archaea predominantly grow through a reverse methanogenesis pathway (similar to the methylotrophic pathway; Fig. 7), through which $F_{420}H_2$ is generated via the Mer and Mtd reactions (137, 212–215). The $F_{420}H_2$ that is produced from this pathway is proposed to be reoxidized by the proton-translocating Fqo complex, with sulfate or nitrate serving as the terminal respiratory electron acceptor (21, 215). This proposal was recently supported by a metagenomic/metatranscriptomic study that showed that the nitrate-reducing methanotroph *Methanoperedens nitroreducens* (part of the ANME-2 lineage) expresses a complete reverse methanogenesis pathway, along with all the F_{420} biosynthesis genes and a putative Fqo complex (137). Environmental sequencing has also inferred a role for F_{420} in other ANME lineages (21, 215, 216). Also consistent with the presence of F_{420}, ANME, like methanogens, are autofluorescent under UV light (217, 218).

3.2. F_{420}-Reducing Dehydrogenases

3.2.1. Frh: F_{420}-reducing hydrogenase

The F_{420}-reducing hydrogenase directly couples H_2 to F_{420} reduction (9, 11, 219, 220). The enzyme is encoded by genes in all classes of methanogens (183) and is the preferred route to F_{420} reduction during hydrogenotrophic methanogenesis (Fig. 7) (221–223). This hydrogenase is essential for growth on H_2/CO_2 in *Methanosarcina barkeri* (*Ms. barkeri*) (224), but it appears to be dispensable in methanogens with genes that encode an alternative pathway for F_{420} reduction such as *Methanococcus maripaludis* (*Mc. maripaludis*) (225). The enzyme complex, encoded by the transcriptional subunit *frhADGB* (222), is a product of the association of an F_{420} reductase subunit of the F_{420}-binding protein family (functionally analogous to F_{420} reductase domains of Fsr, Fpo, and Ffd) with a H_2-oxidizing [NiFe]-hydrogenase of the group 3a family (226). Structural characterization of this complex from *Methanothermobacter marburgensis* through cryo-electron microscopy (167, 227) and X-ray crystallography (150) revealed a large dodecameric complex of heterotrimers (FrhABG), arranged as a shell with a solvent-filled core (Fig. 8). Each heterotrimeric protomer (FrhABG) contains a [NiFe]-hydrogenase large subunit (FrhA; matured by the endopeptidase FrhD), a [NiFe]-hydrogenase small subunit (FrhG), and an F_{420} reductase subunit (FrhB). While the complex is located in the cytoplasm (150), it is often purified from the membrane fraction due to its high molecular mass of 1.2 MDa (228–230).

During the H_2-dependent reduction of F_{420}, H_2 binding and oxidation occur at the buried [NiFe] center of FrhA, which is facilitated by a hydrophobic channel that extends from the [NiFe] center to the outer surface of the enzyme complex (150). On the basis of structural and spectroscopic studies, it is proposed that H_2 is heterolytically cleaved in a mechanism similar to other [NiFe]-hydrogenases (150, 219, 231–233). As with other [NiFe]-hydrogenases, the protons generated are relayed from the [NiFe] center to the outer surface of the complex, where they are released to the bulk solvent near a covalently bound FAD molecule on the FrhB subunit of a neighboring protomer (150). Concomitantly, electrons from the H_2 cleavage reaction are individually transferred via four [4Fe4S] clusters (three on FrhG and one on FrhB) to the FAD molecule bound to FrhB of the same protomer, generating $FADH_2$ (Fig. 8). The terminal step involves hydride transfer from $FADH_2$ to F_{420}, which binds reversibly at a solvent-accessible pocket on FrhB, with the 5-deazaflavin rings (*Si*-face) next to the isoalloxazine of the FAD cofactor (*Si*-face) (150, 234). Kinetic and structural data suggest that hydride transfer to F_{420} occurs rapidly and is rate limited by diffusion, rather than conformational change (227, 235). The remarkable oligomerization of the com-

plex does not appear to influence the reaction kinetics of the hydrogenase and instead may serve to protect metal centers from redox-active compounds of the cytosol (150).

It has been proposed that Frh is physiologically active in both the forward and reverse directions (224, 225). While Frh primarily sustains H_2-mediated F_{420} reduction during hydrogenotrophic growth, it may mediate $F_{420}H_2$-mediated H_2 production during methylotrophic methanogenesis and formate-dependent growth (224, 225). This is consistent with the observations of severe defects of *Ms. barkeri* Δ*frh* mutants during growth on methanol and on H_2 production during formate-dependent growth of *Mc. maripaludis* (225). While F_{420} reduction is more thermodynamically favorable (E_0 F_{420} = −340 mV; E_0 H_2 = −410 mV), the reverse reaction may occur when $F_{420}H_2$ accumulates and H_2 partial pressure [pH_2] is low. This is supported by biochemical data that Frh purified from *Methanobacterium formicum* can sustain a moderate rate of $F_{420}H_2$-mediated H_2 evolution (230). However, genetic dissection experiments will be required to definitively confirm whether Frh-mediated H_2 evolution can occur *in vivo* at physiologically relevant rates.

Several variants of Frh can be encoded by genes in the same genome. Many methanogens carry genes that encode both a selenium-containing F_{420}-reducing hydrogenase (Fru) in addition to a selenium-free one (Frh) (183, 221, 222). Studies on the purified [NiFeSe]-hydrogenase from *Methanococcus voltae* suggest that the selenium-containing isozymes are faster acting and more oxygen tolerant than the selenium-free variant (236, 237). Hence, transcription of Fru over Frh occurs in selenium-containing conditions in this organism (221, 238, 239). In addition, variants of Frh were recently found to be encoded by genes of several non-F_{420}-producing species of the archaeal order *Thermococci* and the bacterial family *Desulfobacteriaceae* (183). Biochemical and sequence analyses indicate that these enzymes cannot reduce F_{420} and instead couple to another electron acceptor, such as a flavin (240); these enzymes and their F_{420}-reducing relatives are capable of reducing FAD and FMN *in vitro* (16, 240).

3.2.2. Ffd: F_{420}-reducing formate dehydrogenase

Many hydrogenotrophic methanogens can also grow using formate as the sole electron donor, including species from the genera *Methanococcus* (241, 242), *Methanobacterium* (243), and *Methanospirillum* (184). This process is especially ecologically significant, given that formate produced by fermentative bacteria can be consumed by methanogens through interspecies transfer (244). It is well established that formatotrophic growth is linked to F_{420} metabolism (17) and that it depends on F_{420}-reducing formate dehydrogenases (called Ffd or Fdh) (242). Although Ffd has not been structurally characterized, biochemical studies on the enzyme from *Methanobacterium formicicum* (*Mb. formicicum*) have revealed its core architecture. Ffd is a membrane-bound heterodimeric enzyme containing several redox centers (190, 245, 246). The large subunit is homologous with the structurally characterized bacterial formate dehydrogenases (247), and it is predicted to contain a molybdopterin guanine nucleotide cofactor (MGD) (248–252) and a [4Fe4S] center (190). The small subunit is unique to methanogenic archaea and is predicted to contain two [4Fe4S] clusters (190), an FAD cofactor (190, 253, 254), and an F_{420}-binding site that is homologous to FrhB (150). It has been proposed that formate is oxidized at the molybdopterin center and that electrons are shuttled via the FeS clusters to the electron gate FAD and finally to F_{420} (254) (Fig. 9). Like most other F_{420}-dependent enzymes (255), hydride transfer to C-5 of F_{420} is *Si*-face stereospecific (254).

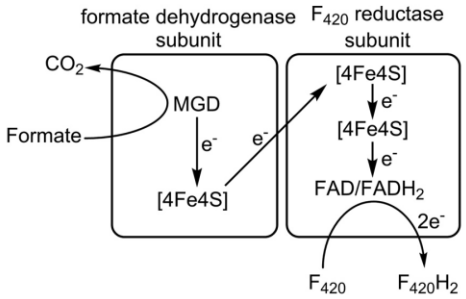

FIG 9 Proposed architecture of Ffd and electron transfer route from formate to F_{420}.

Two pathways that facilitate formate-dependent methanogenesis have been elucidated (Fig. 7). In the first pathway, it has been proposed that electrons derived from formate are funneled through the hydrogenotrophic pathway, with $F_{420}H_2$ and H_2 serving as intermediates (225, 256). First, formate is disproportionated through the combined activity of Ffd (formate + F_{420} → CO_2 + $F_{420}H_2$) and Frh ($F_{420}H_2$ → F_{420} + H_2) (257). Subsequently, the H_2 and CO_2 produced are converted to methane through the hydrogenotrophic pathway (225). More recently, it was proposed that Ffd can form an electron-bifurcating complex with heterodisulfide reductase; in this model, the oxidation of formate simultaneously drives the exergonic reduction of heterodisulfide and endergonic reduction of ferredoxin (258, 259). This pathway is supported through analysis of protein-protein interactions, which indicate that Ffd forms a membrane-bound supercomplex with a heterodisulfide reductase (Hdr) and a hydrogenase subunit (VhuD) (259, 260). Genetic dissection studies likewise show that Ffd but not Frh is essential for formatotrophic growth of *Mc. maripaludis* (259, 261–263). In fact, a suppressor mutant of *Mc. maripaludis* sustains formatotrophic growth when all of its seven hydrogenases are deleted (261). Costa et al. proposed that, in addition to providing electrons to Hdr, Ffd must also provide $F_{420}H_2$ to sustain the central reactions catalyzed by Mer and Mtd in the methanogenesis pathway (259).

As with Frh, methanogens have evolved selenium-free and selenium-containing variants of the Ffd. Whereas *Mb. formicicum* carries a gene that encodes a single Ffd, *Methanococcus vannielii* carries genes that encode both selenium-free and selenium-containing variants of the Ffd (185, 264). Selenium supplementation markedly stimulates formate-driven growth of the organism, suggesting that the selenocysteine-containing Ffd may be the more efficient variant (265). In contrast, both Ffd variants in *Mc. maripaludis* are selenoproteins (266); hence, the organism requires the presence of selenium to grow on formate (267, 268). Genetic dissection has demonstrated that each homolog confers a competitive growth advantage, with single mutants impaired and double mutants unviable for formatotrophic growth (242). Interestingly, while some *Methanosarcina* species carry genes that encode Ffd homologs (269), methanogens with cytochromes cannot sustain formate-dependent growth. Thauer et al. rationalize that the high H_2 threshold of these organisms compared to other methanogens

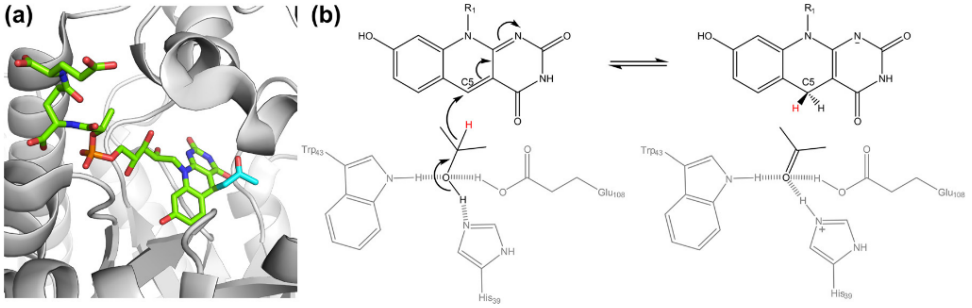

FIG 10 Structure of the active site of Adf. (a) Cartoon representation of the protein (PDB ID 1RHC [49]) showing the bound F_{420}-acetone adduct. (b) Proposed mechanism of isopropanol reduction to acetone (49). R_1 is the ribitylphospholactyl-oligoglutamate chain of F_{420}.

means that they would not be able to competitively oxidize H_2 produced from formate metabolism (182). An alternative explanation is that they lack the electron-bifurcating systems required to efficiently couple formate oxidation to growth (259).

3.2.3. Adf: F_{420}-reducing secondary alcohol dehydrogenase

Some methanogens are capable of low-yield growth using alcohols as electron donors. Whereas methanogens oxidize primary alcohols (e.g., ethanol) using standard NADP-reducing alcohol dehydrogenases (Adh) (22, 270), some can also metabolize secondary and cyclic alcohols using a phylogenetically unrelated class of F_{420}-dependent secondary alcohol dehydrogenases (Adf) (271, 272). The enzymes that mediate this are sparsely distributed, encoded by genes on just six sequenced methanogens in the NCBI database, all of the class *Methanomicrobia*. The $F_{420}H_2$ generated from the reduction of secondary alcohols (e.g., isopropanol, butan-2-ol) to ketones (e.g., acetone, butanone) is, in turn, used to sustain the CO_2-reducing pathway of methanogenesis and other cellular reductive processes (271, 272). Adf belongs to the bacterial luciferase superfamily (TIM barrel protein fold), which also includes other F_{420}-dependent enzymes Fgd (163), Mer (48), and Fht (155). As with other enzymes of the luciferase superfamily, crystallographic analysis shows that Adf from *Methanoculleus thermophilicus* is dimeric, containing a nonprolyl *cis* peptide bond toward the *Re*-face of F_{420} that keeps the 5-deazaflavin rings in a bent "butterfly" conformation (49). The structure contains the inactive F_{420}-acetone adduct (Fig. 10) (thought to form due to acetone accumulation in the presence of oxidized F_{420} in a reductive environment); small secondary alcohol substrates, such as isopropanol, bind in the same pocket in the active enzyme (49). Hydride transfer occurs on the *Si*-face of the cofactor, facilitated by the abstraction of a proton from the alcohol by a catalytic histidine residue and the stabilization of the alcoholate anion transition state by nearby tryptophan and glutamate residues (49, 273).

3.3. $F_{420}H_2$-Dependent Reductases

3.3.1. Mtd: F_{420}-reducing methylene-H_4MPT dehydrogenase/Mer: $F_{420}H_2$-dependent methylene-H_4MPT reductase

In all methanogenesis pathways, tetrahydromethanopterin (H_4MPT) serves as the carrier of one-carbon (1C) units (158, 274). 1C units can be conjugated to H_4MPT in various oxidation states, including formyl (CHO-H_4MPT), methenyl (CH≡H_4MPT), methylene (CH_2=H_4MPT), and methyl (CH_3-H_4MPT). In hydrogenotrophic and formatotrophic methanogenesis, CO_2 is activated through three F_{420}-independent initial steps (Fig. 7). The resultant methenyl-H_4MPT adduct is reduced to methylene-H_4MPT and methyl-H_4MPT via two successive F_{420}-dependent steps. The first is catalyzed by the F_{420}-reducing methylene-H_4MPT dehydrogenase (Mtd; $CH{\equiv}H_4MPT^+ + F_{420}H_2 \rightarrow CH_2{=}H_4MPT + F_{420} + H^+$) (18, 275–278). The second is catalyzed by the $F_{420}H_2$-dependent methylene-H_4MPT reductase (Mer; $CH_2{=}H_4MPT + F_{420}H_2 \rightarrow CH_3\text{-}H_4MPT + F_{420}$) (279–284). Reflecting the standard redox potentials of F_{420}, methylene-H_4MPT, and methenyl-H_4MPT (Table 1), these reactions are physiologically reversible. Hence, Mer and Mtd can also be used to oxidize CH_3-H_4MPT to $CH{\equiv}H_4MPT^+$ with the concomitant reduction of two mole equivalents of F_{420} (156, 157). This is particularly important in the oxidative arm of the methylotrophic methanogenesis pathway, which generates reducing agents ($F_{420}H_2$, Fd_{red}) through the oxidation of CH_3-S-CoM (coenzyme M) to CO_2 (Fig. 7) (157).

A succession of crystal structures of Mtd and Mer have revealed much about their architectures and mechanisms. The structure of Mtd from *Methanopyrus kandleri* revealed a unique protein fold compared to other F_{420}-binding proteins (47, 166, 285, 286). Whereas most F_{420}-binding proteins adopt bacterial luciferase-like (TIM barrel) (163), FDOR-like (split β-barrel) (30), or FdrB-like (novel αβ fold) (150) protein folds, Mtd folds into a unique tertiary structure (47, 166) (Fig. 6). Each protein chain of the homohexameric complex of Mtd (a trimer of dimers) contains an αβ domain, a smaller helical bundle domain, and a C-terminal sheet segment (47). Methenyl-H_4MPT and $F_{420}H_2$ bind opposite each other at the active site, which is located between the two domains and capped by the loop segment of the adjacent chain (Fig. 11) (166). The reaction is catalyzed through a ternary complex mechanism (276, 284), wherein hydride transfer occurs between C-14a of methylene-H_4MPT (*Re*-face stereospecific) and C-5 of $F_{420}H_2$ (*Si*-face stereospecific) (166, 287–289). Crystal structures of Mer homologs have been solved from three organisms, *Methanoplanus kandleri* (159), *Methanothermobacter marburgensis* (159), and *Methanosarcina barkeri* (48). As a member of the bacterial luciferase superfamily, Mer contains a characteristic TIM barrel fold and a nonprolyl *cis*-peptide bond close to the F_{420}-binding site (48, 159). Modeling studies indicate that methylene-H_4MPT and $F_{420}H_2$ are likely to bind opposite each other to

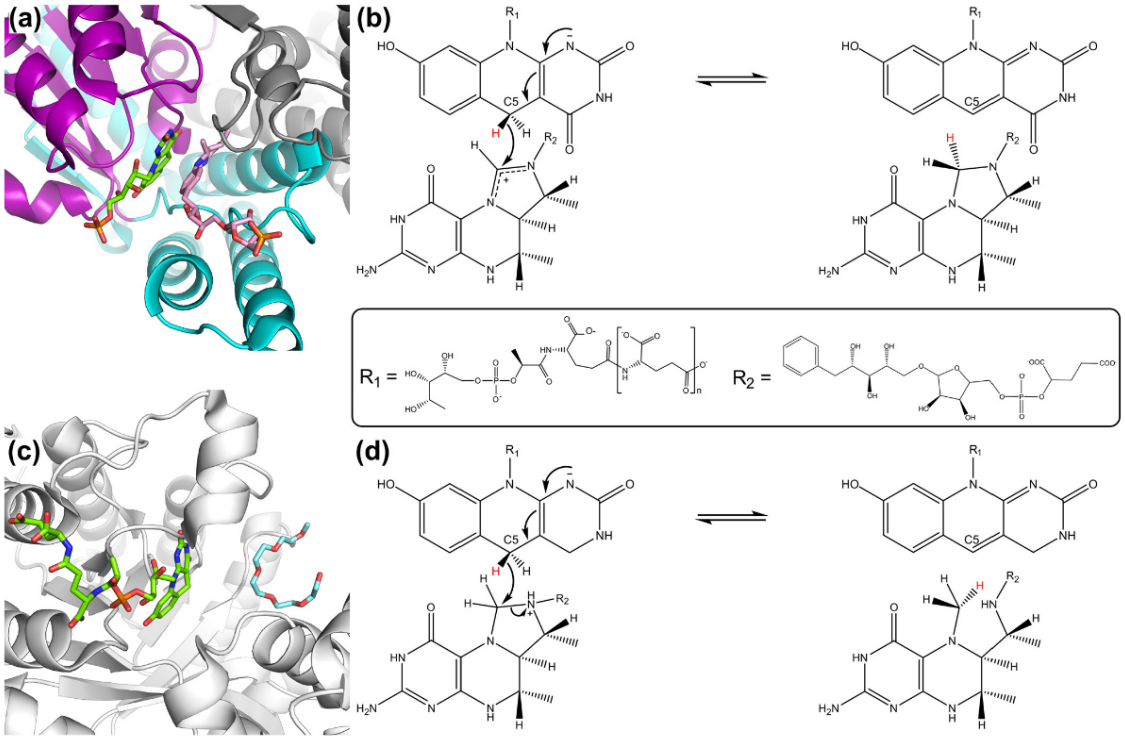

FIG 11 Structure and mechanism of $F_{420}H_2$-dependent hydride transfers to one-carbon compounds conjugated to tetrahydromethanopterin. (a) Structure of Mtd (PDB ID 3IQE [166]) as a ternary complex with F_{420} (green) and methenyl-H_4MPT$^+$ (pink). The large αβ-domain of a single subunit is shown in purple, and the helical bundle domain is shown in cyan. The secondary subunit in the dimer is shown in gray. (b) Mechanism of hydride transfer between $F_{420}H_2$ (*Si*-face) and methenyl-H_4MPT$^+$ (*Re*-face) leading to methylene-H_4MPT production (166). (c) Structure of Mer (PDB ID 1Z69 [48]) as a ternary complex with F_{420} (green) and polyethylene glycol (blue) occupying the methylene-H_4MPT-binding site. (d) Inferred mechanism of hydride transfer between $F_{420}H_2$ (*Si*-face) and methylene-H_4MPT (*Re*-face) leading to methyl-H_4MPT production (166).

form a ternary complex like in Mtd (48), enabling direct hydride transfer in a stereospecific manner (289) (Fig. 11).

In four of the methanogenic orders, the fourth step in the CO_2 reduction pathway can be effected using H_2 instead of F_{420} (Fig. 7) (183). The methylene-H_4MPT hydrogenase (Mth; also known as the [Fe]-hydrogenase, the H_2-forming methylenetetrahydromethanopterin dehydrogenase, and Hmd) directly reduces methenyl-H_4MPT to methylene-H_4MPT using H_2 ($CH{\equiv}H_4MPT^+ + H_2 \rightarrow CH_2{=}H_4MPT + H^+$) (290–292). Several transcriptome analyses have indicated that, while the F_{420}-dependent route is constitutive, the H_2-dependent route predominates at high H_2 partial pressures (pH_2) that induce rapid growth (293–295). Consistently, Mtd mutants of *Methanobacter thermoautotrophicus* are unable to grow at low pH_2 (296). Methanogens can also reduce F_{420} using H_2 through the combined action of Mth ($CH{\equiv}H_4MPT^+ + H_2 \rightarrow CH_2{=}H_4MPT + H^+$) and Mtd ($CH_2{=}H_4MPT + F_{420} + H^+ \rightarrow CH{\equiv}H_4MPT^- + F_{420}H_2$) (the net reaction is $H_2 + F_{420} \rightarrow F_{420}H_2$) (225, 297). Hendrickson and Leigh demonstrated through genetic dissection in *Mc. maripaludis* that this Mth-Mtd cycle can fully compensate for Frh during hydrogenotrophic growth; the pathways could be eliminated separately, but not together (225). Transcriptional and biochemical studies on *Methanothermobacter marburgensis* (*Mt. marburgensis*) have suggested that the Mth-Mtd cycle is particularly important during nickel-limiting conditions when the F_{420}-reducing [NiFe]-hydrogenase cannot be synthesized (297, 298).

Homologs of Mtd and Mer are also present in sulfate-reducing archaea (299, 300). *Archaeoglobus fulgidus* converts lactate to three molecules of carbon dioxide using an Mtd/Mer-facilitated 1C pathway similar to methylotrophic methanogenesis (133, 300). The $F_{420}H_2$ produced by Mtd and Mer can be subsequently respired through a sulfate-reducing electron transport chain (200). It has also been proposed that these enzymes operate during the reverse methanogenesis pathway of anaerobic methanotrophic archaea (ANME). In support of this, genes encoding homologs of Mtd and Mer have been found in some reconstructed ANME metagenomes (21, 137, 215). Heterologously expressed Mtd from an ANME-1 archaeon catalyzed the same reaction as Mtd from methanogens, with similar catalytic specificity and cofactor dependence (214). In addition to F_{420}-dependent enzymes, NAD(P)-dependent methylenetetrahydromethanopterin dehydrogenases have been characterized that have central roles in the formaldehyde assimilation pathways of aerobic methylotrophic bacteria (301, 302).

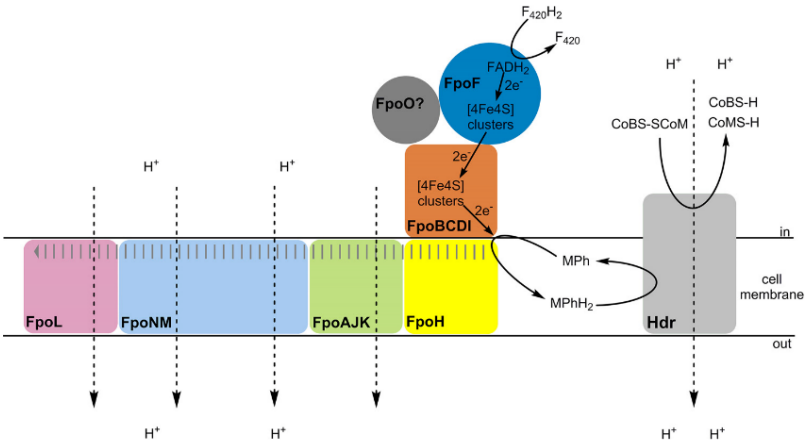

FIG 12 Model of respiration in *Methanosarcina mazei* using $F_{420}H_2$ as an electron donor and heterodisulfide as an electron acceptor. In this system, the primary dehydrogenase is the proton-translocating $F_{420}H_2$-dependent methanophenazine reductase (Fpo) and the terminal reductase is methanophenazine-dependent heterodisulfide reductase (Hdr). Arrangement of Fpo subunits and the proposed electron and proton transfer pathways are inferred from the homology of the system to bacterial complex I (Nuo) (317, 319, 320). Gray lines show the propagation of conformational change in the E channel (FpoAJKH) and antiporter (FpoNML) modules upon electron transfer to methanophenazine ($MPh/MPhH_2$), and dashed arrows show possible routes for proton transfer based on structural analysis of complex I. The protein topology of Hdr is not shown in detail.

3.3.2. Fpo: $F_{420}H_2$-dependent methanophenazine reductase/Fqo: $F_{420}H_2$-dependent quinone reductase

The single order of methanogens containing cytochromes, i.e., the *Methanosarcinales*, can translocate protons by coupling the oxidation of $F_{420}H_2$ to the reduction of heterodisulfide (CoM-S-S-CoB). It was initially thought that this activity was mediated by a single hypothetical enzyme complex, the $F_{420}H_2$:heterodisulfide oxidoreductase (303). However, it is now appreciated that this system is in fact formed from two respiratory complexes (304–306), the $F_{420}H_2$-dependent methanophenazine reductase (Fpo) (162) and the methanophenazine-dependent heterodisulfide reductase (Hdr) (307), which are linked by the redox-active membrane-diffusible cofactor methanophenazine (305, 308–310) (Fig. 10). Constituting the primary dehydrogenase, Fpo is a respiratory proton pump exclusive to the order *Methanosarcinales* (162). Serving as the terminal reductase, Hdr is anchored to the membrane by a *b*-type cytochrome (307, 311, 312). Together, these enzymes translocate four protons (two each through Fpo and Hdr) per molecule of $F_{420}H_2$ that is oxidized (303). In contrast, the Hdr-linked complexes of methanogens without cytochromes are primarily cytosolic and do not serve a respiratory role (182).

The complete Fpo complex has been purified from only a single species, *Methanosarcina mazei* (*Ms. mazei*) (162, 313–315). The complex is very similar to bacterial NADH:ubiquinone oxidoreductase I (Nuo; also known as complex I) in both overall subunit composition and amino acid sequence (316, 317). The Fpo complex is formed of 13 subunits that associate into a hydrophilic portion (FpoFBCDIO) and a transmembrane portion (FpoAHJKNML) (162, 318). The hydrophilic electron input (FpoF) and electron output (FpoBCDI) modules catalyze electron transfer from $F_{420}H_2$ to methanophenazine and are largely conserved with Nuo. However, there are several key differences: an $F_{420}H_2$-oxidizing subunit (FpoF) replaces the NADH-oxidizing module (NuoEFG), the phenazine-reducing subunit (FpoD) has a modified binding pocket compared to its quinone-reducing equivalent (NuoD), and a subunit of unknown function (FpoO) is present. The remaining hydrophobic portion of Fpo is embedded in the membrane, consisting of the proton-translocating E-channels (FpoAJKH) and Mrp antiporter-like channels (FpoNML) that are homologous to those in Nuo (316, 317, 319). Unlike Nuo, which pumps four protons per two input electrons, the Fpo complex is thought to translocate two protons per molecule of $F_{420}H_2$ (162). On the basis of the structure of bacterial Nuo (319, 320), a basic model for the mechanism of Fpo has be proposed (Fig. 12): electrons are transferred from $F_{420}H_2$ to methanophenazine, methanophenazine reduction propagates conformational changes to the E-channel and in turn the antiporter module, and two protons are subsequently translocated through half-channels via conserved lysine and glutamate residues.

During methylotrophic methanogenesis, it is proposed that the $F_{420}H_2$ formed serves as the major respiratory electron donor (Fig. 7). In this pathway, one-carbon compounds (e.g., methanol, methylamine) are activated to produce methyl-coenzyme M (methyl-S-CoM) and thereafter converted to CO_2 or methane; the oxidative branch yields $F_{420}H_2$ via the Mer and Mtd reactions, while the reductive branch generates proton motive force by coupling $F_{420}H_2$ oxidation to heterodisulfide reduction (318, 321). Consistently, trimethylamine-cultured Δ*fpo* mutants of *Ms. mazei* are severely compromised in growth and methane formation compared to the wild-type strain (193). Surprisingly, these findings do not extend to *Ms. barkeri*; in this organism, Fpo appears to be dispensable for methylotrophic growth, whereas Frh is essential (224). On this basis, Kulkarni et al. (224) in Metcalf's laboratory have proposed that H_2 is an intermediate during methylotrophic growth wherein electrons from the $F_{420}H_2$ produced by Mer and Mtd may be used to drive H_2 production by Frh. The H_2 produced is in turn reoxidized via a hydrogenase (Vhu) that can reduce methanophenazine to facilitate heterodisulfide reduction by Hdr,

thereby bypassing the need for Fpo (224). Frh activity is consistently 10-fold higher in *Ms. barkeri* than in *Ms. mazei*; hence, Frh may be able to fully substitute or compensate for loss of Fpo activity only in the former organism (193). Fpo is also likely to be dominant during methylotrophic growth in *Methanosarcina acetivorans*, which exhibits low levels of hydrogenase expression and activity (322, 323).

Beyond methylotrophic methanogenesis, several other roles have been proposed for the Fpo system. For example, the proton gradient generated by Fpo is thought to contribute to ATP synthesis during hydrogenotrophic methanogenesis, while H_2 oxidation can be coupled to methanophenazine reduction directly (via the methanophenazine-reducing hydrogenase), F_{420} is also sometimes preferentially used as an intermediate (through the combined activities of Frh and Fpo) (182, 224). There is also evidence that Fpo contributes to the growth of *Methanosarcina barkeri* on carbon monoxide (324). More recent work also suggests that FpoF may sometimes function as a cytosolic enzyme independently of the other membrane-bound Fpo components in certain methanogens (193, 325). Consistently, the *fpoF* gene is genomically separated from the rest of the *fpo* operon in several *Methanosarcina* species (269, 326), and the protein is expressed at high levels in the cytosolic fraction of *Ms. mazei* cells (193). FpoF from *Ms. mazei* can slowly, but specifically, catalyze electron transfer from Fd_{red} to F_{420} (Fig. 7), which may help to maintain redox balance among methanogenic cofactors (193). Interestingly, members of the genus *Methanosaeta* (part of the order *Methanosarcinales*) contain a variant of Fpo (*fpoABCDHIJKLMNO*) that lacks the $F_{420}H_2$-oxidizing subunit FpoF and instead may be dependent on another reducing agent, e.g., Fd_{red} (196, 327).

A related multimeric membrane-bound proton-translocating complex is also present in some nonmethanogenic archaea (198). The enzyme appears to serve as an $F_{420}H_2$-dependent menaquinone reductase (Fqo) during sulfate respiration of *Archaeoglobi* (198, 199). Transcriptome analysis has shown that Fqo is constitutively expressed at high levels in *Archaeoglobus fulgidus* together with the other respiratory chain components (200). The enzyme is composed of 11 subunits that assemble in a manner similar to Fpo in methanogenic archaea, but it likely reduces menaquinone rather than methanophenazine via the FqoD subunit (199). Homologous enzymes are also encoded by some ANME archaea (e.g., *Methanoperedens nitroreducens*) and are proposed to input electrons derived from methane oxidation into sulfate- and nitrate-reducing respiratory chains (21, 215, 328).

3.3.3. Fpr: $F_{420}H_2$-dependent oxidase

Among the more recently discovered F_{420}-binding proteins, the physiological role of the $F_{420}H_2$-dependent oxidases (Fpr/FprA) is to catalyze the four-electron reduction of dioxygen (O_2) to water (H_2O) in methanogens (161, 192). In contrast to terminal oxidases, these enzymes are not linked to respiratory chains and instead appear to have evolved to detoxify O_2. Encoded in the genomes of five of the six presently recognized orders of methanogens (173), the $F_{420}H_2$ oxidases are part of the flavodiiron protein family, which have been implicated in O_2 and/or NO detoxification in microorganisms across all three domains of life. The methanogen enzymes share particularly high sequence identity (~40%) to the reductases in the anaerobic bacteria *Moorella thermoacetica* and *Desulfovibrio vulgaris* (52, 329), but they use $F_{420}H_2$ rather than an additional rubredoxin domain containing $FMNH_2$ as the reductant. Fpr has been correlated with the ability of methanogens such as *Methanobrevibacter arboriphilus* and *Methanothermobacter marburgensis* (*Mt. marburgensis*) to efficiently scavenge micromolar concentrations of O_2 in their environment (192). Although yet to be confirmed through genetic dissection, it has been hypothesized that such enzymes are responsible for the surprising and potentially ecologically significant aerotolerance of many members of the methanogens (all obligate anaerobes) (192, 330, 331). Some methanogens carry genes that encode multiple isozymes (e.g., *Mt. marburgensis* encodes three FprA homologs) (332), though it has yet to be resolved whether they are differentially regulated and kinetically distinct.

X-ray crystal structures of Fpr from *Methanothermobacter marburgensis* have been determined. They reveal that each monomer of this homotetrameric enzyme binds a diiron center, an FMN cofactor, and a solvent-diffusible $F_{420}H_2$ molecule (161, 192, 255). The enzyme forms a functional homodimer, with the diiron center of one subunit associating with the FMN cofactor of another (161). The structure of this enzyme has been solved in three conformational states (reduced-active, oxidized-active, and oxidized-inactive states) by altering the oxygen exposure of the protein crystals prior to data collection (161). This has enabled the elucidation of the probable catalytic mechanism for this protein (Fig. 13). Dioxygen binding occurs at the reduced-active state [Fe(II)Fe(II)$FMNH_2$], where the $F_{420}H_2$-binding site adjacent to FMN is in a "closed" conformation. The oxygen molecule forms a peroxo intermediate that bridges the diiron center and is reduced to release two water molecules through a diferric transition state. This forms the oxidized-active state of the enzyme [Fe(III)Fe(III)FMN], inducing conformational changes to "open" the $F_{420}H_2$-binding site. Two subsequent $F_{420}H_2$ molecules can then bind in a *Si-Si* conformation adjacent to the oxidized FMN, reducing both the diiron center and FMN to regenerate the reduced-active state. The enzyme also adopts a third oxidized-inactive state where the iron ion closest to FMN is displaced. An additional iron ion is also present, which locks the $F_{420}H_2$-binding site in the "open" state, preventing oxygen binding. This is hypothesized to occur in the presence of excess oxygen to prevent loss of reducing power (161).

3.3.4. Fsr: $F_{420}H_2$-dependent sulfite reductase

The $F_{420}H_2$-dependent sulfite reductase (Fsr) catalyzes the six-electron reduction of sulfite to sulfide (51). Discovered by Johnson and Mukhopadhyay, the enzyme appears to have a dual role in methanogens: detoxification of sulfite and growth on sulfite as the sole sulfur source (51, 191). While sulfite is generally inhibitory for growth of methanogens (e.g., *Methanococcus maripaludis*) (191, 333), diverse species are able to utilize it as a sole sulfur source (e.g., *Methanocaldococcus jannaschii*) (51, 334, 335). *Mc. maripaludis* can be rendered sulfite tolerant through recombinant expression of *Mc. jannaschii* Fsr (191). Fsr purified from *Mc. jannaschii* rapidly catalyzes sulfite reduction using $F_{420}H_2$ (51). The single-subunit enzyme appears to have arisen through the fusion of an $F_{420}H_2$-binding protein with a sulfite reductase (336, 337): the N-terminal domain is homologous to the FhrB-like domains of other $F_{420}H_2$ dehydrogenases, while the C-terminal domain is similar to siroheme-containing dissimilatory sulfite reductases (51). It is therefore proposed that, as in Frh, Ffd, and Fpo (Fig. 8, 9, and 12), $F_{420}H_2$ is oxidized at the N-terminal domain and electrons are funneled to the C-terminal domain via a possible flavin,

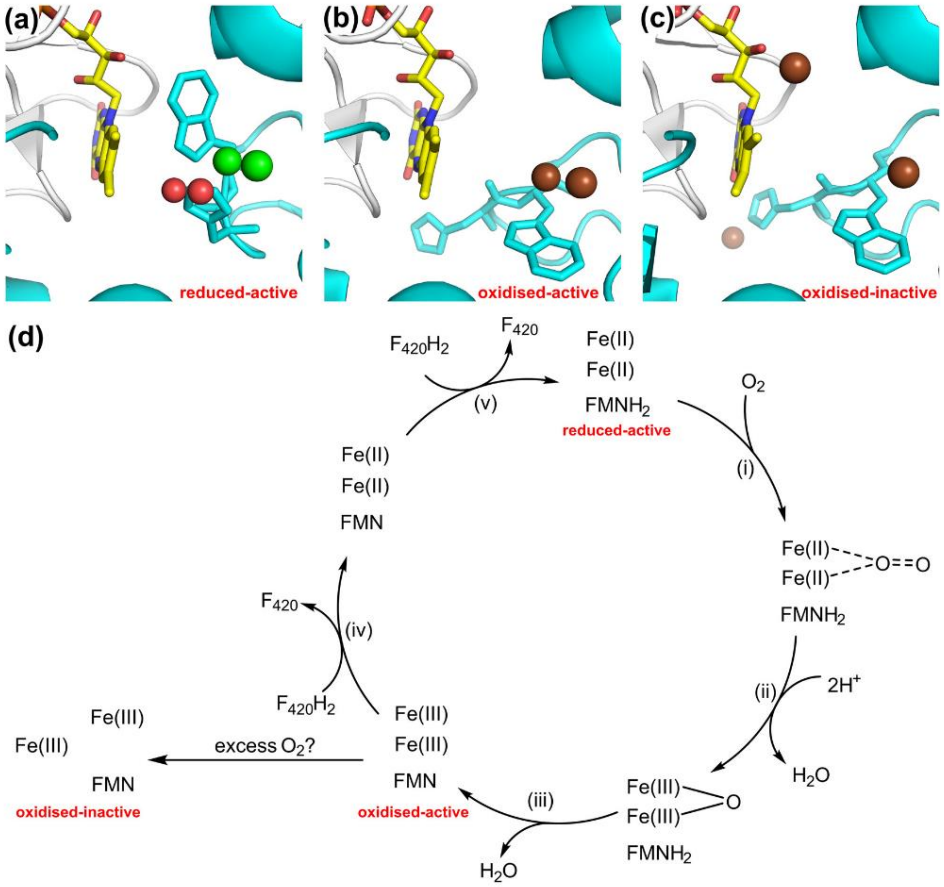

FIG 13 Summary of $F_{420}H_2$-dependent oxygen detoxification by Fpr. The mechanism was inferred based on the three crystallographic states of the active site (161): (a) the reduced-active state where the $F_{420}H_2$-binding site adjacent to FMN is "closed" by a loop with bulky aromatic residues (PDB ID 2OHI), (b) the oxidized-active state where the $F_{420}H_2$-binding site is "open" due to conformational changes in the loop (PDB ID 2OHH), and (c) the oxidized-inactive state where one iron atom in the diiron center is displaced and an additional third iron is present locking the loop in the "open" state (PDB ID 2OHJ). Fe(III) is shown in green, Fe(II) is shown in brown, water molecules at the predicted dioxygen-binding site are red, and FMN is in yellow. (d) Catalytic mechanism of Fpr. The five steps are shown as follows. (i) Transient binding of dioxygen to the reduced-active state; (ii) oxidation of the diiron center with the release of a water molecule; (iii) oxidation of FMN to release the second water molecule; (iv) reduction of the diiron center via FMN at the oxidized-active state, which binds $F_{420}H_2$ as an electron donor; (v) reduction of FMN by a second $F_{420}H_2$ molecule.

an [4Fe4S] cluster, and siroheme, where the sulfite is subsequently reduced (337). The enzyme appears to be sensitive to oxygen, but it can be reactivated by cellular thioredoxins (338). Other than Fsr, some methanogens can also mobilize sulfite using the P_{590}-type sulfite reductases (339), the physiological role of which are still incompletely resolved (336).

3.3.5. Fno: $F_{420}H_2$-dependent NADP reductase

In most cases, the catabolic pathways of methanogens reduce F_{420} and ferredoxin, but not nicotinamides. In order to generate NADPH for biosynthetic processes, methanogens instead transfer electrons from $F_{420}H_2$ to NADP (151). This process depends on $F_{420}H_2$:NADP oxidoreductase (Fno), a physiologically reversible enzyme that primarily acts as an $F_{420}H_2$-dependent NADP reductase in methanogens and an F_{420}-reducing NADPH dehydrogenase in bacteria. Fno is present in all six orders of methanogens and can reduce NADP using electrons derived from $F_{420}H_2$ during hydrogenotrophic, formatotrophic, and methylotrophic growth (16, 152, 340). An exception is those methanogens that grow on primary alcohols (e.g., *Methanoculleus thermophilicus*), which instead use an NADP-reducing primary alcohol dehydrogenase (272); in such organisms, Fno serves as an F_{420}-reducing NADPH dehydrogenase that generates sufficient $F_{420}H_2$ to drive the fourth and fifth steps in the CO_2-reducing pathway of methanogenesis (22). In contrast, methanogens that harbor an F_{420}-reducing secondary alcohol dehydrogenase use Fno in the typical NADP-reducing direction (22). Homologous enzymes also appear to bridge catabolic and anabolic processes in *Archaeoglobi* (201) and *Halobacteria* (136).

One of the best-understood F_{420}-dependent enzymes, Fno has

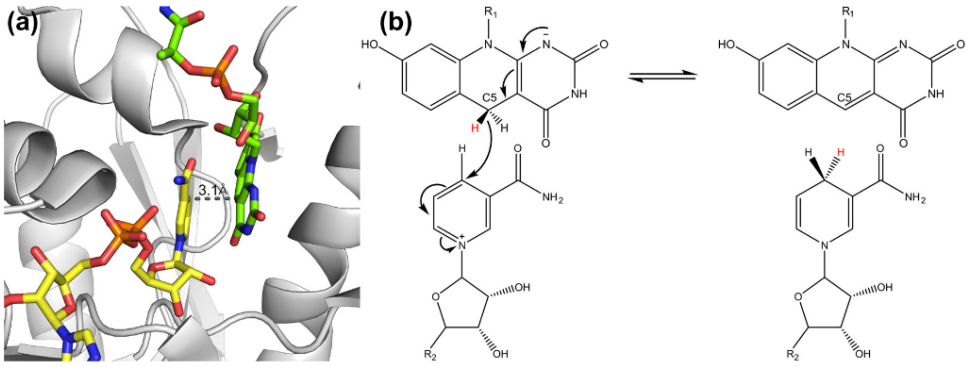

FIG 14 Structure and catalytic mechanism of Fno. (a) Structure of the active site of Fno (PDB ID 1JAY [160]), showing F_{420} and NADP positioned for electron transfer. (b) Hydride transfer mechanism from the *Si*-face of F_{420} to the *Si*-face of $NADP^+$ (160). R_1 is the ribitylphospholactyl-oligoglutamate chain of F_{420}, and R_2 is 2-phosphoadenosine 5-diphosphate.

been purified and characterized from methanogens of the genera *Methanococcus* (341, 342), *Methanothermobacter* (343, 344), *Methanosphaera* (345), and *Methanogenium* (22). The structure of Fno from *Archaeoglobus fulgidus* complexed with F_{420} and NADP gives direct structural insight into its hydride transfer mechanism (Fig. 14). The single-subunit enzyme contains a small C-terminal domain and an N-terminal domain characteristic of a dinucleotide-binding Rossmann fold. The nicotinamide and deazaflavin moieties of the cofactors are bound roughly parallel to each other (*Si*-face to *Si*-face) in a hydrophobic pocket between the domains (160). The aromatic groups are laterally shifted relative to each other, such that the C-4 atom of NADP is positioned exactly above the C-5 atom of F_{420} (201, 346) to allow for hydride transfer at an optimal distance of 3.1 Å. The affinity of F_{420} for Fno increases in the presence of NADP, suggesting that NADP binding facilitates F_{420} binding (160). Consistently, structural comparison between apo- and holoenzymes indicates that NADP binding facilitates a conformational change that induces $F_{420}H_2$ binding and generates a catalytically active ternary complex (160).

3.4. Cofactor F_{390}

Two purinated derivatives of F_{420} are formed in methanogens under certain conditions, and these two derivatives of F_{420} are collectively referred to as F_{390} (347, 348). F_{390}-A and F_{390}-G are formed when F_{420} forms a phosphodiester linkage with AMP and GMP, respectively, via the 8-hydroxy group of the 5-deazaflavin ring (348, 349). Seemingly exclusive to methanogens, F_{390} has been identified in genera as diverse as *Methanothermobacter* (347, 350), *Methanobacterium* (351), *Methanobrevibacter* (330), and *Methanosarcina* (352). Owing to their electron-donating groups, F_{390} compounds have a higher standard redox potential (−320 mV) than F_{420} (−340 mV) and hence may be ideal for sensing or catalytic roles under oxidizing conditions (353). These derivatives are synthesized when methanogens are exposed to oxygen and are hydrolyzed back to F_{420} and AMP/GMP upon reestablishment of anaerobiosis (349). Production depends on an ATP/GTP-dependent F_{390} synthetase of the adenylate-forming superfamily (354–356), while a hydrolase mediates the AMP/GMP-forming hydrolysis reaction (356, 357). As F_{390} synthesis appears to be sensitive to both redox state and oxygenation levels (296, 355), it has been proposed that the cofactor derivative is part of a redox-sensing system that regulates metabolic activity of methanogens. It has been consistently demonstrated that F_{390} synthetase transcription and F_{390} cellular expression levels are correlated with the availability of reductant in *Methanobacterium thermoautotrophicum* (358, 359). However, no genetic or phenotypic studies have been performed to resolve its physiological role. In fact, there has been an almost complete absence of literature on this molecule over the last 2 decades.

4. F_{420} IN MYCOBACTERIA AND OTHER BACTERIA

4.1. Physiological Roles

4.1.1. Mycobacteria

Relatively little is known about the roles of F_{420} in bacteria. The cofactor has been experimentally shown to be synthesized in only one bacterial phylum thus far, *Actinobacteria*, where it has mainly been studied for its roles in secondary, rather than primary, metabolism. Nevertheless, a number of recent phenotypic and biochemical studies have shed light on the endogenous roles of F_{420} in mycobacteria, an actinobacterial genus of major medical and environmental significance (360, 361). F_{420} is synthesized and reduced by all members of the genus *Mycobacterium*, including saprophytes (e.g., *M. smegmatis*, *M. fortuitum*), opportunistic pathogens (e.g., *M. avium*, *M. kansasii*), and the causative agents of tuberculosis (*M. tuberculosis* complex) and leprosy (*M. leprae*) (20, 125, 145). The observation that F_{420} is synthesized even in *M. leprae*, rendered an unculturable, host-dependent organism through massive genome decay (362), suggests that it has an evolutionarily conserved central role in mycobacterial metabolism. In contrast to methanogens, F_{420} is not essential for the viability of mycobacteria under ideal conditions: F_{420} biosynthesis (*fbiC*) and reduction (*fgd*) genes have been successfully deleted or disrupted in *M. smegmatis* (28, 31, 132, 363), *M. tuberculosis* (32, 35), and *M. bovis* (72). However, there is a range of evidence that F_{420} contributes to the notorious ability of mycobacteria to persist in deprived and challenging environments (56). Mycobacteria that are unable to synthesize F_{420} are unable to survive oxygen deprivation, oxi-

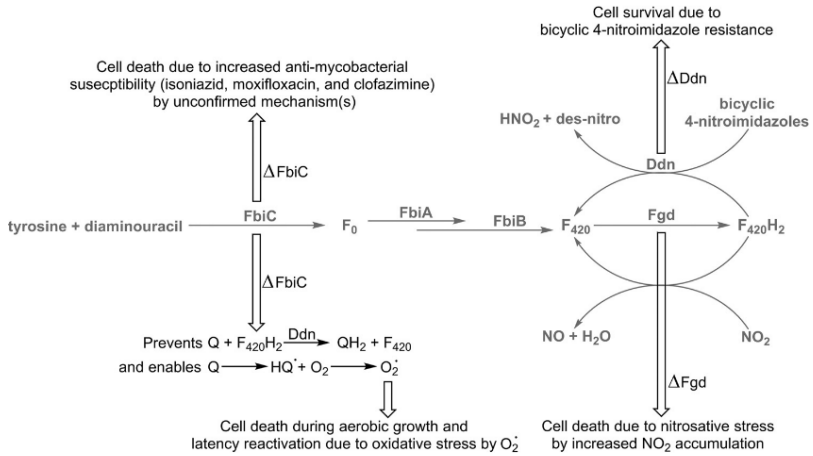

FIG 15 Pleiotropic phenotypes associated with loss of function of F_{420} in mycobacteria. Relevant reactions in the F_{420} biosynthesis and utilization pathway are shown in gray. Hollow arrows show observed chemical and phenotypic effects due to loss-of-function mutations in specific enzymes in the pathway. Q, quinone; QH_2, dihydroquinone; $HQ^{\bullet}$, semiquinone.

dative stress, nitrosative stress, or antibiotic treatment (Fig. 15) (31, 32, 363).

Several F_{420}-dependent enzymes have been functionally annotated in mycobacteria. Pathogenic mycobacteria such as *M. tuberculosis* encode F_{420}-reducing hydroxymycolic acid dehydrogenases (fHMAD) that oxidize hydroxymycolic acids to ketomycolic acids in the cell wall (364, 365). These mycolic acid derivatives appear to influence the integrity and permeability of the cell envelope, which renders them less sensitive to cytotoxic agents such as antibiotics (366–368). Preliminary data indicate that a subgroup of the flavin/deazaflavin oxidoreductase superfamily (FDOR-AAs) may also be involved in fatty acid modification (30). Other members of this superfamily (FDOR-Bs) reduce the degradation products formed during heme oxygenation (30): biliverdin (produced by host heme oxygenase-1 and mycobacterial HugZ in the CO-generating pathway) and possibly mycobilin (produced by mycobacterial MhuD in the CO bypass pathway) (369–371). Our biochemical studies have shown that *M. smegmatis* carries a gene that encodes a conserved $F_{420}H_2$-dependent biliverdin reductase that rapidly reduces biliverdin to bilirubin (30), a potent antioxidant (372, 373).

There is also evidence that F_{420} contributes to an oxidative stress response system in mycobacteria. The survival rate of Δ*fbiC* strains of *M. tuberculosis* is 100- to 1,000-fold lower than wild-type cells following challenge with redox cycling agents (i.e., menadione, plumbagin) and antibiotics (i.e., isoniazid, clofazimine) (32). Δ*fgd* strains of *M. smegmatis* are similarly impaired (363). One explanation is that mycobacteria store electrons as glucose-6-phosphate (G6P) and mobilize them using Fgd (F_{420}-dependent glucose-6-phosphate dehydrogenase) in response to oxidative stress; G6P levels in *M. smegmatis* are consistently approximately 100-fold higher than those of *E. coli* during preferential growth conditions, but the levels become depleted following challenge with redox cycling agents (363). $F_{420}H_2$-derived electrons may be used in endogenous redox processes to prevent or reverse damage from reactive oxygen species. For example, it has been proposed that a subgroup of the flavin/deazaflavin oxidoreductase superfamily (FDOR-As) are $F_{420}H_2$-dependent menaquinone reductases that maintain the respiratory chain in a reduced state in response to oxidative stress (32). Several previous reports have demonstrated that the mycobacterial respiratory chain can be remodeled in response to environmental changes (374, 375), and the ability of $F_{420}H_2$ to serve as a respiratory electron donor has already been demonstrated for respiratory archaea (162, 199). However, this hypothesis has yet to be supported with data on phenotypes or energy, and it remains unclear whether purified FDOR-As are capable of reducing menaquinone (30, 32). There is also evidence that mycobacteria instead use electrons liberated from G6P by Fgd to directly detoxify exogenous agents (363). Two independent studies have demonstrated that FDOR-As rapidly reduce menadione and plumbagin using $F_{420}H_2$ (30, 32), and it is also plausible that these highly promiscuous proteins (28, 55) can directly detoxify certain antibiotics too. However, genetic studies have yet to definitively link FDORs to antibiotic resistance and oxidative stress responses.

The potentially related role of F_{420} in nitrosative stress resistance is also perplexing. *M. tuberculosis* transposon mutants of *fbiC* are hypersusceptible to acidified nitrite (376); this was shown through an *in vitro* screen designed to simulate the environment of an activated macrophage, in which inducible nitric oxide synthase (iNOS)-derived NO is oxidized to NO_2^-, acidified into HNO_2, and dismutated into NO and NO_2 (377), which have antimycobacterial properties (378). One study showed that NO_2 is rapidly nonenzymatically reduced to NO by $F_{420}H_2$ under aerobic conditions (31). However, it is likely that F_{420}-dependent enzymatic mechanisms also contribute to nitrosative stress resistance, either through direct detoxification or indirect mechanisms. Indeed, it is possible that F_{420} may confer protection against cytotoxic agents in multiple ways: enhancing physical barriers through cell wall synthesis, direct detoxification by reducing exogenous agents, and maintaining redox balance through endogenous metabolism. Given the diverse roles of

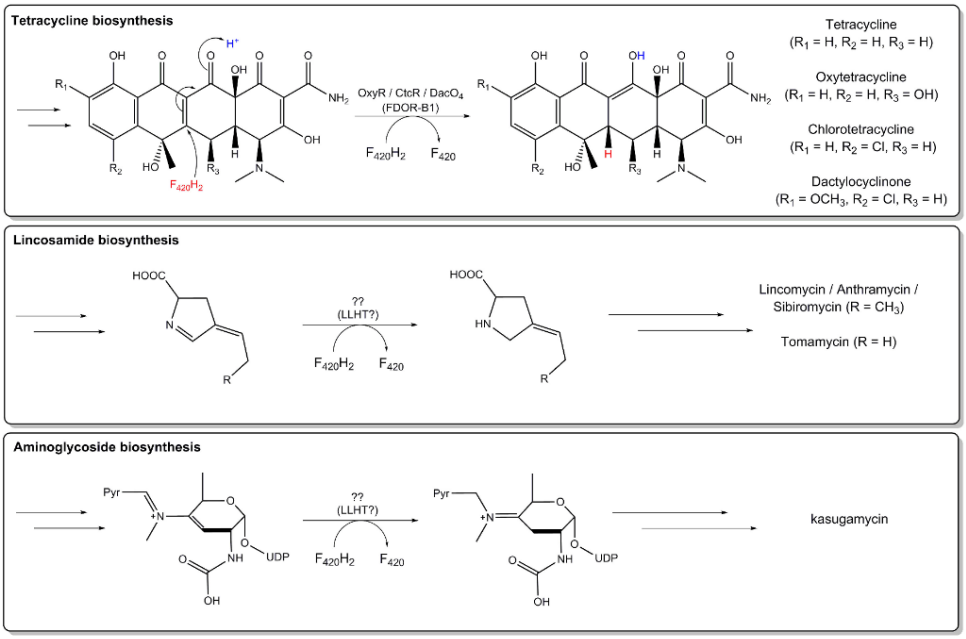

FIG 16 Reactions catalyzed by $F_{420}H_2$-dependent reductases in the biosynthesis pathways of tetracyclines (26), lincosamides (146, 388, 389), and aminoglycosides (394).

F_{420} in mycobacterial metabolism and the pleiotropic phenotypes associated with the cofactor's absence, it seems likely that F_{420} is required for latent tuberculosis infection *in vivo*, though this has yet to be definitively confirmed. In line with this, *M. tuberculosis* strains incapable of synthesizing ketomycolic acids are attenuated in macrophages and mice (366–368). One study surprisingly indicated that transposon mutants of *fbiC* are viable *in vivo* in the murine model of acute infection (379), though it is unclear whether such mutants would be capable of establishing a chronic infection.

4.1.2. Streptomycetes

It is well established that F_{420} is required for the synthesis of tetracycline antibiotics, a group of broad-spectrum aromatic polyketide antibiotics produced by streptomycetes (380). As far back as 1960, McCormick et al. isolated a hydride-transferring cofactor mediating tetracycline biosynthesis (24, 381–383), now known to be F_{420} (29, 122, 384). A combination of genetic and biochemical studies have since shown that an $F_{420}H_2$-dependent reductase (OxyR) catalyzes the final step of oxytetracycline biosynthesis (385), namely, reduction of the C-5a=C-11a double bond of dehydrooxytetracycline (Fig. 16) (29). This enzyme can also perform the equivalent reaction for tetracycline. Closely related enzymes are involved in the same step during biosynthesis of chlorotetracycline (CtcR) and dactylocyclinone (DaCO4) in *Streptomyces aureofaciens* and *Streptomyces rimosus* (29, 386). Encoded by the oxytetracycline (*oxy*), chlorotetracycline (*ctc*), and dactylocyclinone (*dac*) gene clusters (29), these enzymes are members of the flavin/deazaflavin oxidoreductase (FDOR) superfamily (30) and utilize $F_{420}H_2$ reduced through the action of Fno (387).

F_{420} is also required for the synthesis of lincosamide antibiotics by *Streptomyces lincolnensis* strains (146, 388, 389), including lincomycin, the precursor of the clinical semisynthetic antibiotic clindamycin (390). On the basis of the accumulation of 4-propylidene-3,4-dihydropyrrole-2-carboxylic acid by strains unable to biosynthesize F_{420}, it is proposed that an $F_{420}H_2$-dependent reductase catalyzes the reduction of the imine moiety of the dihydropyrrole to tetrapyrrole (Fig. 16) (389, 391). The biosynthesis of other pyrrolobenzodiazepine antibiotics (392) are facilitated by equivalent $F_{420}H_2$-dependent imine reduction steps, namely, tomaymycin (*Streptomyces achromogenes*) (50), sibiromycin (*Streptosporangium sibiricum*) (393), kasugamycin (*Streptomyces kasugaensis*) (394), and anthramycin (*Streptomyces rifuineus*) (395). However, biochemical studies have yet to definitively identify which enzymes are responsible for these reactions. The strongest candidates are the putative $F_{420}H_2$-dependent luciferase-like hydride transferases (LLHTs) encoded in the sequenced antibiotic synthesis gene clusters (50, 391, 393–395) of each of these organisms. Because all research thus far has focused on the roles of F_{420} in the secondary metabolism of streptomycetes, little is known about the roles of this cofactor in central metabolism of this genus; it is likely that streptomycetes use F_{420} to support some important metabolic pathways, as they carry genes that encode homologs of mycobacterial enzymes such as the $F_{420}H_2$-dependent biliverdin reductase (30).

4.1.3. Other actinobacteria

It is established that F_{420} is synthesized in multiple other actinobacterial genera, including *Rhodococcus*, *Nocardia*, and *Nocardioides* (27, 54, 145). However, all studies of such genera have focused on the roles of F_{420} in exogenous substrate reduction, and very little is known about the endogenous roles of F_{420}-dependent processes. The richest literature is on the degradation of picrate (2,4,6-trinitrophenol) and related compounds (e.g., 2,4-dinitrophenol, 2,4-dinitroanisole) (396, 397). A number of actinobacteria, including *Rhodococcus opacus* and *Nocardioides simplex*, are able to mobilize picrate as their sole carbon and nitrogen source (396, 398). This depends on reductive activation of these particularly electron-deficient aromatic compounds using two $F_{420}H_2$-dependent hydride transferases (hydride transferase I [HTI] and hydride transferase II [HTII]) (section 4.3.2) (155). Fno supplies the reductant for this process and is expressed from the same operon as the hydride transferases (54, 155, 396). While polynitroaromatic compounds are anthropogenic, actinobacteria may have evolved the capacity to degrade them from preexisting pathways that metabolize naturally occurring nitroaromatic compounds (e.g., chloramphenicol) (399, 400). It has also been demonstrated that $F_{420}H_2$-dependent oxidoreductases of the flavin/deazaflavin oxidoreductase superfamily have broad substrate specificity; enzymes purified from genera as diverse as *Mycobacterium*, *Frankia*, *Nocardia*, and *Rhodococcus* are capable of reducing coumarin natural products (28, 55). F_{420} may also contribute to the well-reported abilities of soil actinomycetes to biodegrade a wide variety of other polycyclic aromatic hydrocarbons (401). While the physiological advantage of this promiscuity is unclear, it might provide actinobacteria an adaptive or selective advantage to consume or detoxify the wide range of natural products in their respective environments (402, 403).

4.2. F_{420}-Reducing Dehydrogenases

4.2.1. Fno: F_{420}-reducing NADPH dehydrogenase

Fno is the only redox-active F_{420}-dependent protein proven to be conserved between archaea and bacteria. Whereas Fno primarily serves to reduce NADP in methanogens ($F_{420}H_2$-dependent NADP reductases), its homologs generally act in the reverse direction to reduce F_{420} in bacteria (F_{420}-reducing NADPH dehydrogenases) (219); this reflects that, whereas F_{420} is a central catabolic cofactor in methanogens, it is of secondary importance to NADP in the central metabolism of most bacteria (168). While Fno has yet to be structurally characterized in actinobacteria, the enzyme is expected to have a similar structure and mechanism: sequence comparisons and biochemical studies (12) indicate that the overall architecture and cofactor-binding sites are conserved with the archaeal enzyme (section 3.3.5) (160). The $F_{420}H_2$ generated by Fno in bacteria is used for various reductive processes, for example, biosynthesis of tetracycline antibiotics by *Streptomyces* (387) and the mobilization of picrate by *Rhodococcus* and *Nocardioides* species (54, 155).

4.2.2. Fgd: F_{420}-reducing glucose-6-phosphate dehydrogenase

While Fno appears to be the enzyme primarily responsible for F_{420} reduction in most actinobacteria, it is replaced by the F_{420}-reducing glucose-6-phosphate dehydrogenase in several genera, including *Mycobacterium* (Table 2). This enzyme directly links central carbon catabolism in actinobacteria to F_{420} reduction (glucose-6-phosphate + $F_{420} \rightarrow$ 6-phosphogluconolactone + $F_{420}H_2$) (163, 404). First identified in the soil bacterium *M. smegmatis* (148, 404), Fgd has since been identified in multiple other environmental actinobacteria and the obligate pathogens *M. tuberculosis* and *M. leprae* (145). Fgd is either the sole or main source of $F_{420}H_2$ in mycobacteria; neither Δ*fbiC* and Δ*fgd* strains are capable of activating exogenous substrates through $F_{420}H_2$-dependent reactions in *M. tuberculosis* (33, 35) and *M. smegmatis* (28, 363). Fgd therefore appears to have evolved principally as a mechanism to generate $F_{420}H_2$. As elaborated above, there is also evidence that glucose-6-phosphate serves as an electron store in mycobacteria that is mobilized by Fgd in response to oxidative stress (32, 363). The role of Fgd in generating flux through the pentose phosphate pathway appears to be supplementary, given that most mycobacteria also encode conventional NADP-dependent glucose-6-phosphate dehydrogenases (145). An interesting exception may be *M. leprae*, as genome analysis and biochemical studies indicate that it employs F_{420}, but not NADP, for G6P oxidation (145, 362, 405).

The F_{420}-reducing and NADP-reducing glucose-6-phosphate dehydrogenases are not phylogenetically related (148). Fgd is a member of the bacterial luciferase family (163) with a similar TIM barrel structure and catalytic mechanism reminiscent of Adf (49) and Mer (159). The cofactor is accommodated in the active site, with the isoalloxazine rings innermost and the oligoglutamate tail extending into the solvent (Fig. 6), where the isoalloxazine is in a bent butterfly-like conformation due to steric interactions with the protein backbone, including the nonprolyl *cis*-peptide bond behind its *Re*-face (163). The glucose-6-phosphate has been modeled to bind in a positively charged pocket adjacent to the *Si*-face of the deazaflavin (163), similar to what was observed in the ternary complex of the related Adf (Fig. 10). Hydride transfer is thought to occur similarly to Adf (Fig. 17) and is mediated by conserved histidine, tryptophan, and glutamate residues (49, 163): proton abstraction is initiated by the histidine, tryptophan stabilizes the resulting anion transition state, and glutamate is likely to serve as the proton donor for N-2 of the deazaflavin for $F_{420}H_2$ formation (49, 163).

4.2.3. fHMAD: F_{420}-reducing hydroxymycolic acid dehydrogenase

The F_{420}-reducing hydroxymycolic acid dehydrogenase (fHMAD) is responsible for oxidizing hydroxymycolic acids to ketomycolic acids during cell wall biosynthesis (365). A member of the bacterial luciferase family, the enzyme shares 36% sequence identity with Fgd (364). However, in contrast to its original annotation, the enzyme cannot oxidize glucose-6-phosphate (364) and is specific for hydroxymycolic acids (365). The enzyme is translocated through the cell membrane by the Tat pathway and is anchored to the outside of the cell membrane, where it can function in cell wall modification (364). Reflecting the taxonomic distribution of fHMAD (364, 365), ketomycolic acids are distributed in pathogenic mycobacteria (e.g., *M. tuberculosis* complex, *M. avium* complex) but are absent from most soil species (e.g., *M. smegmatis*) (406). Ketomycolic acids appear to be critical for the virulence of *M. tuberculosis*; strains lacking oxygenated mycolic acids have profoundly altered envelope permeability, are hypersusceptible to antibiotics, and are attenuated in macrophages and mice (366–368). Consistent with the synthesis of ketomycolic acids in response to

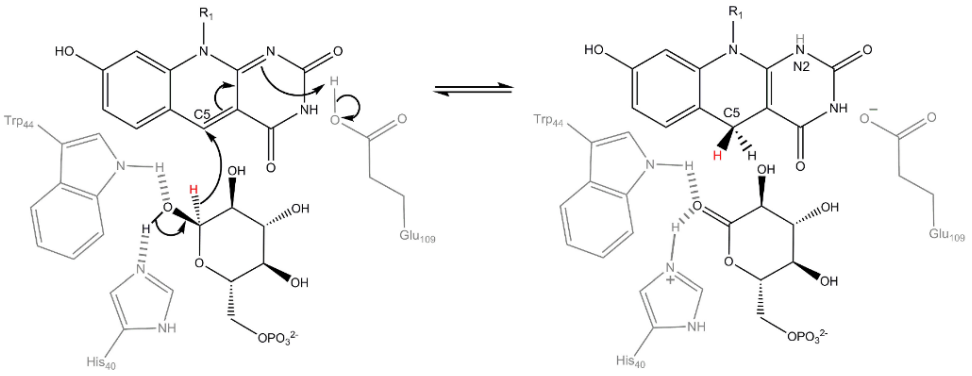

FIG 17 Proposed catalytic mechanism of Fgd (163). F_{420} is reduced to $F_{420}H_2$, and glucose-6-phosphate is oxidized to 6-phosphogluconate.

stress, the gene encoding fHMAD is under the control of the alternative sigma factor SigF in *M. tuberculosis* (407, 408). It was recently confirmed that fHMAD is inhibited by the nitroimidazopyran prodrug pretomanid (PA-824) (365); this interaction may be responsible for the altered mycolic acid composition of pretomanid-treated cells and may contribute to the mode of action of this next-generation bactericidal agent (33).

4.3. $F_{420}H_2$-Dependent Reductases

4.3.1. FDORs: flavin/deazaflavin oxidoreductase superfamily

$F_{420}H_2$-dependent reductases elicit the physiological roles of F_{420} in actinobacteria. They are split into two superfamilies, the flavin/deazaflavin oxidoreductases (FDORs) (30) and the luciferase-like hydride transferases (LLHTs; section 4.3.2) (37). FDORs are small (~150-residue) enzymes that accommodate a cofactor-binding channel and substrate-binding pocket into a split β-barrel fold (30). This superfamily is highly diverse in terms of catalytic activity (reductases, oxidases, and oxygenases), cofactor specificity (F_{420}, FMN, FAD, and heme), and substrate range (30, 409). We have shown that they have diversified into two major families, FDOR-As and FDOR-Bs, that share less than 30% sequence similarity but share the same protein fold (28, 30) (Fig. 18). Proteins from the FDOR-A family are exclusively F_{420}-binding proteins (28, 35, 55, 164, 410) restricted to the phyla *Actinobacteria* and *Chloroflexi* (28, 30, 37). In contrast, FDOR-B proteins are widely distributed, including in bacteria that do not synthesize F_{420}. They include the ubiquitous FMN-dependent pyridoxine/pyridoxamine 5′-phosphate oxidases (PnPOx) involved in vitamin B_6 biosynthesis (411–413), heme oxygenases (HugZ) involved in heme catabolism (414–416), and several groups of uncharacterized FAD-binding proteins (30, 417). *Actinobacteria* and *Chloroflexi* also carry genes that encode multiple $F_{420}H_2$-dependent reductases of the FDOR-B family, which are broadly divided into six subgroups (28, 30, 165, 418, 419). Structural and sequence analyses demonstrate that conserved motifs define cofactor specificity (30); in the case of $F_{420}H_2$-dependent reductases, deazaflavin binding is stabilized by a large hydrophobic groove complementary to the isoalloxazine ring and a positively charged groove that interacts with the oligoglutamate tail (28, 30, 164, 165). Interestingly, unlike all other F_{420}-binding proteins characterized thus far, the most likely substrate-binding pocket of the F_{420}-binding FDORs appears to be toward the *Re*-face of the cofactor (30, 164, 165), similar to the FMN-dependent members of the superfamily (420).

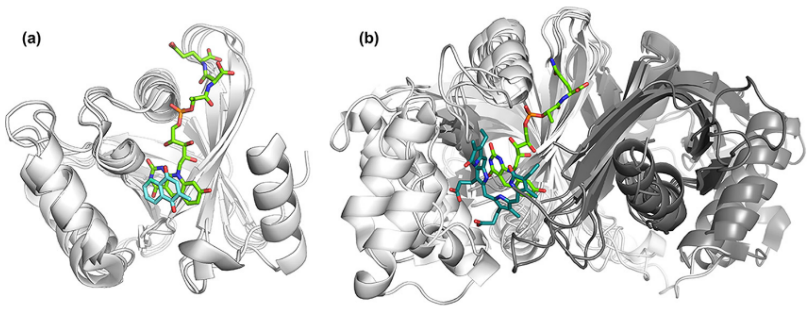

FIG 18 Representative crystal structures of FDOR-A (monomers) and FDOR-B (dimers) proteins. (a) Structures of the quinone-reducing FDOR-A1 proteins MSMEG_2027 (PDB ID 4Y9I [30]) and MSMEG_3356 (PDB ID 3H96 [28]) overlaid with the complex of rv3547 with F_{420} (PDB ID 3R5R [164]) with menadione docked into the active site. (b) Overlay of solved structures of $F_{420}H_2$-dependent FDOR-B proteins. These proteins include the FDOR-B1 proteins rv2991 (PDB ID 1RFE) and MSMEG_3380 (PDB ID 3F7E [28]), FDOR-B2 protein MSMEG_6526 (PDB ID 4ZKY [30]), FDOR-B3 protein rv1155 complexed with F_{420} (PDB ID 4QVB [165]) and FDOR-B4 protein rv2074 (PBD ID 2ASF [419]). Biliverdin, a substrate of FDORs B3 and B4, is docked at the active site (30).

In mycobacteria, there is a multiplicity of $F_{420}H_2$-dependent reductases of the FDOR family: 30 in *M. smegmatis*, 15 in *M. tuberculosis*, and 3 in *M. leprae* (30). As most of these enzymes remain to be functionally annotated, the reasons behind the extreme expansion and diversification of this superfamily remain unclear. The highly diverse architecture of the substrate-binding sites of these proteins, concurrent with a high degree of conservation of the F_{420}-binding site, suggests that they have evolved to catalyze the $F_{420}H_2$-dependent reduction of a variety of substrates (30). Some subgroups (e.g., FDOR-B2s, FDOR-B4s) are tightly phylogenetically clustered and have probably been constrained for a specific function (30). In contrast, representatives of the manifold subgroup FDOR-A1 exhibit broad and overlapping substrate specificities (28, 30). Such enzymes are capable of reducing a wide range of exogenous substrates, including coumarin natural products such as fungus-derived aflatoxins and plant-derived furanocoumarins (e.g., angelicin, methoxsalen) (28, 55). They also show potent activity against redox cycling agents such as menadione and plumbagin (30, 32). The physiological role of these enzymes may therefore be to detoxify a wide range of oxidizing agents in their environment using electrons channeled from G6P. The absence of such detoxification systems may contribute to the profound sensitivity of Δ*fbiC* and Δ*fgd* mutants to redox cycling agents and antibiotics, as discussed in section 4.1.1 (32, 363). Consistent with a role in detoxification or biodegradation, there is some evidence from expression studies (28, 30, 164) and proteome analyses (421, 422) that these enzymes are bound to the membrane through their N termini. Another enzyme of this class, rv3547 (Ddn; deazaflavin-dependent nitroreductase) has also attracted much attention for its role in the activation of nitroimidazole prodrugs (e.g., pretomanid, delamanid) by *M. tuberculosis* (section 5.1) (34, 35, 164).

The endogenous roles of the FDOR-type $F_{420}H_2$-dependent reductases in mycobacteria are presently being resolved. We have shown that a structurally characterized (419) subgroup of this family (FDOR-B4s) are efficient $F_{420}H_2$-dependent biliverdin reductases (30). They convert the heme degradation product biliverdin—produced by HugZ in environmental mycobacteria (30) and host heme oxygenase 1 (HO1) (369) during tuberculosis infection—to bilirubin via hydride transfer to C-10 (30). This may be advantageous for survival of oxidative stress, given that bilirubin is a potent antioxidant that can compensate for 10,000-fold excess in peroxide radicals (372, 373). A recent study showed that addition of bilirubin enhanced the survival of *Mycobacterium abscessus* in HO1-inhibited macrophages, possibly via modulation of intracellular reactive oxygen species (ROS) levels (423). These proteins may also reduce mycobilins (30), the product of the CO bypass pathway of heme oxygenation by mycobacterial MhuD (370). This FDOR group is only the second family of biliverdin reductases to be identified; a previously characterized family of mammalian and cyanobacterial biliverdin reductases employs nicotinamides as an electron source (424, 425). We also observed low-level biliverdin reductase activity in the structurally related FDOR-B3s (30). However, their low catalytic efficiency and suboptimal active site structure for biliverdin binding suggests that this promiscuous activity may result from a common evolutionary origin to the FDOR-B4s; FDOR-B3 enzymes are therefore likely to have a different, currently unidentified physiological substrate (30).

Among other FDORs, there is preliminary evidence that FDOR-AAs are $F_{420}H_2$-dependent fatty acid reductases; these membrane-bound enzymes may contribute to cell wall modification and host invasion, although their substrate specificity has yet to be defined (30). While it has been proposed that FDOR-A proteins are $F_{420}H_2$-dependent menaquinone reductases (32), to date, activity has been observed only with nonphysiological quinones (e.g., menadione), rather than with menaquinone (30, 32); hence, it is unclear whether these enzymes have primarily evolved to input electrons into the respiratory chain or instead detoxify exogenous redox cycling agents (section 4.1.1). Finally, it was recently shown that the $F_{420}H_2$-dependent step in the biosynthesis of antibiotics of the tetracycline, oxotetracycline, and chlortetracycline classes (122, 381, 382, 384) is mediated by enzymes of the FDOR-B1 subgroup in streptomycetes (section 4.1.2) (29).

4.3.2. LLHTs: luciferase-like hydride transferase superfamily

Luciferase-like hydride transferases (LLHTs) are another diverse superfamily of flavin/deazaflavin enzymes. These enzymes were previously defined as luciferase-like monooxygenases (LLMs), but this is inappropriate given that their reaction mechanisms are O_2 independent. Like the FDORs, members of this superfamily vary in their cofactor preferences (F_{420}, FMN, FAD) and catalytic activities (oxidases, reductases, oxygenases) (163, 426–428). F_{420}-binding LLHTs can be distinguished by a conserved glycine residue that binds the phosphate group without steric hindrance, which is not conserved in the FMN-binding proteins of this family (48). The best-characterized F_{420}-dependent LLHTs are the three aforementioned dehydrogenases: F_{420}-reducing methylene-H_4MPT dehydrogenase (Mtd), F_{420}-reducing glucose-6-phosphate dehydrogenase (Fgd), and F_{420}-reducing hydroxymycolic acid dehydrogenase (fHMAD). However, comparative genome analysis indicates that there are numerous other F_{420}-dependent LLHTs in actinomycetes, the majority probably serving as reductases (37). These have been implicated in a variety of roles, ranging from pyrrolobenzodiazepene antibiotic synthesis in streptomycetes (50, 393, 394, 429) to cell wall metabolism in mycobacteria (37) and exogenous substrate mobilization by rhodococci (155). A bioinformatics analysis predicted that there are some 45 F_{420}-binding LLHTs in *M. smegmatis* and 17 in *M. tuberculosis*, though this has yet to be validated experimentally (37). In contrast to the FDOR superfamily (30), to date, no comprehensive analysis of the phylogeny, structure, and function of these enzymes has been performed.

The best-characterized $F_{420}H_2$-dependent reductases of this superfamily are the hydride transferases involved in the biodegradation of the explosive picrate and related compounds (54, 155). In *Rhodococcus opacus*, two LLHTs known as hydride transferase I (HTI) and hydride transferase II (HTII) catalyze the reduction of picrate into hydride-Meisenheimer and dihydride-Meisenheimer complexes (430–432). Subsequent tautomerization, nitrite elimination, reduction, and hydrolysis steps lead to the production of 4,6-dinitrohexanoate, which can then be oxidatively degraded (432). The complete pathway involved is shown in Fig. 19. This pathway enables such organisms to grow using picrate and related compounds as the sole carbon and nitrogen sources (396, 398). The genes encoding the hydride transferases are organized in an operon together with genes encoding other enzymes in the pathway, including Fno which supplies reductant to the pathway (155, 433). Consistent with these genes having a physiological role in the biodegradation of nitroaromatic compounds, the repressor NpdR

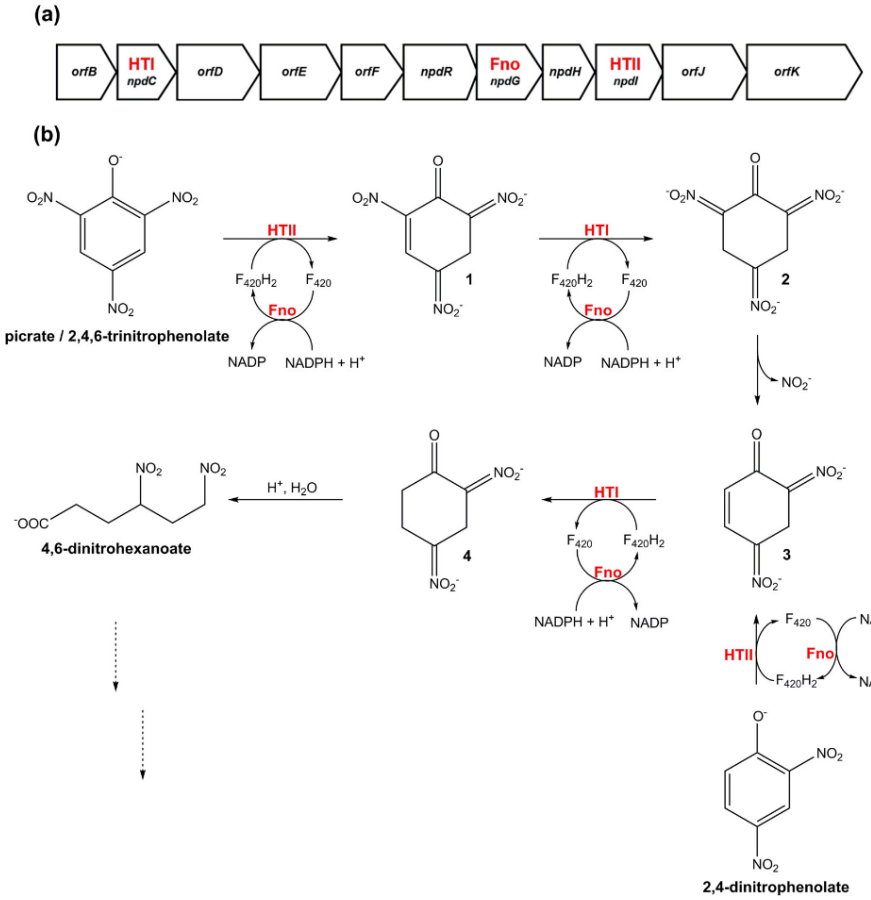

FIG 19 F_{420} dependent degradation of picrate. (a) Genetic determinants of picrate degradation in *Rhodococcus opacus*. F_{420}-utilizing oxidoreductases are highlighted in gray, namely, two luciferase-like hydride transferases (HTI and HTII) and the F_{420}-reducing NADPH dehydrogenase (Fno) (155). Translation of the operon is silenced by the transcription factor NpdR, which is inactivated in the presence of nitroaromatic compounds (434). (b) Mechanism of picrate and 2,4-dinitrophenolate mobilization by *Rhodococcus opacus*. Hydride transfer from $F_{420}H_2$ is catalyzed by HTI and HTII, while $F_{420}H_2$ is regenerated by the F_{420}-reducing NADPH dehydrogenase Fno. The combined action of these enzymes generate hydride-Meisenheimer complex (compound 1 [shown as boldface 1 in the figure]) and dihydride-Meisenheimer complex (compound 2) of picrate and hydride-Meisenheimer complex (compound 3) and dihydride-Meisenheimer complex (compound 4) of 2,4-dinitrophenolate (394, 422).

usually silences these genes, but it is inactivated in the presence of nitroaromatics (434).

The hydride transferases that mediate these reactions share approximately 30% amino acid sequence identity with Mtd of methanogens (435). The results of comparative genomics suggest that homologs of these proteins are exclusively encoded by the genera *Nocardioides*, *Rhodococcus*, and *Nocardia* among presently sequenced organisms. Empirical studies consistently indicate that equivalent enzymatic pathways can degrade nitroaromatic compounds in five additional *Rhodococcus* species (398, 436–438) and three *Nocardioides* species (54, 396, 397, 432, 439). Beyond picrate and 2,4-dinitrophenol, LLHTs are involved in the biodegradation of other nitroaromatic compounds. We recently reported a *Nocardioides* strain that is able to mineralize 2,4-dinitroanisole (DNAN) through an initial O-demethylation step (catalyzed by a novel hydrolase) followed by degradation of the resultant 2,4-dinitrophenol by LLHTs (397). 2,4,6-Trinitrotoluene (TNT) can also be initially reduced to an equivalent hydride-Meisenheimer complex in *Rhodococcus* and *Mycobacterium* strains (440, 441); however, this is unproductive, as the complex cannot be further metabolized to yield carbon or nitrogen sources (441).

5. APPLICATIONS AND IMPLICATIONS

5.1. Tuberculosis Treatment

Globally, tuberculosis (TB) is the most significant bacterial disease in terms of morbidity and mortality, infecting approximately 2 billion individuals and causing approximately 1.5 million deaths in 2013 (442). The standard treatment for tuberculosis relies on a 6-month, four-drug combination therapy (isoniazid, rifampin,

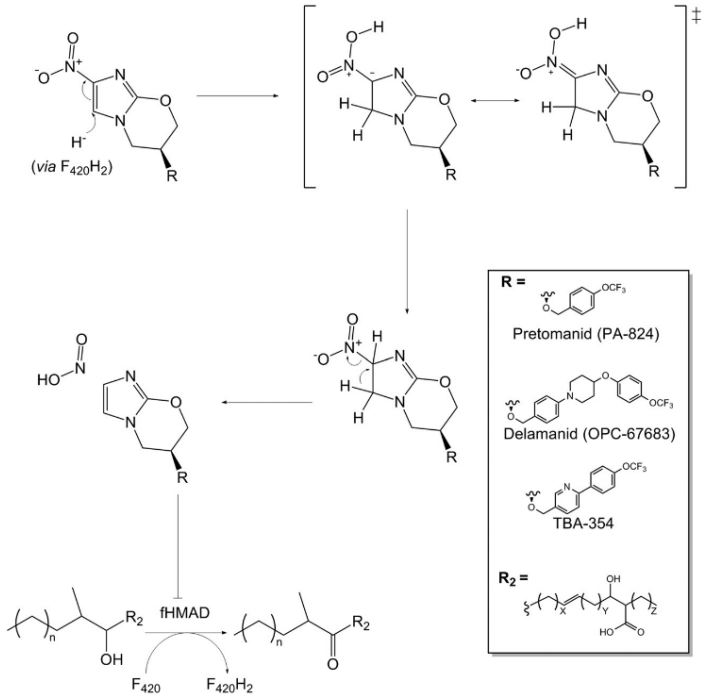

FIG 20 Reductive activation and mode of action of the prodrug pretomanid by the $F_{420}H_2$-dependent reductase rv3547 (FDOR-A1) (33, 34, 365).

pyrazinamide, and ethambutol) (443). There are major issues with this therapy: high cost per patient, poor compliance and management, growing worldwide drug resistance, and extensive drug-drug interactions (444). These problems are a reflection of the extraordinary biology of *M. tuberculosis*, which can transition between chronic and latent infection states that can evade the immune system and resist drug treatment (56), necessitating potent drug regimens to eliminate all tubercle bacilli from infected patients. There is thus an urgent need to develop new antimycobacterials to supplement or replace the current first-line drugs. F_{420} is implicated in the abilities of *M. tuberculosis* to maintain nonreplicating persistent states and resist antibiotic treatment, oxidative stress, and nitrosative stress (section 4.1). Hence, there may be particular promise in developing small-molecule inhibitors of F_{420} biosynthesis and enzymatic pathways in order to target persistent mycobacteria. The pleiotropic importance of F_{420} in *M. tuberculosis* (31, 32), combined with its absence from human cells and commensal microflora, suggest that a specific inhibitor would be highly potent while having few off-target effects. Such an inhibitor is likely to have a synergistic effect if used with existing drug regimens (with the exception of nitroimidazole prodrugs that require $F_{420}H_2$ for activation [33, 34]), given that strains unable to synthesize F_{420} are hypersusceptible to first-line and second-line antimycobacterials (32, 363). There are opportunities to use our knowledge of the F_{420} biosynthesis pathways for fragment-based drug screening and structure-based drug design (445), although no significant progress has been reported in this area thus far. The F_{420} system might also be exploited for the treatment of other serious mycobacterial diseases (145), for example those caused by *M. bovis*, *M. ulcerans*, *M. marinum*, and *M. leprae* (360).

However, there may be even more promise in exploiting the F_{420} system to activate prodrugs. Delamanid (OPC-67683; approved for multidrug-resistant TB [MDR-TB]) (446), pretomanid (PA-824; phase III clinical trials) (33), and the next-generation TBA-354 (phase I clinical trials) (447, 448) are recently developed nitroimidazole prodrugs that are activated by hydride transfer from $F_{420}H_2$ (Fig. 20). These compounds have been shown to inhibit *M. tuberculosis* growth at submicromolar levels and exhibit no cross-resistance with current clinical drugs *in vitro* due to their novel mode of action (33, 34, 446, 449–451). In particular, delamanid shows great promise in the treatment of multi- and extensively drug-resistant TB (MDR-TB and XDR-TB, respectively) (452–454), while combination therapies that incorporate pretomanid exhibited highly promising 14-day bactericidal activity with minimal side effects (455, 456). The mechanism of activation of these prodrugs has been studied primarily with pretomanid (Fig. 20). A member of the FDOR-A1 family (28, 30), rv3547 (deazaflavin-dependent nitroreductase [Ddn]), mediates the hydride transfer from $F_{420}H_2$ to the nitroimidazole (35, 164, 457). Hydride addition leads to the formation of an unstable intermediate, which decomposes into three primary metabolites (predominantly a des-nitro compound) (33–35). During the decomposition, the nitro group is eliminated, resulting in accumulation of reactive nitrogen species (nitric oxide, nitrous acid) in a dose-dependent manner (34, 458). Transcriptome profiling indicates that the prodrug has a dual bactericidal mode of action as a

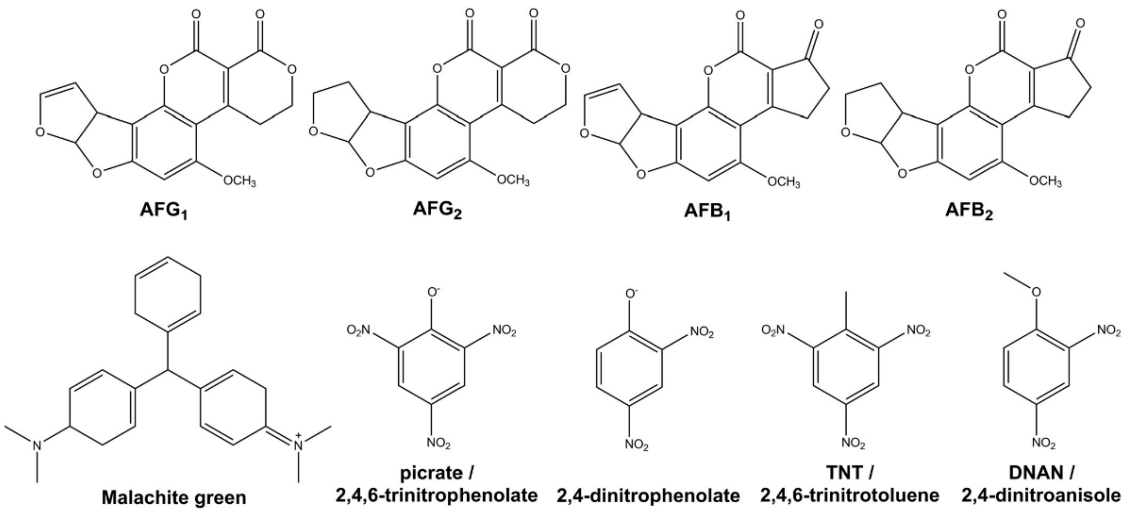

FIG 21 Chemical structures of xenobiotics reduced by actinobacterial $F_{420}H_2$-dependent reductases of the FDOR and LLHT superfamilies. The structures shown are of carcinogenic aflatoxins (aflatoxin G_1 [AFG_1], AFG_2, $AFGB_1$, and $AFGB_2$) (28), nitroaromatic explosives (picrate, 2,4-dinitrophenol, 2,4,6-trinitrotoluene, and 2,4-dinitroanisole) (396), and the toxin malachite green (132).

result of the products formed (33, 459): the primary decomposition products prevent mycolic acid biosynthesis (possibly by inhibiting fHMAD [365, 446]), while reactive nitrogen species (RNS) release causes respiratory poisoning (34). Other mycobacteria are thought to be resistant to pretomanid because they either lack homologs of the activating enzyme rv3547 (i.e., *M. leprae*) (460) or carry genes that encode homologous enzymes with mutations in the nitroimidazole-binding site (e.g., *M. smegmatis*) (30, 164).

There are, however, concerns that *M. tuberculosis* will rapidly develop resistance against nitroimidazoles (35, 461). Point mutations in Ddn may be able to prevent pretomanid activation without inhibiting the protein's native quinone reductase activity (30, 32). Likewise, loss of function of rv3547, *fbiC*, or *fgd* result in cross-resistance to delamanid and pretomanid (458). In the clinic, it was recently reported that an XRD-TB patient rapidly acquired delamanid resistance through loss of function of the F_{420} system (462). Interestingly, the original lead nitroimidazole compound for combating *M. tuberculosis*, CGI-17341 (now abandoned due to safety concerns) (463), depends on the presence of F_{420} but not Ddn for antimicrobial activity (458). As CGI-17341 lacks the hydrophobic tail and phenyloxazole residues of delamanid and pretomanid, it is likely to be activated by a wider range of FDORs (458). It may therefore be possible to develop next-generation nitroimidazoles that are broadly activated by FDORs and hence will have more promising antimicrobial resistance profiles.

5.2. Methane Mitigation

Methane is the second most important anthropogenic greenhouse gas and contributes to about 20% of total anthropogenic climate forcing. Approximately 70% of methane emissions result from the activity of methanogens, the abundance of which has increased as a result of ruminant animal farming, rice paddy agriculture, and solid and liquid waste production (464). As a dominant catabolic cofactor in methanogens, as well as a central mediator in hydrogenotrophic, formatotrophic, and methylotrophic methanogenesis, F_{420} facilitates these emissions. One strategy targeted at reducing methane emissions from ruminant animals and rice paddy fields is to administer methanogen inhibitors (465–467). Economical methanogenesis inhibitors may be particularly attractive in livestock agriculture, as they may simultaneously reduce greenhouse gas emissions while enhancing ruminant productivity (468). Highlighting the potential in this area, a recent study demonstrated that administration of the methyl-CoM reductase inhibitor 3-nitrooxypropanol to dairy cattle feed decreased methane production and increased body weight gain (468, 469). Other highly promising targets for methane mitigation include the F_{420} biosynthesis enzymes CofG/CofH and oxidoreductase Mer, given their presence and predicted essentiality in all methanogens, including obligately aceticlastic species (196). Given that these targets are absent from host cells and other ruminal microbiota (where ANME are not competitive), specific inhibitors are likely to have minimal off-target effects.

5.3. Bioremediation

Many $F_{420}H_2$-dependent reductases have broad substrate specificity and can reductively degrade diverse xenobiotic compounds. For example, mycobacterial flavin/deazaflavin oxidoreductases can degrade coumarin derivatives (28, 55), while rhodococcal luciferase-like hydride transferases can reduce polynitroaromatic compounds (438, 440). While the physiological advantage conferred by this promiscuity has not been fully resolved, it does provide a basis for the exploitation of F_{420} in bioremediation applications (470). It may be possible to deploy F_{420}-dependent organisms to remediate lands and waters contaminated with toxins and explosives. The most significant environmental contaminants that may be remediated through F_{420}-dependent processes are picrate, aflatoxins, and dyes such as malachite green (Fig. 21).

Among the most carcinogenic and hepatotoxic compounds known, aflatoxins are a group of mycotoxins produced by *Aspergillus flavus* and *Aspergillus parasiticus* that contaminate crops in tropical climates (471, 472). As coumarin derivatives, difurocoumarocyclopentenones (aflatoxins B1 and B2) and difurocoumarolactones (aflatoxins G1 and G2) can be efficiently degraded by mycobacterial $F_{420}H_2$-dependent reductases (28, 409). *Rhodococcus erythropolis* and *Nocardia corynebacterioides* can also degrade aflatoxin, possibly through using homologous enzymes (472–474). Environmental mycobacteria are also capable of decolorizing and detoxifying malachite green in an F_{420}-dependent manner (132, 475); while once extensively used as an antiparasitic in aquaculture, this compound has since become regulated against due to its toxicological properties (476).

Picrate and related nitroaromatic compounds are highly toxic explosives that extensively contaminate soils in current and former explosive manufacturing, processing, and storage facilities (477). Luciferase-like hydride transferases from certain actinomycetes can initiate mineralization of such compounds (438, 440). In the case of 2,4,6-trinitrotoluene (TNT), hydride transfer from LLHTs lead to the formation of dead-end products that cannot be further degraded (440, 441). However, multiple strains of *Rhodococcus*, *Nocardia*, and *Nocardioides* can completely mineralize picrate, 2,4-dinitrophenol (DNP), and 2,4-dinitroanisole (DNAP) as the sole carbon and nitrogen sources (396, 397). Administration of such bacteria to nitroaromatic-contaminated sites may be a cheaper and faster alternative to traditional physical remediation methods (477, 478). Consistently, there are reports of *Rhodococcus* sp. strain NJUST16 being used to biodegrade picrate from contaminated soils (437). As with bioremediation of aflatoxins and malachite green, administration of live bacteria is a more promising option than cell-free enzymatic systems, because F_{420} must be enzymatically reduced before it is utilized by $F_{420}H_2$-dependent reductases.

5.4. Industrial Biocatalysis

F_{420} may also prove a useful addition to the toolboxes of synthetic chemists. F_{420}-dependent processes already provide essential steps in some industrial processes, for example in the synthesis of some of the oldest-known antibiotic classes (29, 381), and there is considerable potential to expand the role of F_{420}-dependent enzymes as catalysts for synthetic chemistry. $F_{420}H_2$-dependent reductases of the FDOR and LLHT superfamilies can catalyze the stereospecific reduction of enones (28, 55, 291, 409) and imines (50, 388, 393) in diverse heterocycles. The broad substrate range of these enzymes may be particularly useful for catalyzing hydride addition to nonnatural compounds in a potentially stereospecific manner (479, 480). Such enzymes may be particularly useful in whole-cell biosynthetic cascades if coexpressed with cofactor recycling systems. A promising precedent in this regard is provided by the use of old yellow enzymes (OYEs) for the asymmetric reduction of enone moieties in yeast and bacteria (481). OYEs are mechanistically predisposed to *trans*-hydrogenation, whereby a hydride is delivered to the substrate from the cofactor and a proton is delivered to the opposite face of the substrate from an active site tyrosine (482). As $F_{420}H_2$-dependent reductases deliver hydrides from the cofactor, it is likely that they will provide access to *cis*-hydrogenation of enones for biocatalytic processes (including *in vivo*). Asymmetric imine reduction by enzymes is a promising area for development (483), not least because of the prominence of chiral amines in modern synthetic chemistry: ~40% of pharmaceuticals and ~20% of agrochemicals contain at least one chiral amine (484). However, the toolbox of enzymes available for use in such applications is still small and incomplete; there are few enzymes that will reduce a prochiral imine in a linear molecule, for example (483). The capacity of F_{420}-dependent enzymes to catalyze such imine reductions has, as yet, been explored only superficially (470).

A significant barrier to industrial application of F_{420}-dependent enzymes in biocatalytic applications is the commercial unavailability of F_{420}. While total chemical synthesis has been achieved (485), the most efficient and affordable way to obtain the cofactor is presently through extraction from F_{420} producers. Most laboratory-scale preparations of the cofactor currently rely on *Mycobacterium smegmatis*, a safe "fast"-growing aerobic bacterium that synthesizes micromolar quantities of F_{420} during fermenter growth (96). Bashiri et al. (486) were able to enhance F_{420} production in this organism by overexpressing the *fbiABC* genes in *trans* and inducing F_{420} production in a rich autoinduction medium. F_{420} can subsequently be purified from lysed cells by anion-exchange chromatography, followed by hydrophobic-interaction chromatography (96, 486). In the long-term, it would be preferable to metabolically engineer large-scale recombinant F_{420} production in *Escherichia coli*; however, this depends on the identification of the elusive enzyme responsible for production of 2-phospho-L-lactate (470). The capacity to produce F_{420} in heterologous organisms that do not naturally produce or use the cofactor also raises some interesting possibilities for synthetic biology. "Exotic" cofactors may enable wholly orthogonal synthetic pathways for chemical production in an organism, essentially divorcing the pathway from the central metabolic and regulatory background of the production organism.

6. CONCLUDING REMARKS

On first inspection, it seems surprising that 5-deazaflavins are involved in such disparate processes; very little seems to unify methanogenesis, tetracycline biosynthesis, and DNA photoreactivation other than this class of compounds. Underlying the selection of 5-deazaflavins across biology, however, are the unique properties conferred by the N-5 (flavin) to C-5 (deazaflavin) substitution. The photochemical properties of 5-deazaflavins are crucial for the role of F_o in light capturing and FRET. The electrochemical properties of F_{420} place it at the center of methanogenic redox metabolism and provide actinobacteria with a way of catalyzing low-potential hydride transfer reactions in their primary and secondary metabolism. The enzymes that synthesize 5-deazaflavins share conserved sequences and folds, suggesting that they were either present in the last universal common ancestor or were laterally transferred between archaea and bacteria. However, oxidoreductases appear to have evolved the capacity to utilize F_{420} on multiple occasions from related nicotinamide- or flavin-dependent proteins. Three types of F_{420}-binding sites are nevertheless conserved throughout biology, namely, those in FrhB-like, TIM barrel, and split β-barrel folds. Many F_{420}-dependent enzymes have a modular nature—as particularly evident in Frh, Fpo, and Fsr—suggesting that F_{420} is versatile enough to be accommodated in a wide range of redox enzyme systems.

For the future, there are numerous opportunities to both explore and exploit F_{420}. While we have a relatively rich understanding of the physiology and biochemistry of F_{420} in methanogenesis,

there are still conundrums to solve, for example in relation to the structurally unresolved Ffd, Fpo, and Fsr enzymes. Our understanding of the roles of F_{420} in actinobacteria is much less sophisticated, and there are multiple important questions to resolve. For example, why is F_{420} required for mycobacterial persistence and antibiotic resistance? Why do mycobacteria encode such a multiplicity of FDORs and LLHTs? What are the primary roles of F_{420} in the metabolism of streptomycetes and rhodococci? Looking at the bigger picture, it is still poorly understood how F_{420} biosynthesis pathways have evolved and why F_{420} is distributed in relatively few phyla. However, the finding that F_{420} is likely to be synthesized by ANME, *Chloroflexi*, and *Proteobacteria* indicates that the cofactor may be more important in oxic and anoxic communities than previously anticipated. There is also an urgent need to understand the role of F_{420} at the ecosystem level, particularly in relation to how F_{420}-dependent biodegradation processes influence the community structuring and chemical composition of soils. Fueled by the recent approval of delamanid for treatment of multidrug-resistant tuberculosis, there is also room to explore the application of F_{420} for medical, environmental, and industrial purposes. Half a century since their discovery by the Wolfe laboratory, 5-deazaflavins continue to surprise biologists and chemists alike.

ACKNOWLEDGMENTS

We thank Robyn Russell, Carol Hartley, Trevor Rapson, and the three anonymous reviewers for their useful comments on this review.

This work was supported by Australian Research Council research grants (DE120102673 and DP130102144) awarded to C.J.J., a CSIRO Office of the Chief Executive Postdoctoral Fellowship awarded to C.G., and Australian National University Higher Degree by Research PhD scholarships awarded to F.H.A., A.E.M., and B.M.L.

REFERENCES

1. Hemmerich P, Nagelschneider G, Veeger C. 1970. Chemistry and molecular biology of flavins and flavoproteins. FEBS Lett 8:69–83. http://dx.doi.org/10.1016/0014-5793(70)80229-0.
2. Walsh C. 1980. Flavin coenzymes: at the crossroads of biological redox chemistry. Acc Chem Res 13:148–155. http://dx.doi.org/10.1021/ar50149a004.
3. O'Brien DE, Weinstock LT, Cheng CC. 1967. 10-Deazariboflavin. Chem Ind 48:2044–2045.
4. O'Brien DE, Weinslock LT, Cheng CC. 1970. Synthesis of 10-deazariboflavin and related 2,4-dioxopyrimido[4,5-b]quinolines. J Heterocycl Chem 7:99–105. http://dx.doi.org/10.1002/jhet.5570070114.
5. Cheeseman P, Toms-Wood A, Wolfe RS. 1972. Isolation and properties of a fluorescent compound, Factor420, from Methanobacterium strain MoH. J Bacteriol 112:527–531.
6. Eirich LD, Vogels GD, Wolfe RS. 1978. Proposed structure for coenzyme F_{420} from *Methanobacterium*. Biochemistry 17:4583–4593. http://dx.doi.org/10.1021/bi00615a002.
7. Walsh C. 1986. Naturally occurring 5-deazaflavin coenzymes: biological redox roles. Acc Chem Res 19:216–221. http://dx.doi.org/10.1021/ar00127a004.
8. Jacobson F, Walsh C. 1984. Properties of 7,8-didemethyl-8-hydroxy-5-deazaflavins relevant to redox coenzyme function in methanogen metabolism. Biochemistry 23:979–988. http://dx.doi.org/10.1021/bi00300a028.
9. de Poorter LMI, Geerts WJ, Keltjens JT. 2005. Hydrogen concentrations in methane-forming cells probed by the ratios of reduced and oxidized coenzyme F_{420}. Microbiology 151:1697–1705. http://dx.doi.org/10.1099/mic.0.27679-0.
10. Friedrich W. 1988. Vitamins. Walter de Gruyter & Co., Berlin, Germany.
11. Jacobson FS, Daniels L, Fox JA, Walsh CT, Orme-Johnson WH. 1982. Purification and properties of an 8-hydroxy-5-deazaflavin-reducing hydrogenase from *Methanobacterium thermoautotrophicum*. J Biol Chem 257:3385–3388.
12. Eker AP, Hessels JK, Meerwaldt R. 1989. Characterization of an 8-hydroxy-5-deazaflavin:NADPH oxidoreductase from *Streptomyces griseus*. Biochim Biophys Acta 990:80–86. http://dx.doi.org/10.1016/S0304-4165(89)80015-7.
13. Hossain MS, Le CQ, Joseph E, Nguyen TQ, Johnson-Winters K, Foss FW. 2015. Convenient synthesis of deazaflavin cofactor F_O and its activity in F_{420}-dependent NADP reductase. Org Biomol Chem 13:5082–5085. http://dx.doi.org/10.1039/C5OB00365B.
14. Wolin EA, Wolin MJ, Wolfe RS. 1963. Formation of methane by bacterial extracts. J Biol Chem 238:2882–2886.
15. Eirich LD, Vogels GD, Wolfe RS. 1979. Distribution of coenzyme F_{420} and properties of its hydrolytic fragments. J Bacteriol 140:20–27.
16. Tzeng SF, Wolfe RS, Bryant MP. 1975. Factor 420-dependent pyridine nucleotide-linked hydrogenase system of *Methanobacterium ruminantium*. J Bacteriol 121:184–191.
17. Tzeng SF, Bryant MP, Wolfe RS. 1975. Factor 420-dependent pyridine nucleotide-linked formate metabolism of *Methanobacterium ruminantium*. J Bacteriol 121:192–196.
18. Hartzell PL, Zvilius G, Escalante-Semerena JC, Donnelly MI. 1985. Coenzyme F_{420} dependence of the methylenetetrahydromethanopterin dehydrogenase of *Methanobacterium thermoautotrophicum*. Biochem Biophys Res Commun 133:884–890. http://dx.doi.org/10.1016/0006-291X(85)91218-5.
19. Stetter KO, Lauerer G, Thomm M, Neuner A. 1987. Isolation of extremely thermophilic sulfate reducers: evidence for a novel branch of archaebacteria. Science 236:822–824. http://dx.doi.org/10.1126/science.236.4803.822.
20. Lin XL, White RH. 1986. Occurrence of coenzyme F_{420} and its γ-monoglutamyl derivative in nonmethanogenic archaebacteria. J Bacteriol 168:444–448.
21. Hallam SJ, Putnam N, Preston CM, Detter JC, Rokhsar D, Richardson PM, DeLong EF. 2004. Reverse methanogenesis: testing the hypothesis with environmental genomics. Science 305:1457–1462. http://dx.doi.org/10.1126/science.1100025.
22. Berk H, Thauer RK. 1997. Function of coenzyme F_{420}-dependent NADP reductase in methanogenic archaea containing an NADP-dependent alcohol dehydrogenase. Arch Microbiol 168:396–402. http://dx.doi.org/10.1007/s002030050514.
23. Cousins FB. 1960. The prosthetic group of a chromoprotin from mycobacteria. Biochim Biophys Acta 40:532–534. http://dx.doi.org/10.1016/0006-3002(60)91396-2.
24. Miller PA, Sjolander NO, Nalesnyk S, Arnold N, Johnson S, Doerschuk AP, McCormick JRD. 1960. Cosynthetic factor I, a factor involved in hydrogen-transfer in *Streptomyces aureofaciens*. J Am Chem Soc 82:5002–5003. http://dx.doi.org/10.1021/ja01503a063.
25. Eker APM, Pol A, van der Meyden P, Vogels GD. 1980. Purification and properties of 8-hydroxy-5-deazaflavin derivatives from *Streptomyces griseus*. FEMS Microbiol Lett 8:161–165. http://dx.doi.org/10.1111/j.1574-6968.1980.tb05071.x.
26. Naraoka T, Momoi K, Fukasawa K, Goto M. 1984. Isolation and identification of a naturally occurring 7, 8-didemethyl-8-hydroxy-5-deazaflavin derivative from *Mycobacterium avium*. Biochim Biophys Acta 797:377–380. http://dx.doi.org/10.1016/0304-4165(84)90260-5.
27. Daniels L, Bakhiet N, Harmon K. 1985. Widespread distribution of a 5-deazaflavin cofactor in *Actinomyces* and related bacteria. Syst Appl Microbiol 6:12–17. http://dx.doi.org/10.1016/S0723-2020(85)80004-7.
28. Taylor MC, Jackson CJ, Tattersall DB, French N, Peat TS, Newman J, Briggs LJ, Lapalikar GV, Campbell PM, Scott C, Russell RJ, Oakeshott JG. 2010. Identification and characterization of two families of $F_{420}H_2$-dependent reductases from *Mycobacteria* that catalyse aflatoxin degradation. Mol Microbiol 78:561–575. http://dx.doi.org/10.1111/j.1365-2958.2010.07356.x.
29. Wang P, Bashiri G, Gao X, Sawaya MR, Tang Y. 2013. Uncovering the enzymes that catalyze the final steps in oxytetracycline biosynthesis. J Am Chem Soc 135:7138–7141. http://dx.doi.org/10.1021/ja403516u.
30. Ahmed FH, Carr PD, Lee BM, Afriat-Jurnou L, Mohamed AE, Hong N-S, Flanagan J, Taylor MC, Greening C, Jackson CJ. 2015. Sequence-structure-function classification of a catalytically diverse oxidoreductase superfamily in mycobacteria. J Mol Biol 427:3554–3571. http://dx.doi.org/10.1016/j.jmb.2015.09.021.
31. Purwantini E, Mukhopadhyay B. 2009. Conversion of NO_2 to NO by reduced coenzyme F_{420} protects mycobacteria from nitrosative damage. Proc Natl Acad Sci U S A 106:6333–6338. http://dx.doi.org/10.1073/pnas.0812883106.

32. Gurumurthy M, Rao M, Mukherjee T, Rao SPS, Boshoff HI, Dick T, Barry CE, Manjunatha UH. 2013. A novel F_{420}-dependent anti-oxidant mechanism protects *Mycobacterium tuberculosis* against oxidative stress and bactericidal agents. Mol Microbiol 87:744–755. http://dx.doi.org/10.1111/mmi.12127.
33. Stover CK, Warrener P, VanDevanter DR, Sherman DR, Arain TM, Langhorne MH, Anderson SW, Towell JA, Yuan Y, McMurray DN, Kreiswirth BN, Barry CE, Baker WR. 2000. A small-molecule nitroimidazopyran drug candidate for the treatment of tuberculosis. Nature 405:962–966. http://dx.doi.org/10.1038/35016103.
34. Singh R, Manjunatha U, Boshoff HIM, Ha YH, Niyomrattanakit P, Ledwidge R, Dowd CS, Lee IY, Kim P, Zhang L, Kang S, Keller TH, Jiricek J, Barry CE. 2008. PA-824 kills nonreplicating *Mycobacterium tuberculosis* by intracellular NO release. Science 322:1392–1395. http://dx.doi.org/10.1126/science.1164571.
35. Manjunatha UH, Boshoff H, Dowd CS, Zhang L, Albert TJ, Norton JE, Daniels L, Dick T, Pang SS, Barry CE. 2006. Identification of a nitroimidazo-oxazine-specific protein involved in PA-824 resistance in *Mycobacterium tuberculosis*. Proc Natl Acad Sci U S A 103:431–436. http://dx.doi.org/10.1073/pnas.0508392103.
36. Lewis JM, Sloan DJ. 2015. The role of delamanid in the treatment of drug-resistant tuberculosis. Ther Clin Risk Manag 11:779–791. http://dx.doi.org/10.2147/TCRM.S71076.
37. Selengut JD, Haft DH. 2010. Unexpected abundance of coenzyme F_{420}-dependent enzymes in *Mycobacterium tuberculosis* and other actinobacteria. J Bacteriol 192:5788–5798. http://dx.doi.org/10.1128/JB.00425-10.
38. Hemmerich P, Massey V, Fenner H. 1977. Flavin and 5-deazaflavin: a chemical evaluation of "modified" flavoproteins with respect to the mechanisms of redox biocatalysis. FEBS Lett 84:5–21. http://dx.doi.org/10.1016/0014-5793(77)81047-8.
39. Spencer R, Fisher J, Walsh C. 1976. Preparation, characterization, and chemical properties of the flavin coenzyme analogues 5-deazariboflavin, 5-deazariboflavin 5′-phosphate, and 5-deazariboflavin 5′-diphosphate, 5′ leads to 5′-adenosine ester. Biochemistry 15:1043–1053. http://dx.doi.org/10.1021/bi00650a015.
40. Jorns MS, Hersh LB. 1975. N-methylglutamate synthetase. Substrate-flavin hydrogen transfer reactions probed with deazaflavin mononucleotide. J Biol Chem 250:3620–3628.
41. Averill BA, Schonbrunn A, Abeles RH. 1975. Studies on the mechanism of *Mycobacterium smegmatis* L-lactate oxidase. 5 deazaflavin mononucleotide as a coenzyme analogue. J Biol Chem 250:1603–1605.
42. Jorns MS, Hersh LB. 1976. Nucleophilic addition reactions of free and enzyme-bound deazaflavin. J Biol Chem 251:4872–4881.
43. Fisher J, Spencer R, Walsh C. 1976. Enzyme-catalyzed redox reactions with the flavin analogues 5-deazariboflavin, 5-deazariboflavin 5′-phosphate, and 5-deazariboflavin 5′-diphosphate, 5′→5′-adenosine ester. Biochemistry 15:1054–1064. http://dx.doi.org/10.1021/bi00650a016.
44. Edmondson DE, Barman B, Tollin G. 1972. Importance of the N-5 position in flavin coenzymes. Properties of free and protein-bound 5-deaza analogs. Biochemistry 11:1133–1138.
45. Eker APM, Dekker RH, Berends W. 1981. Photoreactivating enzyme from *Streptomyces griseus*-IV. On the nature of the chromophoric cofactor in *Streptomyces griseus* photoreactivating enzyme. Photochem Photobiol 33:65–72.
46. Xia K, Shen G-B, Zhu X-Q. 2015. Thermodynamics of various F_{420} coenzyme models as sources of electrons, hydride ions, hydrogen atoms and protons in acetonitrile. Org Biomol Chem 13:6255–6268. http://dx.doi.org/10.1039/C5OB00538H.
47. Hagemeier CH, Shima S, Thauer RK, Bourenkov G, Bartunik HD, Ermler U. 2003. Coenzyme F_{420}-dependent methylenetetrahydromethanopterin dehydrogenase (Mtd) from *Methanopyrus kandleri*: a methanogenic enzyme with an unusual quarternary structure. J Mol Biol 332:1047–1057. http://dx.doi.org/10.1016/S0022-2836(03)00949-5.
48. Aufhammer SW, Warkentin E, Ermler U, Hagemeier CH, Thauer RK, Shima S. 2005. Crystal structure of methylenetetrahydromethanopterin reductase (Mer) in complex with coenzyme F_{420}: architecture of the F_{420}/FMN binding site of enzymes within the nonprolyl cis-peptide containing bacterial luciferase family. Protein Sci 14:1840–1849. http://dx.doi.org/10.1110/ps.041289805.
49. Aufhammer SW, Warkentin E, Berk H, Shima S, Thauer RK, Ermler U. 2004. Coenzyme binding in F_{420}-dependent secondary alcohol dehydrogenase, a member of the bacterial luciferase family. Structure 12:361–370. http://dx.doi.org/10.1016/j.str.2004.02.010.
50. Li W, Chou S, Khullar A, Gerratana B. 2009. Cloning and characterization of the biosynthetic gene cluster for tomaymycin, an SJG-136 monomeric analog. Appl Environ Microbiol 75:2958–2963. http://dx.doi.org/10.1128/AEM.02325-08.
51. Johnson EF, Mukhopadhyay B. 2005. A new type of sulfite reductase, a novel coenzyme F_{420}-dependent enzyme, from the methanarchaeon *Methanocaldococcus jannaschii*. J Biol Chem 280:38776–38786. http://dx.doi.org/10.1074/jbc.M503492200.
52. Silaghi-Dumitrescu R, Kurtz DM, Jr, Ljungdahl LG, Lanzilotta WN. 2005. X-ray crystal structures of *Moorella thermoacetica* FprA. Novel diiron site structure and mechanistic insights into a scavenging nitric oxide reductase. Biochemistry 44:6492–6501.
53. Thauer RK, Jungermann K, Decker K. 1977. Energy conservation in chemotrophic anaerobic bacteria. Bacteriol Rev 41:100–180.
54. Ebert S, Rieger P-G, Knackmuss H-J. 1999. Function of coenzyme F_{420} in aerobic catabolism of 2,4,6-trinitrophenol and 2,4-dinitrophenol by *Nocardioides simplex* FJ2-1A. J Bacteriol 181:2669–2674.
55. Lapalikar GV, Taylor MC, Warden AC, Scott C, Russell RJ, Oakeshott JG. 2012. $F_{420}H_2$-dependent degradation of aflatoxin and other furanocoumarins is widespread throughout the Actinomycetales. PLoS One 7:e30114. http://dx.doi.org/10.1371/journal.pone.0030114.
56. Boshoff H, Barry C. 2005. Tuberculosis - metabolism and respiration in the absence of growth. Nat Rev Microbiol 3:70–80. http://dx.doi.org/10.1038/nrmicro1065.
57. Tamada T, Kitadokoro K, Higuchi Y, Inaka K, Yasui A, de Ruiter PE, Eker AP, Miki K. 1997. Crystal structure of DNA photolyase from *Anacystis nidulans*. Nat Struct Biol 4:887–891. http://dx.doi.org/10.1038/nsb1197-887.
58. Malhotra K, Kim ST, Walsh C, Sancar A. 1992. Roles of FAD and 8-hydroxy-5-deazaflavin chromophores in photoreactivation by *Anacystis nidulans* DNA photolyase. J Biol Chem 267:15406–15411.
59. Edwards T, McBride BC. 1975. New method for the isolation and identification of methanogenic bacteria. Appl Microbiol 29:540–545.
60. Doddema HJ, Vogels GD. 1978. Improved identification of methanogenic bacteria by fluorescence microscopy. Appl Environ Microbiol 36:752–754.
61. van Beelen P, Dijkstra AC, Vogels GD. 1983. Quantitation of coenzyme F_{420} in methanogenic sludge by the use of reversed-phase high-performance liquid chromatography and a fluorescence detector. Eur J Appl Microbiol Biotechnol 18:67–69. http://dx.doi.org/10.1007/BF00508132.
62. Dolfing J, Mulder J-W. 1985. Comparison of methane production rate and coenzyme F_{420} content of methanogenic consortia in anaerobic granular sludge. Appl Environ Microbiol 49:1142–1145.
63. Reynolds PJ, Colleran E. 1987. Evaluation and improvement of methods for coenzyme F_{420} analysis in anaerobic sludges. J Microbiol Methods 7:115–130. http://dx.doi.org/10.1016/0167-7012(87)90032-7.
64. Ashby KD, Casey TA, Rasmussen MA, Petrich JW. 2001. Steady-state and time-resolved spectroscopy of F_{420} extracted from methanogen cells and its utility as a marker for fecal contamination. J Agric Food Chem 49:1123–1127. http://dx.doi.org/10.1021/jf000689r.
65. Kim YS, Westerholm M, Scherer P. 2014. Dual investigation of methanogenic processes by quantitative PCR and quantitative microscopic fingerprinting. FEMS Microbiol Lett 360:76–84. http://dx.doi.org/10.1111/1574-6968.12592.
66. Rohde RA, Price PB. 2007. Diffusion-controlled metabolism for long-term survival of single isolated microorganisms trapped within ice crystals. Proc Natl Acad Sci U S A 104:16592–16597. http://dx.doi.org/10.1073/pnas.0708183104.
67. Patiño S, Alamo L, Cimino M, Casart Y, Bartoli F, García MJ, Salazar L. 2008. Autofluorescence of mycobacteria as a tool for detection of *Mycobacterium tuberculosis*. J Clin Microbiol 46:3296–3302. http://dx.doi.org/10.1128/JCM.02183-07.
68. Maglica Ž, Özdemir E, McKinney JD. 2015. Single-cell tracking reveals antibiotic-induced changes in mycobacterial energy metabolism. mBio 6:e02236-14. http://dx.doi.org/10.1128/mBio.02236-14.
69. Fischer M, Bacher A. 2006. Biosynthesis of vitamin B_2 in plants. Physiol Plant 126:304–318. http://dx.doi.org/10.1111/j.1399-3054.2006.00607.x.
70. Graham DE, Xu H, White RH. 2003. Identification of the 7,8-didemethyl-8-hydroxy-5-deazariboflavin synthase required for coen-

zyme F_{420} biosynthesis. Arch Microbiol 180:455–464. http://dx.doi.org/10.1007/s00203-003-0614-8.
71. Decamps L, Philmus B, Benjdia A, White R, Begley TP, Berteau O. 2012. Biosynthesis of F_0, precursor of the F_{420} cofactor, requires a unique two radical-SAM domain enzyme and tyrosine as substrate. J Am Chem Soc 134:18173–18176. http://dx.doi.org/10.1021/ja307762b.
72. Choi K-P, Kendrick N, Daniels L. 2002. Demonstration that *fbiC* is required by *Mycobacterium bovis* BCG for coenzyme F_{420} and F_O biosynthesis. J Bacteriol 184:2420–2428. http://dx.doi.org/10.1128/JB.184.9.2420-2428.2002.
73. Philmus B, Decamps L, Berteau O, Begley TP. 2015. Biosynthetic versatility and coordinated action of 5′-deoxyadenosyl radicals in deazaflavin biosynthesis. J Am Chem Soc 137:5406–5413. http://dx.doi.org/10.1021/ja513287k.
74. Epple R, Carell T. 1998. Flavin- and deazaflavin-containing model compounds mimic the energy transfer step in type II DNA photolyases. Angew Chem Int Ed 37:938–941. http://dx.doi.org/10.1002/(SICI)1521-3773(19980420)37:7<938::AID-ANIE938>3.0.CO;2-P.
75. Sancar A. 2003. Structure and function of DNA photolyase and cryptochrome blue-light photoreceptors. Chem Rev 103:2203–2238. http://dx.doi.org/10.1021/cr0204348.
76. Yasui A, Takao M, Oikawa A, Kiener A, Walsh CT, Eker AP. 1988. Cloning and characterization of a photolyase gene from the cyanobacterium *Anacystis nidulans*. Nucleic Acids Res 16:4447–4463. http://dx.doi.org/10.1093/nar/16.10.4447.
77. Eker AP, Kooiman P, Hessels JK, Yasui A. 1990. DNA photoreactivating enzyme from the cyanobacterium Anacystis nidulans. J Biol Chem 265:8009–8015.
78. Kelner A. 1949. Effect of visible light on the recovery of *Streptomyces griseus* conidia from ultra-violet irradiation injury. Proc Natl Acad Sci U S A 35:73–79. http://dx.doi.org/10.1073/pnas.35.2.73.
79. Kobayashi T, Takao M, Oikawa A, Yasui A. 1989. Molecular characterization of a gene encoding a photolyase from *Streptomyces griseus*. Nucleic Acids Res 17:4731–4744. http://dx.doi.org/10.1093/nar/17.12.4731.
80. Mayerl F, Piret J, Kiener A, Walsh CT, Yasui A. 1990. Functional expression of 8-hydroxy-5-deazaflavin-dependent DNA photolyase from *Anacystis nidulans* in *Streptomyces coelicolor*. J Bacteriol 172:6061–6065.
81. Kiener A, Husain I, Sancar A, Walsh C. 1989. Purification and properties of *Methanobacterium thermoautotrophicum* DNA photolyase. J Biol Chem 264:13880–13887.
82. Kiontke S, Gnau P, Haselsberger R, Batschauer A, Essen L-O. 2014. Structural and evolutionary aspects of antenna chromophore usage by class II photolyases. J Biol Chem 289:19659–19669. http://dx.doi.org/10.1074/jbc.M113.542431.
83. Takao M, Kobayashi T, Oikawa A, Yasui A. 1989. Tandem arrangement of photolyase and superoxide dismutase genes in *Halobacterium halobium*. J Bacteriol 171:6323–6329.
84. Eker APM, Hessels JKC, van de Velde J. 1988. Photoreactivating enzyme from the green alga *Scenedesmus acutus*. Evidence for the presence of two different flavin chromophores. Biochemistry 27:1758–1765.
85. Glas AF, Maul MJ, Cryle M, Barends TRM, Schneider S, Kaya E, Schlichting I, Carell T. 2009. The archaeal cofactor F_0 is a light-harvesting antenna chromophore in eukaryotes. Proc Natl Acad Sci U S A 106:11540–11545. http://dx.doi.org/10.1073/pnas.0812665106.
86. Petersen JL, Ronan PJ. 2010. Critical role of 7,8-didemethyl-8-hydroxy-5-deazariboflavin for photoreactivation in *Chlamydomonas reinhardtii*. J Biol Chem 285:32467–32475. http://dx.doi.org/10.1074/jbc.M110.146050.
87. Selby CP, Sancar A. 2012. The second chromophore in *Drosophila* photolyase/cryptochrome family photoreceptors. Biochemistry 51:167–171. http://dx.doi.org/10.1021/bi201536w.
88. Bennett CJ, Webb M, Willer DO, Evans DH. 2003. Genetic and phylogenetic characterization of the type II cyclobutane pyrimidine dimer photolyases encoded by Leporipoxviruses. Virology 315:10–19. http://dx.doi.org/10.1016/S0042-6822(03)00512-9.
89. van Oers MM, Herniou EA, Usmany M, Messelink GJ, Vlak JM. 2004. Identification and characterization of a DNA photolyase-containing baculovirus from *Chrysodeixis chalcites*. Virology 330:460–470. http://dx.doi.org/10.1016/j.virol.2004.09.032.
90. van Oers MM, Lampen MH, Bajek MI, Vlak JM, Eker APM. 2008. Active DNA photolyase encoded by a baculovirus from the insect Chrysodeixis chalcites. DNA Repair (Amst) 7:1309–1318. http://dx.doi.org/10.1016/j.dnarep.2008.04.013.
91. Biernat MA, Ros VID, Vlak JM, van Oers MM. 2011. Baculovirus cyclobutane pyrimidine dimer photolyases show a close relationship with lepidopteran host homologues. Insect Mol Biol 20:457–464. http://dx.doi.org/10.1111/j.1365-2583.2011.01076.x.
92. Xu F, Vlak JM, van Oers MM. 2008. Conservation of DNA photolyase genes in group II nucleopolyhedroviruses infecting plusiine insects. Virus Res 136:58–64. http://dx.doi.org/10.1016/j.virusres.2008.04.017.
93. Xu F, Vlak JM, Eker APM, van Oers MM. 2010. DNA photolyases of *Chrysodeixis chalcites* nucleopolyhedrovirus are targeted to the nucleus and interact with chromosomes and mitotic spindle structures. J Gen Virol 91:907–914. http://dx.doi.org/10.1099/vir.0.018044-0.
94. Adams MD, Celniker SE, Holt RA, Evans CA, Gocayne JD, Amanatides PG, Scherer SE, Li PW, Hoskins RA, Galle RF, George RA, Lewis SE, Richards S, Ashburner M, Henderson SN, Sutton GG, Wortman JR, Yandell MD, Zhang Q, Chen LX, Brandon RC, Rogers YH, Blazej RG, Champe M, Pfeiffer BD, Wan KH, Doyle C, Baxter EG, Helt G, Nelson CR, Gabor GL, Abril JF, Agbayani A, An HJ, Andrews-Pfannkoch C, Baldwin D, Ballew RM, Basu A, Baxendale J, Bayraktaroglu L, Beasley EM, Beeson KY, Benos PV, Berman BP, Bhandari D, Bolshakov S, Borkova D, Botchan MR, Bouck J, Brokstein P, Brottier P, et al. 2000. The genome sequence of *Drosophila melanogaster*. Science 287:2185–2195. http://dx.doi.org/10.1126/science.287.5461.2185.
95. Peck MW. 1989. Changes in concentrations of coenzyme F_{420} analogs during batch growth of *Methanosarcina barkeri* and *Methanosarcina mazei*. Appl Environ Microbiol 55:940–945.
96. Isabelle D, Simpson DR, Daniels L. 2002. Large-scale production of coenzyme F_{420}-5,6 by using *Mycobacterium smegmatis*. Appl Environ Microbiol 68:5750–5755. http://dx.doi.org/10.1128/AEM.68.11.5750-5755.2002.
97. Kern R, Keller P, Schmidt G, Bacher A. 1983. Isolation and structural identification of a chromophoric coenzyme F_{420} fragment from culture fluid of *Methanobacterium thermoautotrophicum*. Arch Microbiol 136:191–193. http://dx.doi.org/10.1007/BF00409842.
98. Weber S. 2005. Light-driven enzymatic catalysis of DNA repair: a review of recent biophysical studies on photolyase. Biochim Biophys Acta 1707:1–23. http://dx.doi.org/10.1016/j.bbabio.2004.02.010.
99. van der Horst GTJ, Muijtjens M, Kobayashi K, Takano R, Kanno S, Takao M, de Wit J, Verkerk A, Eker APM, van Leenen D, Buijs R, Bootsma D, Hoeijmakers JHJ, Yasui A. 1999. Mammalian Cry1 and Cry2 are essential for maintenance of circadian rhythms. Nature 398:627–630. http://dx.doi.org/10.1038/19323.
100. Johnson JL, Hamm-Alvarez S, Payne G, Sancar GB, Rajagopalan KV, Sancar A. 1988. Identification of the second chromophore of *Escherichia coli* and yeast DNA photolyases as 5,10-methenyltetrahydrofolate. Proc Natl Acad Sci U S A 85:2046–2050. http://dx.doi.org/10.1073/pnas.85.7.2046.
101. Fujihashi M, Numoto N, Kobayashi Y, Mizushima A, Tsujimura M, Nakamura A, Kawarabayasi Y, Miki K. 2007. Crystal structure of archaeal photolyase from *Sulfolobus tokodaii* with two FAD molecules: implication of a novel light-harvesting cofactor. J Mol Biol 365:903–910. http://dx.doi.org/10.1016/j.jmb.2006.10.012.
102. Ueda T, Kato A, Kuramitsu S, Terasawa H, Shimada I. 2005. Identification and characterization of a second chromophore of DNA photolyase from Thermus thermophilus HB27. J Biol Chem 280:36237–36243. http://dx.doi.org/10.1074/jbc.M507972200.
103. Takao M, Oikawa A, Eker AP, Yasui A. 1989. Expression of an *Anacystis nidulans* photolyase gene in *Escherichia coli*; functional complementation and modified action spectrum of photoreactivation. Photochem Photobiol 50:633–637. http://dx.doi.org/10.1111/j.1751-1097.1989.tb04319.x.
104. Miki K, Tamada T, Nishida H, Inaka K, Yasui A, de Ruiter PE, Eker AP. 1993. Crystallization and preliminary X-ray diffraction studies of photolyase (photoreactivating enzyme) from the cyanobacterium *Anacystis nidulans*. J Mol Biol 233:167–169. http://dx.doi.org/10.1006/jmbi.1993.1492.
105. Kort R, Komori H, Adachi S, Miki K, Eker A. 2004. DNA apophotolyase from *Anacystis nidulans*: 1.8 Å structure, 8-HDF reconstitution and X-ray-induced FAD reduction. Acta Crystallogr D Biol Crystallogr 60:1205–1213. http://dx.doi.org/10.1107/S0907444904009321.
106. Mees A, Klar T, Gnau P, Hennecke U, Eker APM, Carell T, Essen L-O. 2004. Crystal structure of a photolyase bound to a CPD-like DNA lesion

after *in situ* repair. Science 306:1789–1793. http://dx.doi.org/10.1126/science.1101598.
107. Kim ST, Heelis PF, Sancar A. 1992. Energy transfer (deazaflavin to $FADH_2$) and electron transfer (FADH2 to TT) kinetics in Anacystis nidulans photolyase. Biochemistry 31:11244–11248. http://dx.doi.org/10.1021/bi00160a040.
108. MacFarlane AW, IV, Stanley RJ. 2003. *Cis-syn* thymidine dimer repair by DNA photolyase in real time. Biochemistry 42:8558–8568. http://dx.doi.org/10.1021/bi034015w.
109. Aubert C, Mathis P, Eker AP, Brettel K. 1999. Intraprotein electron transfer between tyrosine and tryptophan in DNA photolyase from *Anacystis nidulans*. Proc Natl Acad Sci U S A 96:5423–5427. http://dx.doi.org/10.1073/pnas.96.10.5423.
110. Sancar A. 2008. Structure and function of photolyase and *in vivo* enzymology: 50th anniversary. J Biol Chem 283:32153–32157. http://dx.doi.org/10.1074/jbc.R800052200.
111. Ashton WT, Brown RD, Jacobson F, Walsh C. 1979. Synthesis of 7,8-didemethyl-8-hydroxy-5-deazariboflavin. J Am Chem Soc 101:4419–4420. http://dx.doi.org/10.1021/ja00509a083.
112. Pol A, van der Drift C, Vogels GD, Cuppen TJHM, Laarhoven WH. 1980. Comparison of coenzyme F_{420} from *Methanobacterium bryantii* with 7- and 8-hydroxy-10-methyl-5-deazaisoalloxazine. Biochem Biophys Res Commun 92:255–260. http://dx.doi.org/10.1016/0006-291X(80)91546-6.
113. Ashton WT, Brown RD. 1980. Synthesis of 8-demethyl-8-hydroxy-5-deazariboflavins. J Heterocycl Chem 17:1709–1712. http://dx.doi.org/10.1002/jhet.5570170813.
114. Jaenchen R, Schonheit P, Thauer RK. 1984. Studies on the biosynthesis of coenzyme F_{420} in methanogenic bacteria. Arch Microbiol 137:362–365. http://dx.doi.org/10.1007/BF00410735.
115. Reuke B, Korn S, Eisenreich W, Bacher A. 1992. Biosynthetic precursors of deazaflavins. J Bacteriol 174:4042–4049.
116. Graupner M, White RH. 2001. Biosynthesis of the phosphodiester bond in coenzyme F_{420} in the methanoarchaea. Biochemistry 40:10859–10872. http://dx.doi.org/10.1021/bi0107703.
117. Graupner M, Xu H, White RH. 2002. Characterization of the 2-phospho-L-lactate transferase enzyme involved in coenzyme F_{420} biosynthesis in *Methanococcus jannaschii*. Biochemistry 41:3754–3761.
118. Choi K-P, Bair TB, Bae Y-M, Daniels L. 2001. Use of transposon Tn5367 mutagenesis and a nitroimidazopyran-based selection system to demonstrate a requirement for *fbiA* and *fbiB* in coenzyme F_{420} biosynthesis by *Mycobacterium bovis* BCG. J Bacteriol 183:7058–7066. http://dx.doi.org/10.1128/JB.183.24.7058-7066.2001.
119. Forouhar F, Abashidze M, Xu H, Grochowski LL, Seetharaman J, Hussain M, Kuzin A, Chen Y, Zhou W, Xiao R, Acton TB, Montelione GT, Galinier A, White RH, Tong L. 2008. Molecular insights into the biosynthesis of the F_{420} coenzyme. J Biol Chem 283:11832–11840. http://dx.doi.org/10.1074/jbc.M710352200.
120. Li H, Graupner M, Xu H, White RH. 2003. CofE catalyzes the addition of two glutamates to F_{420}-0 in F_{420} coenzyme biosynthesis in *Methanococcus jannaschii*. Biochemistry 42:9771–9778. http://dx.doi.org/10.1021/bi034779b.
121. Rehan AM, Bashiri G, Paterson NG, Baker EN, Squire CJ. 2011. Cloning, expression, purification, crystallization and preliminary X-ray studies of the C-terminal domain of Rv3262 (FbiB) from *Mycobacterium tuberculosis*. Acta Crystallogr Sect F Struct Biol Cryst Commun 67:1274–1277. http://dx.doi.org/10.1107/S1744309111028958.
122. Nakano T, Miyake K, Endo H, Dairi T, Mizukami T, Katsumata R. 2004. Identification and cloning of the gene involved in the final step of chlortetracycline biosynthesis in *Streptomyces aureofaciens*. Biosci Biotechnol Biochem 68:1345–1352. http://dx.doi.org/10.1271/bbb.68.1345.
123. Nocek B, Evdokimova E, Proudfoot M, Kudritska M, Grochowski LL, White RH, Savchenko A, Yakunin A, Edwards FA, Joachimiak A. 2007. Structure of an amide bond forming F420:γγ-glutamyl ligase from Archaeoglobus fulgidus - a member of a new family of non-ribosomal peptide synthases. J Mol Biol 372:456–469. http://dx.doi.org/10.1016/j.jmb.2007.06.063.
124. Gorris LG, van der Drift C. 1994. Cofactor contents of methanogenic bacteria reviewed. Biofactors 4:139–145.
125. Bair TB, Isabelle DW, Daniels L. 2001. Structures of coenzyme F_{420} in *Mycobacterium* species. Arch Microbiol 176:37–43. http://dx.doi.org/10.1007/s002030100290.
126. Graupner M, White RH. 2003. *Methanococcus jannaschii* coenzyme F_{420} analogs contain a terminal α-linked glutamate. J Bacteriol 185:4662–4665. http://dx.doi.org/10.1128/JB.185.15.4662-4665.2003.
127. Kimachi T, Tanaka K, Yoneda F. 1991. Synthesis of a proposed isomer of F_{420} having α-glutamyl bonding. J Heterocycl Chem 28:439–443. http://dx.doi.org/10.1002/jhet.5570280244.
128. Li H, Xu H, Graham DE, White RH. 2003. Glutathione synthetase homologs encode alpha-L-glutamate ligases for methanogenic coenzyme F_{420} and tetrahydrosarcinapterin biosyntheses. Proc Natl Acad Sci U S A 100:9785–9790. http://dx.doi.org/10.1073/pnas.1733391100.
129. Graupner M, Xu H, White RH. 2000. Identification of an archaeal 2-hydroxy acid dehydrogenase catalyzing reactions involved in coenzyme biosynthesis in methanoarchaea. J Bacteriol 182:3688–3692. http://dx.doi.org/10.1128/JB.182.13.3688-3692.2000.
130. Grochowski LL, Xu H, White RH. 2006. Identification of lactaldehyde dehydrogenase in *Methanocaldococcus jannaschii* and its involvement in production of lactate for F_{420} biosynthesis. J Bacteriol 188:2836–2844. http://dx.doi.org/10.1128/JB.188.8.2836-2844.2006.
131. Grochowski LL, Xu H, White RH. 2008. Identification and characterization of the 2-phospho-L-lactate guanylyltransferase involved in coenzyme F_{420} biosynthesis. Biochemistry 47:3033–3037. http://dx.doi.org/10.1021/bi702475t.
132. Guerra-Lopez D, Daniels L, Rawat M. 2007. *Mycobacterium smegmatis* mc^2 155 *fbiC* and MSMEG_2392 are involved in triphenylmethane dye decolorization and coenzyme F_{420} biosynthesis. Microbiology 153:2724–2732. http://dx.doi.org/10.1099/mic.0.2006/009241-0.
133. Möller-Zinkhan D, Börner G, Thauer RK. 1989. Function of methanofuran, tetrahydromethanopterin, and coenzyme F_{420} in *Archaeoglobus fulgidus*. Arch Microbiol 152:362–368. http://dx.doi.org/10.1007/BF00425174.
134. Gorris LG, Voet AC, van der Drift C. 1991. Structural characteristics of methanogenic cofactors in the non-methanogenic archaebacterium *Archaeoglobus fulgidus*. Biofactors 3:29–35.
135. Vornolt J, Kunow J, Stetter KO, Thauer RK. 1995. Enzymes and coenzymes of the carbon monoxide dehydrogenase pathway for autotrophic CO_2 fixation in *Archaeoglobus lithotrophicus* and the lack of carbon monoxide dehydrogenase in the heterotrophic *A. profundus*. Arch Microbiol 163:112–118. http://dx.doi.org/10.1007/BF00381784.
136. de Wit LEA, Eker APM. 1987. 8-Hydroxy-5-deazaflavin-dependent electron transfer in the extreme halophile *Halobacterium cutirubrum*. FEMS Microbiol Lett 48(1-2):121–125. http://dx.doi.org/10.1111/j.1574-6968.1987.tb02527.x.
137. Haroon MF, Hu S, Shi Y, Imelfort M, Keller J, Hugenholtz P, Yuan Z, Tyson GW. 2013. Anaerobic oxidation of methane coupled to nitrate reduction in a novel archaeal lineage. Nature 500:567–570. http://dx.doi.org/10.1038/nature12375.
138. Wu D, Hugenholtz P, Mavromatis K, Pukall RR, Dalin E, Ivanova NN, Kunin V, Goodwin L, Wu M, Tindall BJ, Hooper SD, Pati A, Lykidis A, Spring S, Anderson IJ, D'haeseleer P, Zemla A, Singer M, Lapidus A, Nolan M, Copeland A, Han C, Chen F, Cheng J-F, Lucas S, Kerfeld C, Lang E, Gronow S, Chain P, Bruce D, Rubin EM, Kyrpides NC, Klenk H-P, Eisen JA, D'haeseleer, Zemla PA, Singer M, Lapidus A, Nolan M, Copeland A, Han C, Chen F, Cheng J-F, Lucas S, Kerfeld C, Lang E, Gronow S, Chain P, Bruce D, Rubin EM, Kyrpides NC, Klenk H-P, Eisen JA. 2009. A phylogeny-driven genomic encyclopaedia of *Bacteria* and *Archaea*. Nature 462:1056–1060. http://dx.doi.org/10.1038/nature08656.
139. Rinke C, Schwientek P, Sczyrba A, Ivanova NN, Anderson IJ, Cheng J-F, Darling A, Malfatti S, Swan BK, Gies EA, Dodsworth JA, Hedlund BP, Tsiamis G, Sievert SM, Liu W-T, Eisen JA, Hallam SJ, Kyrpides NC, Stepanauskas R, Rubin EM, Hugenholtz P, Woyke T. 2013. Insights into the phylogeny and coding potential of microbial dark matter. Nature 499:431–437. http://dx.doi.org/10.1038/nature12352.
140. Kozubal MA, Romine M, Jennings RD, Jay ZJ, Tringe SG, Rusch DB, Beam JP, McCue LA, Inskeep WP. 2013. *Geoarchaeota*: a new candidate phylum in the Archaea from high-temperature acidic iron mats in Yellowstone National Park. ISME J 7:622–634. http://dx.doi.org/10.1038/ismej.2012.132.
141. Evans PN, Parks DH, Chadwick GL, Robbins SJ, Orphan VJ, Golding SD, Tyson GW. 2015. Methane metabolism in the archaeal phylum *Bathyarchaeota* revealed by genome-centric metagenomics. Science 350:434–438. http://dx.doi.org/10.1126/science.aac7745.
142. Spang A, Saw JH, Jorgensen SL, Zaremba-Niedzwiedzka K, Martijn J, Lind AE, van Eijk R, Schleper C, Guy L, Ettema TJG. 2015. Complex

archaea that bridge the gap between prokaryotes and eukaryotes. Nature 521:173–179. http://dx.doi.org/10.1038/nature14447.
143. Spang A, Poehlein A, Offre P, Zumbragel S, Haider S, Rychlik N, Nowka B, Schmeisser C, Lebedeva EV, Rattei T, Bohm C, Schmid M, Galushko A, Hatzenpichler R, Weinmaier T, Daniel R, Schleper C, Spieck E, Streit W, Wagner M. 2012. The genome of the ammonia-oxidizing Candidatus *Nitrososphaera gargensis*: insights into metabolic versatility and environmental adaptations. Environ Microbiol 14:3122–3145. http://dx.doi.org/10.1111/j.1462-2920.2012.02893.x.
144. Palatinszky M, Herbold C, Jehmlich N, Pogoda M, Han P, von Bergen M, Lagkouvardos I, Karst SM, Galushko A, Koch H, Berry D, Daims H, Wagner M. 2015. Cyanate as an energy source for nitrifiers. Nature 524:105–108. http://dx.doi.org/10.1038/nature14856.
145. Purwantini E, Gillis TP, Daniels L. 1997. Presence of F_{420}-dependent glucose-6-phosphate dehydrogenase in *Mycobacterium* and *Nocardia* species, but absence from *Streptomyces* and *Corynebacterium* species and methanogenic Archaea. FEMS Microbiol Lett 146:129–134. http://dx.doi.org/10.1111/j.1574-6968.1997.tb10182.x.
146. Kuo MS, Yurek DA, Coats JH, Li GP. 1989. Isolation and identification of 7,8-didemethyl-8-hydroxy-5-deazariboflavin, an unusual cosynthetic factor in streptomycetes, from *Streptomyces lincolnensis*. J Antibiot (Tokyo) 42:475–478. http://dx.doi.org/10.7164/antibiotics.42.475.
147. Janssen PH. 2006. Identifying the dominant soil bacterial taxa in libraries of 16S rRNA and 16S rRNA genes. Appl Environ Microbiol 72:1719–1728. http://dx.doi.org/10.1128/AEM.72.3.1719-1728.2006.
148. Purwantini E, Daniels L. 1998. Molecular analysis of the gene encoding F_{420}-dependent glucose-6-phosphate dehydrogenase from *Mycobacterium smegmatis*. J Bacteriol 180:2212–2219.
149. Mejean A, Paci G, Gautier V, Ploux O. 2014. Biosynthesis of anatoxin-a and analogues (anatoxins) in cyanobacteria. Toxicon 91:15–22. http://dx.doi.org/10.1016/j.toxicon.2014.07.016.
150. Vitt S, Ma K, Warkentin E, Moll J, Pierik AJ, Shima S, Ermler U. 2014. The F_{420}-reducing [NiFe]-hydrogenase complex from *Methanothermobacter marburgensis*, the first X-ray structure of a group 3 family member. J Mol Biol 426:2813–2826. http://dx.doi.org/10.1016/j.jmb.2014.05.024.
151. Thauer RK. 1998. Biochemistry of methanogenesis: a tribute to Marjory Stephenson. Microbiology 144:2377–2406. http://dx.doi.org/10.1099/00221287-144-9-2377.
152. Zeikus JG, Fuchs G, Kenealy W, Thauer RK. 1977. Oxidoreductases involved in cell carbon synthesis of *Methanobacterium thermoautotrophicum*. J Bacteriol 132:604–613.
153. Daniels L, Fuchs G, Thauer RK, Zeikus JG. 1977. Carbon monoxide oxidation by methanogenic bacteria. J Bacteriol 132:118–126.
154. Hedderich R, Whitman W. 2013. Physiology and biochemistry of the methane-producing Archaea, p 635–662. *In* Rosenberg E, DeLong E, Lory S, Stackebrandt E, Thompson F (ed), The prokaryotes. Springer, Berlin, Germany.
155. Heiss G, Hofmann KW, Trachtmann N, Walters DM, Rouvière P, Knackmuss HJ. 2002. npd gene functions of *Rhodococcus* (*opacus*) *erythropolis* HL PM-1 in the initial steps of 2,4,6-trinitrophenol degradation. Microbiology 148:799–806. http://dx.doi.org/10.1099/00221287-148-3-799.
156. Enßle M, Zirngibl C, Linder D, Thauer RK. 1991. Coenzyme F_{420} dependent N^5, N^{10}-methylenetetrahydromethanopterin dehydrogenase in methanol grown *Methanosarcina barkeri*. Arch Microbiol 155:483–490. http://dx.doi.org/10.1007/BF00244966.
157. Mukhopadhyay B, Purwantini E, Daniels L. 1993. Effect of methanogenic substrates on coenzyme F_{420}-dependent N^5,N^{10}-methylene-H_4MPT dehydrogenase, N^5,N^{10}-methenyl-H_4MPT cyclohydrolase and F_{420}-reducing hydrogenase activities in *Methanosarcina barkeri*. Arch Microbiol 159:141–146. http://dx.doi.org/10.1007/BF00250274.
158. Escalante-Semerena JC, Rinehart KL, Wolfe RS. 1984. Tetrahydromethanopterin, a carbon carrier in methanogenesis. J Biol Chem 259:9447–9455.
159. Shima S, Warkentin E, Grabarse W, Sordel M, Wicke M, Thauer RK, Ermler U. 2000. Structure of coenzyme F_{420} dependent methylenetetrahydromethanopterin reductase from two methanogenic archaea. J Mol Biol 300:935–950. http://dx.doi.org/10.1006/jmbi.2000.3909.
160. Warkentin E, Mamat B, Sordel-Klippert M, Wicke M, Thauer RK, Iwata M, Iwata S, Ermler U, Shima S. 2001. Structures of $F_{420}H_2$:NADP$^+$ oxidoreductase with and without its substrates bound. EMBO J 20:6561–6569. http://dx.doi.org/10.1093/emboj/20.23.6561.
161. Seedorf H, Hagemeier CH, Shima S, Thauer RK, Warkentin E, Ermler U. 2007. Structure of coenzyme $F_{420}H_2$ oxidase (FprA), a di-iron flavoprotein from methanogenic *Archaea* catalyzing the reduction of O_2 to H_2O. FEBS J 274:1588–1599. http://dx.doi.org/10.1111/j.1742-4658.2007.05706.x.
162. Bäumer S, Ide T, Jacobi C, Johann A, Gottschalk G, Deppenmeier U. 2000. The $F_{420}H_2$ dehydrogenase from *Methanosarcina mazei* is a redox-driven proton pump closely related to NADH dehydrogenases. J Biol Chem 275:17968–17973. http://dx.doi.org/10.1074/jbc.M000650200.
163. Bashiri G, Squire CJ, Moreland NJ, Baker EN. 2008. Crystal structures of F_{420}-dependent glucose-6-phosphate dehydrogenase FGD1 involved in the activation of the anti-tuberculosis drug candidate PA-824 reveal the basis of coenzyme and substrate binding. J Biol Chem 283:17531–17541. http://dx.doi.org/10.1074/jbc.M801854200.
164. Cellitti SE, Shaffer J, Jones DH, Mukherjee T, Gurumurthy M, Bursulaya B, Boshoff HI, Choi I, Nayyar A, Lee YS, Cherian J, Niyomrattanakit P, Dick T, Manjunatha UH, Barry CE, Spraggon G, Geierstanger BH. 2012. Structure of Ddn, the deazaflavin-dependent nitroreductase from *Mycobacterium tuberculosis* involved in bioreductive activation of PA-824. Structure 20:101–112. http://dx.doi.org/10.1016/j.str.2011.11.001.
165. Mashalidis EH, Gittis AG, Tomczak A, Abell C, Barry CE, Garboczi DN. 2015. Molecular insights into the binding of coenzyme F_{420} to the conserved protein Rv1155 from *Mycobacterium tuberculosis*. Protein Sci 24:729–740. http://dx.doi.org/10.1002/pro.2645.
166. Ceh K, Demmer U, Warkentin E, Moll J, Thauer RK, Shima S, Ermler U. 2009. Structural basis of the hydride transfer mechanism in F_{420}-dependent methylenetetrahydromethanopterin dehydrogenase. Biochemistry 48:10098–10105. http://dx.doi.org/10.1021/bi901104d.
167. Mills DJ, Vitt S, Strauss M, Shima S, Vonck J. 2013. De novo modeling of the F_{420}-reducing [NiFe]-hydrogenase from a methanogenic archaeon by cryo-electron microscopy. eLife 2:e00218. http://dx.doi.org/10.7554/eLife.00218.
168. Liu Y, Whitman WB. 2008. Metabolic, phylogenetic, and ecological diversity of the methanogenic archaea. Ann N Y Acad Sci 1125:171–189. http://dx.doi.org/10.1196/annals.1419.019.
169. Brochier C, Forterre P, Gribaldo S. 2004. Archaeal phylogeny based on proteins of the transcription and translation machineries: tackling the *Methanopyrus kandleri* paradox. Genome Biol 5:R17. http://dx.doi.org/10.1186/gb-2004-5-3-r17.
170. Bapteste E, Brochier C, Boucher Y. 2005. Higher-level classification of the *Archaea*: evolution of methanogenesis and methanogens. Archaea 1:353–363. http://dx.doi.org/10.1155/2005/859728.
171. Gribaldo S, Brochier-Armanet C. 2006. The origin and evolution of *Archaea*: a state of the art. Philos Trans R Soc B Biol Sci 361:1007–1022. http://dx.doi.org/10.1098/rstb.2006.1841.
172. Brochier-Armanet C, Forterre P, Gribaldo S. 2011. Phylogeny and evolution of the *Archaea*: one hundred genomes later. Curr Opin Microbiol 14:274–281. http://dx.doi.org/10.1016/j.mib.2011.04.015.
173. Borrel G, O'Toole PW, Harris HMB, Peyret P, Brugère JF, Gribaldo S. 2013. Phylogenomic data support a seventh order of methylotrophic methanogens and provide insights into the evolution of methanogenesis. Genome Biol Evol 5:1769–1780. http://dx.doi.org/10.1093/gbe/evt128.
174. Whiticar MJ, Faber E, Schoell M. 1986. Biogenic methane formation in marine and freshwater environments: CO_2 reduction vs. acetate fermentation - isotope evidence. Geochim Cosmochim Acta 50:693–709. http://dx.doi.org/10.1016/0016-7037(86)90346-7.
175. Krzycki JA, Kenealy WR, DeNiro MJ, Zeikus JG. 1987. Stable carbon isotope fractionation by *Methanosarcina barkeri* during methanogenesis from acetate, methanol, or carbon dioxide-hydrogen. Appl Environ Microbiol 53:2597–2599.
176. Smith MR, Mah RA. 1978. Growth and methanogenesis by *Methanosarcina* strain 227 on acetate and methanol. Appl Environ Microbiol 36:870–879.
177. Zeikus JG, Kerby R, Krzycki JA. 1985. Single-carbon chemistry of acetogenic and methanogenic bacteria. Sci 227:1167–1173. http://dx.doi.org/10.1126/science.3919443.
178. Ferry JG. 2010. How to make a living by exhaling methane. Annu Rev Microbiol 64:453–473. http://dx.doi.org/10.1146/annurev.micro.112408.134051.
179. Widdel F, Rouvière PE, Wolfe RS. 1988. Classification of secondary alcohol-utilizing methanogens including a new thermophilic isolate. Arch Microbiol 150:477–481. http://dx.doi.org/10.1007/BF00422290.
180. Jablonski PE, DiMarco AA, Bobik TA, Cabell MC, Ferry JG. 1990.

Protein content and enzyme activities in methanol- and acetate-grown *Methanosarcina thermophila*. J Bacteriol 172:1271–1275.
181. Abbanat DR, Ferry JG. 1991. Resolution of component proteins in an enzyme complex from *Methanosarcina thermophila* catalyzing the synthesis or cleavage of acetyl-CoA. Proc Natl Acad Sci U S A 88:3272–3276. http://dx.doi.org/10.1073/pnas.88.8.3272.
182. Thauer RK, Kaster A-K, Seedorf H, Buckel W, Hedderich R. 2008. Methanogenic archaea: ecologically relevant differences in energy conservation. Nat Rev Microbiol 6:579–591. http://dx.doi.org/10.1038/nrmicro1931.
183. Greening C, Biswas A, Carere CR, Jackson CJ, Taylor MC, Stott MB, Cook GM, Morales SE. 2016. Genomic and metagenomic surveys of hydrogenase diversity indicate H2 is a widely utilised energy source for microbial growth and survival. ISME J 10:761–777. http://dx.doi.org/10.1038/ismej.2015.153.
184. Schauer NL, Brown DP, Ferry JG. 1982. Kinetics of formate metabolism in *Methanobacterium formicicum* and *Methanospirillum hungatei*. Appl Environ Microbiol 44:549–554.
185. Jones JB, Stadtman TC. 1981. Selenium-dependent and selenium-independent formate dehydrogenases of *Methanococcus vannielii*. Separation of the two forms and characterization of the purified selenium-independent form. J Biol Chem 256:656–663.
186. Zinder SH, Anguish T. 1992. Carbon monoxide, hydrogen, and formate metabolism during methanogenesis from acetate by thermophilic cultures of *Methanosarcina* and *Methanothrix* strains. Appl Environ Microbiol 58:3323–3329.
187. Miller TL, Wolin MJ. 1985. *Methanosphaera stadtmaniae* gen. nov., sp. nov.: a species that forms methane by reducing methanol with hydrogen. Arch Microbiol 141:116–122. http://dx.doi.org/10.1007/BF00423270.
188. Jetten MSM, Stams AJM, Zehnder AJB. 1992. Methanogenesis from acetate: a comparison of the acetate metabolism in *Methanothrix soehngenii* and *Methanosarcina* spp. FEMS Microbiol Lett 88:181–198. http://dx.doi.org/10.1111/j.1574-6968.1992.tb04987.x.
189. Conrad R. 2009. The global methane cycle: recent advances in understanding the microbial processes involved. Environ Microbiol Rep 1:285–292. http://dx.doi.org/10.1111/j.1758-2229.2009.00038.x.
190. Schauer NL, Ferry JG. 1986. Composition of the coenzyme F_{420}-dependent formate dehydrogenase from *Methanobacterium formicicum*. J Bacteriol 165:405–411.
191. Johnson EF, Mukhopadhyay B. 2008. Coenzyme F_{420}-dependent sulfite reductase-enabled sulfite detoxification and use of sulfite as a sole sulfur source by *Methanococcus maripaludis*. Appl Environ Microbiol 74:3591–3595. http://dx.doi.org/10.1128/AEM.00098-08.
192. Seedorf H, Dreisbach A, Hedderich R, Shima S, Thauer RK. 2004. $F_{420}H_2$ oxidase (FprA) from *Methanobrevibacter arboriphilus*, a coenzyme F_{420}-dependent enzyme involved in O_2 detoxification. Arch Microbiol 182:126–137.
193. Welte C, Deppenmeier U. 2011. Re-evaluation of the function of the F_{420} dehydrogenase in electron transport of *Methanosarcina mazei*. FEBS J 278:1277–1287. http://dx.doi.org/10.1111/j.1742-4658.2011.08048.x.
194. Baresi L, Wolfe RS. 1981. Levels of coenzyme F_{420}, coenzyme M, hydrogenase, and methyl coenzyme M methylreductase in acetate-grown *Methanosarcina*. Appl Environ Microbiol 41:388–391.
195. Barber RD, Zhang L, Harnack M, Olson MV, Kaul R, Ingram-Smith C, Smith KS. 2011. Complete genome sequence of *Methanosaeta concilii*, a specialist in aceticlastic methanogenesis. J Bacteriol 193:3668–3669. http://dx.doi.org/10.1128/JB.05031-11.
196. Zhu J, Zheng H, Ai G, Zhang G, Liu D, Liu X, Dong X. 2012. The genome characteristics and predicted function of methyl-group oxidation pathway in the obligate aceticlastic methanogens, *Methanosaeta* spp. PLoS One 7:e36756. http://dx.doi.org/10.1371/journal.pone.0036756.
197. Nelson-Sathi S, Dagan T, Landan G, Janssen A, Steel M, McInerney JO, Deppenmeier U, Martin WF. 2012. Acquisition of 1,000 eubacterial genes physiologically transformed a methanogen at the origin of *Haloarchaea*. Proc Natl Acad Sci U S A 109:20537–20542. http://dx.doi.org/10.1073/pnas.1209119109.
198. Kunow J, Linder D, Stetter KO, Thauer RK. 1994. $F_{420}H_2$: quinone oxidoreductase from *Archaeoglobus fulgidus*. Eur J Biochem 223:503–511. http://dx.doi.org/10.1111/j.1432-1033.1994.tb19019.x.
199. Brüggemann H, Falinski F, Deppenmeier U. 2001. Structure of the $F_{420}H_2$:quinone oxidoreductase of Archaeoglobus fulgidus: identification and overproduction of the $F_{420}H_2$-oxidizing subunit. Eur J Biochem 5814:5810–5814.
200. Hocking WP, Stokke R, Roalkvam I, Steen IH. 2014. Identification of key components in the energy metabolism of the hyperthermophilic sulfate-reducing archaeon *Archaeoglobus fulgidus* by transcriptome analyses. Front Microbiol 5:95. http://dx.doi.org/10.3389/fmicb.2014.00095.
201. Kunow J, Schwörer B, Stetter KO, Thauer RK. 1993. A F_{420}-dependent NADP reductase in the extremely thermophilic sulfate-reducing *Archaeoglobus fulgidus*. Arch Microbiol 160:199–205.
202. Möller-Zinkhan D, Thauer R. 1990. Anaerobic lactate oxidation to 3 CO_2 by *Archaeoglobus fulgidus* via the carbon monoxide dehydrogenase pathway: demonstration of the acetyl-CoA carbon-carbon cleavage reaction in cell extracts. Arch Microbiol 153:215–218. http://dx.doi.org/10.1007/BF00249070.
203. Klenk H-P, Clayton RA, Tomb J-F, White O, Nelson KE, Ketchum KA, Dodson RJ, Gwinn M, Hickey EK, Peterson JD, Richardson DL, Kerlavage AR, Graham DE, Kyrpides NC, Fleischmann RD, Quackenbush J, Lee NH, Sutton GG, Gill S, Kirkness EF, Dougherty BA, McKenney K, Adams MD, Loftus B, Peterson S, Reich CI, McNeil LK, Badger JH, Glodek A, Zhou L, Overbeek R, Gocayne JD, Weidman JF, McDonald L, Utterback T, Cotton MD, Spriggs T, Artiach P, Kaine BP, Sykes SM, Sadow PW, D'Andrea KP, Bowman C, Fujii C, Garland SA, Mason TM, Olsen GJ, Fraser CM, Smith HO, Woese CR, Venter JC. 1997. The complete genome sequence of the hyperthermophilic, sulphate-reducing archaeon *Archaeoglobus fulgidus*. Nature 390:364–370. http://dx.doi.org/10.1038/37052.
204. Boetius A, Ravenschlag K, Schubert CJ, Rickert D, Widdel F, Gieseke A, Amann R, Jorgensen BB, Witte U, Pfannkuche O. 2000. A marine microbial consortium apparently mediating anaerobic oxidation of methane. Nature 407:623–626. http://dx.doi.org/10.1038/35036572.
205. Raghoebarsing AA, Pol A, van de Pas-Schoonen KT, Smolders AJP, Ettwig KF, Rijpstra WIC, Schouten S, Damste JSS, Op den Camp HJM, Jetten MSM, Strous M. 2006. A microbial consortium couples anaerobic methane oxidation to denitrification. Nature 440:918–921. http://dx.doi.org/10.1038/nature04617.
206. Orphan VJ, House CH, Hinrichs K-U, McKeegan KD, DeLong EF. 2001. Methane-consuming archaea revealed by directly coupled isotopic and phylogenetic analysis. Science 293:484–487. http://dx.doi.org/10.1126/science.1061338.
207. Wegener G, Krukenberg V, Riedel D, Tegetmeyer HE, Boetius A. 2015. Intercellular wiring enables electron transfer between methanotrophic archaea and bacteria. Nature 526:587–590. http://dx.doi.org/10.1038/nature15733.
208. Knittel K, Boetius A. 2009. Anaerobic oxidation of methane: progress with an unknown process. Annu Rev Microbiol 63:311–334. http://dx.doi.org/10.1146/annurev.micro.61.080706.093130.
209. Reeburgh WS. 2007. Oceanic methane biogeochemistry. Chem Rev 107:486–513. http://dx.doi.org/10.1021/cr050362v.
210. Orphan VJ, House CH, Hinrichs K-U, McKeegan KD, DeLong EF. 2002. Multiple archaeal groups mediate methane oxidation in anoxic cold seep sediments. Proc Natl Acad Sci U S A 99:7663–7668. http://dx.doi.org/10.1073/pnas.072210299.
211. Niemann H, Losekann T, de Beer D, Elvert M, Nadalig T, Knittel K, Amann R, Sauter EJ, Schluter M, Klages M, Foucher JP, Boetius A. 2006. Novel microbial communities of the Haakon Mosby mud volcano and their role as a methane sink. Nature 443:854–858. http://dx.doi.org/10.1038/nature05227.
212. Kruger M, Meyerdierks A, Glockner FO, Amann R, Widdel F, Kube M, Reinhardt R, Kahnt J, Bocher R, Thauer RK, Shima S. 2003. A conspicuous nickel protein in microbial mats that oxidize methane anaerobically. Nature 426:878–881. http://dx.doi.org/10.1038/nature02207.
213. Scheller S, Goenrich M, Boecher R, Thauer RK, Jaun B. 2010. The key nickel enzyme of methanogenesis catalyses the anaerobic oxidation of methane. Nature 465:606–608. http://dx.doi.org/10.1038/nature09015.
214. Kojima H, Moll J, Kahnt J, Fukui M, Shima S. 2014. A reversed genetic approach reveals the coenzyme specificity and other catalytic properties of three enzymes putatively involved in anaerobic oxidation of methane with sulfate. Environ Microbiol 16:3431–3442. http://dx.doi.org/10.1111/1462-2920.12475.
215. Wang F-P, Zhang Y, Chen Y, He Y, Qi J, Hinrichs K-U, Zhang X-X, Xiao X, Boon N. 2014. Methanotrophic archaea possessing diverging methane-oxidizing and electron-transporting pathways. ISME J 8:1069–1078. http://dx.doi.org/10.1038/ismej.2013.212.
216. Meyerdierks A, Kube M, Kostadinov I, Teeling H, Glöckner FO,

Reinhardt R, Amann R. 2010. Metagenome and mRNA expression analyses of anaerobic methanotrophic archaea of the ANME-1 group. Environ Microbiol 12:422–439. http://dx.doi.org/10.1111/j.1462-2920.2009.02083.x.
217. Michaelis W, Seifert R, Nauhaus K, Treude T, Thiel V, Blumenberg M, Knittel K, Gieseke A, Peterknecht K, Pape T, Boetius A, Amann R, Jørgensen BB, Widdel F, Peckmann J, Pimenov NV, Gulin MB. 2002. Microbial reefs in the black sea fueled by anaerobic oxidation of methane. Science 297:1013–1015. http://dx.doi.org/10.1126/science.1072502.
218. Knittel K, Lösekann T, Boetius A, Kort R, Amann R. 2005. Diversity and distribution of methanotrophic archaea at cold seeps. Appl Environ Microbiol 71:467–479. http://dx.doi.org/10.1128/AEM.71.1.467-479.2005.
219. Muth E, Mörschel E, Klein A. 1987. Purification and characterization of an 8-hydroxy-5-deazaflavin-reducing hydrogenase from the archaebacterium *Methanococcus voltae*. Eur J Biochem 169:571–577. http://dx.doi.org/10.1111/j.1432-1033.1987.tb13647.x.
220. Fiebig K, Friedrich B. 1989. Purification of the F_{420}-reducing hydrogenase from *Methanosarcina barkeri* (strain Fusaro). Eur J Biochem 184:79–88. http://dx.doi.org/10.1111/j.1432-1033.1989.tb14992.x.
221. Halboth S, Klein A. 1992. Methanococcus voltae harbors four gene clusters potentially encoding two [NiFe] and two [NiFeSe] hydrogenases, each of the cofactor F_{420}-reducing or F_{420}-non-reducing types. Mol Gen Genet 233:217–224. http://dx.doi.org/10.1007/BF00587582.
222. Vaupel M, Thauer RK. 1998. Two F_{420}-reducing hydrogenases in *Methanosarcina barkeri*. Arch Microbiol 169:201–205. http://dx.doi.org/10.1007/s002030050561.
223. Brodersen J, Gottschalk G, Deppenmeier U. 1999. Membrane-bound $F_{420}H_2$-dependent heterodisulfide reduction in *Methanococcus voltae*. Arch Microbiol 171:115–121. http://dx.doi.org/10.1007/s002030050686.
224. Kulkarni G, Kridelbaugh DM, Guss AM, Metcalf WW. 2009. Hydrogen is a preferred intermediate in the energy-conserving electron transport chain of *Methanosarcina barkeri*. Proc Natl Acad Sci U S A 106:15915–15920. http://dx.doi.org/10.1073/pnas.0905914106.
225. Hendrickson EL, Leigh J. 2008. Roles of coenzyme F_{420}-reducing hydrogenases and hydrogen- and F_{420}-dependent methylenetetrahydromethanopterin dehydrogenases in reduction of F_{420} and production of hydrogen during methanogenesis. J Bacteriol 190:4818–4821. http://dx.doi.org/10.1128/JB.00255-08.
226. Vignais PM, Billoud B. 2007. Occurrence, classification, and biological function of hydrogenases: an overview. Chem Rev 107:4206–4272. http://dx.doi.org/10.1021/cr050196r.
227. Allegretti M, Mills DJ, McMullan G, Kühlbrandt W, Vonck J. 2014. Atomic model of the F_{420}-reducing [NiFe] hydrogenase by electron cryomicroscopy using a direct electron detector. eLife 3:e01963. http://dx.doi.org/10.7554/eLife.01963.
228. Lünsdorf H, Niedrig M, Fiebig K. 1991. Immunocytochemical localization of the coenzyme F_{420}-reducing hydrogenase in *Methanosarcina barkeri* Fusaro. J Bacteriol 173:978–984.
229. Baron SF, Brown DP, Ferry JG. 1987. Locations of the hydrogenases of *Methanobacterium formicicum* after subcellular fractionation of cell extract. J Bacteriol 169:3823–3825.
230. Baron SF, Ferry JG. 1989. Purification and properties of the membrane-associated coenzyme F_{420}-reducing hydrogenase from *Methanobacterium formicicum*. J Bacteriol 171:3846–3853.
231. Kojima N, Fox JA, Hausinger RP, Daniels L, Orme-Johnson WH, Walsh C. 1983. Paramagnetic centers in the nickel-containing, deazaflavin-reducing hydrogenase from *Methanobacterium thermoautotrophicum*. Proc Natl Acad Sci U S A 80:378–382. http://dx.doi.org/10.1073/pnas.80.2.378.
232. Lindahl PA, Kojima N, Hausinger RP, Fox JA, Teo BK, Walsh CT, Orme-Johnson WH. 1984. Nickel and iron EXAFS of F_{420}-reducing hydrogenase from *Methanobacterium thermoautotrophicum*. J Am Chem Soc 106:3062–3064. http://dx.doi.org/10.1021/ja00322a068.
233. Fox JA, Livingston DJ, Orme-Johnson WH, Walsh CT. 1987. 8-Hydroxy-5-deazaflavin-reducing hydrogenase from *Methanobacterium thermoautotrophicum*: 1. Purification and characterization. Biochemistry 26:4219–4227.
234. Yamazaki S, Tsai L, Stadtman TC, Teshima T, Nakaji A, Shiba T. 1985. Stereochemical studies of a selenium-containing hydrogenase from *Methanococcus vannielii*: determination of the absolute configuration of C-5 chirally labeled dihydro-8-hydroxy-5-deazaflavin cofactor. Proc Natl Acad Sci U S A 82:1364–1366. http://dx.doi.org/10.1073/pnas.82.5.1364.
235. Livingston DJ, Fox JA, Orme-Johnson WH, Walsh CT. 1987. 8-Hydroxy-5-deazaflavin-reducing hydrogenase from *Methanobacterium thermoautotrophicum*: 2. Kinetic and hydrogen-transfer studies. Derivation of a steady-state rate equation for deazaflavin-reducing hydrogenase. Biochemistry 26:4228–4237.
236. Sorgenfrei O, Müller S, Pfeiffer M, Sniezko I, Klein A. 1997. The [NiFe] hydrogenases of *Methanococcus voltae*: genes, enzymes and regulation. Arch Microbiol 167:189–195. http://dx.doi.org/10.1007/s002030050434.
237. Sorgenfrei O, Duin EC, Klein A, Albracht SP. 1997. Changes in the electronic structure around Ni in oxidized and reduced selenium-containing hydrogenases from *Methanococcus voltae*. Eur J Biochem 247:681–687. http://dx.doi.org/10.1111/j.1432-1033.1997.00681.x.
238. Berghöfer Y, Agha-Amiri K, Klein A. 1994. Selenium is involved in the negative regulation of the expression of selenium-free [NiFe] hydrogenases in *Methanococcus voltae*. Mol Gen Genet 242:369–373.
239. Noll I, Müller S, Klein A. 1999. Transcriptional regulation of genes encoding the selenium-free [NiFe]-hydrogenases in the archaeon *Methanococcus voltae* involves positive and negative control elements. Genetics 152:1335–1341.
240. Jeon JH, Lim JK, Kim M-S, Yang T-J, Lee S-H, Bae SS, Kim YJ, Lee SH, Lee J-H, Kang SG, Lee HS. 2015. Characterization of the *frhAGB*-encoding hydrogenase from a non-methanogenic hyperthermophilic archaeon. Extremophiles 19:109–118. http://dx.doi.org/10.1007/s00792-014-0689-y.
241. Belay N, Sparling R, Daniels L. 1986. Relationship of formate to growth and methanogenesis by *Methanococcus thermolithotrophicus*. Appl Environ Microbiol 52:1080–1085.
242. Wood GE, Haydock AK, John A, Leigh JA. 2003. Function and regulation of the formate dehydrogenase genes of the methanogenic archaeon *Methanococcus maripaludis*. J Bacteriol 185:2548–2554. http://dx.doi.org/10.1128/JB.185.8.2548-2554.2003.
243. Schauer NL, Ferry JG. 1980. Metabolism of formate in *Methanobacterium formicicum*. J Bacteriol 142:800–807.
244. Thiele JH, Zeikus JG. 1988. Control of interspecies electron flow during anaerobic digestion: significance of formate transfer versus hydrogen transfer during syntrophic methanogenesis in flocs. Appl Environ Microbiol 54:20–29.
245. Shuber AP, Orr EC, Recny MA, Schendel PF, May HD, Schauer NL, Ferry JG. 1986. Cloning, expression, and nucleotide sequence of the formate dehydrogenase genes from *Methanobacterium formicicum*. J Biol Chem 261:12942–12947.
246. Baron SF, Williams DS, May HD, Patel PS, Aldrich HC, Ferry JG. 1989. Immunogold localization of coenzyme F_{420}-reducing formate dehydrogenase and coenzyme F_{420}-reducing hydrogenase in *Methanobacterium formicicum*. Arch Microbiol 151:307–313. http://dx.doi.org/10.1007/BF00406556.
247. Boyington JC, Gladyshev VN, Khangulov SV, Stadtman TC, Sun PD. 1997. Crystal structure of formate dehydrogenase H: catalysis involving Mo, molybdopterin, selenocysteine, and an Fe4S4 cluster. Science 275:1305–1308. http://dx.doi.org/10.1126/science.275.5304.1305.
248. Barber MJ, Siegel LM, Schauer NL, May HD, Ferry JG. 1983. Formate dehydrogenase from *Methanobacterium formicicum*. Electron paramagnetic resonance spectroscopy of the molybdenum and iron-sulfur centers. J Biol Chem 258:10839–10845.
249. May HD, Patel PS, Ferry JG. 1988. Effect of molybdenum and tungsten on synthesis and composition of formate dehydrogenase in *Methanobacterium formicicum*. J Bacteriol 170:3384–3389.
250. May HD, Schauer NL, Ferry JG. 1986. Molybdopterin cofactor from *Methanobacterium formicicum* formate dehydrogenase. J Bacteriol 166:500–504.
251. Johnson JL, Bastian NR, Schauer NL, Ferry JG, Rajagopalan KV. 1991. Identification of molybdopterin guanine dinucleotide in formate dehydrogenase from *Methanobacterium formicicum*. FEMS Microbiol Lett 61:213–216.
252. Barber MJ, May HD, Ferry JG. 1986. Inactivation of formate dehydrogenase from *Methanobacterium formicicum* by cyanide. Biochemistry 25:8150–8155. http://dx.doi.org/10.1021/bi00373a004.
253. Schauer NL, Ferry JG. 1983. FAD requirement for the reduction of coenzyme F_{420} by formate dehydrogenase from *Methanobacterium formicicum*. J Bacteriol 155:467–472.

254. Schauer NL, Ferry JG, Honek JF, Orme-Johnson WH, Walsh C. 1986. Mechanistic studies of the coenzyme F_{420} reducing formate dehydrogenase from *Methanobacterium formicicum*. Biochemistry 25:7163–7168. http://dx.doi.org/10.1021/bi00370a059.
255. Seedorf H, Kahnt J, Pierik AJ, Thauer RK. 2005. *Si*-face stereospecificity at C5 of coenzyme F420 for F420H2 oxidase from methanogenic *Archaea* as determined by mass spectrometry. FEBS J 272:5337–5342. http://dx.doi.org/10.1111/j.1742-4658.2005.04931.x.
256. Lupa B, Hendrickson EL, Leigh JA, Whitman WB. 2008. Formate-dependent H_2 production by the mesophilic methanogen *Methanococcus maripaludis*. Appl Environ Microbiol 74:6584–6590. http://dx.doi.org/10.1128/AEM.01455-08.
257. Baron SF, Ferry JG. 1989. Reconstitution and properties of a coenzyme F_{420}-mediated formate hydrogenlyase system in *Methanobacterium formicicum*. J Bacteriol 171:3854–3859.
258. Thauer RK. 2012. The Wolfe cycle comes full circle. Proc Natl Acad Sci U S A 109:15084–15085. http://dx.doi.org/10.1073/pnas.1213193109.
259. Costa KC, Wong PM, Wang T, Lie TJ, Dodsworth JA, Swanson I, Burn JA, Hackett M, Leigh JA. 2010. Protein complexing in a methanogen suggests electron bifurcation and electron delivery from formate to heterodisulfide reductase. Proc Natl Acad Sci U S A 107:11050–11055. http://dx.doi.org/10.1073/pnas.1003653107.
260. Costa KC, Lie TJ, Xia Q, Leigh JA. 2013. VhuD facilitates electron flow from H2 or formate to heterodisulfide reductase in *Methanococcus maripaludis*. J Bacteriol 195:5160–5165. http://dx.doi.org/10.1128/JB.00895-13.
261. Costa KC, Lie TJ, Jacobs MA, Leigh JA. 2013. H_2-independent growth of the hydrogenotrophic methanogen *Methanococcus maripaludis*. mBio 4:e00062-13. http://dx.doi.org/10.1128/mBio.00062-13.
262. Lohner ST, Deutzmann JS, Logan BE, Leigh J, Spormann AM. 2014. Hydrogenase-independent uptake and metabolism of electrons by the archaeon *Methanococcus maripaludis*. ISME J 8:1673–1681. http://dx.doi.org/10.1038/ismej.2014.82.
263. Sattler C, Wolf S, Fersch J, Goetz S, Rother M. 2013. Random mutagenesis identifies factors involved in formate-dependent growth of the methanogenic archaeon *Methanococcus maripaludis*. Mol Genet Genomics 288:413–424. http://dx.doi.org/10.1007/s00438-013-0756-6.
264. Jones JB, Dilworth GL, Stadtman TC. 1979. Occurrence of selenocysteine in the selenium-dependent formate dehydrogenase of *Methanococcus vannielii*. Arch Biochem Biophys 195:255–260. http://dx.doi.org/10.1016/0003-9861(79)90351-5.
265. Jones JB, Stadtman TC. 1977. *Methanococcus vannielii*: culture and effects of selenium and tungsten on growth. J Bacteriol 130:1404–1406.
266. Hendrickson EL, Kaul R, Zhou Y, Bovee D, Chapman P, Chung J, Conway de Macario E, Dodsworth JA, Gillett W, Graham DE, Hackett M, Haydock AK, Kang A, Land ML, Levy R, Lie TJ, Major TA, Moore BC, Porat I, Palmeiri A, Rouse G, Saenphimmachak C, Söll D, Van Dien S, Wang T, Whitman WB, Xia Q, Zhang Y, Larimer FW, Olson MV, Leigh JA. 2004. Complete genome sequence of the genetically tractable hydrogenotrophic methanogen *Methanococcus maripaludis*. J Bacteriol 186:6956–6969. http://dx.doi.org/10.1128/JB.186.20.6956-6969.2004.
267. Rother M, Mathes I, Lottspeich F, Böck A. 2003. Inactivation of the *selB* gene in *Methanococcus maripaludis*: effect on synthesis of selenoproteins and their sulfur-containing homologs. J Bacteriol 185:107–114. http://dx.doi.org/10.1128/JB.185.1.107-114.2003.
268. Stock T, Selzer M, Connery S, Seyhan D, Resch A, Rother M. 2011. Disruption and complementation of the selenocysteine biosynthesis pathway reveals a hierarchy of selenoprotein gene expression in the archaeon *Methanococcus maripaludis*. Mol Microbiol 82:734–747. http://dx.doi.org/10.1111/j.1365-2958.2011.07850.x.
269. Maeder DL, Anderson I, Brettin TS, Bruce DC, Gilna P, Han CS, Lapidus A, Metcalf WW, Saunders E, Tapia R, Sowers KR. 2006. The *Methanosarcina barkeri* genome: comparative analysis with *Methanosarcina acetivorans* and *Methanosarcina mazei* reveals extensive rearrangement within methanosarcinal genomes. J Bacteriol 188:7922–7931. http://dx.doi.org/10.1128/JB.00810-06.
270. Frimmer U, Widdel F. 1989. Oxidation of ethanol by methanogenic bacteria. Arch Microbiol 152:479–483. http://dx.doi.org/10.1007/BF00446933.
271. Widdel F, Wolfe RS. 1989. Expression of secondary alcohol dehydrogenase in methanogenic bacteria and purification of the F_{420}-specific enzyme from *Methanogenium thermophilum* strain TCI. Arch Microbiol 152:322–328. http://dx.doi.org/10.1007/BF00425168.
272. Bleicher K, Winter J. 1991. Purification and properties of F420- and $NADP^+$-dependent alcohol dehydrogenases of Methanogenium liminatans and Methanobacterium palustre, specific for secondary alcohols. Eur J Biochem 200:43–51. http://dx.doi.org/10.1111/j.1432-1033.1991.tb21046.x.
273. Klein AR, Berk H, Purwantini E, Daniels L, Thauer RK. 1996. Si-face stereospecificity at C5 of coenzyme F_{420} for F_{420}-dependent glucose-6-phosphate dehydrogenase from *Mycobacterium smegmatis* and F_{420}-dependent alcohol dehydrogenase from *Methanoculleus thermophilicus*. Eur J Biochem 239:93–97. http://dx.doi.org/10.1111/j.1432-1033.1996.0093u.x.
274. Escalante-Semerena JC, Leigh JA, Rinehart KL, Wolfe RS. 1984. Formaldehyde activation factor, tetrahydromethanopterin, a coenzyme of methanogenesis. Proc Natl Acad Sci U S A 81:1976–1980. http://dx.doi.org/10.1073/pnas.81.7.1976.
275. te Brommelstroet BW, Hensgens CM, Keltjens JT, van der Drift C, Vogels GD. 1991. Purification and characterization of coenzyme F420-dependent 5,10-methylenetetrahydromethanopterin dehydrogenase from *Methanobacterium thermoautotrophicum* strain delta H. Biochim Biophys Acta 1073:77–84. http://dx.doi.org/10.1016/0304-4165(91)90185-J.
276. Klein AR, Koch J, Stetter KO, Thauer RK. 1993. Two N^5, N^{10}-methylenetetrahydromethanopterin dehydrogenases in the extreme thermophile Methanopyrus kandleri: characterization of the coenzyme F_{420}-dependent enzyme. Arch Microbiol 160:186–192.
277. Mukhopadhyay B, Purwantini E, Pihl TD, Reeve JN, Daniels L. 1995. Cloning, sequencing, and transcriptional analysis of the coenzyme F420-dependent methylene-5,6,7,8-tetrahydromethanopterin dehydrogenase gene from Methanobacterium thermoautotrophicum strain Marburg and functional expression in Escherichia coli. J Biol Chem 270:2827–2832. http://dx.doi.org/10.1074/jbc.270.6.2827.
278. Klein AR, Thauer RK. 1997. Overexpression of the coenzyme-F_{420}-dependent N^5,N^{10}-methylenetetrahydromethanopterin dehydrogenase gene from the hyperthermophilic *Methanopyrus kandleri*. Eur J Biochem 245:386–391. http://dx.doi.org/10.1111/j.1432-1033.1997.t01-1-00386.x.
279. Ma K, Thauer RK. 1990. Purification and properties of N^5, N^{10}-methylenetetrahydromethanopterin reductase from Methanobacterium thermoautotrophicum (strain Marburg). Eur J Biochem 191:187–193. http://dx.doi.org/10.1111/j.1432-1033.1990.tb19109.x.
280. te Brömmelstroet BW, Hensgens CM, Keltjens JT, van der Drift C, Vogels GD. 1990. Purification and properties of 5,10-methylenetetrahydromethanopterin reductase, a coenzyme F_{420}-dependent enzyme, from *Methanobacterium thermoautotrophicum* strain delta H. J Biol Chem 265:1852–1857.
281. Ma K, Linder D, Stetter KO, Thauer RK. 1991. Purification and properties of N^5,N^{10}-methylenetetrahydromethanopterin reductase (coenzyme F_{420}-dependent) from the extreme thermophile *Methanopyrus kandleri*. Arch Microbiol 155:593–600. http://dx.doi.org/10.1007/BF00245355.
282. Ma K, Thauer RK. 1990. N^5, N^{10}-Methylenetetrahydromethanopterin reductase from *Methanosarcina barkeri*. FEMS Microbiol Lett 70:119–123. http://dx.doi.org/10.1111/j.1574-6968.1990.tb13963.x.
283. Vaupel M, Thauer RK. 1995. Coenzyme F_{420}-dependent N^5,N^{10}-methylenetetrahydromethanopterin reductase (Mer) from *Methanobacterium thermoautotrophicum* strain Marburg. Cloning, sequencing, transcriptional analysis, and functional expression in *Escherichia coli* of the *mer* gene. Eur J Biochem 231:773–778. http://dx.doi.org/10.1111/j.1432-1033.1995.0773d.x.
284. te Brömmelstroet BWJ, Geerts WJ, Keltjens JT, van der Drift C, Vogels GD. 1991. Purification and properties of 5,10-methylenetetrahydromethanopterin dehydrogenase and 5,10-methylenetetrahydromethanopterin reductase, two coenzyme F_{420}-dependent enzymes, from *Methanosarcina barkeri*. Biochim Biophys Acta 1079:293–302. http://dx.doi.org/10.1016/0167-4838(91)90072-8.
285. Warkentin E, Hagemeier CH, Shima S, Thauer RK, Ermler U. 2005. The structure of F420-dependent methylenetetrahydromethanopterin dehydrogenase: a crystallographic "superstructure" of the selenomethionine-labelled protein crystal structure. Acta Crystallogr Sect D Biol Crystallogr 61:198–202. http://dx.doi.org/10.1107/S0907444904030732.
286. Hagemeier CH, Shima S, Warkentin E, Thauer RK, Ermler U. 2003. Coenzyme F_{420}-dependent methylenetetrahydromethanopterin dehydrogenase from *Methanopyrus kandleri*: the selenomethionine-labelled and non-labelled enzyme crystallized in two different forms. Acta Crys-

tallogr D Biol Crystallogr 59:1653–1655. http://dx.doi.org/10.1107/S0907444903014896.
287. Klein AR, Thauer RK. 1995. Re-face specificity at C14a of methylenetetrahydromethanopterin and Si-face specificity at C5 of coenzyme F_{420} for coenzyme F_{420}-dependent methylenetetrahydromethanopterin dehydrogenase from methanogenic *Archaea*. Eur J Biochem 227:169–174. http://dx.doi.org/10.1111/j.1432-1033.1995.tb20373.x.
288. Bartoschek S, Buurman G, Thauer RK, Geierstanger BH, Weyrauch JP, Griesinger C, Nilges M, Hutter MC, Helms V. 2001. Re-face stereospecificity of methylenetetrahydromethanopterin and methylenetetrahydrofolate dehydrogenases is predetermined by intrinsic properties of the substrate. Chembiochem 2(7-8):530–541. http://dx.doi.org/10.1002/1439-7633(20010803)2:7/8<530::AID-CBIC530>3.0.CO;2-0.
289. Kunow J, Schworer B, Setzke E, Thauer RK. 1993. Si-face stereospecificity at C5 of coenzyme F_{420} for F_{420}-dependent N^5,N^{10}-methylenetetrahydromethanopterin dehydrogenase, F_{420}-dependent N^5,N^{10}-methylenetetrahydromethanopterin. Eur J Biochem 214:641–646. http://dx.doi.org/10.1111/j.1432-1033.1993.tb17964.x.
290. von Bunau R, Zirngibl C, Thauer RK, Klein A. 1991. Hydrogen-forming and coenzyme-F_{420}-reducing methylene tetrahydromethanopterin dehydrogenase are genetically distinct enzymes in *Methanobacterium thermoautotrophicum* (Marburg). Eur J Biochem 202:1205–1208. http://dx.doi.org/10.1111/j.1432-1033.1991.tb16491.x.
291. Shima S, Pilak O, Vogt S, Schick M, Stagni MS, Meyer-Klaucke W, Warkentin E, Thauer RK, Ermler U. 2008. The crystal structure of [Fe]-hydrogenase reveals the geometry of the active site. Science 321:572–575. http://dx.doi.org/10.1126/science.1158978.
292. Zirngibl C, Hedderich R, Thauer RK. 1990. N^5,N^{10}-Methylenetetrahydromethanopterin dehydrogenase from *Methanobacterium thermoautotrophicum* has hydrogenase activity. FEBS Lett 261:112–116. http://dx.doi.org/10.1016/0014-5793(90)80649-4.
293. Hendrickson EL, Haydock AK, Moore BC, Whitman WB, Leigh JA. 2007. Functionally distinct genes regulated by hydrogen limitation and growth rate in methanogenic Archaea. Proc Natl Acad Sci U S A 104:8930–8934. http://dx.doi.org/10.1073/pnas.0701157104.
294. Pennings JL, Vermeij P, de Poorter LM, Keltjens JT, Vogels GD. 2000. Adaptation of methane formation and enzyme contents during growth of *Methanobacterium thermoautotrophicum* (strain deltaH) in a fed-batch fermentor. Antonie Van Leeuwenhoek 77:281–291. http://dx.doi.org/10.1023/A:1002443012525.
295. Nolling J, Pihl TD, Vriesema A, Reeve JN. 1995. Organization and growth phase-dependent transcription of methane genes in two regions of the *Methanobacterium thermoautotrophicum* genome. J Bacteriol 177:2460–2468.
296. Pennings JLA, Keltjens JT, Vogels GD. 1998. Isolation and characterization of *Methanobacterium thermoautotrophicum* ΔH mutants unable to grow under hydrogen-deprived conditions. J Bacteriol 180:2676–2681.
297. Afting C, Hochheimer A, Thauer RK. 1998. Function of H_2-forming methylenetetrahydromethanopterin dehydrogenase from *Methanobacterium thermoautotrophicum* in coenzyme F_{420} reduction with H_2. Arch Microbiol 169:206–210. http://dx.doi.org/10.1007/s002030050562.
298. Afting C, Kremmer E, Brucker C, Hochheimer A, Thauer RK. 2000. Regulation of the synthesis of H_2-forming methylenetetrahydromethanopterin dehydrogenase (Hmd) and of HmdII and HmdIII in Methanothermobacter marburgensis. Arch Microbiol 174:225–232. http://dx.doi.org/10.1007/s002030000197.
299. Schmitz RA, Linder D, Stetter KO, Thauer RK. 1991. N^5,N^{10}-Methylenetetrahydromethanopterin reductase (coenzyme F_{420}-dependent) and formylmethanofuran dehydrogenase from the hyperthermophile *Archaeoglobus fulgidus*. Arch Microbiol 156:427–434. http://dx.doi.org/10.1007/BF00248722.
300. Schworer B, Breitung J, Klein AR, Stetter KO, Thauer RK. 1993. Formylmethanofuran: tetrahydromethanopterin formyltransferase and N^5,N^{10}-methylenetetrahydromethanopterin dehydrogenase from the sulfate-reducing Archaeoglobus fulgidus: similarities with the enzymes from methanogenic Archaea. Arch Microbiol 159:225–232. http://dx.doi.org/10.1007/BF00248476.
301. Vorholt JA, Chistoserdova L, Lidstrom ME, Thauer RK. 1998. The NADP-dependent methylene tetrahydromethanopterin dehydrogenase in *Methylobacterium extorquens* AM1. J Bacteriol 180:5351–5356.
302. Vorholt JA, Kalyuzhnaya MG, Hagemeier CH, Lidstrom ME, Chistoserdova L. 2005. MtdC, a novel class of methylene tetrahydromethanopterin dehydrogenases. J Bacteriol 187:6069–6074. http://dx.doi.org/10.1128/JB.187.17.6069-6074.2005.
303. Deppenmeier U, Blaut M, Mahlmann A, Gottschalk G. 1990. Reduced coenzyme F_{420}: heterodisulfide oxidoreductase, a proton-translocating redox system in methanogenic bacteria. Proc Natl Acad Sci U S A 87:9449–9453. http://dx.doi.org/10.1073/pnas.87.23.9449.
304. Deppenmeier U, Lienard T, Gottschalk G. 1999. Novel reactions involved in energy conservation by methanogenic archaea. FEBS Lett 457:291–297. http://dx.doi.org/10.1016/S0014-5793(99)01026-1.
305. Bäumer S, Murakami E, Brodersen J, Gottschalk G, Ragsdale SW, Deppenmeier U. 1998. The $F_{420}H_2$:heterodisulfide oxidoreductase system from *Methanosarcina* species: 2-hydroxyphenazine mediates electron transfer from $F_{420}H_2$ dehydrogenase to heterodisulfide reductase. FEBS Lett 428:295–298. http://dx.doi.org/10.1016/S0014-5793(98)00555-9.
306. Ide T, Bäumer S, Deppenmeier U. 1999. Energy conservation by the H2:heterodisulfide oxidoreductase from *Methanosarcina mazei* Gö1: identification of two proton-translocating segments. J Bacteriol 181:4076–4080.
307. Heiden S, Hedderich R, Setzke E, Thauer RK. 1994. Purification of a two-subunit cytochrome *b*-containing heterodisulfide reductase from methanol-grown *Methanosarcina barkeri*. Eur J Biochem 221:855–861. http://dx.doi.org/10.1111/j.1432-1033.1994.tb18800.x.
308. Beifuss U, Tietze M, Bäumer S, Deppenmeier U. 2000. Methanophenazine: structure, total synthesis, and function of a new cofactor from methanogenic archaea. Angew Chem Int Ed 39:2470–2472. http://dx.doi.org/10.1002/1521-3773(20000717)39:14<2470::AID-ANIE2470>3.0.CO;2-R.
309. Abken HJ, Tietze M, Brodersen J, Bäumer S, Beifuss U, Deppenmeier U. 1998. Isolation and characterization of methanophenazine and function of phenazines in membrane-bound electron transport of *Methanosarcina mazei* Go1. J Bacteriol 180:2027–2032.
310. Brodersen J, Bäumer S, Abken H-J, Gottschalk G, Deppenmeier U. 1999. Inhibition of membrane-bound electron transport of the methanogenic archaeon *Methanosarcina mazei* Gö1 by diphenyleneiodonium. Eur J Biochem 259:218–224. http://dx.doi.org/10.1046/j.1432-1327.1999.00017.x.
311. Kühn W, Fiebig K, Walther R, Gottschalk G. 1979. Presence of a cytochrome b_{559} in *Methanosarcina barkeri*. FEBS Lett 105:271–274. http://dx.doi.org/10.1016/0014-5793(79)80627-4.
312. Kühn W, Gottschalk G. 1983. Characterization of the cytochromes occurring in *Methanosarcina* species. Eur J Biochem 135:89–94. http://dx.doi.org/10.1111/j.1432-1033.1983.tb07621.x.
313. Abken H-J, Deppenmeier U. 1997. Purification and properties of an $F_{420}H_2$ dehydrogenase from *Methanosarcina mazei* Go1. FEMS Microbiol Lett 154:231–237. http://dx.doi.org/10.1016/S0378-1097(97)00330-3.
314. Haase P, Deppenmeier U, Blaut M, Gottschalk G. 1992. Purification and characterization of $F_{420}H_2$-dehydrogenase from *Methanolobus tindarius*. Eur J Biochem 531:527–531.
315. Westenberg DJ, Braune A, Ruppert C, Müller V, Herzberg C, Gottschalk G, Blaut M. 1999. The $F_{420}H_2$-dehydrogenase from *Methanolobus tindarius*: cloning of the *ffd* operon and expression of the genes in *Escherichia coli*. FEMS Microbiol Lett 170:389–398. http://dx.doi.org/10.1111/j.1574-6968.1999.tb13399.x.
316. Efremov RG, Sazanov LA. 2011. Respiratory complex I: "steam engine" of the cell? Curr Opin Struct Biol 21:532–540. http://dx.doi.org/10.1016/j.sbi.2011.07.002.
317. Efremov RG, Sazanov LA. 2012. The coupling mechanism of respiratory complex I - a structural and evolutionary perspective. Biochim Biophys Acta 1817:1785–1795. http://dx.doi.org/10.1016/j.bbabio.2012.02.015.
318. Deppenmeier U. 2004. The membrane-bound electron transport system of *Methanosarcina* species. J Bioenerg Biomembr 36:55–64. http://dx.doi.org/10.1023/B:JOBB.0000019598.64642.97.
319. Sazanov LA. 2015. A giant molecular proton pump: structure and mechanism of respiratory complex I. Nat Rev Mol Cell Biol 16:375–388. http://dx.doi.org/10.1038/nrm3997.
320. Baradaran R, Berrisford JM, Minhas GS, Sazanov LA. 2013. Crystal structure of the entire respiratory complex I. Nature 494:443–448. http://dx.doi.org/10.1038/nature11871.
321. Galagan JE, Nusbaum C, Roy A, Endrizzi MG, Macdonald P, FitzHugh W, Calvo S, Engels R, Smirnov S, Atnoor D, Brown A, Allen N, Naylor J, Stange-Thomann N, DeArellano K, Johnson R, Linton L, McEwan P, McKernan K, Talamas J, Tirrell A, Ye W, Zimmer A,

Barber RD, Cann I, Graham DE, Grahame DA, Guss AM, Hedderich R, Ingram-Smith C, Kuettner HC, Krzycki JA, Leigh JA, Li W, Liu J, Mukhopadhyay B, Reeve JN, Smith K, Springer TA, Umayam LA, White O, White RH, Conway de Macario E, Ferry JG, Jarrell KF, Jing H, Macario AJL, Paulsen I, Pritchett M, Sowers KR, Swanson RV, Zinder SH, Lander E, Metcalf WW, Birren B. 2002. The genome of *M. acetivorans* reveals extensive metabolic and physiological diversity. Genome Res 12:532–542. http://dx.doi.org/10.1101/gr.223902.

322. Guss AM, Kulkarni G, Metcalf WW. 2009. Differences in hydrogenase gene expression between *Methanosarcina acetivorans* and *Methanosarcina barkeri*. J Bacteriol 191:2826–2833. http://dx.doi.org/10.1128/JB.00563-08.
323. Guss AM, Mukhopadhyay B, Zhang JK, Metcalf WW. 2005. Genetic analysis of *mch* mutants in two *Methanosarcina* species demonstrates multiple roles for the methanopterin-dependent C-1 oxidation/reduction pathway and differences in H_2 metabolism between closely related species. Mol Microbiol 55:1671–1680. http://dx.doi.org/10.1111/j.1365-2958.2005.04514.x.
324. Lessner DJ, Li L, Li Q, Rejtar T, Andreev VP, Reichlen M, Hill K, Moran JJ, Karger BL, Ferry JG. 2006. An unconventional pathway for reduction of CO2 to methane in CO-grown Methanosarcina acetivorans revealed by proteomics. Proc Natl Acad Sci U S A 103:17921–17926. http://dx.doi.org/10.1073/pnas.0608833103.
325. Welte C, Kallnik V, Grapp M, Bender G, Ragsdale S, Deppenmeier U. 2010. Function of Ech hydrogenase in ferredoxin-dependent, membrane-bound electron transport in *Methanosarcina mazei*. J Bacteriol 192:674–678. http://dx.doi.org/10.1128/JB.01307-09.
326. Deppenmeier U, Johann A, Hartsch T, Merkl R, Schmitz RA, Martinez-Arias R, Henne A, Wiezer A, Bäumer S, Jacobi C, Brüggemann H, Lienard T, Christmann A, Bömeke M, Steckel S, Bhattacharyya A, Lykidis A, Overbeek R, Klenk H-P, Gunsalus RP, Fritz H-J, Gottschalk G. 2002. The genome of *Methanosarcina mazei*: evidence for lateral gene transfer between bacteria and archaea. J Mol Microbiol Biotechnol 4:453–461.
327. Welte C, Deppenmeier U. 2011. Membrane-bound electron transport in *Methanosaeta thermophila*. J Bacteriol 193:2868–2870. http://dx.doi.org/10.1128/JB.00162-11.
328. Arshad A, Speth DR, De Graaf RM, den Camp HJM, Jetten MSM, Welte CU. 2015. A metagenomics-based metabolic model of nitrate-dependent anaerobic oxidation of methane by *Methanoperedens*-like archaea. Front Microbiol 6:1423. http://dx.doi.org/10.3389/fmicb.2015.01423.
329. Silaghi-Dumitrescu R, Ng KY, Viswanathan R, Kurtz DM, Jr. 2005. A flavo-diiron protein from *Desulfovibrio vulgaris* with oxidase and nitric oxide reductase activities. Evidence for an *in vivo* nitric oxide scavenging function. Biochemistry 44:3572–3579.
330. Tholen A, Pester M, Brune A. 2007. Simultaneous methanogenesis and oxygen reduction by *Methanobrevibacter cuticularis* at low oxygen fluxes. FEMS Microbiol Ecol 62:303–312. http://dx.doi.org/10.1111/j.1574-6941.2007.00390.x.
331. Angel R, Claus P, Conrad R. 2012. Methanogenic archaea are globally ubiquitous in aerated soils and become active under wet anoxic conditions. ISME J 6:847–862. http://dx.doi.org/10.1038/ismej.2011.141.
332. Kaster AK, Goenrich M, Seedorf H, Liesegang H, Wollherr A, Gottschalk G, Thauer RK. 2011. More than 200 genes required for methane formation from H_2 and CO_2 and energy conservation are present in Methanothermobacter marburgensis and Methanothermobacter thermautotrophicus. Archaea 1:973848.
333. Balderston WL, Payne WJ. 1976. Inhibition of methanogenesis in salt marsh sediments and whole-cell suspensions of methanogenic bacteria by nitrogen oxides. Appl Environ Microbiol 32:264–269.
334. Rothe O, Thomm M. 2000. A simplified method for the cultivation of extreme anaerobic *Archaea* based on the use of sodium sulfite as reducing agent. Extremophiles 4:247–252. http://dx.doi.org/10.1007/PL00010716.
335. Daniels L, Belay N, Rajagopal BS. 1986. Assimilatory reduction of sulfate and sulfite by methanogenic bacteria. Appl Environ Microbiol 51:703–709.
336. Susanti D, Mukhopadhyay B. 2012. An intertwined evolutionary history of methanogenic archaea and sulfate reduction. PLoS One 7:e45313. http://dx.doi.org/10.1371/journal.pone.0045313.
337. Johnson EF, Mukhopadhyay B. 2008. A novel coenzyme F_{420} dependent sulfite reductase and a small sulfite reductase in methanogenic archaea, p 202–216. *In* Dahl C, Friedrich CG (ed), Microbial sulfur metabolism. Springer, Berlin, Germany.
338. Susanti D, Wong JH, Vensel WH, Loganathan U, DeSantis R, Schmitz RA, Balsera M, Buchanan BB, Mukhopadhyay B. 2014. Thioredoxin targets fundamental processes in a methane-producing archaeon, *Methanocaldococcus jannaschii*. Proc Natl Acad Sci U S A 111:2608–2613. http://dx.doi.org/10.1073/pnas.1324240111.
339. Moura JJG, Moura I, Santos H, Xavier AV, Scandellari M, LeGall J. 1982. Isolation of P_{590} from *Methanosarcina barkeri*: evidence for the presence of sulfite reductase activity. Biochem Biophys Res Commun 108:1002–1009. http://dx.doi.org/10.1016/0006-291X(82)92099-X.
340. Eguchi S, Nakata H, Nishio N, Nagai S. 1984. $NADP^+$ reduction by a methanogen using HCOOH or H_2 as electron donor. Appl Microbiol Biotechnol 20:213–217.
341. Jones JB, Stadtman TC. 1980. Reconstitution of a formate-NADP+ oxidoreductase from formate dehydrogenase and a 5-deazaflavin-linked NADP+ reductase isolated from *Methanococcus vannielii*. J Biol Chem 255:1049–1053.
342. Yamazaki S, Tsai L. 1980. Purification and properties of 8-hydroxy-5-deazaflavin-dependent $NADP^+$ reductase from Methanococcus vannielii. J Biol Chem 255:6462–6465.
343. Dudley Eirich L, Dugger RS. 1984. Purification and properties of an F_{420}-dependent NADP reductase from *Methanobacterium thermoautotrophicum*. Biochim Biophys Acta 802:454–458. http://dx.doi.org/10.1016/0304-4165(84)90364-7.
344. Berk H, Thauer RK. 1998. $F_{420}H_2$:NADP oxidoreductase from *Methanobacterium thermoautotrophicum*: identification of the encoding gene via functional overexpression in *Escherichia coli*. FEBS Lett 438:124–126. http://dx.doi.org/10.1016/S0014-5793(98)01288-5.
345. Elias DA, Juck DF, Berry KA, Sparling R. 2000. Purification of the $NADP^+$:F_{420} oxidoreductase of *Methanosphaera stadtmanae*. Can J Microbiol 46:998–1003. http://dx.doi.org/10.1139/w00-090.
346. Yamazaki S, Tsai L, Stadtman TC, Jacobson FS, Walsh C. 1980. Stereochemical studies of 8-hydroxy-5-deazaflavin-dependent $NADP^+$ reductase from Methanococcus vannielii. J Biol Chem 255:9025–9027.
347. Schönheit P, Keweloh H, Thauer RK. 1981. Factor F_{420} degradation in *Methanobacterium thermoautotrophicum* during exposure to oxygen. FEMS Microbiol Lett 12:347–349. http://dx.doi.org/10.1111/j.1574-6968.1981.tb07671.x.
348. Hausinger RP, Orme-Johnson WH, Walsh C. 1985. Factor 390 chromophores: phosphodiester between AMP or GMP and methanogen factor 420. Biochemistry 24:1629–1633. http://dx.doi.org/10.1021/bi00328a010.
349. Kiener A, Orme-Johnson W, Walsh C. 1988. Reversible conversion of coenzyme F420 to the 8-OH-AMP and 8-OH-GMP esters, F390-A and F390-G, on oxygen exposure and reestablishment of anaerobiosis in *Methanobacterium thermoautotrophicum*. Arch Microbiol 150:249–253. http://dx.doi.org/10.1007/BF00407788.
350. Keltjens JT, Vogels GD. 1989. The ATP-dependent synthesis of factor 390 by cell-free extracts of *Methanobacterium thermoautotrophicum* (strain ΔH). FEMS Microbiol Lett 60:5–10. http://dx.doi.org/10.1111/j.1574-6968.1989.tb03409.x.
351. Gloss LM, Hausinger RP. 1988. Methanogen factor 390 formation: species distribution, reversibility and effects of non-oxidative cellular stresses. Biofactors 1:237–240.
352. van de Wijngaard WMH, Vermey P, Van der Drift C. 1991. Formation of factor 390 by cell extracts of *Methanosarcina barkeri*. J Bacteriol 173:2710–2711.
353. Gloss LM, Hausinger RP. 1987. Reduction potential characterization of methanogen factor 390. FEMS Microbiol Lett 48:143–145. http://dx.doi.org/10.1111/j.1574-6968.1987.tb02531.x.
354. Vermeij P, Detmers FJM, Broers FJM, Keltjens JT, Van Der Drift C. 1994. Purification and characterization of coenzyme F_{390} synthetase from *Methanobacterium thermoautotrophicum* (strain ΔH). Eur J Biochem 226:185–191. http://dx.doi.org/10.1111/j.1432-1033.1994.tb20040.x.
355. Vermeij P, van der Steen RJ, Keltjens JT, Vogels GD, Leisinger T. 1996. Coenzyme F_{390} synthetase from *Methanobacterium thermoautotrophicum* Marburg belongs to the superfamily of adenylate-forming enzymes. J Bacteriol 178:505–510.
356. Kengen SW, von den Hoff HW, Keltjens JT, van der Drift C, Vogels GD. 1991. F_{390} synthetase and F_{390} hydrolase from *Methanobacterium thermoautotrophicum* (strain delta H). Biofactors 3:61–65.
357. Vermeij P, Vinke E, Keltjens JT, Van Der Drift C. 1995. Purification

and properties of coenzyme F_{390} hydrolase from *Methanobacterium thermoautotrophicum* (strain Marburg). Eur J Biochem 234:592–597. http://dx.doi.org/10.1111/j.1432-1033.1995.592_b.x.
358. Vermeij P, Pennings JL, Maassen SM, Keltjens JT, Vogels GD. 1997. Cellular levels of factor 390 and methanogenic enzymes during growth of *Methanobacterium thermoautotrophicum* deltaH. J Bacteriol 179:6640–6648.
359. Morgan RM, Pihl TD, Nolling J, Reeve JN. 1997. Hydrogen regulation of growth, growth yields, and methane gene transcription in *Methanobacterium thermoautotrophicum* deltaH. J Bacteriol 179:889–898.
360. Saviola B, Bishai W. 2006. The genus *Mycobacterium* - medical, p 919–933. *In* Dworkin M, Falkow S, Rosenberg E, Schleifer K-H, Stackebrandt E (ed), The prokaryotes. Springer, New York, NY.
361. Hartmans S, de Bont JM, Stackebrandt E. 2006. The genus *Mycobacterium* - nonmedical, p 889–918. *In* Dworkin M, Falkow S, Rosenberg E, Schleifer K-H, Stackebrandt E (ed), The prokaryotes. Springer, New York, NY.
362. Cole ST, Eiglmeier K, Parkhill J, James KD, Thomson NR, Wheeler PR, Honore N, Garnier T, Churcher C, Harris D, Mungall K, Basham D, Brown D, Chillingworth T, Connor R, Davies RM, Devlin K, Duthoy S, Feltwell T, Fraser A, Hamlin N, Holroyd S, Hornsby T, Jagels K, Lacroix C, Maclean J, Moule S, Murphy L, Oliver K, Quail MA, Rajandream M-A, Rutherford KM, Rutter S, Seeger K, Simon S, Simmonds M, Skelton J, Squares R, Squares S, Stevens K, Taylor K, Whitehead S, Woodward JR, Barrell BG. 2001. Massive gene decay in the leprosy bacillus. Nature 409:1007–1011. http://dx.doi.org/10.1038/35059006.
363. Hasan MR, Rahman M, Jaques S, Purwantini E, Daniels L. 2010. Glucose 6-phosphate accumulation in mycobacteria: implications for a novel F_{420}-dependent anti-oxidant defense system. J Biol Chem 285:19135–19144. http://dx.doi.org/10.1074/jbc.M109.074310.
364. Bashiri G, Perkowski EF, Turner AP, Feltcher ME, Braunstein M, Baker EN. 2012. Tat-dependent translocation of an F_{420}-binding protein of *Mycobacterium tuberculosis*. PLoS One 7:e45003. http://dx.doi.org/10.1371/journal.pone.0045003.
365. Purwantini E, Mukhopadhyay B. 2013. Rv0132c of *Mycobacterium tuberculosis* encodes a coenzyme F420-dependent hydroxymycolic acid dehydrogenase. PLoS One 8:e81985. http://dx.doi.org/10.1371/journal.pone.0081985.
366. Yuan Y, Zhu Y, Crane DD, Barry CE, III. 1998. The effect of oxygenated mycolic acid composition on cell wall function and macrophage growth in *Mycobacterium tuberculosis*. Mol Microbiol 29:1449–1458. http://dx.doi.org/10.1046/j.1365-2958.1998.01026.x.
367. Dubnau E, Chan J, Raynaud C, Mohan VP, Lanéelle M-A, Yu K, Quémard A, Smith I, Daffé M. 2000. Oxygenated mycolic acids are necessary for virulence of *Mycobacterium tuberculosis* in mice. Mol Microbiol 36:630–637.
368. Sambandan D, Dao DN, Weinrick BC, Vilchèze C, Gurcha SS, Ojha A, Kremer L, Besra GS, Hatfull GF, Jacobs WR, Jr. 2013. Keto-mycolic acid-dependent pellicle formation confers tolerance to drug-sensitive *Mycobacterium tuberculosis*. mBio 4:e00222-13. http://dx.doi.org/10.1128/mBio.00222-13.
369. Kumar A, Deshane JS, Crossman DK, Bolisetty S, Yan B-S, Kramnik I, Agarwal A, Steyn AJC. 2008. Heme oxygenase-1-derived carbon monoxide induces the *Mycobacterium tuberculosis* dormancy regulon. J Biol Chem 283:18032–18039. http://dx.doi.org/10.1074/jbc.M802274200.
370. Nambu S, Matsui T, Goulding CW, Takahashi S, Ikeda-Saito M. 2013. A new way to degrade heme: the *Mycobacterium tuberculosis* enzyme MhuD catalyzes heme degradation without generating CO. J Biol Chem 288:10101–10109. http://dx.doi.org/10.1074/jbc.M112.448399.
371. Contreras H, Chim N, Credali A, Goulding CW. 2014. Heme uptake in bacterial pathogens. Curr Opin Chem Biol 19:34–41. http://dx.doi.org/10.1016/j.cbpa.2013.12.014.
372. Stocker R, Yamamoto Y, McDonagh AF, Glazer AN, Ames BN. 1987. Bilirubin is an antioxidant of possible physiological importance. Science 235:1043–1046. http://dx.doi.org/10.1126/science.3029864.
373. Barañano DE, Rao M, Ferris CD, Snyder SH. 2002. Biliverdin reductase: a major physiologic cytoprotectant. Proc Natl Acad Sci U S A 99:16093–16098. http://dx.doi.org/10.1073/pnas.252626999.
374. Cook GM, Greening C, Hards K, Berney M. 2014. Energetics of pathogenic bacteria and opportunities for drug development. Adv Microb Physiol 65:1–62. http://dx.doi.org/10.1016/bs.ampbs.2014.08.001.
375. Berney M, Greening C, Conrad R, Jacobs WR, Cook GM. 2014. An obligately aerobic soil bacterium activates fermentative hydrogen production to survive reductive stress during hypoxia. Proc Natl Acad Sci U S A 111:11479–11484. http://dx.doi.org/10.1073/pnas.1407034111.
376. Darwin KH, Ehrt S, Gutierrez-Ramos J-C, Weich N, Nathan CF. 2003. The proteasome of *Mycobacterium tuberculosis* is required for resistance to nitric oxide. Science 302:1963–1966. http://dx.doi.org/10.1126/science.1091176.
377. MacMicking J, Xie Q, Nathan C. 1997. Nitric oxide and macrophage function. Annu Rev Immunol 15:323–350. http://dx.doi.org/10.1146/annurev.immunol.15.1.323.
378. Yu K, Mitchell C, Xing Y, Magliozzo RS, Bloom BR, Chan J. 1999. Toxicity of nitrogen oxides and related oxidants on mycobacteria: *M. tuberculosis* is resistant to peroxynitrite anion. Tuber Lung Dis 79:191–198. http://dx.doi.org/10.1054/tuld.1998.0203.
379. Darwin KH, Nathan CF. 2005. Role for nucleotide excision repair in virulence of *Mycobacterium tuberculosis*. Infect Immun 73:4581–4587. http://dx.doi.org/10.1128/IAI.73.8.4581-4587.2005.
380. Chopra I, Roberts M. 2001. Tetracycline antibiotics: mode of action, applications, molecular biology, and epidemiology of bacterial resistance. Microbiol Mol Biol Rev 65:232–260. http://dx.doi.org/10.1128/MMBR.65.2.232-260.2001.
381. McCormick JRD, Hirsch U, Sjolander NO, Doerschuk AP. 1960. Cosynthesis of tetracyclines by pairs of *Streptomyces aureofaciens* mutants. J Am Chem Soc 82:5006–5007. http://dx.doi.org/10.1021/ja01503a066.
382. Rhodes PM, Winskill N, Friend EJ, Warren M. 1981. Biochemical and genetic characterization of *Streptomyces rimosus* mutants impaired in oxytetracycline biosynthesis. J Gen Microbiol 124:329–338.
383. McCormick JRD, Sjolander NO, Miller PA, Hirsch U, Arnold NH, Doerschuk AP. 1958. The biological reduction of 7-chloro-5A(11A)-dehydrotetracycline to 7-chlorotetracycline by *Streptomyces aureofaciens*. J Am Chem Soc 80:6460–6461. http://dx.doi.org/10.1021/ja01556a080.
384. McCormick JRD, Morton GO. 1982. Identity of cosynthetic factor 1 of *Streptomyces aureofaciens* and fragment F_O from coenzyme F_{420} of *Methanobacterium* species. J Am Chem Soc 104:4014–4015. http://dx.doi.org/10.1021/ja00378a044.
385. Zhang W, Watanabe K, Cai X, Jung ME, Tang Y, Zhan J. 2008. Identifying the minimal enzymes required for anhydrotetracycline biosynthesis. J Am Chem Soc 130:6068–6069. http://dx.doi.org/10.1021/ja800951e.
386. Wang P, Kim W, Pickens LB, Gao X, Tang Y. 2012. Heterologous expression and manipulation of three tetracycline biosynthetic pathways. Angew Chem Int Ed 51:11136–11140. http://dx.doi.org/10.1002/anie.201205426.
387. Novotná J, Neužil J, Hoš'álek Z. 1989. Spectrophotometric identification of 8-hydroxy-5-deazaflavin: NADPH oxidoreductase activity in streptomycetes producing tetracyclines. FEMS Microbiol Lett 59(1-2):241–245. http://dx.doi.org/10.1111/j.1574-6968.1989.tb03118.x.
388. Coats JH, Li GP, Kuo MS, Yurek DA. 1989. Discovery, production, and biological assay of an unusual flavenoid cofactor involved in lincomycin biosynthesis. J Antibiot (Tokyo) 42:472–474. http://dx.doi.org/10.7164/antibiotics.42.472.
389. Kuo MS, Yurek DA, Coats JH, Chung ST, Li GP. 1992. Isolation and identification of 3-propylidene-delta 1-pyrroline-5-carboxylic acid, a biosynthetic precursor of lincomycin. J Antibiot (Tokyo) 45:1773–1777. http://dx.doi.org/10.7164/antibiotics.45.1773.
390. Birkenmeyer RD, Kagan F. 1970. Lincomycin. XI. Synthesis and structure of clindamycin. A potent antibacterial agent. J Med Chem 13:616–619.
391. Peschke U, Schmidt H, Zhang H-Z, Piepersberg W. 1995. Molecular characterization of the lincomycin-production gene cluster of *Streptomyces lincolnensis* 78-11. Mol Microbiol 16:1137–1156. http://dx.doi.org/10.1111/j.1365-2958.1995.tb02338.x.
392. Hurley LH. 1980. Elucidation and formulation of novel biosynthetic pathways leading to the pyrrolo[1,4]benzodiazepine antibiotics anthramycin, tomaymycin, and sibiromycin. Acc Chem Res 13:263–269. http://dx.doi.org/10.1021/ar50152a003.
393. Li W, Khullar A, Chou S, Sacramo A, Gerratana B. 2009. Biosynthesis of sibiromycin, a potent antitumor antibiotic. Appl Environ Microbiol 75:2869–2878. http://dx.doi.org/10.1128/AEM.02326-08.
394. Ikeno S, Aoki D, Hamada M, Hori M, Tsuchiya KS. 2006. DNA sequencing and transcriptional analysis of the kasugamycin biosynthetic gene cluster from *Streptomyces kasugaensis* M338-M1. J Antibiot (Tokyo) 59:18–28. http://dx.doi.org/10.1038/ja.2006.4.

395. Hu Y, Phelan V, Ntai I, Farnet CM, Zazopoulos E, Bachmann BO. 2007. Benzodiazepine biosynthesis in *Streptomyces refuineus*. Chem Biol 14:691–701. http://dx.doi.org/10.1016/j.chembiol.2007.05.009.
396. Ebert S, Fischer P, Knackmuss HJ. 2001. Converging catabolism of 2,4,6-trinitrophenol (picric acid) and 2,4-dinitrophenol by *Nocardioides simplex* FJ2-1A. Biodegradation 12:367–376. http://dx.doi.org/10.1023/A:1014447700775.
397. Fida TT, Palamuru S, Pandey G, Spain JC. 2014. Aerobic biodegradation of 2,4-dinitroanisole by *Nocardioides* sp. strain JS1661. Appl Environ Microbiol 80:7725–7731. http://dx.doi.org/10.1128/AEM.02752-14.
398. Lenke H, Pieper DH, Bruhn C, Knackmuss HJ. 1992. Degradation of 2,4-dinitrophenol by two *Rhodococcus erythropolis* strains, HL 24-1 and HL 24-2. Appl Environ Microbiol 58:2928–2932.
399. Ju K-S, Parales RE. 2010. Nitroaromatic compounds, from synthesis to biodegradation. Microbiol Mol Biol Rev 74:250–272. http://dx.doi.org/10.1128/MMBR.00006-10.
400. Wackett LP. 2009. Questioning our perceptions about evolution of biodegradative enzymes. Curr Opin Microbiol 12:244–251. http://dx.doi.org/10.1016/j.mib.2009.05.001.
401. Haritash AK, Kaushik CP. 2009. Biodegradation aspects of polycyclic aromatic hydrocarbons (PAHs): a review. J Hazard Mater 169:1–15. http://dx.doi.org/10.1016/j.jhazmat.2009.03.137.
402. McLeod MP, Warren RL, Hsiao WWL, Araki N, Myhre M, Fernandes C, Miyazawa D, Wong W, Lillquist AL, Wang D, Dosanjh M, Hara H, Petrescu A, Morin RD, Yang G, Stott JM, Schein JE, Shin H, Smailus D, Siddiqui AS, Marra MA, Jones SJM, Holt R, Brinkman FSL, Miyauchi K, Fukuda M, Davies JE, Mohn WW, Eltis LD. 2006. The complete genome of *Rhodococcus* sp. RHA1 provides insights into a catabolic powerhouse. Proc Natl Acad Sci U S A 103:15582–15587.
403. Martínková L, Uhnáková B, Pátek M, Nešvera J, Køen V. 2009. Biodegradation potential of the genus *Rhodococcus*. Environ Int 35:162–177. http://dx.doi.org/10.1016/j.envint.2008.07.018.
404. Purwantini E, Daniels L. 1996. Purification of a novel coenzyme F_{420}-dependent glucose-6-phosphate dehydrogenase from *Mycobacterium smegmatis*. J Bacteriol 178:2861–2866.
405. Wheeler PR. 1983. Catabolic pathways for glucose, glycerol and 6-phosphogluconate in *Mycobacterium leprae* grown in armadillo tissues. Microbiology 129:1481–1495. http://dx.doi.org/10.1099/00221287-129-5-1481.
406. Minnikin DE, Minnikin SM, Parlett JH, Goodfellow M, Magnusson M. 1984. Mycolic acid patterns of some species of *Mycobacterium*. Arch Microbiol 139:225–231.
407. DeMaio J, Zhang Y, Ko C, Young DB, Bishai WR. 1996. A stationary-phase stress-response sigma factor from *Mycobacterium tuberculosis*. Proc Natl Acad Sci U S A 93:2790–2794. http://dx.doi.org/10.1073/pnas.93.7.2790.
408. Geiman DE, Kaushal D, Ko C, Tyagi S, Manabe YC, Schroeder BG, Fleischmann RD, Morrison NE, Converse PJ, Chen P, Bishai WR. 2004. Attenuation of late-stage disease in mice infected by the *Mycobacterium tuberculosis* mutant lacking the SigF alternate sigma factor and identification of SigF-dependent genes by microarray analysis. Infect Immun 72:1733–1745. http://dx.doi.org/10.1128/IAI.72.3.1733-1745.2004.
409. Lapalikar GV, Taylor MC, Warden AC, Onagi H, Hennessy JE, Mulder RJ, Scott C, Brown SE, Russell RJ, Easton CJ, Oakeshott JG. 2012. Cofactor promiscuity among F_{420}-dependent reductases enables them to catalyse both oxidation and reduction of the same substrate. Catal Sci Technol 2:1560–1567. http://dx.doi.org/10.1039/c2cy20129a.
410. Jackson CJ, Taylor MC, Tattersall DB, French NG, Carr PD, Ollis DL, Russell RJ, Oakeshott JG. 2008. Cloning, expression, purification, crystallization and preliminary X-ray studies of a pyridoxine 5′-phosphate oxidase from *Mycobacterium smegmatis*. Acta Crystallogr Sect F Struct Biol Cryst Commun 64:435–437. http://dx.doi.org/10.1107/S1744309108011512.
411. Pédelacq JD, Rho BS, Kim CY, Waldo GS, Lekin TP, Segelke BW, Rupp B, Hung LW, Kim S-I, Terwilliger TC. 2006. Crystal structure of a putative pyridoxine 5′-phosphate oxidase (Rv2607) from *Mycobacterium tuberculosis*. Proteins Struct Funct Genet 62:563–569.
412. di Salvo ML, Safo MK, Musayev FN, Bossa F, Schirch V. 2003. Structure and mechanism of *Escherichia coli* pyridoxine 5′-phosphate oxidase. Biochim Biophys Acta 1647:76–82. http://dx.doi.org/10.1016/S1570-9639(03)00060-8.
413. Musayev FN, Di Salvo ML, Ko T-P, Schirch V, Safo MK. 2003. Structure and properties of recombinant human pyridoxine 5′-phosphate oxidase. Protein Sci 12:1455–1463. http://dx.doi.org/10.1110/ps.0356203.
414. Guo Y, Guo G, Mao X, Zhang W, Xiao J, Tong W, Liu T, Xiao B, Liu X, Feng Y. 2008. Functional identification of HugZ, a heme oxygenase from *Helicobacter pylori*. BMC Microbiol 8:226. http://dx.doi.org/10.1186/1471-2180-8-226.
415. Hu Y, Jiang F, Guo Y, Shen X, Zhang Y, Zhang R, Guo G, Mao X, Zou Q, Wang D-C. 2011. Crystal structure of HugZ, a novel heme oxygenase from *Helicobacter pylori*. J Biol Chem 286:1537–1544. http://dx.doi.org/10.1074/jbc.M110.172007.
416. Zhang R, Zhang J, Guo G, Mao X, Tong W, Zhang Y, Wang D-C, Hu Y, Zou Q. 2011. Crystal structure of *Campylobacter jejuni* ChuZ: a split-barrel family heme oxygenase with a novel heme-binding mode. Biochem Biophys Res Commun 415:82–87. http://dx.doi.org/10.1016/j.bbrc.2011.10.016.
417. Hilario E, Li Y, Niks D, Fan L. 2012. The structure of a *Xanthomonas* general stress protein involved in citrus canker reveals its flavin-binding property. Acta Crystallogr Sect D Biol Crystallogr 68:846–853. http://dx.doi.org/10.1107/S0907444912014126.
418. Canaan S, Sulzenbacher G, Roig-Zamboni V, Scappuccini-Calvo L, Frassinetti F, Maurin D, Cambillau C, Bourne Y. 2005. Crystal structure of the conserved hypothetical protein Rv1155 from *Mycobacterium tuberculosis*. FEBS Lett 579:215–221. http://dx.doi.org/10.1016/j.febslet.2004.11.069.
419. Biswal BK, Au K, Cherney MM, Garen C, James MNG. 2006. The molecular structure of Rv2074, a probable pyridoxine 5′-phosphate oxidase from *Mycobacterium tuberculosis*, at 1.6 Å resolution. Acta Crystallogr Sect F Struct Biol Cryst Commun 62:735–742. http://dx.doi.org/10.1107/S1744309106025012.
420. Safo MK, Musayev FN, di Salvo ML, Schirch V. 2001. X-ray structure of *Escherichia coli* pyridoxine 5′-phosphate oxidase complexed with pyridoxal 5′-phosphate at 2.0 Å resolution. J Mol Biol 310:817–826. http://dx.doi.org/10.1006/jmbi.2001.4734.
421. de Souza GA, Leversen NA, Malen H, Wiker HG. 2011. Bacterial proteins with cleaved or uncleaved signal peptides of the general secretory pathway. J Proteomics 75:502–510. http://dx.doi.org/10.1016/j.jprot.2011.08.016.
422. He Z, De Buck J. 2010. Cell wall proteome analysis of *Mycobacterium smegmatis* strain mc^2155. BMC Microbiol 10:121. http://dx.doi.org/10.1186/1471-2180-10-121.
423. Abdalla MY, Ahmad IM, Switzer B, Britigan BE. 2015. Induction of heme oxygenase-1 contributes to survival of *Mycobacterium abscessus* in human macrophages-like THP-1 cells. Redox Biol 4:328–339. http://dx.doi.org/10.1016/j.redox.2015.01.012.
424. Yamaguchi T, Komoda Y, Nakajima H. 1994. Biliverdin-IX alpha reductase and biliverdin-IX beta reductase from human liver. Purification and characterization. J Biol Chem 269:24343–24348.
425. Schluchter WM, Glazer AN. 1997. Characterization of cyanobacterial biliverdin reductase: conversion of biliverdin to bilirubin is important for normal phycobiliprotein biosynthesis. J Biol Chem 272:13562–13569. http://dx.doi.org/10.1074/jbc.272.21.13562.
426. Fisher AJ, Thompson TB, Thoden JB, Baldwin TO, Rayment I. 1996. The 1.5-Å resolution crystal structure of bacterial luciferase in low salt conditions. J Biol Chem 271:21956–21968. http://dx.doi.org/10.1074/jbc.271.36.21956.
427. Chaiyen P, Suadee C, Wilairat P. 2001. A novel two-protein component flavoprotein hydroxylase. Eur J Biochem 268:5550–5561. http://dx.doi.org/10.1046/j.1432-1033.2001.02490.x.
428. Kertesz MA, Schmidt-Larbig K, Wuest T. 1999. A novel reduced flavin mononucleotide-dependent methanesulfonate sulfonatase encoded by the sulfur-regulated *msu* operon of *Pseudomonas aeruginosa*. J Bacteriol 181:1464–1473.
429. Flatt PM, Mahmud T. 2007. Biosynthesis of aminocyclitol-aminoglycoside antibiotics and related compounds. Nat Prod Rep 24:358–392. http://dx.doi.org/10.1039/B603816F.
430. Lenke H, Knackmuss HJ. 1992. Initial hydrogenation during catabolism of picric acid by *Rhodococcus erythropolis* HL 24-2. Appl Environ Microbiol 58:2933–2937.
431. Lenke H, Knackmuss H. 1996. Initial hydrogenation and extensive reduction of substituted 2,4-dinitrophenols. Appl Environ Microbiol 62:784–790.
432. Hofmann KW, Knackmuss H, Heiss G. 2004. Nitrite elimination and hydrolytic ring cleavage in 2,4,6-trinitrophenol (picric acid) degrada-

tion. Appl Environ Microbiol 70:2854–2860. http://dx.doi.org/10.1128/AEM.70.5.2854-2860.2004.
433. Walters DM, Russ R, Knackmuss HJ, Rouviere PE. 2001. High-density sampling of a bacterial operon using mRNA differential display. Gene 273:305–315. http://dx.doi.org/10.1016/S0378-1119(01)00597-2.
434. Nga DP, Altenbuchner J, Heiss GS. 2004. NpdR, a repressor involved in 2,4,6-trinitrophenol degradation in *Rhodococcus opacus* HL PM-1. J Bacteriol 186:98–103. http://dx.doi.org/10.1128/JB.186.1.98-103.2004.
435. Heiss G, Trachtmann N, Abe Y, Takeo M, Knackmuss H-J. 2003. Homologous *npdGI* genes in 2,4-dinitrophenol- and 4-nitrophenol-degrading *Rhodococcus* spp. Appl Environ Microbiol 69:2748–2754. http://dx.doi.org/10.1128/AEM.69.5.2748-2754.2003.
436. Ghosh A, Khurana M, Chauhan A, Takeo M, Chakraborti AK, Jain RK. 2010. Degradation of 4-nitrophenol, 2-chloro-4-nitrophenol, and 2,4-nitrophenol by *Rhodococcus imtechensis* strain RKJ300. Environ Sci Technol 44:1069–1077. http://dx.doi.org/10.1021/es9034123.
437. Shen J, Zhang J, Zuo Y, Wang L, Sun X, Li J, Han W, He R. 2009. Biodegradation of 2,4,6-trinitrophenol by *Rhodococcus* sp. isolated from a picric acid-contaminated soil. J Hazard Mater 163:1199–1206. http://dx.doi.org/10.1016/j.jhazmat.2008.07.086.
438. Takeo M, Abe Y, Negoro S, Heiss G. 2003. Simultaneous degradation of 4-nitrophenol and picric acid by two different mechanisms of *Rhodococcus* sp. PN1. J Chem Eng Japan 36:1178–1184. http://dx.doi.org/10.1252/jcej.36.1178.
439. Behrend C, Heesche-Wagner K. 1999. Formation of hydride-Meisenheimer complexes of picric acid (2,4,6-trinitrophenol) and 2,4-dinitrophenol during mineralization of picric acid by *Nocardioides* sp. strain CB 22-2. Appl Environ Microbiol 65:1372–1377.
440. Vorbeck C, Lenke H, Fischer P, Knackmuss HJ. 1994. Identification of a hydride-Meisenheimer complex as a metabolite of 2,4,6-trinitrotoluene by a *Mycobacterium* strain. J Bacteriol 176:932–934.
441. Vorbeck C, Lenke H, Fischer P, Spain JC, Knackmuss HJ. 1998. Initial reductive reactions in aerobic microbial metabolism of 2,4,6-trinitrotoluene. Appl Environ Microbiol 64:246–252.
442. World Health Organization. 2014. Global tuberculosis report 2014. World Health Organization, Geneva, Switzerland.
443. Lienhardt C, Glaziou P, Uplekar M, Lonnroth K, Getahun H, Raviglione M. 2012. Global tuberculosis control: lessons learnt and future prospects. Nat Rev Microbiol 10:407–416.
444. Zumla A, Nahid P, Cole ST. 2013. Advances in the development of new tuberculosis drugs and treatment regimens. Nat Rev Drug Discov 12:388–404. http://dx.doi.org/10.1038/nrd4001.
445. Murray CW, Rees DC. 2009. The rise of fragment-based drug discovery. Nat Chem 1:187–192. http://dx.doi.org/10.1038/nchem.217.
446. Matsumoto M, Hashizume H, Tomishige T, Kawasaki M, Tsubouchi H, Sasaki H, Shimokawa Y, Komatsu M. 2006. OPC-67683, a nitro-dihydro-imidazooxazole derivative with promising action against tuberculosis *in vitro* and in mice. PLoS Med 3:e466. http://dx.doi.org/10.1371/journal.pmed.0030466.
447. Denny WA. 2015. TBA-354: a new drug for the treatment of persistent tuberculosis. Chem New Zeal 1:18–22.
448. Tasneen R, Williams K, Amoabeng O, Minkowski A, Mdluli KE, Upton AM, Nuermberger EL. 2015. Contribution of the nitroimidazoles PA-824 and TBA-354 to the activity of novel regimens in murine models of tuberculosis. Antimicrob Agents Chemother 59:129–135. http://dx.doi.org/10.1128/AAC.03822-14.
449. Saliu OY, Crismale C, Schwander SK, Wallis RS. 2007. Bactericidal activity of OPC-67683 against drug-tolerant *Mycobacterium tuberculosis*. J Antimicrob Chemother 60:994–998. http://dx.doi.org/10.1093/jac/dkm291.
450. Tyagi S, Nuermberger E, Yoshimatsu T, Williams K, Rosenthal I, Lounis N, Bishai W, Grosset J. 2005. Bactericidal activity of the nitroimidazopyran PA-824 in a murine model of tuberculosis. Antimicrob Agents Chemother 49:2289–2293. http://dx.doi.org/10.1128/AAC.49.6.2289-2293.2005.
451. Lenaerts AJ, Gruppo V, Marietta KS, Johnson CM, Driscoll DK, Tompkins NM, Rose JD, Reynolds RC, Orme IM. 2005. Preclinical testing of the nitroimidazopyran PA-824 for activity against *Mycobacterium tuberculosis* in a series of in vitro and in vivo models. Antimicrob Agents Chemother 49:2294–2301. http://dx.doi.org/10.1128/AAC.49.6.2294-2301.2005.
452. Gler MT, Skripconoka V, Sanchez-Garavito E, Xiao H, Cabrera-Rivero JL, Vargas-Vasquez DE, Gao M, Awad M, Park S-K, Shim TS, Suh GY, Danilovits M, Ogata H, Kurve A, Chang J, Suzuki K, Tupasi T, Koh W-J, Seaworth B, Geiter LJ, Wells CD. 2012. Delamanid for multidrug-resistant pulmonary tuberculosis. N Engl J Med 366:2151–2160. http://dx.doi.org/10.1056/NEJMoa1112433.
453. Skripconoka V, Danilovits M, Pehme L, Tomson T, Skenders G, Kummik T, Cirule A, Leimane V, Kurve A, Levina K, Geiter LJ, Manissero D, Wells CD. 2013. Delamanid improves outcomes and reduces mortality in multidrug-resistant tuberculosis. Eur Respir J 41:1393–1400. http://dx.doi.org/10.1183/09031936.00125812.
454. Gupta R, Gao M, Cirule A, Xiao H, Geiter LJ, Wells CD. 2015. Delamanid for extensively drug-resistant tuberculosis. N Engl J Med 373:291–292. http://dx.doi.org/10.1056/NEJMc1415332.
455. Diacon AH, Dawson R, von Groote-Bidlingmaier F, Symons G, Venter A, Donald PR, van Niekerk C, Everitt D, Winter H, Becker P, Mendel CM, Spigelman MK. 2012. 14-day bactericidal activity of PA-824, bedaquiline, pyrazinamide, and moxifloxacin combinations: a randomised trial. Lancet 380:986–993. http://dx.doi.org/10.1016/S0140-6736(12)61080-0.
456. Dawson R, Diacon AH, Everitt D, van Niekerk C, Donald PR, Burger DA, Schall R, Spigelman M, Conradie A, Eisenach K, Venter A, Ive P, Page-Shipp L, Variava E, Reither K, Ntinginya NE, Pym A, von Groote-Bidlingmaier F, Mendel CM. 2015. Efficiency and safety of the combination of moxifloxacin, pretomanid (PA-824), and pyrazinamide during the first 8 weeks of antituberculosis treatment: a phase 2b, open-label, partly randomised trial in patients with drug-susceptible or drug-resistant pul. Lancet 385:1738–1747. http://dx.doi.org/10.1016/S0140-6736(14)62002-X.
457. Mohamed AE, Ahmed FH, Arulmozhiraja S, Lin CY, Taylor MC, Krausz ER, Jackson CJ, Coote ML. 15 February 2016. Protonation state of $F_{420}H_2$ in the prodrug-activating deazaflavin dependent nitroreductase (Ddn) from *Mycobacterium tuberculosis*. Mol Biosyst Epub ahead of print.
458. Gurumurthy M, Mukherjee T, Dowd CS, Singh R, Niyomrattanakit P, Tay JA, Nayyar A, Lee YS, Cherian J, Boshoff HI, Dick T, Barry CE, III, Manjunatha UH. 2012. Substrate specificity of the deazaflavin-dependent nitroreductase from *Mycobacterium tuberculosis* responsible for the bioreductive activation of bicyclic nitroimidazoles. FEBS J 279:113–125. http://dx.doi.org/10.1111/j.1742-4658.2011.08404.x.
459. Manjunatha U, Boshoff HI, Barry CE. 2009. The mechanism of action of PA-824: novel insights from transcriptional profiling. Commun Integr Biol 2:215–218. http://dx.doi.org/10.4161/cib.2.3.7926.
460. Manjunatha UH, Lahiri R, Randhawa B, Dowd CS, Krahenbuhl JL, Barry CE. 2006. *Mycobacterium leprae* is naturally resistant to PA-824. Antimicrob Agents Chemother 50:3350–3354. http://dx.doi.org/10.1128/AAC.00488-06.
461. Haver HL, Chua A, Ghode P, Lakshminarayana SB, Singhal A, Mathema B, Wintjens R, Bifani P. 2015. Mutations in genes for the F_{420} biosynthetic pathway and a nitroreductase enzyme are the primary resistance determinants in spontaneous in vitro-selected PA-824-resistant mutants of *Mycobacterium tuberculosis*. Antimicrob Agents Chemother 59:5316–5323. http://dx.doi.org/10.1128/AAC.00308-15.
462. Bloemberg GV, Keller PM, Stucki D, Trauner A, Borrell S, Latshang T, Coscolla M, Rothe T, Hömke R, Ritter C, Feldmann J, Schulthess B, Gagneux S, Böttger EC. 2015. Acquired resistance to bedaquiline and delamanid in therapy for tuberculosis. N Engl J Med 373:1986–1988. http://dx.doi.org/10.1056/NEJMc1505196.
463. Ashtekar DR, Costa-Perira R, Nagrajan K, Vishvanathan N, Bhatt AD, Rittel W. 1993. *In vitro* and *in vivo* activities of the nitroimidazole CGI 17341 against *Mycobacterium tuberculosis*. Antimicrob Agents Chemother 37:183–186. http://dx.doi.org/10.1128/AAC.37.2.183.
464. Kirschke S, Bousquet P, Ciais P, Saunois M, Canadell JG, Dlugokencky EJ, Bergamaschi P, Bergmann D, Blake DR, Bruhwiler L, Cameron-Smith P, Castaldi S, Chevallier F, Feng L, Fraser A, Heimann M, Hodson EL, Houweling S, Josse B, Fraser PJ, Krummel PB, Lamarque J-F, Langenfelds RL, Le Quere C, Naik V, O'Doherty S, Palmer PI, Pison I, Plummer D, Poulter B, Prinn RG, Rigby M, Ringeval B, Santini M, Schmidt M, Shindell DT, Simpson IJ, Spahni R, Steele LP, Strode SA, Sudo K, Szopa S, van der Werf GR, Voulgarakis A, van Weele M, Weiss RF, Williams JE, Zeng G. 2013. Three decades of global methane sources and sinks. Nat Geosci 6:813–823. http://dx.doi.org/10.1038/ngeo1955.
465. Buddle BM, Denis M, Attwood GT, Altermann E, Janssen PH, Ronimus RS, Pinares-Patiño CS, Muetzel S, Neil Wedlock D. 2011. Strat-

egies to reduce methane emissions from farmed ruminants grazing on pasture. Vet J 188:11–17. http://dx.doi.org/10.1016/j.tvjl.2010.02.019.

466. Cottle DJ, Nolan JV, Wiedemann SG. 2011. Ruminant enteric methane mitigation: a review. Anim Prod Sci 51:491–514. http://dx.doi.org/10.1071/AN10163.
467. Kumar S, Choudhury P, Carro M, Griffith G, Dagar S, Puniya M, Calabro S, Ravella S, Dhewa T, Upadhyay R, Sirohi S, Kundu S, Wanapat M, Puniya A. 2014. New aspects and strategies for methane mitigation from ruminants. Appl Microbiol Biotechnol 98:31–44. http://dx.doi.org/10.1007/s00253-013-5365-0.
468. Hristov AN, Oh J, Giallongo F, Frederick TW, Harper MT, Weeks HL, Branco AF, Moate PJ, Deighton MH, Williams SRO, Kindermann M, Duval S. 2015. An inhibitor persistently decreased enteric methane emission from dairy cows with no negative effect on milk production. Proc Natl Acad Sci U S A 112:10663–10668. http://dx.doi.org/10.1073/pnas.1504124112.
469. Martínez-Fernández G, Abecia L, Arco A, Cantalapiedra-Hijar G, Martín-García AI, Molina-Alcaide E, Kindermann M, Duval S, Yáñez-Ruiz DR. 2014. Effects of ethyl-3-nitrooxy propionate and 3-nitrooxypropanol on ruminal fermentation, microbial abundance, and methane emissions in sheep. J Dairy Sci 97:3790–3799. http://dx.doi.org/10.3168/jds.2013-7398.
470. Taylor MC, Scott C, Grogan G. 2013. F_{420}-dependent enzymes - potential for applications in biotechnology. Trends Biotechnol 31:63–64. http://dx.doi.org/10.1016/j.tibtech.2012.09.003.
471. Wagacha JM, Muthomi JW. 2008. Mycotoxin problem in Africa: current status, implications to food safety and health and possible management strategies. Int J Food Microbiol 124:1–12. http://dx.doi.org/10.1016/j.ijfoodmicro.2008.01.008.
472. Ciegler A, Lillehoj EB, Peterson RE, Hall HH. 1966. Microbial detoxification of aflatoxin. Appl Microbiol 14:934–939.
473. Teniola OD, Addo PA, Brost IM, Farber P, Jany K-D, Alberts JF, van Zyl WH, Steyn PS, Holzapfel WH. 2005. Degradation of aflatoxin B1 by cell-free extracts of *Rhodococcus erythropolis* and *Mycobacterium fluoranthenivorans* sp. nov. DSM44556(T). Int J Food Microbiol 105:111–117. http://dx.doi.org/10.1016/j.ijfoodmicro.2005.05.004.
474. Alberts JF, Engelbrecht Y, Steyn PS, Holzapfel WH, van Zyl WH. 2006. Biological degradation of aflatoxin B_1 by *Rhodococcus erythropolis* cultures. Int J Food Microbiol 109:121–126. http://dx.doi.org/10.1016/j.ijfoodmicro.2006.01.019.
475. Jones JJ, Falkinham JO. 2003. Decolorization of malachite green and crystal violet by waterborne pathogenic mycobacteria. Antimicrob Agents Chemother 47:2323–2326. http://dx.doi.org/10.1128/AAC.47.7.2323-2326.2003.
476. Srivastava S, Sinha R, Roy D. 2004. Toxicological effects of malachite green. Aquat Toxicol 66:319–329. http://dx.doi.org/10.1016/j.aquatox.2003.09.008.
477. Spain JC, Hughes JB, Knackmuss H-J. 2000. Biodegradation of nitroaromatic compounds and explosives. CRC Press, Boca Raton, FL.
478. Snellinx Z, Nepovim A, Taghavi S, Vangronsveld J, Vanek T, van der Lelie D. 2002. Biological remediation of explosives and related nitroaromatic compounds. Environ Sci Pollut Res Int 9:48–61. http://dx.doi.org/10.1007/BF02987316.
479. Schmid A, Dordick JS, Hauer B, Kiener A, Wubbolts M, Witholt B. 2001. Industrial biocatalysis today and tomorrow. Nature 409:258–268. http://dx.doi.org/10.1038/35051736.
480. Bornscheuer UT, Huisman GW, Kazlauskas RJ, Lutz S, Moore JC, Robins K. 2012. Engineering the third wave of biocatalysis. Nature 485:185–194. http://dx.doi.org/10.1038/nature11117.
481. Stuermer R, Hauer B, Hall M, Faber K. 2007. Asymmetric bioreduction of activated C=C bonds using enoate reductases from the old yellow enzyme family. Curr Opin Chem Biol 11:203–213. http://dx.doi.org/10.1016/j.cbpa.2007.02.025.
482. Amato ED, Stewart JD. 2015. Applications of protein engineering to members of the old yellow enzyme family. Biotechnol Adv 33:624–631. http://dx.doi.org/10.1016/j.biotechadv.2015.04.011.
483. Schrittwieser JH, Velikogne S, Kroutil W. 2015. Biocatalytic imine reduction and reductive amination of ketones. Adv Synth Catal 357:1655–1685. http://dx.doi.org/10.1002/adsc.201500213.
484. Ghislieri D, Turner N. 2014. Biocatalytic approaches to the synthesis of enantiomerically pure chiral amines. Top Catal 57:284–300. http://dx.doi.org/10.1007/s11244-013-0184-1.
485. Kimachi T, Kawase M, Matsuki S, Tanaka K, Yoneda F. 1990. First total synthesis of coenzyme factor 420. J Chem Soc Perkin Trans 1 1990:253–256.
486. Bashiri G, Rehan AM, Greenwood DR, Dickson JMJ, Baker EN. 2010. Metabolic engineering of cofactor F420 production in *Mycobacterium smegmatis*. PLoS One 5:e15803. http://dx.doi.org/10.1371/journal.pone.0015803.
487. Buckel W, Thauer RK. 2013. Energy conservation via electron bifurcating ferredoxin reduction and proton/Na^+ translocating ferredoxin oxidation. Biochim Biophys Acta 1827:94–113. http://dx.doi.org/10.1016/j.bbabio.2012.07.002.
488. Née G, Zaffagnini M, Trost P, Issakidis-Bourguet E. 2009. Redox regulation of chloroplastic glucose-6-phosphate dehydrogenase: a new role for f-type thioredoxin. FEBS Lett 583:2827–2832. http://dx.doi.org/10.1016/j.febslet.2009.07.035.
489. Tietze M, Beuchle A, Lamla I, Orth N, Dehler M, Greiner G, Beifuss U. 2003. Redox potentials of methanophenazine and CoB-S-S-CoM, factors involved in electron transport in methanogenic archaea. Chembiochem 4:333–335. http://dx.doi.org/10.1002/cbic.200390053.
490. Wagner GC, Kassner RJ, Kamen MD. 1974. Redox potentials of certain vitamins K: implications for a role in sulfite reduction by obligately anaerobic bacteria. Proc Natl Acad Sci U S A 71:253–256. http://dx.doi.org/10.1073/pnas.71.2.253.

Chapter 7

Conclusions and Future Directions

7.1 Summary

The aim of this thesis was to investigate the function of F_{420}-dependent enzymes to understand their role in *Mycobacteria*, specifically the enzymes that are part of the FDOR super family. In doing so we can expand our understanding of mycobacterial physiology and help in developing treatment against tuberculosis.

In Chapter 2, we defined the role of the nitroimidazole prodrug reducing enzyme Ddn, and demonstrated that mutations can arise that confer pretomanid resistance without substantially affecting fitness. Previous work has shown that Ddn is able to reduce a range of non-physiological quinone analogues, leading to their proposed roles in protection from oxidative stress. We showed direct evidence that Ddn and the *M. smegmatis* orthologues, MSMEG_5998 and MSMEG_2027, can reduce the physiological substrate menaquinone and that this activity is coupled to the electron transport chain via cytochrome bd in a role that enhances respiratory activity. Having further expanded the role of Ddn and knowing that it is the only enzyme to activate the prodrug pretomanid, we sought to understand the fitness cost of mutations that eliminated this activity. We first tested Ddn orthologues from other mycobacterial species, showing that they were able to reduce quinones in a similar manner to Ddn, but lacked activity with pretomanid (consistent with the lack of pretomanid efficacy against these species), demonstrating that it is possible to eliminate pretomanid activity while maintaining its physiological role. The exception to this was the orthologue from *M. marinum* that had activity with both the quinone and pretomanid and was demonstrated to be susceptible to both pretomanid and delamanid. Sequence alignment revealed that Ddn and the *M. marinum* orthologue's active site was homologous whereas the other orthologues lacked key residue, which explained why they lacked activity with pretomanid.

To test whether Ddn could lose pretomanid activity with little to no fitness cost, we mutated the residues in the active site, and other mutations found in clinical strains and tested activity with pretomanid and menadione. We demonstrated that single point mutations in Ddn could remove pretomanid activity and maintain the ability to reduce quinones. We validated this *in vivo* by measuring the MIC of pretomanid and delamanid with a clinically relevant strain that contained one of our tested mutation and showed that it was resistance to pretomanid but that this mutation did not affect delamanid. The reduction of delamanid by this mutant was

confirmed with an enzymatic kinetic fluorescence assay, although full kinetics could not be obtained due to solubility issues. We revealed using computational docking studies that the difference in drug resistance between pretomanid and delamanid is due to the different modes of binding. Finally, we analysed the evolution of Ddn mutations in sequenced strains revealing that every distinct strain of *M. tuberculosis* contains SNPs in Ddn and the chance of resistance causing mutations arising is highly likely.

This chapter has expanded the understanding of Ddn in its physiological role in the cells energetic

In Chapter 3, we have made substantial progress towards characterising the role of MSMEG_6526/Rv0121c. The functions of most of the FDORs are unknown. We attempted to elucidate the role of the *M. smegmatis* FDOR, MSMEG_6526 as a model for Rv012c from *M. tuberculosis*. Using a Δ6526 strain we showed that there was no difference in growth between Δ6526 and wildtype in high nutrient growth media. When we compared the two strains in minimal media with different carbon sources we showed a slower growth rate for Δ6526 compared to wildtype. When acetate or pyruvate was the sole carbon source we observed no growth by Δ6526 revealing that MSMEG_6526 is conditionally essential to *M. smegmatis*.

To understand the biochemical differences resulting in the observed phenotypes, we used proteomics and metabolomics to investigate these changes in the Δ6526 strain. Using proteomics, we observed that proteins from the methylcitrate and glyoxylate cycles were upregulated, while proteins from the Krebs cycle, late stage glycolysis, the glutamate metabolomic pathway, and the aspartate metabolomic pathway were downregulated in the Δ6526 strain. We expanded on this with metabolomics showing the effect of acetate on the *M. smegmatis* metabolome, which revealed the down regulation of the Krebs cycle and the aspartate metabolomic pathway with the accumulation of related metabolites that were not metabolised due to downstream effects. This was interesting as the proteomics revealed that the enzymes involved in these pathways were downregulated in the Δ6526 grown on glycerol. This may explain the difference in growth and maximum cell density between acetate and glycerol as the cell struggles to utilise acetate for energy and amino acid metabolism. Metabolites that had accumulated in the Δ6526 strain metabolome that differed from the wildtype included several metabolites that related to amino acid metabolism. Lysine metabolism and catabolism was particularly affected in the Δ6526 strain, as it is involved in two different biosynthetic pathways where there was an accumulation of metabolites from both,

as well as an accumulation of a lysine degradation product. Altogether, these data suggest that MSMEG_6526 may be involved with amino acid metabolism. The lack of growth by the Δ6526 strain on acetate is most likely due to acetate not allowing for an alternative pathway to the one MSMEG_6526 is involved in, where other carbon sources such as glycerol can allow for an alternative pathway to be utilised. More work will be required to identify the exact physiological substrate and function.

Finally, we solved the structures of Rv0121c and MSMEG_6526 with F_{420} bound. These structures both revealed homodimers and contained the split β-barrel fold that defines the FDOR superfamily. Both structures revealed three extended loops that were unique to these proteins. Two of these loops formed a more defined active site with one of the loops forming a hinge that had an open and closed conformation. We showed that the third loop was not involved in the active site and that this loop is not conserved between the enzymes. Alignment of the structures showed that the active site between the two structures are highly conserved and that the catalytic mechanism should be similar between the two. To identify possible substrates for these enzymes we performed high throughput *in silico* docking. We observed that the common structural feature of high scoring substrates contained aromatic rings due to the pi stacking between F_{420} and a tryptophan present in the active site. The two largest pathways found in the top hits were aromatic amino acid biosynthesis and nucleic acid metabolism. Unfortunately, tested compounds from these pathways revealed no activity or binding. The crystal structure of MSMEG_6526 with F_{420} bound revealed MPD bound in the active site. This reveals that despite the bias towards aromatic rings revealed by the docking, MSMEG_6526 can bind aliphatic compounds such as those found in the Krebs cycle.

In Chapter 4, two papers are presented that definitively classify the FDOR super family and annotated the function of certain enzymes. Although this family had been previously classified, the first paper presented in this chapter further defined each group by revealing amino acid motifs unique to each group. We expanded each group into separate clades revealing the diversity within them. This was especially true of the FDOR-B group as it had the most distinct clades and included proteins that did not have F_{420} as their primary co-factor but still retained the split β-barrel fold that defines this superfamily. We also solved the structures for many proteins of each clade, allowing for structural classification of each clade. The function of some of the clades were discovered, including the confirmation that enzymes within the FDOR-As are quinone reductases, the FDOR-B4s are biliverdin reductases, and the

FDOR-AAs have some fatty acid reductase activity. The second paper presented in this chapter expands on the biliverdin reductases. The first chapter presents enzymes from two different clades (FDOR-B3 and FDOR-B4) that reduced biliverdin but showed a distinct difference in activity between the clades. We concluded that the activity of the FDOR-B4, which had higher activity, was its physiological function and the activity in the FDOR-B3 was promiscuous activity due to being highly related. As the activity of the FDOR- B4 in the first paper was from the *M. smegmatis* enzyme, the second paper confirmed the orthologue from *M. tuberculosis*, Rv2074, was a biliverdin reductase. The structure of Rv2074 was solved with F_{420} bound. This was used to understand the catalytic mechanism of reducing biliverdin, as well as showing that the tail of bound F_{420} is highly dynamic while the rest of the molecule is stable. Finally, we demonstrated that orthologues of this protein are highly conserved throughout actinobacteria.

In Chapter 5, two papers are presented expanding the promiscuous activity of FDORs. Previously it was shown that FDORs could reduce coumarins and aflatoxins. We expanded the list of compounds that FDORs have promiscuous activity with in both papers. In the first paper, we demonstrated that the FDORs can reduce multiple antimicrobials including first line anti-tuberculosis drugs. We demonstrated that *M. smegmatis* is more susceptible to the anti-microbials that are reduced by FDORs when F_{420} is knocked out. In the second paper, we revealed a range of compounds that the FDORs can reduce. We defined the common catalytic mechanism revealing a hydride transfer to an electron deficient alkene group when the C5 of reduced F_{420} is proximal to the acceptor.

Overall the research presented in this thesis has expanded the biological understanding of Mycobacteria of the FDOR super family in mycobacteria and the understanding of drug regimens that target these enzymes. The work done on the nitroimidazoles, pretomanid and delamanid, with Ddn allows for an understanding of resistance towards these compounds and will hopefully help in the understanding of how to administer these drugs that minimalises the amount of resistance that occurs. This research allows further understanding into how to develop the next generation of nitroimidazoles to help eliminate tuberculosis with minimal resistant strains occurring. Previously, little was known about the role of FDORs in Mycobacteria. This research has expanded this especially that of MSMEG_6526/Rv0121c, includes understanding their function, role, structure and has expanded the phylogenetic understanding of the FDORs. Expanding the knowledge of these enzymes will help towards

drug development targeting these enzymes. Elucidating their function will also allow the development of biocatalysts using these enzymes to produce industrially relevant compounds.

7.2 Future Directions

Future work should seek to further the work done in Chapter 2 to expand our knowledge of how nitroimidazole resistance could develop, allowing us to develop more suitable drugs to combat tuberculosis. This could be achieved by exploring mutations throughout the whole sequence of Ddn to fully identify all mutations that will knock out pretomanid activity while maintaining it physiological role. This will allow for physicians to identify resistance strains, so they can avoid overprescribing pretomanid, thereby minimising the rise of resistant tuberculosis. Having identify resistance mutations, it will be important to develop nitroimidazoles that would still be effective against these mutants. As well as testing new nitroimidazoles against these mutants, a structure of Ddn with the nitroimidazoles bound will help to further understand the binding modes of different nitroimidazoles and lead to more rationalised designs. To achieve this, work may need to be done to solve the full-length structure as the current structure of Ddn is truncated. Since we now have evidence that Ddn has a role in respiration, we can expand on this by using a knockout to understand the effect that the loss of Ddn has in infection and respiration of *M. tuberculosis.*

Future directions on the work presented in Chapter 3 will include identifying the exact substrate of MSMEG_6526/Rv0121c and its potential role in metabolism. To show that this activity is conserved in *M. tuberculosis*, experiments analysing the effect on the loss Rv0121c should be done. This would include making a knockout in *M. tuberculosis* and analysing changes in phenotype and what effect it has in infections. Once the role of Rv0121c is established, inhibitors that target Rv0121c should be developed which can be used to develop a novel treatment for tuberculosis, with an emphasis on latent infections. As with the nitroimidazoles, it will be important to understand how resistance can occur to any new inhibitors developed to maximise the potency.

The later chapters of this thesis presented work that expanded on defining the FDOR super family. Therefore, future directions should include understanding the roles of these enzymes in *Mycobacteria* by discovering the function of each clade. This will allow for the

ground work of drug development against tuberculosis if any of the groups outside of FDOR-A (Ddn) and FDOR-B2 (MSMEG_6526/Rv0121c) are found to have any physiological properties that allow them to be targeted. As well as drug development, knowing their physiological function along with expanding the list of compounds that the FDORs have promiscuous activity with can allow for the development of these enzymes as biocatalysts that utilise the low reducing potential of F_{420}.

Previous work on F_{420}-dependent enzymes before this study was focused on Ddn and the mode of action of nitroimidazoles, particularly pretomanid, with some insight into its function in Mycobacteria, or the promiscuous activity of F_{420}-depedndent enzymes, in particular aflatoxins and coumarins. The work presented here has allowed the further validation of the function of Ddn in mycobacteria and expanded it with regards to its role in the electron transport chain. This is important when understanding what happens to the cell when resistance occurs and the decisions made in regards to drug regimes. This work has also shown the effect that nitroimidazole resistance has on the fitness of the cell, the differing binding of pretomanid and delamanid, and the identification of SNPs present in clinical strains of tuberculosis. The translation of this work will help develop regimes in using the current approved nitroimidazole drugs in avoiding resistance and detecting pre-admission resistance. This work can also translate into the development of nitroimidazole pro drugs that will also help to avoid resistance in the future. This study also shows the importance of understanding resistance in new drugs and can be used as a foundation in regards to developing new drugs for tuberculosis and other diseases while avoiding resistance.

This study expanded the understanding of the function of F_{420}-dependent enzymes and the physiological role they have in mycobacteria. As previous work only showed the FDOR's outside of Ddn to have promiscuous activity with aflatoxins and coumarins, the work in this study has expanded the compounds that the FDORs have promiscuous activity with, which can translate into developing new biocatalyst for industrial relevant compounds. This study also revealed the physiological function of serval of the FDORs which has expanded the understanding of the biology of mycobacteria and can translate into helping with the design of new drugs and regimes that can target these FDORs. This is especially true of MSMEG_6526/Rv0121c, as the work done is this study has shown the impact to the cell when this FDOR is inhibited or knocked out. This has validated the enzymes as a drug target which would translate into the development of inhibitors towards Rv0121c that can be used as anti-

tuberculosis drugs. This is enhance with the structures of this enzyme being solved and that work will translate into structure based drug design.

References

Aharoni, A., Gaidukov, L., Khersonsky, O., Gould, S.M.Q., Roodveldt, C., and Tawfik, D.S. (2005) The'evolvability'of promiscuous protein functions. *Nat Genet* **37**: 73–76.

Ahmed, F.H., Carr, P.D., Lee, B.M., Afriat-Jurnou, L., Mohamed, A.E., Hong, N.S., *et al.* (2015) Sequence-Structure-Function Classification of a Catalytically Diverse Oxidoreductase Superfamily in Mycobacteria. *J Mol Biol* **427**: 3554–3571.

Ahmed, F.H., Mohamed, A.E., Carr, P.D., Lee, B.M., Condic-Jurkic, K., O'Mara, M.L., and Jackson, C.J. (2016) Rv2074 is a novel F420H2-dependent biliverdin reductase in Mycobacterium tuberculosis. *Protein Sci* 1692–1709.

Andries, K., Verhasselt, P., Guillemont, J., Göhlmann, H.W.H., Neefs, J.-M., Winkler, H., *et al.* (2005) A diarylquinoline drug active on the ATP synthase of Mycobacterium tuberculosis. *Science* **307**: 223–7.

Ashtekar, D.R., Costa-Perira, R., Nagrajan, K., Vishvanathan, N., Bhatt, a D., and Rittel, W. (1993) In vitro and in vivo activities of the nitroimidazole CGI 17341 against Mycobacterium tuberculosis. *Antimicrob Agents Chemother* **37**: 183–186.

Ashton, W.T., and Brown, R.D. (1980) Synthesis of 8-demethyl-8-hydroxy-5-deazariboflavins. *J Heterocycl Chem* **17**: 1709–1712.

Ashton, W.T., Brown, R.D., Jacobson, F., and Walsh, C. (1979) Synthesis of 7,8-didemethyl-8-hydroxy-5-deazariboflavin and confirmation of its identity with the deazaisoalloxazine chromophore of Methanobacterium redox coenzyme F420. *J Am Chem Soc* **101**: 4419–4420.

Aufhammer, S.W., Warkentin, E., Ermler, U., Hagemeier, C.H., Thauer, R.K., and Shima, S. (2005) Crystal structure of methylenetetrahydromethanopterin reductase (Mer) in complex with coenzyme F420: Architecture of the F420/FMN binding site of enzymes within the nonprolyl cis-peptide containing bacterial luciferase family. *Protein Sci* **14**: 1840–1849.

Bair, T.B., Isabelle, D.W., and Daniels, L. (2001) Structures of coenzyme F420 in Mycobacterium species. *Arch Microbiol* **176**: 37–43.

Bankevich, A., Nurk, S., Antipov, D., Gurevich, A.A., Dvorkin, M., Kulikov, A.S., *et al.* (2012) SPAdes: A New Genome Assembly Algorithm and Its Applications to Single-Cell Sequencing. *J Comput Biol* **19**: 455–477.

Bashiri, G., Perkowski, E.F., Turner, A.P., Feltcher, M.E., Braunstein, M., and Baker, E.N. (2012) Tat-dependent translocation of an F420-binding protein of Mycobacterium tuberculosis. *PLoS One* **7**: e45003.

Bashiri, G., Rehan, A.M., Greenwood, D.R., Dickson, J.M.J., and Baker, E.N. (2010) Metabolic engineering of cofactor F 420 production in Mycobacterium smegmatis. *PLoS One* **5**: e15803.

Bashiri, G., Rehan, A.M., Sreebhavan, S., Baker, H.M., Baker, E.N., and Squire, C.J. (2016) Elongation of the poly-gamma-glutamate tail of F420 requires both domains of the F420:gamma-glutamyl ligase (FbiB) of Mycobacterium tuberculosis. *J Biol Chem* **291**: 6882–6894.

Bashiri, G., Squire, C.J., Moreland, N.J., and Baker, E.N. (2008) Crystal structures of F420-

dependent glucose-6-phosphate dehydrogenase FGD1 involved in the activation of the anti-tuberculosis drug candidate PA-824 reveal the basis of coenzyme and substrate binding. *J Biol Chem* **283**: 17531–17541.

Beelen, P. van, Dijkstra, A.C., and Vogels, G.D. (1983) Quantitation of coenzyme F 420 in methanogenic sludge by the use of reversed-phase high-performance liquid chromatography and a fluorescence detector. *Appl Microbiol Biotechnol* **18**: 67–69.

Benson, D.A., Cavanaugh, M., Clark, K., Karsch-Mizrachi, I., Lipman, D.J., Ostell, J., and Sayers, E.W. (2013) GenBank. *Nucleic Acids Res* **41**: D36–D42.

Berk, H., and Thauer, R.K. (1997) Function of coenzyme F420-dependent NADP reductase in methanogenic archaea containing an NADP-dependent alcohol dehydrogenase. *Arch Microbiol* **168**: 396–402.

Berney, M., Weimar, M.R., Heikal, A., and Cook, G.M. (2012) Regulation of proline metabolism in mycobacteria and its role in carbon metabolism under hypoxia. *Mol Microbiol* **84**: 664–681.

Berteau, O. (2012) Biosynthesis of F 0 , Precursor of the F 420 Cofactor, Requires a Unique Two Radical-SAM Domain Enzyme and Tyrosine as Substrate. *J Am Chem Soc* **134**: 5–8.

Biswal, B.K., Au, K., Cherney, M.M., Garen, C., James, M.N.G., Wang, M., *et al.* (2006) The molecular structure of Rv2074, a probable pyridoxine 5′-phosphate oxidase from Mycobacterium tuberculosis, at 1.6 Å resolution. *Acta Crystallogr Sect F Struct Biol Cryst Commun* **62**: 735–742.

Bloemberg, G. V., Keller, P.M., Stucki, D., Trauner, A., Borrell, S., Latshang, T., *et al.* (2015) Acquired Resistance to Bedaquiline and Delamanid in Therapy for Tuberculosis. *N Engl J Med* **373**: 1986–1988.

Boshoff, H.I.M., and Barry, C.E. (2005) Tuberculosis—metabolism and respiration in the absence of growth. *Nat Rev Microbiol* **3**: 70–80.

Buckel, W., and Thauer, R.K. (2013) Energy conservation via electron bifurcating ferredoxin reduction and proton/Na+ translocating ferredoxin oxidation. *Biochim Biophys Acta (BBA)-Bioenergetics* **1827**: 94–113.

Canaan, S., Sulzenbacher, G., Roig-Zamboni, V., Scappuccini-Calvo, L., Frassinetti, F., Maurin, D., *et al.* (2005) Crystal structure of the conserved hypothetical protein Rv1155 from Mycobacterium tuberculosis. *FEBS Lett* **579**: 215–221.

Carroll, A.J., Zhang, P., Whitehead, L., Kaines, S., Tcherkez, G., and Badger, M.R. (2015) PhenoMeter: a metabolome database search tool using statistical similarity matching of metabolic phenotypes for high-confidence detection of functional links. *Front Bioeng Biotechnol* **3**.

Cellitti, S.E., Shaffer, J., Jones, D.H., Mukherjee, T., Gurumurthy, M., Bursulaya, B., *et al.* (2012) Structure of Ddn, the deazaflavin-dependent nitroreductase from Mycobacterium tuberculosis involved in bioreductive activation of PA-824. *Structure* **20**: 101–112.

Chaiyen, P., Suadee, C., and Wilairat, P. (2001) A novel two-protein component flavoprotein hydroxylase. *FEBS J* **268**: 5550–5561.

Cheeseman, P., Toms-wood, A., and Wolfe, R.S. (1972) Isolation and Properties of a

Fluorescent Compound, Factor420, from Methanobacterium Strain M.o.H. *Microbiology* **112**: 527–531.

Chen, V.B., Davis, W., Echols, N., Headd, J.J., Hung, L., Kapral, G.J., *et al.* (2010) PHENIX : a comprehensive Python-based system for macromolecular structure solution Paul D . Adams , Pavel V . Afonine , G ´ PHENIX : a comprehensive Python-based system for macromolecular structure solution. *Acta Crystallogr Sect D* **d66**: 213–221.

Chen, X., Hashizume, H., Tomishige, T., Nakamura, I., Matsuba, M., Fujiwara, M., *et al.* (2017) Delamanid Kills Dormant Mycobacteria in Vitro and in the Guinea Pig Model of Tuberculosis. *Antimicrob Agents Chemother* AAC-02402.

Choi, K.P., Bair, T.B., Bae, Y.M., and Daniels, L. (2001) Use of transposon Tn5367 mutagenesis and a nitroimidazopyran-based selection system to demonstrate a requirement for fbiA and fbiB in coenzyme F420 biosynthesis by Mycobacterium bovis BCG. *J Bacteriol* **183**: 7058–7066.

Colditz, G.A., Brewer, T.F., Berkey, C.S., Wilson, M.E., Burdick, E., Fineberg, H. V, and Mosteller, F. (1994) Efficacy of BCG vaccine in the prevention of tuberculosis: meta-analysis of the published literature. *Jama* **271**: 698–702.

Cole, S.T., Brosch, R., Parkhill, J., Garnier, T., Churcher, C., Harris, D., *et al.* (1998) Deciphering the biology of Mycobacterium tuberculosis from the complete genome sequence. *Nature* **393**: 537–544.

Cole, S.T., Eiglmeier, K., Parkhill, J., James, K.D., Thomson, N.R., Wheeler, P.R., *et al.* (2001) Massive gene decay in the leprosy bacillus. *Nature* **409**: 1007–1011.

Comas, I., Coscolla, M., Luo, T., Borrell, S., Holt, K.E., Kato-Maeda, M., *et al.* (2013) Out-of-Africa migration and Neolithic coexpansion of Mycobacterium tuberculosis with modern humans. *Nat Genet* **45**: 1176–1182.

Cook, G.M., Greening, C., Hards, K., and Berney, M. (2014) Chapter One-Energetics of Pathogenic Bacteria and Opportunities for Drug Development. *Adv Microb Physiol* **65**: 1–62.

Cowtan, K. (2006) The Buccaneer software for automated model building. 1. Tracing protein chains. *Acta Crystallogr Sect D Biol Crystallogr* **62**: 1002–1011.

Cox, E., and Laessig, K. (2014) FDA approval of bedaquiline—the benefit–risk balance for drug-resistant tuberculosis. *N Engl J Med* **371**: 689–691.

Croucher, N.J., Page, A.J., Connor, T.R., Delaney, A.J., Keane, J.A., Bentley, S.D., *et al.* (2015) Rapid phylogenetic analysis of large samples of recombinant bacterial whole genome sequences using Gubbins. *Nucleic Acids Res* **43**: e15–e15.

Daffé, M., Lacave, C., Lanéelle, M., and Lanéelle, G. (1987) Structure of the major triglycosyl phenol-phthiocerol of Mycobacterium tuberculosis (strain Canetti). *Eur J Biochem* **167**: 155–160.

Dawson, R., Diacon, A.H., Everitt, D., Niekerk, C. Van, Donald, P.R., Burger, D.A., Schall, R., Spigelman, M., Pym, A., Groote-bidlingmaier, F. Von, Mendel, C.M., *et al.* (2015) Efficiency and safety of the combination of moxifloxacin, pretomanid (PA-824), and pyrazinamide during the first 8 weeks of antituberculosis treatment: a phase 2b, open-label, partly randomised trial in patients with drug-susceptible or drug-resistant pul. *Lancet* **385**: 1738–1747.

Dawson, R., Diacon, A.H., Everitt, D., Niekerk, C. Van, Donald, P.R., Burger, D.A., Schall, R., Spigelman, M., Pym, A., Groote-bidlingmaier, F. Von, and Mendel, C.M. (2015) Effi ciency and safety of the combination of moxifl oxacin , pretomanid (PA-824), and pyrazinamide during the fi rst 8 weeks of antituberculosis treatment : a phase 2b , open-label , partly randomised trial in patients with drug-susceptible or drug-resi. *Lancet* **385**: 1738–1747.

Day, T.A., Mittler, J.E., Nixon, M.R., Thompson, C., Miner, M.D., Hickey, M.J., *et al.* (2014) Mycobacterium tuberculosis strains lacking surface lipid phthiocerol dimycocerosate are susceptible to killing by an early innate host response. *Infect Immun* **82**: 5214–5222.

DeLano, W.L. (2002) The PyMOL molecular graphics system. *http//pymol org* .

DeMaio, J., Zhang, Y., Ko, C., Young, D.B., and Bishai, W.R. (1996) A stationary-phase stress-response sigma factor from Mycobacterium tuberculosis. *Proc Natl Acad Sci U S A* **93**: 2790–2794.

Deoghare, S. (2013) Bedaquiline: a new drug approved for treatment of multidrug-resistant tuberculosis. *Indian J Pharmacol* **45**: 536.

Diacon, A.H., Dawson, R., Groote-Bidlingmaier, F. von, Symons, G., Venter, A., Donald, P.R., *et al.* (2015) Bactericidal activity of pyrazinamide and clofazimine alone and in combinations with pretomanid and bedaquiline. *Am J Respir Crit Care Med* **191**: 943–953.

Diacon, A.H., Pym, A., Grobusch, M., Patientia, R., Rustomjee, R., Page-Shipp, L., *et al.* (2009) The Diarylquinoline TMC207 for Multidrug-Resistant Tuberculosis. *N Engl J Med* **360**: 2397–2405.

Diacon, A.H., Pym, A., Grobusch, M.P., Los Rios, J.M. de, Gotuzzo, E., Vasilyeva, I., *et al.* (2014) Multidrug-resistant tuberculosis and culture conversion with bedaquiline. *N Engl J Med* **371**: 723–732.

Dolfing, J., and Mulder, J.-W. (1985) Comparison of methane production rate and coenzyme F420 content of methanogenic consortia in anaerobic granular sludge. *Appl Environ Microbiol* **49**: 1142–1145.

Dubnau, E., Chan, J., Raynaud, C., Mohan, V.P., Lanéelle, M., Yu, K., *et al.* (2000) Oxygenated mycolic acids are necessary for virulence of Mycobacterium tuberculosis in mice. *Mol Microbiol* **36**: 630–637.

Ebert, S., Rieger, P.-G., and Knackmuss, H.-J. (1999) Function of coenzyme F420 in aerobic catabolism of 2, 4, 6-trinitrophenol and 2, 4-dinitrophenol by Nocardioides simplex FJ2-1A. *J Bacteriol* **181**: 2669–2674.

Edgar, R.C. (2008) MUSCLE : multiple sequence alignment with high accuracy and high throughput. *Nucleic Acids Res* **32**: 1792–1797.

Edmondson, D.E., Barman, B., and Tollin, G. (1972) Importance of the N-5 position in flavin coenzymes. Properties of free and protein-bound 5-deaza analogs. *Biochemistry* **11**: 1133–1138.

Eirich, L.D., Vogels, G.D., and Wolfe, R.S. (1976) Proposed structure for coenzyme F420 from Methanobacterium. *Biochem J Prog Surf Membr Sci Methods Enzym J Bioi Chem Anal Biochem Biophys Acta Natl AcadSci USA USA J J Bioi Chem chim Biophys Acta Biochim Biophys Acta Biochem* **71**: 18–324.

Eirich, L.D., Vogels, G.D., and Wolfe, R.S. (1979) Distribution of coenzyme F420 and properties of its hydrolytic fragments. *J Bacteriol* **140**: 20–27.

Emsley, P., Lohkamp, B., Scott, W.G., Cowtan, K., IUCr, W., G.-K.R., *et al.* (2010) Features and development of Coot. *Acta Crystallogr Sect D Biol Crystallogr* **66**: 486–501.

Evans, P.N., Parks, D.H., Chadwick, G.L., Robbins, S.J., Orphan, V.J., Golding, S.D., and Tyson, G.W. (2015) Methane metabolism in the archaeal phylum Bathyarchaeota revealed by genome-centric metagenomics. *Science (80-)* **350**: 434–438.

Evans, P.R., Murshudov, G.N., K., C., K., D., K., D., A., K.P., *et al.* (2013) How good are my data and what is the resolution? *Acta Crystallogr Sect D Biol Crystallogr* **69**: 1204–1214.

Feuerriegel, S., Köser, C.U., Baù, D., Rüsch-Gerdes, S., Summers, D.K., Archer, J.A.C., *et al.* (2011) Impact of fgd1 and ddn diversity in Mycobacterium tuberculosis complex on in vitro susceptibility to PA-824. *Antimicrob Agents Chemother* **55**: 5718–5722.

Fischer, M., and Bacher, A. (2011) Biosynthesis of Vitamin B2 and Flavocoenzymes in Plants. *Adv Bot Res* **58**: 93–152.

Fisher, A.J., Thompson, T.B., Thoden, J.B., Baldwin, T.O., and Rayment, I. (1996) The 1.5-Å resolution crystal structure of bacterial luciferase in low salt conditions. *J Biol Chem* **271**: 21956–21968.

Fisher, J., Spencer, R., and Walsh, C. (1976) Enzyme-catalyzed redox reactions with the flavin analogues 5-deazariboflavin, 5-deazariboflavin 5'-phosphate, and 5-deazariboflavin 5'-diphosphate, 5' →5'-adenosine ester. *Biochemistry* **15**: 1054–1064.

Forouhar, F., Abashidze, M., Xu, H., Grochowski, L.L., Seetharaman, J., Hussain, M., *et al.* (2008) Molecular insights into the biosynthesis of the F420 coenzyme. *J Biol Chem* **283**: 11832–11840.

Friesner, R.A., Banks, J.L., Murphy, R.B., Halgren, T.A., Klicic, J.J., Mainz, D.T., *et al.* (2004) Glide: a new approach for rapid, accurate docking and scoring. 1. Method and assessment of docking accuracy. *J Med Chem* **47**: 1739–1749.

Garrison, E., and Marth, G. (2012) Haplotype-based variant detection from short-read sequencing. *arXiv Prepr arXiv12073907* .

Gebhard, S., Tran, S.L., and Cook, G.M. (2006) The Phn system of Mycobacterium smegmatis: a second high-affinity ABC-transporter for phosphate. *Microbiology* **152**: 3453–3465.

Geiman, D.E., Kaushal, D., Ko, C., Tyagi, S., Manabe, Y.C., Schroeder, B.G., *et al.* (2004) Attenuation of Late-Stage Disease in Mice Infected by the Mycobacterium tuberculosis Mutant Lacking the SigF Alternate Sigma Factor and Identification of SigF-Dependent Genes by Microarray Analysis. *Infect Immun* **72**: 1733–1745.

Gibson, D.G., Young, L., Chuang, R.-Y., Venter, J.C., Hutchison, C. a, Smith, H.O., *et al.* (2009) Enzymatic assembly of DNA molecules up to several hundred kilobases. *Nat Methods* **6**: 343–5.

Gorris, L.G., and Drift, C. Van der (1994) Cofactor contents of methanogenic bacteria reviewed. *Biofactors* **4**: 139–145.

Gould, T.A., Langemheen, H. Van De, Muñoz-Elías, E.J., McKinney, J.D., and Sacchettini, J.C. (2006) Dual role of isocitrate lyase 1 in the glyoxylate and methylcitrate cycles in

Mycobacterium tuberculosis. *Mol Microbiol* **61**: 940–947.

Graham, D.E., Xu, H., and White, R.H. (2003) Identification of the 7,8-didemethyl-8-hydroxy-5-deazariboflavin synthase required for coenzyme F420 biosynthesis. *Arch Microbiol* **180**: 455–464.

Graupner, M., and White, R.H. (2001) Biosynthesis of the phosphodiester bond in coenzyme F420 in the methanoarchaea. *Biochemistry* **40**: 10859–10872.

Graupner, M., and White, R.H. (2003) Methanococcus jannaschii coenzyme F420 analogs contain a terminal α-linked glutamate. *J Bacteriol* **185**: 4662–4665.

Graupner, M., Xu, H., and White, R.H. (2000) Identification of an archaeal 2-hydroxy acid dehydrogenase catalyzing reactions involved in coenzyme biosynthesis in methanoarchaea. *J Bacteriol* **182**: 3688–3692.

Graupner, M., Xu, H., and White, R.H. (2002) Characterization of the 2-phospho-L-lactate transferase enzyme involved in coenzyme F420 biosynthesis in Methanococcus jannaschii. *Biochemistry* **41**: 3033–3037.

Greening, C., Ahmed, F.H., Mohamed, A.E., Lee, B.M., Pandey, G., Warden, A.C., *et al.* (2016) Physiology, Biochemistry, and Applications of F420 - and Fo -Dependent Redox Reactions. *Microbiol Mol Biol Rev* **80**: 451–493.

Greening, C., Jirapanjawat, T., Afroze, S., Ney, B., Scott, C., Pandey, G., *et al.* (2017) Mycobacterial F420H2-dependent reductases promiscuously reduce diverse compounds through a common mechanism. *Front Microbiol* **8**: 1000.

Grochowski, L.L., Xu, H., and White, R.H. (2006) Identification of lactaldehyde dehydrogenase in Methanocaldococcus jannaschii and its involvement in production of lactate for F420 biosynthesis. *J Bacteriol* **188**: 2836–2844.

Guenin-Macé, L., Simeone, R., and Demangel, C. (2009) Lipids of pathogenic Mycobacteria: contributions to virulence and host immune suppression. *Transbound Emerg Dis* **56**: 255–268.

Guerra-Lopez, D., Daniels, L., and Rawat, M. (2007) Mycobacterium smegmatis mc2 155 fbiC and MSMEG_2392 are involved in triphenylmethane dye decolorization and coenzyme F420 biosynthesis. *Microbiology* **153**: 2724–2732.

Guo, Y., Guo, G., Mao, X., Zhang, W., Xiao, J., Tong, W., *et al.* (2008) Functional identification of HugZ, a heme oxygenase from Helicobacter pylori. *BMC Microbiol* **8**: 226.

Gupta, R., Gao, M., Cirule, A., Xiao, H., Geiter, L.J., and Wells, C.D. (2015) Delamanid for Extensively Drug-Resistant Tuberculosis. *N Engl J Med* **373**: 291–292.

Gurumurthy, M., Mukherjee, T., Dowd, C.S., Singh, R., Niyomrattanakit, P., Tay, J.A., *et al.* (2012) Substrate specificity of the deazaflavin-dependent nitroreductase from Mycobacterium tuberculosis responsible for the bioreductive activation of bicyclic nitroimidazoles. *FEBS J* **279**: 113–125.

Gurumurthy, M., Rao, M., Mukherjee, T., Rao, S.P.S., Boshoff, H.I., Dick, T., *et al.* (2013) A novel F420-dependent anti-oxidant mechanism protects Mycobacterium tuberculosis against oxidative stress and bactericidal agents. *Mol Microbiol* **87**: 744–755.

Haagsma, A.C., Abdillahi-Ibrahim, R., Wagner, M.J., Krab, K., Vergauwen, K., Guillemont, J., *et al.* (2009) Selectivity of TMC207 towards mycobacterial ATP synthase compared with

that towards the eukaryotic homologue. *Antimicrob Agents Chemother* **53**: 1290–1292.

Hards, K., Robson, J.R., Berney, M., Shaw, L., Bald, D., Koul, A., *et al.* (2015) Bactericidal mode of action of bedaquiline. *J Antimicrob Chemother* **70**: 2028–2037.

Haroon, M.F., Hu, S., Shi, Y., Imelfort, M., Keller, J., Hugenholtz, P., *et al.* (2013) Anaerobic oxidation of methane coupled to nitrate reduction in a novel archaeal lineage. *Nature* **500**: 567–570.

Hart, K.M., Ho, C.M.W., Dutta, S., Gross, M.L., and Bowman, G.R. (2016) Modelling proteins' hidden conformations to predict antibiotic resistance. *Nat Commun* **7**: 12965.

Hartzell, P.L., Zvilius, G., Escalante-Semerena, J.C., and Donnelly, M.I. (1985) Coenzyme F420 dependence of the methylenetetrahydromethanopterin dehydrogenase of Methanobacteriumthermoautotrophicum. *Biochem Biophys Res Commun* **133**: 884–890.

Hasan, M.R., Rahman, M., Jaques, S., Purwantini, E., and Daniels, L. (2010) Glucose 6-phosphate accumulation in mycobacteria: implications for a novel F420-dependent anti-oxidant defense system. *J Biol Chem* **285**: 19135–19144.

Haver, H., Chua, A., and Ghode, P. (2015) Mutations in genes for the F420 biosynthetic pathway and a nitroreductase enzyme are the primary resistance determinants in spontaneous in vitro-selected PA-824-. *Antimicrob agents* **59**: 5316–5323.

He, Z., and Buck, J. De (2010) Cell wall proteome analysis of Mycobacterium smegmatis strain MC2 155. *BMC Microbiol* **10**: 121.

Heikal, A., Hards, K., Cheung, C.Y., Menorca, A., Timmer, M.S.M., Stocker, B.L., and Cook, G.M. (2016) Activation of type II NADH dehydrogenase by Quinolinequinones mediates antitubercular cell death. *J Antimicrob Chemother* **71**: 2840–2847.

Hemmerich, P., Nagelschneider, G., and Veeger, C. (1970) Chemistry and molecular biology of flavins and flavoproteins. *FEBS Lett* **8**: 69–83.

Ho, S.N., Hunt, H.D., Horton, R.M., Pullen, J.K., and Pease, L.R. (1989) Site-directed mutagenesis by overlap extension using the polymerase chain reaction. *Gene* **77**: 51–59.

Hoffmann, H., Borroni, E., Schena, E., Nedialkova, L., Hofmann-Thiel, S., and Cirillo, D. (2016) Delamanid susceptibility testing of Mycobacterium tuberculosis using the resazurin microtitre assay and the BACTEC^{TM} MGIT^{TM} 960 system—authors' response. *J Antimicrob Chemother* **71**: 3625–3625.

Hoffmann, H., Kohl, T.A., Hofmann-Thiel, S., Merker, M., Beckert, P., Jaton, K., *et al.* (2016) Delamanid and bedaquiline resistance in MTB ancestral Beijing genotype causing extensive drug-resistant TB in a tibetan refugee. *Am J Respir Crit Care Med* **193**: 337–340.

Hossain, M.S., Le, C.Q., Joseph, E., Nguyen, T.Q., Johnson-Winters, K., and Foss, F.W. (2015) Convenient synthesis of deazaflavin cofactor FO and its activity in F420-dependent NADP reductase. *Org Biomol Chem* **13**: 5082–5085.

Irwin, J.J., and Shoichet, B.K. (2005) ZINC − A Free Database of Commercially Available Compounds for Virtual Screening ZINC - A Free Database of Commercially Available Compounds for Virtual Screening. *J Chem Inf Model* **45**: 177–182.

Jacobson, F., and Walsh, C. (1984) Properties of 7,8-Didemethyl-8-hydroxy-5-deazaflavins Relevant to Redox Coenzyme Function in Methanogen Metabolism. *Biochemistry* **23**: 979–

988.

Jain, S.K., Lamichhane, G., Nimmagadda, S., Pomper, M.G., and Bishai, W.R. (2008) Antibiotic treatment of tuberculosis: old problems, new solutions. *Microbe* **3**: 285.

Ji, B., Lefrançois, S., Robert, J., Chauffour, A., Truffot, C., and Jarlier, V. (2006) In vitro and in vivo activities of rifampin, streptomycin, amikacin, moxifloxacin, R207910, linezolid, and PA-824 against Mycobacterium ulcerans. *Antimicrob Agents Chemother* **50**: 1921–1926.

Jindani, A., Harrison, T.S., Nunn, A.J., Phillips, P.P.J., Churchyard, G.J., Charalambous, S., *et al.* (2014) High-dose rifapentine with moxifloxacin for pulmonary tuberculosis. *N Engl J Med* **371**: 1599–1608.

Jirapanjawat, T., Ney, B., Taylor, M.C., Warden, A.C., Afroze, S., Russell, R.J., *et al.* (2016) The redox cofactor F420 protects mycobacteria from diverse antimicrobial compounds and mediates a reductive detoxification system. *Appl Environ Microbiol* **82**: 6810–6818.

Johnson, E.F., and Mukhopadhyay, B. (2005) A new type of sulfite reductase, a novel coenzyme F420-dependent enzyme, from the methanarchaeon Methanocaldococcus jannaschii. *J Biol Chem* **280**: 38776–38786.

Jonge, M.R. de, Koymans, L.H.M., Guillemont, J.E.G., Koul, A., and Andries, K. (2007) A computational model of the inhibition of Mycobacterium tuberculosis ATPase by a new drug candidate R207910. *PROTEINS Struct Funct Bioinforma* **67**: 971–980.

Kabsch, W. (2010) Xds. *Acta Crystallogr Sect D Biol Crystallogr* **66**: 125–132.

Kana, B.D., Weinstein, E.A., Avarbock, D., Dawes, S.S., Rubin, H., and Mizrahi, V. (2001) Characterization of the cydAB -Encoded Cytochrome bd Oxidase from Mycobacterium smegmatis. *J Bacteriol* **183**: 7076–7086.

Kertesz, M.A., Schmidt-Larbig, K., and Wüest, T. (1999) A Novel Reduced Flavin Mononucleotide-Dependent Methanesulfonate Sulfonatase Encoded by the Sulfur-Regulatedmsu Operon of Pseudomonas aeruginosa. *J Bacteriol* **181**: 1464–1473.

Kornberg, H.L. (1966) The role and control of the glyoxylate cycle in Escherichia coli. *Biochem J* **99**: 1.

Koul, A., Dendouga, N., Vergauwen, K., Molenberghs, B., Vranckx, L., Willebrords, R., *et al.* (2007) Diarylquinolines Target Subunit c of Mycobacterial ATP Synthase. *Nat Chem Biol* **3**: 323–324.

Koul, A., Vranckx, L., Dendouga, N., Balemans, W., Wyngaert, I. Van Den, Vergauwen, K., *et al.* (2008) Diarylquinolines are bactericidal for dormant mycobacteria as a result of disturbed ATP homeostasis. *J Biol Chem* **283**: 25273–25280.

Koul, A., Vranckx, L., Dhar, N., Göhlmann, H.W.H., Özdemir, E., Neefs, J.-M., *et al.* (2014) Delayed bactericidal response of Mycobacterium tuberculosis to bedaquiline involves remodelling of bacterial metabolism. *Nat Commun* **5**.

Kozubal, M.A., Romine, M., deM Jennings, R., Jay, Z.J., Tringe, S.G., Rusch, D.B., *et al.* (2013) Geoarchaeota: a new candidate phylum in the Archaea from high-temperature acidic iron mats in Yellowstone National Park. *ISME J* **7**: 622–634.

Kuo, M.-S.T., Yurek, D.A., Coats, J.H., and Li, G.P. (1989) Isolation and identification of 7, 8-didemethyl-8-hydroxy-5-deazariboflavin, an unusual cosynthetic factor in streptomycetes,

from Streptomyces lincolnensis. *J Antibiot (Tokyo)* **42**: 475–478.

Lamprecht, D.A., Finin, P.M., Rahman, M.A., Cumming, B.M., Russell, S.L., Jonnala, S.R., *et al.* (2016) Turning the respiratory flexibility of Mycobacterium tuberculosis against itself. *Nat Commun* **7**: 12393.

Lapalikar, G. V., Taylor, M.C., Warden, A.C., Scott, C., Russell, R.J., and Oakeshott, J.G. (2012) F 420H 2-dependent degradation of aflatoxin and other furanocoumarins is widespread throughout the Actinomycetales. *PLoS One* **7**: e30114.

Li, H. (2013) Aligning sequence reads, clone sequences and assembly contigs with BWA-MEM. *arXiv Prepr arXiv13033997* .

Li, H., Graupner, M., Xu, H., and White, R.H. (2003) CofE catalyzes the addition of two glutamates to F420-0 in F420 coenzyme biosynthesis in Methanococcus jannaschii. *Biochemistry* **42**: 9771–9778.

Li, H., Xu, H., Graham, D.E., and White, R.H. (2003) Glutathione synthetase homologs encode α-L-glutamate ligases for methanogenic coenzyme F420 and tetrahydrosarcinapterin biosyntheses. *Proc Natl Acad Sci* **100**: 9785–9790.

Li, W., Cowley, A., Uludag, M., Gur, T., McWilliam, H., Squizzato, S., *et al.* (2015) The EMBL-EBI bioinformatics web and programmatic tools framework. *Nucleic Acids Res* **43**: W580–W584.

Lienhardt, C., Glaziou, P., Uplekar, M., Lönnroth, K., Getahun, H., and Raviglione, M. (2012) Global tuberculosis control: lessons learnt and future prospects. *Nat Rev Microbiol* **10**: 407–416.

Lin, X.L., and White, R.H. (1986) Occurrence of coenzyme F420 and its gamma-monoglutamyl derivative in nonmethanogenic archaebacteria. *J Bacteriol* **168**: 444–448.

Lorenz, M.C., and Fink, G.R. (2002) Life and death in a macrophage: role of the glyoxylate cycle in virulence. *Eukaryot Cell* **1**: 657–662.

Mahajan, R. (2013) Bedaquiline: First FDA-approved tuberculosis drug in 40 years. *Int J Appl Basic Med Res* **2**: 124–128.

Makarov, V., Lechartier, B., Zhang, M., Neres, J., Sar, A.M. van der, Raadsen, S.A., *et al.* (2014) Towards a new combination therapy for tuberculosis with next generation benzothiazinones. *EMBO Mol Med* e201303575.

Manjunatha, U., Boshoff, H.I.M., and Barry, C.E. (2009) The mechanism of action of PA-824: Novel insights from transcriptional profiling. *Commun Integr Biol* **2**: 215–218.

Manjunatha, U.H., Boshoff, H., Dowd, C.S., Zhang, L., Albert, T.J., Norton, J.E., *et al.* (2006) Identification of a nitroimidazo-oxazine-specific protein involved in PA-824 resistance in Mycobacterium tuberculosis. *Proc Natl Acad Sci U S A* **103**: 431–436.

Manjunatha, U.H., Lahiri, R., Randhawa, B., Dowd, C.S., Krahenbuhl, J.L., and Barry, C.E. (2006) Mycobacterium leprae is naturally resistant to PA-824. *Antimicrob Agents Chemother* **50**: 3350–3354.

Marrero, J., Rhee, K.Y., Schnappinger, D., Pethe, K., and Ehrt, S. (2010) Gluconeogenic carbon flow of tricarboxylic acid cycle intermediates is critical for Mycobacterium tuberculosis to establish and maintain infection. *Proc Natl Acad Sci* **107**: 9819–9824.

Mashalidis, E.H., Gittis, A.G., Tomczak, A., Abell, C., Barry 3rd, C.E., and Garboczi, D.N. (2015) Molecular insights into the binding of coenzyme F to the conserved protein Rv1155 from Mycobacterium tuberculosis. *Protein Sci* .

Mashalidis, E.H., Mukherjee, T., Śledź, P., Matak-Vinković, D., Boshoff, H., Abell, C., and Barry III, C.E. (2011) Rv2607 from Mycobacterium tuberculosis is a pyridoxine 5′-phosphate oxidase with unusual substrate specificity. *PLoS One* **6**: e27643.

Matsumoto, M., Hashizume, H., Tomishige, T., Kawasaki, M., Tsubouchi, H., Sasaki, H., *et al.* (2006) OPC-67683, a nitro-dihydro-imidazooxazole derivative with promising action against tuberculosis in vitro and in mice. *PLoS Med* **3**: 2131–2144.

Mawuenyega, K.G., Forst, C. V, Dobos, K.M., Belisle, J.T., Chen, J., Bradbury, E.M., *et al.* (2005) Mycobacterium tuberculosis functional network analysis by global subcellular protein profiling. *Mol Biol Cell* **16**: 396–404.

McCoy, A.J. et al. (2007) PHASER crystallographic software. *J Appli Cryst* **40**: 658–674.

McPhillips, T.M., McPhillips, S.E., Chiu, H.-J., Cohen, A.E., Deacon, A.M., Ellis, P.J., *et al.* (2002) Blu-Ice and the Distributed Control System: software for data acquisition and instrument control at macromolecular crystallography beamlines. *J Synchrotron Radiat* **9**: 401–406.

Mohamed, A.E., Condic-Jurkic, K., Ahmed, F.H., Yuan, P., O'Mara, M.L., Jackson, C.J., and Coote, M.L. (2016) Hydrophobic Shielding Drives Catalysis of Hydride Transfer in a Family of F420H2-Dependent Enzymes. *Biochemistry* **55**: 6908–6918.

Mohamed, A.E., Condic-Jurkic, K., Ahmed, F.H., Yuan, P., O'Mara, M.L., Jackson, C.J., and Coote, M.L. (2016) Hydrophobic shielding drives catalysis of hydride transfer in a family of $F_{420}H_2$-dependent enzymes. *Biochemistry* .

Mohamed, E., Ahmed, F.H., Arulmozhiraja, S., Lin, C.Y., Taylor, M.C., Krausz, E.R., *et al.* (2016) Protonation state of F 420 H 2 in the prodrug-activating deazaflavin dependent nitroreductase (Ddn) from Mycobacterium tuberculosis. *Mol BioSyst* **12**: 1110–1113.

Möller-Zinkhan, D., Börner, G., and Thauer, R.K. (1989) Function of methanofuran, tetrahydromethanopterin, and coenzyme F 420 in Archaeoglobus fulgidus. *Arch Microbiol* **152**: 362–368.

Morris, G., and Huey, R. (2009) AutoDock4 and AutoDockTools4: Automated docking with selective receptor flexibility. *J ...* **30**: 2785–2791.

Muñoz-Elías, E.J., Upton, A.M., Cherian, J., and McKinney, J.D. (2006) Role of the methylcitrate cycle in Mycobacterium tuberculosis metabolism, intracellular growth, and virulence. *Mol Microbiol* **60**: 1109–1122.

Murray, S., Mendel, C., and Spigelman, M. (2016) TB Alliance regimen development for multidrug-resistant tuberculosis. *Int J Tuberc Lung Dis* **20**: 38–41.

Murshudov, G.N., Skubák, P., Lebedev, A.A., Pannu, N.S., Steiner, R.A., Nicholls, R.A., *et al.* (2011) REFMAC5 for the refinement of macromolecular crystal structures. *Acta Crystallogr Sect D Biol Crystallogr* **67**: 355–367.

Nakano, T., Miyake, K., Dairi, T., Mizukami, T., and Katsumata, R. (2004) Identification and cloning of the gene involved in the final step of chlortetracycline biosynthesis in Streptomyces

aureofaciens. *Biosci Biotechnol Biochem* **68**: 1345–1352.

Nelson-Sathi, S., Sousa, F.L., Roettger, M., Lozada-Chávez, N., Thiergart, T., Janssen, A., *et al.* (2015) Origins of major archaeal clades correspond to gene acquisitions from bacteria. *Nature* **517**: 77–80.

Ney, B., Ahmed, F.H., Carere, C.R., Biswas, A., Warden, A.C., Morales, S.E., *et al.* (2017) The methanogenic redox cofactor F420 is widely synthesized by aerobic soil bacteria. *ISME J* **420**: In press.

Nguyen, Q.-T., Trinco, G., Binda, C., Mattevi, A., and Fraaije, M.W. (2016) Discovery and characterization of an F420-dependent glucose-6-phosphate dehydrogenase (Rh-FGD1) from Rhodococcus jostii RHA1. *Appl Microbiol Biotechnol* 1–12.

Nocek, B., Evdokimova, E., Proudfoot, M., Kudritska, M., Grochowski, L.L., White, R.H., *et al.* (2007) Structure of an Amide Bond Forming F 420: γγ-glutamyl Ligase from Archaeoglobus Fulgidus-A Member of a New Family of Non-ribosomal Peptide Synthases. *J Mol Biol* **372**: 456–469.

Onwueme, K.C., Vos, C.J., Zurita, J., Ferreras, J.A., and Quadri, L.E.N. (2005) The dimycocerosate ester polyketide virulence factors of mycobacteria. *Prog Lipid Res* **44**: 259–302.

Orencia, M.C., Yoon, J.S., Ness, J.E., Stemmer, W.P.C., and Stevens, R.C. (2001) Predicting the emergence of antibiotic resistance by directed evolution and structural analysis. *Nat Struct Mol Biol* **8**: 238–242.

Oyugi, M.A., Bashiri, G., Baker, E.N., and Johnson-Winters, K. (2017) Mechanistic insights into F 420-dependent glucose-6-phosphate dehydrogenase using isotope effects and substrate inhibition studies. *Biochim Biophys Acta (BBA)-Proteins Proteomics* .

Oyugi, M.A., Bashiri, G., Baker, E.N., and Johnson-Winters, K.L. (2016) Investigating the reaction mechanism of F420-dependent glucose-6-phosphate dehydrogenase from Mycobacterium tuberculosis: kinetic analysis of the wild-type and mutant enzymes. *Biochemistry* .

Patterson, S., Wyllie, S., Norval, S., Stojanovski, L., Simeons, F.R.C., Auer, J.L., *et al.* (2016) The anti-tubercular drug delamanid as a potential oral treatment for visceral leishmaniasis. *Elife* **5**: e09744.

Patterson, S., Wyllie, S., Stojanovski, L., Perry, M.R., Simeons, F.R.C., Norval, S., *et al.* (2013) The R enantiomer of the antitubercular drug PA-824 as a potential oral treatment for visceral Leishmaniasis. *Antimicrob Agents Chemother* **57**: 4699–4706.

Pecsi, I., Hards, K., Ekanayaka, N., Berney, M., Hartman, T., Jacobs, W.R., and Cook, G.M. (2014) Essentiality of succinate dehydrogenase in Mycobacterium smegmatis and its role in the generation of the membrane potential under hypoxia. *MBio* **5**: e01093-14.

Pédelacq, J.D., Rho, B.S., Kim, C.Y., Waldo, G.S., Lekin, T.P., Segelke, B.W., *et al.* (2006) Crystal structure of a putative pyridoxine 5′-phosphate oxidase (Rv2607) from Mycobacterium tuberculosis. *Proteins Struct Funct Genet* **62**: 563–569.

Pethe, K., Bifani, P., Jang, J., Kang, S., Park, S., Ahn, S., *et al.* (2013) Discovery of Q203, a potent clinical candidate for the treatment of tuberculosis. *Nat Med* **19**: 1157–1160.

Philmus, B., Decamps, L., Berteau, O., and Begley, T.P. (2015) Biosynthetic versatility and coordinated action of 5′-deoxyadenosyl radicals in deazaflavin biosynthesis. *J Am Chem Soc* **137**: 5406.

Pol, A., Drift, C. van der, Vogels, G.D., Cuppen, T.J.H.M., and Laarhoven, W.H. (1980) Comparison of coenzyme F420 from Methanobacterium bryantii with 7-and 8-hydroxy-10-methyl-5-deazaisoalloxazine. *Biochem Biophys Res Commun* **92**: 255–260.

Preiss, L., Langer, J.D., Yildiz, Ö., Eckhardt-Strelau, L., Guillemont, J.E.G., Koul, A., and Meier, T. (2015) Structure of the mycobacterial ATP synthase Fo rotor ring in complex with the anti-TB drug bedaquiline. *Sci Adv* **1**: e1500106.

Purwantini, E., and Daniels, L. (1996) Purification of a novel coenzyme F420-dependent glucose-6-phosphate dehydrogenase from Mycobacterium smegmatis. *J Bacteriol* **178**: 2861–2866.

Purwantini, E., Daniels, L., and Mukhopadhyay, B. (2016) F 420 H 2 is required for phthiocerol dimycocerosates synthesis in mycobacteria. *J Bacteriol* JB.01035-15.

Purwantini, E., Gillis, T.P., and Daniels, L. (1997) Presence of F420-dependent glucose-6-phosphate dehydrogenase in Mycobacterium and Nocardia species, but absence from Streptomyces and Corynebacterium species and methanogenic Archaea. *FEMS Microbiol Lett* **146**: 129–134.

Purwantini, E., and Mukhopadhyay, B. (2009) Conversion of NO2 to NO by reduced coenzyme F420 protects mycobacteria from nitrosative damage. *Proc Natl Acad Sci U S A* **106**: 6333–6338.

Purwantini, E., and Mukhopadhyay, B. (2013) Rv0132c of Mycobacterium tuberculosis encodes a coenzyme F 420-dependent hydroxymycolic acid dehydrogenase. *PLoS One* **8**: e81985.

Purwantini, E., Mukhopadhyay, B., Spencer, R.W., and Daniels, L. (1992) Effect of temperature on the spectral properties of coenzyme F420 and related compounds. *Anal Biochem* **205**: 342–350.

Rinke, C., Schwientek, P., Sczyrba, A., Ivanova, N.N., Anderson, I.J., Cheng, J.-F., *et al.* (2013) Insights into the phylogeny and coding potential of microbial dark matter. *Nature* **499**: 431–437.

Rohde, K., Yates, R.M., Purdy, G.E., and Russell, D.G. (2007) Mycobacterium tuberculosis and the environment within the phagosome. *Immunol Rev* **219**: 37–54.

Rustad, T.R., Harrell, M.I., Liao, R., and Sherman, D.R. (2008) The enduring hypoxic response of Mycobacterium tuberculosis. *PLoS One* **3**: e1502.

Ryan, N.J., and Lo, J.H. (2014) Delamanid: first global approval. *Drugs* **74**: 1041–1045.

Safo, M.K., Musayev, F.N., Salvo, M.L. di, and Schirch, V. (2001) X-ray structure of Escherichia coli pyridoxine 5'-phosphate oxidase complexed with pyridoxal 5'-phosphate at 2.0 Å resolution. *J Mol Biol* **310**: 817–826.

Sambandan, D., Dao, D.N., Weinrick, B.C., Vilchèze, C., Gurcha, S.S., Ojha, A., *et al.* (2013) Keto-mycolic acid-dependent pellicle formation confers tolerance to drug-sensitive Mycobacterium tuberculosis. *MBio* **4**: e00222-13.

Sambrook, J., Fritsch, E.F., and Maniatis, T. (1989) *Molecular cloning: a laboratory manual.* Cold spring harbor laboratory press, .

Sastry, G.M., Adzhigirey, M., Day, T., Annabhimoju, R., and Sherman, W. (2013) Protein and ligand preparation: parameters, protocols, and influence on virtual screening enrichments. *J Comput Aided Mol Des* **27**: 221–234.

Schauer, N.L., Ferry, J.G., Honek, J.F., Orme-Johnson, W.H., and Walsh, C. (1986) Mechanistic studies of the coenzyme F420 reducing formate dehydrogenase from Methanobacterium formicicum. *Biochemistry* **25**: 7163–7168.

Schrödinger, L. (2017) Biologics Suite 2017-4. *Schrödinger, LLC, New York, NY* .

Schrödinger Release (2016) LigPrep. *Schrödinger, LLC, New York, NY* .

Seedorf, H., Dreisbach, A., Hedderich, R., Shima, S., and Thauer, R.K. (2004) F420H2 oxidase (FprA) from Methanobrevibacter arboriphilus, a coenzyme F420-dependent enzyme involved in O2 detoxification. *Arch Microbiol* **182**: 126–137.

Segala, E., Sougakoff, W., Nevejans-Chauffour, A., Jarlier, V., and Petrella, S. (2012) New mutations in the mycobacterial ATP synthase: new insights into the binding of the diarylquinoline TMC207 to the ATP synthase C-ring structure. *Antimicrob Agents Chemother* **56**: 2326–2334.

Selengut, J.D., and Haft, D.H. (2010) Unexpected abundance of coenzyme F420-dependent enzymes in Mycobacterium tuberculosis and other actinobacteria. *J Bacteriol* **192**: 5788–5798.

Sievers, F., Wilm, A., Dineen, D., Gibson, T.J., Karplus, K., Li, W., *et al.* (2011) Fast, scalable generation of high-quality protein multiple sequence alignments using Clustal Omega. *Mol Syst Biol* **7**.

Simeone, R., Constant, P., Malaga, W., Guilhot, C., Daffe, M., and Chalut, C. (2007) Molecular dissection of the biosynthetic relationship between phthiocerol and phthiodiolone dimycocerosates and their critical role in the virulence and permeability of Mycobacterium tuberculosis. *Febs J* **274**: 1957–1969.

Singh, A.R., Strankman, A., Orkusyan, R., Purwantini, E., and Rawat, M. (2016) Lack of mycothiol and ergothioneine induces different protective mechanisms in Mycobacterium smegmatis. *Biochem Biophys Reports* **8**: 100–106.

Singh, R., Manjunatha, U., Boshoff, H.I.M., Ha, Y.H., Niyomrattanakit, P., Ledwidge, R., *et al.* (2008) PA-824 kills nonreplicating Mycobacterium tuberculosis by intracellular NO release. *Science* **322**: 1392–5.

Sinha, S., Kosalai, K., Arora, S., Namane, A., Sharma, P., Gaikwad, A.N., *et al.* (2005) Immunogenic membrane-associated proteins of Mycobacterium tuberculosis revealed by proteomics. *Microbiology* **151**: 2411–2419.

Smeulders, M.J., Keer, J., Speight, R.A., and Williams, H.D. (1999) Adaptation of Mycobacterium smegmatis to stationary phase. *J Bacteriol* **181**: 270–283.

Snapper, S.B., Melton, R.E., Mustafa, S., Kieser, T., and WR Jr, J. (1990) Isolation and characterization of efficient plasmid transformation mutants of Mycobacterium smegmatis. *Mol Microbiol* **4**: 1911–1919.

Souza, G.A. de, Leversen, N.A., Målen, H., and Wiker, H.G. (2011) Bacterial proteins with

cleaved or uncleaved signal peptides of the general secretory pathway. *J Proteomics* **75**: 502–510.

Spang, A., Poehlein, A., Offre, P., Zumbrägel, S., Haider, S., Rychlik, N., *et al.* (2012) The genome of the ammonia-oxidizing Candidatus Nitrososphaera gargensis: insights into metabolic versatility and environmental adaptations. *Environ Microbiol* **14**: 3122–3145.

Spang, A., Saw, J.H., Jørgensen, S.L., Zaremba-Niedzwiedzka, K., Martijn, J., Lind, A.E., *et al.* (2015) Complex archaea that bridge the gap between prokaryotes and eukaryotes. *Nature* **521**: 173–179.

Stamatakis, A. (2014) RAxML version 8: a tool for phylogenetic analysis and post-analysis of large phylogenies. *Bioinformatics* **30**: 1312–1313.

Stein, N. (2008) CHAINSAW: a program for mutating pdb files used as templates in molecular replacement. *J Appl Crystallogr* **41**: 641–643.

Steiner, A., Stucki, D., Coscolla, M., Borrell, S., and Gagneux, S. (2014) KvarQ: targeted and direct variant calling from fastq reads of bacterial genomes. *BMC Genomics* **15**: 881.

Sterling, T., and Irwin, J.J. (2015) ZINC 15–ligand discovery for everyone. *J Chem Inf Model* **55**: 2324–2337.

Stover, C.K., Warrener, P., VanDevanter, D.R., Sherman, D.R., Arain, T.M., Langhorne, M.H., *et al.* (2000) A small-molecule nitroimidazopyran drug candidate for the treatment of tuberculosis. *Nature* **405**: 962–966.

Tasneen, R., Betoudji, F., Tyagi, S., Li, S.-Y., Williams, K., Converse, P.J., *et al.* (2016) Contribution of oxazolidinones to the efficacy of novel regimens containing bedaquiline and pretomanid in a mouse model of tuberculosis. *Antimicrob Agents Chemother* **60**: 270–277.

Tasneen, R., Williams, K., Amoabeng, O., Minkowski, A., Mdluli, K.E., Upton, A.M., and Nuermbergera, E.L. (2015) Contribution of the nitroimidazoles PA-824 and TBA-354 to the activity of novel regimens in murine models of tuberculosis. *Antimicrob Agents Chemother* **59**: 129–135.

Taylor, M., Scott, C., and Grogan, G. (2013) F420-dependent enzymes-potential for applications in biotechnology. *Trends Biotechnol* **31**: 63.

Taylor, M.C., Jackson, C.J., Tattersall, D.B., French, N., Peat, T.S., Newman, J., *et al.* (2010) Identification and characterization of two families of F420H2-dependent reductases from Mycobacteria that catalyse aflatoxin degradation. *Mol Microbiol* **78**: 561–575.

Thauer, R.K., Jungermann, K., and Decker, K. (1977) Energy conservation in chemotrophic anaerobic bacteria. *Bacteriol Rev* **41**: 100.

Thauer, R.K., Kaster, A.K., Seedorf, H., Buckel, W., and Hedderich, R. (2008) Methanogenic archaea: ecologically relevant differences in energy conservation. *Nat Rev Microbiol* **6**: 579–591.

Tian, J., Bryk, R., Itoh, M., Suematsu, M., and Nathan, C. (2005) Variant tricarboxylic acid cycle in Mycobacterium tuberculosis: identification of α-ketoglutarate decarboxylase. *Proc Natl Acad Sci U S A* **102**: 10670–10675.

Tran, S.L., and Cook, G.M. (2005) The F1Fo-ATP synthase of Mycobacterium smegmatis is essential for growth. *J Bacteriol* **187**: 5023–5028.

Treangen, T.J., Ondov, B.D., Koren, S., and Phillippy, A.M. (2014) The Harvest suite for rapid core-genome alignment and visualization of thousands of intraspecific microbial genomes. *Genome Biol* **15**: 524.

Trott, O., and Olson, A.J. (2010) AutoDock Vina: Improving the Speed and Accuracy of Docking with a New Scoring Function, EfficientOptimization, and Multithreading. *J Comput Chem* **31**: 455–61.

Tzeng, S.F., Wolfe, R.S., and Bryant, M.P. (1975) Factor 420-dependent tyridine nucleotide-linked hydrogenase system of Methanobacterium ruminantium. *J Bacteriol* **121**: 184–191.

Tzing, S.F., Bryant, M.P., and Wolfe, R.S. (1975) Factor 420-dependent pyridine nucleotide-linked formate metabolism of Methanobacterium ruminantium. *J Bacteriol* **121**: 192–196.

Upton, A.M., Cho, S., Yang, T.J., Kim, Y., Wang, Y., Lu, Y., *et al.* (2015) In vitro and in vivo activities of the nitroimidazole TBA-354 against Mycobacterium tuberculosis. *Antimicrob Agents Chemother* **59**: 136–144.

Upton, A.M., and McKinney, J.D. (2007) Role of the methylcitrate cycle in propionate metabolism and detoxification in Mycobacterium smegmatis. *Microbiology* **153**: 3973–3982.

Vagin, A., and Teplyakov, A. (1997) MOLREP: an automated program for molecular replacement. *J Appl Crystallogr* **30**: 1022–1025.

Vornolt, J., Kunow, J., Stetter, K.O., and Thauer, R.K. (1995) Enzymes and coenzymes of the carbon monoxide dehydrogenase pathway for autotrophic CO 2 fixation in Archaeoglobus lithotrophicus and the lack of carbon monoxide dehydrogenase in the heterotrophic A. profundus. *Arch Microbiol* **163**: 112–118.

Walsh, C. (1986) Naturally occurring 5-deazaflavin coenzymes: biological redox roles. *Acc Chem Res* **19**: 216–221.

Wang, F., Jain, P., Gulten, G., Liu, Z., Feng, Y., Ganesula, K., *et al.* (2010) Mycobacterium tuberculosis dihydrofolate reductase is not a target relevant to the antitubercular activity of isoniazid. *Antimicrob Agents Chemother* **54**: 3776–3782.

Wang, P., Bashiri, G., Gao, X., Sawaya, M.R., and Tang, Y. (2013) Uncovering the enzymes that catalyze the final steps in oxytetracycline biosynthesis. *J Am Chem Soc* **135**: 7138–7141.

Wang, Z.-X., Brämer, C.O., and Steinbüchel, A. (2003) The glyoxylate bypass of Ralstonia eutropha. *FEMS Microbiol Lett* **228**: 63–71.

WHO (2016) Global Tuberculosis Report 2016. *Cdc 2016* 214.

Wickham, H. (2016) tidyverse: Easily Install and Load "Tidyverse" Packages. *R Packag version* **1**.

Wiegand, I., Hilpert, K., and Hancock, R.E.W. (2008) Agar and broth dilution methods to determine the minimal inhibitory concentration (MIC) of antimicrobial substances. *Nat Protoc* **3**: 163–75.

Williams, K.J., and Duncan, K. (2007) Current strategies for identifying and validating targets for new treatment-shortening drugs for TB. *Curr Mol Med* **7**: 297–307.

Williams, K.N., Stover, C.K., Zhu, T., Tasneen, R., Tyagi, S., Grosset, J.H., and Nuermberger, E. (2009) Promising antituberculosis activity of the oxazolidinone PNU-100480 relative to that

of linezolid in a murine model. *Antimicrob Agents Chemother* **53**: 1314–1319.

Winn, M.D., Ballard, C.C., Cowtan, K.D., Dodson, E.J., Emsley, P., Evans, P.R., *et al.* (2011) Overview of the CCP4 suite and current developments. *Acta Crystallogr Sect D Biol Crystallogr* **67**: 235–242.

Wit, L.E.A. De, and Eker, A.P.M. (1987) 8-Hydroxy-5-deazaflavin-dependent electron transfer in the extreme halophile Halobacterium cutirubrum. *FEMS Microbiol Lett* **48**: 121–125.

Wood, D.E., and Salzberg, S.L. (2014) Kraken: ultrafast metagenomic sequence classification using exact alignments. *Genome Biol* **15**: R46–R46.

Wu, D., Hugenholtz, P., Mavromatis, K., Pukall, R., Dalin, E., Ivanova, N.N., *et al.* (2009) A phylogeny-driven genomic encyclopaedia of Bacteria and Archaea. *Nature* **462**: 1056–1060.

Wyllie, S., Roberts, A.J., Norval, S., Patterson, S., Foth, B.J., Berriman, M., *et al.* (2016) Activation of Bicyclic Nitro-drugs by a Novel Nitroreductase (NTR2) in Leishmania. *PLOS Pathog* **12**: e1005971.

Xia, K., Shen, G.-B., and Zhu, X.-Q. (2015) Thermodynamics of various F420 coenzyme models as sources of electrons, hydride ions, hydrogen atoms and protons in acetonitrile. *Org Biomol Chem* **13**: 6255–6268.

Yamazaki, S., Tsai, L., Stadtman, T.C., Jacobson, F.S., and Walsh, C. (1980) Stereochemical studies of 8-hydroxy-5-deazaflavin-dependent NADP+ reductase from Methanococcus vannielii. *J Biol Chem* **255**: 9025–9027.

Yuan, Y., Zhu, Y., Crane, D.D., and Barry III, C.E. (1998) The effect of oxygenated mycolic acid composition on cell wall function and macrophage growth in Mycobacterium tuberculosis. *Mol Microbiol* **29**: 1449–1458.

Zumla, A., Nahid, P., and Cole, S.T. (2013) Advances in the development of new tuberculosis drugs and treatment regimens. *Nat Rev Drug Discov* **12**: 388–404.

Zuniga, E.S., Early, J., and Parish, T. (2015) The future for early-stage tuberculosis drug discovery. *Future Microbiol* **10**: 217–229.